N° d'ordre : 2766

THÈSE

présentée à

L'UNIVERSITÉ BORDEAUX I

ÉCOLE DOCTORALE DES SCIENCES CHIMIQUES

par M^elle Marie-Christine DANIEL

POUR OBTENIR LE GRADE DE

DOCTEUR

SPÉCIALITÉ : CHIMIE ORGANIQUE

****

RECONNAISSANCE ELECTROCHIMIQUE SUPRAMOLECULAIRE D'ANIONS D'INTÉRÊT BIOLOGIQUE À L' AIDE DE RÉCEPTEURS DENDRITIQUES ET À BASE DE NANOPARTICULES D'OR

****

Soutenue le : **22 décembre 2003**

Après avis de :

M. Bernard MEUNIER, Directeur de Recherche CNRS (LCC, Toulouse) **Rapporteurs**
M. Jean-René HAMON, Directeur de Recherche CNRS (Université Rennes 1)

Devant la commission d'examen formée de :

M. Stéphane GRELIER, Professeur (Université Bordeaux 1) **Président**
M. Bernard MEUNIER, Directeur de Recherche CNRS (LCC, Toulouse) **Rapporteurs**
M. Jean-René HAMON, Directeur de Recherche CNRS (Université Rennes 1)
M. Alexander KUHN, Professeur (Université Bordeaux 1) **Examinateurs**
M. Jaime RUIZ, Ingénieur de Recherche CNRS (Université Bordeaux 1)
M. Didier ASTRUC, Professeur (Université Bordeaux 1)

- 2003 -

"La pierre n'a point d'espoir d'être autre chose que pierre.
Mais de collaborer, elle s'assemble et devient temple."

Antoine de Saint-Exupéry

Citadelle, ch. 9.

A mes parents.

A ma famille.

A tous mes amis.

Ce travail a été effectué au Laboratoire de Chimie Organique et Organométallique de l'Université Bordeaux 1 (CNRS U.M.R. 5802), sous la direction scientifique du Professeur Didier Astruc.

☺ ☺ ☺ ☺ ☺ ☺ ☺ ☺ ☺ ☺ ☺ ☺

Je remercie M. le Professeur Didier Astruc pour m'avoir accueillie dans son équipe de recherche et pour m'avoir donné l'opportunité de réaliser ma thèse sur un sujet porteur. J'ai ainsi pu me familiariser avec la chimie organométallique. Je le remercie pour l'enthousiasme avec lequel il a dirigé cette thèse, pour les nombreux conseils et idées qu'il m'a donnés mais aussi pour son attention quotidienne à l'évolution des travaux et pour son souci permanent de me faire progresser et de valoriser le travail accompli.

J'adresse mes sincères remerciements à M. Bernard Meunier, Directeur de Recherche CNRS au Laboratoire de Chimie de Coordination de Toulouse et membre de l'Académie, et M. Jean-René Hamon, Directeur de Recherche CNRS à l'Université de Rennes 1, pour avoir accepté d'être rapporteurs de ce manuscrit.

J'exprime toute ma reconnaissance à M. Alexander Kuhn et à M. Stéphane Grelier, Professeurs à l'Université de Bordeaux 1, ainsi qu'à M. Jaime Ruiz, Ingénieur de Recherche CNRS, qui m'ont fait l'honneur de bien vouloir participer à mon jury.

☺ ☺ ☺ ☺ ☺ ☺ ☺ ☺ ☺ ☺ ☺ ☺

Je remercie de tout cœur chaque personne que j'ai côtoyée pendant ma thèse au laboratoire et qui a apporté sa pierre à l'édifice, tant au niveau matériel que psychologique:

J'exprime, en particulier, toute ma gratitude à M. Jaime Ruiz, Ingénieur de Recherche CNRS, qui m'a encadrée tout au long de ma thèse avec enthousiasme et dynamisme, et a su composer avec mon caractère… J'ai beaucoup apprécié sa grande disponibilité, son altruisme, son soutien constant et son sens de la transmission du savoir, plus spécialement dans l'initiation à la voltammétrie cyclique. De plus, ses nombreux conseils, ses encouragements et sa faculté d'écoute m'ont permis de progresser et de me surpasser. Aussi, il n'a pas hésité à s'investir dans les travaux de ma thèse, sans quoi les résultats n'auraient pu être si nombreux, et je lui en suis très reconnaissante. Merci pour tout.

Je remercie également M. Sylvain Nlate, Maître de Conférence, pour avoir apporté sa contribution aux travaux de ma thèse par la synthèse des dendrons silylferrocényles et pour ses conseils concernant l'enseignement.

En ce qui concerne les analyses des produits synthétisés, je remercie sincèrement Jean-Claude BLAIS, Directeur de Recherche à l'Université de Pierre et Marie Curie, pour les analyses en spectroscopie de masse.

Je remercie aussi Mme Karine Heuzé, Chargée de Recherche CNRS, pour ses conseils, sa franchise et son sens de l'humour toujours bien dosé.

Je remercie encore Agnès Labande, à qui j'ai succédé et qui m'a gentiment passé le flambeau.

Je tiens également à remercier Sylvain Gatard pour son soutien, son écoute et sa compréhension dans les moments difficiles. Merci beaucoup.

Je dois aussi un grand merci à Victor Martinez (qui m'a accompagné de ses taquineries pendant ces trois ans: sans rancune!), pour toutes les fois où il a résolu mes problèmes informatiques, et il sait qu'il y en a eu... Muchas gracias!

Quiero agradecer a Gustavo Lafuente y Yolanda Nieto quienes generaron un ambiente convivial y solidario en el grupo; además me ayudaron a aprender la langua española mundana. Seran por siempre mis amigos.

Je voudrais aussi remercier Catiá Ornelas pour son amitié sincère et sa présence toujours solidaire. Elle reste pour moi un modèle de sérénité à toute épreuve. Obrigada!

J'exprime ma reconnaissance à María-Jesus Ruiz-Medel et Fatou Bá qui ont aidé à la progression des travaux de ma thèse avec gentillesse et dévouement.

Je remercie également Denise Mery qui a partagé un bureau avec moi pendant quelques mois et dont j'ai apprécié la compagnie amicale et réconfortante si besoin durant ces deux dernières années.

De même, je remercie Julietta Lemo, Lauriane Plault, Andreas Haeuseler, Ignacio Quiros et Magali Szlosek-Pinaud, qui ont contribué, chacun à leur manière à un bon climat pendant ma dernière année de thèse. Je n'oublie pas non plus Santi et Bénédicte, Ricardo, Veronicá et Dominik pour leur sympathie lors de leur passage au laboratoire.

Merci aussi à Jocelyne Moncada, à qui je dois d'avoir tapé les 700 références de la revue sur les nanoparticules d'or. Je la remercie pour sa gentillesse et sa patience.

Enfin, je n'oublie pas Michel Colomes, Jacky Handy et Fabrice Forlini pour les fois où ils m'ont aidée face à un ennui technique.

Pour terminer, je remercie tous les autres membres du personnel du laboratoire qui ont permis que je travaille dans de meilleures conditions.

☺ ☺ ☺ ☺ ☺ ☺ ☺ ☺ ☺ ☺ ☺ ☺

SOMMAIRE

PARTIE 3: Assemblages nanoscopiques de métallodendrons électroactifs et de nanoparticules d'or pour la reconnaissance d'$H_2PO_4^-$, d'HSO_4^- et de l'ATP^{2-}.

Introduction

Note préliminaire:

Gold nanoparticles containing redox-active supramolecular dendrons that recognize $H_2PO_4^-$.

Mémoire:

Nanoscopic Assemblies between Supramolecular Redox Active Metallodendrons and Gold Nanoparticles: Synthesis, Characterization, and Selective Recognition of $H_2PO_4^-$, HSO_4^- and adénosine-5'-triphosphate (ATP^{2-}) Anions.

RESUME – CONCLUSION

PERSPECTIVES

ANNEXES:

***Annexe 1*:** Nano-Scale Metallodendritic Complexes in Electron-Transfer Processes and Catalysis.

Annexe 2: Gold Nanoparticles: Assembly, Supramolecular Chemistry, Quantum-size Related Properties and Applications towards Biology, Catalysis and Nanotechnology**.**

INTRODUCTION GENERALE

INTRODUCTION GENERALE

En ce début du XXI^{ème} siècle, un domaine d'actualité et d'avenir est celui des nanosciences. En effet, ces dernières sont en pleine expansion et présentent déjà des résultats très prometteurs. En chimie plus particulièrement, les colloïdes, les dendrimères et les monocouches auto-assemblées connaissent actuellement un véritable essor. Les deux premiers types d'entités, de tailles nanoscopiques, présentent une potentialité importante: elles ont des applications diverses et variées telles que la catalyse, la mise au point de matériaux, la biologie et la reconnaissance moléculaire entre autres.

Un dendrimère, aussi appelé arbre moléculaire, est une macromolécule arborescente parfaitement définie, composé d'un cœur dendritique et d'un nombre plus ou moins élevé de fonctions à sa périphérie.[1] Plusieurs méthodes permettent de les préparer. Dans cette thèse, trois voies ont été explorées: la formation de dendrimères de manière covalente, de façon supramoléculaire et à partir d'un cœur colloïdal.

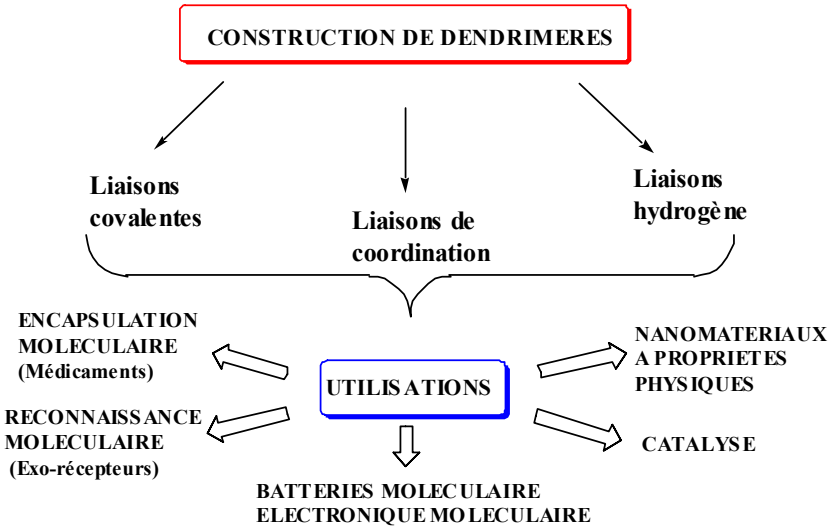

Un colloïde (ou nanoparticule) se définit comme un assemblage constitué d'un agrégat métallique (or, argent, platine, palladium, cadmium, etc…) stabilisé par des ligands organiques.[2] Dans cette thèse, nous avons choisi de travailler avec des nanoparticules d'or car ce sont les nanoparticules métalliques très stables. Les ligands choisis pour leur stabilisation sont des ligands thiols puisque ce sont ceux qui ont la plus forte interaction avec l'or. Ceux-ci

permettent d'empêcher l'agrégation extensive des particules qui formerait de l'or métallique massif.

Colloïdes et dendrimères ont en commun leur taille nanoscopique ainsi que leur haute ramification et leur forme globulaire. Cependant, leur principale différence réside dans le fait que les ligands du colloïde s'écartent en s'éloignant du noyau métallique alors que, dans le dendrimère, les branches se resserrent en s'éloignant du cœur. Ces caractéristiques confèrent à ces deux types d'objets nanoscopiques des propriétés bien particulières, ce qui permet, entre autre, de les utiliser comme capteurs pour la reconnaissance d'anions.

Les anions ont un rôle important dans notre environnement car on les retrouve tant dans l'industrie pharmaceutique ou agricole que dans le monde du vivant. En effet, les médicaments contiennent des chlorhydrates et des carboxylates, et les engrais renferment des phosphates et des nitrates. De plus l'acide désoxyribonucléique (ADN), support de l'information génétique et l'ATP (adénosine-5'-triphosphate), avec lequel nous avons travaillé pendant cette thèse, sont des polyanions d'importance centrale en biologie.

En effet, l'ATP est un coenzyme transporteur d'énergie universel, par hydrolyse d'une de ses liaisons P-O riches en énergie. Sa présence dans le métabolisme de tous les êtres vivants souligne l'intérêt de cette molécule comme carrefour métabolique de tous les échanges d'énergie. Cette énergie peut apparaître sous de multiples formes: en énergie mécanique, comme dans la contraction musculaire; en énergie osmotique, comme dans les échanges Na^+/K^+ au niveau des membranes cellulaires; en énergie chimique, pour effectuer des synthèses de produits biologiques; en énergie calorique, pour maintenir la température de 37°C; en énergie électrique, pour la propagation de l'influx nerveux; et enfin en énergie lumineuse, chez le vers luisant, par exemple.

En plus de l'énergie, les enzymes transfèrent souvent une partie de la structure chimique de l'ATP. Ainsi, l'ATP peut être donneur:

-de phosphate, avec la plupart des enzymes de phosphorylation ou kinases;

-de pyrophosphate, comme dans l'activation de la vitamine B_1 ou thiamine;

-d'adénosine, comme dans la synthèse des coenzymes B12 ou adénosyl-méthionine;

-d'adénosine monophosphate , comme dans l'activation des acides gras ou des acides aminés. C'est aussi l'un des quatre nucléotides qui composent l'ADN.

D'autre part, certains anions sont en partie responsables de la pollution des cours d'eau à cause de l'emploi massif de fertilisants (phosphates, nitrates). Toutes ces constatations nous convainquent donc de la réelle nécessité de pouvoir détecter et capter les anions.

Bien que la reconnaissance des anions soit moins développée et plus récente (fin des années 60 mais surtout depuis 20 ans) que celle des cations, plusieurs approches ont été abordées. D'une part, deux principaux types de récepteurs sont utilisés: les endorécepteurs et les exo récepteurs. Les endorécepteurs présentent des cavités internes capables d'accueillir les anions et les exorécepteurs possèdent des cavités externes dans lesquelles les anions vont se loger. D'autre part, plusieurs méthodes sont utilisées pour signaler l'interaction anion-récepteur.

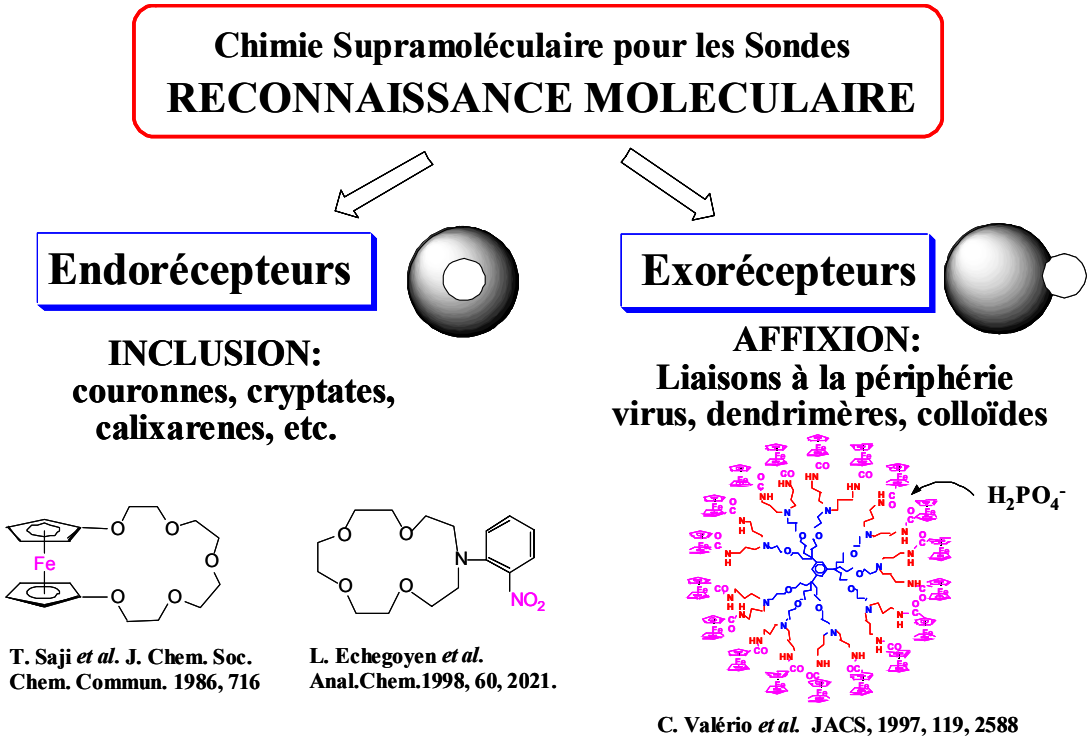

Ces dernières années, principalement deux revues ont parcouru le sujet.[3] D'un côté, des méthodes optiques ont été employées, telles que la fluorescence[4] (P. Turkewitsch *et al.* ont travaillé sur des polymères comportant des cavités réceptrices d'anion) et la luminescence[5] (l'équipe de R. S. Dickins a utilisé des complexes de lanthanides cationiques). A. W. Czarnik *et al.* ont, quant à eux, fabriqué des récepteurs mettant en jeu un processus de transfert d'électrons photoinduits,[6] c'est-à-dire qu'on assiste à une modulation de la luminescence du récepteur par association avec l'anion. De plus, E. V. Anslyn a imaginé une méthode de compétition qui met en jeu un assemblage récepteur-indicateur[7] et où l'indicateur sera déplacé par l'anion ajouté en solution (impliquant un changement de couleur si on dispose d'un

indicateur colorimétrique). D'un autre côté, le groupe de J.-M. Lehn[8] a conçu une panoplie d'endorécepteurs macrocycliques et macropolycycliques contenant des ammoniums et interagissant avec l'anion par liaison hydrolyse et par attraction électrostatique. Celui de Y. Umezawa a créé une série de récepteurs (bis)thio-urées acycliques en forme de pince: certains s'associent fortement au dihydrogénophosphate grâce à des liaisons hydrogène et à un système hautement préorganisé;[9] d'autres, incorporés dans une membrane électroactive (électrode sélective d'ions), détectent sélectivement les chlorures. Reinhoudt *et al.* ont introduit des dérivés uranylsalophanes dans des membranes de transistors à effet de champs chimiquement modifié,[10] ce qui forme des sondes sélectives d'anions. D'autre part, l'équipe de P. D. Beer[11] a préparé une variété de récepteurs acycliques, macrocycliques, et à base de calixarènes, comportant des fonctions cobalticiniums mais aussi plus récemment des fonctions ferrocénylamines. Ces fonctions électroactives permettent une détection par voltammétrie cyclique.

La voltammétrie cyclique est une méthode d'analyse électrochimique à potentiel contrôlé, qui permet de détecter des composés oxydables et réductibles en solution. Pour une explication détaillée et complète de cet outil de mesure, il est possible de se référer au livre d'Alan Bard[12] ou à celui de Didier Astruc.[13]

Dans notre groupe, des travaux concernant la reconnaissance d'anions par voltammétrie cyclique ont été réalisés depuis quelques années.[14] En effet, certains thèmes de recherche de l'équipe de D. Astruc impliquent les métallocènes, les dendrimères et, plus récemment, les colloïdes d'or. Fort de ces acquis, une série de dendrimères à base de dérivés du ferrocène a d'abord été développée, en utilisant le composé ferrocénique soit comme cœur dendritique, soit comme fonction terminale à la périphérie du dendrimère. Une première approche de la reconnaissance d'oxo anions a mis en jeu des dendrimères 9-amidoferrocényles et 18-amidoferrocényles à cœur aromatique.[15]

Une comparaison des dendrimères avec les colloïdes d'or a ensuite été réalisée c'est-à-dire que des nanoparticules d'or comportant des ligands amidoferrocényles ont été synthétisées et leur pouvoir de reconnaissance des oxoanions a été testé.[16] Les résultats acquis montrent un comportement comparable à celui des dendrimères.

Ces colloïdes, comme les dendrimères homologues, donnent lieu à un voltammogramme présentant une seule vague d'oxydo-réduction correspondant à toutes les

fonctions ferrocényles terminales. En fait, tous les ferrocènes sont équivalents. A l'échelle de temps électrochimique, ils apparaissent dans une seule vague réversible de voltammétrie cyclique, du fait de la rotation rapide des molécules en solution.

La détection des anions se matérialise de deux manières selon les anions ajoutés. Soit une nouvelle vague se forme à des potentiels moins positifs que la vague initiale, ce qui traduit une interaction forte entre anion et récepteur. Soit la vague de départ se déplace peu à peu vers des potentiels moins positifs, ce qui reflète une interaction plus faible entre anion et récepteur.

A partir de la différence de potentiel entre les deux vagues, ou du déplacement total de la vague, on peut accéder aux constantes d'association entre l'anion et le groupement ferrocényle, ceci grâce au schéma carré de L. Echegoyen /A. E. Kaifer.[17] Dans le cas d'une interaction faible (donc avec un déplacement ΔE_1 de la vague), l'équation utilisée est la suivante: $\Delta E_1 = 0{,}058.\log (K^+ c)$ où c est la concentration en anion à saturation. Si l'interaction anion-récepteur est forte (donc avec un écart entre les deux vagues ΔE_2), voici l'équation qui convient: $\Delta E_2 = 0{,}058.\log (K^+ / K^0)$.

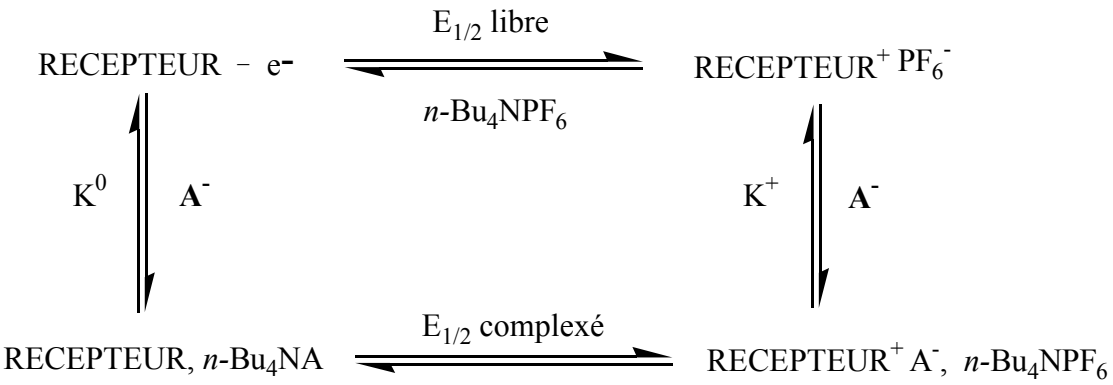

Schéma carré représentant le comportement électrochimique d'un récepteur électroactif en présence d'un anion.[17]

Le phénomène de reconnaissance résulte de la synergie de trois effets décrits dans le schéma ci-après. Il implique la formation de liaisons hydrogènes entre les atomes d'oxygènes et d'hydrogènes de l'oxoanion d'une part et des fonctions du récepteur. Quand le couple rédox est sous sa forme oxydée, une attraction électrostatique se crée entre le cation formé et l'anion. Enfin, vient s'ajouter à cela un effet dendritique dû à la forme particulière des dendrimères qui présentent des cavités périphériques dans lesquelles les anions vont s'insérer. Les deux premières interactions sont alors consolidées.

PHENOMENE DE RECONNAISSANCE:
Synergie de trois effets

- Double liaison hydrogène :

x = 0 or +1

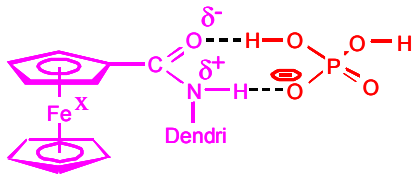

- Attraction électrostatique avec la forme ferricinium:

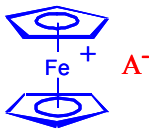

- Topologie. **Effet dendritique**
  Compression stérique et effet tunnel / cavité
  à la périphérie du dendrimère

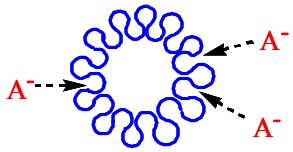

Cette thèse s'inscrit donc dans ce contexte. Son objectif est la reconnaissance électrochimique supramoléculaire d'anions d'intérêt biologique à l'aide d'exorécepteurs dendritiques et à base de nanoparticules d'or. Le manuscrit est composé de trois parties. Les premières et troisième parties sont constituées d'une note préliminaire et d'un mémoire, la présente introduction servant de canevas général. Pour la seconde partie, seule la note préliminaire est disponible et un mémoire a été rédigé à l'occasion de cette thèse.

La première partie sera dédiée aux travaux menés sur des métallodendrimères formés par liaisons covalentes. Il est constitué d'une note préliminaire suivie d'un mémoire qui détaillent l'élaboration, par voie covalente, de dendrimères pentaméthylamidoferrocényles robustes permettant une reconnaissance des oxoanions plus propre en voltammétrie cyclique et montrant aussi une certaine sélectivité envers le dihydrogénophosphate et l'adénosine-5'-triphosphate.

La seconde partie décrit la préparation de métallodendrimères par voie supramoléculaire et leurs propriétés en reconnaissance des oxoanions. Elle est composée d'une note préliminaire s'intéressant au dihydrogénophosphate et qui devance un mémoire en français présentant la description détaillée des travaux complémentaires effectués et dont une version en anglais sera rapidement soumise à publication.

La troisième partie traitera de la préparation de nanoparticules d'or contenant des dendrons à terminaisons ferrocényles et de leur utilisation en voltammétrie cyclique pour la reconnaissance d'anions tels que le dihydrogénophosphate $H_2PO_4^-$, l'adénosine-5'-triphosphate ATP^{2-} et l'hydrogénosulfate HSO_4^-. On y trouvera une note préliminaire concernant la synthèse et l'utilisation de colloïdes d'or possédant des dendrons de première génération et reconnaissant $H_2PO_4^-$. Suivra un mémoire développant l'élargissement des travaux à la synthèse de dendrons de seconde génération, à la reconnaissance de l'ATP^{2-} et d'HSO_4^- et à la fabrication d'électrodes chimiquement modifiées.

L'annexe 2 sera consacrée à la bibliographie relative aux nanoparticules d'or. Cette recherche a fait l'objet d'une revue intitulée "Gold Nanoparticles: Assembly, Supramolecular Chemistry, Quantum-size Related Properties and Applications toward Biology, Catalysis and Nanotechnology.".

Enfin, un résumé-conclusion et quelques perspectives seront proposés. Pour clôturer ce manuscrit, vous trouverez, en annexe de ce fascicule, une revue des travaux de notre groupe de recherche sur les fonctions des métallodendrimères.

Références:

1- V. Ardoin, D. Astruc. *Bull. Chim. Soc. Fr.*, **1995**. *132,* 875.

2- D. Astruc. *Chimie Organométallique*, EDP Sciences, Les Ullis, 2000.

3- T. S. Snowden, E. V. Anslyn. Curr. *Opin. Chem. Biol.*, **1999**, *3*, 740; P. D. Beer, P. A. Gale. *Angew. Chem. Int. Ed. Engl*. **2001**, *40*, 486.

4- P. Turkewitsch, B. Wandelt, G. D. Darling, W. S. Powell. *Anal. Chem.*, **1998**, *70*, 2025.

5- R. S. Dickins, T. Gunnlaugsson, D. Parker, R. D. Peacock. *Chem. Commun.*, **1998**, 1643.

6- A. W. Czarnik. *Acc. Chem. Res.,* **1994**, *27*, 302.

7- K. Niikura, A. Metzger, E. V. Anslyn. *J. Am. Chem. Soc.,* **1998**, *120*, 8533.

8- E. Graf, J.-M. Lehn. *J. Am. Chem. Soc.*, **1976**, *98*, 6403; J.-M. Lehn, E. Souveaux, A. K. Willard. *J. Am. Chem. Soc.*, **1978**, *100*, 4914; B. Dietrich, J. Guilhem, J.-M. Lehn, C. Pascard, E. Souveaux. *Helv. Chim. Acta.*, **1984**, *67*, 91; M. W. Hosseini, J.-M. Lehn. *J. Am. Chem. Soc.*, **1982**, *104*, 3525; M. W. Hosseini, J.-M. Lehn. *Helv. Chim. Acta*, **1986**, *69*, 587.

9- P. Buhlmann, S. Nishizawa, K. P. Xiao, Y. Umezawa. *Tetrahedron*, **1997**, *53*, 1647.

10- M. M. G. Antonisse, B. H. M. Snellink-Ruel, A. C. Ion, J. F. J. Engbersen, D. N. Reinhoudt. *J. Chem. Soc. Perkin Trans. 2*, **1999**, 1211.

11- P. D. Beer, M. G. B. Drew; J. Hodacova; S. E. Stokes. *J. Chem. Soc., Dalton Trans.* **1995**, 3447; P. D. Beer, *J. Chem. Soc. Chem. Commun.* **1996**, 689; P. D. Beer. *Acc. Chem. Res.* **1998**, *31*, 71; P. D. Beer. P. A. Gale, Z. Chen. *Adv. Phys. Org. Chem*. **1998**, *31*, 1; P. D. Beer, J. Cadman, J. M. Lloris, R. Martinez-Mànez, M. E. Padilla, T. Pardo, D. K. Smith, J. Soto. *J. Chem. Soc., Dalton Trans.* **1999**, 127; P. D. Beer, J. Davis, D. A. Drillsma-Millgrom, F. Szemes. *Chem. Commun*. **2002**, 1716.

12- A. J. Bard, L. R. Faulkner. *Electrochemical Methods*. Wiley, New York, 1980.

13- D. Astruc. *Electron-Transfer and Radical Processes in Transition-Metal Chemistry*, VCH, New York, 1995, Chapitre 2.

14- D. Astruc. *Pure Appl. Chem.* **2003**, *79*, 461.

15- C. Valério, J.-L. Fillaut, J. Ruiz, J. Guittard., J.-C. Blais, D. Astruc. *J. Am. Chem. Soc.* **1997**, *119*, 2588.

16- A. Labande, J. Ruiz, D. Astruc. *J. Am. Chem. Soc.* **2002**, *124*, 1782.

17- S. R Miller, D. A. Gustowski, Z.-H. Chen, G. W. Gokel, L. Echegoyen, A. E. Kaifer. *Anal. Chem*. **1988**, *60*, 2021.

PARTIE 1:

ETUDE COMPARATIVE DE DENDRIMERES PENTAMETHYLAMIDOFERROCENYLES ET AMIDOFERROCENYLES EN TANT QUE SONDES ELECTROCHIMIQUES POUR LES ANIONS $H_2PO_4^-$, HSO_4^- et ATP^{2-}.

.

Etude comparative de dendrimères pentaméthylamidoferrocényles et amidoferrocényles en tant que sondes électrochimiques pour les anions $H_2PO_4^-$, HSO_4^- et ATP^{2-}.

De nouveaux dendrimères, portant des fonctions amidoferrocényles perméthylées ont été synthétisés et comparés à leurs homologues non perméthylés en ce qui concerne la voltammétrie cyclique.

Dans un premier temps, la reconnaissance du dihydrogénophosphate dans le dichlorométhane et dans le diméthylformamide a fait l'objet d'une note préliminaire publiée à *Chemical Communication* et intitulée:

Redox-robust pentamethylamidoferrocenyl metallodendrimers that cleanly and selectively recognize the $H_2PO_4^-$.

Dans un deuxième temps, ces études ont été étendues à la reconnaissance de l'hydrogénosulfate et de l'ATP^{2-}, ainsi qu'à la sélectivité de cette reconnaissance. Ceci a donné lieu à l'élaboration d'un mémoire publié à *Chemistry, European Journal* et intitulé:

Synthesis of Five Generations of Redox-Stable Pentamethylamidoferrocenyl Dendrimers and Comparison of amidoferrocenyl- and Pentamethylamido-ferrocenyl Dendrimers as electrochemical exoreceptors for the selective recognition of $H_2PO_4^-$, HSO_4^-, and Adénosine-5'-Triphosphate (ATP) Anions: Stereoelectronic and Hydrophobic Roles of Cyclopentadienyl Permethylation.

Les principes mis en jeu ainsi que les résultats obtenus sont résumés respectivement dans l'introduction générale et dans le résumé final de ce manuscrit.

COMMUNICATION

ChemComm
www.rsc.org/chemcomm

Redox-robust pentamethylamidoferrocenyl metallodendrimers that cleanly and selectively recognize the $H_2PO_4^-$ anion†

Jaime Ruiz,[a] Maria Jesus Ruiz Medel,[a] Marie-Christine Daniel,[a] Jean-Claude Blais[b] and Didier Astruc*[a]

[a] *LCOO, UMR CNRS N° 5802, Université Bordeaux I, 33405 Talence Cedex, France*
[b] *LCSOB, UMR CNRS N° 7613, Université Paris VI, 75252 Paris, France*

Received (in Cambridge, UK) 26th November 2002, Accepted 10th January 2003
First published as an Advance Article on the web 27th January 2003

The first pentamethylferrocenyl (Fc*) dendrimers are synthesized from DSM polyamine dendrimers (generations 1 to 5) and cleanly and selectively recognize the $H_2PO_4^-$ anion.

Nanoreceptors for anion recognition should have practical applications but are so far much less common than the model molecular systems.[1] Nanoscopic exoreceptors have recently been designed with dendrimers[2a] and gold nanoparticles[2b] terminated with amidoferrocenyl groups that bring the supramolecular basis for the recognition of $H_2PO_4^-$ anion. A key drawback is that these systems are marred by adsorption peaks in the cyclovoltammograms and by chemical irreversibility due to instability upon oxidation. The stabilizing C_5Me_5 (Cp*) ligand has already been introduced in pentamethylferrocenyl (Fc*) termini on thiol ligands of nanoparticles in order to study the electronic consequence of Cp permethylation on the recognition parameters.[2b] Metallodendrimers[3] are especially attractive, and positive dendritic effects enhance the recognition of this anion for high generations.[2a] Whereas there are numerous ferrocenyl (Fc) dendrimer families,[4] we are reporting here the first examples of Fc* dendrimer and their excellent and selective sensing properties.

The new compounds are derived from DSM's polyamine dendrimers DAB-dend-$(NH_2)_x$ (x = 4, 8, 16, 32, 64).[5] These five generations G_1 (x = 4) to G_5 (x = 64) of metallodendrimers are easily available by reactions between these polyamines and Fc*COCl[2b] in CH_2Cl_2 at RT overnight in the presence of triethylamine. The parent amidoferrocenyl dendrimers (Fc series) are known from the work of Cuadrado's group who has also reported their electrochemistry in order to examine their deposition on platinum surfaces.[6] Since no molecular recognition studies have been published with these compounds, we have undertaken anion recognition studies with both Fc* and Fc series for comparison. We now report that both families can recognize $H_2PO_4^-$ using the variation of Fe^{II}/Fe^{III} redox potentials of these metallodendrimers, and that this new Fc* series shows much less adsorption and no chemical irreversibility that prevent a clean recognition in the Fc series. The dramatic advantage of the Fc* series over the parent one for redox recognition is due to both the stabilization of the 17-electron form and the lipophilicity brought about by the numerous methyl groups located at the dendrimer periphery.

These new dendrimers were suitably characterized by the standard analytical and spectroscopic techniques (including molecular peaks that are prominent in the MALDI TOF mass spectra and sharp for G_1 to G_4†) and by cyclic voltammetry (CV, Table 1). The fact that there is only one CV wave is attributable to the rotation of the dendrimers that is much more rapid than the electrochemical time scale, as for other Fc dendrimers.[7] Their $E_{1/2}$ value is 0.405 ± 0.005 V *vs.* [FeCp*$_2$] in CH_2Cl_2, and thus does not significantly vary from G_1 to G_5. This value is compared to that of the parent series that is 0.690

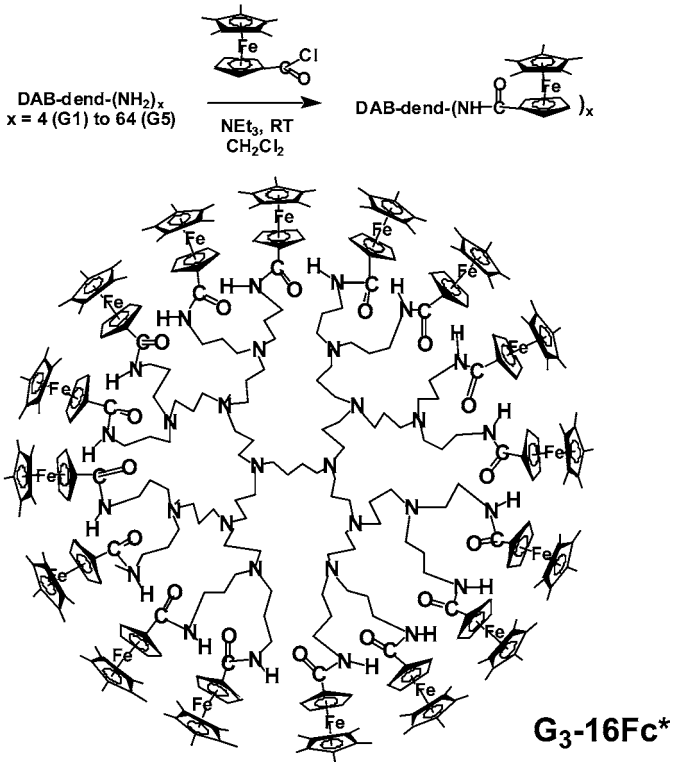

± 0.010 V *vs.* [FeCp*$_2$].[6] [FeCp*$_2$] is a much better reference than ferrocene[8] (because ferrocenium is sensitive to the medium) for the investigation of possible small dendritic effects, and we conclude here to their absence using [FeCp*$_2$] as the reference ($E_{1/2}$ *vs.* $FeCp_2$ = $E_{1/2}$ *vs.* FeCp*$_2$ + 0.545 V in CH_2Cl_2, or + 0.595 V in DMF[8]).

The comparison of these CV with those of the parent series shows that the permethylated Fc* dendrimers behave in a much better fashion than the parent Fc series. One of the dramatic differences between the CV of the dendritic Fc* and parent Fc series is that the Fc* series shows almost no adsorption in CH_2Cl_2, the i_{pc}/i_{pa} values being 1.00 ± 0.03 for G_1, G_2 and G_3, 1.1 for G_4 and 1.2 for G_5. On the contrary, the parent Fc series shows i_{pc}/i_{pa} values between 2 and 3.4 under the same conditions (0.2 V s^{-1}, 20 °C, Pt anode, CH_2Cl_2, 0.1 M nBu$_4$NPF$_6$) indicating strong adsorption (Fig. 1). This difference of behavior towards adsorption is confirmed by the $E_{pc} - E_{pa}$ values which are 0.06 V for G_1, G_2 and G_3, 0.05 V for G_4 and 0.035 V for G_5 for the Fc* series and only 0.03 V for G_1 to G_5 in the parent Fc series. In DMF, the i_{pc}/i_{pa} value is 1.05 ± 0.05 for the Fc* series, but it decreases from 0.9 for G_1 to 0.4 for G_2, G_3 and G_4 in the parent Fc series under these conditions. This shows chemical irreversibility in the Fc series, *i.e.* decomposition of the parent ferrocenium dendrimers is all the more rapid in this solvent as the generation number increases, even on the short CV time scales (Fig. 1). The measured values of the number n of electrons correspond to the theoretical numbers[9] within 10% in either CH_2Cl_2 or DMF for the generations G_1 to G_4 (Table 1).

† Electronic supplementary information (ESI) available: experimental procedures, spectroscopic and analytical data of the Fc* dendrimers, and titration graph of [nBu$_4$N][H_2PO_4] by G_2-8Fc* using the variations of current intensities of the initial and new waves by cyclic voltammetry. See http://www.rsc.org/suppdata/cc/b2/b211772j/

DOI: 10.1039/b211772j

Table 1 Cyclovoltammetry data for G_1–G_5 (both Fc and Fc* series) before and after titration of $[n\text{Bu}_4\text{N}][H_2PO_4]$

	$E_{1/2}{}^a$ (Ep_a-Ep_c)		ip_c/ip_a		n^b		$\Delta E_{1/2}(H_2PO_4^-)^a$ ($Ep_a - Ep_c$)		$K_{(+)}/K_{(o)}{}^c$ $K_{(+)}{}^d$	
	CH_2Cl_2	DMF	CH_2Cl_2	DMF	CH_2Cl_2	DMF	CH_2Cl_2	DMF	CH_2Cl_2	DMF
G_0-1Fc	0.700 (0.06)	0.615 (0.06)	1.1	0.92	1.1	1.1	0.155 (0.15)	0.65 (0.09)	470	
G_1-4Fc	0.695 (0.03)	0.645 (0.07)	3.2	0.75	3.5		0.310 (0.09)	0.265 (0.16)	$2.2.10^5$	
G_2-8Fc	0.675 (0.03)	0.650 (0.08)	2.2	0.46	7.2		0.250 (0.11)	**	$2.0.10^4$	
G_3-16Fc	0.690 (0.03)	0.650 (0.08)	3.5	0.42	16.0		0.170 (0.15)	**	850	
G_4-32Fc	0.690 (0.04)	0.650 (0.08)	1.9	0.40	32	31.5	**	**		
G_5-64Fc	0.680 (0.03)	0.670 (0.10)	3.4	0.62		53	**	**		
G_1-4Fc*	0.406 (0.06)	0.360 (0.07)	1.05	1.07	3.8	4.2	0.155 (0.16)	0.115 (0.06)	470	$9.6.10^3$
G_2-8Fc*	0.395 (0.06)	0.370 (0.08)	1.02	1.1	7.9	8.0	0.160 (0.11)	0.125 (0.07)	570	14.10^3
G_3-16Fc*	0.410 (0.06)	0.370 (0.07)	1.01	1.12	15.1		0.130 (0.13)	0.145 (0.08)	170	32.10^3
G_4-32Fc*	0.400 (0.05)	0.390 (0.07)	1.1	1.05	32		0.140 (0.17)	0.165 (0.06)	260	70.10^3
G_5-64Fc*	0.410 (0.035)	0.375 (0.03)	1.2	1.06	55		0.160 (0.17)	0.140 (0.03)	570	26.10^3

[a] $E_{1/2} = (Ep_a + Ep_c)/2$ *vs.* $FeCp_2^*$, in Volts. Electrolyte: $[n\text{-Bu}_4\text{N}][PF_6]$ 0.1 M; working and counter electrodes: Pt; reference electrode: Ag; (internal reference: $FeCp^*_2$); scan rate: 0.200 V s^{-1}; 20 °C; [b] Values of the number of electrons involved calculated from the Anson–Bard equation[9] using anodic intensities; [c] Error = 10%; $\Delta E_{1/2} = 0.058 \log (K_{(+)}/K_{(o)})$[11] at 20 °C; [d] Error = 10%; progressive shift of the wave: $K_{(o)} << 1$, $\Delta E_{1/2} = 0.058 \log [c.\ K_{(+)}]$;[11] **no cathodic wave (no accessible $\Delta E_{1/2}$ value).

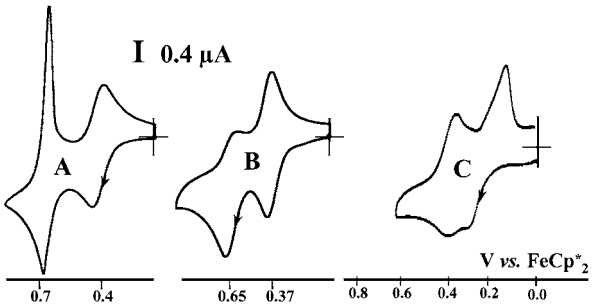

Fig. 1 Cyclovoltammograms of a mixture of G_3-16Fc and G_3-16Fc* (10^{-4} M, Pt anode; 0.1 M $[n\text{-Bu}_4\text{N}][PF_6]$, 20 °C). **A**: in CH_2Cl_2 showing the extensive adsorption only for G_3-16Fc; **B**: in DMF showing the chemical irreversibility only for G_3-16Fc that perturbs access to $E_{1/2}$ and K; **C**: CV of G_3-16Fc* in CH_2Cl_2 with 0.5 eq. $[n\text{Bu}_4\text{N}][H_2PO_4]$.

The addition of $[n\text{Bu}_4\text{N}][H_2PO_4]$ to the electrochemical cell containing the CH_2Cl_2 solution of the dendrimer (Fig. 1C) provokes the apparition of a new wave at a potential less positive than the initial one whose intensity decreases along with the intensity increase of the new wave. The equivalence point is reached as indicated by the complete replacement of the initial wave by the new one.[2] In the case of the parent Fc dendrimer series, however, this phenomenon is marred by both the chemical and electrochemical irreversibilities[10] of the new wave. Gratifyingly, there is no chemical irreversibility with the Fc* dendrimers and the new wave is electrochemically quasi-reversible (Fig. 1C, and Table 1). The use of the parent Fc dendrimer series is difficult again in DMF, because of the complete chemical irreversibility except with the first generation. On the contrary, all the Fc* dendrimer show CV waves that are fully chemically reversible and progressively shifted upon addition of $[n\text{Bu}_4\text{N}][H_2PO_4]$. This shift of $E_{1/2}$ values is the subject of a small dendritic effect: 115 mV (G_1), 125 mV (G_2), 145 mV (G_3), 165 mV (G_4) (all values ± 10 mV) and 140 mV (G_5 with more adsorption). The largest shift is that observed in the parent Fc series between FcCONHPr (65 mV) and G_1 (265 mV). These shifts provide direct access to the apparent association constants $K_{(+)}$ in DMF (±20%) for the whole Fc* series only: 9600 (G_1), 14000 (G_2), 32000 (G_3), 70000 (G_4) according to the Echegoyen–Kaifer model.[11]

The addition of $n\text{-Bu}_4N^+$ salts of chloride or hydrogensulfate only has a minute influence, provoking a shift of the Fe^{II}/Fe^{III} wave by 40 mV for Cl^- and 80 mV for HSO_4^- after addition of one equiv. of each anion to G_2-8Fc*. Indeed, the recognition of dihydrogenphosphate can be carried out in the presence of these anions. Instead of provoking the appearance of a new Fe^{II}/Fe^{III} wave as when Cl^- and HSO_4^- are not in the solution, the addition of $H_2PO_4^-$, when Cl^- and HSO_4^- are both present, induces a shift of this wave by $\Delta E_{1/2}$ = 180 mV for $H_2PO_4^-$.

In conclusion, these new Fc* dendrimers are redox robust and selectively recognize $H_2PO_4^-$ much more cleanly (no chemical irreversibility, much less adsorption) than the compared Fc series due to enhanced stability of the 17-electron form and lipophilicity provided by permethylation of the Cp ligands. A modest positive dendritic effect (*i.e.* larger shift of potential provoked by the addition of the anion when the generation is higher) is found in DMF whereas no dendritic effect is noted in CH_2Cl_2. This situation contrasts with the large dendritic effect found for the redox recognition of $H_2PO_4^-$ with other Fc dendrimers[2a] showing that these effects are dependent on the dendritic structure.

Notes and references

1 (*a*) P. D. Beer and P. A. Gale, *Angew. Chem., Int. Ed. Engl.*, 2001, **40**, 486; (*b*) P. D. Beer, J. Davis, D. A. Drillsma-Millgrom and F. Szemes, *Chem. Commun.*, 2002, 1716.

2 (*a*) C. Valério, J.-L. Fillaut, J. Ruiz, J. Guittard., J.-C. Blais and D. Astruc, *J. Am. Chem. Soc.*, 1997, **119**, 2588; (*b*) A. Labande, J. Ruiz and D. Astruc, *J. Am. Chem. Soc.*, 2002, **124**, 1782.

3 G. R. Newkome, C. N. Moorefield and F. Vögtle, *Dendrimers and Dendrons. Concepts, Synthesis and Applications*, Wiley, Weinheim, 2001; H. M. Janssen and E. W. Meijer, *Chem. Rev.*, 1999, **99**, 1665.

4 (*a*) C. M. Casado, M. Cuadrado, M. Morán, B. Alonso, B. Garcia, J. Gonzales and J. Losada, *Coord. Chem. Rev.*, 1999, **185**/**186**, 53; (*b*) A. E. Kaifer and M. Gomez-Kaifer, *Supramolecular Electrochemistry*, Wiley-VCH, Weinheim, 1999, ch. 16, p. 207.

5 (*a*) E. M. M. de Brabander-van den Berg and E. W. Meijer, *Angew. Chem. Int. Ed. Engl.*, 1993, **32**, 1308; (*b*) J. C. Hummelen, J. L. J. van Dongen and E. W. Meijer, *Chem. Eur. J.*, 1997, **3**, 1489.

6 K. Takada, D. J. Diaz, H. Abruña, I. Cuadrado, C. M. Casado, B. Alonso, M. Morán and J. Losada, *J. Am. Chem. Soc.*, 1997, **119**, 10763.

7 C. B. Gorman, J. C. Smith, B. L. Parkhurst, H. Sierzputowska-Gracz and C. A. Haney, *J. Am. Chem. Soc.*, 1999, **121**, 9958.

8 D. Astruc, in *Electron Transfer in Chemistry*, ed. V. Balzani, Wiley-VCH, New York, 2001, vol. 2, section 2, Chapter 4, p. 728.

9 J. B. Flanagan, S. Margel, A. J. Bard and F. C. Anson, *J. Am. Chem. Soc.*, 1978, **100**, 4248.

10 (*a*) D. Astruc, *Electron Transfer and Radical Processes in Transition-Metal Chemistry*, VCH, New York, 1995, ch. 2; (*b*) E_{pc} and E_{pa} are the cathodic and anodic peak potentials respectively. If $E_{pa} - E_{pc} > 58$ mV at 20 °C, the heterogeneous electron transfer is slow (signifying structural reorganization upon electron transfer). If $E_{pa} - E_{pc} < 58$ mV, it means that some adsorption occurs.

11 Seminal report: S. R. Miller, D. A. Gustowski, Z.-H. Chen, G. W. Gokel, L. Echegoyen and A. E. Kaifer, *Anal. Chem.*, 1988, **60**, 2021. When a new wave appears, $K_o > 1$ and only the ratio K_+/K_o is determined whereas, when the initial wave is only shifted, $K_0 << 1$, and access to K_+ is provided (see text and Table 1).

Synthesis of Five Generations of Redox-Stable Pentamethylamidoferrocenyl Dendrimers and Comparison of Amidoferrocenyl- and Pentamethylamidoferrocenyl Dendrimers as Electrochemical Exoreceptors for the Selective Recognition of $H_2PO_4^-$, HSO_4^-, and Adenosine 5′-Triphosphate (ATP) Anions: Stereoelectronic and Hydrophobic Roles of Cyclopentadienyl Permethylation

Marie-Christine Daniel,[a] Jaime Ruiz,[a] Jean-Claude Blais,[b] Nathalie Daro,[c] and Didier Astruc*[a]

Abstract: A family of five metallodendrimers with pentamethylamidoferrocenyl termini were synthesized from the DSM dendrimers G_n-DAB-dend-$(NH_2)_x$ ($x = 4$, 8, 16, 32, 64) and characterized by standard techniques, including prominent molecular peaks (broad for $x = 64$) in their MALDI-TOF mass spectra. Oxidation of G_4-DAB-dend-$(NHCOFc^*)_x$ ($Fc^* = C_5H_4FeCp^*$, $Cp^* = \eta^5$-C_5Me_5) with $SbCl_5$ in CH_2Cl_2 yields the stable 17-electron pentamethylferrocenium analogue, which can be characterized by ESR and Mössbauer spectroscopy and reduced back to the initial Fe^{II} dendrimer, the cycle being carried out without decomposition. The cyclic voltammograms (CVs) of all dendrimers, recorded in CH_2Cl_2 or DMF, show a fully reversible ferrocenyl wave without adsorption. They are much cleaner than those of the parent ferrocenyl analogues previously synthesized and studied by Cuadrado et al. These properties allow much easier recognition and titration of $H_2PO_4^-$ and ATP^{2-} by CV with the permethylated series than with the parent series. On the other hand, permethylation reduces the difference between the potentials recorded before and after titration. This is not crucial for $H_2PO_4^-$ and ATP^{2-}, but it is for HSO_4^-, because of the weak interaction in this case. Thus recognition and titration in CH_2Cl_2 proceeds best with the parent series, and a positive dendritic effect is revealed by the appearance of a new wave whose difference in potential relative to the initial wave increases with increasing generation number. In DMF, recognition and titration are only possible with the permethylated series and are subject to a dramatic dendritic effect. Indeed, the titration is followed by only a shift of the initial wave with G_1 and by the appearance of a new wave with G_2 and G_3. In conclusion, the permethylated dendrimers allow excellent recognition and titration of the oxoanions by CV due to the stereoelectronic stabilization of the 17-electron form and their hydrophobic effect. The magnitude of the recognition and positive dendritic effects is very sensitive to the dendrimer structure and to the nature of the solvent. The recognition is of the strong-interaction type (square scheme) between these dendrimers and ATP^{2-} with a stoichiometry of 0.5 equiv ATP^{2-} per ferrocenyl branch.

Keywords: cyclic voltammetry · dendrimers · metallocenes · molecular recognition · receptors

Introduction

Molecular recognition by means of weak supramolecular interactions is a key area,[1] because it opens a route to sensors that work in a reversible and thus practical way. Application of this principle to the recognition and sensing of anions is especially crucial in view of their role in biology. Beer et al. have developed electrochemical sensors with a rich variety of endoreceptors by modulation of the redox potential of ferrocenyl systems.[2] We are interested in dendritic and colloidal exoreceptors that, like viruses, recognize anions at their periphery.[3] In particular, the dendritic organization[4] involves channels and microcavities at the surface that

[a] Prof. Dr. D. Astruc, M.-C. Daniel, Dr. J. Ruiz
Groupe Nanosciences Moléculaires et Catalyse
LCOO, UMR CNRS No. 5802
Université Bordeaux I, 33405 Talence Cedex (France)
Fax: (+33) 5-40-00-69-94
E-mail: d.astruc@lcoo.u-bordeaux1.fr

[b] Dr. J.-C. Blais
LCOSB, UMR CNRS No. 7613, Université Paris VI
75252 Paris (France)

[c] Dr. N. Daro
ICMCB, Université Bordeaux I
33608 Pessac Cedex (France)

Supporting information for this article is available on the WWW under http://www.chemeurj.org/ or from the author.

 DOI: 10.1002/chem.200304886

provide useful topological conditions for the function as an exoreceptor.

Amidoferrocenyl dendrimers were independently reported by Cuadrado et al.[5] and by us[3a] with two different families of cores. Cuadrado et al. reported amidoferrocenyl dendrimers based on the well-known commercial DSM polyamine dendrimers DAB-dend-$(NH_2)_x$ ($x = 4$, 8, 16, 32, 64),[6] and studied their electrochemistry in the context of deposition on metal surfaces.[5] For our dendrimers, made with different cores, we reported the recognition of $H_2PO_4^-$ and HSO_4^- anions by means of the dendritic effect, that is, the increase in perturbation of the ferrocenyl redox potential with increasing generation, using cyclic voltammetry.[3a]

There were two major drawbacks in using amidoferrocenyl dendrimers[7] for electrochemical recognition of anions: 1) the cyclic voltammetry wave of the amidoferrocenyl system was not reversible, due to decomposition of the amidoferrocenium species, and 2) the cyclic voltammetry waves were marred by considerable adsorption. Therefore, given the well-known stabilizing effect of Cp permethylation,[8] we synthesized pentamethylamidoferrocenyl dendrimers from the DSM family, starting from the previously disclosed complex $[Fe(\eta^5\text{-}C_5Me_5)(CO)_3](PF_6)$.[3c, 9] It was shown that the cyclic voltammetric recognition of $H_2PO_4^-$ was much easier with these compounds than with the ferrocenyl derivatives.[10]

Here we report 1) the full characterization of five generations of these metallodendrimers and spectroscopic data for their 17-electron pentamethylamidoferrocenium forms, 2) new recognition studies on the HSO_4^- anion that, surprisingly, are best performed with the parent amidoferrocenyl dendrimers, and 3) details and extension of the recognition of $H_2PO_4^-$ to the recognition of the biologically important adenosyltriphosphate dianion, including the selectivity of this recognition in the presence of other anions such as HSO_4^- and Cl^-.

Results

Syntheses and oxidation of the pentamethylamidoferrocenyl-dendrimers: The five generations of metallodendrimers were synthesized by reactions of DSM's polyamine dendrimers DAB-dend-$(NH_2)_x$ ($x = 4$, 8, 16, 32, 64) with pentamethylferrocenoyl chloride in dichloromethane at room temperature overnight in the presence of triethylamine and obtained after purification as yellow-orange powders [Eq. (1) and Scheme 1].

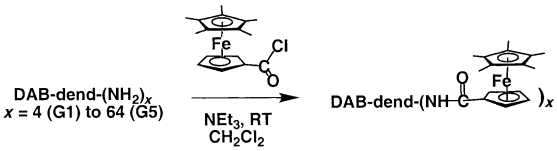

(1)

All dendrimers were characterized by standard analytical and spectroscopic techniques, including MALDI-TOF mass spectrometry, which showed prominent and sharp molecular peaks except for G_5-DAB-dend-{[NHCOCpFeCp*][PF_6]}$_{64}$, for which the molecular signal was broad, like that of the parent Cp compound.[5, 11] The dendrimer G_5-DAB-dend-(NHCOCpFeCp*)$_{64}$ was oxidized by $SbCl_5$ in CH_2Cl_2 to the

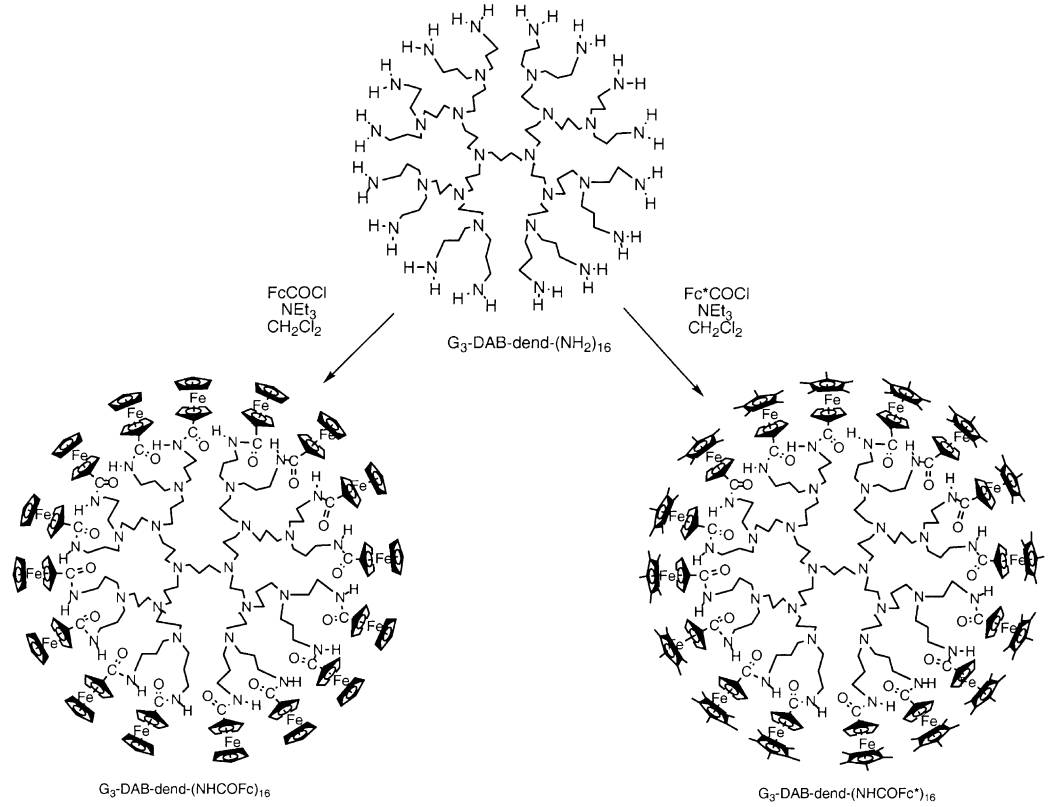

Scheme 1. Synthesis of G_1-G_5 (Fc and Fc* series) from the DSM dendrimers G_n-DAB-dend-$(NH_2)_x$ ($\times = 4$, 8, 16, 32, 64).

blue-green 17-electron complex G_5-DAB-dend-{[NHCOCp-FeCp*][$SbCl_6$]}$_{64}$. The Mössbauer and EPR spectra of the oxidized dendrimer are shown in Figure 1 and confirm that its

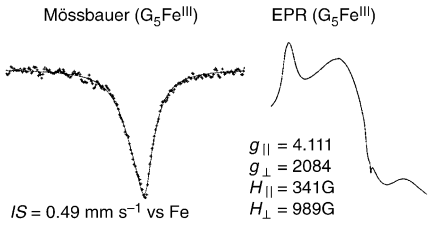

Figure 1. Mössbauer (left, $QS = 0$) and EPR (right) spectra of [G_5-64-Fc*][$SbCl_6$]$_{64}$ at 4 K for neat samples.

electronic structure is identical to that of the ferrocenium cation[12] and that this 17-electron dendrimer is thermally stable. This stability is confirmed by the quantitative exergonic reduction back to the pentamethylamidoferrocene dendrimer with decamethylferrocene in CH_2Cl_2 [Eq. (2)].

$$G_5\text{-64-NHCOFc}^{\star} \underset{[FeCp^{\star}_2],\ CH_2Cl_2,\ RT}{\overset{SbCl_5,\ CH_2Cl_2,\ RT}{\rightleftharpoons}} G_5\text{-64-\{[NHCOFc}^{\star}\text{][SbCl}_6\text{]\}} \quad (2)$$

Cyclic voltammetry of the dendrimers G_n-DAB-dend-(NHCOCpFeCp*)$_x$: Cyclic voltammetry (Table 1) was performed for all dendrimers with a Pt anode in CH_2Cl_2 or DMF. The fact that only one CV wave is observed is attributable to the following factors: First, the electrostatic factor is very weak, since two ferrocenyl groups are separated by at least 11 atoms in the metallodendritic molecules. Then, the rotation of the dendrimers is much more rapid relative to the electrochemical timescale than for other ferrocenyl dendrimers.[13] The redox potentials of the different ferrocenyl centers do not have exactly the same value, but the differences, due to the electrostatic factor, must be on the order of a fraction of millivolt or a few millivolts. Therefore, they are negligible and, in any case, not observed. The $E_{1/2}$ values are 0.405 ± 0.05 V versus [$FeCp_2^*$], and thus do not significantly vary from G_1 to G_5. The value for the parent series is 0.690 ± 0.010 V versus [$FeCp_2^*$] under the present conditions (Table 1). The internal [$FeCp_2^*$] reference is much better than ferrocene, as we have already reported.[14] Indeed, ferrocenium is too sensitive to the medium. Possible small dendritic effects were investigated, and we conclude that they are absent here with [$FeCp_2^*$] as internal reference ($E_{1/2}$ vs $FeCp_2 = E_{1/2}$ vs $FeCp_2^* + 0.545$ V in CH_2Cl_2, or $+0.595$ V in DMF[14]).

The comparison of these CV data with those of the parent series shows that the permethylated dendrimers (Fc*) behave in a much better fashion than the parent series (Fc). One of the dramatic differences between the CV of the dendritic Cp* and parent Cp series is that the Cp* series shows no or almost no adsorption in CH_2Cl_2, the i_{pc}/i_{pa} values being 1.00 ± 0.03 for G_1, G_2, and G_3, 1.1 for G_4, and 1.2 for G_5. In contrast, the parent Cp series shows i_{pc}/i_{pa} values between 2 and 3.4 under the same conditions (0.2 V s^{-1}, 20 °C, Pt anode, CH_2Cl_2, 0.1 M nBu_4NPF_6), which are indictive of strong adsorption (Figure 2 A). This difference of behavior toward adsorption is confirmed by $E_{pc} - E_{pa}$ values of 0.06 V for G_1, G_2, and G_3, 0.05 V for G_4, and 0.035 V for G_5 for the Cp* series, but only 0.03 V for G_1 to G_5 in the parent Cp series. In DMF, the i_{pc}/i_{pa} value is 1.05 ± 0.05 for the Cp* series, but it decreases from 0.9 for G_1 to 0.4 for G_2, G_3, and G_4 in the parent Cp series under these conditions. This indicates chemical irreversibility in the Cp series, that is, decomposition of the parent ferrocenium dendrimers becomes faster in this solvent with increasing generation number, even on the short CV timescale (Figure 2 B).

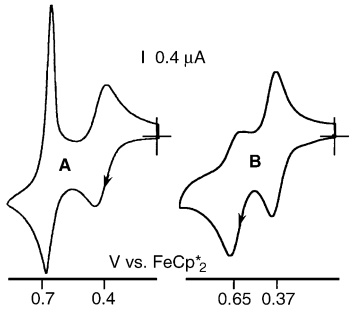

Figure 2. Cyclic voltammograms of a mixture of G_3-16Fc and G_3-16Fc* (10^{-4} M, Pt anode; 0.1 M [nBu_4N][PF_6], 20 °C). A) In CH_2Cl_2 showing the extensive adsorption only for G_3-16Fc. B) In DMF showing the chemical irreversibility for G_3-16Fc which perturbs access to $E_{1/2}$ and K.

The number n of electrons involved in the CV waves for ferrocenyl dendrimers is usually determined by using the Bard–Anson formula, which gives fairly correct results.[15–17] For the dendritic Cp* series it gave values of n that correspond to the theoretical numbers to within 5% in CH_2Cl_2 or DMF for generations G_1 to G_4, but significantly lower for G_5 (Table 1).[11]

Electrochemical recognition and titration of the oxoanions $H_2PO_4^-$, HSO_4^-, and ATP^{2-}

$H_2PO_4^-$: Numerous studies by Beer et al. with endoreceptors to which one or more ferrocenyl groups are attached have paved the way for the recognition of oxoanions. Addition of [nBu_4N][H_2PO_4] to an electrochemical cell containing a solution of amidoferrocenyl or pentamethylamidoferrocenyl dendrimer in CH_2Cl_2 leads to the appearence of a new wave at a potential less positive than the initial wave, the intensity of which decreases while that of the new wave increases. The equivalence point is reached when the initial wave is completely replaced by the new wave, as is already known for endoreceptors and another ferrocenyldendrimer structures.[2, 3] This was rationalized by Echegoyen and Kaifer using the square scheme in a seminal article.[18] We used this analysis to determine the ratio of apparent equilibrium constants $K_{(+)}$ and K_0 related to the strong interaction of the anion with the cationic ferrocenium form of the redox system, but also with the neutral ferrocenyl form ($K \gg 1$).

There are large differences in behavior between the amidoferrocenyl dendrimers and the pentamethylamidoferrocenyl series. In the case of the parent Cp dendrimer series, the cyclic voltammograms are marred by both chemical and,

Table 1. Cyclic voltammetry data for G_1-G_5 (both Fc and Fc* series) before and after titration of $[n\mathrm{Bu_4N}][H_2PO_4]$, $[n\mathrm{Bu_4N}]_2[ATP]$, and $[n\mathrm{Bu_4N}][HSO_4]$.

	$E_{1/2}$[a] ($E_{pa}-E_{pc}$) [V]		i_{pc}/i_{pa}		n[b]		$\Delta E_{1/2}(H_2PO_4^-)$[a] ($E_{pa}-E_{pc}$) [V]		$H_2PO_4^-$		
	CH_2Cl_2	DMF	CH_2Cl_2	DMF	CH_2Cl_2	DMF	CH_2Cl_2	DMF	$K_{(+)}/K_{(o)}$[c] CH_2Cl_2	$K_{(+)}/K_{(o)}$[c] DMF	$K_{(+)}$[d] DMF
G_0-1Fc	0.700 (0.06)	0.615 (0.06)	1.1	0.92	1.1	1.1	0.155 (0.15)	0.065 (0.09)	470	13	
G_1-4Fc	0.695 (0.03)	0.645 (0.07)	3.2	0.75	3.5		0.310 (0.09)	0.150 (0.16)	2.2×10^5	386	
G_2-8Fc	0.675 (0.03)	0.650 (0.08)	2.2	0.46	7.2		0.250 (0.11)	–[e]	2.0×10^4		
G_3-16Fc	0.690 (0.03)	0.650 (0.08)	3.5	0.42	16.0		0.170 (0.15)	–[e]	850		
G_4-32Fc	0.690 (0.04)	0.650 (0.08)	1.9	0.40	32	31.5	–[e]	–[e]			
G_5-64Fc	0.680 (0.03)	0.670 (0.10)	3.4	0.62		53	–[e]	–[e]			
G_1-4Fc*	0.406 (0.06)	0.360 (0.07)	1.05	1.07	3.8	4.2	0.155 (0.16)	0.115 (0.06)	470		9.6×10^3
G_2-8Fc*	0.395 (0.06)	0.370 (0.08)	1.02	1.1	7.9	8.0	0.160 (0.11)	0.125 (0.07)	570		14×10^3
G_3-16Fc*	0.410 (0.06)	0.370 (0.07)	1.01	1.12	15.1		0.130 (0.13)	0.145 (0.08)	170		32×10^3
G_4-32Fc*	0.400 (0.05)	0.390 (0.07)	1.1	1.05	32		0.140 (0.17)	0.165 (0.06)	260		70×10^3
G_5-64Fc*	0.410 (0.035)	0.375 (0.03)	1.2	1.06	55		0.160 (0.17)	0.140 (0.03)	570		26×10^3

[a] $E_{1/2}=(E_{pa}+E_{pc})/2$ vs $FeCp_2^*$ (in V). Electrolyte: $[n\mathrm{Bu_4N}][PF_6]$ 0.1M; working and counterelectrodes: Pt; reference electrode: Ag; internal reference: $FeCp_2^*$; scan rate: 0.200 V s^{-1}; 20 °C. [b] Values of the number of electrons involved calculated from the Anson–Bard equation[9] using anodic intensities. [c] Error = 10%; $\Delta E_{1/2}=0.058\log(K_{(+)}/K_{(o)})$[11] at 20 °C. [d] Error = 10%; progressive shift of the wave: $K_{(o)}\ll1$, $\Delta E_{1/2}=0.058\log(cK_{(+)})$. [e] No cathodic wave (no accessible $\Delta E_{1/2}$ value).

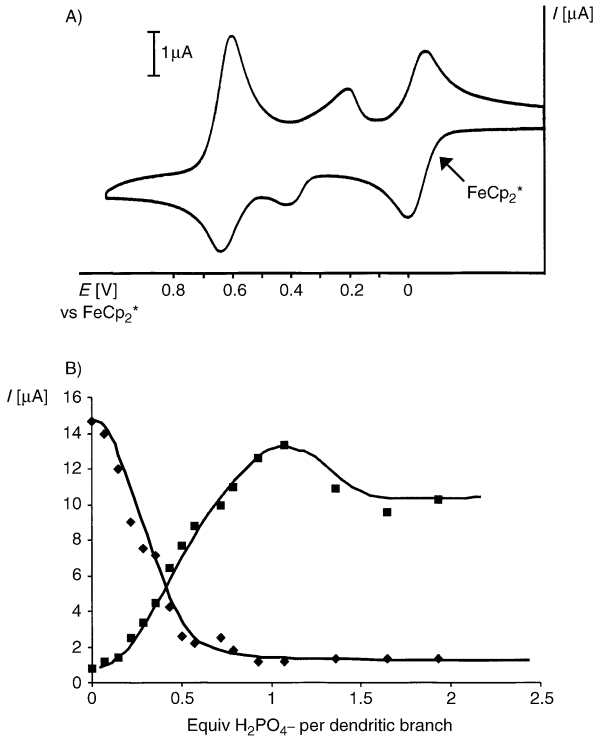

Figure 3. Titration of a 9.7×10^{-4}M solution of G_1-4Fc with a 10^{-3}M solution of $[n\mathrm{Bu_4N}][H_2PO_4]$ in CH_2Cl_2 in the presence of 0.1M $[n\mathrm{Bu_4N}][PF_6]$, Pt anode, 20 °C. A) Cyclic voltammogram obtained after addition of 0.5 equiv $[n\mathrm{Bu_4N}][H_2PO_4]$ per dendritic branch. B) Variation of the intensities of the initial (●) and new (◆) waves during the titration.

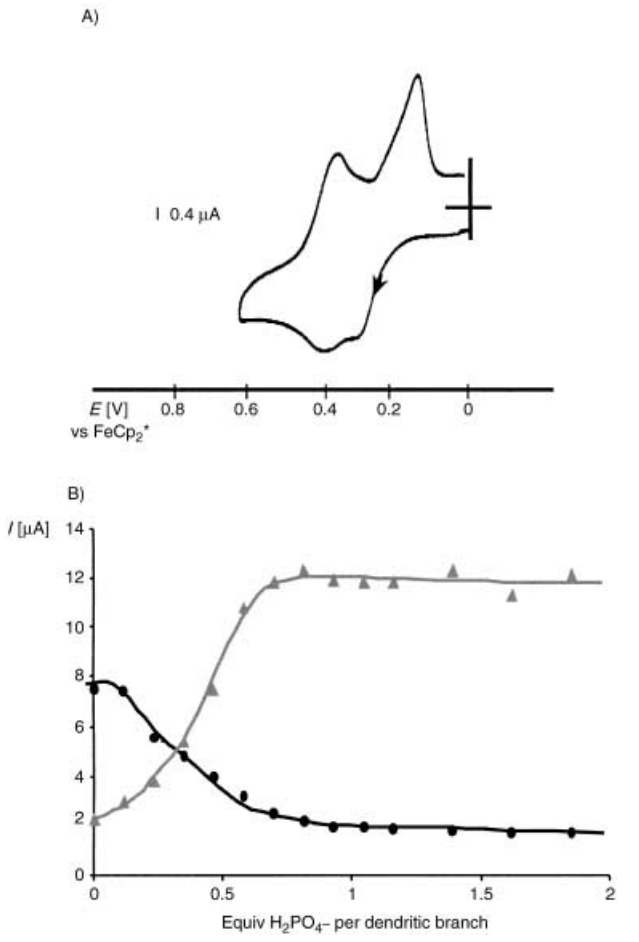

Figure 4. Titration of a 2.7×10^{-4}M solution of G_3-16Fc* by a 10^{-3}M solution of $[n\mathrm{Bu_4N}][H_2PO_4]$ in CH_2Cl_2 in the presence of 0.1M $[n\mathrm{Bu_4N}][PF_6]$, Pt anode, 20 °C. A) Cyclic voltammogram obtained after addition of 0.5 equiv $[n\mathrm{Bu_4N}][H_2PO_4]$ per dendritic branch. B) Variation of the intensities of the initial (●) and new (▲) waves along the titration.

electrochemical irreversibility[11b, 14] of the new wave (Figure 3 and Figure S5 in the Supporting Information). Gratifyingly the chemical irreversibility is not found with the new Cp* dendrimer series, and this allows a much easier analysis of this electrochemical recognition phenomenon (Figure 4 and Figure S6 in the Supporting Information). The electrochemical irreversibility is characterized by $E_{pc}-E_{pa}$ values[14] of 0.150 ± 0.010 V without significant dendritic effect, and adsorption by i_{pc}/i_{pa} values of 4 ± 1, also without significant dendritic effect. The difference in $E_{1/2}$ values between the initial and the new wave (determined after addition of 0.5 equiv $[n\mathrm{Bu_4N}][H_2PO_4]$, in order to observe both waves at the same time) is 0.150 ± 0.010 V without significant dendritic effect. This corresponds to a ratio of apparent

association constants $K_{(+)}/K_{(0)}$ of 400 ± 100 (resp. 170 ± 40) according to the Echegoyen–Kaifer model.[18]

Interestingly, a different phenomenon is found in DMF as solvent. Again, use of the parent Cp dendrimer series is difficult in this solvent because of the complete chemical irreversibility, except for the first generation. In contrast, the whole Cp* dendrimer series shows a CV wave that is fully chemically reversible and progressively shifted upon addition of $[n\mathrm{Bu_4N}][\mathrm{H_2PO_4}]$, with an adsorption characterized by an i_{pc}/i_{pa} ratio of 3 ± 1 without significant dendritic effect. This shift in $E_{1/2}$ values is subject to a small dendritic effect, for instance, with $[n\mathrm{Bu_4N}][\mathrm{H_2PO_4}]$: 115 mV ($G_1$), 125 mV ($G_2$), 145 mV ($G_3$), 165 mV ($G_4$) (all values ± 0.010 V), 140 mV (G_5, with more adsorption; see Figure S1 in the Supporting Information). The largest shift is that observed in the parent Cp series between FcCONHPr (65 mV) and G_1 (150 mV). These shifts provide direct access to the apparent association constants $K_{(+)}$ in DMF ($\pm 20\%$) only for the whole Cp* series: 9600 (G_1), 14000 (G_2), 32000 (G_3), 70000 (G_4) according to the Echegoyen–Kaifer model.[15]

ATP^{2-}: Electrochemical recognition was first studied in CH_2Cl_2. In this solvent, the trends found for ATP^{2-}[19, 20] closely follow those found for $H_2PO_4^-$ (Table 2). The addition of $[n\mathrm{Bu_4N}]_2[\mathrm{ATP}]$ to the electrochemical cell containing the amidoferrocenyl- or pentamethylamidoferrocenyl dendrimer causes, as with $[n\mathrm{Bu_4N}][\mathrm{H_2PO_4}]$, the appearance of a new wave at a potential less positive than the initial one, whose intensity decreases while that of the new wave increases (Figure 5A and Figure S2A in the Supporting Information). Thus, this is a case of strong-type interaction and can be treated by using the square scheme, as with $[n\mathrm{Bu_4N}]_2[\mathrm{H_2PO_4}]$. As for $[n\mathrm{Bu_4N}][\mathrm{H_2PO_4}]$, the pentamethylamidoferrocenyl dendrimers were greatly superior to the parent dendrimers with regard to the quality of the CVs, and consequently the study was carried out with this permethylated series (see Table 2). The difference in ferrocenyl redox potential between the initial wave and the new wave is of the same order of magnitude as with $[n\mathrm{Bu_4N}][\mathrm{H_2PO_4}]$, but slightly lower than for the latter (0.130 mV for $[n\mathrm{Bu_4N}]_2[\mathrm{ATP}]$, i.e., 20 mV less than with $[n\mathrm{Bu_4N}][\mathrm{H_2PO_4}]$; see Table 2). The corresponding ratio of apparent association constants is $K_{(+)}/K_{(0)} = 170 \pm 40$. The equivalence point is reached when 0.5 equiv $[n\mathrm{Bu_4N}]_2[\mathrm{ATP}]$ has been added, which is in accordance with the double negative charge of this anion (Figure 5B and Figure S5B in the Supporting Information). Other large stoichiometries have been found for ATP^{2-} with receptors based on other functional groups such as amines.[19]

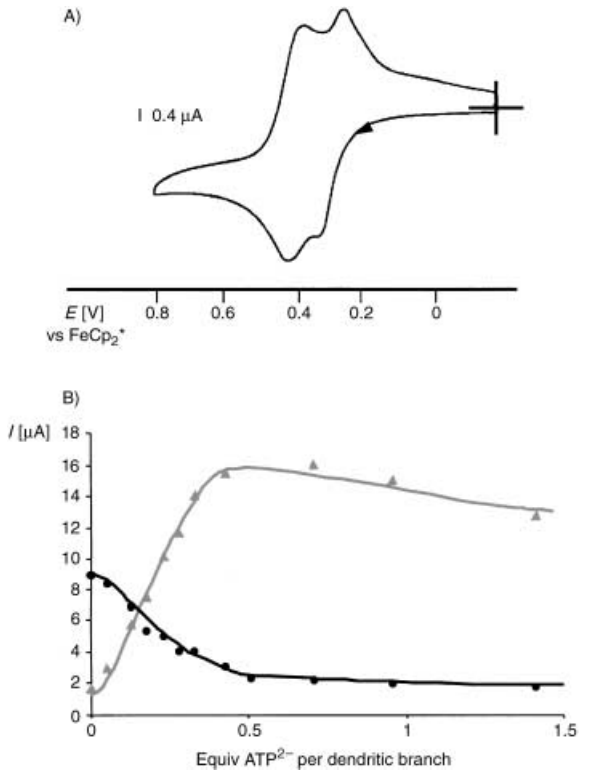

Figure 5. Titration of a 1.25×10^{-4} M solution of G_2-32Fc* with a 10^{-3} M solution of $[n\mathrm{Bu_4N}]_2[\mathrm{ATP}]$ in CH_2Cl_2 in the presence of 0.1 M $[n\mathrm{Bu_4N}][\mathrm{PF_6}]$, Pt anode, 20 °C. A) Cyclovoltammogram obtained after addition of 0.25 equiv $[n\mathrm{Bu_4N}]_2[\mathrm{ATP}]$ per dendritic branch; B) Variation of the intensities of the initial (●) and new (▲) waves during the titration.

A study in DMF revealed remarkable dendritic effects. With the first generation (G_1-4Fc*), the addition of $[n\mathrm{Bu_4N}]_2[\mathrm{ATP}]$ does not lead to the appearance of a new CV wave, but only a progressive shift of the wave (see Figure 6). The overall shift up to the equivalence point is $\Delta E_{1/2} = 145$ mV. Although the initial CV wave does not show adsorption, an adsorption phenomenon appears with increasing intensity along the titration. For the 2nd and 3rd generations G_2-8Fc* and G_3-16Fc, addition of $[n\mathrm{Bu_4N}]_2[\mathrm{ATP}]$ to the electrochem-

Table 2. Cyclic voltammetry data for G_1–G_4 (both Fc and Fc* series) after titration of ATP^{2-} and HSO_4^-.

	$\Delta E_{1/2}(ATP^{2-})$[a] ($E_{pa} - E_{pc}$) [V]		ATP^{2-}			$\Delta E_{1/2}(HSO_4^-)$[a] ($E_{pa} - E_{pc}$) [V]		HSO_4^-	
		$K_{(+)}/K_{(o)}$[b]		$K_{(+)}/K_{(o)}$[b]		$K_{(+)}$[c]		$K_{(+)}/K_{(o)}$[b]	$K_{(+)}$[c]
	CH_2Cl_2	DMF	CH_2Cl_2	DMF	DMF	CH_2Cl_2	DMF	CH_2Cl_2	DMF
G_1-4Fc	–[d]					0.120 (0.06)		140	
G_2-8Fc									
G_3-16Fc	–[d]					0.165 (0.10)		700	
G_4-32Fc						0.110 (0.14)		80	
G_1-4Fc*	0.130 (0.09)	0.145 (0.06)	170		24.10^4	0.080 (0.06)		24	
G_2-8Fc*	0.130 (0.10)	0.065 (0.10)	170	13		0.105 (0.07)	0.05 (0.06)	65	2.8×10^3
G_3-16Fc*	0.130 (0.09)	0.065 (0.07)	170	13		0.100 (0.06)		53	
G_4-32Fc*	0.110 (0.10)		80			0.095 (0.06)		44	

[a] $E_{1/2} = (E_{pa} + E_{pc})/2$ vs $FeCp_2^*$(in V). Electrolyte: $[n\mathrm{Bu_4N}][\mathrm{PF_6}]$ 0.1 M; working and counterelectrodes: Pt; reference electrode: Ag; internal reference: $FeCp_2^*$; scan rate: 0.200 V s^{-1}; 20 °C. [b] Error = 10%; $\Delta E_{1/2} = 0.058 \lg (K_{(+)}/K_{(o)})$[11] at 20 °C. [c] Error = 10%; progressive shift of the wave: $K_{(o)} \ll 1$, $\Delta E_{1/2} = 0.058 \lg (cK_{(+)})$. [d] No cathodic wave (no accessible $\Delta E_{1/2}$ value).

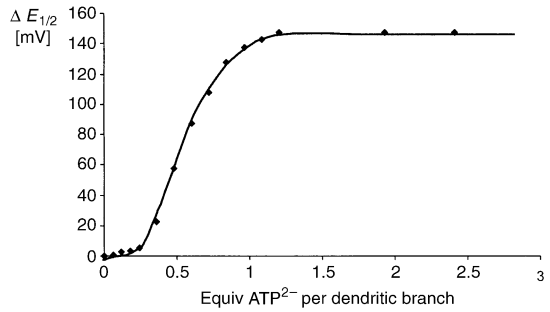

Figure 6. Titration of a 4.1×10^{-4} M solution of G_1-4Fc* with a 10^{-3} M solution of $[n\mathrm{Bu_4N}]_2[\mathrm{ATP}]$ in DMF in the presence of 0.1 M $[n\mathrm{Bu_4N}][\mathrm{PF_6}]$, Pt anode, 20 °C: shift of $E_{1/2}$ toward positive potentials recorded by CV as a function of the number of equivalents of $[n\mathrm{Bu_4N}]_2[\mathrm{ATP}]$ added per dendritic branch.

ical cell leads to the appearance of a new wave at a potential 65 mV less positive than that of the initial wave. This new wave is also accompanied by some adsorption. Thus, this change in behavior from G_1 to G_2 and G_3 means that the interaction between the neutral ferrocenyl form of the dendrimer and $[n\mathrm{Bu_4N}]_2[\mathrm{ATP}]$ progresses from weak for G_1 ($K_{(0)} \ll 1$) to relatively strong for G_2 and G_3 ($K_{(0)} \gg 1$).

HSO_4^-: This is the only anion for which the electrochemical recognition is sometimes easier with the amidoferrocenyl dendrimers than with the permethylated dendrimers. Indeed, the addition of $[n\mathrm{Bu_4N}][\mathrm{HSO_4}]$ to G_1-G_4 amidoferrocenyl dendrimers in CH_2Cl_2 solution leads to the appearance of a new wave, contrary to what is observed with other amidoferrocenyl dendrimers, for which only a shift of the wave was observed. The difference in potential between the new and initial waves increases from the first to the third generation, that is, this recognition is subject to a positive dendritic effect. The maximum $\Delta E_{1/2}$ value (3rd generation, G_3-16Fc) is 165 mV. Figure 7 shows the titration of HSO_4^- with G_3-16Fc in CH_2Cl_2 (see also Figure S7 in the Supporting Information). As usual, adsorption is found on the new wave and on the initial wave, but recognition and titration are possible.

With the new permethylated metallodendrimer series, this adsorption is observed neither at the beginning of nor during the titration. A new wave is observed when $[n\mathrm{Bu_4N}][\mathrm{HSO_4}]$ is added to the electrochemical cell containing permethylated metallodendrmer in CH_2Cl_2, but the difference in potential between the new wave and the initial wave is only 105 mV (max.) for G_2-8Fc*. This $\Delta E_{1/2}$ value is relatively small, so that there is much overlap between the two waves. Figure S3 (Supporting Information) shows the cyclovoltammogram of G_4-32Fc* in the presence of HSO_4^- in CH_2Cl_2, and Figure S4 (Supporting Information) shows the variation of the intensities of the initial and new waves during the titration of HSO_4^- with G_3-16Fc* in CH_2Cl_2.

In DMF, the irreversibility of the redox process does not allow a correct CV analysis with the parent amidoferrocenyl dendrimer series. In this solvent, the CV of the pentamethylamidoferrocenyl dendrimers is not marred by adsorption either, but it is only shifted upon addition of $[n\mathrm{Bu_4N}][\mathrm{HSO_4}]$, and this shift is rather modest ($\Delta E_{1/2} = 50$ mV). Nevertheless,

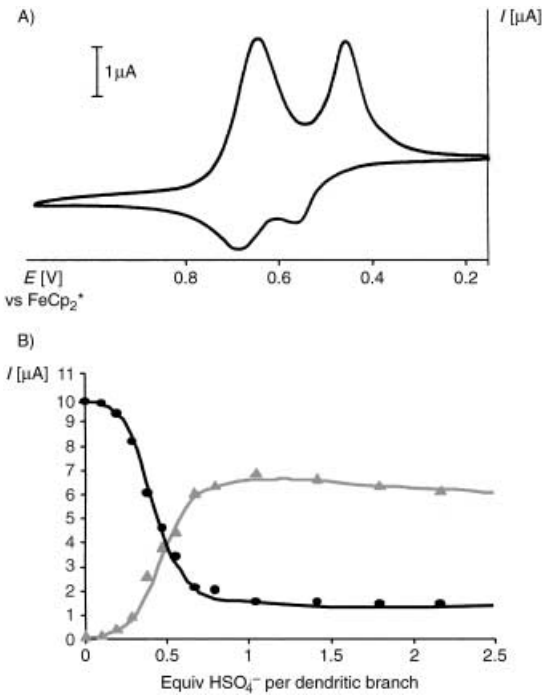

Figure 7. Titration of a 3.3×10^{-4} M solution of G_3-16Fc with a 10^{-3} M solution of $[n\mathrm{Bu_4N}][\mathrm{HSO_4}]$ in CH_2Cl_2 in the presence of 0.1 M $[n\mathrm{Bu_4N}][\mathrm{PF_6}]$, Pt anode, 20 °C. A) Cyclic voltammogram obtained after addition of 0.5 equiv $[n\mathrm{Bu_4N}][\mathrm{HSO_4}]$ per dendritic branch. B) Variation of the intensities of the initial (●) and new (▲) waves during the titration.

it allows a titration to be performed by plotting this potential shift as a function of the amount of $[n\mathrm{Bu_4N}][\mathrm{HSO_4}]$ added, especially because the shape of the CV wave is not perturbed from the beginning to the very end of the titration.

Selective recognition and titration of $H_2PO_4^-$ and ATP^{2-} in the presence of $[n\mathrm{Bu_4N}][\mathrm{HSO_4}]$ and $[n\mathrm{Bu_4N}][\mathrm{Cl}]$: Since addition of $n\mathrm{Bu_4N^+}$ salts of Cl^- or HSO_4^- only has a slight influence, provoking a weak shift in the Fe^{II}/Fe^{III} wave of the pentamethylamidoferrocenyl dendrimers by 40 mV for Cl^- and 50 mV for HSO_4^-, selective recognition and titration were investigated after addition of 1 equiv of each anion to G_2-8Fc*. Indeed, the recognition of $H_2PO_4^-$ or ATP^{2-} can be carried out in the presence of these anions. Instead of leading to the appearance of a new Fe^{II}/Fe^{III} wave, as in the absence of Cl^- and HSO_4^-, the addition of $H_2PO_4^-$ or ATP^{2-} when Cl^- and HSO_4^- are both present induces a shift of this wave by $\Delta E_{1/2} = 180$ mV for $H_2PO_4^-$ and 160 mV for ATP^{2-}. Figure 8 shows that titration of ATP^{2-} proceeds smoothly in the presence of these anions.

Discussion

Several reports have already appeared on the recognition of various anions by metallodendrimers.[3a, 21, 22] In particular, the recognition of $H_2PO_4^-$ has been shown to result from a strong interaction with ferrocenyl derivatives. These first pentamethylferrocenyl dendrimers have two favorable properties derived from the presence of a permethylated cyclopentadienyl ligand that clearly distinguish them from ferrocenyl

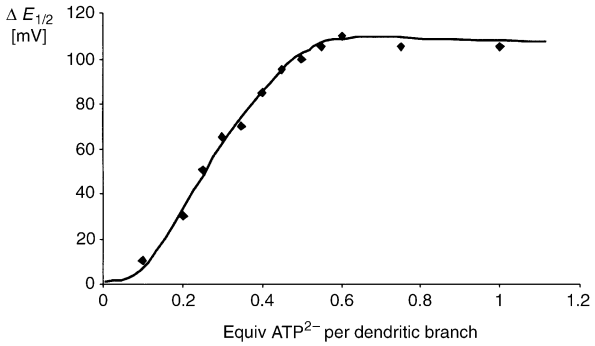

Figure 8. Titration of a 4×10^{-4} M solution of G_2-8Fc* with a 10^{-3} M solution of $[n\mathrm{Bu_4N}]_2[\mathrm{ATP}]$ in CH_2Cl_2 in the presence of 0.1 M $[n\mathrm{Bu_4N}][PF_6]$, 2.10^{-4} M $[n\mathrm{Bu_4N}][\mathrm{Cl}]$, and 2.10^{-4} M $[n\mathrm{Bu_4N}][HSO_4]$, Pt anode, 20 °C. Shift of $E_{1/2}$ toward positive potentials, recorded by CV, as a function of the number of equivalents of $[n\mathrm{Bu_4N}]_2[\mathrm{ATP}]$ added per dendritic branch.

dendrimers: stabilization of the oxidized 17-electron ferrocenium form and hydrophobicity bestowed on the periphery of the dendrimers by methyl substituents on the Cp rings. Both properties are essential in overcoming the problems encountered with amidoferrocenyl dendrimers: the instability of the oxidized ferrocenium form, largely due to the presence of the electron-withdrawing amido group, and adsorption due to the polarity of the amidoferrocenium groups. Indeed the comparison of the CV waves before and during the recognition and titration of the oxoanions clearly shows that the permethylated dendrimers are no longer marred by the problems encountered in the Cp series. The result is that the recognition and titration of $H_2PO_4^-$ and ATP^{2-} are clean with the permethylated series.

Another difference between permethylated Cp* and Cp is the increased donor strength due to the electron-releasing methyl groups. In recognition studies with thiolate–gold nanoparticles,[2a] it was shown that this factor weakens the key hydrogen bond between the amido group and $H_2PO_4^-$ and thus decreases the difference in potential $\Delta E_{1/2}$ between the initial ferrocenyl wave and the new wave. We have the same situation here, but this $\Delta E_{1/2}$ value is large anyway, so that these two waves are distinct. Thus, the recognition and titration of $H_2PO_4^-$ do not really suffer from this factor. In the case of HSO_4^- in DMF, however, for which the interaction of the amido group with the oxoanion is not as strong as with $H_2PO_4^-$, the difference in potential between the new wave and the initial wave is generally much smaller. Then, the decrease in this difference becomes a decisive factor that leads to a preference for the parent amidoferrocenyl dendrimers (early generation) over the permethylated dendrimers, because the small difference in potential in the latter series causes overlap of the two waves.

Various dendritic effects on $\Delta E_{1/2}$ are evident in the present study. A distinction can be made between the dendritic effect in comparing a monoamidoferrocenyl compound with G_1-4-NHCOFc, and the dendritic effects among dendrimers of different generations. Whereas the former is always significant, the latter varies from negligible to very significant. No dendritic effect of the second type is found for $H_2PO_4^-$ and ATP^{2-} in CH_2Cl_2, whereas a modest dendritic effect is observed in DMF. A significant dendritic effect is found for the recognition of HSO_4^- in CH_2Cl_2 by the amidoferrocenyl dendrimers. The most spectacular dendritic effect of the second type is found in the recognition of ATP^{2-} in DMF by pentamethylamidoferrocenyl dendrimers, since the recognition goes from the weak type for G_1-4-NHCOFc* (only shift of the wave) to the strong type with G_2-8-NHCOFc* and G_3-16-NHCOFc* (new wave). In these studies of dendritic effects, it is not possible to compare the amidoferrocenyl dendrimers with the pentamethylamidoferrocenyl dendrimers. Indeed, the former series does not present CVs that are clean enough for a family of several generations (the study of the first generation G_1-4-NHCOFc is most often possible, but usually not those of higher generations).

Finally, one can try to compare the amidoferrocenyl dendrimers to those previously reported with a different core, which showed strong dendritic effects. These dendritic effects are always positive in both families, although of different nature and magnitude. They are also very sensitive to many factors, especially to the solvent and the dendrimer structure. Thus, a comparison between two series of different structure is all the more delicate as the dendritic effects are very variable even within a single family, as shown in the present study. Thus, one can simply underline their great sensitivity to the structural variations from one dendrimer family to another, even with the same terminal amidoferrocenyl groups.

Conclusion

The synthesis of the first pentamethylamidoferrocenyl dendrimers has facilitated the clean recognition of oxoanions including ATP^{2-} due to stabilization of the 17-electron ferrocenium form and the hydrophobicity of the many methyl groups of the Cp* ligands around the dendrimers.

The relatively strong interaction between the hydrogenphosphate anions (including ATP^{2-}) and the amido group allows analysis according to the square scheme with very distinct initial and new ferrocenyl waves. The effect of ATP^{2-} is almost as strong as that of the $H_2PO_4^-$ anion itself, but the stoichiometry in the titration is halved.

With HSO_4^-, the donor strength of the methyl groups of the Cp* groups brings the two waves close to each other, so that the parent amidoferrocenyl dendrimers are more suitable than the permethylated dendrimers in CH_2Cl_2 (but not in DMF). With these dendrimers, recognition is also of the strong-interaction type in CH_2Cl_2.

In the permethylated series, recognition and titration are subject to a remarkable dendritic effect in DMF: from the weak-type with G_1, the interaction changes to the strong-interaction type with G_2 and G_3. The dendritic effects are strongly dependent on the structure and solvent and range from negligible to dramatic as a function of these factors.

Experimental Section

NEt_3 (2 mmol), CH_2Cl_2 (20 mL), and then $[FeCp^*(C_5H_4COCl)]$ (1.2 mmol), prepared according to ref. [3b], were added to the commercial

DSM polyamine dend-DAB$(NH_2)_x$ (1 mmol). After stirring overnight at room temperature, the solution was washed with a saturated aqueous solution of K_2CO_3 and then with distilled water, and dried over Na_2SO_4, filtered, and concentrated. Addition of diethyl ether led to precipitation of a yellow-orange powder of the metallodendrimer, which was further purified by dissolution in CH_2Cl_2 and reprecipitation by addition of diethyl ether.

G_1: ^{1}H NMR ($CDCl_3$): $\delta = 6.65$ (t, 4H, NH), 4.24 (br, 8H, C_5H_4), 3.88 (br, 8H, C_5H_4), 3.43 (br, 8H, $NHCH_2$), 2.47 (br, 12H, CH_2N), 1.85 (s, 60H, $C_5(CH_3)_5$), 1.51 (br, 8H, CH_2), 1.48 (br, 4H, CH_2); ^{13}C NMR ($CDCl_3$): $\delta =$ 169.28 (CO), 82.07 (Cq, C_5H_4), 81.06 (Cq, CCH_3), 76.05 and 70.21 (C_5H_4), 52.81 (CH_2), 38.92 (CH_2), 27.92 (CH_2), 10.67 (CH_3); IR (Nujol): $\tilde{\nu} = 1623$ (ν(CO)), 1539 cm^{-1} (ν(CN)); MS (MALDI-TOF): *m*/*z*: calcd for $C_{80}H_{112}N_6Fe_4O_4$: 1445.163; found: 1445.72; elemental analyis (%) calcd for $C_{80}H_{112}N_6Fe_4O_4$: C 66.48, H 7.81; found: C 66.05, H 7.36.

G_2: ^{1}H NMR ($CDCl_3$): $\delta = 6.90$ (br, 8H, NH), 4.31 (br, 16H, C_5H_4), 3.86 (br, 16H, C_5H_4), 3.43 (br, 16H, $NHCH_2$), 2.35 (br, 36H, CH_2N), 1.84(s, 120H, $C_5(CH_3)_5$), 1.68 (br, 28H, CH_2), 1.48 (br, 4H, CH_2); ^{13}C NMR ($CDCl_3$): $\delta =$ 170.28 (CO), 81.16 (Cq, CCH_3), 76.40 and 70.32 (C_5H_4), 53.21(CH_2), 39.12(CH_2), 28.45 (CH_2), 10.31 (CH_3); IR (Nujol): $\tilde{\nu} = 1620$ (ν(CO)), 1539 cm^{-1} (ν(CN)); MS (MALDI-TOF): *m*/*z*: calcd for $C_{168}H_{240}N_{14}Fe_8O_8$: 3028; found: 3029; elemental analyis (%) calcd for $C_{168}H_{240}N_{14}Fe_8O_8$: C 66.58, H 7.98; found: C 65.12, H 7.28.

G_3: ^{1}H NMR ($CDCl_3$): $\delta = 7.16$ (br, 16H, NH), 4.31 (br, 32H, C_5H_4), 3.86 (br, 32H, C_5H_4), 3.43 (br, 32H, $NHCH_2$), 2.35 (br, 84H, CH_2N), 1.84 (s, 240H, $C_5(CH_3)_5$), 1.68 (br, 56H, CH_2), 1.48 (br, 4H, CH_2); ^{13}C NMR ($CDCl_3$): $\delta = 170.28$ (CO), 80.98 (Cq, CCH_3), 76.40, 70.45 (C_5H_4), 53.21 (CH_2), 39.08 (CH_2), 28.36 (CH_2), 10.52 (CH_3); IR (Nujol): $\tilde{\nu} = 1620$ (ν(CO)), 1540 cm^{-1} (ν(CN)); MS (MALDI-TOF): *m*/*z*: calcd for $C_{344}H_{496}N_{30}Fe_{16}O_{16}$: 6201.33; found: 6204.3; elemental analyis (%) calcd for $C_{344}H_{496}N_{30}Fe_{16}O_{16}$: C 66.62, H 8.06; found: C 65.32, H 7.28.

G_4: ^{1}H NMR ($CDCl_3$): $\delta = 7.21$ (br, 32H, NH), 4.31 (br, 64H, C_5H_4), 3.86 (br, 64H, C_5H_4), 3.43 (br, 64H, $NHCH_2$), 2.35 (br, 180H, CH_2N), 1.84 (s, 480H, $C_5(CH_3)_5$), 1.68 (br, 60H, CH_2), 1.48 (br, 4H, CH_2); ^{13}C NMR ($CDCl_3$): $\delta = 169.87$ (CO), 80.97 (Cq, CCH_3), 76.40, 70.40 (C_5H_4), 53.21 (CH_2), 39.01(CH_2), 28.42 (CH_2), 10.31(CH_3); IR (Nujol): $\tilde{\nu} = 1622$ (ν(CO)), 1540 cm^{-1} (ν(CN)); MS (MALDI-TOF): *m*/*z*: calcd for $C_{696}H_{1008}N_{62}Fe_{32}O_{32}$: 12542.89; found: 12544.9; elemental analyis (%) calcd for $C_{696}H_{1008}N_{62}Fe_{32}O_{32}$: C 66.64, H 8.10; found: C 65.10, H 7.78.

G_5: ^{1}H NMR ($CDCl_3$): $\delta = 7.43$ (br, 64H, NH), 4.41 (br, 128H, C_5H_4), 3.82 (br, 128H, C_5H_4), 3.43 (br, 128H, $NHCH_2$), 2.37 (br, 372H, CH_2N), 1.84 (s, 960H, C_5CH_3), 1.51 (br, 252H, CH_2); ^{13}C NMR ($CDCl_3$): $\delta = 170.15$ (CO), 81.16 (Cq, CCH_3), 76.47 and 70.46 (C_5H_4), 53.21(CH_2), 39.23 (CH_2), 2838 (CH_2), 10.50 (CH_3); IR (Nujol): $\tilde{\nu} = 1622$ (ν(CO)), 1540 cm^{-1} (ν(CN)); MS (MALDI-TOF): *m*/*z*: calcd for $C_{1400}H_{2032}N_{126}Fe_{64}O_{64}$: 25226; found: ≈25000 (br).

Titrations by cyclic voltammetry: *Conditions*: Solvent: distilled dichloromethane or anhydrous DMF; 20 °C; supporting electrolyte: [*n*Bu$_4$N][PF_6], 0.1M; internal reference: $FeCp_2^*$; reference electrode: Ag; auxiliary and working electrodes: Pt; scan rate: 0.2 V s^{-1}; [*n*Bu$_4$N][H_2PO_4] or [*n*Bu$_4$N]$_2$[ATP]: 5×10^{-3}M; *n*Bu$_4$NCl and [*n*Bu$_4$N][HSO_4]: 5×10^{-2}M.

General method for the titration of $H_2PO_4^-$, ATP^{2-}, or HSO_4^-: First, [*n*Bu$_4$N][PF_6] was introduced into the electrochemical cell containing the working electrode, the reference electrode, and the counterelectrode and dissolved in dichloromethane or DMF. A blank voltammogram was recorded without dendrimer to check the working electrode. Then, the dendrimer was dissolved in a minimum amount of dichloromethane or DMF and added to the cell. About 1 mg decamethylferrocene (3×10^{-6} mol) was also added. The solution was degassed by flushing with dinitrogen, and the CV of the dendrimer alone was recorded. Then, the anion $H_2PO_4^-$, ATP^{2-},or HSO_4^- was added in small quantities with a microsyringe). After each addition, the solution was degassed, and a CV was recorded. The appearance and progressive increase of a new wave was observed, while the initial wave decreased and finally disappeared. When the initial wave had completely disappeared, addition of the salt of the anion was continued until twice the volume already introduced was reached. The titration of $H_2PO_4^-$ (or ATP^{2-}) in the presence of Cl^- and HSO_4^- was carried out similarly, the salts [*n*Bu$_4$N][Cl] and [*n*Bu$_4$N][HSO_4] being added before [*n*Bu$_4$N][H_2PO_4] (or [*n*Bu$_4$N]$_2$[ATP]).

Acknowledgement

Helpful assistance of Professor François Varret (Université de Versailles, Mössbauer spectroscopy), contribution of Maria Jesus Ruiz Medel (Bordeaux group) to preliminary experiments, and financial support from the Institut Universitaire de France (IUF, DA), the Centre National de la Recherche Scientifique (CNRS), the Universities Bordeaux I and Paris VI, and the Ministère de la Recherche et de la Technologie (MRT, Ph.D. grant to M.-C.D.) are gratefully acknowledged.

[1] J.-M. Lehn, *Supramolecular Chemistry: Concepts and Perspectives* VCH, Weinheim, **1995**; K. D. Schierbaum, T. Weiss, E. U. Thorden - van Zelzen, J. F. G. Engberson, D. N. Reinhoudt, W. Göpel, *Science* **1994**, *265*, 1413; A. Kumar, N. L. Arbott, E. Kim, A. Biebuyck, G. M. Whitesides, *Acc. Chem. Res.* **1995**, *28*, 219; J. Atwood, K. T. Holman, G. W. Steed, *Chem. Commun.* **1996**, 1401; C. Seel, J. de Mendoza in *Comprehensive Supramolecular Chemistry*, *Vol. 2* (Eds.: J. Atwood, J. E. D. Davies, D. D. McNichol, F. Vögtle), Elsevier, New York, **1996**, Chapter 17, pp. 519–552; *Supramolecular Chemistry of Anions* (Eds.: A. Bianchi, K. Bowman-James, E. Garcia-Espana), Wiley, New York, **1997**; M. Berger, F. P. Schmidtchen, *Chem. Rev.* **1997**, *97*, 1609.

[2] a) P. D. Beer, *Acc. Chem. Res.* **1998**, *31*, 71; b) P. D. Beer, P. A. Gale, Z. Chen, *Adv. Phys. Org. Chem.* **1998**, *31*, 1; c) P. D. Beer, P. A. Gale, *Angew. Chem.* **2001**, *113*, 502; *Angew. Chem. Int. Ed.* **2001**, *40*, 486; d) P. D. Beer, J. Davis, D. A. Drillsma-Millgrom, F. Szemes, *Chem. Commun.* **2002**, 1716.

[3] a) C. Valério, J.-L. Fillaut, J. Ruiz, J. Guittard, J.-C. Blais, D. Astruc, *J. Am. Chem. Soc.* **1997**, *119*, 2588; b) A. Labande, J. Ruiz, D. Astruc, *J. Am. Chem. Soc.* **2002**, *124*, 1782; c) M.-C. Daniel, J. Ruiz, D. Astruc, *J. Am. Chem. Soc.* **2003**, *125*, 1150; d) M.-C. Daniel, J. Ruiz, S. Nlate, J.-C. Blais, D. Astruc, *J. Am. Chem. Soc.* **2003**, *125*, 2617.

[4] Recent reviews on dendrimers: G. R. Newkome, C. N. Moorefield, F. Vögtle, *Dendrimers and Dendrons, Concepts, Synthesis and Applications*, Wiley-VCH, Weinheim, **2001**; *Dendrimers and other Dendritic Polymers* (Eds.: D. Tomalia, J. M. J. Fréchet), Wiley-VCH, New York, **2002**; recent reviews on metallodendrimers: G. R. Newkome, E. He, C. N. Moorefield, *Chem. Rev.* **1999**, *99*, 1689; H. M. Janssen, E. W. Meijer, *Chem. Rev.* **1999**, *99*, 1665; I. Cuadrado, I. M. Morán, C. M. Casado, B. Alonso, J. Losada, *Coord. Chem. Rev.* **1999**, *189*, 123; M. A. Hearshaw, J. R. Moss, *Chem. Commun.* **1999**, 1; D. Astruc, F. Chardac, *Chem. Rev.* **2001**, *101*, 2991.

[5] a) I. Cuadrado, M. Morán, C. M. Casado, B. Alonso, F. Lobete, B. Garcia, M. Ibisate, J. Losada, *Organometallics* **1996**, *119*, 5278; b) K. Takada, D. J. Diaz, H. Abruna, I. Cuadrado, C. M. Casado, B. Alonso, M. Morán, J. Losada, *J. Am. Chem. Soc.* **1997**, *119*, 19763.

[6] E. M. M. de Brabander-van den Berg, E. W. Meijer, *Angew. Chem.* **1993**, *105*, 1370; *Angew. Chem. Int. Ed. Engl.* **1993**, *32*, 1308.

[7] For reviews on ferrocenyl dendrimers and their electrochemistry, see refs. [4b], [5] and C. M. Casado, M. Cuadrado, M. Morán, B. Alonso, B. Garcia, J. Gonzales, J. Losada, *Coord. Chem. Rev.* **1999**, *185/186*, 53; A. E. Kaifer, M. Gomez-Kaifer, *Supramolecular Electrochemistry*, Wiley-VCH, Weinheim, **1999**, Chapter 16, p. 207.

[8] R. H. Crabtree, *The Organometallic Chemistry of the Transition Metals*, 3rd ed., Wiley, New York, **2001**.

[9] D. Catheline, D. Astruc, *Organometallics* **1984**, *3*, 1094–1100.

[10] J. Ruiz, M.-J. Ruiz Medel, M.-C. Daniel, J.-C. Blais, D. Astruc, *Chem. Commun.* **2003**, 464.

[11] Mass spectrometric characterization showing the purity of the DSM polyamines[6] from G_1 to G_4 has been reported. Note, however, that deviation from the theoretical number of 64 branches in G_5 has also been shown: J. C. Hummelen, J. L. J. van Dongen, E. W. Meijers, *Chem. Eur. J.* **1997**, *3*, 1489.

[12] a) R. L. Collins, *J. Chem. Phys.* **1965**, *42*, 1072; b) R. Prins, *Mol. Phys.* **1970**, *19*, 603.

[13] C. B. Gorman, J. C. Smith, M. W. Hager, B. L. Parkhurst, H. Sierzputowska-Gracz, C. A. Haney, *J. Am. Chem. Soc.* **1999**, *121*, 9958.

[14] J. Ruiz, D. Astruc, *C.R. Acad. Sci. Paris Ser. IIc* **1998**, 21; D. Astruc in *Electron Transfer in Chemistry* (Ed.: V. Balzani), *Vol. 2*, *Organic, Inorganic and Organometallic Molecules* (Eds.: J. Mattay, D. Astruc), Wiley, New York, **2001**, Section 2, Chapter 4, p. 728.

[15] J. B. Flanagan, S. Margel, A. J. Bard, F. C. Anson, *J. Am. Chem. Soc.* **1978**, *100*, 4248.
[16] D. Astruc, *Electron Transfer and Radical Processes in Transition-Metal Chemistry*, VCH, New York, **1995**, Chapter 2 (Electrochemistry).
[17] a) J.-L. Fillaut, J. Linares, D. Astruc, *Angew. Chem.* **1994**, *106*, 2540; *Angew. Chem. Int. Ed. Engl.* **1994**, *33*, 2460; b) S. Nlate, J. Ruiz, V. Sartor, R. Navarro, J.-C. Blais, D. Astruc, *Chem. Eur. J.* **2000**, *6*, 2544.
[18] Seminal report: S. R. Miller, D. A. Gustowski, Z.-H. Chen, G. W. Gokel, L. Echegoyen, A. E. Kaifer, *Anal. Chem.* **1988**, *60*, 2021.
[19] For previous studies on recognition of ATP^{2-} by a mononuclear ferrocenyl derivative, see a) P. D. Beer, J. Cadman, J. M. Lloris, R. Martinez-Mànez, M. E. Padilla, T. Pardo, D. K. Smith, J. Soto, *J. Chem. Soc. Dalton Trans.* **1999**, 127; b) O. Reynes, F. Maillard, J.-C. Moutet, G. Royal, E. Saint-Aman, G. Stanciu, J.-P. Dutasta, I. Gosse, J.-C. Mulatier, *J. Organomet. Chem.* **2001**, *637–639*, 356; c) O. Reynes, J.-C. Moutet, J. Pecaut, G. Royal, E. Saint-Aman, *New J. Chem.* **2002**, *26*, 9.
[20] E_{pc} and E_{pa} are the cathodic and anodic peak potentials, respectively. If their difference is less than than 58 mV at 20 °C, then some adsorption occurs. If it is larger than 58 mV at 20 °C, heterogeneous electron transfer is slow (signifying structural reorganization of the supramolecular assembly upon electron transfer).
[21] a) D. Astruc, C. Valério, J.-L. Fillaut, J. Ruiz, J.-R. Hamon, F. Varret in *Supramolecular Magnetism* (Ed.: O. Kahn), NATO ASI Series, Kluwer, Dordrecht, **1996**, pp. 107–127; see also refs. [3a,c]; b) C. Valério, E. Alonso, J. Ruiz, J.-L. Fillaut, D. Astruc, *Pure Appl. Chem.* **1998**, *70*, 809; c) C. Valério, E. Alonso, J. Ruiz, J.-C. Blais, D. Astruc *C. R. Acad. Sci. Paris Ser. IIc* **1999**, *2*, 79; d) C. Valério, E. Alonso, J. Ruiz, J.-C. Blais, D. Astruc, *Angew. Chem.* **1999**, *111*, 1855; *Angew. Chem. Int. Ed. Engl.* **1999**, *38*, 1747.
[22] a) J. Losada, B. Alonso, I. Cuadrado, C.-M. Casado, M. Morán, *J. Electroanal. Chem.* **1999**, *463*, 87; b) B. Alonso, C.-M. Casado, I. Cuadrado, M Morán, A. Kaifer, *Chem. Commun.* **2002**, 1778.

Received: February 26, 2003 [F4886]

PARTIE 2:

ASSEMBLAGES SUPRAMOLECULAIRES PAR LIAISONS HYDROGENE DE METALLODENDRIMERES ELECTROACTIFS: CARACTERISATION ET RECONNAISSANCE DES ANIONS $H_2PO_4^-$ et ATP^{2-}.

Assemblages supramoléculaires par liaisons hydrogène de métallodendrimères électroactifs: caractérisation et reconnaissance des anions $H_2PO_4^-$ et ATP^{2-}.

Des dendrimères ont aussi été formés au moyen de liaisons hydrogène entre des amines primaires et des phénols.

En premier lieu, les assemblages comportant des fonctions terminales amidoferrocényles ont été étudiés en reconnaissance du dihydrogénophosphate par voltammétrie cyclique dans le dichlorométhane, ce qui a permis la publication au *Journal of American Chemical Society* d'une note préliminaire intitulée:

Supramolecular H-Bonded Assemblies of Redox-Active Metallodendrimers and Positif and Unusual Dendritic Effect on the Recognition of $H_2PO_4^-$.

Les récents travaux complémentaires, concernant la reconnaissance de l'ATP^{2-}, ont permis la rédaction d'un mémoire en français, mémoire destiné à être rapidement soumis à publication après traduction en anglais (la partie expérimentale étant déjà en anglais). Son titre est le suivant:

Assemblages supramoléculaires par liaisons hydrogène de métallodendrimères électroactifs: caractérisation et reconnaissance des anions $H_2PO_4^-$ et adénosine-5'-triphosphate (ATP^{2-}).

J|A|C|S
COMMUNICATIONS

Published on Web 01/10/2003

Supramolecular H-Bonded Assemblies of Redox-Active Metallodendrimers and Positive and Unusual Dendritic Effects on the Recognition of $H_2PO_4^-$

Marie-Christine Daniel, Jaime Ruiz, and Didier Astruc*

Groupe Nanosciences Moléculaires et Catalyse, LCOO, UMR CNRS N° 5802, Université Bordeaux I, 33405 Talence Cedex, France

Received June 11, 2002; E-mail: d.astruc@lcoo.u-bordeaux.fr

The recognition of anions such as $H_2PO_4^-$ is of interest in the biological and environmental contexts and has been investigated using a variety of *endo*receptors.[1] We have recently addressed the recognition of small anions using metallodendrimers[2a] and gold nanoparticles[2b] as *exo*receptors. Because topological effects were found to be essential factors in these studies, we envisaged assembling redox-active metallodendrimers by multiple H-bonding to possibly benefit from positive dendritic effects.[2a] We now report our first findings along this line that involve the dramatic influence of these supramolecular assemblies on the recognition of $H_2PO_4^-$. Although dendrimers are a well-established field,[2,3] there are still only very few examples of dendrimers assembled using H-bonding.[4,5] Simple alcohols mixed with primary amines are known to form complementary O- -H- -N bonds with tetrahedral disposition of both O and N valences and 1:1 stoichiometry[6] (e.g., minimal melting point for this stoichiometry[6b]), a property that has been astutely used in crystal engineering[6c] and chiral recognition.[6d] We applied this principle to the association of the AB_3 phenol units *p*-OH−$C_6H_4C(CH_2CH{=}CH_2)_3$, **1**, and *p*-OH−$C_6H_4C\{(CH_2)_3SiMe_2$-$CH_2NHCOFc\}_3$, **2** (Fc = ferrocenyl), with the dendritic DAB polyamines of generations 1 to 4 (G_1−G_4, see G_1 in Chart 1).[7] The ^{1}H NMR signals of the phenolic H in **1** and **2** at 5 ppm and of the NH_2 amine protons of DAB-G_1 to G_4 at 1.5 ppm are strongly shifted to a common signal between 2.4 and 4.1 ppm (broad, concentration-dependent, see the Supporting Information) for the H-bonded, assembled dendrimers.

The recognition of $H_2PO_4^-$ by monomeric amidoferrocenes using cyclic voltammetry is weak, but it is enhanced when amidoferrocenes are attached to receptors.[1,2] In the latter, a new amidoferrocenyl wave at less positive potential progressively replaces the initial one in the course of the addition of $H_2PO_4^-$, until the initial wave disappears when a 1:1 stoichiometry is reached.[2a] For instance, the difference $\Delta E_{1/2}$ between the potential of the initial ferrocenyl wave[8] and that of the new wave reached after addition of 1 equiv of $H_2PO_4^-$ *per* amidoferrocenyl branch is 150 mV with FcCONHPr and is raised to 205 mV with **1** alone (apparition of a new wave along with the intensity decrease of the original wave in CH_2Cl_2 (Pt anode, [*n*-Bu_4N][PF_6])). The addition of propylamine to **2** does not change this $\Delta E_{1/2}$ value, but it is then necessary to add 2.5 equiv of $H_2PO_4^-$ instead of 1 equiv per ferrocenyl branch, because the amine strongly competes with the amidoferrocenyl group in $H_2PO_4^-$ binding. The addition of a stoichiometric amount of [*n*-Bu_4N][H_2PO_4] to a DAB dendritic amine enhances the $\Delta E_{1/2}$ value from 205 mV for $PrNH_2$ to 250 mV for DAB-G_1 and 280 mV for DAB-G_2. The larger DAB dendritic polyamines DAB-G_3 and -G_4 also give a value of 280 mV, indicating that saturation is obtained with DAB-G_2. An increase of the $\Delta E_{1/2}$ values upon increasing the generation is the signature of a *positive dendritic effect*.[2a] The number of equivalents of $H_2PO_4^-$ *per* dendritic branch found at the equivalent point dramatically varies from *n*-$PrNH_2$ to the DAB series. It drops from 2.5 for $PrNH_2$ to 0.5 for DAB-G_1, and then raises to 0.8 for DAB-G_2 and 2.0 for DAB-G_3 and DAB-G_4. The considerable drop of this value from $PrNH_2$ to DAB-G_1 and -G_2 seemingly results from difficult access of the guest to the core amines and from the chelation of $H_2PO_4^-$ to two amidoferrocenyl groups. The increase of the value from DAB-G_1 to -G_2 and -G_3 indicates progressive steric congestion and/or destabilization of the H-bonding as the dendritic size increases, which is consistent with the limit of the $\Delta E_{1/2}$ increase. The increased number of tertiary amines upon generation increase might also be responsible for the binding of more $H_2PO_4^-$. Thus, the most dramatic supramolecular dendritic effect combining both values of $\Delta E_{1/2}$ and of the variation of number of equivalents of $H_2PO_4^-$ per amidoferrocenyl branch is found for G_1 and G_2, for which 12 and 24 amidoferrocenyl groups, respectively, are present at the dendrimer periphery. For G_1, the fact that the equivalent point is reached for 0.5 equiv of $H_2PO_4^-$ shows that a single unit is interacting with two amidoferrocenyl arms (also by H-bonding), a unique situation. In addition, for G_1 and G_2, a dramatic cooperative effect is found in the course of the titration: the replacement of the initial ferrocenyl wave by the incoming wave during the titration is very sudden. It occurs within the addition of about 0.1 equiv of $H_2PO_4^-$ (Figure 1), whereas it is normally proportional to the quantity of added $H_2PO_4^-$

Chart 1. Supramolecular Assembly between the AB_3 Unit **2** and the G_1 DAB Dendrimer Characterized by the Concentration-Dependent Single Phenolic + Amine ^{1}H NMR Broad Signal between 2.4 and 4.1 ppm versus TMS in $CDCl_3$ (see Supporting Information)[a]

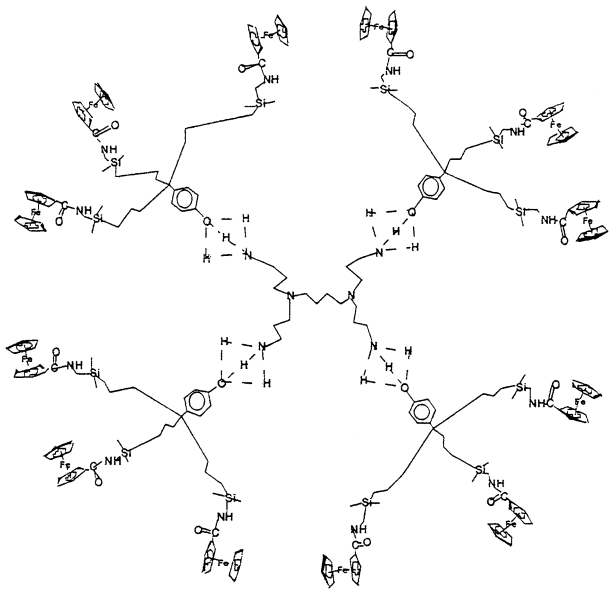

[a] The H-bonding representation is arbitrary.

10.1021/ja020833k CCC: $25.00

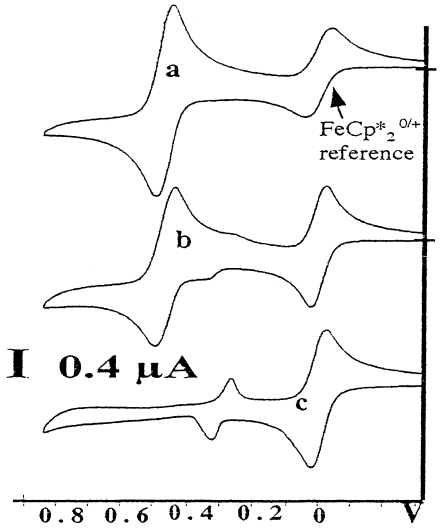

Figure 1. Titration of DAB-G_1 in CH_2Cl_2 (Pt, 0.1 M [*n*Bu_4N][PF_6], 20 °C; reference: $FeCp_2$* = decamethylferrocene) by [*n*Bu_4N][H_2PO_4]: (a) before addition, (b) 0.4 equiv, (c) 0.5 equiv.

Chart 2. Supramolecular Assembly between **2** + DAB-G_1 and 0.5 equiv of [*n*-Bu_4N][H_2PO_4] Characterized by Its Large Diffusion Coefficient (i.e., Reduced Intensity in the CV, See Figure 1c)

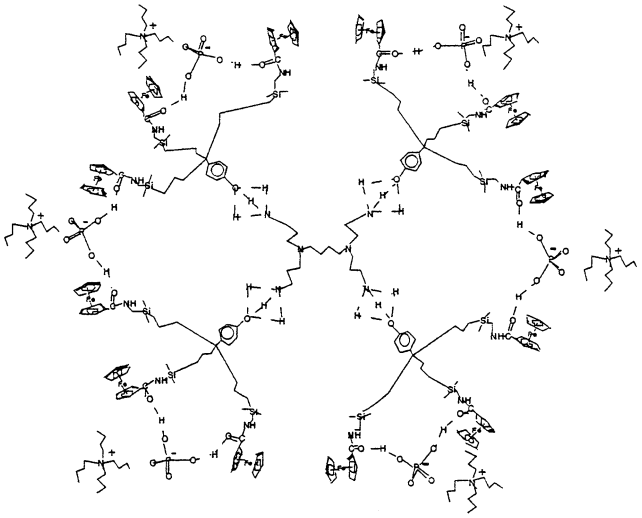

in the absence of DAB.[2a] This means that, for **2** + DAB-G_1, the six $H_2PO_4^-$ units probably cooperatively bind the 12 amidoferrocenyl groups of G_1 when the correct 1:2 stoichiometry is reached (Chart 2). About the same event is noted with **2** + DAB-G_2; that is, the 12 $H_2PO_4^-$ units cooperatively bind 24 amidoferrocenyl groups of G_2, although the increase of the $H_2PO_4^-$ stoichiometry from 0.5 to 0.8 for this generation indicates that competition among several phenomena is beginning. Finally, an exceptional drop from the intensity of the initial wave to that of the incoming wave (4 times weaker) is noted during the titration of $H_2PO_4^-$ with **2** + DAB-G_1 or **2** + DAB-G_2. This shows a large difference in the diffusion coefficients, that is, in the size of the electroactive species before and after addition of $H_2PO_4^-$. Thus, the electroactive assembly is considerably larger when $H_2PO_4^-$ is present than when it is absent. *Because H-bonding equilibria are much faster than the electrochemical time scale*, the electroactive species involved before $H_2PO_4^-$ titration is a mixture of free **2** and DAB-bonded **2**, and the electrochemical response is an average of these two situations. On the other hand, after titration, the fact that the new wave intensity is so much smaller than before shows that each $H_2PO_4^-$ unit links two amidoferrocenyl groups around the dendritic periphery to form a large dendritic assembly whose lifetime is larger than the electrochemical time scale. The absence of such a phenomenon during the titration of $H_2PO_4^-$ with reported covalent amidoferrocenyl dendrimers[2a] indicates that no interdendritic linking by $H_2PO_4^-$ significantly occurs and that this linking of two amidoferrocenyl branches by each $H_2PO_4^-$ unit is thus intradendritic as shown in Chart 2.

In summary, $H_2PO_4^-$ titrations by **2** + DAB-G_1 and **2** + DAB-G_2 show new positive dendritic effects[2a] characteristic of amidoferrocenyl dendrimers assembled by H-bonding. The completely unusual trends found during electrochemical monitoring of the titration (half-stoichiometry, sudden wave change, dramatic intensity decrease) are rationalized in terms of the formation of a dendritic assembly in which each $H_2PO_4^-$ unit links two amidoferrocenyl groups at the dendrimer periphery. The characteristics found for the higher DAB generations (G_3 and G_4) show saturation, indicating that the above trend, pure only with DAB-G_1, is less efficient for these high generations because of steric congestion and/or competition of $H_2PO_4^-$ binding between the amido and amino groups. Practically, the addition of DAB-G_1 to **2** for the titration of $H_2PO_4^-$ has the best positive effects facilitating this titration (large $\Delta E_{1/2}$ and sudden potential change at the equivalent point).

Acknowledgment. This communication is dedicated to our distinguished colleague and friend Professor Pierre Gouzerh (Université Paris VI) on the occasion of his 60th birthday. Financial support from the Institut Universitaire de France (IUF), the Ministère de la Recherche et de la Technologie (Ph.D. grant to M.-C.D.), the CNRS, and the Université Bordeaux I is gratefully acknowledged.

Supporting Information Available: Compared 400 MHz ^{1}H NMR spectra of **1**, **2**, G_3-DAB-16NH_2 and their dendritic H-bonded assemblies at different concentrations in $CDCl_3$ (PDF). This material is available free of charge via the Internet at http://pubs.acs.org.

References

(1) Beer, P. D.; Gale, P. A. *Angew. Chem., Int. Ed.* **2001**, *40*, 486.
(2) (a) Valério, C.; Fillaut, J.-L.; Ruiz, J.; Guittard, J.; Blais, J.-C.; Astruc, D. *J. Am. Chem. Soc.* **1997**, *119*, 2588. (b) Labande, A.; Ruiz, J.; Astruc, D. *J. Am. Chem. Soc.* **2002**, *124*, 1782.
(3) (a) Newkome, G. R.; Moorefield, C. N.; Vögtle, F. *Dendrimers and Dendrons: Concepts, Syntheses, Applications*; Wiley-VCH: Weinheim, 2001. (b) Matthews, O. A.; Shipway, A. N.; Stoddart, J. F. *Prog. Polym. Chem*. **1998**, *23*, 1. (c) Smith, D. K.; Diederich, F. *Angew. Chem. Eur. J.* **1998**, *4*, 1353. (d) Bosman, A. W.; Jansen, E. W.; Meijer, E. W. *Chem. Rev.* **1999**, *99*, 1665. (e) Hecht, S.; Fréchet, J. M. J. *Angew. Chem., Int. Ed.* **2001**, *40*, 74.
(4) Newkome, G. R.; Woosley, B. D.; He, E.; Moorefield, C. N.; Guther, R.; Baker, G. R.; Escamilla, G. H.; Merrill, J.; Lufmann, H. *Chem. Commun*. **1996**, 2737. Zimmerman, S. C.; Zeng, F.; Reichert, D. E. C.; Kolotuchin, S. V. *Science* **1996**, *271*, 1095. Wang, Y.; Zeng, S. C.; Zimmermann, S. C. *Tetrahedron Lett*. **1997**, *38*, 5459. Zeng, F.; Zimmermann, S. C. *Chem. Rev*. **1997**, *97*, 1681.
(5) Meijer's group has functionalized the DAB dendrimers using hydrogen bonding, see ref 3d and: Jansen, J. F. G. A.; de Brabander-van den Berg, E. M. M.; Meijer, E. W. *Science* **1994**, *265*, 1226. Jansen, J. F. G. A.; Meijer, E. W. *J. Am. Chem. Soc*. **1995**, *117*, 4417.
(6) (a) For a seminal article on the complementary H-bonding between alcohol and amines, see: Ermer, O.; Eling, A. *J. Chem. Soc., Perkin Trans. 2* **1994**, 925. (b) Melwyn-Hugues, E. A. *Physical Chemistry*, 2nd ed.; Pergamon: Oxford, 1961, 1060. (c) Desiraju, G. R. *Crystal Engineering: The Design of Organic Solids*; Elsevier: New York, 1989. (d) Hanessian, S.; Simard, M.; Roelens, S. *J. Am. Chem. Soc*. **1995**, *117*, 7630.
(7) De Brabander-van den Berg, E. M. M.; Meijer, E. W. *Angew. Chem., Int. Ed. Engl*. **1993**, *32*, 1308. See also the Supporting Information.
(8) (a) For a review on ferrocenyl dendrimers and their electrochemistry, see: Casado, C. M.; Cuadrado, M.; Moran, M.; Alonso, B.; Garcia, B.; Gonzales, J.; Losada, J. *Coord. Chem. Rev*. **1999**, *185/186*, 53.

JA020833K

Assemblages supramoléculaires par liaisons hydrogène de métallodendrimères électroactifs: caractérisation et reconnaissance des anions $H_2PO_4^-$ et adénosine-5'-triphosphate (ATP^{2-})

Résumé: Deux familles de cinq métallodendrimères supramoléculaires ont été assemblées à partir de dendrimères DSM G_n-DAB-dend-$(NH_2)_x$ (x = 4, 8, 16, 32, 64) et de dendrons phénols comportant en para un tripode triallyle ou triferrocényle puis elles ont été caractérisées par spectroscopie RMN^{1}H. Les études en voltammétrie cyclique des dendrimères à fonctions terminales amidoferrocényles dans CH_2Cl_2 montrent la présence d'une seule vague réversible du groupement ferrocényle. La reconnaisance des anions $H_2PO_4^-$ et ATP^{2-} (sous la forme de leurs sels de tétrabutylammonium) est excellente avec ces dendrimères supramoléculaires. Ces derniers présentent, pour certains, un comportement inhabituel dans le cas d'$H_2PO_4^-$ avec une très brusque disparition de la vague initiale et une saturation pour un demi-équivalent d'anion par branche dendritique. On note aussi un effet dendritique positif. En ce qui concerne l'adénosine-5'-triphosphate, ce comportement est analogue mais un peu moins marqué et un léger effet dendritique négatif est constaté.

Introduction

Le rôle des anions dans notre environnement est très important car ils interviennent aussi bien dans les milieux biologiques que dans l'industrie agricole ou pharmaceutique. Leur reconnaissance a fait l'objet d'investigations au moyen d'endorécepteurs variés.[1] Beer, en particulier, a construit des endorécepteurs à base de ferrocène[1d-g] ou de cobalticinium[1b] utilisés comme sondes rédox. Nous nous sommes intéressés à des exorécepteurs tels que les colloïdes[2] et les dendrimères[3], qui, grâce aux tunnels ou cavités qu'ils présentent en périphérie, vont reconnaître les anions. La reconnaissance d'oxoanions a déjà été réalisée dans notre groupe de recherche avec des dendrimères ainsi que des colloïdes à fonctions terminales amidoferrocényles.[4, 17] Des assemblages à base de colloïdes d'or et de dendrons ont aussi montré de bonnes aptitudes comme sondes rédox d'oxo-anions.[4c-d]

Nous avons maintenant exploré un nouveau type de dendrimères, formés de manière supramoléculaire par liaisons hydrogène entre des fonctions phénols et des fonctions amines primaires. Peu de travaux de ce type sont actuellement connus en ce qui concerne les dendrimères.[5, 6] Zimmerman a construit des auto-assemblages de dendrimères en utilisant des molécules tétraacides dendritiques dont les fonctions acides forment des paires de liaisons hydrogène mais aucune fonction particulière n'a été recherchée.[6]

Notre stratégie a consisté à assembler des dendrons comportant une fonction phénol autour d'un dendrimère aux extrémités amines primaires. Les dendrimères commerciaux DSM polyaminés G_n-DAB-dend-$(NH_2)_x$ (x = 4, 8, 16, 32, 64) ont été utilisés,[7] ainsi que les dendrons triallylés,[8] ou triamidoferrocéniques.[4d] Les dendrimères obtenus ont été caractérisés par spectroscopie RMN ^{1}H.

Grâce aux dendrons triferrocéniques, nous avons utilisé ces assemblages dendritiques supramoléculaires pour la reconnaissance électrochimique d'oxoanions tels que $H_2PO_4^-$ et ATP^{2-}. Les résultats ont montré un comportement inhabituel pendant les titrages, surtout avec la première génération de dendrimères lors de la titration d'$H_2PO_4^-$. On assiste en fait à une disparition brutale de la vague initiale à une demi-stœchiométrie d'anion par rapport au nombre de branches dendritiques et à l'apparition d'une nouvelle vague à un potentiel moins positif et beaucoup moins intense que la première. Ces caractéristiques se retrouvent lors des titrages de l'ATP^{2-} mais avec un caractère moins accentué. De plus, on note un effet dendritique positif pour la reconnaissance d' $H_2PO_4^-$ et un effet dendritique légèrement négatif pour l'ATP^{2-}.

Résultats

Synthèse et caractérisation

Les assemblages supramoléculaires ont été obtenus à partir des dendrimères commerciaux DSM polyaminés G_n-DAB-dend-$(NH_2)_x$ (x = 4, 8, 16, 32, 64) associés par liaisons hydrogène aux dendrons *p*-HO-$C_6H_4C(CH_2CH{=}CH_2)_3$ (**1**) ou *p*-HO-$C_6H_4C\{(CH_2)_3SiMe_2\text{-}CH_2NHCOFc\}_3$ (**2**), déjà connus au laboratoire. Ils seront notés respectivement DAB-(3x)-allyle (voir schéma 1) et DAB-(3x)-Fc (Fc = ferrocényle) (voir schéma 2 et 3). La synthèse des dendrons a été effectuée d'après les références 8 et 4d. La formation des dendrimères supramoléculaires a été réalisée en mélangeant des quantités équimolaires de G_n-DAB-dend-$(NH_2)_x$ et de dendrons en solution dans le chloroforme

deutérié. Plus précisément, dans le cas du G_1-DAB-dend-$(NH_2)_4$, porteur de quatre fonctions amines, on ajoute quatre équivalents de dendron.

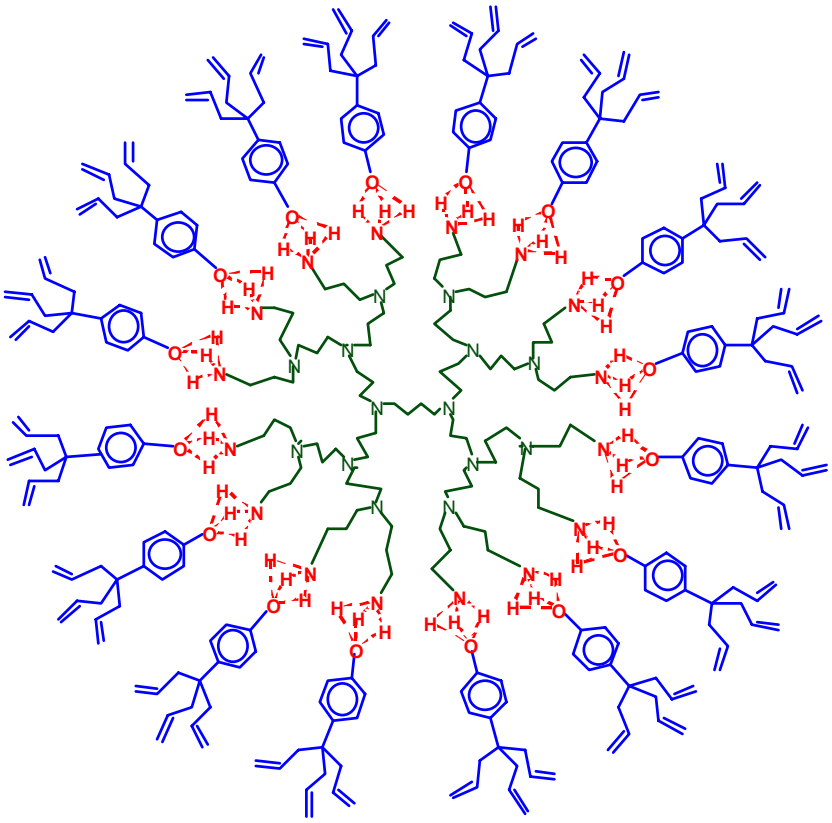

Schéma 1: Représentation schématique de DAB-48-allyles formé à partir de G_3-DAB-dend-$(NH_2)_{16}$ et du dendron **1**.

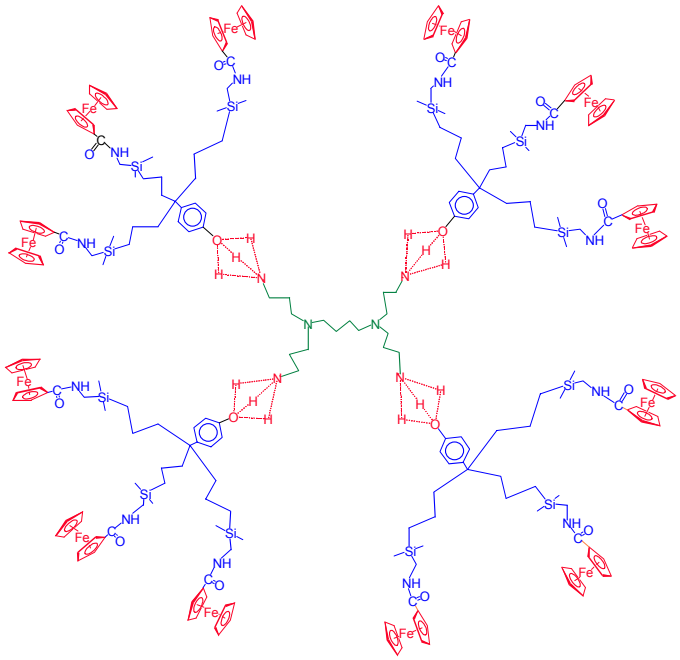

Schéma 2: Représentation schématique de DAB-12-Fc formé à partir de G_1-DAB-dend-$(NH_2)_4$ et du dendron **2**.

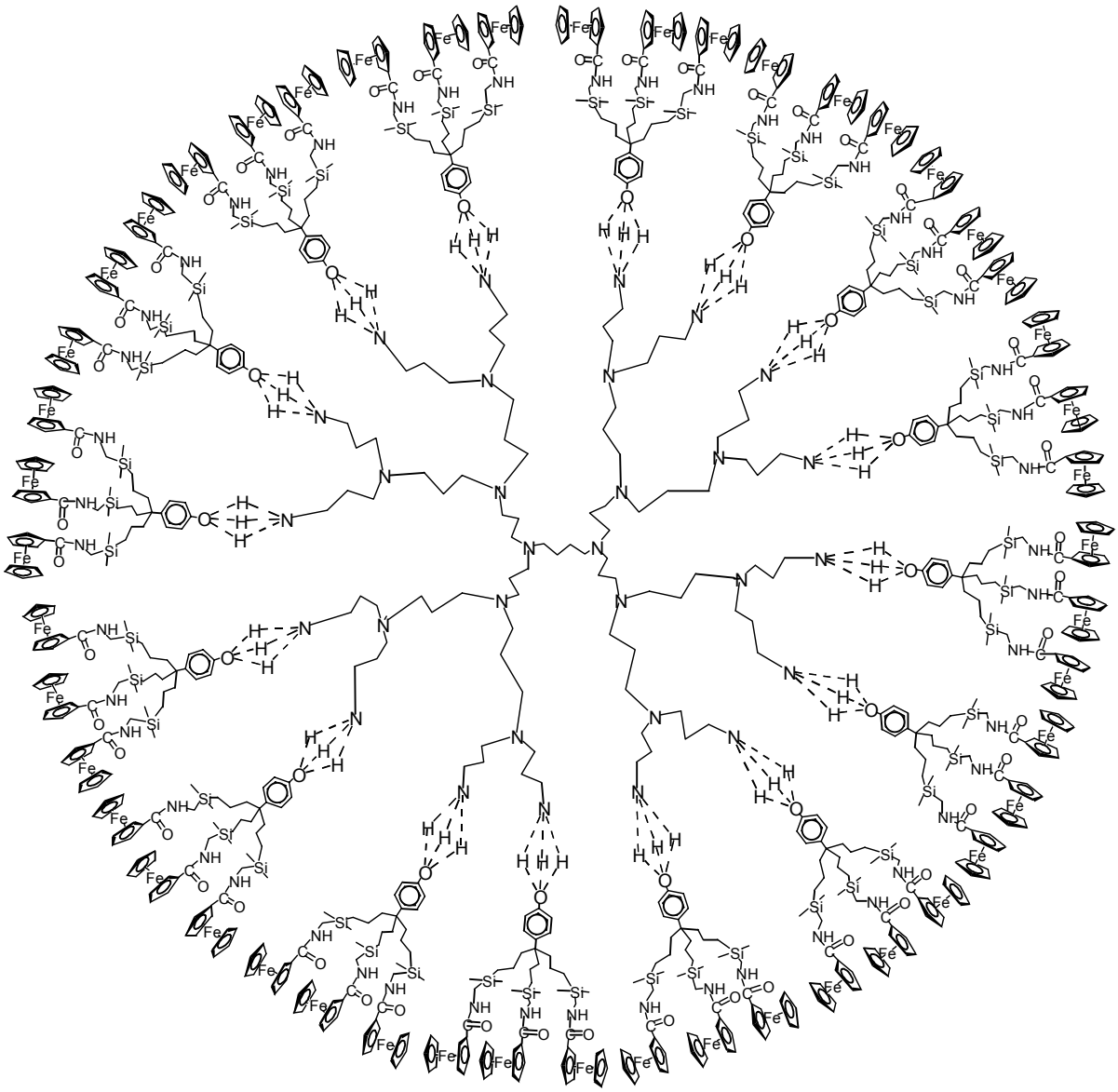

Schéma 3: Représentation schématique de DAB-48-Fc formé à partir de G_3-DAB-dend-$(NH_2)_{16}$ et du dendron **2**.

Les solutions sont préparées dans $CDCl_3$ pour permettre la caractérisation par RMN ^1H. Le spectre RMN ^1H du dendron **1** présente un pic à 4,8 ppm correspondant à la fonction phénol. Les fonctions amines des dendrimères G_n-DAB-dend-$(NH_2)_x$ donnent naissance à un signal à 1,5 ppm. L'association entre les dendrimères polyaminés et le dendron **1** provoque un blindage du signal du proton phénolique et un déblindage de celui des protons des amines pour former un signal unique situé entre 2,4 et 4,1 ppm selon la concentration (voir figure 1). Ce nouveau signal, matérialisant la création des liaisons hydrogène entre phénols et amines, est large. On le retrouve aussi dans les spectres RMN ^1H relatifs aux assemblages impliquant le dendron 2 (Voir figures 2 et 3).

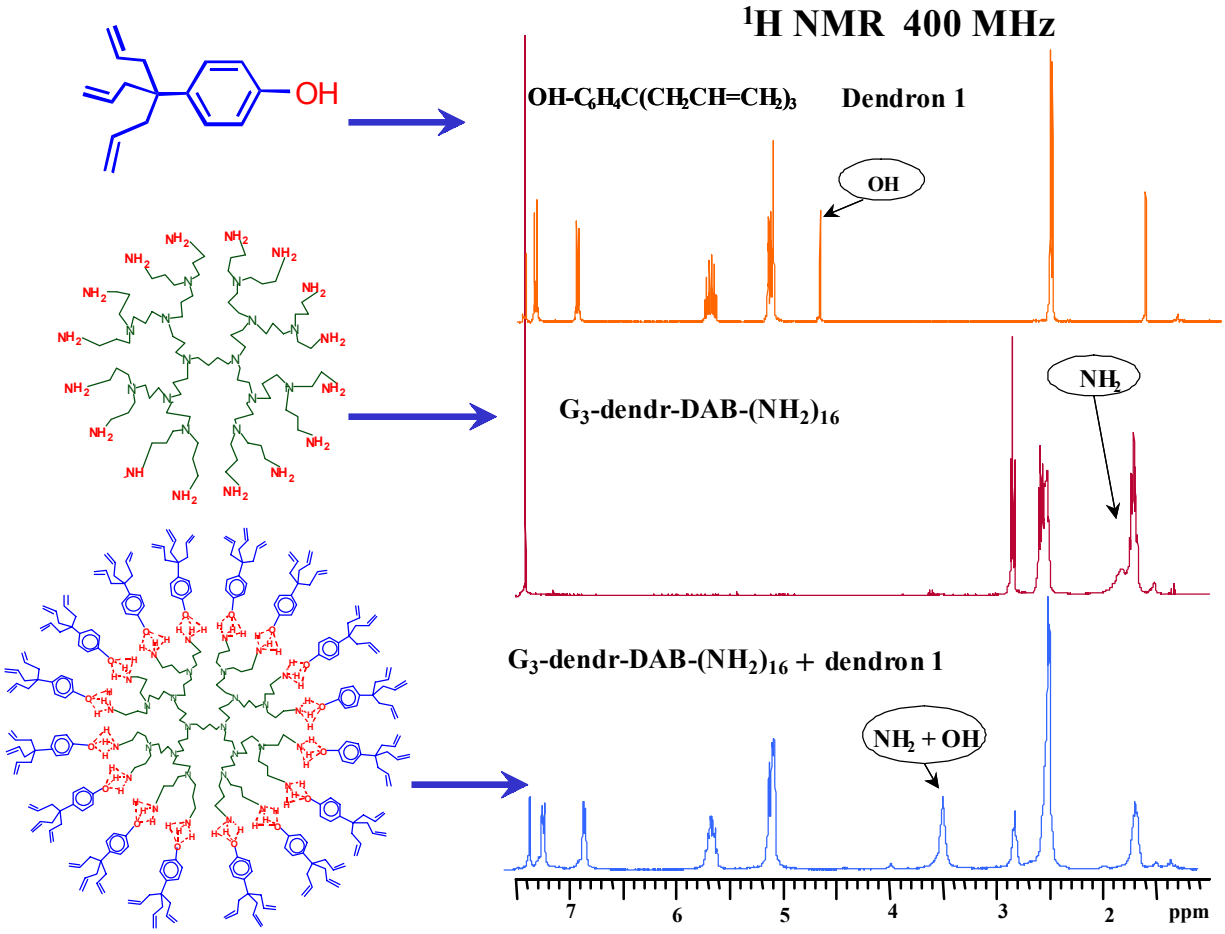

Figure 1: Spectres RMN ^1H (400 MHz) du dendron **1**, du G_3-DAB-dend-$(NH_2)_{16}$ et de leur assemblage par liaisons hydrogène.

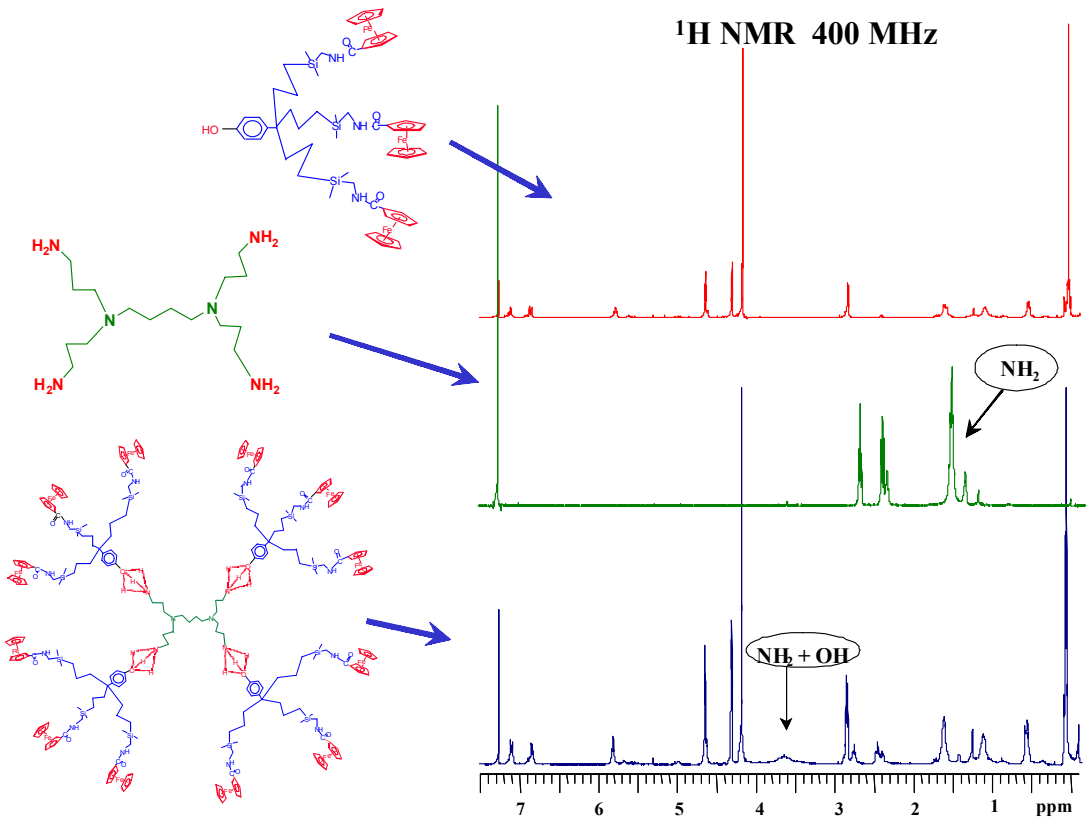

Figure 2: Spectres RMN ^{1}H (400 MHz) du dendron **2**, du G_1-DAB-dend-$(NH_2)_4$ et de leur assemblage par liaisons hydrogène (DAB-12-Fc).

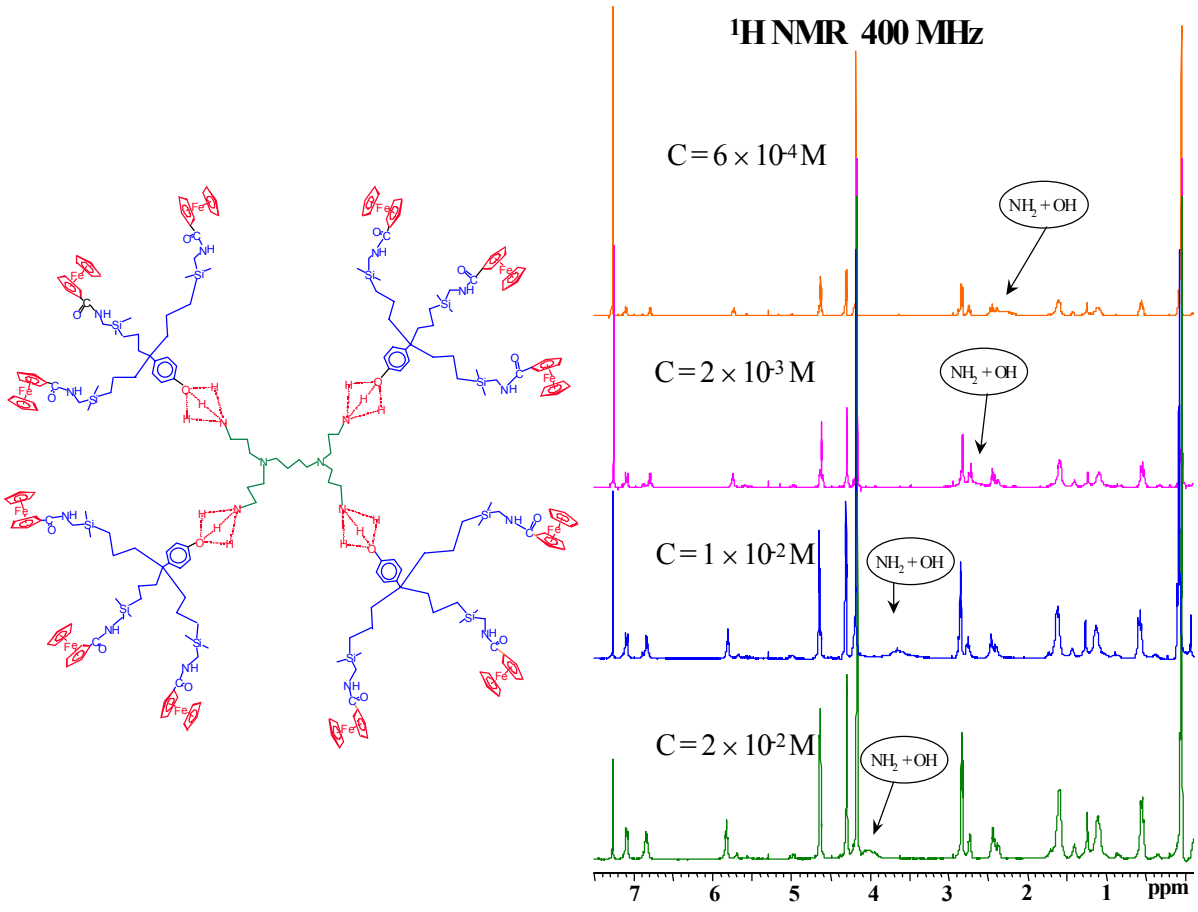

Figure 3: Spectres RMN ^{1}H (400 MHz) de DAB-12-Fc à différentes concentrations.

Voltammétrie cyclique des assemblages supramoléculaires DAB-(3x)-Fc

Les dendrimères étant construits par liaisons hydrogène avec le dendron **2** électroactif du fait des fonctions amidoferrocényles, ils ont pu être étudiés en voltammétrie cyclique.[9-11] Les voltammogrammes réalisés dans le dichlorométhane à température ambiante montrent une vague d'oxydo-réduction unique, réversible chimiquement et électrochimiquement. Seule la dernière génération, DAB-192-Fc, présente un léger phénomène d'adsorption car ΔE_p = 45 mV au lieu de 58 mV pour un composé réversible électrochimiquement. Les potentiels de demi-vague des différentes générations de DAB-G_n (n = 1 à 4) sont répertoriés dans le tableau 1, par rapport à Ag/ AgCl.

Reconnaissance électrochimique et titrages d'oxo-anions: $H_2PO_4^-$ et ATP^{2-}

$H_2PO_4^-$: Les interactions entre nos nouveaux dendrimères, formés par liaisons hydrogène, et $H_2PO_4^-$ ont été examinées par voltammétrie cyclique. L'ajout de sel de dihydrogénophosphate dans une cellule électrochimique contenant un des dendrimères DAB-(3x)-Fc dissout dans le dichlorométhane provoque l'apparition d'une nouvelle vague d'oxydo-réduction à des potentiels moins positifs que la vague de départ. Au fur et à mesure de l'ajout d'anion dans la cellule, l'intensité de la vague initiale diminue pendant que celle de la nouvelle vague augmente. Tous les résultats sont rassemblés dans le tableau 1.

Cependant, des phénomènes inhabituels se produisent pour les deux premières générations (DAB-12-Fc et DAB-24-Fc). En effet, on observe une brusque disparition de la vague initiale entre 0,4 et 0,5 équiv. d'anion par branche dendritique (Figure 4) alors que, normalement,[4a] la diminution d'intensité de la vague initiale est proportionnelle à la quantité d'anion en solution. De plus, la saturation a lieu pour 0,5 équiv. d'anion par unité amidoferrocényle pour DAB-12-Fc alors que des études antérieures avec d'autres dendrimères ont décrit une saturation à 1 équiv. d' $H_2PO_4^-$ par branche dendritique.[4a]

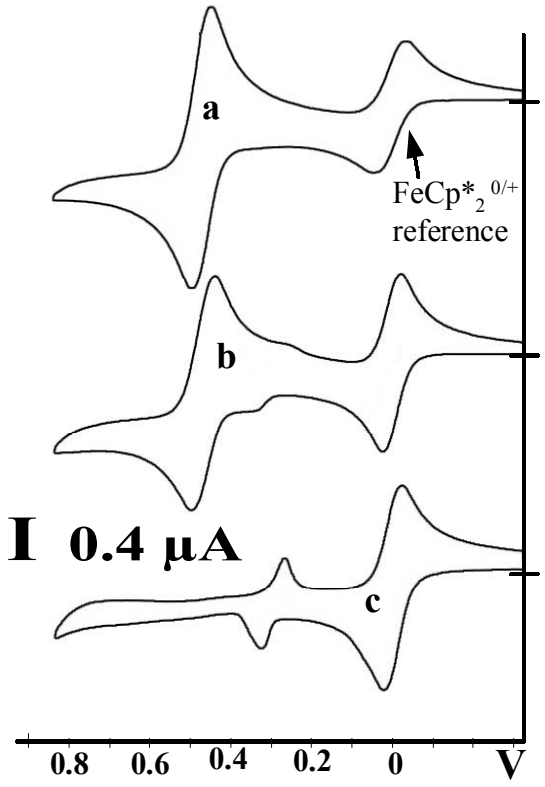

Figure 4. Titrage de DAB-12-Fc dans CH_2Cl_2 (Pt, [*n*-Bu_4N][PF_6] 0,1 M, 20°C, référence : $FeCp^*_2$ = décaméthylferrocène) par [*n*-Bu_4N][H_2PO_4]: cyclovoltammogrammes a) avant l'addition, b) avec 0,4 équiv. d'anion; c) avec 0,5 équiv. d'anion.

Dans le cas de DAB-24-Fc, le système sature avec 0,8 équiv. d' $H_2PO_4^-$ par fonction ferrocénique (Figure 5). Pour ce qui est des générations suivantes (DAB-48-Fc, DAB-96-Fc et DAB-192-Fc), la saturation est observée respectivement à 1,85 équiv., 1,7 équiv. et 0,95 équiv. par branche.

Le pouvoir de reconnaissance des DAB-3x-Fc présente un effet dendritique positif. Le dendron **2** seul reconnaît $H_2PO_4^-$ avec un écart entre la vague initiale et la nouvelle vague de 205 mV. Or, quand il est associé au dendrimère G_1-DAB-dend-$(NH_2)_4$ pour former DAB-12-Fc, la différence entre les deux vagues passe à 250 mV, et elle devient 280 mV à partir de la deuxième génération (DAB-24-Fc).

Le modèle d'Echegoyen-Kaifer[12] nous permet d'accéder aux rapports des constantes d'association K^+/ K^0 entre l'anion et les fonctions amidoferrocényles: ils sont détaillés dans le tableau 1 et atteignent la valeur de 67230. Une dernière caractéristique particulière à la reconnaissance d'$H_2PO_4^-$ par ces dendrimères est la forte diminution d'intensité de la nouvelle vague à saturation par rapport à la vague de départ. Les rapports d'intensité entre la vague finale et la vague avant titrage sont de 0,25 pour les deux premières générations, puis il augmente pour les dernières générations. De plus, la vague formée présente une irréversibilité

électrochimique avec un écart ΔE_p entre 90 et 140 mV selon la génération. On peut enfin noter que, si on essaie d'utiliser le décaméthylferrocène comme référence interne,[13] la vague de ce dernier est irréversible chimiquement et électrochimiquement en début de titrage. Par contre, elle devient réversible après que l'on ait ajouté un excès d'anion en solution.

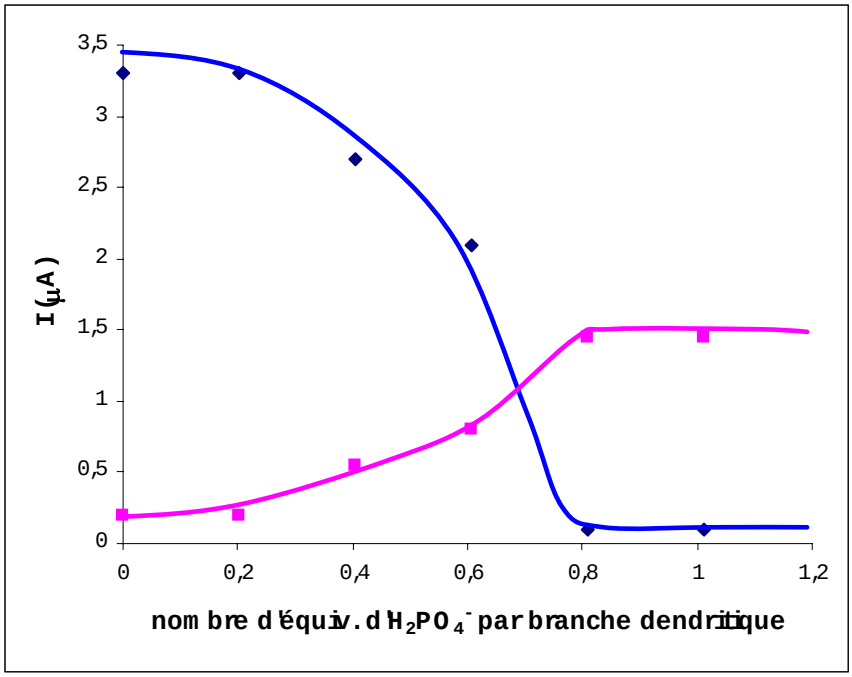

Figure 5: Titrage de DAB-24-Fc dans CH_2Cl_2 (Pt, 0.1M [*n*-Bu_4N][PF_6], 20°C, référence : $FeCp^*_2$ = décaméthylferrocène) par [*n*-Bu_4N][H_2PO_4]: variation des intensités des pics anodiques initial (♦) et nouveau (■) au cours du titrage.

Tableau 1: Données en voltammétrie cyclique concernant le dendron **2** et les DAB-3x-Fc avant et pendant le titrage d'$H_2PO_4^-$ dans CH_2Cl_2..

	$E_{1/2}$ (libre) (mV)[a]	ΔEp(libre) (mV)[b]	$H_2PO_4^-$			I_{final} / I_0[d]	Saturation (eq. d'$H_2PO_4^-$)
			$\Delta E_{1/2}$ (mV)	ΔEp (mV)	K^+/K^{0}[c]		
Dendron 2	750	55	205	115	3420	0.5	1
DAB-12-Fc	725	60	250	90	20430	0.25	0,50
DAB-24-Fc	780	55	280	90	67230	0.25	0.80
DAB-48-Fc	785	55	280	140	67230	1	1,85
DAB-96-Fc	745	55	280	110	67230	0.8	1,50
DAB-192-Fc	745	45	280	115	67230	0.66	0.95

(a) $E_{1/2}$ = (Ep_a+ Ep_c) / 2 vs. Ag/AgCl , en mV; électrolyte support: [*n*-Bu_4N][PF_6] 0,1 M; électrode de travail et électrode auxiliaire: Pt; électrode de référence: Ag; vitesse de balayage: 200 mV/s; 20 °C.

(b) ΔEp = Ep_a- Ep_c avec Ep_a le potentiel du pic anodique et Ep_c celui du pic cathodique.

(c) $\Delta E_{1/2}$ = 0,058 log (K^+/ K^0) à 20 °C selon la ref. 12.

(d) I_{final} : intensité de la nouvelle vague à saturation; I_0 : intensité de la vague initiale avant l'ajout d'anion.

***ATP*$^{2-}$**: Nos dendrimères constitués par assemblage supramoléculaire reconnaissant efficacement $H_2PO_4^-$, nous avons alors envisagé de les étudier en reconnaissance de l'adénosine-5'-triphosphate (ATP^{2-}).[14] En effet, l'ATP^{2-} est un anion dérivé du phosphate qui joue un rôle très important dans les organismes vivants. D'une part, c'est un des quatre nucléotides formant l'ADN, d'autre part, il constitue le réservoir d'énergie des cellules. Il est donc important de pouvoir le reconnaître et le titrer.

Le comportement des dendrimères DAB-3x-Fc observé envers l'ATP^{2-} est de même type qu'avec $H_2PO_4^-$ c'est-à-dire qu'on assiste à l'émergence d'une nouvelle vague à des potentiels plus faibles. La vague produite conserve une irréversibilité électrochimique conduisant à un ΔE_p du même ordre de grandeur que dans le cas de l'hydrogénophosphate (Voir le tableau 2). Cette vague garde aussi une intensité plus faible que celle de la vague de départ. Cependant, quelques différences sont à noter: l'écart de potentiels entre les deux vagues, $\Delta E_{1/2}$, est en effet un petit peu moins important puisqu'il varie de 200 mV pour le DAB-12-Fc à 180 mV pour DAB-192-Fc (Figure 6).

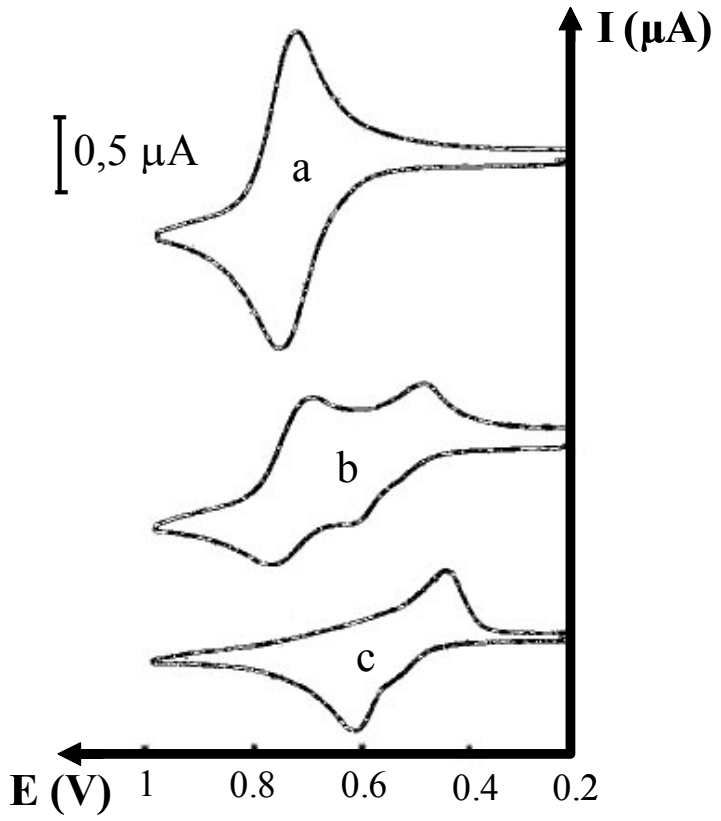

Figure 6: Titrage de DAB-192-Fc dans CH_2Cl_2 (Pt, [*n*-Bu_4N][PF_6] 0,1 M, 20°C, référence : $FeCp^*_2$ = décaméthylferrocène) par [*n*-Bu_4N]$_2$[ATP]: cyclovoltammogrammes a) avant l'addition, b) avec 0,26 équiv. d'anion; c) avec 0,35 équiv. d'anion.

On constate donc ici un léger effet dendritique négatif. De plus, le phénomène de chute brutale d'intensité de la vague initiale est moins marqué que dans les titrages d'$H_2PO_4^-$ (Figure 7) mais il reste présent pour toutes les générations de dendrimères supramoléculaires. Quant à la saturation, elle intervient avant 0,5 équivalent d'ATP^{2-} par branche dendritique (de 0,35 équiv. pour DAB-12-Fc à 0,45 équiv. pour DAB-96-Fc). On ne remarque pas de phénomène d'adsorption, même avec les dernières générations. Par contre, la nouvelle vague perd sa réversibilité chimique après saturation c'est-à-dire que le pic anodique disparaît peu à peu à partir de 0,5 équiv. d'ATP^{2-} ajouté en solution. Enfin, la vague induite présente une allure particulière car son pic anodique se découpe en deux pics en cascade qui, après saturation, finissent par ne plus former qu'un seul pic pour 1 équiv. d'ATP^{2-} par branche dendritique.

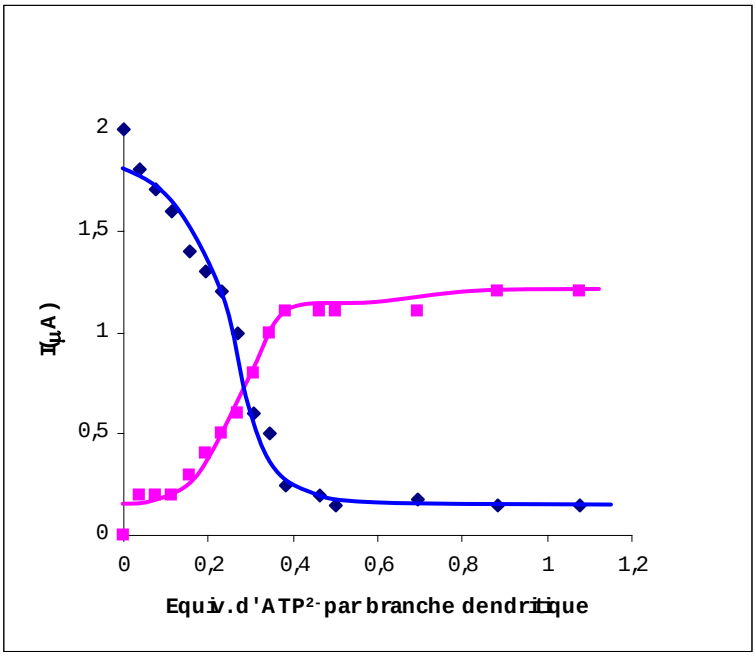

Figure 7: Titrage de DAB-24-Fc dans CH_2Cl_2 (Pt, 0.1M [*n*-Bu_4N][PF_6], 20°C, référence : $FeCp^*_2$ = décaméthylferrocène) par [*n*-Bu_4N]$_2$[ATP]: variation des intensités des pics anodiques initial (♦) et nouveau (■) au cours du titrage.

Tableau 2: Données en voltammétrie cyclique concernant le dendron **2** et les DAB-3x-Fc pendant le titrage de l'ATP^{2-} dans CH_2Cl_2.

	ΔEp(seul) (mV)[(a)]	ATP^{2-}			I_{final} / I_0[(c)]	Saturation (eq. d'ATP^{2-})
		$\Delta E_{1/2}$(mV)	ΔEp (mV)	$K^+/K^{0(b)}$		
Dendron 2	55	200	115	2810	0.40	0.5
DAB-12-Fc	60	200	120	2810	0.35	0.36
DAB-24-Fc	55	200	130	2810	0.46	0.40
DAB-48-Fc	55	180	115	1270	0.53	0.35
DAB-96-Fc	55	180	120	1270	0.47	0.45
DAB-192-Fc	45	180	115	1270	0.47	0.35

(a) $\Delta Ep = Ep_a - Ep_c$ avec Ep_a le potentiel du pic anodique et Ep_c celui du pic cathodique.

(b) $\Delta E_{1/2} = 0{,}058 \log (K^+/K^0)$ à 20 °C selon la ref. 12.

(c) I_{final} : intensité de la nouvelle vague à saturation; I_0 : intensité de la vague initiale avant l'ajout d'anion

Discussion

Des études de reconnaissance d'anions par des métallodendrimères ont déjà été menées et ont montré une affinité particulière des dendrimères à terminaisons amidoferrocényles envers l'hydrogénophosphate.[4,15-17]

$H_2PO_4^-$: En ce qui concerne les nouveaux dendrimères DAB-3x-Fc que nous avons préparés, la vague unique observée sur les voltammogrammes nous indique de l'équivalence des unités ferrocényles.[4,15,17] Ceci s'explique par un faible facteur électrostatique car les fonctions ferrocényles sont séparés par au moins onze atomes dans le dendron. A cela s'ajoute une vitesse de rotation des assemblages très rapide par rapport à l'échelle de temps électrochimique.[18] Au niveau reconnaissance, on retrouve une interaction forte entre les fonctions amidoferrocényles et $H_2PO_4^-$, déduite de l'apparition d'une nouvelle vague distinguant les amidoferrocényles complexés à l'anion de ceux restés libres.[12]

De plus, un effet dendritique positif (c'est-à-dire une meilleure reconnaissance quand la génération augmente) est remarqué, surtout entre le dendron **2** seul et DAB-12-Fc. Ceci s'explique par un espace inter-branches qui, en diminuant, devient plus approprié à la taille de l'anion, ce qui permet de mieux le piéger. La meilleure reconnaissance est obtenue avec DAB-24-Fc et stagne ensuite, quand la génération devient plus élevée. On arrive donc à une saturation de l'effet dendritique, ce qui peut signifier que la place offerte à $H_2PO_4^-$ est idéale dans le cas de DAB-24-Fc et que la reconnaissance se stabilise avec les générations suivantes, même si la cavité devient un peu petite pour l'anion.

D'autre part, nos dendrimères obéissent à un phénomène d'adsorption à partir de la troisième génération (DAB-48-Fc): les assemblages devenant plus gros, ils ont tendance à se déposer à la surface de l'électrode, surtout sous la forme oxydée car le ferricinium diminue leur solubilité dans CH_2Cl_2. Quant à l'irréversibilité électrochimique de la vague créée, elle est due à une réorganisation structurale du fait des interactions avec les anions.

Cependant, si ces aspects sont relativement classiques pour ce qui est de la reconnaissance d'$H_2PO_4^-$, les dendrimères supramoléculaires présentent des propriétés inattendues. D'abord, la disparition brutale de la vague initiale correspondant à une saturation à un demi-équivalent d'anion laisse imaginer et spéculer un effet coopératif d'association de six $H_2PO_4^-$ avec les 12 terminaisons amidoferrocényles de DAB-12-Fc au moment où la quantité d'anion nécessaire est atteinte en solution (schéma 4).

L'augmentation du nombre d'équivalent d'anion pour saturer les générations suivantes peut venir d'une compétition entre les fonctions amides et les fonctions amines. Ces dernières étant de plus en plus nombreuses quand la génération de dendrimère augmente, la compétiton peut devenir plus favorable aux amines (pour se lier à $H_2PO_4^-$) car l'effet stérique croissant peut déstabiliser les liaisons hydrogène.

La faible intensité de la nouvelle vague nous indique la diminution du coefficient de diffusion entre l'assemblage dendritique sans anion et celui complexé aux anions. En effet, l'intensité d'une vague est proportionnelle à la racine carrée du coefficient de diffusion D selon l'équation de Sevick-Randles[19]: $i = kA\, n^{3/2}\, D^{1/2}\, v^{1/2}\, C$ où A désigne l'aire de l'électrode, k un coefficient numérique, n le nombre d'électrons mis en jeu, v la vitesse de balayage et C la concentration du substrat. Or, l'assemblage est beaucoup plus gros quand les anions sont présents à la périphérie et bloquent l'ensemble supramoléculaire (schéma 4). Ils diffuse alors bien moins facilement vers l'électrode.

Enfin, l'équilibre des liaisons hydrogène entre les G_n-DAB-dend-$(NH_2)_x$ et le dendron **2** est rapide à l'échelle de temps électrochimique. Par conséquent, la réponse électrochimique, avant le titrage, représente une moyenne entre les dendrimères aminés libres d'une part et les dendrimères aminés liés à **2** d'autre part. Donc, on peut penser que les DAB-dend-$(NH_2)_x$ s'adsorbent sur l'électrode et perturbent le signal du décaméthylferrocène alors que celui du dendron **2** est intact grâce aux liaisons hydrogène avec les DAB-dend-$(NH_2)_x$. La présence des anions va déplacer l'équilibre vers la formation des liaisons hydrogène entre les dendrimères polyaminés et **2**, ce qui va empêcher le phénomène d'adsorption et rendre une vague réversible pour le décaméthylferrocène. Ainsi, l'observation de l'irréversibilité de la vague de [$FeCp_2$*] avant addition d'anion ajouté à celle de sa réversibilité avec l'excès d'$H_2PO_4^-$ constitue un argument supplémentaire de la cohésion de l'ensemble supramoléculaire que nous suggérons en présence d'un demi-équivalent d'$H_2PO_4^-$.

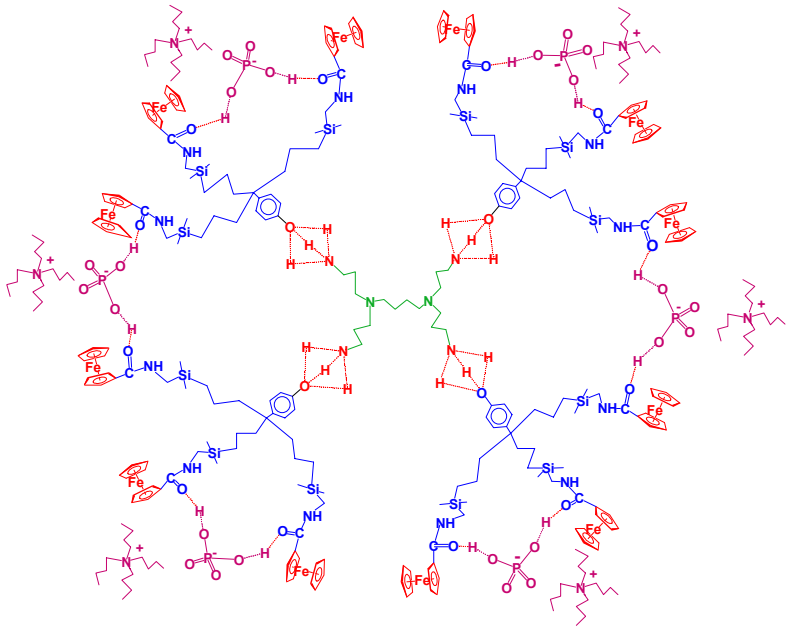

Schéma 4: Représentation schématique de DAB-12-Fc + 0,5 équiv. d'$H_2PO_4^-$ par branche dendritique.

***ATP*$^{2-}$**: Comme pour le dihydrogénophosphate, on note une interaction forte entre les fonctions amidoferrocényles et l'ATP^{2-}, mais cette interaction demeure un peu plus faible qu'avec $H_2PO_4^-$. De plus, le léger effet dendritique négatif peut signifier, qu'à partir de 48 branches, l'espace inter-branches devient trop petit pour que l'anion puisse s'insérer correctement.

Comme expliqué ci-dessus, la petite taille de la nouvelle vague témoigne de la formation d'un gros assemblage et son irréversibilité électrochimique atteste d'une réorganisation structurale pendant la réduction. La stœchiométrie obtenue rappelle le fait qu'elle varie suivant le type de récepteur.[14]

Le remplacement de la vague initiale est moins brusque qu'avec $H_2PO_4^-$: en effet, l'ATP^{2-}, de par ses deux charges négatives, a une meilleure tendance à se lier à deux groupements ferrocényles à la fois, d'où, au début, un mélange entre ATP^{2-} monocomplexés et ATP^{2-} bi-complexés. Quand la stœchiométrie est atteinte, la vague initiale disparaît, nous indiquant que chaque dianion complexe alors deux fonctions amidoferrocényles.

A ce stade, le pic anodique, en cascade, suggère une valence mixte des deux ferrocènes reliés par l'ATP^{2-} avec coopération de deux potentiels successifs en raison essentiellement du facteur électrostatique . Puis, l'apport supplémentaire d'anion nous amène à un pic anodique unique pour un équivalent d'anion par branche dendritique car on peut penser, qu'avec cet excès, chaque entité ferrocényle complexe deux phosphates d'un seul

ATP^{2-}. La perte progressive du pic cathodique pourrait être expliquée par une dégradation des fonctions ferriciniums due à une trop forte concentration en anion dans la solution.

Conclusion

Un nouveau type de métallodendrimères a été réalisé par assemblage supramoléculaire, à l'aide de liaisons hydrogène, entre les dendrimères G_n-DAB-dend-$(NH_2)_x$ et un dendron trisallyle ou tris-amidoferrocényle. Les dendrimères formés par liaisons hydrogène avec le dendron tris-amidoferrocényle ont permis de reconnaître le dihydrogénophosphate et l'adénosine-5'-triphosphate avec des aspects très intéressants, même inattendus pour certains:

- L'interaction anion-récepteur est de type fort envers $H_2PO_4^-$ mais aussi envers l'ATP^{2-}.
- On constate un remplacement soudain de la vague initiale pour un demi équivalent d'anion par branche dendritique, ce qui correspond à une association coopérative des anions autour du dendrimère.
- L'intensité de la nouvelle vague est bien inférieure à celle de la vague de départ, ce que nous interprétons par la création d'un assemblage supramoléculaire beaucoup plus volumineux que les espèces initiales.
- Un effet dendritique positif est observé envers $H_2PO_4^-$ et un effet dendritique légèrement négatif est constaté dans le cas de l'ATP^{2-}. Ces effets témoignent probablement de l'encombrement stérique influençant la compétition amide/amine pour les liaisons hydrogène avec $H_2PO_4^-$.

Experimental Section

General data. Dichloromethane (CH_2Cl_2) was distilled from calcium hydride just before use. DSM polyamines G_n-DAB-dend-$(NH_2)_x$ were purchased from Aldrich and used as received. 1H NMR spectra were recorded with a Brucker AC 400 (400 MHz) spectrometer. All chemical shifts are reported in parts per million (δ, ppm) with reference to the solvent or Me_4Si. Cyclic voltammetry data were recorded with a PAR 273 potentiostat galvanostat. Care was taken in the CV experiments to minimise the effects of solution resistance on the measurements of potentials peaks (the use of positive feedback IR compensation and dilute

solution (≈ 10^{-4} mol/L) maintained currents between 1 and 10 μA). The reference electrode was an Ag quasi-reference electrode (QRE). The QRE potential was calibrated by adding the reference couple [$FeCp_2$*]/ [$FeCp_2$*]$^+$. The working electrode (platinum) was treated by immersion in 0.1 M HNO_3 then polished before use and between each recording if necessary.

Synthesis of the dendron **2**. It was carried out as reported in reference 4d.

Preparation of the supramolecular assembly {G_1-DAB-dend-$(NH_2)_4$ + dendron **2**}. 2.25 mg (7.11 x 10^{-6} mol.) of the commercial DSM polyamine G_1-DAB-dend-$(NH_2)_4$ were weighed in a NMR tube with a microbalance and dissolved in 0.6 mL of $CDCl_3$. Then, 32.17 mg (4 eq., 28.43 x 10^{-6} mol.) of dendron **2** were weighed in an essay tube and transferred in a NMR tube with 0.6 mL of $CDCl_3$. The formation of the supramolecular assembly is observed by ^{1}H NMR. Spectra of each product were monitored before mixing them and after. Then, the solvent was removed and the assembly was dissolved in CH_2Cl_2 and adjusted at 25 mL in a volumetric flask.

^{1}H NMR (400 MHz, $CDCl_3$) δ (ppm): 0.05 (s, 72H, $(CH_3)_2Si$); 0.55 (t, 24H, CH_2Si); 1.10 (br, 24H, CH_2CH_2Si); 1.40 (br, 4H, CH_2CH_2N central); 1.58-1.61 (m, 12H, $CH_2CH_2NH_2$ and $ArC(CH_2)_3$); 2.43 (m, 12H, CH_2NCH_2); 2.72 (t, 8H, CH_2NH_2); 2.84 (d, 24H, $SiCH_2N$); 3.11 (br, 12H, NH_2 + OH); 4.17 (s, 60H, Cp); 4.30 (s, 24H, C_5H_4CO); 4.64 (s, 24H, C_5H_4CO); 5.81 (t, 12H, NHCO); 6.83 (d, 8H, Ar); 7.10 (d, 8H, Ar).

The formation of supramolecular dendrimers with the other four generations of the DSM dendrimers were carried out as described above.

For DAB-24-Fc: ^{1}H NMR (400 MHz, $CDCl_3$) δ (ppm): 0.05 (s, 144H, $(CH_3)_2Si$); 0.55 (t, 48H, CH_2Si); 1.10 (br, 48H, CH_2CH_2Si); 1.38 (br, 4H, CH_2CH_2N central); 1.58-1.61 (m, 72H, $CH_2CH_2NH_2$ and $ArC(CH_2)_3$); 2.42 (m, 36H, CH_2NCH_2); 2.72 (t, 16H, CH_2NH_2); 2.84 (d, 48H, $SiCH_2N$); 3.19 (br, 24H, NH_2 + OH); 4.17 (s, 120H, Cp); 4.30 (s, 48H, C_5H_4CO); 4.64 (s, 48H, C_5H_4CO); 5.82 (t, 24H, NHCO); 6.83 (d, 16H, Ar); 7.10 (d, 16H, Ar).

For DAB-48-Fc: ^{1}H NMR (400 MHz, $CDCl_3$) δ (ppm): 0.05 (s, 288H, $(CH_3)_2Si$); 0.55 (t, 96H, CH_2Si); 1.10 (br, 96H, CH_2CH_2Si); 1.38 (br, 4H, CH_2CH_2N central); 1.58 (m, 152H, $CH_2CH_2NH_2$ and $ArC(CH_2)_3$); 2.41 (m, 88H, CH_2NCH_2); 2.72 (t, 32H, CH_2NH_2); 2.84 (d, 96H, $SiCH_2N$); 3.02 (br, 48H, NH_2 + OH); 4.17 (s, 240H, Cp); 4.30 (s, 96H, C_5H_4CO); 4.64 (s, 96H, C_5H_4CO); 5.82 (t, 48H, NHCO); 6.83 (d, 32H, Ar); 7.10 (d, 32H, Ar).

For DAB-96-Fc: ^{1}H NMR (400 MHz, $CDCl_3$) δ (ppm): 0.04 (s, 576H, $(CH_3)_2Si$); 0.55 (t, 192H, CH_2Si); 1.10 (br, 192H, CH_2CH_2Si); 1.59 (m, 316H, $CH_2CH_2NH_2$ + CH_2CH_2N central and $ArC(CH_2)_3$); 2.41 (m, 180H, CH_2NCH_2); 2.68 (t, 64H, CH_2NH_2); 2.84 (d, 192H,

$SiCH_2N$); 3.05 (br, 96H, NH_2 + OH); 4.17 (s, 480H, Cp); 4.30 (s, 192H, C_5H_4CO); 4.63 (s, 192H, C_5H_4CO); 5.80 (t, 96H, NHCO); 6.82 (d, 64H, Ar); 7.10 (d, 64H, Ar).

For DAB-192-Fc: ^{1}H NMR (400 MHz, $CDCl_3$) δ (ppm): 0.05 (s, 1152H, $(CH_3)_2Si$); 0.55 (t, 384H, CH_2Si); 1.10 (br, 384H, CH_2CH_2Si); 1.58 (m, 636H, $CH_2CH_2NH_2$ + CH_2CH_2N central and $ArC(CH_2)_3$); 2.41 (m, 372H, CH_2NCH_2); 2.72 (t, 128H, CH_2NH_2); 2.85 (d, 384H, $SiCH_2N$); 3.20 (br, 192H, NH_2 + OH); 4.17 (s, 960H, Cp); 4.30 (s, 384H, C_5H_4CO); 4.63 (s, 384H, C_5H_4CO); 5.82 (t, 192H, NHCO); 6.84 (d, 128H, Ar); 7.10 (d, 128H, Ar).

Titrations using cyclic voltammetry: commun conditions for all the captions of the figures.

Solvent: distilled CH_2Cl_2; temperature: 20 °C; supporting electrolyte: [*n*-Bu_4N][PF_6] 0.1 M; internal reference: $FeCp_2$*; reference electrode: Ag; auxiliary and working electrodes: Pt; scan rate: 0.2 V/s; anion concentration ([*n*-Bu_4N][H_2PO_4] or [*n*-Bu_4N]$_2$[ATP]): 5 x 10^{-2} M.

General method for the titration of $H_2PO_4^-$ or ATP^{2-}. First, [*n*-Bu_4N][PF_6] was introduced in the electrochemical cell (that contained the working electrode, the reference electrode and the counter electrode) and dissolved in freshly distilled dichloromethane. A blank voltammogram was recorded without dendrimer in order to check the working electrode. Then, 2 mL of the solution of supramolecular dendrimer in dichloromethane was added into the cell. About 1 mg (3 x 10^{-6} mol) of decamethylferrocene was also added. After degassing the solution by flushing dinitrogen, the CV of the dendrimer alone was recorded. Then, the anion $H_2PO_4^-$ or ATP^{2-} was added as the *n*-Bu_4N^+ salts by small quantities using a microseringe. After each addition, the solution was degassed, and a CV was recorded. The appearance and progressive increase of a new wave was observed while the initial wave decreased and finally disappeared (see the titration graphs). When the initial wave had completely disappeared, addition of the salt of the anion was continued until reaching twice the volume already introduced.

Références:

[1] (a) P. D. Beer. *Advan. Inorg. Chem.* **1992**, *39*, 79; (b) P. D. Beer, M. G. B. Drew; J. Hodacova, S.E. Stokes. *J. Chem. Soc., Dalton Trans.* **1995**, 3447; (c) P. D. Beer, *J. Chem. Soc., Chem. Commun.* **1996**, 689; (d) P. D. Beer. *Acc. Chem. Res.* **1998**, *31*, 71; (e) P. D. Beer, P. A. Gale, Z. Chen. *Adv. Phys. Org. Chem*. **1998**, *31*, 1; (f) P. D. Beer, P. A. Gale. *Angew. Chem. Int. Ed. Engl*. **2001**, *40*, 486; (g) P. D. Beer, J. Davis, D. A. Drillsma-Millgrom, F. Szemes. *Chem. Commun*. **2002**, 1716.

[2] (a) G. Schmid. *Chem. Rev*. **1992**, *92*, 1709; (b) J. S. Bradley, in *Clusters and Colloïds*, G. Schmid, Ed., VCH, Weinheim, 1995, Chapter 6; (c) G. Schmid, L. F. Chi. *Adv. Mater*. **1998**, *18*, 515.

[3] For recent reviews on dendrimers [3a] and metallodendrimers, [3b] see; (a) G. R. Newkome, C. N. Moorefield, F. Vögtle. *Dendrimers and Dendrons, Concepts, Synthesis and Applications*, VCH-Wiley, Weinheim, 2001; Dendrimers and other Dendritic Polymers, (Eds.: D. Tomalia, J. M. J. Fréchet), Wiley-VCH, New York, 2002; (b) G. R. Newkome, E. He, C. N. Moorefield. *Chem. Rev.* **1999**, *99,* 1689; H. M. Janssen, E. W. Meijer. *Chem. Rev*. **1999**, *99*, 1665; I. Cuadrado, M. Morán, C. M. Casado, B. Alonso, J. Losada. *Coord. Chem. Rev.* **1999**, *189*, 123; M.A. Hearshaw, J. R. Moss. *Chem. Commun.* **1999**, 1; D. Astruc, F. Chardac. *Chem. Rev*. **2001**, *101*, 2991.

[4] (a) C. Valério, J.-L. Fillaut, J. Ruiz, J. Guittard., J.-C. Blais, D. Astruc. *J. Am. Chem. Soc.* **1997**, *119*, 2588; (b) A. Labande, J. Ruiz, D. Astruc. *J. Am. Chem. Soc.* **2002**, *124*, 1782; (c) M.-C. Daniel, J. Ruiz, S. Nlate, J. Palumbo, J.-C. Blais, D. Astruc. *Chem. Commun.*, **2001**, 2000; (d) M.-C. Daniel, J. Ruiz, S. Nlate, J.-C. Blais, D. Astruc. *J. Am. Chem. Soc*., **2003**, *125*, 2617.

[5] Meijer's group has functionalized the DAB dendrimers using hydrogen bonding: (a) A. W. Bosman, J. F. G. A. Jansen, E. W. Meijer. *Chem. Rev.* **1999**, *99*, 1665; (b) J. F. G. A. Jansen, E. M. M. de Brabander-van den Berg, E. W. Meijer. *Science* **1994**, *265*, 1226; (c) J. F. G. A. Jansen, E. W. Meijer. *J. Am. Chem. Soc*. **1995**, *117*, 4417.

[6] (a) G. R. Newkome, B. D. Woosley, E. He, C. N. Moorefield, R. Guther, G. R. Baker, G. H. Escamilla, J. Merrill, H. Lufmann. *Chem. Commun*. **1996**, 2737; (b) S. C. Zimmerman, F. Zeng, D. E. C. Reichert, S. V. Kolotuchin. *Science*, **1996**, *271*, 1095; (c) Y. Wang, F. Zeng, S. C. Zimmermann. *Tetrahedron Lett*. **1997**, *38*, 5459; (d) F. Zeng,; S. C. Zimmermann. *Chem. Rev*. **1997**, *97*, 1681.

[7] E. M. M. de Brabander-van den Berg, E. W. Meijer. *Angew. Chem. Int. Ed. Engl*. **1993**, *32*, 1308.

[8] (a) V. Sartor, L. Djakovitch, J.-L. Fillaut, F. Moulines, F. Neveu, V. Marvaud, J. Guittard, J.-C. Blais, D.Astruc. *J. Am. Chem. Soc*. **1999**, *121*, 2929; (b) V. Sartor, S. Nlate, L. Djakovitch, J.-L. Fillaut, F. Moulines, F. Neveu, V. Marvaud, J. Guittard, J.-C. Blais, D. Astruc. *New. J. Chem*. **2000**, *24*, 351; (c) S. Nlate, J.-C. Blais, D. Astruc. *New J. Chem*. **2003**, *27*, 178.

[9] (a) A. J. Bard, L. R. Faulkner, *Electrochemical Methods*. Wiley, New York, 1980 ; (b) J. B. Flanagan, S. Margel, A. J. Bard, F. C. Anson. *J. Am.Chem. Soc*. **1978**, *100*, 4248.

[10] (a) D. Astruc. *Electron-Transfer and Radical Processes in Transition-Metal Chemistry*, VCH, New York, 1995, Chapters 2 and 7**;** (b) D. Astruc, In *Electron Transfer in Chemistry* (Ed.: V. Balzani), Wiley-VCH, New York, 2001, *Vol. 2*, *Organic, Inorganic and Organometallic Molecules* (Eds.: J. Mattay, D. Astruc,) *section 2, Chapter 4*, p. 728.

[11] A. E. Kaifer, M. Gomez-Kaifer. *Supramolecular Electrochemistry*, Wiley-VCH, Weinheim, 1999, Chapter 16, p. 207.

[12] Seminal report: S. R Miller, D. A. Gustowski, Z.-H. Chen, G. W. Gokel, L. Echegoyen, A. E. Kaifer. *Anal. Chem*. **1988**, *60*, 2021.

[13] La référence interne décaméthylferrocène, [$FeCp^*_2$], est une meilleure référence que le ferrocène: voir J. Ruiz, D. Astruc. *C. R. Acad. Sci. Paris, Ser. II c*, **1998**, 21.

[14] Pour des études antérieures sur la reconnaissance de l'ATP^{2-} par un dérivé ferrocényle mononucléaire, voir: (a) P. D. Beer, J. Cadman, J. M. Lloris, R. Martinez-Mànez, M. E. Padilla, T. Pardo, D. K. Smith, J. Soto. *J. Chem. Soc., Dalton Trans.* **1999**, 127; (b) O. Reynes, F. Maillard, J.–C. Moutet, G. Royal, E. Saint-Aman., G. Stanciu, J.-P. Dutasta, I. Gosse, J.-C. Mulatier. *J. Organomet. Chem*. **2001**, *637-639*, 356; (c) O. Reynes, J.–C. Moutet, J. Pecaut, G. Royal, E. Saint-Aman. *New J. Chem*., **2002**, *26*, 9.

[15] a) D. Astruc, C. Valério, J.-L. Fillaut, J. Ruiz, J.-R. Hamon, F. Varret. In Supramolecular Magnetism, O. Kahn Ed., NATO ASI Series, Kluwer, Dordrecht, 1996, pp. 107-127; voir aussi réf. [3a, c]; b) C. Valério, E. Alonso, J. Ruiz, J.-L. Fillaut, D. Astruc. *Pure Appl. Chem*. **1998**, *70*, n°4, 809; c) C. Valério, E. Alonso, J. Ruiz, J.-C. Blais, D. Astruc. *C. R. Acad. Sci. Paris*, **1999**, *2*, Série IIc, 79; d) C. Valério, E. Alonso, J. Ruiz, J.-C. Blais, D. Astruc. *Angew. Chem. Int. Ed. Engl*. **1999**, *38*, 1747.

[16] a) J. Losada, B. Alonso, I. Cuadrado, C.-M. Casado, M. Morán. *J. Electroanal. Chem*. **1999**, *463***,** 87; b) B. Alonso, C.-M. Casado, I. Cuadrado, M Morán, A. Kaifer. *Chem. Commun*. **2002**, 1778.

[17] M.-C. Daniel, J. Ruiz, J.-C. Blais, N. Daro, D. Astruc. *Chemistry, Eur. J.*, **2003**, *9*, 4371.

[18] C. B. Gorman, J. C. Smith, M. W. Hager, B. L. Parkhurst, H. Sierzputowska-Gracz, C. A. Haney. *J. Am. Chem. Soc*. **1999**, *121*, 9958.

[19] A. Tallec. *Electrochimie organique*, Masson, Paris, 1995, chapitre 3, p. 59.

PARTIE 3:

ASSEMBLAGES NANOSCOPIQUES DE METALLODENDRONS ELECTROACTIFS ET DE NANOPARTICULES D'OR POUR LA RECONNAISSANCE D'$H_2PO_4^-$, D'HSO_4^- ET DE L'ATP^{2-}.

Assemblages nanoscopiques de métallodendrons électroactifs et de nanoparticules d'or pour la reconnaissance d'$H_2PO_4^-$, d'HSO_4^- et de l'ATP^{2-}.

Des dendrimères à cœur colloïdal ont été formés en associant des dendrons thiols autour de nanoparticules d'or de 2,5 à 3 nm de diamètre.

L'utilisation de dendrons triferrocényles et la reconnaissance d'$H_2PO_4^-$ dans le dichlorométhane par les colloïdes obtenus a fait l'objet d'une note préliminaire publiée à *Chemical Communication* et intitulée:

Gold nanoparticles containing redox-active supramolecular dendrons that recognize $H_2PO_4^-$.

L'extension des travaux avec des dendrons nonaferrocényles, ainsi que la reconnaissance d'HSO_4^- et de l'ATP^{2-}, l'étude de la sélectivité, le travail dans le diméthylformamide et la création d'électrodes modifiées ont été rassemblés dans un mémoire publié au *Journal of American Chemical Society* et intitulé:

Nanoscopic Assemblies between Supramolecular Redox Active Metallodendrons and Gold Nanoparticles: Synthesis, Characterization, and Selective Recognition of $H_2PO_4^-$, HSO_4^- and adénosine-5'-triphosphate (ATP^{2-}) Anions.

Les résultats de ces investigations sont récapitulés en français dans le résumé-conclusion à la fin de ce manuscrit.

CHEMCOMM
Communication
www.rsc.org/chemcomm

Gold nanoparticles containing redox-active supramolecular dendrons that recognize $H_2PO_4^-$

Marie-Christine Daniel,[a] Jaime Ruiz,[a] Sylvain Nlate,[a] Jennifer Palumbo,[a] Jean-Claude Blais[b] and Didier Astruc*[a]

[a] *Groupe de Chimie Supramoléculaire des Métaux de Transition, LCOO, UMR CNRS, 5802, 33405 Talence Cedex, France. E-mail: d.astruc@lcoo.u-bordeaux.fr*
[b] *Laboratoire de Chimie Structurale Organique et Biologique, EP CNRS N° 103, Université Paris VI, 4 Place Jussieu, 75252 Paris, France*

Received (in Cambridge, UK) 27th July 2001, Accepted 16th August 2001
First published as an Advance Article on the web 18th September 2001

Gold nanoparticles have been functionalized with thiol dendrons containing three redox active amidoferrocenyl or silylferrocenyl units; using cyclic voltammetry, these dendronized gold nanoparticles recognize $H_2PO_4^-$

The scope of supramolecular chemistry[1] involves nanoscience including dendrimers[2] and nanoparticles[3] with applications to the field of sensors.[1,4] Beer *et al*. have shown various examples of redox anion recognition by amidoferrocenes bound to endoreceptors,[4] a concept that we have extended to dendrimers[5a] and colloids[5b] as exoreceptors. So far, only a few other reports of molecular recognition by nanoparticles have appeared,[6] althought ferrocenylalkylthiol ligands bonded to surfaces in self-assembled monolayers and colloids have been known for some time.[7] Dendrimer-colloid assemblies have also been successfully designed for the fabrication of a new generation of catalysts and sensors.[3b] We now report the synthesis of dendrons containing silylferrocenyl or amidoferrocenyl termini, their functionalization by thiol ligands, fixation of these dendron-thiol ligands onto gold colloids[8] and recognition of $H_2PO_4^-$ by these thiol-functionalized gold colloids.

Our strategy has consisted of performing ligand exchange reactions between alkylthiol–gold colloids of the Brust type[9] and the thiol dendron, a method that keeps the size of the colloids constant during the ligand exchange reactions, thus retaining their narrow polydispersity.[5b,9] The two syntheses of the triferrocenyl dendron–gold particle assemblies are represented in Scheme 1. Both syntheses represent the first routes to ferrocenyl-containing dendrons, although numerous ferrocenyl- and amidoferrocenyl-containing dendrimers are known.[10–13a] The key to rapid entry into the chemistry of such functionalized dendrons is the direct hydrosilylation of the three allyl groups of the dendron **1**[12] using various silanes[11–13] without any protection of the phenol function (Scheme 1).[14] The two air-sensitive thiol dendrons **8** and **10** were fully characterized by elemental analysis, NMR and the molecular peaks in their MALDI TOF mass spectra. We synthesized gold colloids with 2.1 nm diameter core and approximately 108 ± 5 dodecanethiolate ligands using the method of Brust *et al*.[9] Ligand-exchange reactions between these gold–dodecanethiolate particles and the thiol ligands **8** and **10** were carried out under ambient conditions in CH_2Cl_2 using 2/3 equiv. functional thiol per dodecane thiol

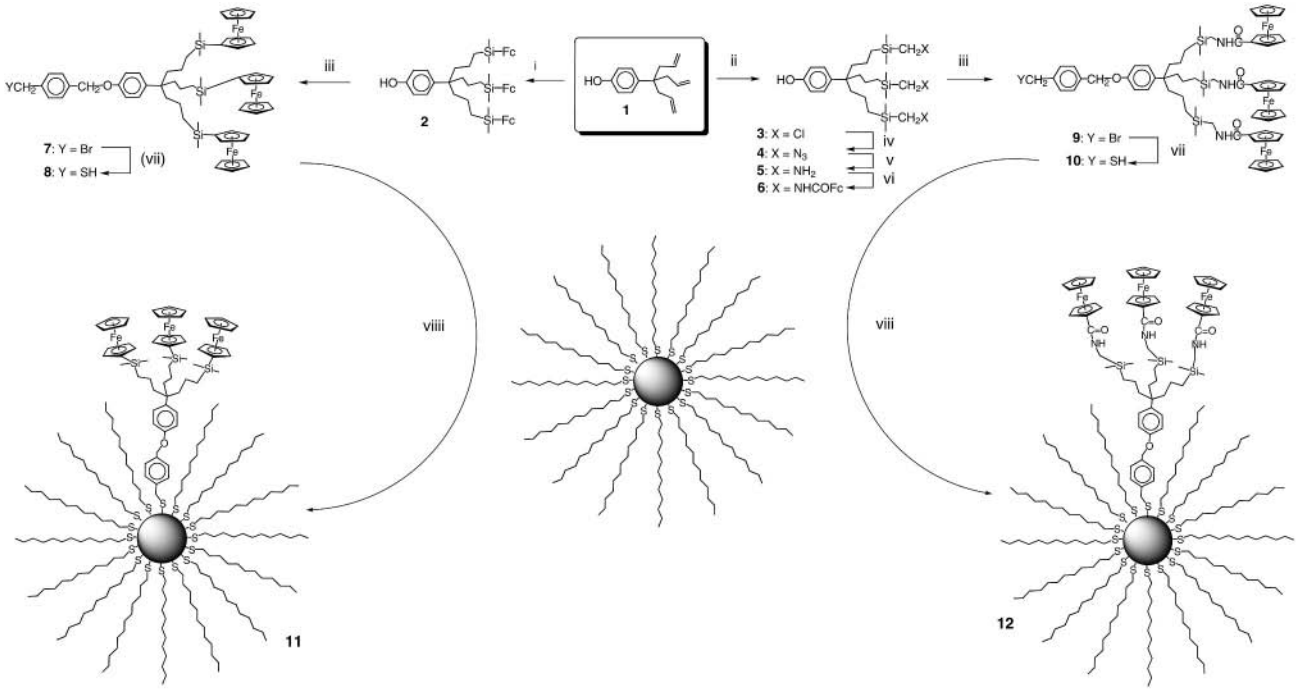

Scheme 1 Syntheses of the dendronized gold colloids. *Reagents and conditions*: i, Karstedt cat., $HSiMe_2Fc$ (Fc = ferrocenyl), Et_2O, reflux, 1 d, 90%; ii, Karstedt cat., $HSiMe_2(CH_2Cl)$, Et_2O, 1 d at room temp., then 1 d at reflux, 85%; iii, 1,1′-dibromo-*p*-xylene, K_2CO_3, MeCN, room temp., 3 d; **7**: 76%; **9**: 70%; iv, NaI, NaN_3, anhydrous DMF, 80 °C, 1 d, 90%; v, PPh_3, H_2O, THF, 80 °C, 1 d, 70%; vi, conc. aq. HCl, then NEt_3, FcCOCl, CH_2Cl_2, 16 h, room temp., 45%; vii, NaSH, THF, 50 °C, 1 d; **8**: 76%, **10**: 90%; viii, thiol dendron (2/3 equiv./equiv. dodecanethiolate ligand), CH_2Cl_2, 3 d, room temp.

 DOI: 10.1039/b106805a

ligand. This led to the dendronized particles **11** and **12**, and the excess of functional ligand was removed by washing **11** and **12** with methanol. The percentage of functional thiolate dendrons introduced as ligands in **11** and **12**, determined by combined HRTEM, ^{1}H NMR spectroscopy and elemental analysis, was 4.8 and 3%, respectively (a little more than five and three dendrons per particle for **11** and **12**, respectively). TEM images confirm that the sizes of the gold cores of the particles remain unchanged after the ligand-substitution reactions.

The cyclovoltammograms of the dendronized colloids **11** and **12** (Pt, CH_2Cl_2, 0.1 M [*n*-Bu_4N][PF_6]) show a chemically (i_a/i_c = 1) and electrochemically ($\Delta E_p \leq 50$ mV) reversible ferrocene/ferrocenium wave.[14] Thus, all the ferrocenyl units appear equivalent in each type of particles, which is due, in particular, to the fact that rotation of the particles is faster than the electrochemical time scale.[15] The separation between the anodic and cathodic peaks is 50 mV for **11**, which almost corresponds to the value expected at 20 °C for a single-electron wave (58 mV). In the case of **12**, however, this peak separation is only 20 mV. This indicates some adsorption, although this phenomenon is not accompanied by an enhanced intensity of the adsorbed species. The $E_{1/2}$ value is 0 V *vs.* $Cp_2Fe^{0/+}$ for **11** and 0.145 V *vs.* $Cp_2Fe^{0/+}$ for **12**.

We then added [*n*-Bu_4N][H_2PO_4] to the electrochemical cell containing **12**, which led to a decrease of the intensity of the amidoferrocene wave of **12** (Fig. 1). The growth of another wave was then observed at a less positive potential until the initial wave had disappeared when the amount of [*n*-Bu_4N][H_2PO_4] added corresponded to 1 equiv. per amidoferrocenyl branch. Thus, the new wave is the signature of a strong amidoferrocenium–$H_2PO_4^-$ interaction. Contrary to the initial wave, it shows the characteristic of slow electron transfer since the ΔE_p value is larger than 60 mV and depends on the scan rate, indicating structural reorganization in the course of the heterogeneous electron transfer.[14] The value of $E_{1/2}$ for each wave does not vary during the titration, the difference remaining equal to 210 ± 10 mV (as for the dendron **8** alone). This corresponds to an apparent association constant K_{app} between the ferrocenium form of **12** and $H_2PO_4^-$ that is 5200 ± 1000 times larger than that between the neutral form of **12** and $H_2PO_4^-$.[16] This shift is very large compared to monomeric amidoferrocenes ($E_{1/2(free)} - E_{1/2(bound)}$ = 45 mV) and even to tripodal tris-amidoferrocenes such as PhC{$(CH_2)_3O(CH_2)_3$NHCOFc}$_3$ ($E_{1/2(free)} - E_{1/2(bound)}$ = 110 mV), and is about as large as with a nona-amidoferrocene dendrimer.[5a] The known factors involved in the recognition of $H_2PO_4^-$ by amidoferrocenyl-containing receptors are the double hydrogen bonding between this anion and the amido groups, the enhanced electrostatic attraction in the oxidized ferrocenium form and the topographical effect of the receptor.[4]

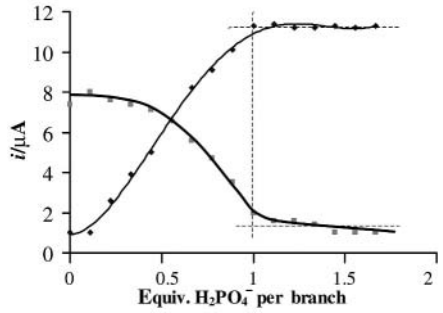

Fig. 1 Titration of **12** (10^{-6} M in CH_2Cl_2) with [*n*-Bu_4N][H_2PO_4] (10^{-2} M in CH_2Cl_2) monitored by CV. Decrease of the intensity of the initial wave at $E_{1/2}$ = 0.145 V *vs.* $FeCp_2^{+/0}$ and increase of the intensity of the new wave at $E_{1/2}$ = –0.065 V *vs.* $FeCp_2^{+/0}$ *vs.* the number of equivalents of [*n*-Bu_4N][H_2PO_4] added per ferrocenyl branch of **12**. [*n*-Bu_4N][PF_6] 0.1 M, 20 °C; internal reference: [Fe(η^5-$C_5Me_5)_2$]; reference electrode: Ag; auxiliary and working electrodes: Pt; scan rate: 0.2 V s^{-1}. A similar response was obtained with **11**.

Interestingly, the silylferrocene-containing colloids **11** also recognize $H_2PO_4^-$. Addition of [*n*-Bu_4N][H_2PO_4] to an electrochemical cell containing **11** provokes the same effect as with **12**, *i.e.* the appearance of a new wave at less positive potential than the original one, while the disappearance of the initial wave is observed for 1 equiv. of anion per silylferrocenyl branch. The difference of potential between the two waves is 110 ± 10 mV, which corresponds to a K_{app} value 85 ± 30 times larger for the ferrocenium form than for the ferrocenyl form. So far, only $H_2PO_4^-$ is recognized, the anions HSO_4^-, Cl^-, Br^- and NO_3^-, for instance, having no significant effect using either **11** or **12**.

It is likely that the supramolecular redox properties of dendronized colloids can be developed for sensoring, catalysis and molecular electronics in the near future.

Notes and references

1 J.-M. Lehn, *Supramolecular Chemistry: Concepts and Perspectives*, VCH, Weinheim, 1995.

2 G. R. Newkome, C. N. Moorefield and F. Vögtle, *Dendritic Molecules: Concepts, Syntheses and Perspectives*, VCH, New York, 1996.

3 (*a*) J. S. Bradley, in *Clusters and Colloïds*, ed. G. Schmid, VCH, Weinheim, 1995, ch. 6 (*b*) R. M. Crooks, M. Zhao, L. Sun, V. Chechik and L. K. Yeung, *Acc. Chem. Res*., 2001, **34**, 181.

4 P. D. Beer, *Adv. Inorg. Chem*., 1992, **39**, 79; P. D. Beer, *Chem. Commun*., 1996, 689; P. D. Beer, *Acc. Chem. Res*., 1998, **31**, 71; P. D. Beer, P. A. Gale and Z. Chen, *Adv. Phys. Org. Chem*., 1998, **31**, 1.

5 (*a*) C. Valério, J.-L. Fillaut, J. Ruiz, J. Guittard, J.-C. Blais and D. Astruc, *J. Am. Chem. Soc*., 1997, **119**, 2588; (*b*) A. Labande and D. Astruc, *Chem. Commun*., 2000, 1007.

6 R. Elghanian, J. J. Storhoff, R. C. Mucic, R. L. Letsinger and C. A. Mirkin, *Science*, 1997, **277**, 1078; S. Sampath and O. Lev, *Adv. Mater*., 1997, **9**, 410; D. Fitzmaurice, S. N. Rao, J. Preece, J. F. Stoddart, S. Wenger and N. Zaccheroni, *Angew. Chem., Int. Ed*., 1999, **38**, 1147; A. Niemz and V. M. Rotello, *Acc. Chem. Res*., 1999, **32**, 44; W. Shenton, D. A. Davis and S. Mann, *Adv. Mater*., 1999, **119**, 11132.

7 K. Weber and S. E. Creager, *Anal. Chem*., 1994, **66**, 3164; K. Weber, L. Hockett and S. E. Creager, *J. Phys. Chem. B*., 1997, **101**, 8286; M. J. Hosteler, S. J. Green, J. J. Stockes and R. W. Murray, *J. Am. Chem. Soc*., 1996, **118**, 4212; T. Horikoshi, M. Itoh, M. Kurihara, K. Kubo and H. Nishihara, *J. Electroanal. Chem*., 1999, **473**, 113; A. C. Templeton, W. P. Wuelfing and R. W. Murray, *Acc. Chem. Res*., 2000, **33**, 27.

8 M.-K. Kim, Y.-M. Jeon, W. S. Jeon, H.-J. Kim, S. G. Hong, C. G. Park and K. Kim, *Chem. Commun*., 2001, 667; R. Wang, J. Yang, Z. Zheng, M. D. Carducci, J. Jiao and S. Searaphin, *Angew. Chem., Int. Ed*., 2001, **40**, 549.

9 M. Brust, M. Walker, D. Bethell, D. J. Schiffrin and R. Whyman, *J. Chem. Soc., Chem. Commun*., 1994, 801; M. Brust, J. Fink, D. Bethell, D. J. Schiffrin and C. Kiely, *J. Chem. Soc., Chem. Commun*., 1995, 1655.

10 A. E. Kaifer and M. Gomez-Kaifer, *Supramolecular Electrochemistry*, Wiley-VCH, Weinheim, 1999, ch. 16, p. 207

11 Review: C. M. Casado, I. Cuadrado, M. Morán, B. Alonso, B. Garcia, B. Gonzales and J. Losada, *Coord. Chem. Rev*., 1999, **185**, 53.

12 (*a*) S. Nlate, J. Ruiz, J.-C. Blais and D. Astruc, *Chem. Eur. J*., 2000, **6**, 2544; (*b*) V. Sartor, L. Djakovitch, J.-L. Fillaut, F. Moulines, F. Neveu, V. Marvaud, J. Guittard, J.-C. Blais and D. Astruc, *J. Am. Chem. Soc*., 1999, **121**, 2929.

13 (*a*) P. Jutzi, C. Batz, B. Neumann and H. G. Stammler, *Angew. Chem., Int. Engl*., 1996, **35**, 2118; (*b*) S. W. Krsda and D. Seyferth, *J. Am. Chem. Soc*., 1998, **120**, 3604.

14 D. Astruc, *Electron-Transfer and Radical Processes in Transition-Metal Chemistry*, VCH, New York, 1995, chapters 2 and 7

15 C. B. Gorman, *Adv. Mater*., 1997, **9**, 1117; C. B. Gorman, *Adv. Mater*., 1998, **10**, 295.

16 S. R. Miller, D. A. Gustowski, Z.-H. Chen, G. W. Gokel, L. Echegoyen and A. E. Kaifer, *Anal. Chem*., 1988, **60**, 2021.

J|A|C|S
ARTICLES
Published on Web 02/04/2003

Nanoscopic Assemblies between Supramolecular Redox Active Metallodendrons and Gold Nanoparticles: Synthesis, Characterization, and Selective Recognition of $H_2PO_4^-$, HSO_4^-, and Adenosine-5′-Triphosphate (ATP^{2-}) Anions

Marie-Christine Daniel,[†] Jaime Ruiz,[†] Sylvain Nlate,[†] Jean-Claude Blais,[‡] and Didier Astruc*[,†]

Contribution from the Groupe Nanoscience et Catalyse, LCOO, UMR CNRS No. 5802, Université Bordeaux I, 33405 Talence Cedex, France and LCSOB, UMR CNRS No. 7613, Université Paris VI, 75252 Paris, France

Received November 1, 2002; E-mail: d.astruc@lcoo.u-bordeaux.fr

Abstract: Tri- and nonaferrocenyl thiol dendrons have been synthesized and used to assemble dendronized gold nanoparticles either by the ligand-substitution method from dodecanethiolate−gold nanoparticles (AB_3 units) or Brust-type direct synthesis from a 1:1 mixture of dodecanethiol and dendronized thiol (AB_9 units). The dendronized colloids are a new type of dendrimers with a gold colloidal core. Two colloids containing a nonasilylferrocenyl dendron have been made; they bear respectively 180 and 360 ferrocenyl units at the periphery. These colloids selectively recognize the anions $H_2PO_4^-$ and adenosine-5′-triphosphate (ATP^{2-}) with a positive dendritic effect and can be used to titrate these anions because of the shift of the CV wave even in the presence of other anions such as Cl^- and HSO_4^-. Recognition is monitored by the appearance of a new wave at a less positive potential in cyclic voltammetry (CV). The anion HSO_4^- is also recognized and titrated by the dendronized colloid containing the tris-amidoferrocenyl units, because of the progressive shift of the CV wave until the equivalence point. These dendronized colloids can form robust modified electrodes by dipping the naked Pt electrode into a CH_2Cl_2 solution containing the colloids. The robustness is all the better as the dendron is larger. These modified electrodes can recognize $H_2PO_4^-$, ATP^{2-} and HSO_4^-, be washed with minimal loss of adsorbed colloid, and be reused.

Introduction

Nanoscopic supramolecular assemblies[1] between dendrimers[2] and colloids[3] should be fruitful to provide a new generation of materials that are likely to give applications as sensors,[1,4,5] catalysts,[1,3,6] and components for molecular electronics.[1,7] So far, only very few examples of assemblies between dendrimers or dendrons[8] and colloids are known.[1,9] We have been interested in such assemblies disclosing supramolecular properties in order to provide means to approach new sensors. The recognition of anions has indeed been the subject of special scrutiny, given their role in biology.[10] In particular, Beer has shown various examples of redox anion recognition by amidoferrocenes bound to endoreceptors.[11] We have addressed the use of redox-active

[†] University Bordeaux I. This article is part of the Ph.D. thesis of M.-C.D.

[‡] University Paris VI (MALDI TOF mass spectroscopy).

(1) (a) Balogh, L.; Tomalia, D. A. *J. Am. Chem. Soc*. **1998**, *120*, 7355. (b) Zhao, M.; Crooks, R. M. *Angew. Chem., Int. Ed*. **1999**, *38*, 364. (c) Niu, Y.; Yeung, L. K.; Crooks, R. M. *J. Am. Chem. Soc* **2001**, *123*, 6840. (d) Crooks, R. M.; Zhao, M.; Sun, L.; Chechik, V.; Yeung, L. K. *Acc. Chem. Res*. **2001**, *34*, 181.

(2) (a) Tomalia, D. A.; Naylor, A. N.; Goddard, W. A., III *Angew. Chem., Int. Ed. Engl*. **1990**, *29*, 138. (b) Ardoin, N.; Astruc, D. *Bull. Soc. Chim. Fr*. **1995**, *132*, 875. (c) Matthews, O. A.; Shipway, A. N.; Stoddart, J. F. *Prog. Polym. Chem*. **1998**, *23*, 1. (d) Smith, D. K.; Diederich, F. *Angew. Chem. Eur. J*. **1998**, *4*, 1353. (e) Balzani, V.; Campagna, S.; Denti, G.; Juris, A.; Serroni, S.; Venturi, M. *Acc. Chem. Res*. **1998**, *31*, 26. (f) Gossage, R. A.; van de Kuil, L. A.; van Koten, G. *Acc. Chem. Res*. **1998**, *31*, 423. (g) Bosman, A. W.; Jansen, E. W.; Meijer, E. W. *Chem. Rev*. **1999**, *99*, 1665. (h) Fisher, M.; Vögtle, F. *Angew. Chem., Int. Ed*. **1999**, *38*, 884. (i) Hecht, S.; Fréchet, J. M. J. *Angew. Chem., Int. Ed*. **2001**, *40*, 74. (j) Balzani, V.; Ceroni, P.; Juris, A.; Venturi, M.; Campagna, S.; Puntoriero, F.; Serroni, S. *Coord. Chem. Rev*. **2001**, 219−221, 545. (k) Newkome, G. R.; Moorefield, C. N.; Vögtle, F. *Dendrimers and Dendrons: Concepts, Syntheses, Applications;* Wiley-VCH: Weinheim, Germany, 2001.

(3) (a) Schmid, G. *Chem. Rev*. **1992**, *92*, 1709. (b) Bradley, J. S. In *Clusters and Colloïds*; Schmid, G., Ed.; VCH: Weinheim, Germany, 1995; Chapter 6. (c) Schmid, G.; Chi, L. F. *Adv. Mater*. **1998**, *18*, 515.

(4) (a) Schierbaum, K. D.; Weiss, T.; Thorden van Zelzen, E. U.; Engberson, J. F. G.; Reinhoudt, D. N.; Göpel, W. *Science* **1994**, *265*, 1413. (b) Chechik, V.; Crooks, R. M. *Langmuir* **1999**, *15*, 6364. (c) Garcia, M. E.; Baker, L. A.; Crooks, R. M. *Anal. Chem*. **1999**, *71*, 256.

(5) Daniel, M.-C.; Ruiz, J.; Nlate, S.; Palumbo, J.; Blais, J.-C.; Astruc, D. *Chem. Commun*. **2001**, 2000.

(6) Astruc, D.; Chardac, F. *Chem. Rev*. **2001**, *101*, 2991.

(7) (a) Lehn, J.-M. *Supramolecular Chemistry: Concepts and Perspectives;* VCH: Weinheim, Germany, 1995. (b) Kumar, A.; Arbott, N. L.; Kim, E.; Biebuyck, A.; Whitesides, G. M. *Acc. Chem. Res*. **1995**, *28*, 219. (c) *Nanosystems, Molecular Machinery, Manufactoring and Computation;* Drexler, K. E., Ed.; Wiley: New York, 1992. (d) Willner, I.; Willner, B. *Adv. Mater*. **1997**, *9*, 351.

(8) For a comprehensive review on dendrons, see: Grayson, S. M.; Fréchet, J. M. J. *Chem. Rev*. **2001**, *101*, 3819.

(9) For previous dendron-colloid assemblies, see: ref 5 and (a) Kim, M. K.; Jeon, Y.-M.; Jeon, W. S.; Kim, H.-J.; Hong, S. G.; Park, C. G.; Kim, K. *Chem. Commun*. **2001**, 667. (b) Wang, R.; Yang, J.; Zheng, Z.; Carducci, M. D. *Angew. Chem., Int. Ed*. **2001**, *40*, 549.

(10) Seel, C.; de Mendoza, J. In *Comprehensive Supramolecular Chemistry*; Atwood, J., Davies, J. E. D., McNichol, D. D., Vögtle, F. Eds.; Elsevier: New York, 1996; Vol. 2, Chapter 17, pp 519−552.

(11) (a) Beer, P. D. *Adv. Inorg. Chem*. **1992**, *39*, 79. (b) Beer, P. D. *J. Chem. Soc., Chem. Commun*. **1996**, 689. (c) Beer, P. D. *Acc. Chem. Res*. **1998**, *31*, 71. (d) Beer, P. D.; Gale, P. A.; Chen, Z. *Adv. Phys. Org. Chem*. **1998**, *31*, 1. (e) Beer, P. D.; Gale, P. A. *Angew. Chem., Int. Ed*. **2001**, *40*, 486.

metallodendrimers[12a,b] and colloids[5,12c,d] as *exo*-receptors for the recognition of anions. Dendrimers show positive dendritic effects, that is, the recognition improves as the generation number increases, because the redox centers become close to one another at the periphery for high generations.[12a,b] On the other hand, colloids are also relatively good sensors that present the advantage over dendrimers that they are rapidly prepared, although the magnitude of the recognition phenomena only reaches that of low-generation dendrimers.[5,12c,d] Thus, the novel assemblies between supramolecular dendrons containing redox-active groups and colloids should disclose new features involving hopefully good recognition properties. We already know that AB_3 units bearing thiol functions and three amido- or silylferrocenyl groups can be introduced to a certain extent onto gold colloids by the classic ligand-substitution procedure that leaves the core intact.[5] These colloids do recognize $H_2PO_4^-$ as well as or slightly better than gold colloids containing thiol ligands bearing a single amidoferrocenyl unit.[12c] We now report the extension of these studies to direct synthetic methods of assemblies between gold colloids and two real dendrons (AB_9 units) containing nine ferrocenyl groups. This allows us to compare assemblies containing colloid-AB_3 units and colloid-AB_9 dendrons for the recognition of $H_2PO_4^-$. We have also now applied these principles to the recognition of the biologically important adenosine-5′-triphosphate anion (ATP^{2-}). Finally, we also present here successful attempts specific to these assemblies to prepare stable derivatized electrodes that also recognize these anions. So far, only very few other examples of molecular recognition by nanoparticles have been reported,[13−17] although ferrocenyl-alkylthiol ligands bonded to surfaces in self-assembled monolayers and particles have been known for some time.[18] Fitzmaurice and Stoddart et al. have shown the recognition of dibenzylammonium cation using crown ethers located at the periphery of nanoparticles.[13] Rotello et al. have investigated supramolecular recognition between flavin and the diacetyl derivative of diamidopyridine.[15] Thiol-modified oligonucleotides have been fixed onto gold nanoclusters. In particular, Mirkin and Letsinger have used such modified nanoparticles for several studies involving DNA analysis,[16] and Mann et al have built three-dimensional networks by antigen−antibody associations.[17] Recently, Nishihara has reported a series of studies on gold nanoparticles bonded to thiolate ligands bearing mixed-valent biferrocenyl (AB_2) units.[19]

Results and Discussions

We have used two synthetic strategies to introduce the AB_3 and AB_9 units onto the colloids. The first one is the exchange of a limited proportion of alkylthiol ligands in Brust-type alkylthiol−gold colloids.[18c,20] This method was already involved to introduce amidoferrocenylalkylthiols in our preliminary work.[12c] It has the advantage of keeping the core size unchanged during the ligand-substitution reaction, but the proportion of substituted ligands can be small with dendrons that are much bulkier than linear thiols. The other one is new, exploratory, and consists of a direct synthesis,[20] derived from Brust's method, for which both dodecanelthiol and dendronized alkylthiols are allowed to competitively react during the direct colloid synthesis. These two synthetic approaches of the supramolecular colloids have been applied to the AB_3 and AB_9 units and compared.

Synthesis of the Dendronized Thiol Ligands. (a) AB_3 Units. The synthesis starts with the phenoltriallyl derivative **1**. This compound is an AB_3 unit that is now easily available in good yield from $[FeCp(\eta^6\text{-}p.MeC_6H_4OEt)][PF_6]$, itself synthesized in large scale from $[FeCp(\eta^6\text{-}p.MeC_6H_4Cl)][PF_6]$, ethanol, and potassium carbonate.[21] A convenient entry into functionalized dendrons derived from **1** is the direct hydrosilylation with various silanes[22,23] of the three allyl groups of **1** without any protection of the phenol function, as exemplified in Scheme 1 for the synthesis of **2** and **3** (top). The following organic reactions also proceed in good yields to provide the phenol compound **6** derived with three amidoferrocenyl groups. The introduction of the thiol group into these dendrons **2** and **6** was achieved by selective reaction with *p*.di(bromomethyl)benzene (in excess) giving **7** and **9** followed by reaction with NaSH which finally yielded **8** and **10**. These new functional thiols are very air sensitive and are quickly oxidized to the corresponding disulfide in air, possibly because the ferrocenyl groups act as redox catalysts for this aerobic oxidation process.

However, the two thiol dendrons **8** and **10** were fully characterized by analytical and spectroscopic techniques including the molecular peaks in their MALDI TOF mass spectra (see the experimental procedures in the Supporting Information).

B. AB_9 Dendrons. From the AB_3 unit **1**, two phenolic nona-allyl AB_9 dendrons were synthesized using convergent strategies (Scheme 2). The allyl branches of **1** were either hydroborated, and then oxidized to alcohol and transformed into iodo termini, or catalytically hydrosilylated by dimethylchloromethylsilane followed by halogen exchange for iodo. These two triodo derivatives were protected at the phenol focal point by reaction with propionyl iodide, which gave the protected triodo derivatives **13** and **14**. These two compounds reacted with **1** to give nona-allyl AB_9 units **15** and **16** after deprotection. These two phenol nona-allyl derivatives were hydrosilylated using ferrocenyldimethylsilane yielding **17** and **18**, then reaction of the phenol group with *p*.dibromoxylene gave the bromomethyl

(12) (a) Valério, C.; Fillaut, J.-L.; Ruiz, J.; Guittard, J.; Blais, J.-C.; Astruc, D. *J. Am. Chem. Soc.* **1997**, *119*, 2588. (b) Valério, C.; Alonso, E.; Ruiz, J.; Blais, J.-C.; Astruc, D. *Angew. Chem., Int. Ed.* **1999**, *38*, 1747. (c) Labande, A.; Astruc, D. *Chem. Commun*. **2000**, 1007. (d) Nlate, S.; Ruiz, J.; Sartor, V.; Navarro, R.; Blais, J.-C.; Astruc, D. *Chem.—Eur. J*. **2000**, *6*, 2544. (e) Labande, A.; Ruiz, J.; Astruc, D. *J. Am. Chem. Soc.* **2002**, *124*, 1782.
(13) Fitzmaurice, D.; Rao, S. N.; Preece, J.; Stoddart, J. F.; Wenger, S.; Zaccheroni, N. *Angew. Chem., Int. Ed.* **1999**, *38*, 1147.
(14) Sampath, S.; Lev, O. *Adv. Mater*. **1997**, *9*, 410.
(15) (a) Boal, A. K.; Rotello, V. M. *J. Am. Chem. Soc*. **1999**, *121*, 4914. (b) Boal, A. K.; Rotello, V. M. *J. Am. Chem. Soc.* **2000**, *122*, 734. (c) Niemz, A.; Rotello, V. M. *Acc. Chem. Res*. **1999**, *32*, 44.
(16) (a) Storhoff, J. J.; Elghanian, R.; Mucic, R. C.; Mirkin, C. A.; Letsinger, R. L. *J. Am. Chem. Soc.* **1998**, *120*, 1959. (b) Mucic, R. C.; Storhoff, J. J.; Mirkin, C. A.; Letsinger, R. L. *J. Am. Chem. Soc*. **1998**, *120*, 12674. (c) Elghanian, R.; Storhoff, J. J.; Mucic, R. C.; Letsinger, R. L.; Mirkin, C. A. *Science*, **1997**, *277*, 1078.
(17) Shenton, W.; Davis, D. A.; Mann, S. *Adv. Mater*. **1999**, *119*, 11132.
(18) (a) Weber, K.; Creager, S. E. *Anal. Chem.* **1994**, *66*, 3164. (b) Weber, K.; Hockett, L.; Creager, S. E. *J. Phys. Chem. B.* **1997**, *101*, 8286. (c) Hosteler, M. J.; Green, S. J.; Stockes, J. J.; Murray, R. W. *J. Am. Chem. Soc*. **1996**, *118*, 4212.
(19) (a) Horikoshi, T.; Itoh, M.; Kurihara, M.; Kubo, K.; Nishihara, H. *J. Electroanal. Chem*. **1999**, *473*, 113. (b) Yamada, M.; Tadera, T.; Kubo, K.; Nishihara, H. *Langmuir*, **2001**, *17*, 2263.
(20) (a) Brust, M.; Walker, M.; Bethell, D.; Schiffrin, D. J.; Whyman, R. *J. Chem. Soc., Chem. Commun.* **1994**, 801. (b) Brust, M.; Fink, J.; Bethell, D.; Schiffrin, D. J.; Kiely, C. *J. Chem. Soc., Chem. Commun.* **1995**, 1655.
(21) Sartor, V.; Djakovitch, L.; Fillaut, J.-L.; Moulines, F.; Neveu, F.; Marvaud, V.; Guittard, J.; Blais, J.-C.; Astruc, D. *J. Am. Chem. Soc*. **1999**, *121*, 2929. Sartor, V.; Nlate, S.; Djakovitch, L.; Fillaut, J.-L.; Moulines, F.; Neveu, F.; Marvaud, V.; Guittard, J.; Blais, J.-C.; Astruc, D. *New J. Chem*. **2000**, *24*, 351. Nlate, S.; Blais, J.-C.; Astruc, D. *New J. Chem*. **2003**, *27*, 178.
(22) Jutzi, P.; Batz, C.; Neumann, B.; Stammler, H. G. *Angew. Chem., Int. Ed. Engl.* **1996**, *35*, 2118.
(23) Krsda, S. W.; Seyferth, D. *J. Am. Chem. Soc.* **1998**, *120*, 3604.

Scheme 1. Synthesis of the AB_3 Thiol Ligands **8** and **10** Containing Ferrocenyl Groups

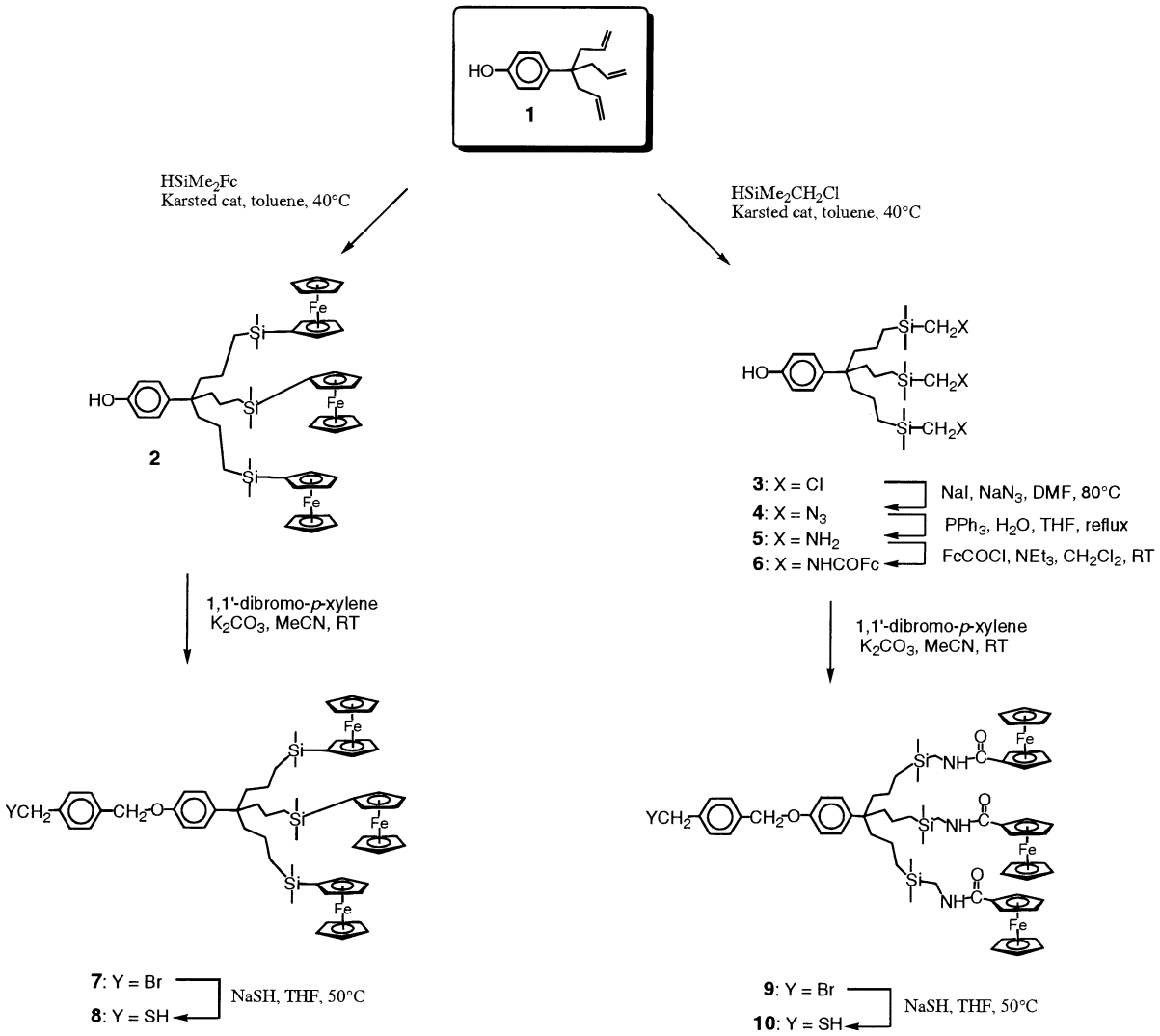

derivatives **19** and **20**, and finally substitution of Br^- by SH^- yielded the desired thiol dendrons **21** and **23**.

The AB_9 thiols **21** and **23** were fully characterized including by the prominent molecular peak in their MALDI TOF mass spectra. The thiol dendrons are air sensitive and show a strong tendency to oxidize to disulfide (see Scheme 3 where **21** is oxidized to **22**). Thus, reduction of the eventually partly oxidized thiols was systematically carried out just before dendron-colloid assembly in order to optimize the colloid yields whatever the type of colloid synthesis.

Colloid-Dendron Assemblies. Brust's method reproducibly leads to the synthesis of gold−dodecanethiolate particles of various sizes with narrow polydispersities,[20] and we chose to synthesize such colloids with a 2.3-nm diameter core and approximately 150 thiol ligands, which was checked by combined HRTEM and elemental analysis. Ligand-exchange reactions between these gold−dodecanethiolate particles and the thiol ligands **8** and **10** were carried out under ambient conditions in dichloromethane (Scheme 4). The functional thiol dendrons were used in excess (1 equiv of functional thiol *per* dodecanethiol ligand) leading to the dendron-functionalized particles **11** and **12**, and the excess of functional ligand was removed by washing **11** and **12** with methanol. The percentages of functional thiol dendrons introduced as ligands in **11** and **12**, determined by combined HRTEM (see the TEM pictures and histograms in the Supporting Information, Figures SI 1 to SI 4), ^{1}H NMR, and elemental analysis, were 4.8% and 3%, respectively. This corresponds, in average, to a little less than seven dendrons for **11** and five dendrons for **12**. The TEM pictures confirm that the sizes of the gold cores of the particles remain unchanged after the ligand-substitution reactions.

The limit of the ligand-substitution reaction was noted with larger dendrons. For instance, attempts to synthesize dendron-colloid assemblies using the nona-allyl dendron $HSCH_2p.C_6H_4$-$CH_2p.OC_6H_4C[C(CH_2)_3OC_6H_4C(CH_2CHCH_2)_3]_3$ resulted in the incorporation of very little dendron, that is, less than one per colloid particle. Under these conditions, reactions with even larger nonametallic dendrons containing nine ferrocenyl groups for recognition purpose appeared hopeless. Therefore, we embarked into a different strategy that consisted in carrying out direct Brust-type nanoparticle syntheses using mixtures of linear dodecanethiols and dendronized thiols containing nine ferrocenyl groups. The direct synthesis was first successfully attempted using the trisilylferrocenyl thiol which gave **11a**, whose characteristics turned out to be similar to those of the colloid **11** obtained by the previous ligand-substitution procedure. It was expected that linear dodecanethiol molecules would become thiolate ligands of gold particles more easily than the den-

Scheme 2. Synthesis of the Two Nonasilylferrocenyl Thiol Dendrons (AB_9 Units) **21** and **23** Starting from the Triallylphenol Molecular Brick **1**

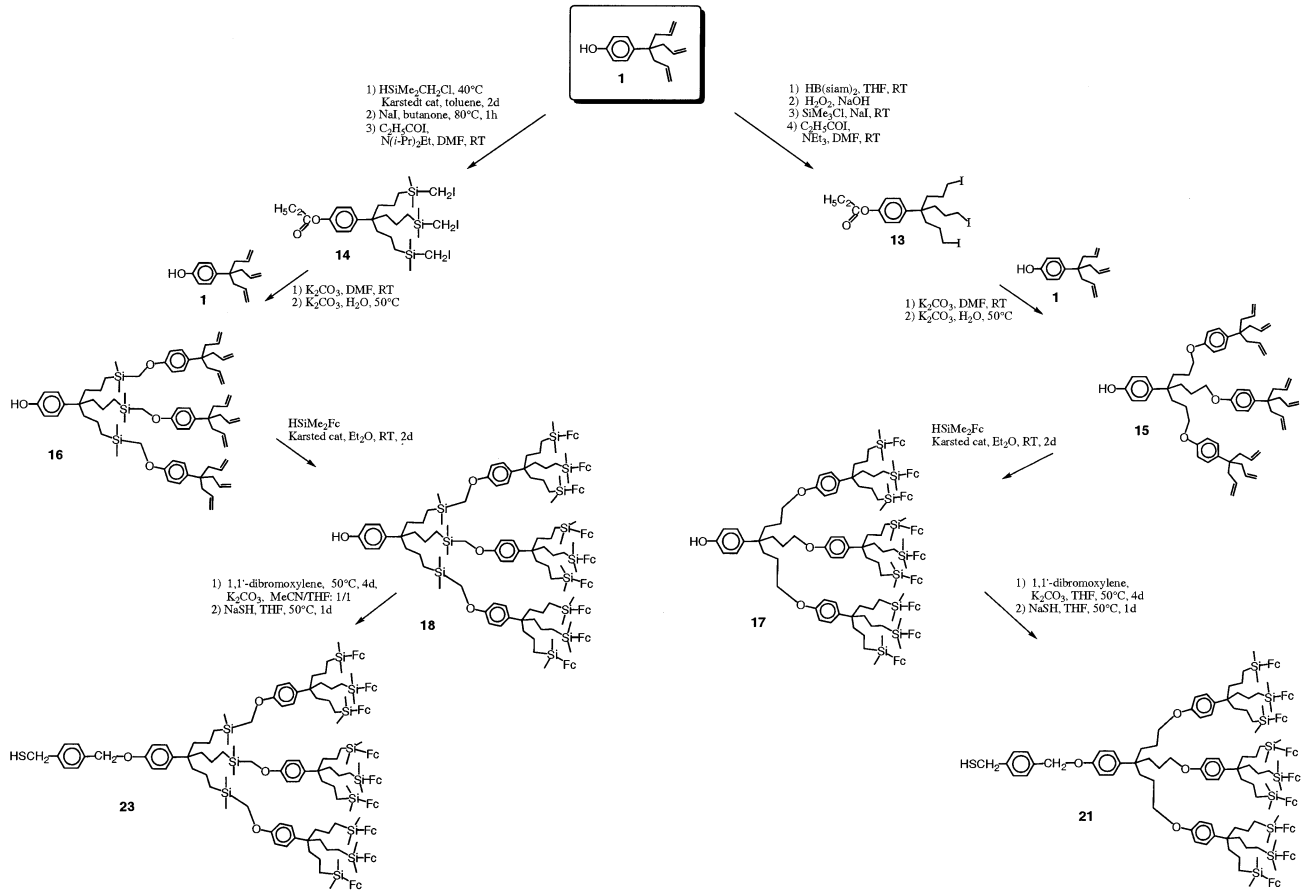

Scheme 3. Reversible Dimerization of the Nonaferrocenyl Thiol Dendrons upon Exposure to Air

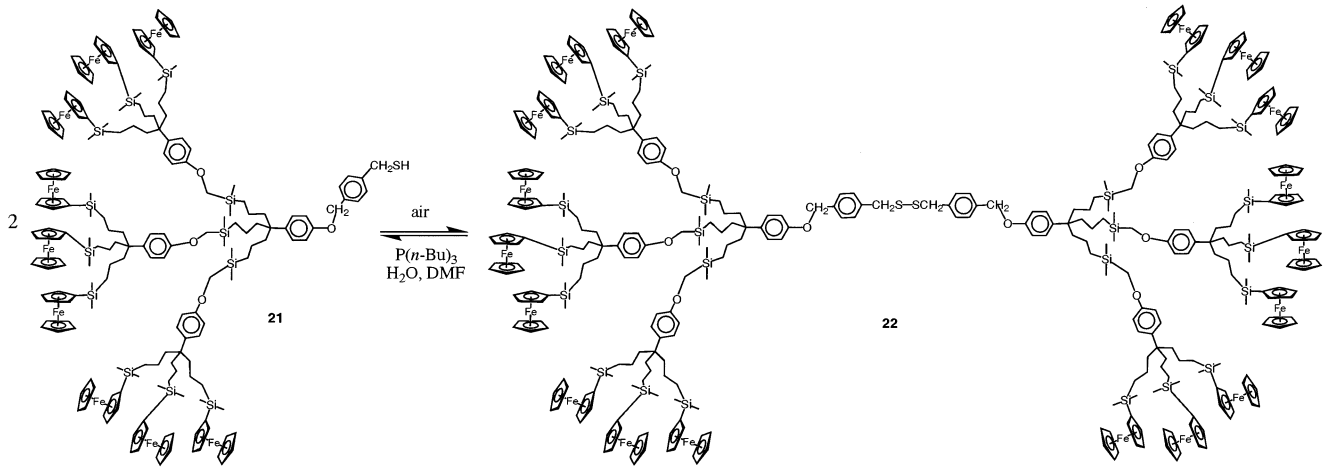

dronized thiols, especially with the bulky nonaferrocenylthiol dendrons. Indeed, their proportion found in the nanoparticles obtained was higher than that in the reaction mixture that systematically contained an equimolar ratio of both dodecanethiol and dendronized thiol. Nevertheless, this technique is very successful and allows efficient synthesis of colloids **24** and **25** with good amounts of nonaferrocenyl dendronized thiols (Schemes 5 and 6). Adjusting the proportion of ligands and gold source can control the size of the particles, although the particles made in this way are larger (2.9 nm diameter) than those synthesized by the substitution method. We first attempted it using the trisilyl dendron that could be introduced in a proportion of 25%. Then, the two nonaferrocenylthiol dendrons could form dendronized nanoparticles containing, respectively, 10 and 20% of dendrons among the thiol ligands. This means that, for a colloid of a 2.9-nm diameter bearing around 200 thiolate ligands, there are about 20 and 40, respectively, dendronized thiolates bearing around 180 and 360, respectively, ferrocenyl units linked to the colloidal core, which makes a rather bulky periphery. The cavities near the core, located between the particle surface and the ferrocenyl layer at the periphery, are filled with about 180 and 160, respectively, linear dodecanethiolate ligands, as schematically represented on Schemes 5 and 6. The proportions of dendronized and linear ligands in **24** and **25** were determined

Scheme 4. Synthesis of the Dendronized Gold Colloids **11** and **12** Using the Thiol-Ligand Substitution Procedure

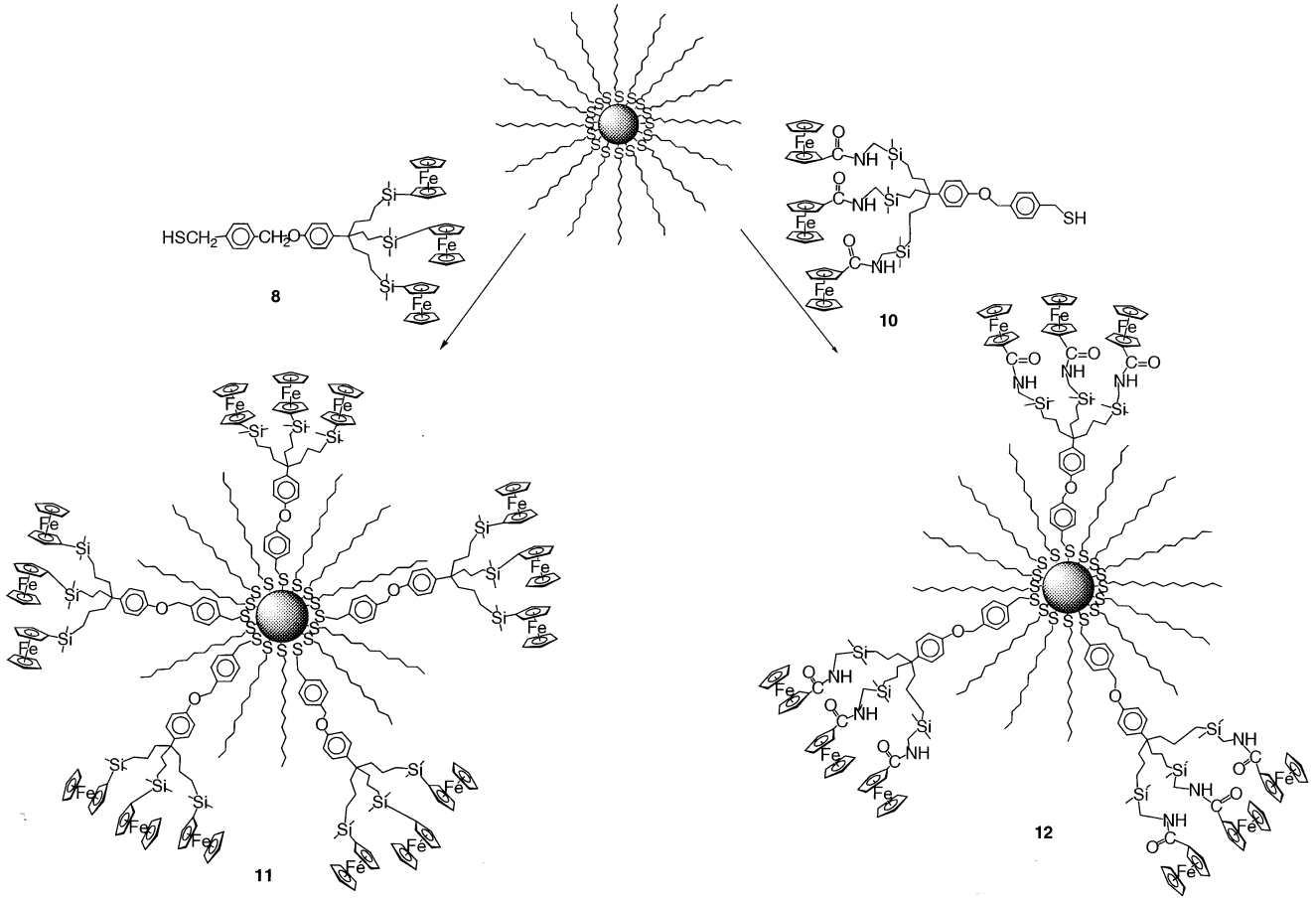

Scheme 5. Direct Synthesis of the Dendronized Gold Colloid **24** Containing the Nonaferrocenyl Thiol Dendron **21** (About 180 Ferrocenyl Groups)

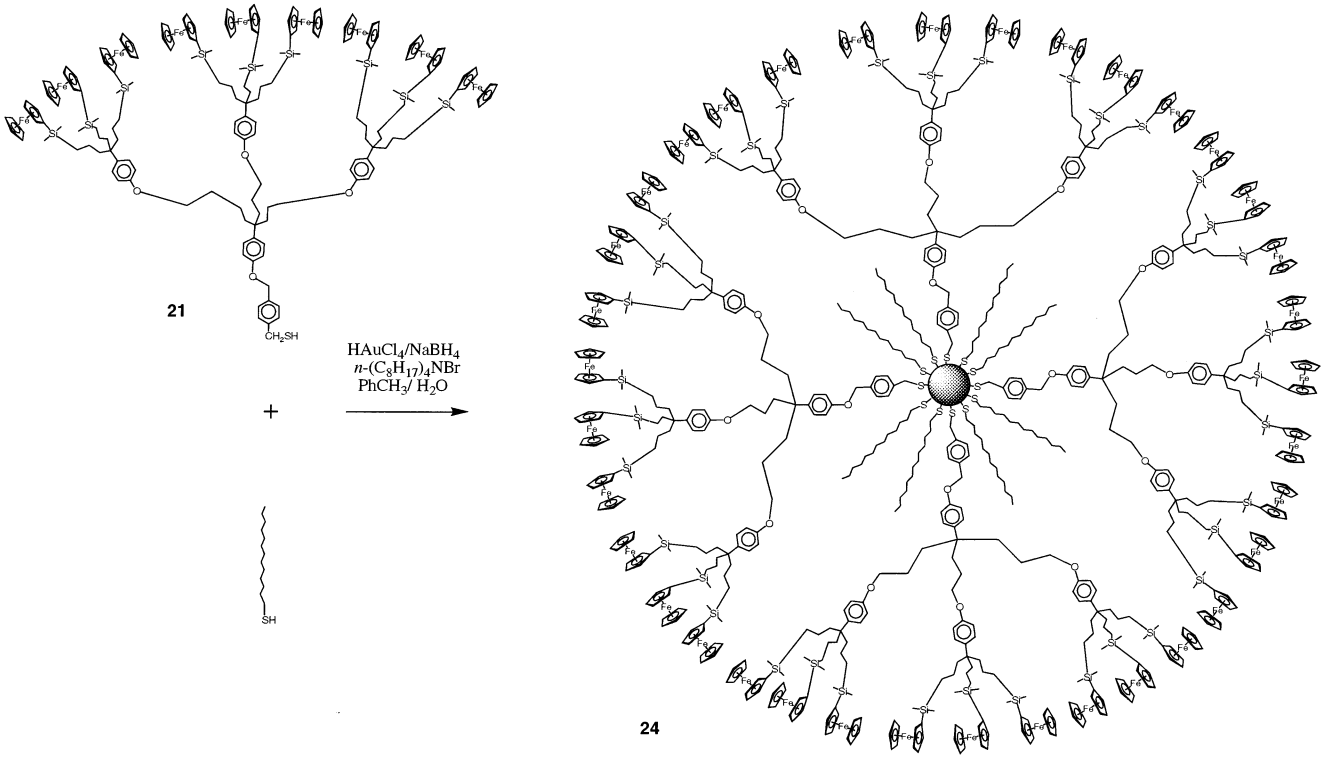

by integration of the respective ^{1}H NMR signals of these ligands and by electrochemical titration (vide infra).

Cyclic Voltammetry Studies of the Metallodendron-Colloid Assemblies. The cyclovoltammograms (CV) of the

Scheme 6. Direct Synthesis of Dendronized Gold Colloid **25** Containing the Nonaferrocenyl Thiol Dendron **23** (About 360 Ferrocenyl Groups)

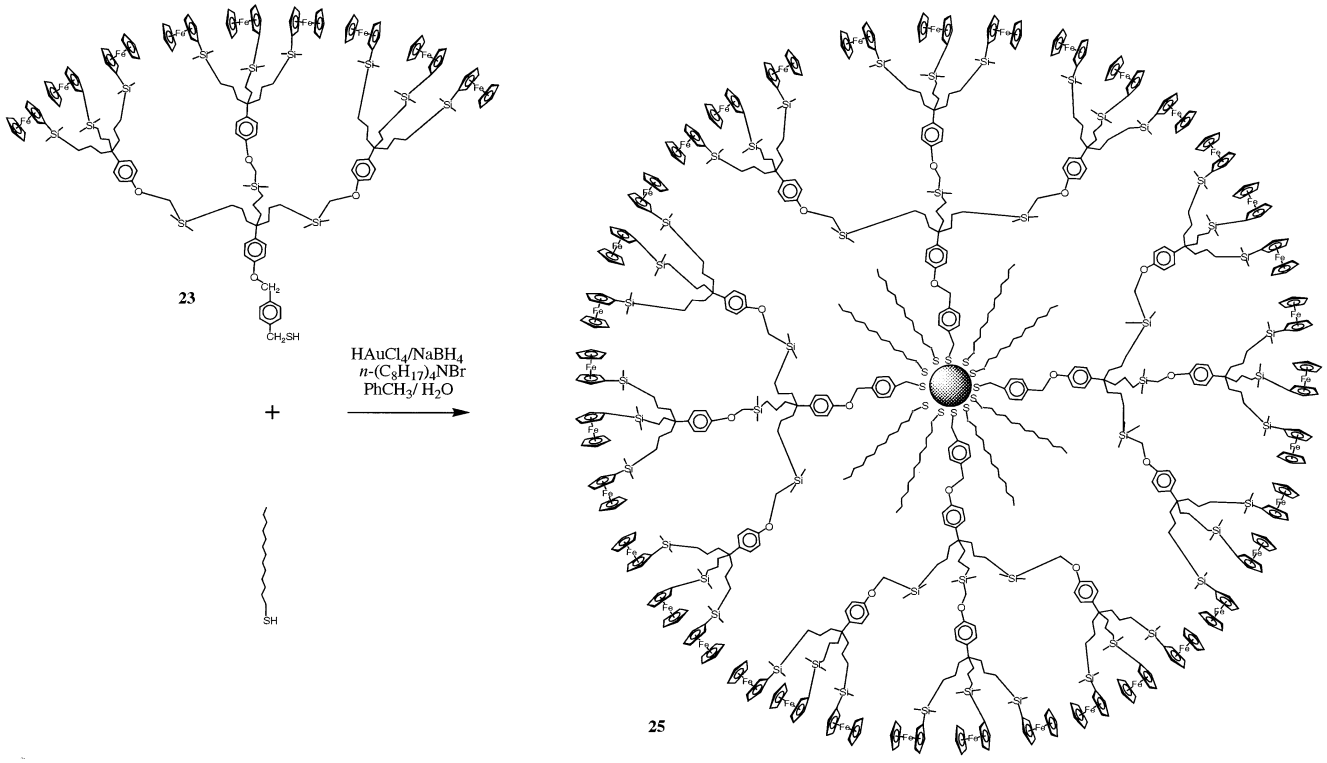

dendronized gold nanoparticles **11**, **12**, **24**, and **25** (Pt, CH_2Cl_2, 0.1 M $[NBu_4][PF_6]$) show a chemically ($i_a/i_c = 1$) and electrochemically ($\Delta E_p \leq 50$ mV) reversible ferrocene/ferrocenium wave.[24−26] Although these waves look like single-electron waves, the total number of electrons exchanged per particles corresponds to the total number of ferrocenyl units per particle, that is, for instance about 30 for **11** and 18 for **12**. These numbers cannot be determined using the Bard−Anson formula,[24b] which is working well with polymers including dendrimers, however, contrary to what could be achieved with metallodendrimers,[12] because the gold core is too large and heavy. All the ferrocenyl units look equivalent, in each type of particle, which is due, in particular, to the fact that rotation of the particles is faster than the electrochemical time scale.[27] The separation between the anodic and cathodic peaks is 50 mV for **11** and **12**, which almost corresponds to the 58-mV value expected at 20 °C for a single-electron wave. Values lower than 58 mV indicate that some adsorption[27b,c] occurs, although this phenomenon is weak and not accompanied by an enhanced intensity of the adsorbed dendronized colloids alone (see Table 1).

The $E_{1/2}$ value is 0 V versus $Cp_2Fe^{0/+}$ for **11** and 0.145 V versus $Cp_2Fe^{0/+}$ for **12**.[25b] The dendronized colloids **24** and **25** containing the nonaferrocenyl dendrons adsorb more strongly than the colloids **11** and **12** that contain AB_3 units when the CV are recorded using CH_2Cl_2 solutions. This latter parameter can eventually influence the choices of conditions for the recognition experiments in solution or at modified electrodes (vide infra).

Recognition of $H_2PO_4^-$, HSO_4^-, and ATP^{2-}. (a) $H_2PO_4^-$. We have examined the interaction between $H_2PO_4^-$ and the new dendronized colloids by adding $[n\text{-}Bu_4N][H_2PO_4]$ to the electrochemical cell containing one of the dendronized colloids. This led to the decrease of the intensity of the ferrocenyl wave and to the concomitant appearance and growth of another wave at a less positive potential until the initial wave disappeared when the amount of $[n\text{-}Bu_4N][H_2PO_4]$ added corresponded to 1 equiv *per* amidoferrocenyl branch. Thus, the new wave corresponds to the interaction between $H_2PO_4^-$ and the branch containing the ferrocenyl group, and this appearance of a new wave is the signature of a strong interaction. This new wave, contrary to the initial one, shows the characteristic of a slow electron transfer, since the ΔE_p value is more or less larger than 60 mV and depends on the scan rate, meaning that some structural reorganization intervenes in the course of the heterogeneous electron transfer.[24,25] The value of $E_{1/2}$ for each wave does not vary during the titration. For instance, with the dendronized colloid **12** containing AB_3 units that bear three amidoferrocenyl groups, the difference remains equal to 210 ± 10 mV. Yet, in this particular case, the recognition is marred by the partial chemical irreversibility of the system in solution, contrary to

(24) (a) Bard, A. J.; Faulkner, L. R. *Electrochemical Methods*; Wiley: New York, 1980. (b) Flanagan, J. B; Margel, S.; Bard, A. J.; Anson, F. C. *J. Am. Chem. Soc.* **1978**, *100*, 4248.

(25) (a) Astruc, D. *Electron-Transfer and Radical Processes in Transition-Metal Chemistry;* VCH: New York, 1995; Chapters 2 and 7. (b) the internal reference was decamethylferrocene, $[FeCp^*_2]$, a much better reference than ferrocene (the $E°$ values are then converted vs $[FeCp_2]$, however). See: Ruiz, J.; Astruc, D. *C. R. Acad. Sci., Ser. IIc: Chim.* **1998**, 21. Astruc, D. In *Electron Transfer in Chemistry*; Balzani, V., Mattay, J., Astruc, D., Eds.; Vol. 2. Organic, Inorganic and Organometallic Molecules; Wiley-VCH: New York, 2001; section 2, Chapter 4, p 728.

(26) Kaifer, A E.; Gomez-Kaifer, M. *Supramolecular Electrochemistry*; Wiley-VCH: Weinheim, Germany, 1999; Chapter 16, p 207.

(27) (a) Gorman, C. B.; Smith, J. C.; Hager, M. W.; Parkhurst, B. L.; Sierzputowsska-Gracz, H.; Haney, C. A. *J. Am. Chem. Soc.* **1999**, *121*, 9958. (b) For the adsorption of organothiol dendrons on a gold surface, see: Gorman, C. B.; Miller, R. L.; Chen, K. Y.; Bishop, A. R.; Haasch, R. T.; Nuzzo, R. G. *Langmuir*, **1998**, *14*, 3312. (c) For a review on dendritic thin films and monolayers, see: Schenning, A. P. H. J.; Weener, J. W.; Meijers, E. W. In *Conjugated Polymers and Molecular Interfaces*; Salaneck, W. R. R., Seki, K., Kahn, A., Pireaux, J.-J., Eds.; Marcel Dekker: New York, 2001, p 1.

Table 1. Electrochemical Characteristics of the Dendronized Gold Colloids **11**, **12**, **24**, and **25** before and after Titration of the $H_2PO_4^-$ and ATP^{2-} Anions and of the Stable Modified Electrodes Obtained with Colloids **12**, **24**, and **25**

	$E_{1/2}$[a] ($E_{pa} - E_{pc}$)	i_{pc}/i_{pa}[b]	$E_{1/2initial} - E_{1/2new}$[c] with $H_2PO_4^-$	$K_{(+)}/K_{(0)}$[d]	$E_{1/2initial} - E_{1/2new}$[c] with ATP^{2-}	$K_{(+)}/K_{(0)}$[e]
colloid-3-amido-Fc **12**	0.680 (0.050)	1.0	0.200 (0.130)	2800 ± 600	0.170 (0.170)	850 ± 200
colloid-3-silyl-Fc **11**	0.545 (0.050)	1.0	0.115 (0.070)	96 ± 20	0.080 (0.070)	24 ± 5
colloid-3-silyl-Fc **24**	0.545 (0.025)	1.2	0.135 (0.060)	210 ± 40	0.100 (0.070)	53 ± 10
colloid-9-silyl-silyl-Fc **25**	0.545 (0.025)	1.2	0.125 (0.050)	140 ± 30	0.090 (0.050)	36 ± 7
modified Pt electrode with the colloid-3-amido-Fc **12**	0.680 (0.0) $\Delta E_{FWHM} = 0.100$[f]	1.0	0.160 (0.070) $\Delta E_{FWHM} = 0.150$	600 ± 100	0.175 (0.110) $\Delta E_{FWHM} = 0.150$	1040 ± 200
modified Pt electrode with the colloid-9-silyl-Fc **24**	0.530 (0.0) $\Delta E_{FWHM} = 0.060$	1.0	0.120 (0.070) $\Delta E_{FWHM} = 0.100$	120 ± 30	0.090 (0.050) $\Delta E_{FWHM} = 0.100$	36 ± 7
modified Pt electrode with the colloid-9-silyl-silyl-Fc **25**	0.540 (0.0) $\Delta E_{FWHM} = 0.060$	1.0	0.130 (0.040) $\Delta E_{FWHM} = 0.100$	170 ± 40	0.090 (0.060) $\Delta E_{FWHM} = 0.100$	36 ± 7

[a] $E_{1/2}$ vs $FeCp^*_2$; electrolyte, [*n*-Bu_4N][PF_6]; working electrode, Pt. [b] Intensity ratio i_{pc}/i_{pa}, whose unity value shows the chemical reversibility and lack of adsorption. [c] Difference of $E_{1/2}$ value between the initial wave and the new wave at half titration in order to observe and compare both waves (see Figures 1−3). [d] Ratio between the apparent association constants $K_{(+)}/K_{(0)}$ of the cationic and neutral forms with the $H_2PO_4^-$ anion. [e] Ibid with the ATP^{2-} anion. [f] Full width of potential at half-maximum.

the other dendronized colloids that bear silylferrocenyl groups. This corresponds to an apparent association constant *K* between the ferrocenium form of **12** and $H_2PO_4^-$ that is 4200 times larger than the same constant between the neutral form of **11** and $H_2PO_4^-$.[28] This ratio is very large compared to that with monomeric amidoferrocenes ($E_{1/2free} - E_{1/2bound} = 45$ mV) and even that with tripodal tris-amidoferrocenes ($E_{1/2\ free} - E_{1/2bound} = 110$ mV) and is about as large as that with a nona-amidoferrocene dendrimer.[12a] The recognition of $H_2PO_4^-$ is very selective. We have tested other anions (HSO_4^-, Cl^-, Br^-, NO_3^-) which did not provoke the appearance of a new wave or a significant shift of the ferrocenyl wave. In particular, it is noteworthy that the other oxo-anion HSO_4^- did not interact significantly, whereas it is recognized by amidoferrocene dendrimers and colloid **12**.[12a]

With the dendronized colloids **11** containing AB_3 units bearing three silylferrocenyl groups, the difference between the potentials $E_{1/2}$ of the initial and new waves is smaller (110 mV) than that with **12**. The chemical reversibility obtained under ambient condition, however, was encouraging to investigate further such silylferrocenyl systems with AB_9 dendrons and especially with electrodes modified with dendronized colloids bearing such large dendrons (vide infra). Gratifyingly, this difference of potentials appears to be somewhat larger with the two dendronized colloids bearing these AB_9 silylferrocenyl units, meaning that the recognition is subjected to a positive dendritic effect. The characteristics of the electrochemical recognition features by all the dendronized colloids are gathered in Table 1. The potential differences between the two waves show the magnitude of the recognition. The differences ΔE_p between the anodic and cathodic peaks of each wave indicate whether the heterogeneous electron transfer is fast ($\Delta E_p = 60$ mV) or slowed by the structural reorganization ($\Delta E_p > 60$ mV), especially during the increase of interaction with the anion upon oxidation of the ferrocenyl unit to ferrocenium. The intensity i_c/i_a ratio shows cases for which one is dealing with chemical irreversibility ($i_c/i_a < 1$) or adsorption ($i_c/i_a > 1$). The comparison between the colloid dendronized with the AB_3 units and those dendronized with the AB_9 units shows the advantage of the AB_9 dendronized colloid with silylferrocenyl groups disclosing a larger potential shift due to the positive dendritic effect (Figure SI 5). These two dendrons show identical characteristics for the recognition of these anions. Given these satisfactory redox recognition features, titration of [*n*-Bu_4N][H_2PO_4] can be carried out. The equivalence points of these titrations can be determined either from the decrease of intensity of the initial ferrocenyl wave or increase of intensity of the new ferrocenyl−$H_2PO_4^-$ wave at less positive potential. Both variations yield close results, and the data obtained also corresponded with 5−10% errors to the amount of redox active species. Indeed, this amount was also determined by integration of the ^1H NMR signals, in the dendrons coordinated to the colloidal core (assuming a one-to-one interaction of the ferrocenyl group with $H_2PO_4^-$ and two-to-one for ATP^{2-}). All the dendronized colloids gave satisfactory titration graphs (see all the titration graphs in the Supporting Information, Figures SI 7 to SI 15), since the separation between the initial and new wave is relatively large and the intensities are not much marred by adsorption in the beginning or during the titration.

(b) Adenosine-5′-triphosphate, ATP^{2-}. The addition of [*n*-Bu_4N]$_2$[ATP] to the electrochemical cell containing the dendronized colloid provokes the apparition of a new wave, just as with the [*n*-Bu_4N][H_2PO_4] salt. The potential difference between the initial and new wave is of the same order of magnitude with those of [*n*-Bu_4N]$_2$[ATP] and [*n*-Bu_4N][H_2PO_4] (slightly smaller for [Bu_4N]$_2$[ATP] than for [*n*-Bu_4N][H_2PO_4]) with all the dendronized colloids studied here. Table 1 also gathers the data of this recognition of [*n*-Bu_4N] $_2$[ATP] in the same fashion as for [*n*-Bu_4N][H_2PO_4]. Figure 1 shows the CVs in the course of the titrations; that is, both the initial and new waves are visible at this stage.

Thus, these waves can be compared for the tris-amidoferrocenyl-dendronized colloid **12** (Figure SI 6) and a nonaferrocenyl-dendronized colloid (good wave separation and chemical

(28) Reynes, O.; Moutet, J.-C.; Pecaut, J.; Royal, G.; Saint-Aman E. *Chem.—Eur*. J. **2000**, *6*, 2544.

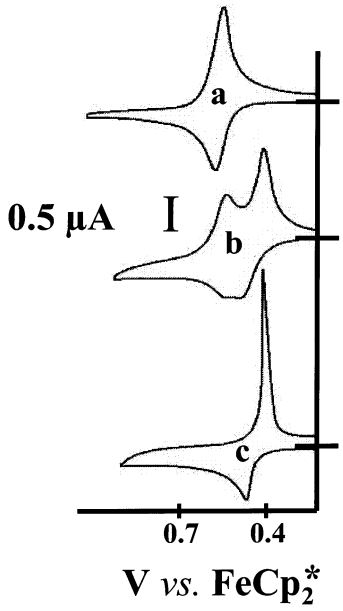

Figure 1. Titration of ATP^{2-} with **24** (colloid 9-silyl-Fc) in CH_2Cl_2. Cyclic voltammograms: electrolyte support, 0.1 M [*n*-Bu_4N][PF_6]; reference electrode, Ag; auxiliary and working electrodes, Pt; scan rate, 0.2 V/s; solution of [*n*-Bu_4N]$_2$[ATP], 5×10^{-3} M; internal reference, $FeCp_2$*. (a) nanoparticle alone; (b) in the course of the titration (note the two close waves on the cathodic side); (c) with an excess of [*n*-Bu_4N]$_2$[ATP].

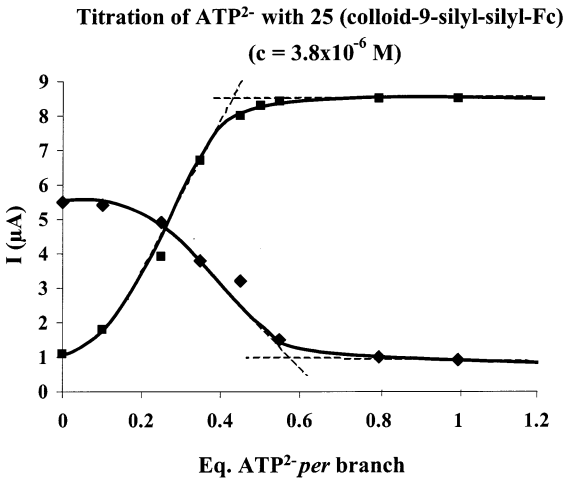

Figure 2. Titration of ATP^{2-} with **25** (colloid-9-silyl-silyl-Fc). Decrease of the intensity of the initial CV wave (◆) and increase of the intensity of the new CV wave (■) vs the number of equiv of [*n*-Bu_4N]$_2$[ATP] added per ferrocenyl branch. Nanoparticles: 3.8×10^{-6} M in CH_2Cl_2. See the caption to Figure 1 for the conditions.

reversibility, Figure 1). A key difference between $H_2PO_4^-$ and ATP^{2-} resides in the stoichiometry obtained in the titration of ATP^{2-} that is half that of [*n*-Bu_4N][H_2PO_4] because of the double anionic charge of ATP^{2-}. This finding is not trivial, however, since recent ATP^{2-} titration with monoferrocenyl derivatives led to very different ATP^{2-} stoichiometries.[28] An example of CV obtained during ATP^{2-} titration with the colloid **24** dendronized with the AB_9 unit **21** is shown in Figure 1, whereas the corresponding titration graph is shown in Figure 2 for colloid **25**.

The selective recognition and titration of ATP^{2-} can also be carried out in the presence of [*n*-Bu_4N][Cl] and [*n*-Bu_4N][HSO_4] using colloid **24**. The addition of these latter salts to **24** does not provoke the appearance of a new CV wave or a shift of the

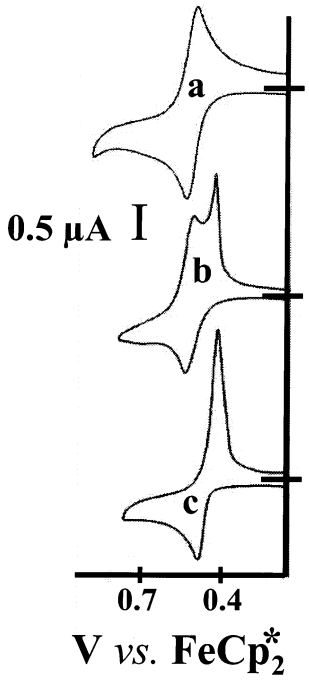

Figure 3. Titration of ATP^{2-} with **24** (colloid-9-silyl-Fc) in the presence of [*n*-Bu_4N][Cl] and [*n*-Bu_4N][HSO_4] (both anions, 5×10^{-2} M, 0.5 equiv *per* ferrocenyl branch): cyclic voltammograms (see Figure 1 for the experimental conditions). (a) nanoparticle **24** alone; (b) in the course of the titration; (c) with an excess of [*n*-Bu_4N]$_2$[ATP].

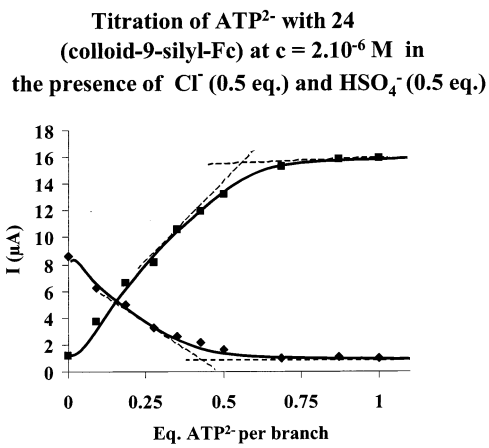

Figure 4. Titration of ATP^{2-} with **24** (colloid-9-silyl-Fc) in the presence of [*n*-Bu_4N][Cl] and [*n*-Bu_4N][HSO_4] (both anions, 0.5 equiv *per* ferrocenyl branch). Decrease of the intensity of the initial CV wave (◆) and increase of the intensity of the new CV wave (■) vs the number of equiv of [*n*-Bu_4N]$_2$[ATP] added per ferrocenyl branch. Nanoparticles: 2×10^{-6} M in CH_2Cl_2. See also Figure 1 for the conditions.

initial CV wave. A new wave appears, upon addition of [*n*-Bu_4N]$_2$[ATP], only on the cathodic side at a potential 100 mV less positive than that of the initial wave. On the anodic side, the initial wave is progressively shifted until the equivalent point is reached, the total shift along the titration being 50 mV. These features are original. Figure 3 shows the CV before, during, and after titration, and Figure 4 shows the titration graph using the changes of intensities of the initial and new wave.

(c) HSO_4^-. The interaction of the silylferrocenyl-containing colloids **11**, **24**, and **25** with HSO_4^- is negligible, but recognition and titration can be carried out using the colloid **12** that bears the tris-amidoferrocenyl units. The latter provides a stronger interaction than those of the other colloids with HSO_4^-. The

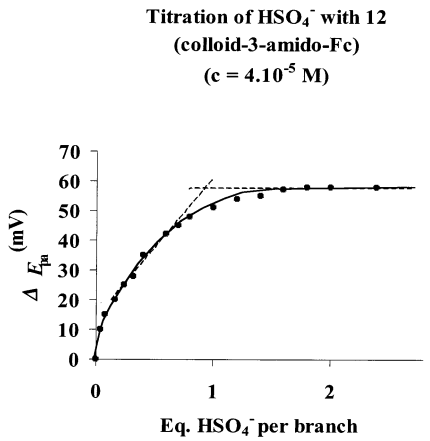

Figure 5. Titration of HSO_4^- with **12** (colloid-3-amido-Fc): shift of E_{pa} toward positive potentials recorded by CV as a function of the number of equiv [*n*-Bu_4N][HSO_4] added *per* amidoferrocenyl branch of the colloid. Nanoparticles: 4×10^{-5} M in CH_2Cl_2. See also Figure 1 for experimental conditions.

addition of [*n*-Bu_4N][HSO_4] to the electrochemical cell containing **12** does not provoke the apparition of a new CV wave, however, and only a shift of the CV wave is observed. The maximum shift of 60 mV for the anodic wave potential and 25 mV for the cathodic one are reached around the equivalent point, which allows titrating [*n*-Bu_4N][HSO_4], as shown in Figure 5. The absolute apparent association constant K^+ between **12** and the anion HSO_4^- is then defined by $\log K^+c = \Delta E_{1/2}/0.058$[33] at 20 °C, giving $K^+ = (18 \pm 4) \times 10^3$ L mol^{-1}. The weaker interaction of the amidoferrocenyl group with HSO_4^- than that with $H_2PO_4^-$ has already been discussed.[12e] It is due to the fact that the negative charge density on the oxygen atoms is weaker in HSO_4^- than in $H_2PO_4^-$. The H bonding between these O atoms and the positively polarized nitrogen atom of the amido group dominates the overall H-bonding interaction. The silicon atom plays this role of the positively polarized nitrogen atom in the silylferrocenyl-branched dendrons because of the stabilization of a positive charge in the β position relative to the metal. This difference in H-bonding abilities of the functional ferrocenyl branch with HSO_4^- and H_2PO_4 is seemingly responsible for the observed selectivity.

Modified Electrodes. Electrodes modified by polymers containing ferrocenyl units have been known for a long time.[29] More recently, Cuadrado et al. have extensively studied the derivatization of silylferrocenyl-terminated and other ferrocenyl dendrimers.[30,31] The only report of modified electrodes with thiol−gold colloid assemblies functionalized by ferrocenyl dendrimers, however, is that of Nishihara's group.[32] To test the possible applications of dendronized colloids, we attempted to modify platinum electrodes by depositing these polyferrocenyl dendronized colloids. Previous attempts to do so with amidoferrocenylalkylthiol−gold colloids that were recently reported met with failure, because they resulted in unstable modified electrodes. Nishihara has prepared modified electrodes with alkylthiol−gold colloids terminated by biferrocenyl units that may be considered as AB_2 units.[32] The seminal works of Crooks and Tomalia, who prepared dendrimer-colloid assemblies, showed that such assemblies are stable.[1] In the previous electrochemical study of the polyferrocenyl dendronized gold colloids, we could note the tendency of these nanoscopic assemblies to adsorb on electrodes. Indeed, we found that the adsorption of the dendronized gold colloids was all the better, as the thiols contained a larger number of ferrocenyl groups. The dendronized colloids bearing three ferrocenyl groups in AB_3 units adsorb better than monoferrocenylalkylthiols and allow preparing modestly stable electrodes. In this respect, the tris-amidoferrocenyl branching was found to give better results than the tri-silylferrocenyl one. The most stable modified electrodes were those prepared with the dendronized gold colloids containing either of the nonaferrocenyl dendrons. Indeed, the dendronized colloids containing the nonasilylferrocenylthiolate dendron give excellent modified electrodes, whereas the intensities and stabilities observed with those containing the trisilylferrocenylthiolate dendron are much weaker. These modified electrodes were prepared by simply dipping a platinum electrode into a CH_2Cl_2 solution of the dendronized colloid and scanning the potential back and forth around the ferrocenyl wave. This scanning provoked the appearance of the classic symmetric CV wave with the same anodic and cathodic potential disclosing an increase of its current intensity until saturation was reached after about fifty scans. These modified electrodes were perfectly stable (including in air), and they also showed a remarkable change when the $H_2PO_4^-$ or ATP^{2-} anion was introduced into the CH_2Cl_2 solution. Figure 6 shows the progress of the CV waves from the initial one to the new one.

The new wave seen in the presence of one of these anions is largely shifted to a less positive potential as noted for the dendronized colloids in solution (see the potential shifts in Table 1 for the modified electrodes with the various dendronized colloids). The anodic and cathodic peak potentials are no longer identical; this indicates electrochemical irreversibility, that is, strong structural rearrangement due to the supramolecular interactions (hydrogen bonding and especially electrostatic interaction) in the course of electron transfer. Remarkable features were the following:

(i) The stability of these CV waves upon multiple scanning the potentials around the waves.

(ii) The selective recognition of $H_2PO_4^-$ or ATP^{2-} in the presence of other anions, such as HSO_4^- and Cl^-.

(iii) The possibility to selectively wash the salts from these modified electrodes, leaving only the dendronized colloid on the electrode surface (Figure 6d). This allowed sensing this anion again in another solution or another anion. These experiments

(29) (a) Brown, A. P.; Anson, F. C. *Anal. Chem.* **1977**, *49*, 1589. (b) Peerce, P. J.; Bard, A. J. *Electroanal. Chem.* **1980**, *114*, 89. (c) Laviron, E. *J. Electroanal. Chem.* **1981**, *122*, 37. (d) Abruna, H. D. In *Electroresponsive Molecular and Polymeric Systems*; Stotheim, T. A., Ed.; Dekker: New York, 1988; Vol. 1, p 97. (e) Murray, R. W. In *Molecular Design of Electrode Surfaces*; Murray, R. W., Ed.; Techniques of Chemistry XXII; Wiley: New York, 1992; p 1. (f) Morán, M.; Casado, C. M.; Cuadrado, I. *Organometallics* **1993**, *12*, 4327. (g) Audebert, P.; Cerveau, G.; Corriu, R. J. P.; Costa, N. *J. Electroanal. Chem.* **1996**, *413*, 89.

(30) (a) Alonso, B.; Morán, M.; Casado, C.; Lobete, F.; Losada, J.; Cuadrado, I. *Chem. Mat.* **1995**, *7*, 1440. (b) Cuadrado, I.; Morán, M.; Losada, J.; Casado, M.; Pascual, C.; Alonso, B.; Lobete, F. In *Advances in Dendritic Macromolecules*; Newkome, G., Ed.; Jai Press: Stanford, CT, 1996; Vol. 3, p 151. (c) Cuadrado, I.; Casado, M.; Alonso, B.; Morán, M.; Losada, J.; Belsky, V. *J. Am. Chem. Soc.* **1997**, *119*, 7673.

(31) Reviews on ferrocenyl dendrimers and their electrochemistry:(a) Cuadrado, I.; Morán, M.; Casado, C. M.; Alonso, B.; Losada, J. *Coord. Chem. Rev.* **1999**, *193*−*195*, 395−445. (b) Casado, C. M.; Cuadrado, I.; Morán, M.; Alonso, B.; Garcia, B.; Gonzales, B.; Losada, J. *Coord. Chem. Rev.* **1999**, *185*−*186*, 53.

(32) (a) Biferrocenyl-substituted thiol-nanoparticles deposited on metal surfaces: Yamada, M.; Quiros, I.; Mizutani, J.; Kubo, K.; Nishihara, I. *Phys. Chem. Chem. Phys.* **2001**, *3*, 3377. (b) Yamada, M.; Kuzume, A.; Kurihara, M.; Kubo, K.; Nishihara, H. *Chem. Commun.* **2001**, 2476. (c) Yamada, M.; Nishihara, H. *Chem. Commun.* **2002**, 2578.

(33) Miller, S. R.; Gustowski, D. A.; Chen, Z.-H.; Gokel, G. W.; Echegoyen, L.; Kaifer, A. E. *Anal. Chem.* **1988**, *60*, 2021.

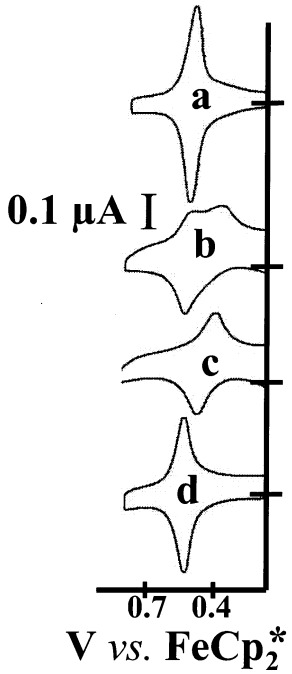

Figure 6. Recognition of ATP^{2-} with a Pt electrode modified: with 24 (colloid 9-silyl-Fc). Cyclic voltammograms: (a) 24-modified electrode alone; (b) in the course of the titration; (c) with an excess of $[n\text{-}Bu_4N]_2[ATP]$; (d) after removing ATP^{2-} by washing the 24-modified electrode with CH_2Cl_2. See experimental conditions in the caption to Figure 1.

show that adsorption is very strong upon scanning around the ferrocenyl potential area with such dendronized colloids loaded with a large number of ferrocenyl units, a feature that is very profitable for practical use of such modified electrodes.

Finally, the Pt electrode modified with **12** is also rather stable with a larger full width at half-maximun (100 mV) larger than the 90 mV value above which the adsorbed sites exert repulsive interactions among one another. This modified electrode also recognizes HSO_4^-, the potential being also shifted by 60 mV at the anode and by 25 mV at the cathode upon addition of this anion in solution (vide supra), which makes the signal slightly disymmetrical. As with $H_2PO_4^-$ and ATP^2, the modified electrode can be rinsed with CH_2Cl_2, after recognition of HSO_4^-, with minimal loss of adsorbed colloid for reuse. After using and washing 5 times, half the adsorbed redox active species is left, but further cycling and washing does not modify this amount any longer; the modified electrode is then stable.

Concluding Remarks

(a) Gold nanoparticles have been synthesized with both dodecanethiolate and the dendronized thiolate that contained triferrocenyl or nonaferrocenyl units either by the ligand-substitution procedure (AB_3 units) or by direct synthesis from mixtures of functional and nonfunctional thiols (AB_9 dendrons). The latter route is remarkably efficient for the nanoparticle−nonaferrocenyl dendronized assemblies when the substitution procedure is marred by the steric inhibition with large dendrons. With a gold nanoparticle−nonaferrocenylthiolate assembly, the colloidal gold core is surrounded by 180 or 360 silylferrocenyl units, so that these assemblies closely resemble large metallodendrimers in which the core is the gold nanoparticle.

(b) These dendronized gold nanoparticles combine the advantages of dendrimers and gold nanoparticles as sensors for the selective recognition and titration of $H_2PO_4^-$ and ATP^{2-} anions even in the presence of other anions. Their recognition properties are the subject of dendritic effect; that is, the shift of the ferrocenyl redox potential observed upon introduction of the anion is larger as the generation number increases. The assembly around the core provoking the clusterification of a large number of peripheral ferrocenyl groups induces the formation of narrow channels that facilitate the appearance of microcavities at the dendritic surface for a tighter supramolecular interaction with the anion. The silylferrocenyl system presents the advantage, over the amidoferrocenyl one, that its oxidation is fully reversible, although the provoked shift by addition of an anion is slightly larger with the amido group than with the silyl group. Although structural and electronic variations were designed concerning the size of the tethers and the number of Lewis-acidic silicon atoms in the dendrons **21** and **23**, the colloids **24** and **25** obtained with these two dendrons give similar recognition properties.

(c) The fabrication of modified electrodes is very successful only with the dendronized nanoparticles that contain the triamidoferrocenyl and nonaferrocenyl dendrons. This specific property cannot be obtained with the linear thiolate ligands and only begins to appear more or less weakly with the nanoparticles dendronized by the thiolate ligand containing the trisilylferrocenyl units. These modified electrodes recognize the $H_2PO_4^-$ and ATP^{2-} anions even in the presence of other anions such as HSO_4^- and Cl^-. HSO_4^- can also be recognized. Moreover, the salt of these anions can be easily removed after rinsing simply by dipping the used electrode a few minutes in CH_2Cl_2. In this way, the modified electrode with either of the dendronized nanoparticles can be reused many times.

Experimental Section

The synthesis of the AB_3 units from **1** is described in the Supporting Information. The preparation of the organic intermediates **13**−**17** was carried out as reported in ref 21.

Dendron 18. Karstedt catalyst (250 μL) was added to a mixture of nona-allyl dendron **16** (0.5 g, 0.44 mmol) and ferrocenyldimethylsilane (1.5 g, 6 mmol) in Et_2O, and this reaction mixture was stirred for 4 days at ambient temperature. The solution was filtered on Celite, and the solvent was removed under vacuum. After chromatographic separation on silica gel using a pentane/Et_2O (95:5) mixture as eluent, dendron **18** was obtained as an orange oil (1.2 g, 83%). Elemental analysis calcd for $C_{181}H_{248}Si_{12}Fe_9O_4$: H, 7.51; C, 65.33. Found: H, 7.59; C, 65.11. MALDI TOF mass spectrum, *m*/*z*: 3327.08 $[M]^+$ (calcd 3327.60). ^{1}H NMR ($CDCl_3$): δ_{ppm} 7.20 (d, C_6H_4, 6H); 7.09 (d, C_6H_4, 2H); 6.87 (d, C_6H_4, 6H); 6.67 (d, C_6H_4, 2H); 4.30 (s, C_5H_4, 2H); 4.09 (s, C_5H_5, 5H); 4.02 (s, C_5H_4, 2H); 3.51 (s, CH_2O, 6H); 1.61 (m broad, CH_2, 18H); 1.14 (m broad, CH_2, 18H); 0.62 (m broad, CH_2, 18H); 0.17 (s, SiMe, 54H); 0.08 (s, SiMe, 18H). ^{13}C NMR ($CDCl_3$): δ_{ppm} 159.38 (C_q, ArO); 152.84 (C_q, ArO); 139.77 (C_q, Ar); 137.17 (C_q, Ar); 127.51 (CH_{Ar}); 127.40 (CH_{Ar}); 114.65 (CH_{Ar}); 113.52 (CH_{Ar}); 73.04 (C_5H_4); 72.91 (C_q, C_5H_4); 70.69 (C_5H_4); 68.17 (C_5H_5); 60.09 (CH_2O); 43.13 (C_q-CH_2); 41.96 (CH_2); 17.90 (CH_2); 17.40 (CH_2Si); 14.58 (CH_2); −2.05 (SiMe); − 4.61 (SiMe).

Dendron 20. A mixture of **18** (0.600 g, 0.180 mmol), K_2CO_3 (0.076 g, 0.540 mmol), and 4, 4′-dibromomethylbenzene (0.476 g, 0.900 mmol) in CH_3CN/THF (50:50) was stirred for 4 days at 50 °C. After removal of the solvent under vacuum, the product was extracted with 3 × 30 mL of Et_2O, and the solvent was removed under vacuum. The residue was chromatographed on silica gel using a pentane/ether mixture (20:80) as eluent, and **20** was obtained as a yellow oil (0.600 g, 95%). Elemental analysis calcd for $C_{189}H_{255}O_4Si_{12}BrFe_9$: H, 7.32; C, 64.66. Found: H, 7.50; C, 64.33. MALDI TOF mass spectrum, *m*/*z*: 3510.07 $[M^+]$ (calcd 3510.65). ^{1}H NMR ($CDCl_3$): δ_{ppm} 7.38 (s, C_6H_4, 4H); 7.18

(d, C_6H_4, 10H); 6.86 (d, C_6H_4, 10H); 5.04 (s, OCH_2, 2H); 4.51 (s, BrCH_2, 2H); 4.31 (s, C_5H_4, 18H); 4.18 (s, C_5H_5, 45H); 4.02 (s, C_5H_4, 18H); 1.61 (m broad, CH_2, 18H); 1.14 (m broad, CH_2, 18H); 0.62 (m broad, CH_2, 18H); 0.17 (s, SiMe, 54H); 0.08 (s, SiMe, 18H). ^{13}C NMR ($CDCl_3$): δ_{ppm} 159.30 (C_q, ArO); 156.84 (C_q, ArO); 139. 70 (C_q, Ar); 137. 17 (C_q, Ar); 130.60 (C_q, Ar); 129.10 (C_q, Ar); 128.60 (CH_{Ar}); 127.40 (CH_{Ar}); 127.10 (CH_{Ar}); 114.65 (CH_{Ar}); 113.50 (CH_{Ar}); 72.97 (C_5H_4); 71.44 (C_q, C_5H_4); 70.62 (C_5H_4); 68.13 (C_5H_5); 66.10 (CH_2O); 60.09 (CH_2O); 43.13 (C_q-CH_2); 42.22 (CH_2); 33.09 (CH_2Br); 18.11 (CH_2); 17.59 (CH_2Si); 15.18 (CH_2); −1.85 (SiMe); −4.50 (SiMe).

Dendron 19. A mixture of **17** (0.500 g, 0.160 mmol), K_2CO_3 (0.045 g, 0.320 mmol), and 4,4′-dibromomethylbenzene (0.211 g, 0.800 mmol) in a CH_3CN was stirred for 4 days at 50 °C. After removal of the solvent under vacuum, the product was extracted with 2 × 20 mL of Et_2O. The solvent was removed in a vacuum. After chromatographic separation on silica gel using a pentane/ether mixture (20:80) as eluent, the bromobenzyl derivative **19** was obtained as a yellow oil (0.406 g, 77%). Elemental analysis calcd for $C_{180}H_{231}O_4Si_9BrFe_9$: H, 7.07; C, 65.63. Found: H, 7.51; C, 66.32. MALDI TOF mass spectrum, *m*/*z*: 3294.64 [M^+] (calcd 3294.11). ^{1}H NMR ($CDCl_3$): δ_{ppm} 7.42 (s, C_6H_4, 4H); 7.15 (d, C_6H_4, 10H); 6.80 (d, C_6H_4, 10H); 5.04 (s, OCH_2, 2H); 4.51 (s, BrCH_2, 2H); 4.30 (s, C_5H_4, 18H); 4.08 (s, C_5H_5, 45H); 4.01(s, C_5H_4, 18H); 3.87 (s, OCH_2, 6H); 1.61 (m broad, CH_2, 18H); 1.11 (m broad, CH_2, 18H); 0.59 (m broad, CH_2, 18H); 0.15 (s, SiMe, 54H). ^{13}C NMR ($CDCl_3$): δ_{ppm} 156.50 (C_q, ArO); 156.42 (C_q, ArO); 139.74 (C_q, Ar); 138.90 (C_q, Ar); 130.82 (C_q, Ar); 129. 19 (C_q, Ar); 128.73 (CH_{Ar}); 127.82 (CH_{Ar}); 127.28 (CH_{Ar}); 114.27 (CH_{Ar}); 113.55 (CH_{Ar}); 72.92 (C_5H_4); 71.40 (C_q, C_5H_4); 70.57 (C_5H_4); 68.20 (C_5H_5); 68.09 (CH_2O); 60.10 (CH_2O); 43.07 (C_q-CH_2); 42.04 (CH_2); 33.13 (CH_2-Br); 29.60 (CH_2); 17.95 (CH_2); 17.41 (CH_2Si); −2.03 (SiMe).

Dendron 21. A mixture of **19** (0.396 g, 0.120 mmol) and NaSH (0.068 g, 1.200 mmol) in THF was stirred for 24 h at 50 °C. After removal of the solvent under vacuum, the reaction product was extracted with 2 × 20 mL of Et_2O and chromatographed on a silica column using Et_2O, providing **21** as a yellow-orange oil (0.370 mg, 0.114 mmol, 95%). Elemental analysis calcd for $C_{180}H_{232}O_4Si_9Fe_9S$: H, 7.20; C, 66.58. Found: H, 7.61; C, 66.91. MALDI TOF mass spectrum, *m*/*z*: 3247.27 [M^+] (calcd 3445.60). ^{1}H NMR ($CDCl_3$): δ_{ppm} 7.38 (s, C_6H_4, 4H); 7.15 (d, C_6H_4, 8H); 6.69 (d, C_6H_4, 8H); 5.01 (s, OCH_2, 2H); 4.29 (s, C_5H_4, 2H); 4.08 (s, C_5H_5, 5H); 4.01 (s, C_5H_4, 2H); 3.87 (s, OCH_2, 6H); 3.60 (d, HSCH_2, 2H); 1.60 (m, CH_2, 18H); 1.13 (m, CH_2, 18H); 0.60 (m, CH_2, 18H); 0.16 (s, SiCH_3, 54H). ^{13}C NMR ($CDCl_3$): δ_{ppm} 156.70 (C_q, ArO); 156.42 (C_q, ArO); 139.74 (C_q, Ar); 138.90 (C_q, Ar); 130.80 (C_q, Ar); 129. 20 (C_q, Ar); 128.70 (CH_{Ar}); 127.82 (CH_{Ar}); 127.28 (CH_{Ar}); 114.26 (CH_{Ar}); 113.55 (CH_{Ar}); 73.04 (C_5H_4); 71.43 (C_q, C_5H_4); 70.70 (C_5H_4); 68.21 (C_5H_5); 66.01 (CH_2O); 60.10 (CH_2O); 43.05 (C_q-CH_2); 42.00 (CH_2); 35.50 ($HSCH_2$); 29.60 (CH_2); 17.95 (CH_2); 17.41 (CH_2Si); −1.88 (SiMe).

Reduction of Disulfides to Thiols. The dendron **21** oxidized by air to disulfide **22** (250 mg, 0.038 mmol) was dissolved with 10 mL of DMF in a Schlenk flask. Water (70 μL, 100 equiv) was added, then the reaction mixture was degassed, tris-*n*-butylphosphine (100 μL, 10 equiv) was introduced, and the mixture was stirred at room temperature for 3 h. Then, 50 mL of ethyl acetate was added, and the mixture was washed with 1 N HCl. The organic layer was separated, degassed, dried under Na_2SO_4, and filtered. The solvent was then removed under vacuum, and the solid residue was rinsed under positive nitrogen pressure using degassed petroleum ether. The orange solid thiol **21** (220 mg, 0.067 mmol, 88%) was dried under vacuum. The same procedure was applied to all the thiol dendrons just before the synthesis of dendronized nanoparticles.

Dendron 23. A mixture of **20** (0.300 g, 0.085 mmol) and NaSH (0.048 g, 0.854 mmol) in THF was stirred for 24 h at 50 °C. After removal of the solvent under vacuum, the reaction product was extracted with 2 × 20 mL Et_2O and chromatographed on a silica column using a pentane/Et_2O (90:10) mixture, providing **23** as a yellow-orange oil (0.277 mg, 0.080 mmol, 94%). Elemental analysis calcd for $C_{189}H_{256}O_4Si_{12}Fe_9S$: H, 7.45; C, 65.54. Found: H, 7.88; C, 65.90. MALDI TOF mass spectrum, *m*/*z*: 3463.66 [M^+] (calcd 3463.81); 6927.21 [$2M^+$] (calcd 3927.62). ^{1}H NMR ($CDCl_3$): δ_{ppm} 7.38 (s, C_6H_4, 4H); 7.18 (d, C_6H_4, 8H); 6.87 (d, C_6H_4, 8H); 5.01 (s, OCH_2, 2H); 4.29 (s, C_5H_4, 2H); 4.08 (s, C_5H_5, 5H); 4.01 (s, C_5H_4, 2H); 3.60 (d, HSCH_2, 2H); 3.51 (s, OCH_2, 6H); 1.59 (m, CH_2, 18H); 1.13 (m, CH_2, 18H); 0.61 (m, CH_2, 18H); 0.16 (s, SiCH_3, 54H); 0.07 (s, SiCH_3, 18H). ^{13}C NMR ($CDCl_3$): δ_{ppm} 158.86 (C_q, ArO); 156.60 (C_q, ArO); 140.30 (C_q, Ar); 138.10 (C_q, Ar); 136.53 (C_q, Ar); 129.23 (C_q, Ar); 127.75 (CH_{Ar}); 127.10 (CH_{Ar}); 113.29 (CH_{Ar}); 72.95 (C_5H_4); 71.43 (C_q, C_5H_4); 70.60 (C_5H_4); 68.11 (C_5H_5); 66.11 (CH_2O); 60.10 (CH_2O); 43.04 (C_q-CH_2); 42.07 (CH_2); 35.50 ($HSCH_2$); 17.96 (CH_2); 15.18 (CH_2); −2.02 (SiMe); −4.64 (SiMe).

Ligand Substitution in Alkylthiol−Gold Nanoparticles. A CH_2Cl_2 (20 mL) solution of alkylthiol−gold nanoparticles (0.080 g, 10^{-6} mmol) and tris-ferrocenyl thiol dendron (see amounts later) was stirred under positive nitrogen pressure at room temperature. After 3 days, the solvent was evaporated under reduced pressure. The dark brown product was washed 3 times with 10 mL of methanol and then 3 times with 10 mL of acetone in order to remove the noncoordinated thiols, the desired colloids being not soluble in these two solvents (the washing solvents were finally colorless). The black solid was dried under vacuum.

(a) Dendron 11 (0.080 g, 0.073 mmol) gives 0.065 g of **11** (85% yield) and 4.8% of substitution in alkylthiol−gold nanoparticles. ^{1}H NMR (250 MHz, $CDCl_3$) δ_{ppm}: 7.33 (CH($C_6H_4CH_2S$)); 7.21 (CH-(C_6H_4O)); 6.91 (CH(C_6H_4O)); 4.94 (CH_2O); 4.31 (CH(C_5H_4Si)); 4.10 (Cp); 4.03 ($CH(C_5H_4Si$); 3.51 (SCH_2−arom.); 1.27 (CH_2 alkylthiol); 0.89 (CH_3 alkylthiol); 0.62 (CH_2Si); 0.08 (CH_3Si). ^{13}C NMR (62.9 MHz, $CDCl_3$) δ_{ppm}: 156.41 (C(C_6H_4O)); 142.13 (C($SCH_2(C_6H_4)CH_2$); 133.01 ($CH(C_6H_4CH_2S$)); 132.3 ($CH(C_6H_4O$)); 112.4 ($CH(C_6H_4O$)); 72.5 (CH-(C_5H_4Si)); 70.5 ($CH(C_5H_4Si$)); 69.6 (CH(Cp)); 63.8 (CH_2O); 31.90−29.4 (CH_2 alkylthiol); 28.82 (SCH−arom.); 22.56 (CH_2 alkylthiol); 17.92 (CH_2C−arom.); 15.23 (CH_2CH_2Si); 14.1 (CH_3 alkylthiol); 3.11 (CH_2CH_2Si); −4.0 (CH_3Si). $E_{1/2}$ (V vs Fc; CH_2Cl_2; 20 °C) 0.00 (r) (see text).

(b) Dendron 12. (0.080 g, 0.063 mmol) gives 0.073 g of **12** (90% yield) and 3% of ligand substitution in alkylthiol−gold nanoparticles. ^{1}H NMR (250 MHz, $CDCl_3$) δ (ppm): 7.37 (CH($C_6H_4CH_2S$)); 7.15 (CH(C_6H_4O)); 6.91 (CH(C_6H_4O)); 4.64 ($CH_2(C_5H_4CO)$); 4.31 (CH-(C_5H_4CO)); 4.19 (Cp); 3.62 (SCH_2−arom.); 2.86 ($SiCH_2N$); 1.27 (CH_2 alkylthiol); 0.89 (CH_3 alkylthiol); 0.08 (CH_3Si). ^{13}C NMR (62.9 MHz, $CDCl_3$) δ(ppm): 170.00 (*C*ONH); 156.41(C(C_6H_4O)); 139.13 (C(SCH_2-(C_6H_4)CH_2)); 129.71 ($CH(C_6H_4CH_2S$)); 127.3 ($CH(C_6H_4O$)); 114.4 ($CH(C_6H_4C$)); 70.0 ($CH(C_5H_4CO$)); 69.6 (CH(Cp)); 67.9 (CH(C_5H_4-CO)); 42.0 ($SiCH_2N$); 32.0−29.4 (CH_2 alkylthiol); 28.7 (SCH−arom.); 22.6 (CH_2 alkylthiol); 17.7 (CH_2C−arom.); 15.2 (CH_2CH_2Si); 14.1 (CH_3 alkylthiol); −4.0 (CH_3Si). IR (KBr, cm^{-1}): ν_{CON} 1625.3, 1542.5. $E_{1/2}$ (V vs Fc; CH_2Cl_2; 20 °C) 0.145 (r) (see text and Scheme 4).

Direct Brust Colloid Synthesis. General Method. (a). A colorless solution of N(*n*-C_8H_{17})$_4$Br (0.524 g, 0.959 mmol) in 10 mL of toluene was added to a yellow water solution (10 mL) of $HAuCl_4$ (0.093 g, 0.274 mmol). The mixture was stirred under positive nitrogen pressure, and separation between the red organic phase (top) and colorless aqueous phase (bottom) resulted. A mixture of dodecanethiol $C_{12}H_{25}$-SH (0.028 g, 0.137 mmol) and dendronized-thiol containing the trisilyl ferrocenyl unit (0.150 g, 0.137 mmol) in 10 mL of toluene was added to the organic phase. Then, $NaBH_4$ (0.114 g, 3.04 mmol) in 10 mL of water was slowly added to the stirred reaction mixture. The red color turned to black brown, and the reaction mixture was vigorously stirred for 3 h. The organic phase was separated from the aqueous phase, its volume was reduced to 3 mL, and 100 mL of ethanol was added. The mixture was kept at −20 °C for 12 h. The resulting dark brown-black precipitate was filtered on Celite and then washed twice with ethanol and twice with acetone to remove excess thiol. The crude product was dissolved in CH_2Cl_2 and precipitated again with methanol.

The dark black colloid containing the mixture of ligands $C_{12}H_{25}S$/dendron-thiol tri-silyl ferrocene = 75:25 (ratio determined by ^1H NMR) was then dried under vacuum, which gave 0.085 g. ^1H NMR (250 MHz, $CDCl_3$) δ_{ppm}: 7.33 (C*H*($C_6H_4CH_2S$)); 7.21 (C*H*(C_6H_4O)); 6.91 (C*H*(C_6H_4O)); 4.94 (CH_2O); 4.31 (C*H*(C_5H_4Si)); 4.10 (Cp); 4.03 (C*H*(C_5H_4Si)); 3.51 (SCH_2−arom.); 1.27 (CH_2 alkylthiol); 0.89 (CH_3 alkylthiol); 0.62 (CH_2Si); 0.08 (CH_3Si). ^{13}C NMR (62.9 MHz, $CDCl_3$) δ_{ppm}: 156.41 (C(C_6H_4O)); 142.13 (C($SCH_2(C_6H_4)CH_2$)); 133.01 (C*H*($C_6H_4CH_2S$)); 132.3 (C*H*(C_6H_4O)); 112.4 (C*H*(C_6H_4O)); 72.5(CH-(C_5H_4Si)); 70.5 (CH(C_5H_4Si)); 69.6 (CH (Cp)); 63.8 (CH_2O); 31.90−29.4 (CH_2 alkylthiol); 28.82 (SCH−arom.); 22.56 (CH_2 alkylthiol); 17.92 (CH_2C−arom.); 15.23 (CH_2CH_2Si); 14.1 (CH_3 alkylthiol); 3.11 (CH_2CH_2Si); −4.0 (CH_3Si).

(b). A reaction between $HAuCl_4$ (0.031 g, 0.092 mmol), N(*n*-$C_8H_{17})_4$-Br (0.176 g, 0.322 mmol), $C_{12}H_{25}SH$ (0.0094 g 0.046 mmol) dendron **21** (0.150 g, 0.046 mmol), and $NaBH_4$ (aq) solution (0.038 g, 1.00 mmol) was carried out as in procedure (**a**) which gave nanoparticle **24**. ^1H NMR integration indicated that the ratio of ligands $C_{12}H_{25}S$ and **21** was 80:20. ^1H NMR (250 MHz, $CDCl_3$) δ_{ppm}: 7.33 (C*H*(C_6H_4-CH_2S)); 7.21 (C*H*(C_6H_4O)); 7.01 (C*H*($C_6H_4CH_2S$)); 6.91 (C*H*(C_6H_4O)); 5.05 (CH_2O); 4.29 (C*H*(C_5H_4Si)); 4.10 (Cp); 4.01 (CH(C_5H_4Si)); 3.87 (O−C*H*$_2$); 1.90 (C*H*$_2$); 1.27 (CH_2 alkylthiol); 0.89 (CH_3 alkylthiol); 0.62 (CH_2Si); 0.16 (CH_3Si). ^{13}C NMR (62.9 MHz, $CDCl_3$) δ_{ppm}: 155.91 (C_{qAr}); 139.58 (C_{qAr}); 127.15 (CH_{Ar}); 113.40 (CH_{Ar}); 72.68 (CH (C_5H_4-Si)); 70.5 (CH (C_5H_4Si)); 69.6 (CH (Cp)); 65.52 (CH_2O); 42.94 (C_q−CH_2); 41.89 (CH_2); 29.4 (CH_2 alkylthiol); 17.82; 17.28; 15.03 (CH_2); 14.30 (CH_3 alkylthiol); −2.14.0 (CH_3Si).

(c). Procedure (**a**) applied to the mixture of $HAuCl_4$ (0.029 g, 0.086 mmol), N(*n*-$C_8H_{17})_4Br$ (0.165 g, 0.301 mmol), $C_{12}H_{25}SH$ (0.009 g 0.043 mmol), dendron **23** (0.150 g, 0.043 mmol), and aq $NaBH_4$ solution (0.036 g, 0.95 mmol) gave nanoparticle **25**. The proportion of ligands $C_{12}H_{25}S$ and **23** in the mixture was 90:10. ^1H NMR (250 MHz, $CDCl_3$) δ_{ppm}: 7.33 (C*H*($C_6H_4CH_2S$)); 7.15 (C*H*(C_6H_4O)); 6.55 (C*H*(C_6H_4O)); 5.05 (CH_2O); 4.29 (C*H*(C_5H_4Si)); 4.08 (Cp); 4.01 (C*H*(C_5H_4Si)); 3.52 (OCH_2); 1.58 (CH_2); 1.27 (CH_2 alkylthiol); 1.14 (CH_2); 0.89 (CH_3 alkylthiol); 0.62 (CH_2Si); 0.16 (CH_3Si). ^{13}C NMR (62.9 MHz, $CDCl_3$) δ_{ppm}: 158.96 (*C*(C_6H_4O)); 139.45 ($C_q(SCH_2(C_6H_4)CH_2)$; 127.19 (CH_{Ar}); 113.39 (*CH* (C_6H_4O)); 72.90 (*CH*(C_5H_4Si)); 70.57 (*CH* (C_5H_4Si)); 68.07 (CH (Cp)); 60.15 (CH_2O); 43.12 (C_q−CH_2); 42.16 (CH_2); 29.93 (CH_2 alkylthiol); 18.04, 17.52 (CH_2); 14.21 (CH_3 alkylthiol); 3.11 (CH_2CH_2-Si); −1.19 (CH_3Si).

Determination of the Number of Ligands in the Dendronized Gold Nanoparticles. Elemental analysis found for **11**: S, 3.41; Au, 54.68. Atomic ratio Au/S = 2.6. HRTEM: average diameter = 2.3 ± 0.4 nm. Number of gold atoms *per* core: 375. $n_s = 144$. Proportion of dendron **8** = 25%. Average number of dendron **8** *per* particle: $n_{\text{dendron}\mathbf{8}} = 36$; $n_{\text{alkylthiolate}} = 108$. MW = 135 072 g/mol.

Elemental analysis found for **12**: S, 4.39; Au, 67.52. Atomic ratio Au/S = 2.5. HRTEM: average diameter = 2.3 ± 0.7 nm. Number of gold atoms *per* core: 375. $n_s = 150$. Proportion of dendrons **10** = 3%. Average number of dendron **10** *per* particle: $n_{\text{dendron}\mathbf{10}} = 4.5$; $n_{\text{alkylthiolate}} = 145.5$. MW = 108 868 g/mol.

Elemental analysis found for **25**: S, 2.53; Au, 57.68. This elemental analysis provides the atomic ratio Au/S = 3.7 = *X*. HRTEM: average diameter *D* (gold core): 2.9 ± 0.5 nm. Number of gold atoms *per* core:[34] $N_{Au} = 4\pi R^3/3\nu_g = 4\pi(D/2)^3/51 = 751$ Au atoms *per* particle in average ($\nu_g = 17$ Å^3 for a gold atom). The number n_s of thiolate ligand *per* particle can then be deduced: $n_s = N_{Au}/X = 751/3.7 = 203$. The proportion of dendron **23** is given by the ^1H NMR spectrum of **25**: 10%. The average number of dendron **23** *per* particle is $n_{\text{dendron}\mathbf{23}} = 10/100 \times 203 = 20.3$ The average number of remaining dodecanethiolate ligands is $n_{\text{alkylthiolate}} = 203 - 20.3 = 182.7$. The average molecular weight *per* dendronized particle is MW = $N_{Au} \times 196.97 + n_{\text{dendron}}MW_{\text{dendron}} + n_{\text{alkylthiolate}}MW_{\text{alkylthiolate}} = 254\,157$ g/mol.

(34) Leff, D. V.; Ohara, P. C.; Heath, J. R.; Gelbart, W. M. *J. Phys. Chem.* **1995**, 99, 7036.

Elemental analysis found for **24**: S, 2.25; Au, 42.80. Atomic ratio Au/S = 3.1. HRTEM: average diameter: 2.8 ± 0.5 nm. Number of gold atoms *per* core: 676. $n_s = 218$. Proportion of dendron **21** = 20%. The average number of dendron **21** *per* particle is $n_{\text{dendron}21} = 43.6$; $n_{\text{alkylthiolate}} = 174.4$. MW = 309 806 g/mol.

General Method for the Titration of $H_2PO_4^-$ or ATP^{2-}: First, [*n*-Bu_4N][PF_6] was introduced in the electrochemical cell (that contained the working electrode, the reference electrode, and the counter electrode) and dissolved in freshly distillated dichloromethane. A blank voltammogram was recorded without colloid in order to check the working electrode. Then, the colloid was solubilized in a minimum of dichloromethane and added into the cell. About 1 mg (3×10^{-6} mol) of decamethylferrocene was also added. After the solution was degassed by dinitrogen flushing, the CV of the nanoparticle alone was recorded. Then, the anion $H_2PO_4^-$ or ATP^{2-} was added by small quantities using a microsyringe. After each addition, the solution was degassed, and a CV was recorded. The appearance and progressive increase of a new wave was observed while the initial wave decreased and finally disappeared (see all the titration graphs in the Supporting Information). When the initial wave had completely disappeared, addition of the salt of the anion was continued until reaching twice the volume already introduced. The titration of ATP^{2-} in the presence of Cl^- and HSO_4^- was carried out similarly, the salts [*n*-Bu_4N][Cl] and [*n*-Bu_4N][HSO_4] being added before [*n*-$Bu_4N]_2$[ATP].

Modification of Electrodes with the Dendronized Gold Nanoparticles. A platinum electrode (Sodimel, Pt 30) was dipped into 10% aq HNO_3 for 3 h, then rinsed with distilled water, dried in air, and polished using cerium oxide pulver (5 MU). The nanoparticles were electrodeposited onto such platinum-disk electrodes ($A = 0.078$ cm^2) from degassed CH_2Cl_2 solutions of metallodendron gold nanoparticles (10^{-6} M) and [*n*-Bu_4N][PF_6] (0.1 M) by continuous scanning (0.10 V s^{-1}) up to 50 cycles between 0.0 and 0.80 V vs $FeCp^*_2$. The coated electrode was washed with CH_2Cl_2 in order to remove the solution of material and dried in air. This modified electrode was characterized by CV in freshly distilled CH_2Cl_2 as containing only the supporting electrolyte. It showed a single symmetrical CV wave, and the linear relationship of the peak current with potential sweep rate was verified. The surface coverage Γ (mol cm^{-2}) by the dendronized gold nanoparticles was determined from the integrated charge of the CV wave. $\Gamma = Q/nFA$, where *Q* is the charge, *n* is the number of electrons transferred, *F* is the Faraday constant, and *A* is the area. Thus, the surface coverage for the electrode modified with **12** was 2.3×10^{-10} mol cm^{-2} (ferrocenyl sites), corresponding to 1.7×10^{-11} mol cm^{-2} of colloid-3-amido-Fc. The coverage surface Γ for the electrode modified with **24** was 5.6×10^{-10} mol cm^{-2} (ferrocenyl sites) or 1.55×10^{-12} mol cm^{-2} of colloid-9-silyl-Fc **24**. The nanoparticle **25** electrodeposited onto the Pt-disk electrode showed a surface coverage of $\Gamma = 1 \times 10^{-10}$ mol cm^{-2}, corresponding to a number of colloid-9-silyl-silyl-Fc **25** of 5.5×10^{-13} mol cm^{-2}.

Acknowledgment. We are grateful to Prof. J.-C. Moutet (University of Grenoble) for helpful discussions and the Institut Universitaire de France (IUF, grant to D. A.), the Centre National de la Recherche Scientifique (CNRS), the Ministère de la Recherche et de la Technologie (MRT, Ph. D. grant to M.-C. D.), and the Universities Bordeaux I and Paris VI for financial support.

Supporting Information Available: Syntheses of the AB_3 derivatives leading to thiols containing three ferrocenyl groups; histograms and TEM pictures of the dendronized gold nanoparticles (Figures SI 1 to SI 4) and CVs (Figures SI 5 and SI 6) and graphs of current variations (Figures SI 7 to SI 13) for the anion titrations by the dendronized gold nanoparticles. This material is available free of charge via the Internet at http://pubs.acs.org.

JA021325D

Nanoscopic Assemblies between Supramolecular Redox Active Metallodendrons and Gold Nanoparticles: Synthesis, Characterization and Selective Recognition of $H_2PO_4^-$, HSO_4^-, and Adenosine-5'-Triphosphate (ATP^{2-}) Anions

Marie-Christine Daniel, Jaime Ruiz, Sylvain Nlate, Jean-Claude Blais, Didier Astruc*
Contribution from the Groupe Nanoscience et Catalyse, LCOO, UMR CNRS N°5802, Université Bordeaux I, 33405 Talence Cedex, France and LCSOB, UMR CNRS N° 7613, Université Paris VI, 75252 Paris, France

SUPPORTING INFORMATION

Dendron 3. 1 g of phenoltriallyl **1** synthesized according to reference 12a (4.38 mmol) was dissolved in 40 mL of anhydrous ether. Then, 10 drops of Karstedt catalyst and 1.76 mL of dimethyl(chloromethyl)silane (14.4 mmol, 3.3 equiv.) were added. The mixture was stirred for 1 day at room temperature, then 1 day at 50°C. Excess of silane was removed under vacuum. The residue was redissolved in ether and filtered on silica in order to remove the catalyst. After flash chromatography on silica-gel column with petroleum ether/Et_2O (95/5), the yellow oil **3** was obtained with a yield of 85% (2.055 g)

^{1}H NMR (200 MHz, $CDCl_3$), δ(ppm): 0.057 (s, 18H, $SiCH_3$); 0.59 (t, 6H, CH_2Si); 1.08 (m, 6H, CH_2CH_2Si); 1.62 (t, 6H, $C(CH_2)_3$); 2.74 (s, 6H, CH_2Cl); 6.76-6.80 (d, 2H, CH_{Ar}); 7.11-7.15 (d, 2H, CH_{Ar}). ^{13}C NMR ($CDCl_3$), δ(ppm): -4.46 ($SiCH_3$); 15.07 (CH_2Si); 17.82 (CH_2CH_2Si); 28.4 ($C(\underline{C}H_2)_3$); 30.42 (CH_2Cl); 45.9 ($\underline{C}(CH_2)_3$); 115.1 (CH, Ar); 127.4 (CH, Ar); 138.6 (C_q, Ar); 155.3 (phenolic C).

Dendron 4 A mixture of **3** (2 g, 3.6 mmol), NaI (4.84 g, 9 equiv.) and NaN_3 (3.50 g, 15 equiv.) in anhydrous DMF (20 mL) was stirred and heated at 80°C for 24 h in the dark. The solvent was evaporated under vacuum. The white powder obtained was treated with Et_2O and water. The extracted organic layer was washed twice again with water and evaporated under vacuum. The organic layer was dried over Na_2SO_4 , filtrated and the solvent was removed under vacuum: **4** was obtained as a yellow oil with a yield of 90% (1.852 g).

^{1}H NMR (250 MHz, $CDCl_3$), δ(ppm): 0.050 (s, 18H, $SiCH_3$); 0.56 (t, 6H, CH_2Si); 1.08 (m, 6H, CH_2CH_2Si); 1.62 (t, 6H, $C(CH_2)_3$); 2.73 (s, 6H, CH_2N_3); 6.76-6.80 (d, 2H, CH_{Ar}); 7.10-7.15 (d, 2H, CH_{Ar}). ^{13}C NMR ($CDCl_3$), δ(ppm): -4.48 ($SiCH_3$); 15.1 (CH_2Si); 17.80 (CH_2CH_2Si); 28.5 ($C(\underline{C}H_2)_3$); 30.1 (CH_2Cl); 45.9 ($\underline{C}(CH_2)_3$); 115 (CH, Ar); 127.2 (CH, Ar); 138.3 (C_q, Ar); 155.3 (phenolic C). FTIR (KBr), ν (cm^{-1}): 2092.8 (azide).

Dendron 5. The compound **4** (1.80 g, 3.15 mmol) was dissolved in 20 mL of THF. Then, PPh_3 (4.96 g, 6 eq) and water (0.68 mL, 12 eq) were added. The mixture was stirred at reflux for 24 h and the solvent was removed under vacuum. The residue was dissolved in Et_2O then acidified with conc. HCl. After the removal of solvent under vacuum, the white powder was washed with CH_3CN, then Et_2O. The yellow solid **5** was obtained with a yield of 70% (1.34 g).

^{1}H NMR (250 MHz, D_2O), δ(ppm): 0.099 (s, 18H, $SiCH_3$); 0.63 (t, 6H, CH_2Si); 1.12 (m, 6H, CH_2CH_2Si); 1.68 (t, 6H, $C(CH_2)_3$); 2.38 (s, 6H, $CH_2NH_3^+$); 6.87-6.90 (d, 2H, CH_{Ar}); 7.31-7.35 (d, 2H, CH_{Ar}). ^{13}C NMR (D_2O), δ(ppm): -4.24 ($SiCH_3$); 14.61 (CH_2Si); 18.1 (CH_2CH_2Si); 28.6 ($C(\underline{C}H_2)_3$); 42.2 ($CH_2NH_3^+$); 46.0 ($\underline{C}(CH_2)_3$); 115.3 (CH, Ar); 129.2 (CH, Ar); 142 (C_q, Ar); 156 (phenolic C). FTIR (KBr), ν (cm^{-1}): 2921.9 and 1508.5 (ammonium). MALDI TOF mass spectrum (m/z): 496.41 (calcd 498.37), $(M-2H)^+$.

Dendron 6. A mixture of **5** (0.900 g, 1.48 mmol) and NEt_3 (2.5 mL, 12 equiv.) in anhydrous CH_2Cl_2 (20 mL) was stirred, then ferrocenoyl chloride in CH_2Cl_2 (3.3 equiv.) was added. After stirring for 16 h, the solvent was removed under vacuum. The residue was washed with a saturated solution of K_2CO_3, then filtrated over celite and washed with Et_2O. The product was dissolved with CH_2Cl_2 and dried over Na_2SO_4. It was finally purified by chromatography on a silica-gel column with CH_2Cl_2/methanol (97/3) as eluent. The compound **6** was obtained as an orange solid with a yield of 45% (750 mg).

^{1}H NMR (250 MHz, $CDCl_3$), δ(ppm): 0.063 (s, 18H, $SiCH_3$); 0.56 (t, 6H, CH_2Si); 1.11 (m, 6H, CH_2CH_2Si); 1.63 (t, 6H, $C(CH_2)_3$); 2.85 (s, 6H, CH_2NH); 4.18 (s, 15H, CH of Cp); 4.31 (s, 6H, CH of C_5H_4CO); 4.64 (s, 6H, CH of C_5H_4CO); 5.75 (t, 3H, CONH); 6.89 (d, 2H, CH_{Ar}); 7.12 (d, 2H, CH_{Ar}). ^{13}C NMR ($CDCl_3$), δ(ppm): -5.6 ($SiCH_3$); 8.7 (CH_2Si); 15.2 (CH_2CH_2Si); 17.7 ($C(\underline{C}H_2)_3$); 41.9 (CH_2NH); 46 ($\underline{C}(CH_2)_3$); 68.1 (CH of C_5H_4CO); 69.6 (Cp); 70.2 (C of C_5H_4CO); 115 (CH of C_6H_4OH); 127.1 (CH of C_6H_4OH); 138 (C of C_6H_4OH); 155 (C of C_6H_4OH); 170.2 (CONH). FTIR (KBr), ν (cm^{-1}): 3307.1 (NH), 1624 and 1544 (amide). MALDI TOF mass spectrum (m/z): 1132.40 (MH^+) (calcd 1132.35). Elemental analysis calcd for $C_{58}H_{79}Fe_3N_3O_5Si_3$: H 6.92, C 60.57; found: H 6.89, C 60.16.

Dendron 7. A mixture of 2 synthesized according to reference 12a (0.486 g, 0.5 mmol), K_2CO_3 (0.085 g, 0.607 mmol), and 4, 4'–dibromomethylbenzene in CH_3CN, was stirred for 72 h at ambient temperature. After removal of the solvent under vacuum, 30 mL of pentane was added, and the mixture was filtered. The solvent was removed under vacuum. After chromatography on a silica-gel column using Et_2O and pentane (10/90) as eluent, 7 was obtained as a yellow oil (0.439 g, 76%).

Elemental analysis calcd for $C_{60}H_{75}Si_3Fe_3Br$: H 6.60, C 62.99; found: H 7.07, C 63.94. MALDI TOF mass spectrum, m/z: 1143.52 [M^+] (calcd 1143.93). ^{1}H NMR ($CDCl_3$): δ(ppm) 7.47 (s, $C_6\underline{H}_4$, 4H); 7.30 (d, $C_6\underline{H}_4$, 2H); 6.90 (d, $C_6\underline{H}_4$, 2H); 5.10 (s, $OC\underline{H}_2$, 2H); 4.50 (s, $BrC\underline{H}_2$, 3H); 4.30 (s, C_5H_4, 2H); 4.08 (s, C_5H_5, 5H); 4.01 (s, C_5H_4, 2H); 1.60 (m, $C\underline{H}_2$, 6H); 1.15 (m, $C\underline{H}_2$, 6H); 0.60 (m, $C\underline{H}_2$, 6H); 0.15 (s, $SiC\underline{H}_3$, 6H). ^{13}C NMR ($CDCl_3$): δ(ppm) 156.28 (C_q, ArO); 140.31 (C_q, Ar); 130.66 (C_q, Ar); 129.09 (C_q, Ar); 128,65 (CH, Ar); 127,78 (CH, Ar); 127,07 (CH, Ar); 113.73 (CH, Ar); 72.95 (C_5H_4); 72.91 (C_q, C_5H_4); 70.58 (C_5H_4); 69.44 (CH_2O); 68.09 (C_5H_5); 43.00 (C_q-CH_2); 42.20 (CH_2); 33.00 (CH_2Br); 17.96 (CH_2CH_2Si); 17.40 (CH_2Si); -2.05 (SiMe).

Dendron 8. A mixture of **7** (0.200 g, 0.175 mmol), NaSH (0.098 g, 1.745 mmol) in THF, was stirred for 24 h at 40°C. After removal of the solvent under vacuum, the reaction product was extracted with 30 mL of pentane/Et_2O (90/10) and chromatographed on a silica-gel column using a 9/1 pentane/Et_2O mixture providing **8** as a yellow-orange oil (146 mg, 0.133 mmol, 76%). Elemental analysis calcd for $C_{60}H_{76}Si_3Fe_3S$: H 6.98, C 65.69; found : H 7.49, C 66.09. MALDI TOF mass spectrum, m/z: 2191.67 (calcd 2192.23), [2M-2H, disulfide] $^+$, 2159.69 [2M-S-2H, disulfide-S] $^+$, 1101.87 [M, thiol] $^+$, 1069.89 [M-S, thiol-S] $^+$. ^{1}H NMR ($CDCl_3$): δ(ppm) 7.47 (m, $C_6\underline{H}_4$, 4H); 7.15 (m, $C_6\underline{H}_4$, 2H); 6.92 (m, $C_6\underline{H}_4$, 2H); 5.01 (s, $OC\underline{H}_2$, 2H); 4.29 (s, C_5H_4, 2H); 4.08 (s, C_5H_5, 5H); 4.01 (s, C_5H_4, 2H); 3.64 (d, $HSC\underline{H}_2$, 2H); 1.60 (m, $C\underline{H}_2$, 6H); 1.15 (m, $C\underline{H}_2$, 6H); 0.60 (m, $C\underline{H}_2$, 6H); 0.15 (s, $SiC\underline{H}_3$, 6H). ^{13}C NMR ($CDCl_3$): δ(ppm) 156.55 (C_q, ArO); 140.37 (C_q, Ar); 138.04 (C_q, Ar); 136.53 (C_q, Ar); 129.23 (CH, Ar); 127.85 (CH, Ar); 127.51 (CH, Ar); 114.37 (CH, Ar); 72.95 (C_5H_4); 71.30 (Cq, C_5H_4); 70.61 (C_5H_4); 70.09 (CH_2O); 68.12 (C_5H_5); 43.25 (C_q-CH_2); 42.16 (CH_2); 35.54 ($HSCH_2$); 18.11 (CH_2CH_2Si); 17.56 (CH_2Si); -1.90 (SiMe).

Dendron 9. A mixture of **6** (0.180 g, 0.158 mmol), K_2CO_3 (0.030 g, 0.214 mmol), and α, α' – dibromo-*p*-xylene (0.168 g, 0.634 mmol), in CH_3CN, was stirred for 5 days at ambient temperature. After removing the solvent under vacuum , the residue was washed with diethyl ether (3 x 20mL), and **9** was extracted with CH_2Cl_2 and obtained as a yellow-orange solid (0.147 g, 70%).

Elemental analysis calcd for $C_{66}H_{84}Si_3Fe_3O_4N_3Br$: H 6.43, C 60.27; found: H 6.38, C 59.95. MALDI TOF mass spectrum, m/z: 1316.57 [MH^+], 1338.56 [M + Na^+] (calcd 1315.08). ^{1}H NMR ($CDCl_3$): δ (ppm) 7.38 (s, $C_6\underline{H}_4$, 4H); 7.16 (d, $C_6\underline{H}_4$, 2H); 6.87 (d, $C_6\underline{H}_4$, 2H); 5.70 (t, $N\underline{H}CH_2$, 3H); 5.00 (s, $OC\underline{H}_2$, 2H); 4.62 (s, C_5H_4, 6H); 4.50 (s, CH_2Br, 2H); 4.30 (s, C_5H_4, 6H); 4.18 (s, C_5H_5, 15H); 2.84 (d, $NHC\underline{H}_2$, 6H); 1.59 (m, $C\underline{H}_2$, 6H); 1.09 (m, $C\underline{H}_2$, 6H); 0.56 (m, $C\underline{H}_2$, 6H); 0.06 (s, $SiC\underline{H}_3$, 18H). ^{13}C NMR ($CDCl_3$): δ ppm 170.02 (CO); 156.08 (C_q, ArO); 140.00 (C_q, Ar); 137.78 (C_q, Ar); 129.14 (C_q, Ar); 127.78 (CH, Ar); 127,22 (CH, Ar); 127,10 (CH, Ar); 114.12 (CH, Ar); 70.02 (C_5H_4); 69.51 (C_q, C_5H_4); 70.58 (C_5H_4); 69.31 (CH_2O); 67.88 (C_5H_5); 43.01; (C_q-CH_2); 41.82 (CH_2); 33.16 (CH_2Br); 28.63 (CH_2NH); 17.59 (CH_2CH_2Si); 15.04 (CH_2Si); -4.06 (SiMe).

Dendron 10. A mixture of **9** (0.126 g, 0.95 mmol), NaSH (0.054 g, 0.964 mmol) in THF, was stirred for 1 day at 50°C. After removal of the solvent under vacuum, the residue was washed with diethyl ether (3 x 20 ml), and **10** was extracted with CH_2Cl_2 and obtained as a yellow-orange solid (0.108 g, 0.085 mmol, 90%).

Elemental analysis calcd for $C_{66}H_{85}Si_3Fe_3O_4N_3S$: H 6.75, C 62.50; found: H 6.97, C 59.68. MALDI TOF mass spectrum, m/z: 1290.49 (calcd 1268.25) [M + Na^+], 2557.60 [2M + Na^+]. ^{1}H NMR ($CDCl_3$): δ(ppm) 7.35 (m, $C_6\underline{H}_4$, 4H); 7.14 (d, $C_6\underline{H}_4$, 2H); 6.84 (d, $C_6\underline{H}_4$, 2H); 5.72 (broad, $N\underline{H}CH_2$, 3H); 4.98 (s, $OC\underline{H}_2$, 2H); 4.62 (s, C_5H_4, 6H); 4.29 (s, C_5H_4, 6H); 4.16 (s, C_5H_5, 15H); 3.61 (d, $HSC\underline{H}_2$, 2H); 2.84 (d, $NHC\underline{H}_2$, 6H); 1.61 (m, $C\underline{H}_2$, 6H); 1.09 (m, $C\underline{H}_2$, 6H); 0.56 (m, $C\underline{H}_2$, 6H); 0.06 (s, $SiC\underline{H}_3$, 18H). ^{13}C NMR ($CDCl_3$): δ(ppm) 170.00 (CO); 156.18 (C_q, ArO); 139.61 (C_q, Ar); 137.67 (C_q, Ar); 129.44 (C_q, Ar); 129.06 (CH, Ar); 127,64 (CH, Ar); 127,08 (CH, Ar); 114.10 (CH, Ar); 69.99 (C_5H_4); 69.51 (C_5H_5 and CH_2O); 67.87 (C_5H_4); 43.01 (C_q-CH_2); 41.84 (CH_2); 28.65 ($HSCH_2$ and CH_2NH); 17.60 (CH_2CH_2Si); 15.06 (CH_2Si); -4.04 (SiMe).

CAPTIONS OF THE SUPPORTING INFORMATION

HISTOGRAMS, CYCLOVOLTAMMOGRAMS AND TITRATION GRAPHS

Figure SI 1: Histogram of size repartition of nanoparticle **11** (colloid 3-silyl-Fc)

Figure SI 2: Histogram of size repartition of nanoparticle **12** (colloid 3-amido-Fc)

Figure SI 3: Histogram of size repartition of nanoparticle **24** (colloid 9-silyl-Fc)

Figure SI 4: Histogram of size repartition of nanoparticle **25** (colloid 9-silyl-silyl-Fc)

Titrations using cyclic voltammetry: commun conditions for all the captions of the SI Figures: Solvent: distilled CH_2Cl_2; temperature: 20 °C; supporting electrolyte: [*n*-Bu_4N] [PF_6] , 0.1 M; internal reference: $FeCp_2$*; reference electrode: Ag; auxiliary and working electrodes: Pt; scan rate: 0.2 V/s; anion concentration ([n-Bu_4N][H_2PO_4] or [n-Bu_4N]$_2$[ATP]): 5.10^{-3} M; concentration of [*n*-Bu_4N]Cl and [*n*-Bu_4N][HSO_4]: 5.10^{-2} M.

Figure SI 5: Titration of $H_2PO_4^-$ with **25** (colloid 9-silyl-silyl-Fc). Cyclic voltammograms:

a) nanoparticle **25** alone
b) in the course of the titration
c) after saturation with $H_2PO_4^-$

Figure SI 6: Titration of ATP^{2-} with **12** (colloid 3-amido-Fc). Cyclic voltammograms:

a) nanoparticle **12** alone
b) in the course of the titration
c) after saturation with ATP^{2-}

Figure SI 7: Titration of $H_2PO_4^-$ with **11** (colloid 3-silyl-Fc) in CH_2Cl_2 at R.T.

Figure SI 8: Titration of $H_2PO_4^-$ with **12** (colloid 3-amido-Fc) in CH_2Cl_2 at R.T.

Figure SI 9: Titration of $H_2PO_4^-$ with **24** (colloid 9-silyl-Fc) in CH_2Cl_2 at R.T.

Figure SI 10: Titration of $H_2PO_4^-$ with **25** (colloid 9-silyl-silyl-Fc) in CH_2Cl_2 at R.T.

Figure SI 11: Titration of ATP^{2-} with **11** (colloid 3-silyl-Fc) in CH_2Cl_2 at R.T.

Figure SI 12: Titration of ATP^{2-} with **12** (colloid 3-amido-Fc) in CH_2Cl_2 at R.T.

Figure SI 13: Titration of ATP^{2-} with **24** (colloid 9-silyl-Fc) in CH_2Cl_2 at R.T.

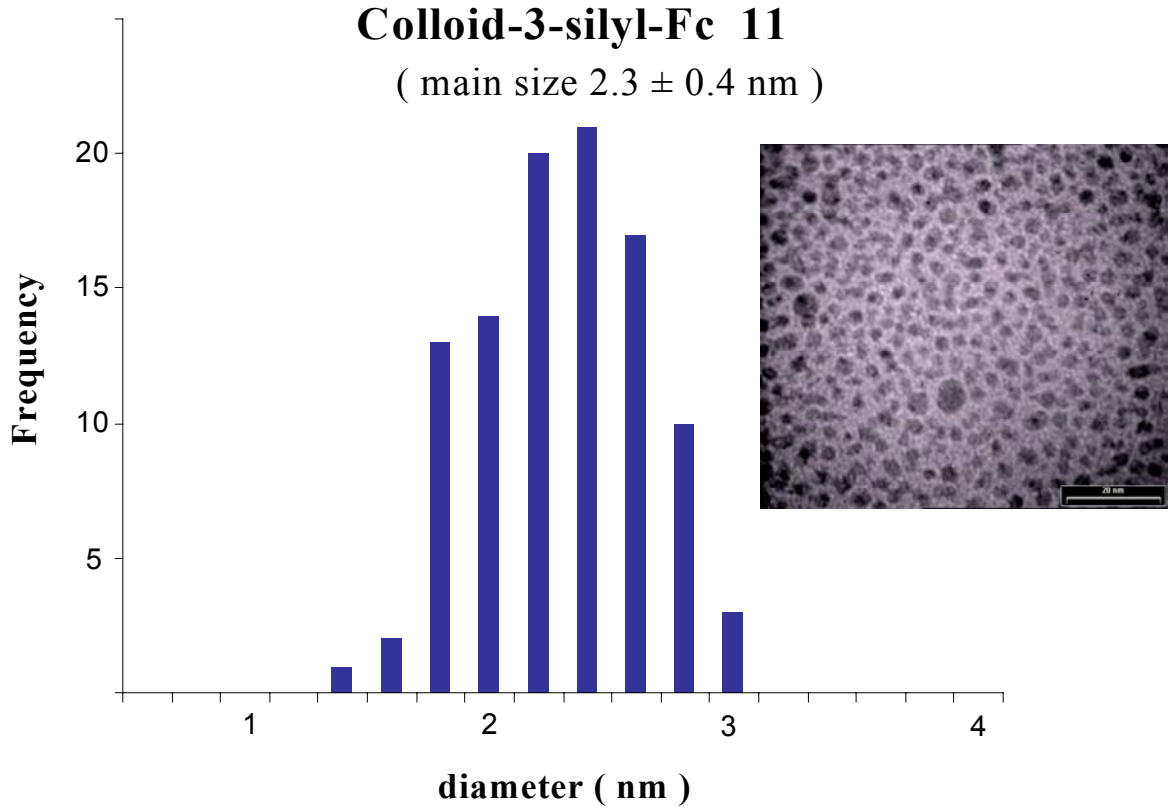

Figure SI 1: Histogram of size repartition of nanoparticle **11** (colloid 3-silyl-Fc)

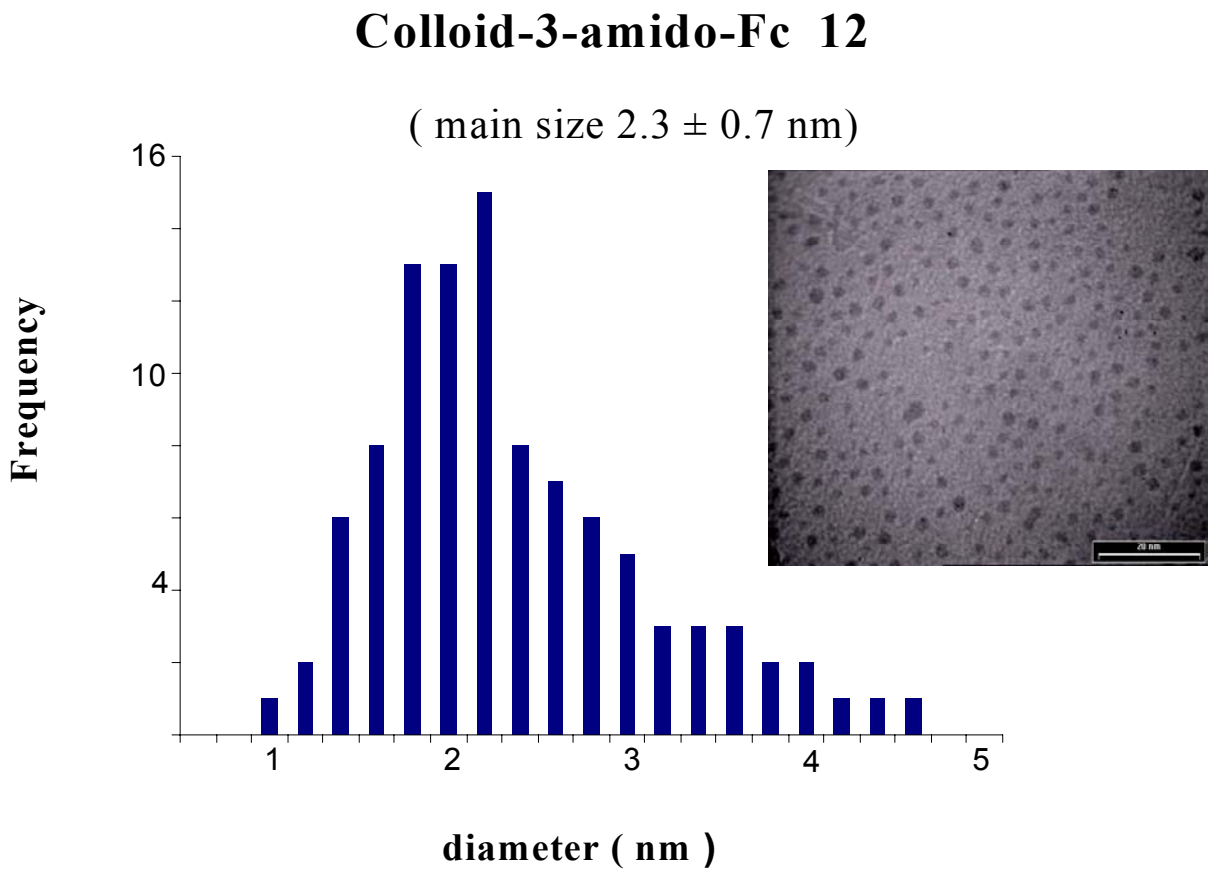

Figure SI 2: Histogram of size repartition of nanoparticle **12** (colloid 3-amido-Fc)

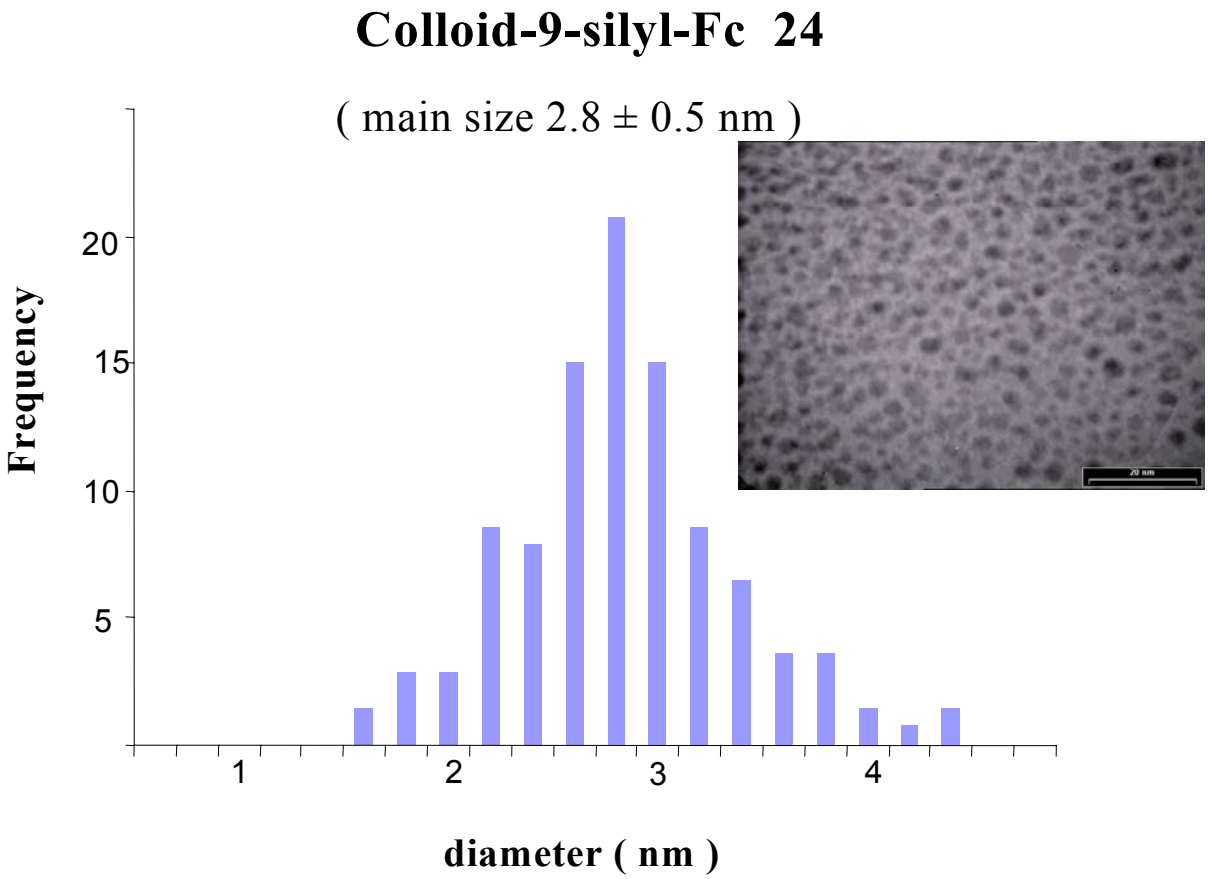

Figure SI 3: Histogram of size repartition of nanoparticle **24** (colloid 9-silyl-Fc)

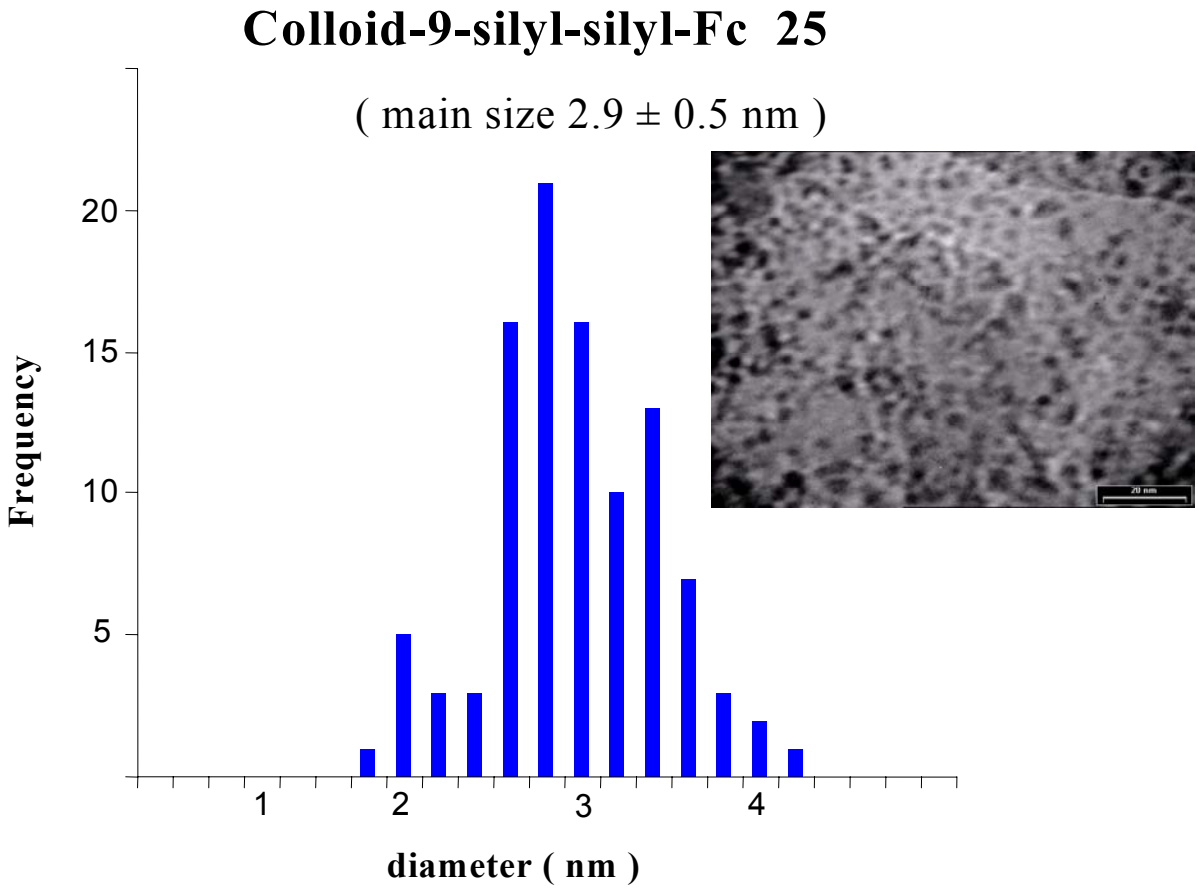

Figure SI 4: Histogram of size repartition of nanoparticle **25** (colloid 9-silyl-silyl-Fc)

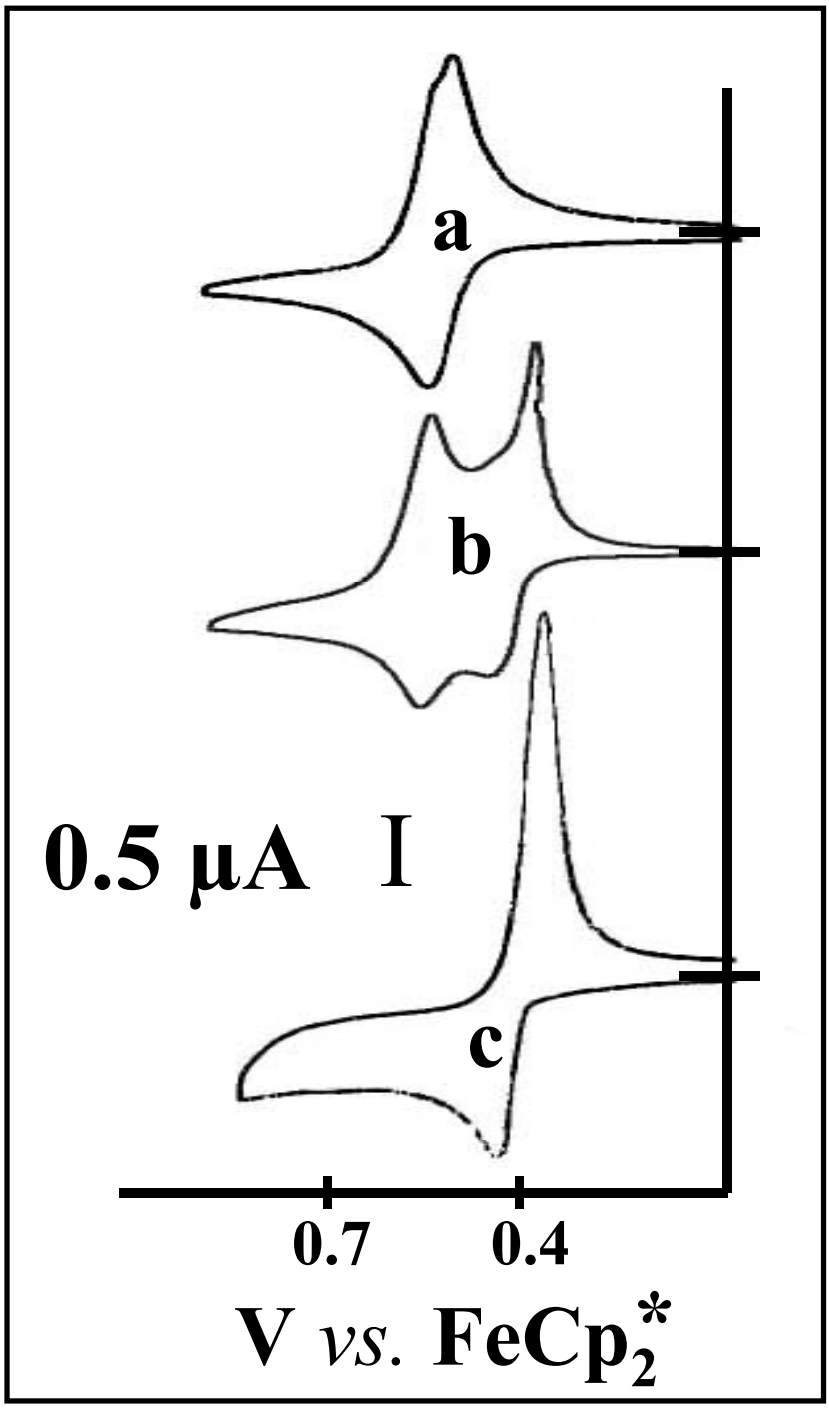

Figure SI 5: Titration of $H_2PO_4^-$ with **25** (colloid 9-silyl-silyl-Fc).

Cyclic voltammograms:

a) nanoparticle **25** alone

b) in the course of the titration

c) after saturation with $H_2PO_4^-$

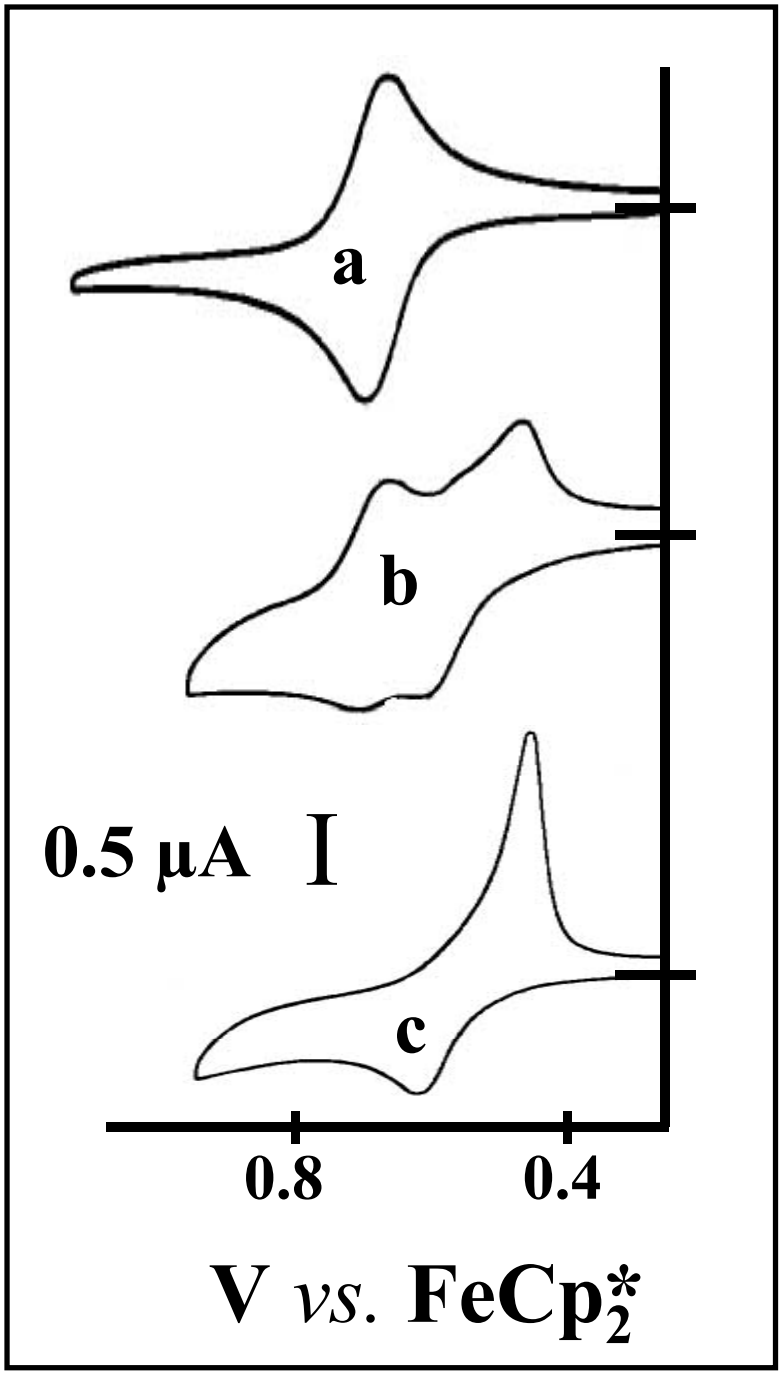

Figure SI 6: Titration of ATP^{2-} with **12** (colloid 3-amido-Fc).

Cyclic voltammograms:

a) nanoparticle **12** alone

b) in the course of the titration

c) after saturation with ATP^{2-}

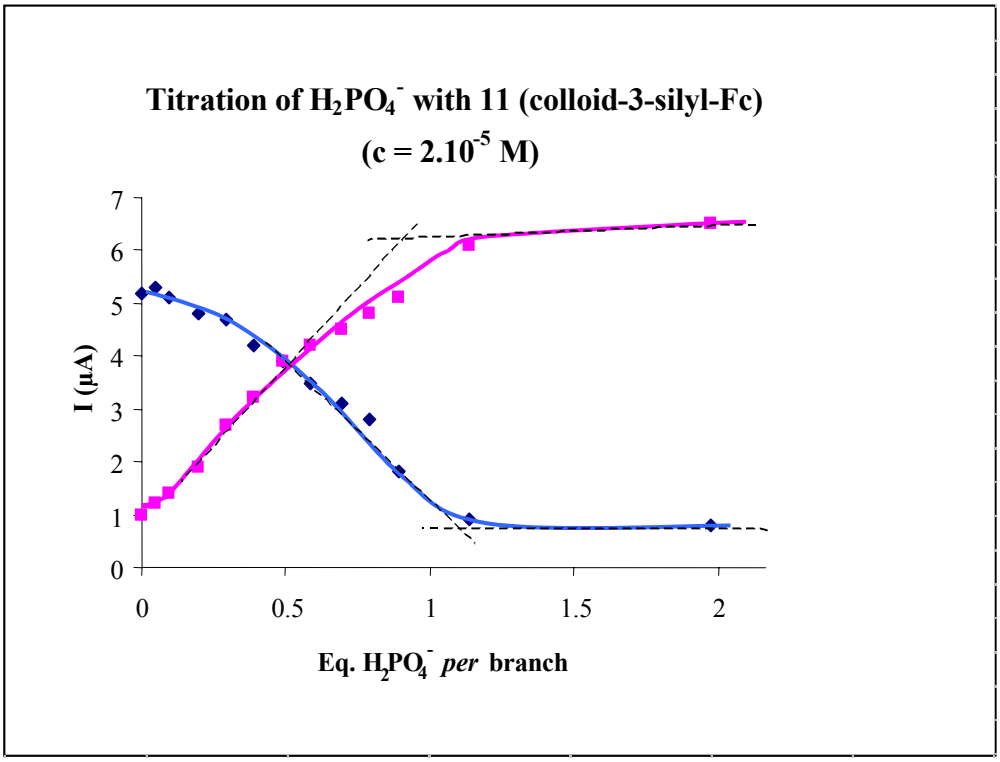

Figure SI 7: Titration of $H_2PO_4^-$ with **11** (colloid 3-silyl-Fc) in CH_2Cl_2 at R.T.

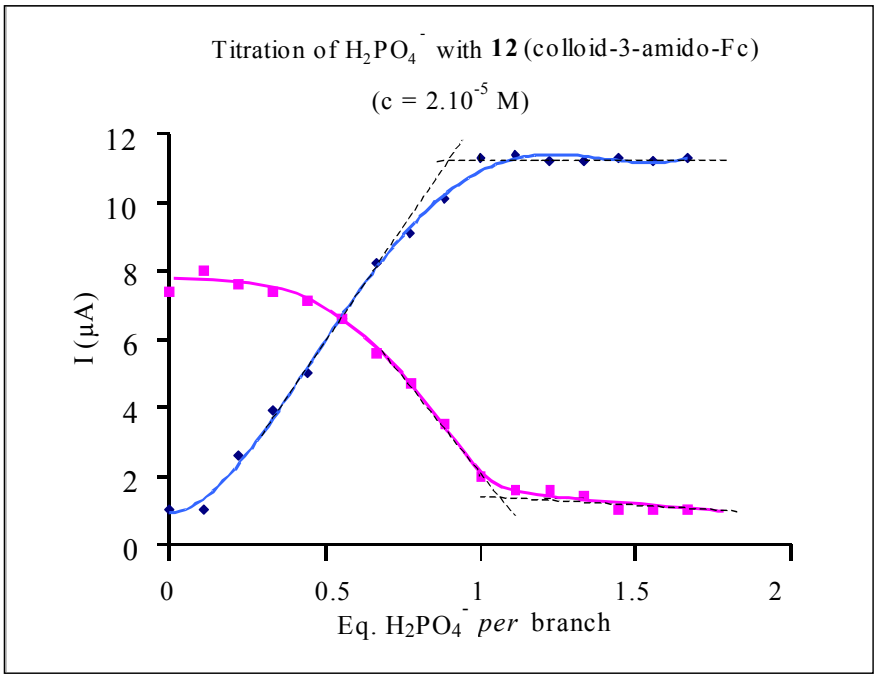

Figure SI 8: Titration of $H_2PO_4^-$ with **12** (colloid 3-amido-Fc) in CH_2Cl_2 at R.T.

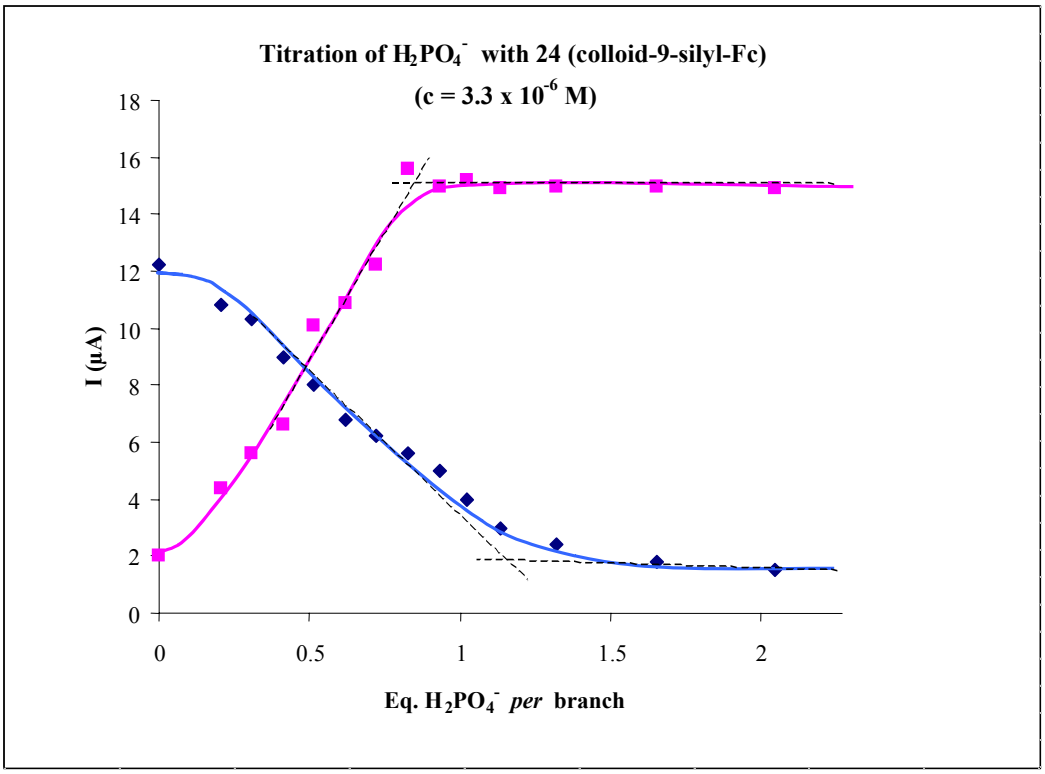

Figure SI 9: Titration of $H_2PO_4^-$ with **24** (colloid 9-silyl-Fc) in CH_2Cl_2 at R.T.

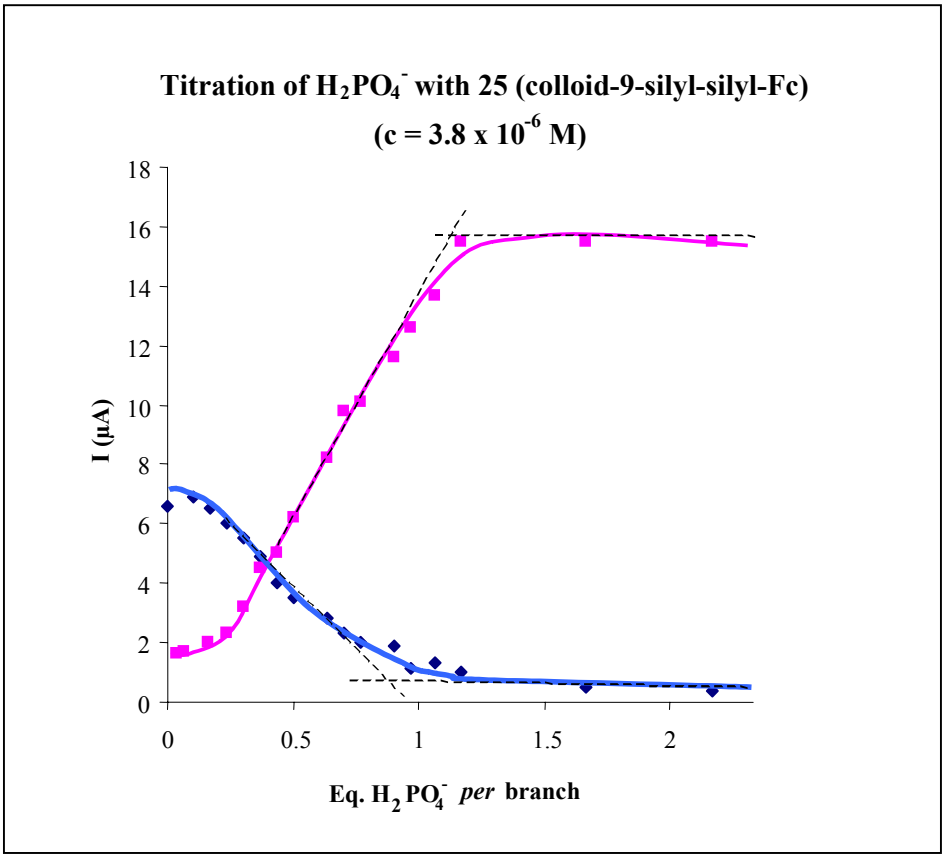

Figure SI 10: Titration of $H_2PO_4^-$ with **25** (colloid 9-silyl-silyl-Fc) in CH_2Cl_2 at R.T.

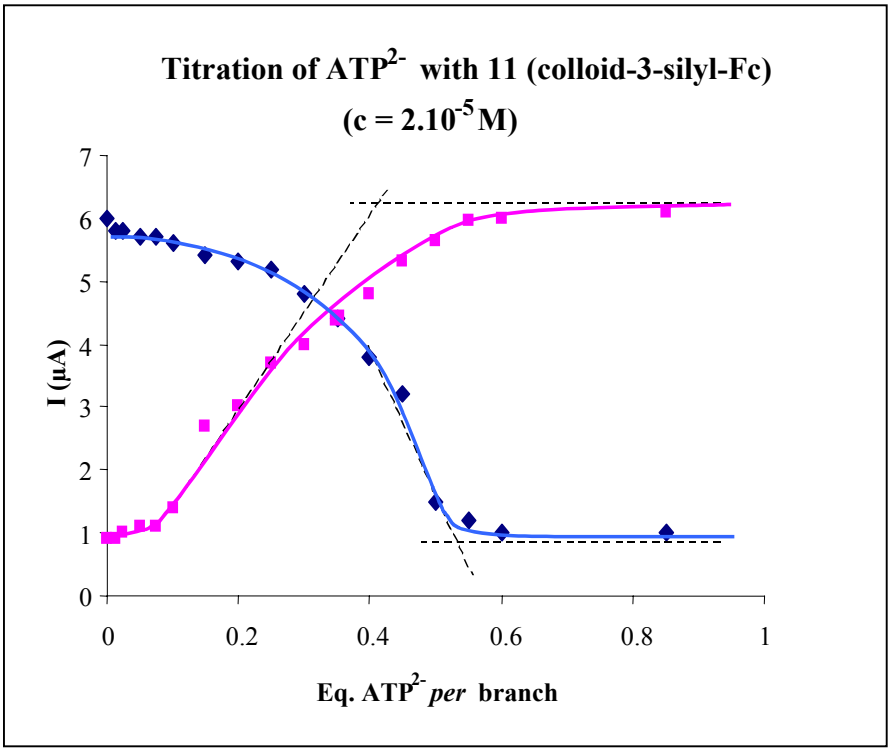

Figure SI 11: Titration of ATP^{2-} with **11** (colloid 3-silyl-Fc) in CH_2Cl_2 at R.T.

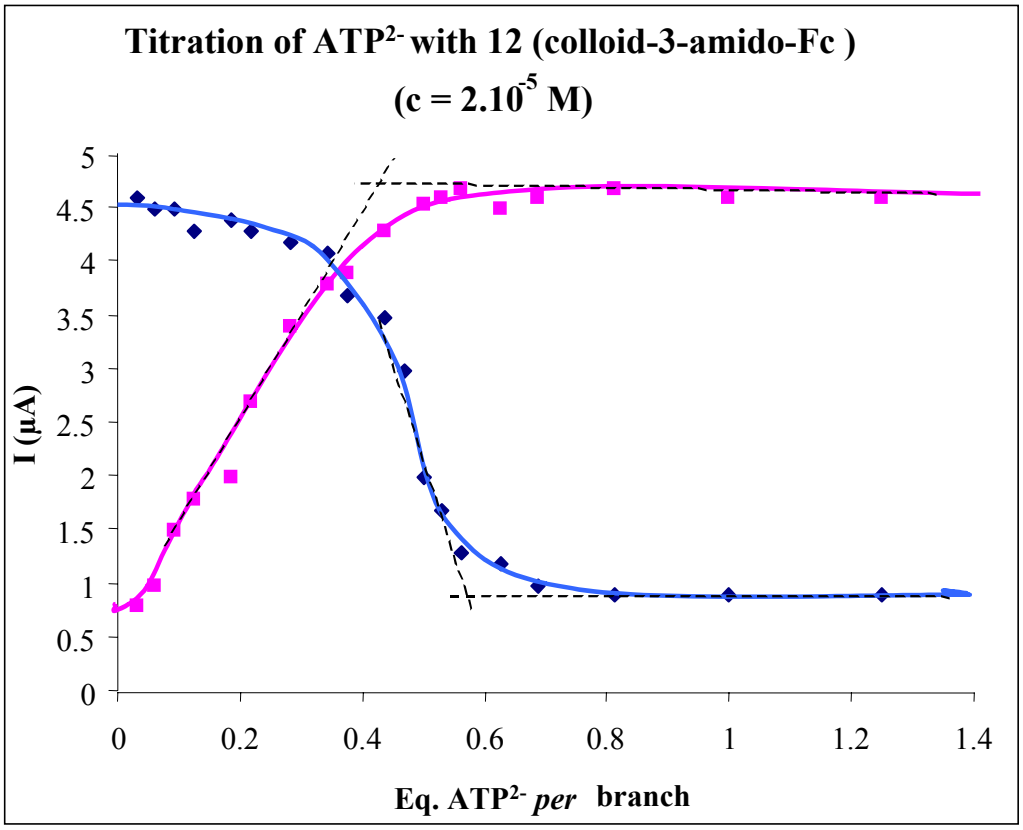

Figure SI 12: Titration of ATP^{2-} with **12** (colloid 3-amido-Fc) in CH_2Cl_2 at R.T.

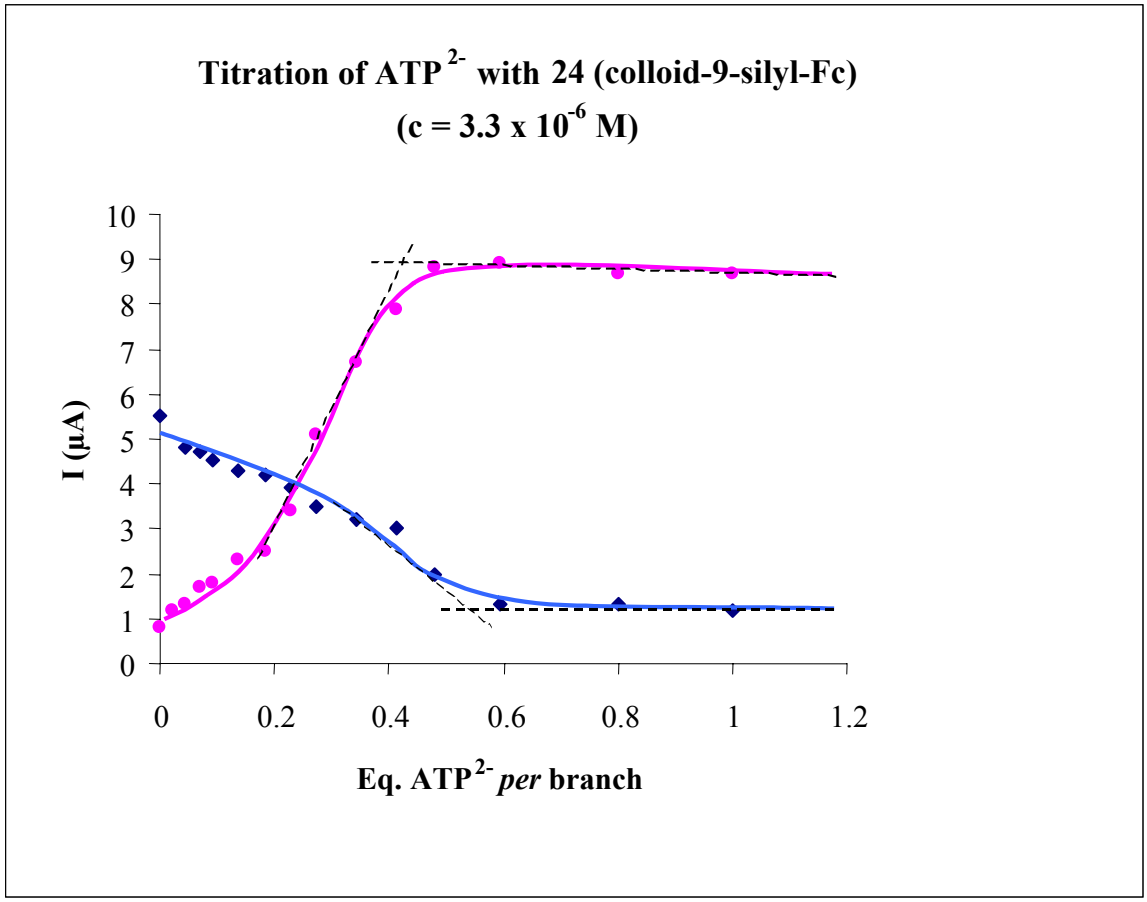

Figure SI 13: Titration of ATP^{2-} with **24** (colloid 9-silyl-Fc) in CH_2Cl_2 at R.T.

RESUME – CONCLUSION

PERSPECTIVES

RESUME - CONCLUSION

Introduction

Dans le domaine des nanosciences, la chimie des colloïdes ainsi que celle des dendrimères ont connu un véritable essor depuis quelques années. Ces deux entités macroscopiques ont des applications diverses et variées telles que la catalyse, la science des matériaux, la biologie et la reconnaissance entre autre.

Un colloïde (ou nanoparticule) se définit comme un cluster géant constitué d'un centre métallique (or, argent, platine, palladium, cadmium, césium…) stabilisé par des ligands organiques. Et un dendrimère aussi appelé arbre moléculaire, est une macromolécule parfaitement définie, formée d'un cœur dendritique sur lequel sont greffés des motifs d'arborescence multifonctionnels nommés dendrons.

Colloïde et dendrimère ont en commun leur taille nanoscopique ainsi que leur haute ramification. Mais leur principale différence réside dans le fait que les ligands du colloïde s'écartent en s'éloignant du noyau métallique alors que, dans le dendrimère, les branches se resserrent en s'éloignant du cœur.

Les thématiques de recherche de notre groupe sont surtout axées sur les métallodendrimères. Mais récemment, un intérêt particulier s'est porté sur les nanoparticules d'or de part leurs similitudes avec les dendrimères et pour effectuer une étude comparative.

L'objectif de cette thèse est donc d'aller plus loin dans la reconnaissance électrochimique d'anions avec des nanoparticules d'or fonctionnalisées et des métallodendrimères. La première partie concerne donc la reconnaissance de l'anion dihydrogénophosphate ($H_2PO_4^-$), de l'hydrogénosulfate et de l'adénosine-5'-triphosphate (ATP^{2-}) par des dendrimères pentaméthylamidoferrocényles Un second point traite de la reconnaissance d'$H_2PO_4^-$ et de l'ATP^{2-} par des dendrimères supramoléculaires. Une troisième partie détaille la reconnaissance de ces mêmes anions et d'HSO_4^- à l'aide de colloïdes d'or dendronisés.

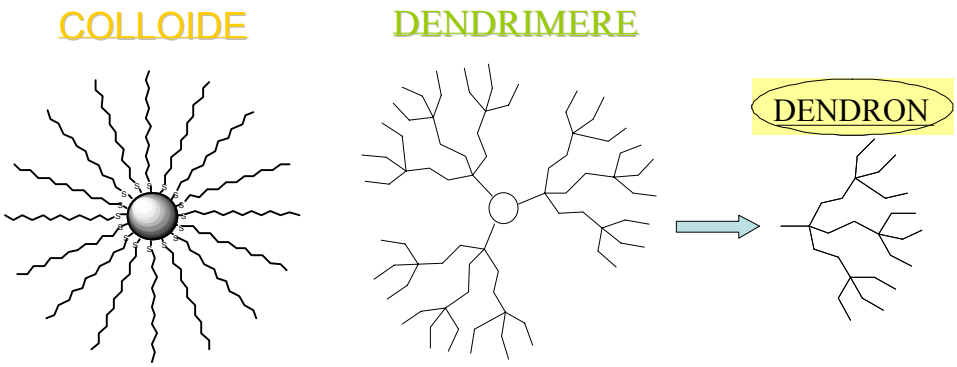

I. Etude comparative de dendrimères pentaméthylamidoferrocényles et amidoferrocényles utilisés comme sonde électrochimique pour $H_2PO_4^-$, HSO_4^- et ATP^{2-}

Deux familles de métallodendrimères à fonctions terminales respectivement amidoferrocényles et pentaméthylamidoferrocényles ont été synthétisées à partir des dendrimères commerciaux DAB-Am puis comparés.[1]

La reconnaissance d'$H_2PO_4^-$ ou d'ATP^{2-} avec les dendrimères perméthylés est plus "propre" qu'avec leurs homologues amidoferrocényles car les voltammogrammes présentent des vagues réversibles chimiquement et électrochimiquement et sans adsorption. Ceci s'explique par la stabilisation de la forme ferricinium due aux groupes méthyles des $Cp(Me)_5$. L'existence d'une interaction forte entre anions et groupements amidoferrocényles est matérialisée par la présence d'une nouvelle vague d'oxydoréduction à des potentiels plus négatifs (l'anion renforce la densité électronique du ferrocène et le rend donc plus facile à oxyder).

Dans le CH_2Cl_2, la reconnaissance est meilleure pour la série amidoferrocényle car un effet dendritique positif est observé c'est-à-dire que la différence de potentiel entre les deux vagues augmente avec la génération du dendrimère. Dans le DMF, la titration est seulement possible avec la série pentaméthylferrocène et montre un effet dendritique remarquable. En effet, avec la première génération, la vague de départ se déplace (intéraction faible) alors qu'à partir de la deuxième génération, on constate l'apparition d'une seconde vague (intéraction forte).

Pour ce qui est de l'hydrogénosulfate, les deux types de dendrimères montrent une intéraction forte avec l'anion, comportement nouveau par rapport aux colloïdes.

Toutefois, ils conservent une reconnaissance sélective d'$H_2PO_4^-$ ou d'ATP^{2-} en présence d' HSO_4^- et de Cl^- mais dans ce cas c'est un déplacement de la vague initiale qui est observé et non plus une nouvelle vague.

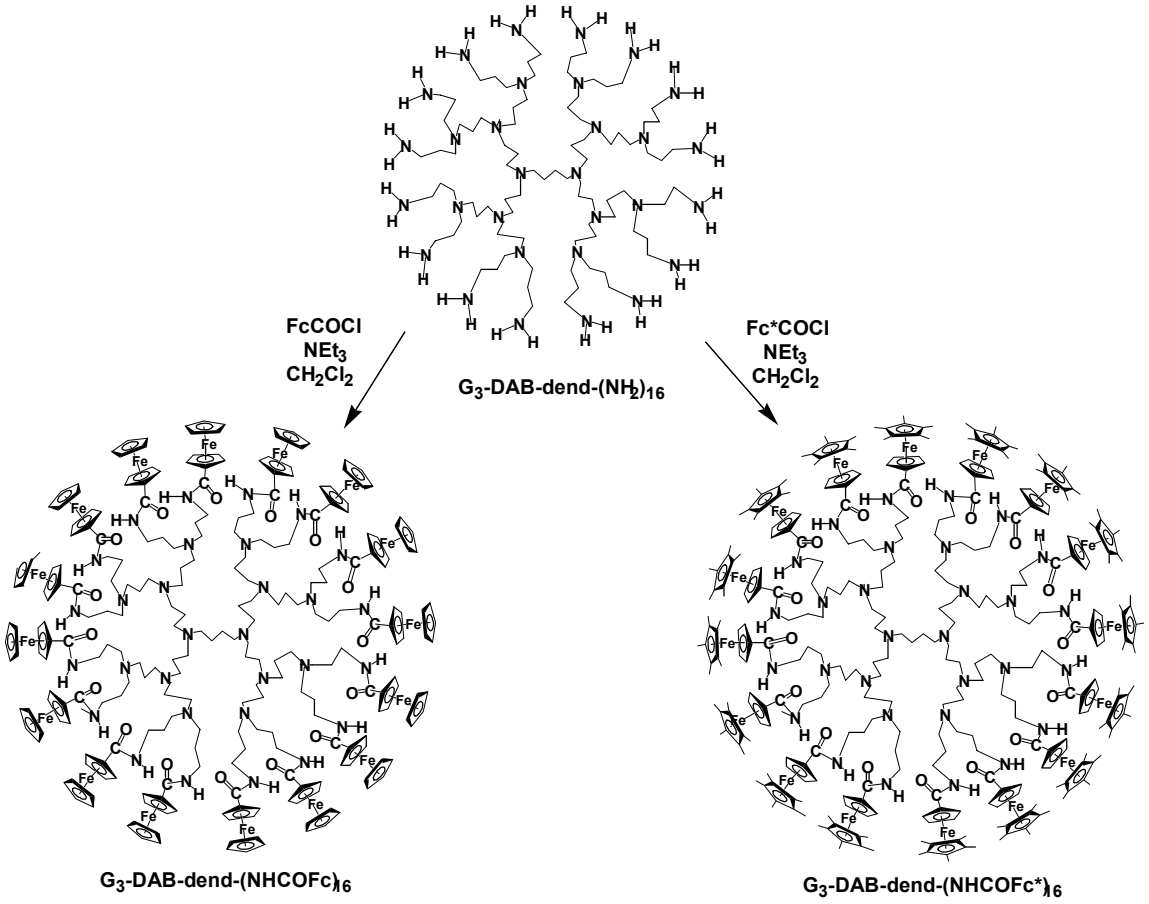

Synthèse des dendrimères amidoferrocényles et pentaméthylamidoferrocényles.

II. Assemblages supramoléculaires par liaisons hydrogène de métallodendrimères électroactifs et leur utilisation pour la reconnaissance d'$H_2PO_4^-$ et de l'ATP^{2-}.

La partie I traitait de dendrimères formés par des liaisons covalentes. Cette partie va avoir pour sujet des dendrimères créés par liaisons hydrogène.[2] Pour ce faire, nous avons utilisé le dendron phénol trisamidoferrocényle et les dendrimères commerciaux DAB-Am.
L'assemblage se fait par liaisons hydrogène entre les protons d'une amine et l'oxygène d'un phénol d'une part et entre l'azote d'une amine et le proton d'un phénol d'autre part. Les liaisons hydrogène peuvent être visualisées en ^1H RMN par le regroupement des signaux des protons phénoliques et des protons des amines en un signal unique avec un déplacement chimique plus blindé que le phénol et moins que l'amine.

La reconnaissance d'$H_2PO_4^-$ et de l'ATP^{2-} présentent des effets inhabituels. En effet, l'ajout des oxoanions, donne naissance, comme vu précédemment, à une nouvelle vague. Mais, lors du titrage, on assiste d'abord à une légère diminution d'intensité de la vague initiale puis à la soudaine disparition de cette dernière. De plus, dans le cas de la première génération (12 branches amidoferrocènes), la saturation a lieu pour un demi-équivalent d'$H_2PO_4^-$: on peut expliquer ce phénomène par la formation d'un assemblage dendritique dans lequel chaque anion est lié à deux branches amidoferrocènes. L'intensité de la nouvelle vague est beaucoup moins importante que celle de la première vague car la taille de l'espèce électroactive saturée en anions est plus grande que celle du dendrimère de départ. Un effet dendritique positif est remarqué pour la reconnaissance d'$H_2PO_4^-$ alors qu'un léger effet dendritique négatif est noté dans le cas de l'ATP^{2-}.

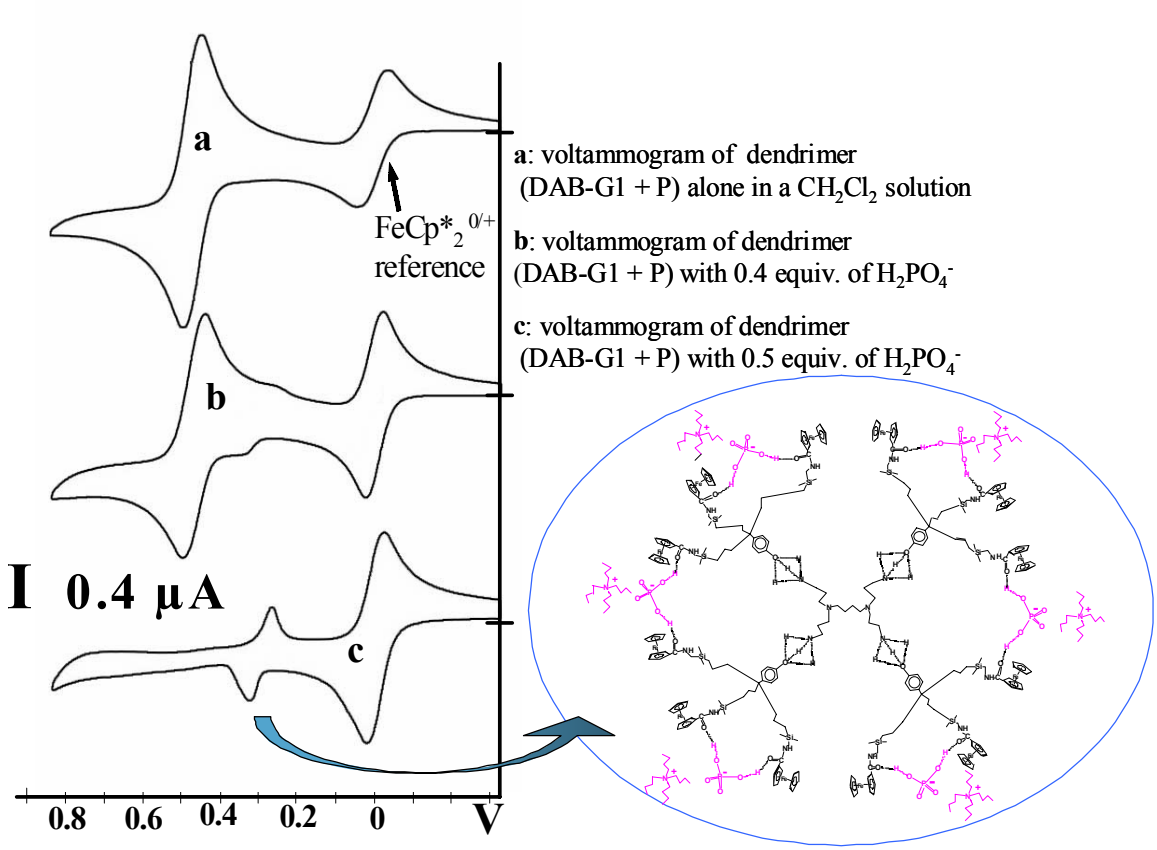

Titrage par voltampérométrie cyclique du dendrimère supramoléculaire de première génération dans le dichlorométhane avec $[Bu_4N][H_2PO_4]$.

III. Assemblages nanoscopiques de métallodendrons électroactifs et de nanoparticules d'or pour la reconnaissance du dihydrogénophosphate ($H_2PO_4^-$), de l'hydrogénosulfate (HSO_4^-) et de l'adénosine-5'-triphosphate (ATP^{2-})[3]

Nous avons synthétisé des dendrons thiol tri- et nonaferrocényles qui ont été utilisés pour la formation de nanoparticules d'or dendronisées. Cet assemblage a été fait par échange de ligands à partir de nanoparticules d'or stabilisées par des dodécanethiols mais aussi par synthèse directe de type Brust à partir d'un mélange 1/1 de dodécanethiols et de dendrons thiols. En fait, on peut considérer que les colloïdes dendronisés sont un nouveau type de dendrimères avec un cœur colloïdal d'or.

Dans un premier temps, des nanoparticules d'or contenant des dendrons trisilyl- et triamidoferrocényles ont été préparés par réaction d'échange de ligands. Ils portent respectivement cinq et trois dendrons, donc quinze et neuf fonctions ferrocényles. En voltampérométrie cyclique, ces colloïdes présentent une seule vague d'oxydoréduction correspondant au couple ferrocène/ferricinium car tous les groupements d'une même particule sont équivalents à l'échelle de temps électrochimique.

L'ajout de l'anion dihydrogénophosphate dans une solution de ces nanoparticules d'or dendronisées provoque l'apparition d'une nouvelle vague d'oxydoréduction à des potentiels plus négatifs: celle-ci matérialise une complexation forte de l'anion avec les fonctions silylferrocènes ou amidoferrocènes du colloïde. Plus on ajoute d'$H_2PO_4^-$, plus l'intensité de la nouvelle vague augmente et plus celle de la vague initiale diminue. Pour un équivalent d'anion par branche dendritique, on constate la disparition de la vague de départ, ce qui nous indique la saturation. Il est donc possible d'effectuer un titrage.

Cette reconnaissance d'$H_2PO_4^-$ est spécifique au phosphate car on ne note pas d'effet significatif avec les anions HSO_4^-, Cl^-, Br^- et NO_3^- alors que l'adénosine-5'-triphosphate (ATP^{2-}) est aussi reconnu mais avec un écart entre les deux vagues un peu moins important et une demi-stoechiométrie. En ce qui concerne l'hydrogénosulfate HSO_4^-, il n'y a pas d'effet avec le colloïde d'or portant des dendrons silylferrocènes. Par contre, pour la nanoparticule d'or contenant des dendrons amidoferrocènes, la reconnaissance d'HSO_4^- se traduit par un déplacement progressif de la vague initiale.

Dans un second temps, des nanoparticules d'or contenant des dendrons nonasilylferrocényles ont été préparés par synthèse directe en utilisant la méthode de type Brust. Ceci a permis d'optimiser le nombre de dendrons sur les nanoparticules d'or et d'obtenir

des colloïdes d'or comprenant jusqu'à 360 fonctions ferrocényles à leurs périphéries. Les mêmes études ont été effectuées sur ces nanoparticules d'or, concluant à un effet dendritique positif. Le mélange d'$H_2PO_4^-$ ou d' ATP^{2-} avec des anions chlorures et hydrogénosulfates, a démontré la sélectivité de reconnaissance des deux premiers anions par ces colloïdes dendronisés.

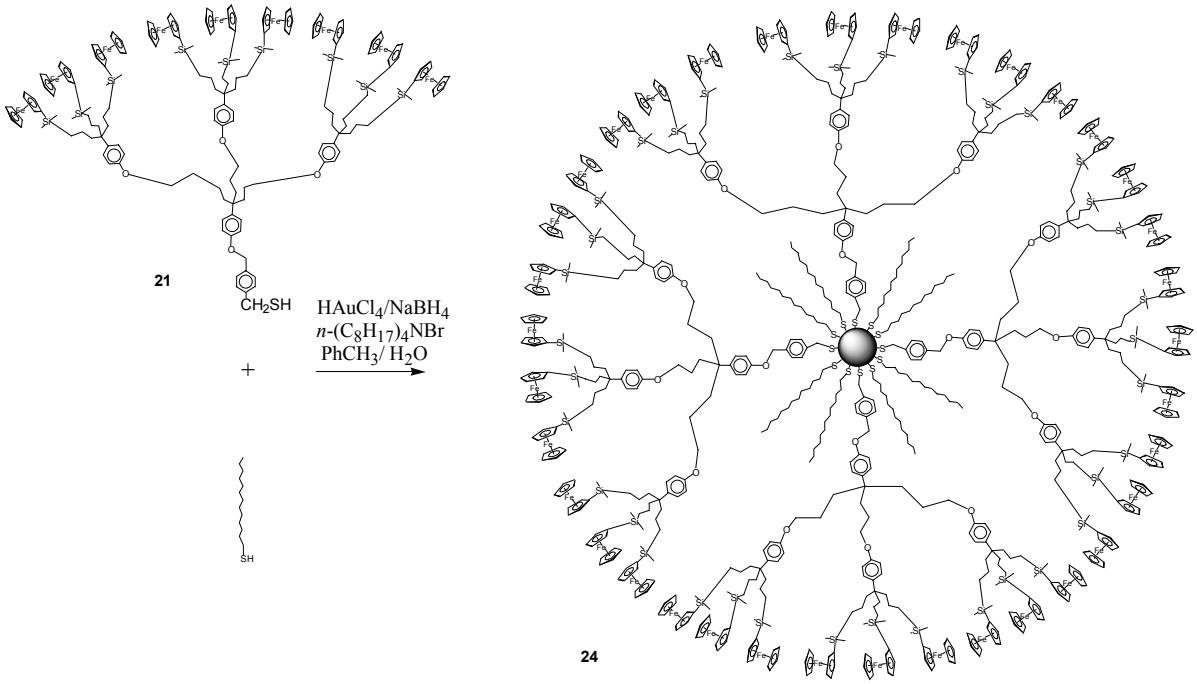

Synthèse directe d'un colloïde dendronisé à partir de dodécanethiols et de dendrons nonasilylferrocényles

Dans un troisième temps, des électrodes modifiées ont été préparées par trempage d'électrodes de platine dans des solutions de dichlorométhane contenant les nanoparticules d'or dendronisées et en effectuant des cycles de potentiels continus. Ces électrodes modifiées sont stables et permettent aussi la reconnaissance sélective d'$H_2PO_4^-$ ou d'ATP^{2-}. Mais l'avantage est leur recyclabilité car après titrage, on peut les laver sans perdre beaucoup de colloïdes adsorbés, puis les réutiliser.

Conclusion

Nous avons synthétisé trois types de dendrimères différents:

- ✓ des dendrimères à cœur colloïdal d'or (liaison de coordination),
- ✓ des dendrimères "classiques" (liaisons covalentes),
- ✓ des dendrimères supramoléculaires (liaisons hydrogène).

Leur étude pour la reconnaissance d'oxoanions, principalement d'$H_2PO_4^-$ et de l'ATP^{2-}, a montré quelques différences intéressantes:

- Les nanoparticules d'or dendronisées peuvent être utilisées pour la préparation d'électrodes modifiées recyclables.
- Les dendrimères possédant des fonctions ferrocényles perméthylées sont plus stables et permettent un titrage plus "propre" des anions.
- Les dendrimères formés par liaisons hydrogène possèdent des propriétes particulières de reconnaissance au cours du titrage des anions étudiés.

La facilité d'accès à des objets moléculaires avec un grand nombre de fonctions périphériques, offertes par les colloïdes d'or dendronisés et par les dendrimères supramoléculaires nous ouvre le champs à de nombreuses autres idées d'assemblages. Et la reconnaissance de l'ATP^{2-} nous invite à tendre encore plus vers la biologie et vers des études en milieu aqueux.

Listes des publications issues de la thèse:

1 a) J. Ruiz, M.-J. Ruiz Medel, M.-C. Daniel, J.-C. Blais, D. Astruc. Redox-Robust Pentamethylamidoferrocenyl Metallodendrimers that cleanly and selectively Recognize the $H_2PO_4^-$Anion. *Chem. Commun.*, **2003**, 464. b) M.-C. Daniel, J. Ruiz, J.-C. Blais, N. Daro, D. Astruc. Synthesis of Five Generations of Redox Stable Pentamethylamidoferrocenyl Dendrimers As Electrochemical Exoreceptors for the selective recognition of $H_2PO_4^-$, $HSO4^-$ and Adenosyl-5'-Triphosphate (ATP) Anions. Stereoelectronic and hydrophobic Role of the Cp Permethylation. *Chemistry, Eur. J.*, **2003**, 4371.

2 M.-C. Daniel, J. Ruiz, D. Astruc. Supramolecular H-Bonded Assemblies of Redox Active Metallodendrimers and Positive and Unusual Dendritic Effects on the Recognition of $H_2PO_4^-$. *J. Am. Chem. Soc*., **2003**, *125*, 1150.

3 a) M.-C. Daniel, J. Ruiz, S. Nlate, J. Palumbo, J.-C. Blais, D. Astruc. Gold nanoparticles containing redox active supramolecular dendrons that recognise $H_2PO_4^-$, *Chem. Commun.*, **2001**, 2000; b) M.-C. Daniel, J. Ruiz, S. Nlate, J.-C. Blais, D. Astruc. Nanoscopic Assemblies between Supramolecular Redox Active Metallodendronsand Gold Nanoparticles: synthesis, Characterisation and Selective Recognition of $H_2PO_4^-$, HSO_4^- and Adenosine-5'-Triphosphate (ATP^{2-}) Anions**,** *J. Am. Chem. Soc*., **2003**, *125*, 2617.

PERSPECTIVES

Dans cette thèse, les travaux réalisés ont permis de montrer une bonne reconnaissance des oxoanions par différents types d'assemblages dendritiques en voltammétrie cyclique. On peut imaginer de nombreuses perspectives en faisant varier les fonctions terminales, la structure des composés ou l'anion à détecter.

Un aspect important est l'approche biologique. En particulier, l'ATP, qui est une molécule biochimique, a pu être reconnue. Ceci nous encourage donc à poursuivre les recherches plus avant en direction de la reconnaissance d'anions biologiques. Si on considère que l'ATP, en tant que nucléotide, était un premier pas vers des entités plus complexes, on peut, par exemple, envisager d'étudier le comportement des systèmes dendritiques envers des brins d'ADN. Dans ce cas, il faut viser un travail en milieu aqueux pour reproduire au mieux le milieu naturel, ce qui est actuellement un véritable enjeu. Une approche par les dendrimères ou par les colloïdes va donc d'abord nécessiter la synthèse de récepteurs hydrosolubles. Il nous faudra aussi optimiser les interactions récepteur-anion car les constantes d'association chutent largement quand on passe en milieu aqueux. Une manière de répondre à ces exigences est la préparation de composés polycationiques, comportant par exemple, des ammoniums.

Outre la voltammétrie cyclique, d'autres outils peuvent être utilisés pour visualiser la reconnaissance. On peut penser, entre autre, à la spectroscopie UV / visible. Cette dernière demande bien sûr un capteur possédant un spectre UV / visible avec une bande significative, telle que, par exemple, celle d'une fonction carbonylée. Les colloïdes d'or de diamètre supérieur ou égal à 5 nm présentent aussi une bande plasmon très intéressante qui évolue suivant l'environnement.

La reconnaissance d'anions jouant un rôle important dans l'environnement pourra aussi ëtre considérée (NO_3^-, TcO_4^-, etc…).

Résumé

Nous avons synthétisé trois types de dendrimères différents:

- ✓ des dendrimères à cœur colloïdal d'or (liaisons de coordination),
- ✓ des dendrimères "classiques" (liaisons covalentes),
- ✓ des dendrimères supramoléculaires (liaisons hydrogène).

Leur étude pour la reconnaissance d'oxoanions, principalement d'$H_2PO_4^-$ et de l'ATP^{2-}, a montré quelques différences intéressantes:

- ➢ Les nanoparticules d'or dendronisées peuvent être utilisées pour la préparation d'électrodes modifiées recyclables.
- ➢ Les dendrimères possédant des fonctions ferrocényles perméthylées sont plus stables et permettent un titrage plus "propre" des anions.
- ➢ Les dendrimères formés par liaisons hydrogène possèdent des propriétés particulières de reconnaissance au cours du titrage des anions étudiés.

La facilité d'accès à des objets moléculaires avec un grand nombre de fonctions périphériques, offertes par les colloïdes d'or dendronisés et par les dendrimères supramoléculaires nous ouvre le champs à de nombreuses autres idées d'assemblages. Et la reconnaissance de l'ATP^{2-} nous invite à tendre encore plus vers la biologie et vers des études en milieu aqueux.

Mots clés: métallodendrimères, nanoparticules d'or, reconnaissance anionique, ATP, voltammétrie cyclique, sondes rédox, ferrocènes

ANNEXES

ANNEXE 1:

NANO-SCALE METALLODENDRITIC COMPLEXES
IN ELECTRON-TRANSFER PROCESSES
AND CATALYSIS

Nano-Scale Metallodendritic Complexes in Electron-Transfer Processes and Catalysis

Didier Astruc,*[a] *Jean-Claude Blais*,[b] *Marie-Christine Daniel*,[a] *Victor Martinez*,[a] *Sylvain Nlate*,[a] *Jaime Ruiz*[a]

[a]Groupe Nanosciences Moléculaires et Catalyse, LCOO, UMR CNRS N° 5802, Université Bordeaux I, 33405 Talence Cedex., France
E-mail : d.astruc@lcoo.u-bordeaux1.fr
[b]LCSOB, UMR CNRS N° 7613, Université Paris VI, 75252 Paris, France

Summary: Nano-sized metallodendrimers in which the equivalent metal fragments are located at the periphery can be assembled covalently, by H-bonding (supramolecular) or onto dendronized nanoparticles. They can be used as electron-reservoirs, i.e. molecular batteries, redox catalysts and sensors for the recognition of biologically relevant anions. They can also be deposited on metal surfaces or electrodes, which optimizes their use as recoverable sensors.

Keywords: catalysis; dendrimers, nanocomposites; sensors; transition metal chemistry

Content

Introduction

Metallodendrimers [1-10] with redox stability are electron-reservoir systems that should prove useful as molecular batteries, catalysts and sensors. With a low polydispersity, their molecular definition is much more precise than that of organometallic polymers, yet they can be very large. Moreover, their use in molecular electronics is promising in the context of nano-technology.

 CCC 1022-1360/00/$ 17,50+.50/0

Ferrocenyl dendrimers are now a well-spread field of dendrimer research to which we have contributed.[11-14] In this chapter, we review our strategy as well as electron-transfer processes in other metallodendrimers involving monomeric electron-reservoir iron-sandwich complexes.

Organo-Iron Syntheses of Dendritic Cores, Dendrons and Large Dendrimers

In the robust, very easily accessible cationic complexes [FeCp(arene)][PF_6)], the benzylic protons are more acidic than in the free arene because of the electron-withdrawing character of the 12-electron $CpFe^+$ moiety. For instance, [FeCp(C_6Me_6)][PF_6)] is more acidic by 15 p*K*a units (p*K*a = 28 in DMSO) than in the corresponding free arene (p*K*a = 43 in DMSO). As a result, these complexes are much more easily deprotonated than the free arene. [15,16] This key proton-reservoir property led us to synthesize stars and dendrimers in an easy way. [15] Indeed, reaction of [FeCp(C_6Me_6)][PF_6)],[17-19] with excess KOH (or *t*-BuOK) in THF or DME and excess methyl iodide, alkyl iodide, allyl bromide or benzylbromide result in the one-pot hexasubstitution (Scheme 1a).[20-22] With allyl bromide (or iodide) in DME, the hexaallylated complex has also been easily isolated and its X-ray crystal structure determined. With alkyliodides, the reaction using *t*-BuOK only leads to dehalogenation of the alkyl iodide giving the terminal olefin. Thus, one must use KOH, and the reactions with various alkyl iodides (even long-chain ones) were shown to work very well with this reagent to give the hexaalkylated Fe^{II}-centered complexes. The hexa-alkylation was also performed with alkyl iodides containing functional groups at the alkyl chain termini. [23] For instance, 1-ferrocenylbutyliodide reacts nicely to give the hexaferrocene star containing the $CpFe^+$ center.[24] The reaction with excess benzylbromide, [20,24] *p*-alkoxybenzylbromide [24] or *p*-bromobenzylbromide [24] only gives the hexabenzylated, hexa-*p*-alkoxybenzylated or hexa *p*-bromobenzylated complex as the ultimate reaction product. Cleavage of the methyl group in the *p*.methoxybenzyl derivatives synthesized in this way yields the hexaphenolate stars that could be combined with halogen containing organometallic compounds.[24b,c]

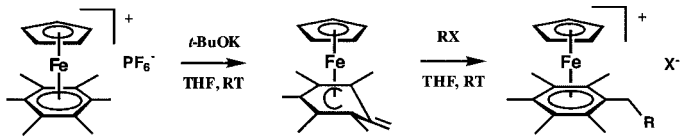

RX = CH_3I, $PhCH_2Br$, $SiMe_3Cl$, PPh_2Cl, $FeCp(CO)_2Br$ (also CO_2 and metal carbonyls)

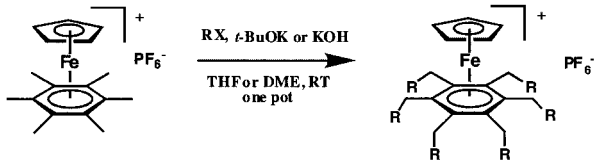

R = CH_3, $(CH_2)_nCH_3$, $(CH_2)_4Fc$ (X = I), CH_2Ph, p-CH_2PhOR', $CH_2CH{=}CH_2$,(X = Br)

Scheme 1: Deprotonation of $[FeCp(\eta^6\text{-}C_6Me_6)][PF_6]$ followed by reactions with electrophiles (top) and one-pot hexafunctionalization of this complex under ambient conditions (bottom). The top reaction illustrates the mechanism of the bottom one.

It is remarkable that the allyl group (as allyl bromide or iodide) is the only one leading to complete double branching of the C_6Me_6 complex. $CpFe^+$-induced dodecaallylation of C_6Me_6 indeed gives the extremely bulky dodeca-allylation product [26] that can be reached when the reaction is prolonged for two weeks at 40°C. The chains are blocked in a directionality that cannot convert into its enantiomer and makes the metal complex chiral. Both the hexa- and dodeca-allylation reactions are well controlled.

Alkynyl halides cannot be used in the $CpFe^+$-induced hexafunctionalization reaction, but alkynyl substituents can be introduced from the hexa-alkene derivative by bromination followed by dehydrohalogenation of the dodecabromo compound.[27] The hexa-alkene is also an excellent starting point for further syntheses, especially using hydroelementation reactions. Hydrosilylation reactions catalyzed by Speir's reagent led to long-chain hexasilanes [28] and hydrometallations were also achieved using $[ZrCp_2(H)(Cl)]$.[29] The hexa-zirconium compound obtained is an intermediate for the synthesis of the hexa-iodo derivative.[29] One of most useful

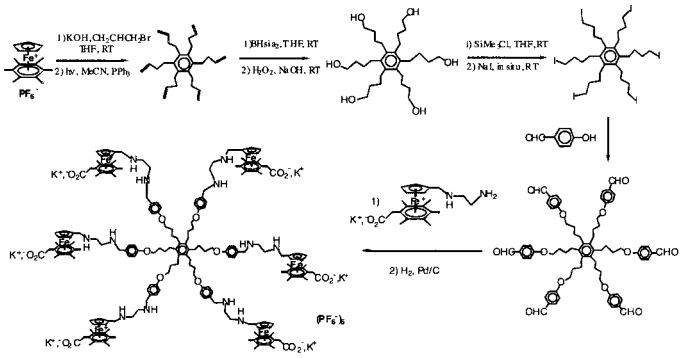

Scheme 2: $CpFe^+$-induced hexa-allylation of C_6Me_6 and subsequent hexafunctionalization of the aromatic stars with the heterodifunctional, water soluble organometallic redox catalyst (bottom) for the cathodic reduction of nitrates and nitrites to ammonia in water).

hydroelementation reactions of the hexabutenyl derivatives is the hydroboration leading to the hexaborane. The latter is oxidized to the hexa-ol using H_2O_2 under basic condition.[21] This chemistry can be carried out on the iron complex or alternatively on the free hexa-alkene which may be liberated from the metal by photolysis in CH_2Cl_2 or MeCN using visible light.[20] The polyol stars and dendrimers can be transformed into mesilates and iodo derivatives that are useful for further functionalization. The hexa-ol is indeed the best source of hexa-iodo derivative either using HI in acetic acid or even better by trimethylsilylation using $SiMe_3Cl$ followed by iodination using NaI.[30] Williamson coupling reactions between the hexa-ol and 4-bromomethylpyridine or -polypyridine led to hexa-pyridine and hexa-polypyridine and to their ruthenium complexes (31,32). This hexa-iodo star was condensed with *p*-hydroxybenzaldehyde to give an hexa-benzaldehyde star, which could further react with substrates bearing a primary amino group. Indeed, this reaction yielded a water-soluble hexametallic redox catalysts which was active in the electroreduction of nitrate and nitrite to ammonia in basic aqueous solution, *vide infra*.[33-35]

If the hexafunctionalization of hexamethylbenzene leads to stars, the octafunctionalization of durene leads to dendritic cores. The first of these octa-alkylation reactions was reported as early

as 1982, and led to a primitive dendritic core containing a metal-sandwich unit.[20] Thus, as the hexafunctionalization, this reaction is very specific. Two hydrogen atoms of each methyl group are now replaced by two methyl, allyl or benzyl groups.[26] Applications to the synthesis of dendrimers containing 8 [36] or 24 redox-active groups has recently been reported. Double branching, *i.e.* replacement of two out of three hydrogen atoms by two groups on each methyl substituent of an aromatic ligand coordinated to an activating cationic group CpM^+ in an 18-electron complex is also easily obtained in the pentamethylcyclopentadienyl ligand (in pentamethyl cobaltocenium [37] and in penta- [38] and decamethylrhodocenium [39]). The interconversion of the two directionalities of decafunctionalized ligands coordinated to $CpCo^+$ or $CpRh^+$ whose could be observed by ^1H NMR for the decaisopropyl- and decaisopentyl cyclopentadienyl cobalt and rhodium complexes [37-39] (Scheme 3).

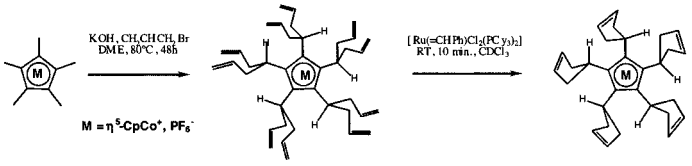

Scheme 3: Deca-allylation of 1,2,3,4,5-pentamethylcobaltocenium in a one-pot reaction consisting in 10 deprotonation-allylation sequences (steric constraints inhibit further reaction, and the 10 groups introduced are self-organized according to a single directionality) and follow-up RCM of the deca-allylated complex.

In all the above examples, the polybranching reaction of arene ligands was limited by the steric bulk. In the toluene and mesitylene ligands, the deprotonation-allylation reactions are no longer restricted by the neighborhood of other alkyl groups. All the benzylic protons, *i.e.* three per benzylic carbon, can be replaced by methyl or allyl groups in the one-pot iterative methylation or allylation reactions.[30] Thus, the toluene complex can be triallylated and the resulting tripod can be disymetrized by stoichiometric [40] or catalytic reaction [41] with transition metals shown in Scheme 18. The metathesis reaction, in particular, is complete in 5 min. at room temperature using the first-generation Grubb's catalyst $[Ru(=CHPh)Cl_2(PCy_2)_2]$ [2] with many polyallylated

complexes $[FeCp(arene)]^+$ described above as well as to the decaallylated cobalt complex.[41] The reaction is very selective and terminal double bonds remain unreacted using this catalyst at room temperature.

The mesitylene complex can be nonaallylated, these reactions being carried out smoothly at room temperature in the presence of excess KOH and allyl bromide. The nonaallyl complex was photolyzed using visible light to remove the metal group $CpFe^+$, then hydroborated using 9-BBN, and the nonaborane was oxidized using H_2O_2/OH^- to the nona-ol.[30]

The triple branching reaction being very straightforward, we sought a more sophisticated version compatible with a functional group in the para position of the tripod in order to open the access to a functional dendron. Serendipitously, we found that KOH or *t*-BuOK easily cleaved the iron complexes of aromatic ethers under very mild conditions. The activating $CpFe^+$ group again induces this reaction, which is very general for a variety of aromatic ether complexes (42,43).

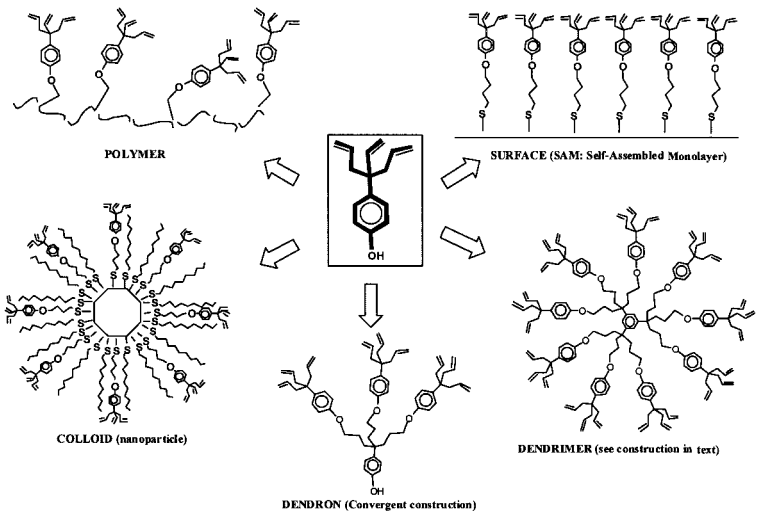

Scheme 4: Example of the linkage of the phenoltriallyl dendron to various nanostructures.

Since this cleavage reaction is carried out with the same reagent and solvent as the one used in the trialkylation reaction (ideally *t*-BuOK in THF), we have attempted to perform both reactions in a well-defined order (triallylation before ether cleavage) in a one-pot reaction. Indeed, this works out well and the $CpFe^{II}$ complex of the phenol tripod was made in 50% yield in this way. This complex can be photolyzed in the usual way using visible light, which yields the free phenol tripod. However, we have also further investigated the possibility to obtain the cleavage of the arene ligand *in situ* at the end of the phenol tripod construction; *t*-BuOK is a reductant when it cannot perform other reactions. Since the two important reactions are over, then comes the third role of *t*-BuOK: single-electron reductant. Reasoning in this way turned out to be correct: the cleavage of the arene intervenes rapidly at the 19-electron stage because 19-electron complexes of this kind are not stable with an heteroatom located in exocyclic position (most probably because the heteroatom coordinates to the metal from the labile 19-electron structure). After optimizing the reaction conditions, a 50%-yield of free phenol dendron from the ethoxytoluene complex could be reproducibly obtained,[44,45] and this reaction is now currently used in our laboratory to synthesize this very useful dendron as a starting material.

This phenoltriallyl dendron has been functionalized at both the phenolic and allylic positions. For instance, the dendron can be bound, after suitable molecular engineering, to the branches of a phenolic-protected dendron (convergent construction) onto stars and dendritic cores (divergent construction), nonaparticles, surfaces and polymers. An example is provided by the $CpFe^{+}$-induced hexafunctionalization by a phenol-nonaallyl dendron (prepared according to such a convergent synthesis) that was functionalized in phenolic position by a tail terminated by a benzylbromide group. This type of strategy allows direct access to large dendrimers by simply using the $CpFe^{+}$-induced hexafunctionalization reaction that gives hexa-branch stars with linear organic halides.

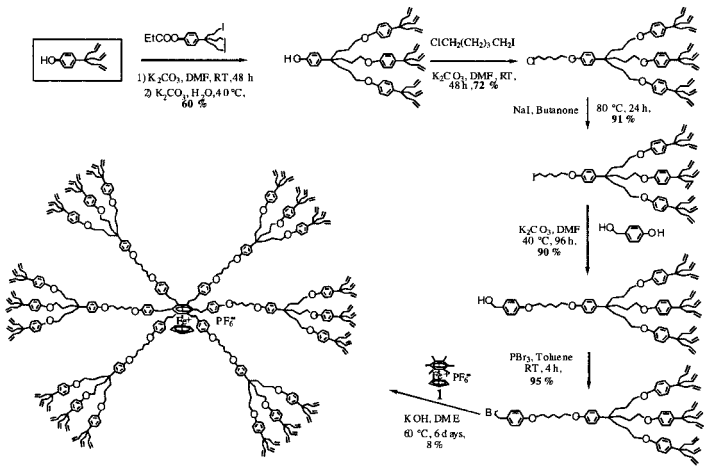

Scheme 5: $CpFe^+$-induced hexabenzylation of C_6Me_6 applied to direct convergent dendrimer synthesis of a 54-allyl dendrimer.

Decoration of Dendrimers with Redox-Active Groups: Towards Molecular Batteries

The functionalization of the three allyl chains of the phenol dendron could be achieved by hydrosilylation reaction catalyzed by the Karsted catalyst.[46] Indeed, it is very interesting that there is no need to protect the phenol group before performing these reactions. For instance, catalyzed hydrosilylation using ferrocenyldimethylsilane gives a high yield of the triferrocenyl dendron $HOp\text{-}C_6H_4C(CH_2CH_2CH_2SiMe_2Fc)_3$ that is easily purified by column chromatography.[46,47] Protection of the phenol dendron using propionyliodide gave the phenolate ester which was hydroborated. Oxidation of the triborane using H_2O_2/OH^- gave the triol, then reaction with $SiMe_3Cl$ gave the tris-silyl derivative. Reaction with NaI yielded the tri-iodo compound, and reaction with the tri-ferrocenyl dendron provided the nona-ferrocenyl dendron that was deprotected using K_2CO_3 in DMF. The nona-ferrocenyl dendron was allowed to react with hexakis(bromomethyl)benzene, which gave the 54-ferrocenyl dendrimer. This convergent synthesis is clean and the 54-ferrocenyl dendrimer gave correct analytical data, although a mass spectrum could not be obtained (Scheme 6).This approach is somewhat limited, however, since

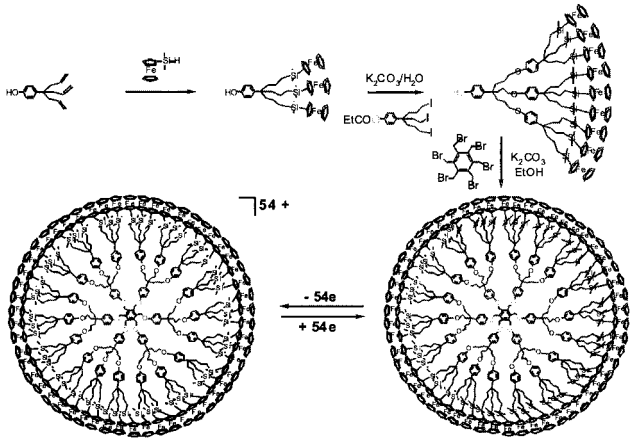

Scheme 6: Convergent synthesis of a redox-robust 54-silylferrocenyl dendrimer.

larger dendrons, which one would like to synthesize in this way, cannot be made because dehydrohalogenation becomes faster than nucleophilic substitution of the iodo by phenolate for bulkier higher generations of dendrons. Although this problem might be overcome by modifying the iodo branch in such a way that there would be no hydrogens in β positions, the condensation of higher dendrons onto a core would become tedious or impossible for steric reasons. This well known inconvenient is intrinsic to the convergent dendritic synthesis. On the other hand, divergent syntheses are not marred by such a problem since additional generations and terminal groups are added at the periphery of the dendrimer. The limit is that indicated by De Gennes, *i. e.* the steric congestion encountered at a generation where the peripheral branches can no longer by divided. Another obvious limit intervenes if the molecular objects added onto the termini of the branches are large and interfere with one another. We have developed a divergent synthesis of polyallyl dendrimers indicated on *Scheme 20* whereby each generation consists in hydroboration, oxidation of the borane to the alcohol, formation of the mesylate, and reaction of the phenol dendron with the mesylate. This strategy has allowed us to synthesize dendrimers of generation 0, 1, 2 and 3 with respectively 9 (G_0), 27 (G_1), 81 (G_2) and 243 branches (G_3) (Scheme 7 and Chart 1).

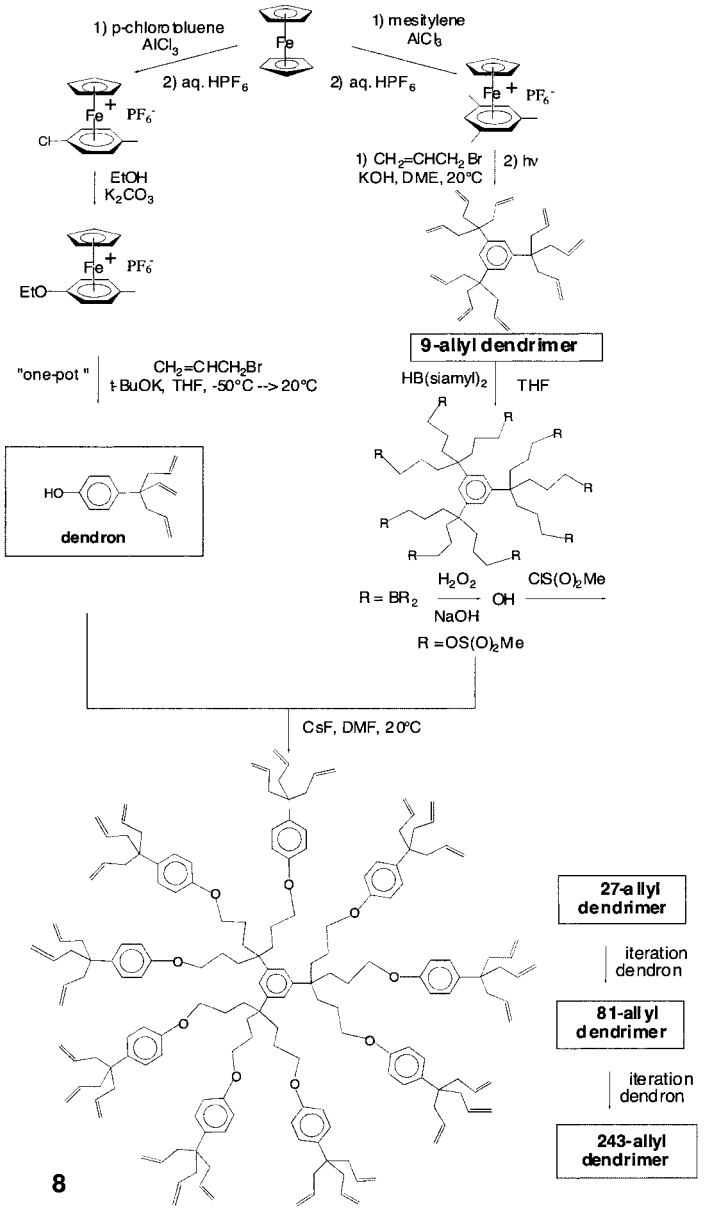

Scheme 7: Strategy for the construction of large dendrimers starting from ferrocene.

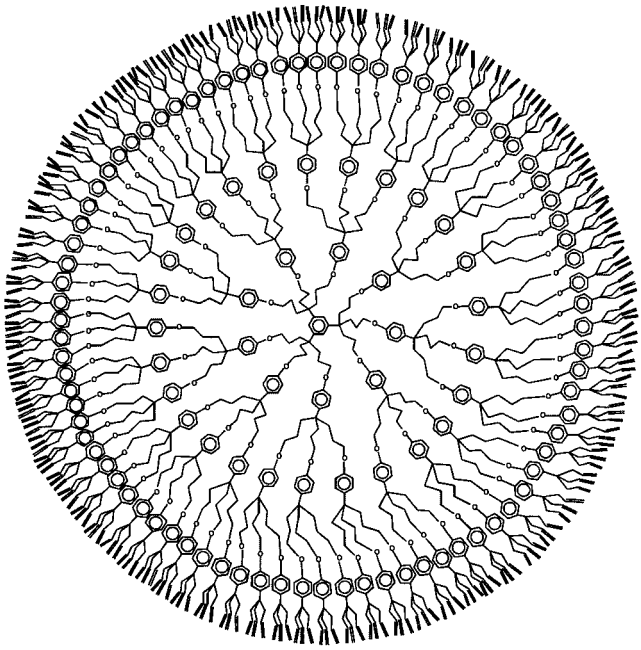

Chart 1: 243-allyl dendrimer (3rd generation, see the construction on Scheme 7).

The MALDI TOF mass spectrum of the 27-allyl dendrimer only shows the molecular peak with only traces of side product. That of the 81-allyl shows a dominant molecular peak, but also important side products resulting from incomplete branching. That of the 243-allyl could not be obtained possibly signifying that this dendrimer is polydisperse (correct ^{1}H and ^{13}C NMR spectra were obtained, however, indicating that the ultimate reactions had proceeded to completion). This dendrimer was soluble which indicated that this generation is not the last one, which might be reached. Larger dendrimers have recently been synthesized using a slightly diferent strategy. The ferrocenylsilylation of all these polyallyl dendrimers was carried out using ferrocenyldimethylsilane in ether or toluene and was catalyzed by the Karsted catalyst [48,49] at 40-45°C. The reactions were complete after two or three days except for the ferrocenylsilylation

of 243-allyl that required a reaction time of one weeks indicating some degree of steric congestion (Scheme 8).

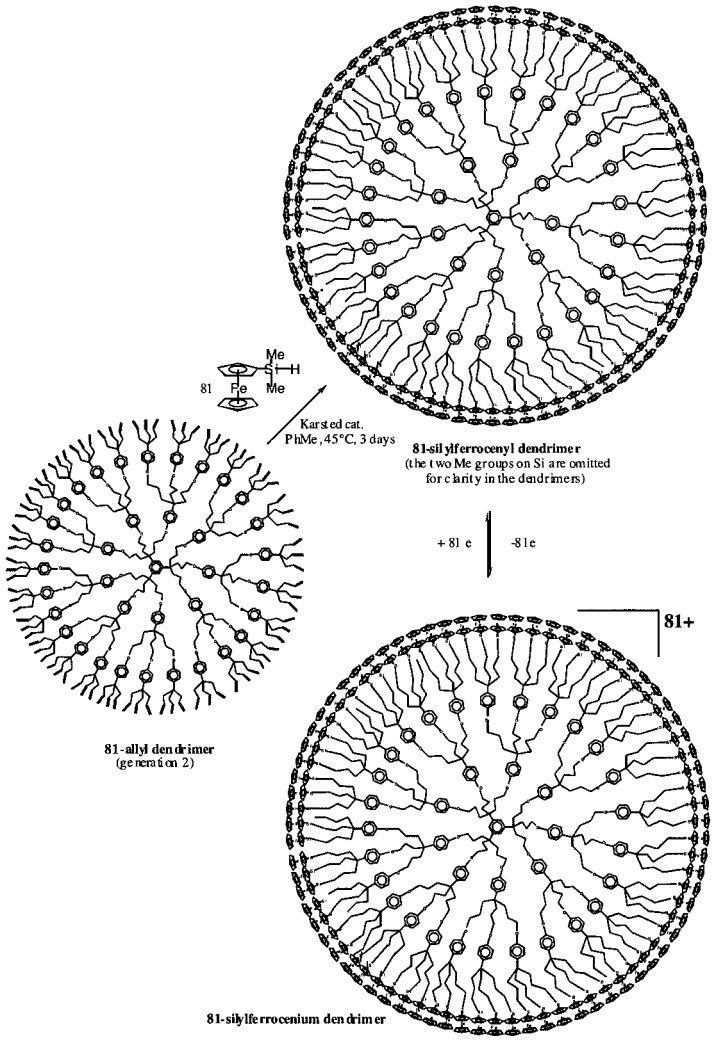

Scheme 8: Ferrocenylsilylation of the polyallyl dendrimers synthesized. Example of the 2nd generation 81-allyl dendrimer.

The ^{1}H and ^{13}C spectra indicated the absence of regioisomer. The solubility in pentane decreased from good for the 9-Fc dendrimer to low for the 27-Fc dendrimer and nil for the superior dendrimers, but the solubility in ether remained good for all the ferrocenyl dendrimers. Likewise, the retention times on plate or column chromatography increased with generation and no migration was observed for the "243-Fc" dendrimer. The silane use here, $HSi(Fc)Me_2Cl$, reported by Pannel and Sharma,[50] was already used by Jutzi [51] to synthesize the decaferrocenyl dendrimer $[Fe(CCH_2CH_2SiMe_2Fc)_{10}]$ (with Fc = ferrocenyl) from deca-allylferrocene.

The cyclic voltammetry of all the ferrocenyl dendrimers on Pt anode shows that all the ferrocenyl centers are equivalent and only one wave was observed. It was possible to avoid adsorption using even CH_2Cl_2 for the small ferrocenyl dendrimers, but it was required to use MeCN for the medium size ones (27-Fc, 54-Fc and 81-Fc). Finally, adsorption was not avoided even with MeCN for the "243-Fc" dendrimer. From the intensity of the wave, the number of ferrocenyl units could be estimated using the Anson-Bard equation,[52] and the number found were within 5% of the branch numbers except for the "243-Fc"dendrimer, for which the experimental number was too high (250) because of the adsorption.

The first polyferrocenium dendrimers reported by our group in 1994 and characterized *inter alia* by Mössbauer spectroscopy (a "quantitative" technique) were mixed valence Fe^{II}/Fe^{III} complexes.[23] Since then, we have been seeking to synthesize larger ferrocenyldendrimers, which could also withstand oxidation to their ferrocenium analogues. The syntheses of amidoferrocene dendrimers were reported five years ago simultaneously by our group [11,53] and the Madrid group using different cores.[54,55] In our reports, we were able to show the use of these metallodendrimers as redox sensors for the recognition of oxo-anions, with remarkable positive dendritic effects when the generation increased. The amidoferrocenyl dendrimers are not the best candidates for a stable redox activity on the synthetic scale, however, and thus even less so for molecular batteries. Indeed, although they give fully reversible cyclic voltammetry waves, it is known that ferrocenium derivatives bearing an electron-withdrawing substituent are at least fragile, if stable at all. This inconvenient is probably enhanced in the dendritic structures because

of the steric effect which forces ferrocenium groups to encounter one another more easily than as monomers. Thus, we have oxidized our silylferrocenyl dendrimers using $[NO][PF_6]$ in CH_2Cl_2 and obtained stable polyferrocenium dendrimers as dark-blue precipitates, as expected from the known characteristic color of ferrocenium itself. These polyferrocenium dendrimers were reduced back to soluble orange polyferrocenyl dendrimers using decamethylferrocene as the reductant.[56] No decomposition was observed either in the oxidation or in the reduction reactions which were very clean, and this redox cycle could be achieved in quantitative yield even with the "243-ferrocenyl" dendrimer. The zero-field Mössbauer spectrum of the 243-ferrocenium dendrimer (Figure 1) showed a single line corresponding to the expected spectrum known for ferrocenium itself,[57] confirming its electronic structure. Thus, these polyferrocenyl dendrimers are molecular batteries, which could be used, in specific devices. Indeed, as large as they may be, they transfer a very large number of electrons rapidly and "simultaneously" with the electrode. By "simultaneously", we mean that, visually, the cyclic voltammogram looks as if it were that of a monoelectronic wave. One must question the notion of the isopotential for the many ferrocenyl units at the periphery of a dendrimer. In theory, all the standard potentials of the n ferrocenyl units of a single dendrimer are distinct even if all of them are equivalent and independent. This situation arises since the charge of the overall dendrimer molecule increases by one unit of charge every time one of its ferrocenyl units is oxidized to ferrocenium. The next single-electron oxidation is more difficult than the preceding one since, the dendritic molecule having one more unit of positive charge, it is more difficult to oxidize because of the increased electrostatic factor. Thus, the potentials of the n redox units are statistically distributed around an average standard potential centered at the average potential (Gaussian distribution).[52] In practice, the situation is complicated by the fact that the dendritic molecule, as large as it may be, is rotating much more rapidly than the usual electrochemical time scales.[58,59] Under these conditions, all the potentials are probably averaged. The fast rotation is also responsible for the fact that all the ferrocenyl units come close to the electrode within the electrochemical time scale. Consequently, there is no slowing down of the electron transfer due to long distance from the electrode even in large dendrimers. Indeed, the waves of the ferrocenyl dendrimers always appear fully electrochemically

reversible indicating fast electron transfer.

The ferrocenyl dendrimers also adsorb readily on electrodes, a phenomenon already well known with various kinds of polymers.[60] When polymers contain redox centers, the adsorbed polymer have long been shown to disclose a redox wave for which the cathodic and anodic waves are located at exactly the same potential and the intensity of each wave is proportional to scan rate. Continuous cycling shows the stability of the adsorption of the electrode modified in this way. The ferrocenyl dendrimers described show this phenomenon as expected. The stability of the electrode modified by soaking the Pt electrode in a CH_2Cl_2 solution containing the ferrocenyl dendrimer and cyclic scanning between the ferrocenyl and ferrocenium regions is all the better as the ferrocenyl dendrimer is larger. For instance, in the case of the 9-ferrocenyl dendrimer, scanning twenty times is necessary before obtaining a constant intensity, and this intensity is weak. With the 27-, 54-, 81-, and 243-ferrocenyl dendrimers, only approximately ten cyclic scans are necessary before obtaining a constant wave, and the intensity is much larger. When such derivatized electrodes are washed with CH_2Cl_2 and re-used with a fresh, dendrimer-free CH_2Cl_2 solution, the cyclic voltammogram is obtained with $\Delta E_p = 0$. Other characteristic features are the linear relationship between the intensity and scan rate and the constant stability after cycling many times with no sign of diminished intensity (Figure 1).

Under these conditions, one may note that the argument of the fast rotation of the dendritic molecule to bring all the redox centers in turn close to the electrode does not hold for modified electrodes. Some redox centers must be close to the electrode and some must be far. It is probable that a hoping mechanism in the solid state is responsible for fast electron transfer and for averaging all the potentials of the different ferrocenyl groups of a single dendritic molecule around a mean value. The proximity of the ferrocenyl groups at the periphery of the dendrimer is a key factor allowing this hoping to occur since it is known that electron transfer with redox sites which are remote or buried inside a molecular framework is slow, if at all observable.[61-67]

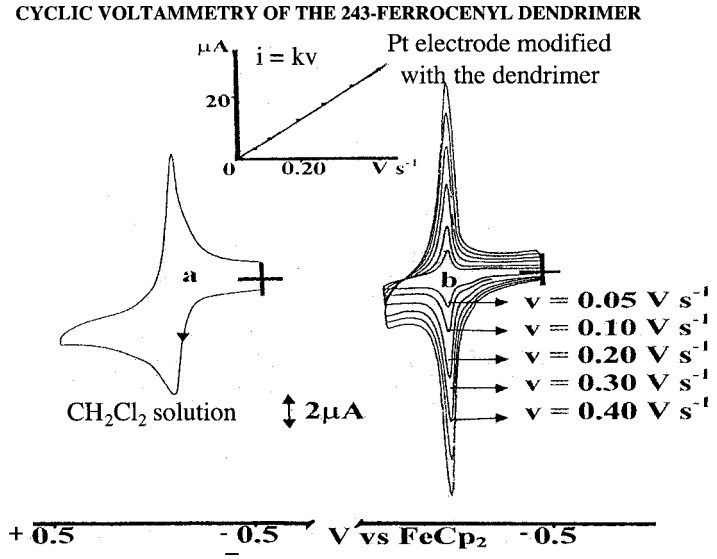

Figure 1: Cyclic voltammogram of the 243-ferrocenyl dendrimer ("243-Fc") in CH_2Cl_2 solution containing 0.1M [n-Bu_4N][PF_6]: a) in solution (10-4 M) at 100 mV. s-1 on Pt anode; b) Pt anode modified with "243-Fc" at various scan rates, dendrimer-free clear CH_2Cl_2 solution (inset: intensity as a function of scan rate: the linearity shows the expected behavior of a modified electrode with a fully adsorbed dendrimer).

Ferrocenes and ferrocenyl dendrimers are poor reductants. On the other hand, the complexes $[Fe(\eta^5\text{-}C_5R_5)(\eta^6\text{-}C_6Me_6)]^{2+/+/0}$ (R = H or Me) have been shown to be efficient for various stoichiometric and catalytic electron-transfer reactions.[16,68] The covalent linkage of this sandwich complex to the Cp ligand by means of a chlorocarbonyl substituent leads, upon reaction with dendritic polyamines, to soluble Fe^{II} metallodendrimers. Moreover, these Fe^{II} metallodendrimers can be reduced to Fe^{I} by $[Fe^{I}Cp(\eta^6\text{-}C_6Me_6)]$, **1**. Reduction of the monomeric model $[Fe^{II}(\eta^5\text{-}C_5H_4CONH\text{-}n\text{-}Pr)(\eta^6\text{-}C_6Me_6)][PF_6]$ by Na/Hg in THF (RT) gives the deep-blue-green, thermally stable 19-electron complex $[Fe^{I}(\eta^5\text{-}C_5H_4CONH\text{-}n\text{-}Pr)(\eta^6\text{-}C_6Me_6)]$ that shows the classic rhombic distorsion of the Fe^{I} sandwich family, observable by EPR in frozen THF at 77K (3 g values around 2).[69] Given this stability, we carried out the same reaction of $[Fe^{II}(\eta^5\text{-}C_5H_4COCl)(\eta^6\text{-}$

C_6Me_6)][PF_6] with the commercial polypropyleneimine dendrimer of generation 5 (64 amino termini) in MeCN/CH_2Cl_2: 2/1 in the presence of NEt_3. The polycationic metallodendrimer DAB *dendr*-64--NHCOCpFe^{II}(η^6-C_6Me_6), was obtained as the PF_6^- salt, soluble in MeCN and DMF (Equation 1).

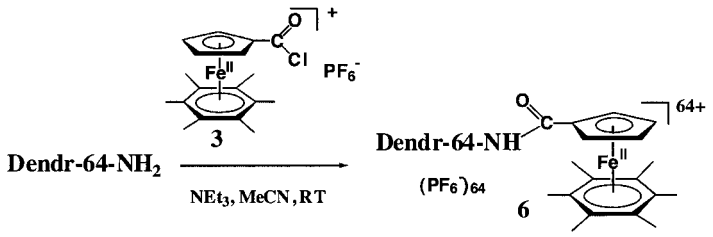

Equation 1: Covalent linkage of the complex [FeCpCOCl(η^6-C_6Me_6)][PF_6] to the DSM polyamine dendrimer of generation 5 (64 branches). Example of the 64-NH_2 dendrimer (generation 5).

This dendritic complex was characterized by ^1H and ^{13}C NMR and IR spectroscopies and cyclovoltammetry (a single reversible wave in DMF, at $E_{1/2}$ = -1.84 V *vs.* $FeCp_2^{0/+}$; ΔE = 70 mV). Attempts to reduce it with the classic reductants that reduce monomeric complexes [Fe^{II}(η^5-Cp)(η^6-arene)][PF_6] such as Na sand, Na/Hg or $LiAlH_4$ in THF or DME failed due to the insolubility of both the metallodendrimer and the reductant in the required solvents. The only successful reductant was the parent 19-electron complex [Fe^{I}Cp(η^6-C_6Me_6)] [70,71] (in pentane or THF) that reduced the metallodendrimer in MeCN at –30°C to the neutral, deep-green-blue 19-electron Fe^{I} dendrimer **6** in a few minutes (Equation 2).[72]

The exoergonicity of this electron-transfer reaction is 0.16 V, which is due to the electron-withdrawing effect of the juxta-cyclic carbonyl group on the Cp ring that lowers the reduction potential of the metallodendrimer as compared to that [Fe^{I}Cp(η^6-C_6Me_6)]. Although the Fe^{I} dendrimer decomposes a 0°C, it was also characterized by its EPR spectrum at 10 K confirming, as the deep-blue-green color, the Fe^{I} -sandwich structure analogous to that of the monomeric model.

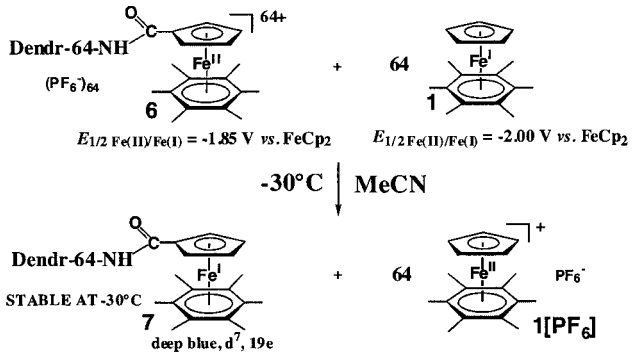

Equation 2: Exergonic reduction of the cationic Fe^{II} dendritic sandwich groups by the parent 19-electron complex [FeICp(η^6-C_6Me_6)] to the Fe^{I} dendrimer complex.

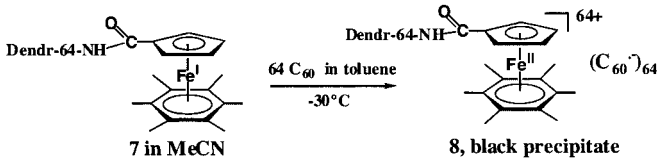

Equation 3: Dendr-64-NHCOCpFe(C_6Me_6)$^{64+}$, 64 $C_{60}^{\cdot-}$ resulting from the reaction of the 64-Fe^{I} dendrimer with C_{60} in MeCN/toluene at –30°C yielding the 64-Fe^{II}-C_{60} - dendrimer with EPR spectrum (bottom, right) in MeCN at 10K and Mössbauer spectrum at 77K (bottom, left) of the latter.

Contrary to the case of [Fe^{I}Cp(η^6-C_6Me_6)],[69] however, it was not possible to record the EPR spectrum of the solution of the Fe^{I} dendrimer above 10 K. This is presumably due to the intramolecular relaxation among the peripheral Fe^{I} sandwich units. The intermolecular version of this relaxation effect is known to preclude observation of the spectrum of monomeric Fe^{I} sandwich complexes in the solid state above 4K and in solution above 77K.[69] This acetonitrile solution of the 64-Fe^{I} dendrimer was used for the reaction with C_{60}, the stoichiometry being Fe^{I}/C_{60}: 1/1 (64 C_{60} *per* dendrimer). Upon reaction with a toluene solution of C_{60}, the deep-blue-

green color of the Fe^{I} dendrimer disappeared, leaving a yellow solution that contained $[Fe^{II}Cp(\eta^6\text{-}C_6Me_6)][PF_6]$ and a black precipitate (Equation 3). Tentative extraction of this precipitate with toluene yielded a colorless solution, which indicated that no C_{60} was present. The Mössbauer spectra of this black solid at 298K discloses parameters that show the presence of an Fe^{II} sandwich complex of the same family as $[Fe^{II}Cp(\eta^6\text{-}C_6Me_6)]^+$.[69-71] Its EPR spectrum recorded at 77 K shows the same EPR spectrum as that of $[Fe^{II}Cp(\eta^6\text{-}C_6Me_6)]^+$ C_{60}.[73] It could thus be concluded that C_{60} had been reduced to its monoanion, as designed for a process that is exergonic by 0.9 V (74). The [dendr-Fe^{II}]$^+$ C_{60}^- units being very large, they must be located at the dendrimer periphery, presumably with rather tight ion pairs although the number of fullerene layers and

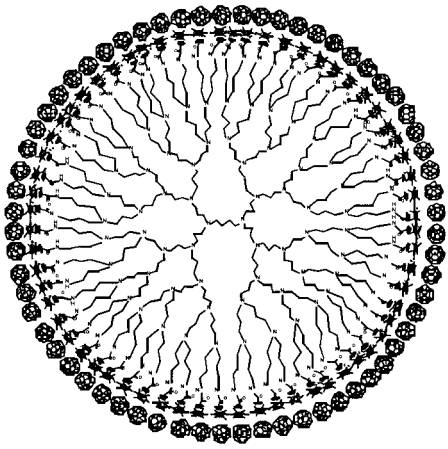

overall molecular size are unknown (Figure 2).

Figure 2 : Dendr-[NHCOCp-$Fe^{II}C_6Me_6$]$_{64}$[C60]64 (top) ; Mössbauer (left, bottom) and EPR (right, bottom) spectra.

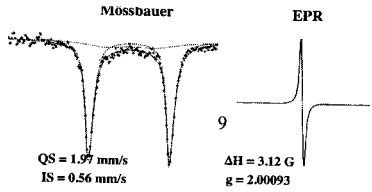

Decoration of Dendrimers with Ruthenium Clusters: Towards Dendritic Catalysts

The clean introduction of clusters onto the termini of polyphosphine dendrimers is a real challenge because of the current interest of dendritic clusters in catalysis and the mixtures usually obtained in thermal reactions of $[Ru_3(CO)_{12}]$ with phosphines. The diphosphine $CH_3(CH_2)_2N(CH_2PPh_2)_2$ (abbreviated P-P below) was used as a simple, model ligand. The reaction between P-P and $[Ru_3(CO)_{12}]$ [75] (molar ratio: 1/1.05) in the presence of 0.1 equiv. $[Fe^{I}Cp(\eta^6\text{-}C_6Me_6)]$ in THF at 20°C led to the complete disappearance of $[Ru_3(CO)_{12}]$ in a few minutes and the appearance of a mixture of chelate [P-P. $Ru_3(CO)_{10}$], monodentate [P-P. $Ru_3(CO)_{11}$] and bis-cluster [P-P. $\{Ru_3(CO)_{11}\}_2$]. These reactions were reported by Bruce with simple diphosphines.[76] On the other hand, the reaction of P-P with $[Ru_3(CO)_{12}]$ in excess (1/4) and only 0.01 equiv. $[Fe^{I}Cp(\eta^6\text{-}C_6Me_6)]$ in THF at 20°C led, in 20 minutes, to the formation of the air-stable, light-sensitive bis-cluster [P-P. $\{Ru_3(CO)_{11}\}_2$] as the only reaction product. Given the simplicity of the above characterization of the reaction product by ^{31}P NMR and the excellent selectivity of this model reaction when excess $[Ru_3(CO)_{12}]$ was used, the same reaction between Reetz's dendritic phosphines,[77a] derived from DSM's dendritic amines,[77b] and $[Ru_3(CO)_{12}]$ could be more confidently envisaged. This reaction, catalyzed by 1% equiv. $[Fe^{I}Cp(\eta^6\text{-}C_6Me_6)]$ was carried out in THF at 20°C. The dendrimer-cluster assembly was obtained in 50% yield. This shows the selectivity and completion of the coordination of each of the 32 phosphino

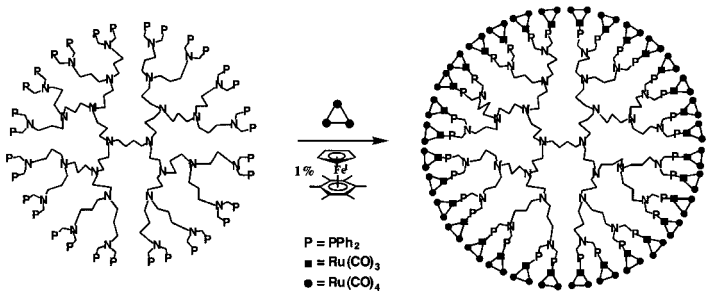

Scheme 9: Electron-Transfer-Chain catalyzed ligand substitution of one Ru-coordinated CO by a dendritic phosphine termini in Reetz's 32-phosphine dendrimer under ambiant conditions leading to the 32-$Ru_3(CO)_{11}$ dendrimer-cluster.

ETC mechanism [78-80] proceeds for the introduction of the 32 cluster fragments in the dendrimer for ligation of the first $Ru_3(CO)_{11}$ fragment to the dendritic phosphine. Then, this first complex [dendriphosphine.$Ru_3(CO)_{11}$] would undergo the same ETC cycle as [$Ru_3(CO)_{12}$] initially does to generate the bis-cluster complex [dendriphosphine.{$Ru_3(CO)_{11}$}$_2$], and so on (Scheme 10).

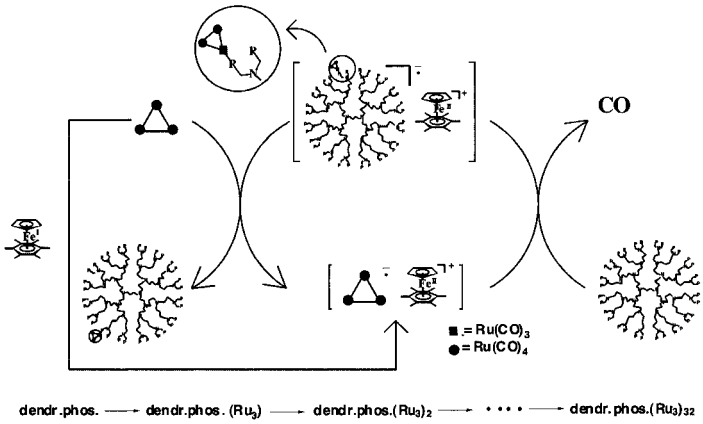

Scheme 10: Electron-Transfer-Chain mechanism for the synthesis of the 96-Ru dendrimer-cluster complex.

Finally, the 64-branch phosphine DAB-*dendr*-G4-[$N(CH_2PPh_2)_2]_{32}$ analogously reacts with [$Ru_3(CO)_{12}$] and 1% [$Fe^ICp(\eta^6\text{-}C_6Me_6)$] (20°C, THF, 20 min.) to give the dark-red 192-Ru dendrimer. Characterization of the purity of these dendrimer-cluster assemblies is conveniently monitored by ^{31}P NMR. This application should find extension to other metal-carbonyl clusters and other families of phosphine dendrimers.

Dendritic Catalysts and Sensors

It is of interest to compare the efficiency of homologous metallo-stars and metallo-dendrimers in catalysis and sensing. Recently, we were able to compare the rate of the redox catalyzed cathodic

reduction of nitrate and nitrite to ammonia using metallo-stars and cyclic voltammetry. It was found that the metallo-stars in which the catalytic metal centers were located at the periphery of the metallo-stars showed about the same rate of reduction of the nitrogen oxides NO_2^- and NO_3^- by the 19-electron form of the catalysts as mononuclear complexes with the same driving force. On the other hand, those containing the redox-active site at the center of the dendritic- or star core showed rates that were at least an order of magnitude lower.[81]

In another example using dendritic ruthenium carbene dendrimers for the living ROMP of norbornene, it was found that the most efficient dendrimer was that of first generation (4 arms) whereas the efficiency decreased as the generation increased. This finding is due to the increasing steric bulk around the ruthenium-carbene centers that increases with the dendrimer generation.[82] This type of steric congestion is not found is metallostars. Thus, first-generation dendrimers (which are in fact stars rather than dendrimers) are best for catalytic activity as long as they are large enough to be removed by ultra-filtration or centrifugation.[8-10]

For dendritic amido- or silylferrocene nano-sensors, stars show some activity, but dendrimers are far better, and their efficiency increases as the dendritic generation increases. In this case, the steric bulk at the dendrimer periphery provides narrow channels that are desired and ideal with an optimized topology in view of efficient recognition.[83-85]

Outlook

Very large dendrimers [86] have been synthesized and functionalized with transition metal fragments including ferrocenyl and other metal-sandwich type complexes that include a supramolecular function (amide, silicon center).[87] Their large size is a very important parameter for improved adsorption on metal surfaces and electrodes. It is also essentiel to have in hands nano-sized, well defined macromolecules for integration in devices as nano-wires. For instance, comparison of surfaces and electrodes modified with several layers and average-size metallodendrimers with those modified with giant metallodendrimers should provide insight into the mechanism of electron-hoping in the solid (compare intramolecular vs. intermolecular hoping). It is also essential to control reactions such as those involving metal-ligand bond formation at the

nanoscale. The behavior of nano-catalysts is highlighted in this review and different topologies have been compared in term of efficiency. These studies are needed in order to make progress in green catalysis.[88] Applications of these fundamental studies are awaited in the fields of catalysts, sensors and nano-devices.

Acknowledgement

We are grateful to the colleagues, students and post-docs cited in the references who have contributed to the ideas and efforts of this research program. We are especially indebted in this respect to Dr Sylvain Lazarre (AFM: LCPT, University Bordeaux I), Dr Eric Cloutet (SEC: LCPO, University Bordeax I) and Prof. François Varret (Mössbauer spectroscopy: University of Versailles). Financial support from the Institut Universitaire de France (IUF), the University Bordeaux I, the Centre National de la Recherche Scientifique (CNRS), the Alexander von Humboldt Fundation, Iberdrola, the Picasso and Erasmus-Socrates programs, the European Community and the Region Aquitaine is gratefully acknowledged.

[1] G. R. Newkome, C. N. Moorefield, F. Vögtle, *"Dendrimers and Dendrons. Concept, Syntheses, Applications"*, Wiley-VCH, Weinheim, 2001.
[2] Dendrimers and other Dendritic Polymers, (Eds.: Tomalia, D.; Fréchet, J. M. J.), Wiley-VCH, New York, 2002.
[3] V. Balzani, S. Campagna, G. Denti, A. Juris, S. Serrini, M. Venturi, *Acc. Chem. Res.* **1998,** 31, 26.
[4] G. R. Newkome, E. He, C. N. Moorefield, *Chem. Rev.* **1999**, 99, 1689.
[5] A. W. Bosman, E. W. Jansen, E. W. Meijers, *Chem. Rev.* **1999**, 99, 1665.
[6] I. Cuadrado, M. Morán, C. M. Casado, B. Alonso, J. Losada, *Coord. Chem. Rev.* **1999**, 193-195, 395-445.
[7] M. A. Hearshaw, J. R. Moss, *Chem. Commun.* **1999,** 1.
[8] G. E. Oosterom, J. N. H. Reek, P. C. J. Kamer, P. W. N. M. van Leeuwen, *Angew. Chem. Intern. Ed. Engl.* **2001**, 40, 1828.
[9] R. Kreiter, A. W. Kleij, R. J. M. Klein Gebbink, G. van Koten In Dendrimers IV: Metal Coordination, Self Assembly, Catalysis, (Eds.: F. Vögtle, C.A. Schalley) Top. Curr. Chem. Springer-Verlag, Berlin, 2001, 217, 163.
[10] D. Astruc, F. Chardac, *Chem. Rev.* **2001**, 101, 2991; N. Ardoin, D. Astruc, *Bull. Soc. Chim. Fr.* **1995**, 132, 875 (review).
[11] C. Valério, J-L. Fillaut, J. Ruiz, J.-C. Guittard, J.-C. Blais, D. Astruc, *J. Am. Chem. Soc.* **1997**, 117, 2588.
[12] C. Valério, E. Alonzo, J. Ruiz, J.-C. Blais, D. Astruc, *Angew. Chem. Int. Ed. Engl.* **1999**, 38, 1747.
[13] a) A. Labande, J. Ruiz, D. Astruc, *J. Am. Chem. Soc.* **2002**, 124, 1782; b) A. Labande, D. Astruc, *Chem.Commun.* **2000**, 1007.
[14] E. Alonso, A. Labande, L. Raehm, J.-M. Kern, D. Astruc, *C. R. Acad. Sci. Ser. IIc* **1999**, 2, 209.
[15] a) H. Trujillo, C. Casado, J. Ruiz, D. Astruc, *J. Am. Chem. Soc.* **1999**, 121, 5674; b) D. Astruc *Acc. Chem. Res.* **2000**, 33, 287.
[16] C. C. Lee, B. R. Steele, K. J. Demchuk, R. G. Sutherland, *Can. J. Chem.* **1979**, 57, 946.
[17] For the synthesis of $[Fe^{II}Cp(\eta^6\text{-}C_6Me_6)][PF_6]$, see references 18,19 and 35.
[18] P. L. Pauson, W. E. Watts, *J. Chem. Soc.* **1963**, 2990.
[19] D. Astruc, J.-R. Hamon, M. Lacoste, M.-H. Desbois, E. Román, *Organometallic Synthesis* (Ed.: R. B. King), 1988, Vol. IV, p. 172.

[20] J.-R. Hamon, J.-Y. Saillard, A. Le Beuze, M. McGlinchey, D. Astruc, *J. Am. Chem. Soc.* **1982**, 104, 3755.
[21] F. Moulines, D. Astruc, *Angew. Chem. Int. Ed. Engl.* **1988**, 27, 1347.
[22] F. Moulines, D. Astruc, *J. Chem. Soc. Chem. Commun.* **1989**, 614.
[23] See also: B. R. Steele, C. G. Screttas, *J. Am. Chem. Soc.* **2000**, 122, 2391.
[24] a) J.-L. Fillaut, J. Linares, D. Astruc, *Angew. Chem. Int. Ed. Engl.* **1994**, 33, 2460; b) J.-L. Fillaut, R. Boese, D. Astruc, *Synlett* **1992**, 55; c) J.-L. Fillaut, D. Astruc, *New J. Chem.* **1996**, 20, 945.
[25] B. Alonso, J.-C. Blais, D. Astruc, *Organometallics* **2000**, 21, 1001.
[26] F. Moulines, B. Gloaguen, D. Astruc, *Angew. Chem. Int. Ed. Engl.* **1992**, 28, 458.
[27] H. W. Marx, F. Moulines, T. Wagner, D. Astruc, *Angew. Chem. Int. Engl.* **1996**, 35, 1701.
[28] J. Ruiz, E. Alonso, J. Guittard, J.-C. Blais, D. Astruc, *J. Organomet. Chem.* **1999**, 582/1, 139 (issue dedicated to Alan H. Cowley).
[29] F. Moulines, L. Djakovitch, J.-L. Fillaut, D. Astruc, *Synlett* **1992**, 57.
[30] F. Moulines, L. Djakovitch, R. Boese, B. Gloaguen, W. Thiel, J.-L. Fillaut, M.-H. Delville, D. Astruc, *Angew. Chem. Int. Ed. Engl.* **1993**, 105, 1132.
[31] V. Marvaud, D. Astruc, *Chem. Commun.* **1997**, 773.
[32] V. Marvaud, D. Astruc, *New J. Chem.* **1997**, 21, 1309.
[33] S. Rigaut, M.-H. Delville, D. Astruc, *J. Am. Chem. Soc.* **1997**, 119, 1132.
[34] S. Rigaut, M.-H. Delville, J. Losada, D. Astruc, *Inorg. Chim. Acta* **2002**, *334*, 225.
[35] D. Astruc In *Electron Transfer in Chemistry* (Ed.: V. Balzani), Vol II (J. Matay, D. Astruc Vol. Eds.), Wiley, Weinheim, 2001, pp 714-803.
[36] C. Valério, F. Moulines, J. Ruiz, J.-C. Blais, D. Astruc, *J. Org. Chem.* **2000**, 65, 1996.
[37] B. Gloaguen, D. Astruc, *J. Am. Chem. Soc.* **1990**, 112, 4607.
[38] D. Buchholz, B. Gloaguen, J.-L. Fillaut, M. Cotrait, D. Astruc, *Chem. Eur. J.* **1995**, 1, 374.
[39] D. Buchholz, D. Astruc, *Angew. Chem. Int. Ed. Engl.* **1994**, *33*, 1637.
[40] S. Marcen, S. Jimenez, M. V. Dobrinovitch, F. Lahoz, L. Oro, J. Ruiz, D. Astruc *Organometallics* **2002**, 21, 326.
[41] V. Martinez, J.-C. Blais, D. Astruc, *Org. Lett.* **2002**, 4, 651.
[42] F. Moulines, L. Djakovitch, M.-H. Delville, F. Robert, P. Gouzerh, D. Astruc, *J. Chem. Soc., Chem. Commun.* **1995**, 463.
[43] F. Moulines, L. Djakovitch, D. Astruc, *New J. Chem.* **1996**, 20, 1071.
[44] a)V. Sartor, L. Djakovitch, J.-L. Fillaut, F. Moulines, F. Neveu, V. Marvaud, J. Guittard, J.-C. Blais, D. Astruc, *J. Am. Chem. Soc.* **1999**, 121, 2929; b) V. Sartor, S. Nlate, J.-L. Fillaut, F. Djakovitch, F. Moulines, V. Marvaud, F. Neveu, J.-C. Blais, *New J. Chem.* **2000**, 24, 351.
[45] S. Nlate, Y. Neto, J.-C. Blais, J. Ruiz, D. Astruc *Chemistry Eur. J.*, **2002**, 8, 171.
[46] S. Nlate, J. Ruiz, D. Astruc, *Chem. Commun.* **2000**, 417.
[47] S. Nlate, J. Ruiz, V. Sartor, R. Navarro, J.-C. Blais, D. Astruc *Chemistry Eur. J.* **2000**, 6, 2544.
[48] B. Marciniec, In "*Applied Homogeneous Catalysis with Organometallic Compounds*" (Eds.: B. Cornils, W. A. Herrmann), VCH, Weinheim, 1996, Vol. 1, Chap. 2.6.
[49] L. N. Lewis, J. Stein, K. A. Smith, In *Progress in Organosilicon Chemistry* (Eds.: B. Marciniec, J Chojnowski) Gordon and Breach, Langhorne, USA, 1995, p. 263.
[50] K. H. Pannel, H. Sharma, *Organometallics* **1991**, 10, 954.
[51] P. Jutzi, C. Batz, B. Neumann, H. G. Stammler, *Angew. Chem. Int. Engl.* **1996**, 35, 2118.
[52] J. B. Flanagan, S. Margel, A. J. Bard, F. C. Anson, *J. Am. Chem. Soc.* **1978**, 100, 4248.
[53] a) D. Astruc, C. Valério, J.-L. Fillaut, J.-R. Hamon, F. Varret, In *Magnetism, a Supramolecular Function* (Ed.: O. Kahn), NATO ASAI Series, Kluver, Dordrecht, 1996, p. 1107; b) C. Valério, *PhD Thesis*, Université Bordeaux I, 1996.
[54] a) I. Cuadrado, M. Morán, C. M. Casado, B. Alonso, F. Lobete, B. Garcia, J. Losada, *Organometallics* **1996**, 15, 5278; b) K. Takada, D. J. Diaz, H. Abruña, I. Cuadrado, C. M. Casado, B. Alonso, M. Morán, J. Losada, *J. Am. Chem. Soc.* **1997**, 119, 10763.
[55] Review: C. M. Casado, I. Cuadrado, M. Moran, B. Alonso, B. Garcia, B. Gonzales, J Losada, *Coord. Chem. Rev.* **1999**, 185-6, 53.
[56] J. Ruiz, D. Astruc, *C. R. Acad. Sci.* Paris, t. 1, Série II *c*, **1998**, 21.
[57] R. L. Collins, *J. Chem. Phys.* **1965**, 42, 1072.
[58] S. J. Green, J. J. Pietron, J. J. Stokes, M. J. Hostetler, H. Vu, W. P. Wuelfing, R. W. Murray, *Langmuir* **1998**, 14, 5612.
[59] C. B. Gorman, J. C. Smith, M. W. Hager, B. L. Parhurst, H. Sierzputowska-Gracz, C. A. Haney *J. Am. Chem. Soc.* **1999**, 121, 9958.
[60] R. Murray In *Molecular Design of Electrode Surfaces* (Ed.: R. Murray), Wiley, New York, 1992, p. 1.
[61] P. J. Dandliker, F. Diederich, M. Gross, B. Knobler, A. Louati, E. M. Stanford, *Angew. Chem. Int. Ed. Engl.*

1994, 33, 1739.
[62] G. R. Newkome, R. Güther, C. N. Moorefield, F. Cardullo, L. Echegoyen, F. Pérez-Cordero, H. Luftmann, *Angew. Chem. Int. Ed. Engl.* **1995**, 34, 2023.
[63] H.-F. Chow, I. Y.-K. Chan, D. T. W. Chan, R. W. M. Kwok, *Chem. Eur. J.* **1996**, 2, 1085.
[64] P. J. Dandliker, F. Diederich, H.-F. Chow, I. Y.-K. Chan, R. W. M. Kwok *Chem. Eur. J.* **1996**, 2, 1085.
[65] J. Issberner, F. Vögtle, L. De Cola, V. Balzani, *Chem. Eur. J.* **1997**, 3, 706.
[66] C. B. Gorman, B. L. Parkhurst, W. Y. Su, K. Y. Chen, *J. Am. Chem. Soc.* **1997**, 119, 1141.
[67] D. K. Smith, F. Diederich, *Chem. Eur. J.* **1998**, 4, 2353.
[68] J. Ruiz, F. Ogliaro, J.-Y. Saillard, J.-F. Halet, F. Varret, D. Astruc, *J. Am. Chem. Soc.* **1998**, 120, 11693.
[69] M. V. Rajasekharan, S. Giesynski, J. H. Ammeter, N. Oswald, J.-R. Hamon, P. Michaud, D. Astruc *J. Am. Chem. Soc.* **1982**, 104, 129.
[70] D. Astruc, J.-R. Hamon, G. Althoff, E. Roman, P. Batail, P. Michaud, J;_P. Mariot, F. Varret, D. Cozak, *J. Am. Chem. Soc.* **1979**, 101, 5445. This paper also reports the first $CpFe^{+}$-induced iterative starburst hexa-alkylation of C_6Me_6.
[71] J.-R. Hamon, D. Astruc, P. Michaud, *J. Am. Chem. Soc.* **1981**, 103, 758.
[72] J. Ruiz, C. Pradet, F. Varret, D. Astruc, *Chem. Commun.* **2002**, 1108.
[73] C. Bossard, S. Rigaut, D. Astruc, M.-H. Delville, G. Félix, A. Février-Bouvier, J. Amiell, S. Flandrois, P. Delhaès, *J. Chem. Soc., Chem. Commun.* **1993**, 333.
[74] Redox potentials of the six cathodic monoelectronic reductions of C_{60}: A. Xie, E. Pérez-Cordero, L. Echegoyen, *J. Am. Chem. Soc.* **1992**, 114, 3978.
[75] E. Alonso, D. Astruc, *J. Am. Chem. Soc.* **2000**, 122, 3222.
[76] a) M. I. Bruce, D. C. Kehoe, J. G. Matisons, B. K. Nicholson, P. H. Rieger, M. L. J. Williams, *J. Chem. Soc. Chem. Commun.* **1982**, 442; b) M. I. Bruce, J. G. Mattisons, B. K. Nicholson, *J. Organomet. Chem.* **1983**, 247, 321.
[77] a) M. T. Reetz, G. Lohmer, R. Scwickardi, *Angew. Chem. Int. Ed. Engl.* **1997**, 36, 1526. b) E. M. M. de Brabander-van den Berg, E. W. Meijers, *Angew. Chem. Int. Ed. Engl.* **1993**, 32, 1308.
[78] For pioneering work in the field of ETC catalysis, see: R. Rich, H. Taube, *J. Am. Chem. Soc.* **1954**, 76, 2608.
[79] Review on ETC catalysis: D. Astruc, *Angew. Chem. Int. Ed. Engl.* **1988**, 27, 643. See also ref. 80.
[80] a) D. Astruc, *"Electron Transfer and Radical Processes in Transition-Metal Chemistry"*, VCH, New York, 1995; b) ref. 80 a), chapter 6: Chain Reactions, pp. 413-478.
[81] S. Rigaut, M.-H. Delville, J. Losada, D. Astruc, *Inorg. Chim. Acta*, **2000**, 334, 225 (issue dedicated to Andrew Wojcicki).
[82] S.Gatard , S. Nlate, E. Cloutet , G. Bravic, J.-C. Blais, D. Astruc, *Angew. Chem. Int. Ed.* **2003**, 42, 452.
[83] A. Labande, J. Ruiz, D. Astruc, *J. Am. Chem. Soc.* **2002**, 124, 1782.
[84] M.-C. Daniel, J. Ruiz, D. Astruc, *J. Am. Chem. Soc.* **2003**, 125, 1150.
[85] M.-C. Daniel, J. Ruiz, S. Nlate, J.-C. Blais, D. Astruc, *J. Am. Chem. Soc.* **2003**, 125, 2617.
[86] J. Ruiz, G. Lafuente, S. Marcen, C. Ornela, S. Lazarre, J.-C. Blais, E. Cloutet, D. Astruc, *J. Am. Chem. Soc.* **2003**, 125, ASAP.
[87] S. Nlate, J. Ruiz, V. Sartor, R. Navarro, J.-C. Blais, D. Astruc, *Chem. Eur. J.* **2000**, 6, 2544.
[88] "Green Chemistry" P. T. Anastas, T. C. Williamson Eds., *ACS Symp. Ser.* 626, ACS. Washington DC, 1996.

ANNEXE 2:

GOLD NANOPARTICLES: ASSEMBLY, SUPRAMOLECULAR CHEMISTRY, QUANTUM-SIZE RELATED PROPERTIES AND APPLICATIONS TOWARDS BIOLOGY, CATALYSIS AND NANOTECHNOLOGY.

Gold Nanoparticles: Assembly, Supramolecular Chemistry, Quantum-Size-Related Properties, and Applications toward Biology, Catalysis, and Nanotechnology

Marie-Christine Daniel and Didier Astruc*

Molecular Nanosciences and Catalysis Group, LCOO, UMR CNRS No. 5802, Université Bordeaux I, 33405 Talence Cedex, France

Received August 6, 2003

Contents

1. Historic Introduction

Although gold is the subject of one of the most ancient themes of investigation in science, its renaissance now leads to an exponentially increasing number of publications, especially in the context of emerging nanoscience and nanotechnology with nanoparticles and self-assembled monolayers (SAMs). We will limit the present review to gold nanoparticles (AuNPs), also called gold colloids. AuNPs are the most stable metal nanoparticles, and they present fascinating aspects such as their assembly of multiple types involving materials science, the behavior of the individual particles, size-related electronic, magnetic and optical properties (quantum size effect), and their applications to catalysis and biology. Their promises are in these fields as well as in the bottom-up approach of nanotechnology, and they will be key materials and building block in the 21st century.

Whereas the extraction of gold started in the 5th millennium B.C. near Varna (Bulgaria) and reached 10 tons per year in Egypt around 1200−1300 B.C. when the marvelous statue of Touthankamon was constructed, it is probable that "soluble" gold appeared around the 5th or 4th century B.C. in Egypt and China. In antiquity, materials were used in an ecological sense for both aesthetic and curative purposes. Colloidal gold was used to make ruby glass

10.1021/cr030698+ CCC: $48.50
Published on Web 12/20/2003

Marie-Christine Daniel was born in Vannes, France. She graduated from the University of Rennes (France). She is now finishing her Ph.D. on exoreceptors at the Bordeaux 1 University in the research group of Professor Didier Astruc. Her doctoral research is concerned with the recognition of anions of biological interest using functionnalized gold nanoparticles and redox-active metallodendrimers.

Didier Astruc is Professor of Chemistry at the University Bordeaux I and has been a Senior Member of the Institut Universitaire de France since 1995. He studied in Rennes (thesis with R. Dabard), and then did his postdoctoral research at MIT with R. R. Schrock. He is the author of *Electron Transfer and Radical Processes in Transition-Metal Chemistry* (VCH, 1995, prefaced by Henry Taube) and *Chimie Organométallique* (EDP Science, 2000; Spanish version in 2003). His research interests are in organometallic chemistry at the interface with nanosciences, including sensing, catalysis, and molecular electronics.

and for coloring ceramics, and these applications are still continuing now. Perhaps the most famous example is the Lycurgus Cup that was manufactured in the 5th to 4th century B.C. It is ruby red in transmitted light and green in reflected light, due to the presence of gold colloids. The reputation of soluble gold until the Middle Ages was to disclose fabulous curative powers for various diseases, such as heart and venereal problems, dysentery, epilepsy, and tumors, and for diagnosis of syphilis. This is well detailed in what is considered as the first book on colloidal gold, published by the philosopher and medical doctor Francisci Antonii in 1618.[1] This book includes considerable information on the formation of colloidal gold sols and their medical uses, including successful practical cases. In 1676, the German chemist Johann Kunckels published another book,[2a] whose chapter 7 concerned "drinkable gold that contains metallic gold in a neutral, slightly pink solution that exert curative properties for several diseases". He concluded, well before Michael Faraday (vide infra), that "gold must be present in such a degree of communition that it is not visible to the human eye". A colorant in glasses, "Purple of Cassius", is a colloid resulting from the heterocoagulation of gold particles and tin dioxide, and it was popular in the 17th century.[2b] A complete treatise on colloidal gold was published in 1718 by Hans Heinrich Helcher.[3] In this treatise, this philosopher and doctor stated that the use of boiled starch in its drinkable gold preparation noticeably enhanced its stability. These ideas were common in the 18th century, as indicated in a French dictionary, dated 1769,[4] under the heading "or potable", where it was said that "drinkable gold contained gold in its elementary form but under extreme sub-division suspended in a liquid". In 1794, Mrs. Fuhlame reported in a book[5] that she had dyed silk with colloidal gold. In 1818, Jeremias Benjamin Richters suggested an explanation for the differences in color shown by various preparation of drinkable gold:[6] pink or purple solutions contain gold in the finest degree of subdivision, whereas yellow solutions are found when the fine particles have aggregated.

In 1857, Faraday reported the formation of deep-red solutions of colloidal gold by reduction of an aqueous solution of chloroaurate ($AuCl_4^-$) using phosphorus in CS_2 (a two-phase system) in a well-known work. He investigated the optical properties of thin films prepared from dried colloidal solutions and observed reversible color changes of the films upon mechanical compression (from bluish-purple to green upon pressurizing).[7] The term "colloid" (from the French, *colle*) was coined shortly thereafter by Graham, in 1861.[8] Although the major use of gold colloids in medicine in the Middle Ages was perhaps for the diagnosis of syphilis, a method which remained in use until the 20th century, the test is not completely reliable.[9−11]

In the 20th century, various methods for the preparation of gold colloids were reported and reviewed.[11−17] In the past decade, gold colloids have been the subject of a considerably increased number of books and reviews,[15−44] especially after the breakthroughs reported by Schmid[17,19,21] and Brust et al.[22,27] The subject is now so intensively investigated, due to fundamental and applied aspects relevant to the quantum size effect, that a majority of the references reported in the present review article have appeared in the 21st century. Readers interested in nanoparticles in general can consult the excellent books cited in refs 15, 24, 28, 33, and 43. The book by Hayat, published in 1989,[14] essentially deals with biological aspects and imaging of AuNPs.

2. General Background: Quantum Size Effect and Single-Electron Transitions

Physicists predicted that nanoparticles in the diameter range 1−10 nm (intermediate between the size of small molecules and that of bulk metal) would display electronic structures, reflecting the electronic band structure of the nanoparticles, owing to quantum-mechanical rules.[29] The resulting physical properties are neither those of bulk metal nor those of molecular compounds, but they strongly depend on

the particle size, interparticle distance, nature of the protecting organic shell, and shape of the nanoparticles.[27] The few "last metallic electrons" are used for tunneling processes between neighboring particles, an effect that can be detected by impedance measurements that distinguish intra- and intermolecular processes. The *quantum size effect* is involved when the de Broglie wavelength of the valence electrons is of the same order as the size of the particle itself. Then, the particles behave electronically as zero-dimensional quantum dots (or quantum boxes) relevant to quantum-mechanical rules. Freely mobile electrons are trapped in such metal boxes and show a characteristic collective oscillation frequency of the plasma resonance, giving rise to the so-called plasmon resonance band (PRB) observed near 530 nm in the 5−20-nm-diameter range. In nanoparticles, there is a gap between the valence band and the conduction band, unlike in bulk metals. The size-induced metal−insulator transition, described in 1988, is observed if the metal particle is small enough (about 20 nm) that size-dependent quantization effects occur. Then, standing electron waves with discrete energy levels are formed. *Single-electron transitions* occur between a tip and a nanoparticle, causing the observation of so-called Coulomb blockades if the electrostatic energy, $E_{el} = e^2/2C$, is larger than the thermal energy, $E_T = kT$. The capacitance C becomes smaller with smaller particles. This means that single-electron transitions can be observed at a given temperature only if C is very small, i.e., for nanoparticles since they are small enough ($C < 10^{-18}$ F). Large variations of electrical and optical properties are observed when the energy level spacing exceeds the temperature, and this flexibility is of great practical interest for applications (transistors, switches, electrometers, oscillators, biosensors, catalysis).[32−38] For instance, single-electron tunneling related to the electrical resistance of a single rod-shaped molecule provided a value of 18 ± 12 MΩ for self-assembled monolayers on gold (1,1,1) substrate used to tether AuNPs deposited from a cluster beam.[32] The transition from metal-like capacitive charging to redox-like charging was observed with alkanethiolate−gold nanoparticles of low dispersity in an electrochemical setup for Coulomb staircase experiments.[39,40] Indeed, it was initially indicated that these AuNPs could accommodate 10 redox states.[39a] In a subsequent paper published in 2003, it was shown that lower temperatures enhance the resolution of quantized double-layer charging peaks in differential pulse voltammetry (DPV) observations. This led to the resolution of 13 peaks in CH_2Cl_2 at 263 K for Au_{140} particles.[39b] At the same time, however, a publication by Quinn's group revealed remarkably well-resolved DPV of analogous Au_{147} particles, showing 15 evenly spaced peaks at room temperature (295 K) corresponding to 15 oxidation states (Figure 1). It was also anticipated that, the number of observable charge states being limited by the size of the available potential window, additional peaks should be observed in controlled atmosphere and reduced temperature conditions.[40] Thus, AuNPs behave as other delocalized redox molecules, disclosing redox cascades that are well known in inorganic and organometallic electrochemistry for other transition metal clusters and bi-sandwich complexes.

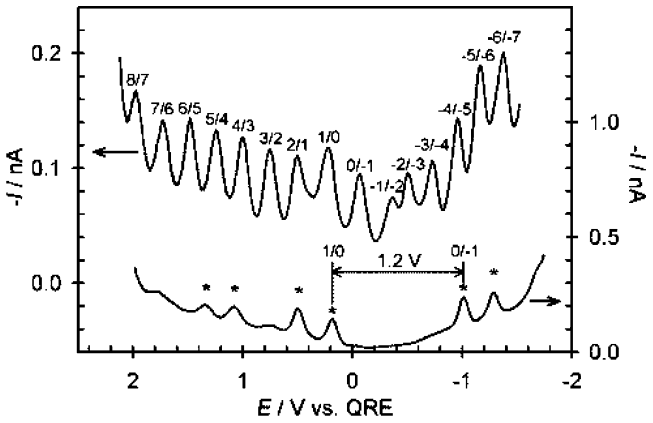

Figure 1. Differential pulse voltammetry (DPV) responses for AuNP solutions measured at a Pt microelectrode; (upper) as-prepared 177 μM hexanethiol-capped Au_{147} showing 15 high-resolution quantized double-layer charging (QDL) peaks and (lower) 170 μM hexanethiol-capped Au_{38} showing a HOMO−LUMO gap. It can be seen that the as-prepared solution contains a residual fraction of Au_{38} that smears out the charging response in E regions where QDL peaks overlap. The electrode potential scanned negative to positive. Reprinted with permission from ref 40 (Quinn's group). Copyright 2003 American Chemical Society.

The pioneering work by Schmid and co-workers on well-defined phosphine-stabilized gold clusters showed the properties of quantum-dot particles for the first time.[30] The number of atoms in these gold clusters is based on the dense packing of atoms taken as spheres, each atom being surrounded by 12 nearest neighbors. Thus, the smallest cluster contains 13 atoms, and the following layers contain $10n^2 + 2$ atoms, n being the layer number. For instance, the second layer contains 42 atoms, which leads to a total of 55 atoms for a gold cluster, and the compound $[Au_{55}(PPh_3)_{12}Cl_6]$ has been well characterized by Schmid's group. Recently, spectroscopic data have revealed discrete energy level spacings of 170 meV that can be attributed to the Au_{55} core.[30c] Larger clusters containing, respectively, 147, 309, 561, 923, 1415, or 2057 ($n = 3−8$) atoms have been isolated.[30,31] Discrete organogold clusters are also well known with small numbers of atoms and various geometries, and they will not be reviewed here.[41,42] Large ones form a fuzzy frontier between clusters and colloids (AuNPs), the latter being defined by some dispersity materialized by a histogram determined using transmission electron microscopy (TEM) data.

Despite the considerable variety of contributions, we will focus first on synthesis, stabilization, and various types of assemblies, and then on physical properties and on chemical, supramolecular, and sensor properties, and finally on applications to biochemistry, catalysis, and nonlinear optical properties before concluding on the perspectives of AuNPs in nanosciences and nanotechnology. Many publications involve two or even sometimes several of these topics. Thus our classification is arbitrary, but the reader will often better understand the spirit of each paper from its title given in the reference section.

3. Synthesis and Assembly

3.1. Citrate Reduction

Among the conventional methods of synthesis of AuNPs by reduction of gold(III) derivatives, the most popular one for a long time has been that using citrate reduction of $HAuCl_4$ in water, which was introduced by Turkevitch in 1951.[12] It leads to AuNPs of ca. 20 nm. In an early effort, reported in 1973 by Frens,[13] to obtain AuNPs of prechosen size (between 16 and 147 nm) via their controlled formation, a method was proposed where the ratio between the reducing/stabilizing agents (the trisodium citrate-to-gold ratio) was varied. This method is very often used even now when a rather loose shell of ligands is required around the gold core in order to prepare a precursor to valuable AuNP-based materials. Recently, a practical preparation of sodium 3-mercaptopropionate-stabilized AuNPs was reported in which simultaneous addition of citrate salt and an amphiphile surfactant was adopted; the size could be controlled by varying the stabilizer/gold ratio (Figure 2).[44]

3.2. The Brust–Schiffrin Method: Two-Phase Synthesis and Stabilization by Thiols

Schmid's cluster $[Au_{55}(PPh_3)_{12}Cl_6]$, reported in 1981, long remained unique with its narrow dispersity (1.4 ± 0.4 nm) for the study of a quantum-dot nanomaterial, despite its delicate synthesis.[45] The stabilization of AuNPs with alkanethiols was first reported in 1993 by Mulvaney and Giersig, who showed the possibility of using thiols of different chain lengths and their analysis.[46a] The Brust−Schiffrin method for AuNP synthesis, published in 1994, has had a considerable impact on the overall field in less than a decade, because it allowed the facile synthesis of thermally stable and air-stable AuNPs of reduced dispersity and controlled size for the first time (ranging in diameter between 1.5 and 5.2 nm). Indeed, these AuNPs can be repeatedly isolated and

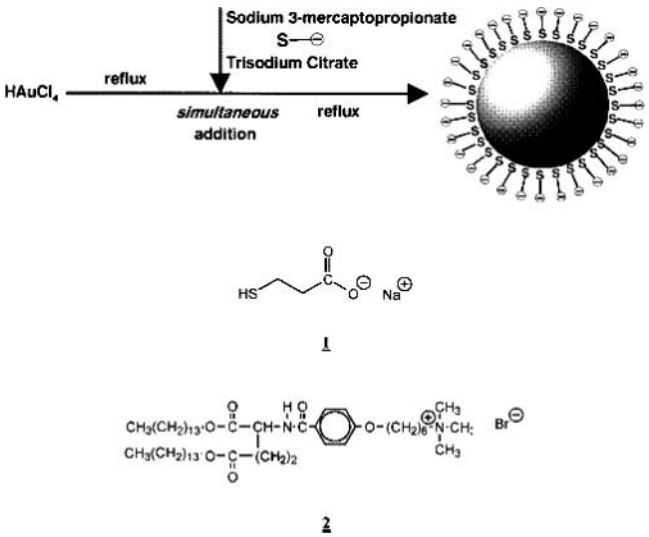

Figure 2. Preparation procedure of anionic mercapto-ligand-stabilized AuNPs in water. Reprinted with permission from ref 44 (Kunitake's group). Copyright 1999 Elsevier.

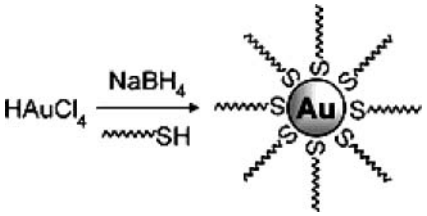

Figure 3. Formation of AuNPs coated with organic shells by reduction of Au^{III} compounds in the presence of thiols. Reprinted with permission from ref 73 (Crooks's group). Copyright 2001 Royal Society of Chemistry.

redissolved in common organic solvents without irreversible aggregation or decomposition, and they can be easily handled and functionalized just as stable organic and molecular compounds. The technique of synthesis is inspired by Faraday's two-phase system[7] and uses the thiol ligands that strongly bind gold due to the soft character of both Au and S.[47] $AuCl_4^-$ is transferred to toluene using tetraoctylammonium bromide as the phase-transfer reagent and reduced by $NaBH_4$ in the presence of dodecanethiol (Figure 3).[47a] The organic phase changes color from orange to deep brown within a few seconds upon addition of $NaBH_4$:

$$AuCl_4^-(aq) + N(C_8H_{17})_4^+(C_6H_5Me) \rightarrow N(C_8H_{17})_4^+AuCl_4^-(C_6H_5Me)$$

$$mAuCl_4^-(C_6H_5Me) + nC_{12}H_{25}SH(C_6H_5Me) + 3m\ e^- \rightarrow 4m\ Cl^-(aq) + [Au_m(C_{12}H_{25}SH)_n](C_6H_5Me)$$

The TEM photographs showed that the diameters were in the range 1−3 nm, with a maximum in the particle size distribution at 2.0−2.5 nm, with a preponderance of cuboctahedral and icosahedral structures. Larger thiol/gold mole ratios give smaller average core sizes, and fast reductant addition and cooled solutions produced smaller, more monodisperse particles. A higher abundance of small core sizes (≤2 nm) is obtained by quenching the reaction immediately following reduction or by using sterically bulky ligands.[48−50] Brust et al. extended this synthesis to *p*-mercaptophenol-stabilized AuNPs in a single-phase system,[47b] which opened an avenue to the synthesis of AuNPs stabilized by a variety of functional thiol ligands.[47,48] Subsequently, many publications appeared describing the use of the Brust−Schiffrin procedure for the synthesis of other stable AuNPs, also sometimes called monolayer-protected clusters (MPCs), of this kind that contained functional thiols.[49−53] The proportion thiol:$AuCl_4^-$ used in the synthesis controls the size of the AuNPs (for instance, a 1:6 ratio leads to the maximum average core diameter of 5.2 nm, i.e., ca. 2951 Au atoms and ca. 371 thiolate ligands; core diameter dispersity of ∼ ±10%). Murray et al. reported and studied the "place exchange" of a controlled proportion of thiol ligands by various functional thiols[52] (Figures 4 and 5) and the subsequent reactions of these functional AuNPs.[50,52] Schiffrin reported the purification of dodecanethiol-stabilized AuNPs from tetraoctylam-

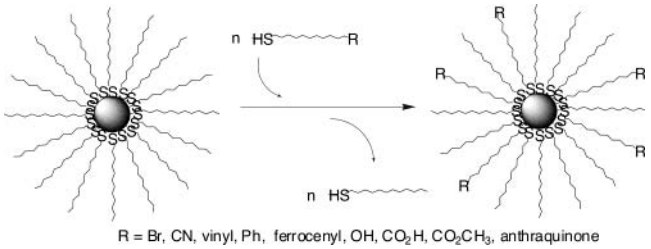

Figure 4. General scheme for the ligand-exchange reaction between alkanethiol-AuNPs of the Brust type and various functionalized thiols.

monium impurities by Soxhlet extraction.[54] The influence of nonionic surfactant polyoxoethylene(20) sorbitan monolaurate (Tween 20) on surface modification of AuNPs was studied with mercaptoalkanoic acids.[55] Digestive ripening, i.e., heating a colloidal suspension near the boiling point in the presence of alkanethiols (for instance, 138 °C for 2 min, followed by 5 h at 110 °C), significantly reduced the average particle size and polydispersity in a convenient and efficient way. This technique also led to the formation of 2D and 3D superlattices,[56,57] a subject of intense investigation (see also section 3.13 on materials).[58−63] For instance, AuNPs obtained using acid-facilitated transfer are free of tetraalkylammonium impurity, are remarkably monodisperse, and form crystalline superstructures.[63a] The truncated icosahedron structure is formed in growth conditions in which the equilibrium shape is achieved.[63b] Molecular dynamics simulations showed that AuNPs with 1157 Au atoms attained an icosahedral structure upon freezing.[63c] A single-toluene phase method was also reported whereby the ammonium salt-stabilized AuNPs were synthesized, followed by an exchange reaction with dodecanethiol.[58] Superhydride[64a] and hexadecylaniline[64b] (inter alia) have been used as alternative reagents to $NaBH_4$ for the reduction of gold(III) in the synthesis of thiol-stabilized AuNPs. Shape separation of suspended AuNPs by size-exclusion chromatography was monitored by examining the 3D chromatograms obtained by employing a diode-array detection system.[65]

3.3. Other Sulfur Ligands

Other sulfur-containing ligands,[67−70] such as xanthates[66] and disulfides,[67−69] di-[70a] and trithiols,[70b] and resorcinarene tetrathiols,[70d] have been used to stabilize AuNPs. Disulfides are not as good stabilizing agents as thiols,[67−70] which is eventually useful for catalysis.[70] Similarly, thioethers do not bind AuNPs strongly,[71] but the use of polythioethers by Rheinhout's group astutely circumvented this problem.[72a] Tetradentate thiethers have also been used to reversibly form AuNP assemblies.[72b] On the other hand, oxidation of thiol-stabilized AuNPs by iodine provokes their decomposition to gold iodide with formation of disulfides, which led Crooks to form polycyclodextrin hollow spheres by templating AuNPs.[73]

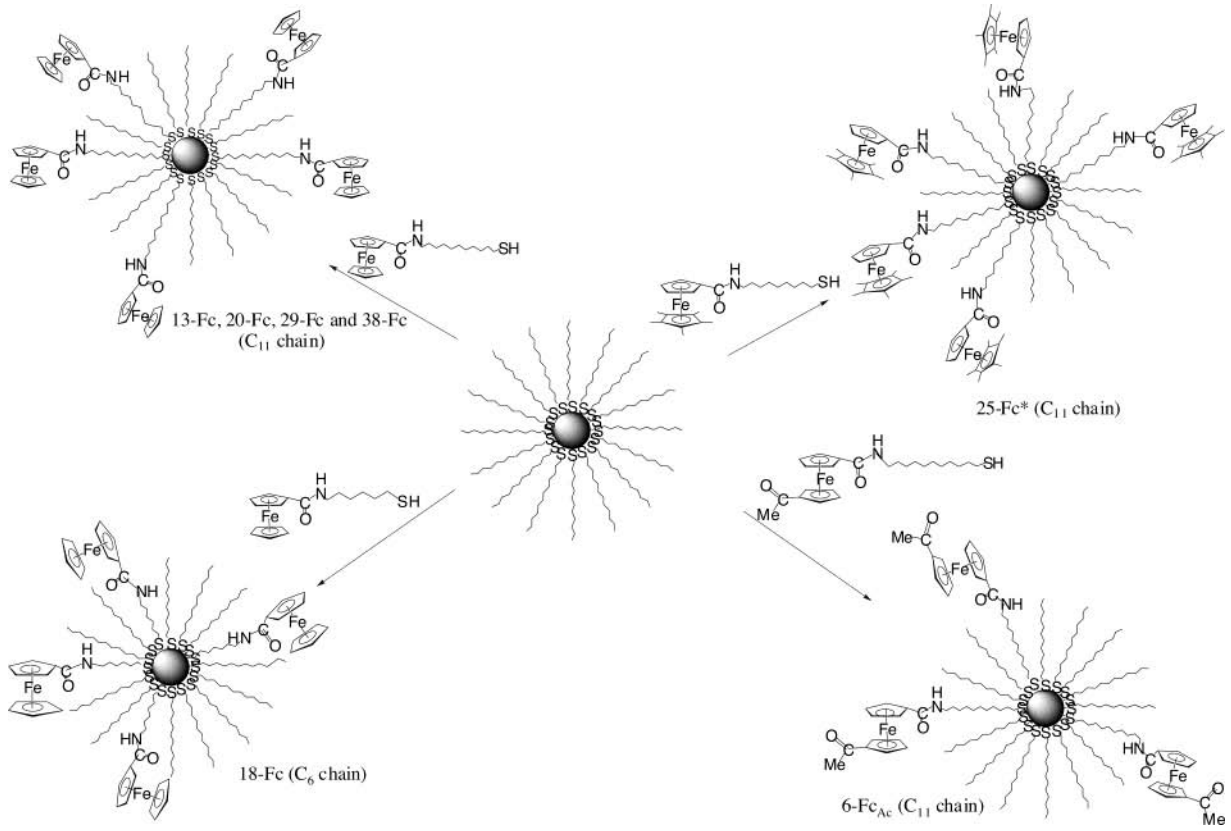

Figure 5. Ligand substitution reactions (CH_2Cl_2, 2 d, room temperature) for the syntheses of the AuNPs containing mixed dodecanethiol and (amidoferrocenyl) alkanethiol-type ligands with variation of the chain length (C_{11} vs C_6) and ring structure of the ferrocenyl motif (Cp, Cp*, C_5H_4COMe). Reprinted with permission from ref 140 (Astruc's group). Copyright 2002 American Chemical Society.

3.4. Other Ligands

3.4.1. Phosphine, Phosphine Oxide, Amine, and Carboxylate Ligands

The Brust biphasic method of synthesis was applied to PPh_3 in order to improve the synthesis of Schmid's cluster $[Au_{55}(PPh_3)_{12}Cl_6]$, using $HAuCl_4 \cdot 3H_2O$ and $N(C_8H_{15})_4Br$ in a water−toluene mixture to which PPh_3 and then $NaBH_4$ were added. It was estimated that the cluster synthesized in this way had the formula $[Au_{101}(PPh_3)_{21}Cl_5]$ and contained 3.7 mass percent of $[Au(PPh_3)Cl]$ as an impurity.[74a] Thermolysis of $[Au^I(C_{13}H_{27}COO)(PPh_3)]$ at 180 °C under N_2 yielded monodispersed AuNPs capped by myristate and a small amount of PPh_3 ligands; the AuNP diameter increased with reaction time, from 12 nm for 1 h to 28 nm for 10 h, and with increasing temperature (42 nm for 5 h at 200 °C).[74b] Various other gold complexes, in particular gold(I) amine complexes, have been used as precursors for the synthesis of amine-stabilized AuNPs.[75,76a,b] Reduction of $Au^{IV}Cl_4$ by $NaBH_4$ in a mixture of tri-*n*-octylphosphine oxide (TOPO) and octadecylamine (1:0.57 molar ratio) at 190 °C resulted in the controlled growth of spherical AuNPs (8.59 ± 1.09 nm diameter) that are stable for months in toluene and were manipulated into crystals and 2D arrays (Figure 6).[76c] Capping aqueous AuNPs with the amino acid lysine stabilizes the AuNPs in solution electrostatically and renders them air-stable and water-dispersible, a finding that is promising toward biologically relevant research.[76d] Efficient synthesis of stable AuNPs by reaction of $AuCl_4^-$ ions with the alkalothermophilic actinomycete *Thermomonospora* sp. has been described.[76e]

3.4.2. Isocyanide

Aryl isocyanide thin films have attracted some attention, due to their potential application as molecular wires,[76f] and 1,4-diisocyanide−AuNP forms large aggregate superstructures that have been examined by IR and Raman spectroscopy, showing bonding to the AuNP core via the carbon lone pair.[76g,h]

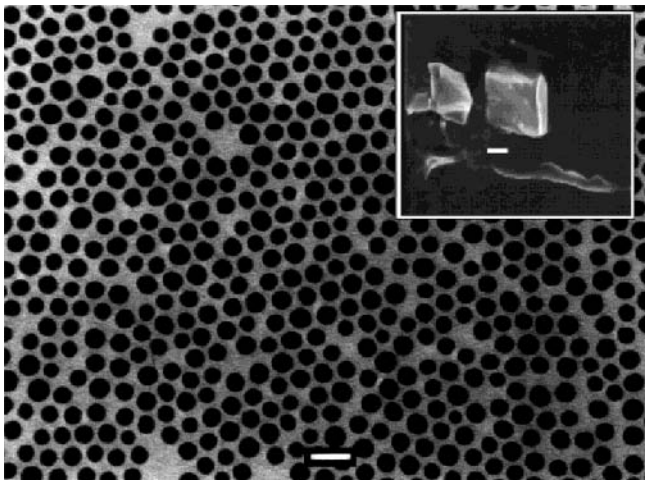

Figure 6. 2D lattice of octadecylamine/TOPO-capped AuNPs spontaneously formed when the latter are deposited on a copper grid; bar = 20 nm. (Inset) Scanning electron microscopy (SEM) image of a cubic colloidal crystal prepared from octadecylamine/TOPO-capped AuNPs (190 °C); bar = 80 μm. Reprinted with permission from ref 76c (O'Brien's group). Copyright 2000 The Royal Society of Chemistry.

3.4.3. Acetone

Pure Au^0NPs, obtained by replacement of citrate by acetone, were shown to be stable against attack by BH_4^- or HCl.[76i]

3.4.4. Iodine

Iodine adsorption was shown to displace citrate ions from AuNPs, leading to superstructures that are also formed upon addition of KI.[76j]

3.5. Microemulsion, Reversed Micelles, Surfactants, Membranes, and Polyelectrolytes

The use of microemulsions,[77] copolymer micelles,[78] reversed micelles,[77] surfactant, membranes, and other amphiphiles is a significant research field for the synthesis[38] of stabilized AuNPs in the presence or in the absence of thiol ligands.[77−95] The syntheses involve a two-phase system with a surfactant that causes the formation of the microemulsion or the micelle maintaining a favorable microenvironment, together with the extraction of metal ions from the aqueous phase to the organic phase. This is an advantage over the conventional two-phase system. This dual role of the surfactant and the interaction between the thiol and the AuNP surface control the growth and stabilization of the AuNP or nanocrystal. The narrow size distribution allows the ordering of the particles into a 2D hexagonal close-packed array. AuNP sizes of the order of 4 nm diameter have been found.[79] Polyelectrolytes have also been extensively used for the synthesis of AuNPs (Figure 7).[94,98−102] The polyelectrolyte coating of carboxylic acid-derivatized AuNPs with diameters less than 10 nm has been achieved by electrostatic self-assembly of oppositely charged polyelectrolytes.[102b]

3.6. Seeding Growth

The seeding-growth procedure is another popular technique that has been used for a century. Recent studies have successfully led to control of the size distribution (typically 10−15%) in the range 5−40 nm, whereas the sizes can be manipulated by varying the ratio of seed to metal salt (Figure 8).[103−105] The step-by-step particle enlargement is more effective than a one-step seeding method to avoid secondary nucleation.[87a] Gold nanorods have been conveniently fabricated using the seeding-growth method.[87b]

3.7. Physical Methods: Photochemistry (UV, Near-IR), Sonochemistry, Radiolysis, and Thermolysis

UV irradiation is another parameter that can improve the quality of the AuNPs,[86,104,105] including when it is used in synergy with micelles[86] or seeds.[104] Near-IR laser irradiation provokes an enormous size growth of thiol-stabilized AuNPs.[106] The presence of an ultrasonic field (200 kHz) allowed the control of the rate of $AuCl_4^-$ reduction in an aqueous solution containing only a small amount of 2-propanol and the

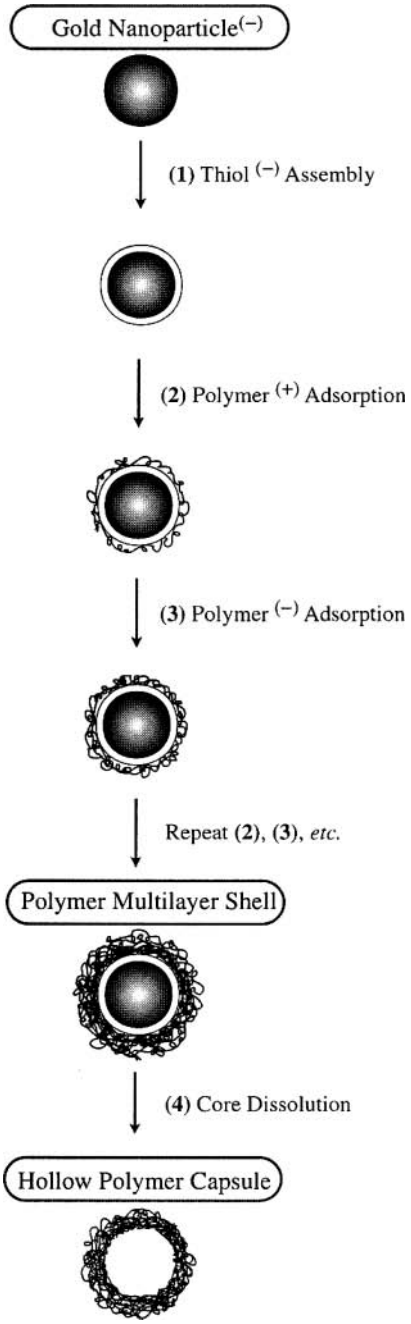

Figure 7. Schematic diagram illustrating the layer-by-layer polymer deposition process applied to AuNPs. Reprinted with permission from ref 98 (Caruso's group). Copyright 2001 American Chemical Society.

sizes of the formed AuNPs by using parameters such as the temperature of the solution, the intensity of the ultrasound, and the positioning of the reactor.[107,108] Sonochemistry was also used for the synthesis of AuNPs within the pores of silica[111−113] and for the synthesis of Au/Pd bimetallic particles.[114] Radiolysis has been used to control the AuNP size[115a] or to synthesize them in the presence of specific radicals,[115b] and the mechanism of AuNP formation upon γ-irradiation has been carefully examined (Figure 9).[116]

AuNPs have been fabricated via decomposition of $[AuCl(PPh_3)]$ upon reduction in a monolayer at the gas/liquid interface.[117] The thermolysis of $[C_{14}H_{29}Me_3N][Au(SC_{12}H_{25})_2]$ at 180 °C for 5 h under N_2

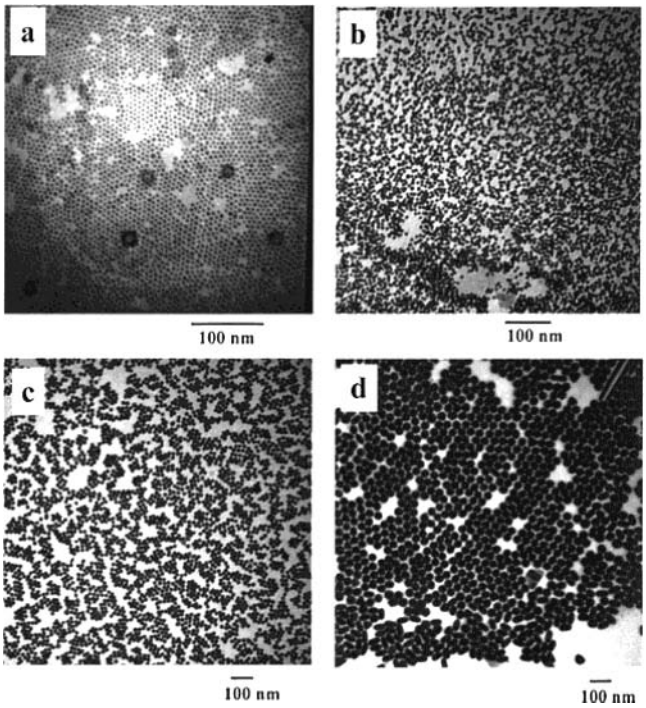

Figure 8. TEM image of larger gold particles prepared from seed: (a) 5.5 ± 0.6, (b) 8.0 ± 0.8, (c) 17 ± 2.5, and (d) 37 ± 5 nm after separation of rods. The 5.5 ± 0.6-nm AuNPs were extracted into toluene after thiol capping for TEM in order to remove excess surfactant. The other particles were separated from excess surfactant by centrifugation. Reprinted with permission from ref 89 (Murphy's group). Copyright 2001 American Chemical Society.

produced alkyl-groups-passivated AuNPs of 26 nm.[118a] Thermolysis of crude preparations of Brust's AuNPs without removing the phase-transfer reagent, tetraoctylammonium bromide, to 150−25 °C led to an increase of the particle sizes to 3.4−9.7 nm, and this size evolution was discussed on the basis of a thermodynamic model. The heat-treated AuNPs formed 2D superlattices with hexagonal packing. The conformation of the alkanethiol is all-trans, and these ligands interpenetrate each other (Figure 10).[118b] Laser photolysis has been used to form AuNPs in block copolymer micelles.[119] Laser ablation is another technique of AuNP synthesis that has been used under various conditions whereby size control can be induced by the laser.[120−122] The evolution of thiol-stabilized AuNPs has been induced by and observed upon heating.[123−126,135] Structural changes of spherical aggregates composed of mercaptoacetate-stabilized AuNPs suspended in water were monitored by maintaining the spheroid suspension at a constant temperature, ranging from 65 to 91 °C, for 2−12 h. The spheroid diameter was reduced to almost 70% of the original size, due to an irreversible "coagulative" transition resulting from fusion among the nanocolloids in spheroids.[126b] Morphology changes of AuNPs were also shown during sintering.[126c] Sputtering AuNPs by single ions and clusters was shown to eject AuNPs.[178]

3.8. Solubilization in Fluorous and Aqueous Media

AuNPs stabilized by perfluorodecanethiol or 1*H*,1*H*,2*H*,2*H*-perfluorooctathiol, with an average

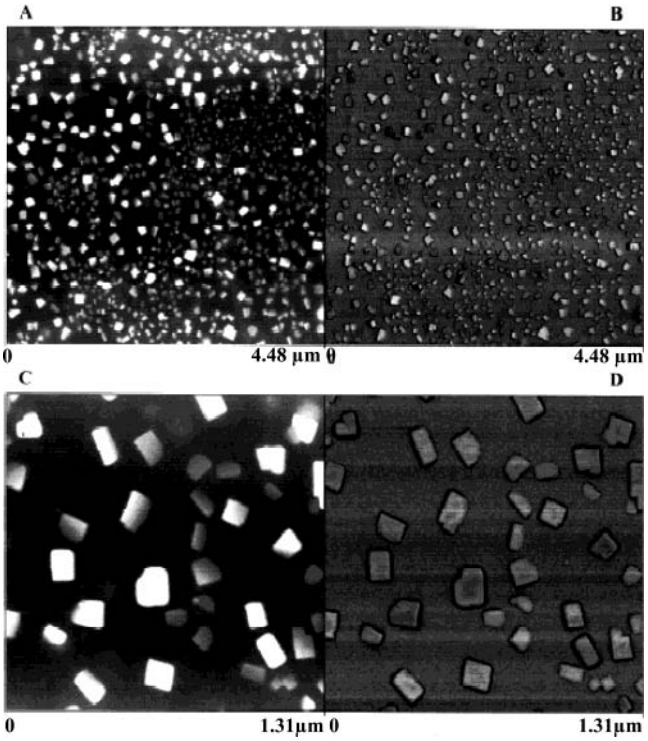

Figure 9. Taping-mode AFM images of the species formed in a solution irradiated with γ rays (1.5 kGy) and then deposited on highly ordered pyrolytic graphite (HOPG) 30 days after the irradiation and dried under a mild N_2 stream for visualization. The solution contains 10^{-3} mol·L^{-1} Au^{III} and poly(vinyl alcohol) but no alcohol. (A) Height-mode (*z* range 80.0 nm) image and (B) phase (*z* range 42.2°) image, run simultaneously on the same area of the sample. (C, D) Close-up images showing the same area as in (A) and (B), respectively. Reprinted from ref 116 (Belloni's group) by permission of The Royal Society of Chemistry (RSC) on behalf of the Centre National de la Recherche Scientifique (CNRS). Copyright 1998.

diameter of 2.4−2.6 nm, were prepared by reduction of $HAuCl_4$ by $NaBH_4$ (dropwise addition) in ethanol and were soluble only in fluorocarbon media.[127]

Special emphasis has been placed on the synthesis of stable water-soluble thiol-stabilized AuNPs[128−134] using thiols containing poly(ethylene oxide) chains[128−130a] (Figure 11) or carboxylate modification (Figure 12).[130b,134] Poly(*N*-vinyl-2-pyrrolidone) (PVP) is the polymer of choice for the stabilization in water of AuNPs prepared by reduction of $HAuCl_4$ (see the section on polymers).

3.9. Characterization Techniques

The most common characterization technique is high-resolution transmission electron microscopy (HRTEM), which gives a photograph of the gold core of the AuNPs,[46] but the core dimensions can also be determined using scanning tunneling microscopy (STM), atomic force microscopy (AFM), small-angle X-ray scattering (SAXS),[50,137a] laser desorption−ionization mass spectrometry (LDI-MS),[137b−139] and X-ray diffraction.[136] A detailed high-resolution study of the AuNP shape using HRTEM, reported by Brust et al., revealed that the truncated cuboctahedron predominated, and that decahedra, dodecahedra and icosahedra were also present in the same preparation of alkanethiol-stabilized AuNPs.[47] The histogram

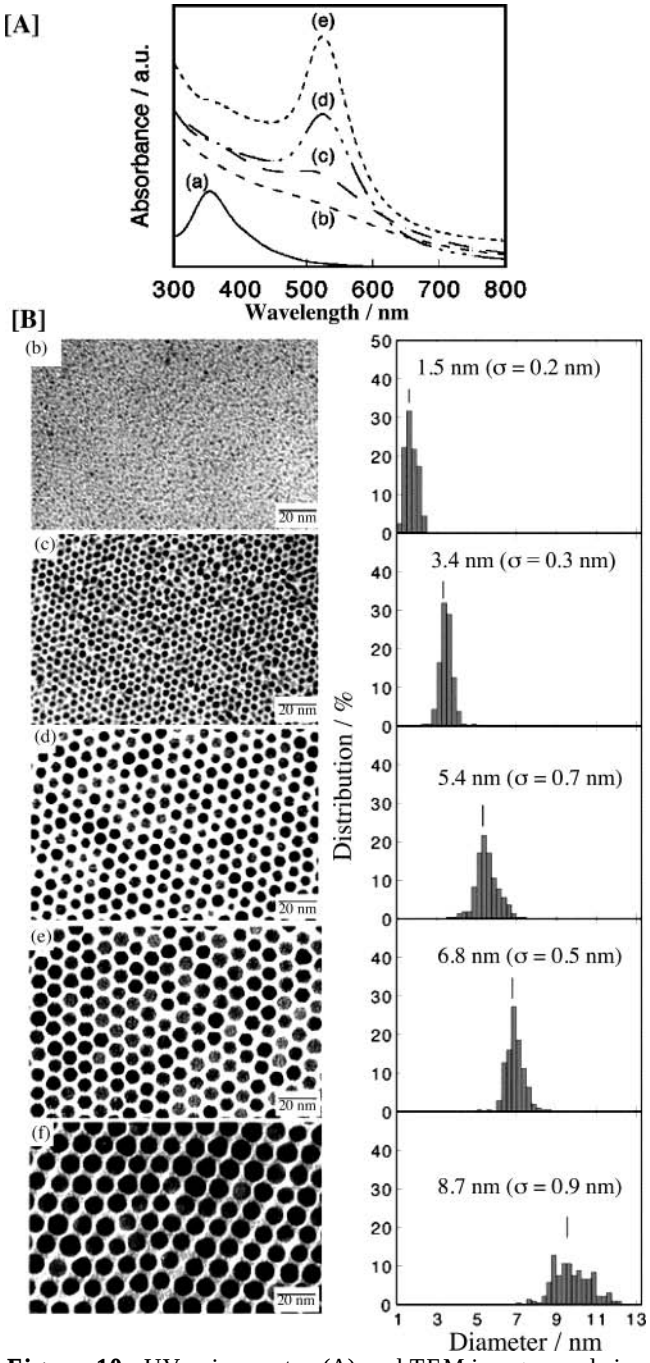

Figure 10. UV−vis spectra (A) and TEM images and size distributions (B) of (a) $[AuCl_4]^-$ before reduction; dodecanethiol-AuNPs (b) as prepared and after heat treatment at (c) 150, (d) 190, and (e) 230 °C; and (f) octadecanethiol-AuNPs heat-treated at 250 °C. Reprinted with permission from ref 188b (Miyake's group). Copyright 2003 American Chemical Society.

providing the size distribution of these cores gives crucial information on the dispersity of the sample that is usually obtained from TEM pictures.[47] The mean diameter, *d*, of the cores allows determination of the mean number of gold atoms, N_{Au}, in the cores:[47] $N_{Au} = 4\pi(d/2)^3/v_{Au}$. For instance, with d = 2.06 nm, $N_{Au} = 269$.[140] From these data, the elemental analysis, giving the Au/S ratio, allows calculation of the average number of S ligands. This number can also be deduced from X-ray photoelectron spectroscopy (XPS) or thermogravimetric analysis (TGA).[50]

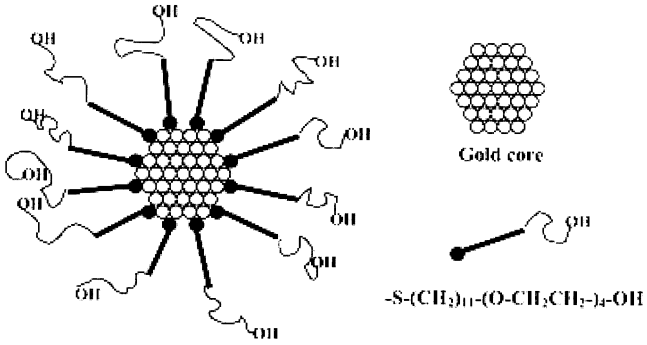

Figure 11. Schematic representation of a AuNP protected by a monolayer of monohydroxy (1-mercaptoundec-11-yl) tetraethylene glycol. The hydrophobic C_{11} chain confers extreme stability to the cluster, while the hydrophilic tetraethylene glycol unit ensures solubility in water. Reprinted with permission from ref 129 (Brust's group). Copyright 2002 The Royal Society of Chemistry.

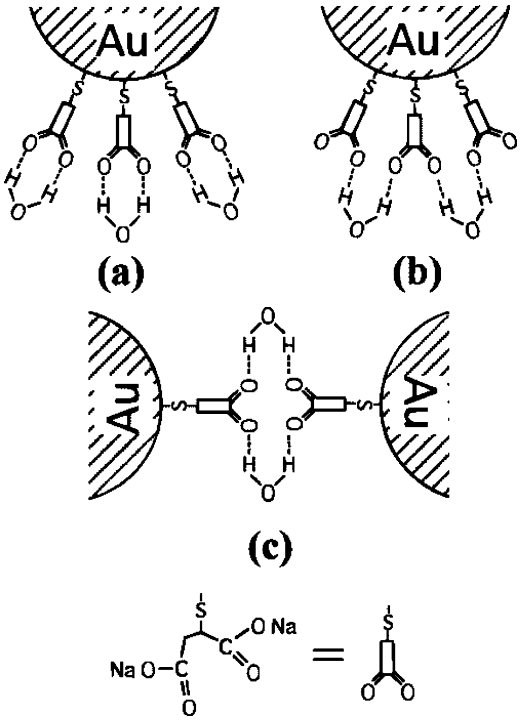

Figure 12. Possible combinations of H_2O molecules with mercaptosuccinic acid (MSA)-capped AuNPs: one H_2O molecule connected with two carbonyl groups in either (a) one MSA molecule, (b) adjoining MSA molecules on one AuNP, making a successive hydrogen-bonding network, or (c) MSA molecules from different AuNPs, the water acting as "glue" to join two neighboring particles. Reprinted with permission from ref 130b (Chen's group). Copyright 1999 American Chemical Society.

The oxidation state of the gold atoms of the core has been examined by Brust et al in their seminal article using X-ray photoelectron spectra that showed the binding energies of the doublet for Au $4f_{7/2}$ (83.8 eV) and Au $4f_{5/2}$ (87.5 eV) characteristic of Au^0. No band was found for Au^I at 84.9 eV, although one-third of the gold atoms are located at the surface and bonded to thiols for 2.0−2.5 nm sized particle cores. On this basis, Brust et al. suggested that the gold-thiol bond does not have the character of gold sulfide.[46b] This matter of a thiol vs thiolate bond to the gold core atoms, however, has been debated. For instance, it was suggested that a high coverage of gold cores by thiolate ligands[139] was due to large ligand/Au binding ratios on core edges and vertexes (Figure 13), in accord with theoretical calculations.[140] Moreover, it was reported that thermolysis of the thiolate-stabilized AuNPs produces only the corresponding disulfide. The absence of thiol by thermal desorption mass spectrometry was considered to be evidence that the chemisorbed ligand consisted of an alkanethiolate (not thiol) fragment. This would mean that H_2 is produced during the reductive synthesis from thiols, but this formation has never been detected. Theoretical calculations suggested the formation of disulfides when the number of thiol molecules around a AuNP was enough to saturate the flat planes, whereas thiolate behavior was observed when the sulfur atoms were not enough.[139a] This finding was reported[139] to corroborate the observation of a S−S distance of 2.32 Å from grazing incidence X-ray in self-assembly of *n*-alkanethiols on a (1,1,1) gold crystal surface.[139b] Brust et al. recently provided ^{1}H NMR evidence for intact thiols adsorbed on AuNPs. They showed that the loss of hydrogen could be prevented to some extent as long as there is no easy reaction path for hydrogen removal.[140]

X-ray diffraction also demonstrated the striking tendency of thiolates−AuNPs to spontaneously form highly ordered superlattices[141−144] with periodicity extending to three dimensions up to several tens of micrometers.[143] These superlattices were obtained upon slow evaporation of the organic solvent or even water on a suitable surface.[144b] Such self-organized superlattices of AuNPs on highly ordered pyrolytic graphite (HOPG) are also observable by STM (Figure 14).[27] Monodispersity is a very important criterion for the formation of ordered superlattices.[145a] When the gas phase at the gas−suspension interface of a synthetic medium leading to sodium mercaptosuccinate−AuNPs contained nonpolar organic molecules, spherical AuNPs formed. On the other hand, when the gas phase contained polar organic vapors such as MeCN or $CHCl_3$, irregular-shaped AuNPs formed.[145b]

Langmuir−Blodgett (LB) films of Schmid's Au_{55} cluster were characterized by STM, Brewter angle microscopy (BAM), and scanning force microscopy (SFM). These techniques showed that the cluster formed monolayers, as indicated by the surface pressure−area ($\pi-A$) isotherms and the area−time ($A-t$) isobars between 20 and 30 °C and 15−30 nN/m of surface pressure, and the cluster size could be estimated from the $\pi-A$ isotherms as 2.17 nm (calcd 2.1 nm).[19] The Au_{55} cluster has also been studied by Mössbauer spectroscopy, extended X-ray absorption fine structure (EXAFS), electron spectroscopy for chemical analysis (ESCA), and conductivity measurements. These techniques show that the Au_{55} particles behave like a system with a few "last metallic electrons" that are used for tunneling between neighboring clusters. This "metallizing" situation was observed by applying an alternating current in the 10-kHz range as for impedance measurements.[146,147] Scanning tunneling spectroscopy (STS) had been used to observe Coulomb blockade in metal nanoparticles. The tunneling current is induced by an

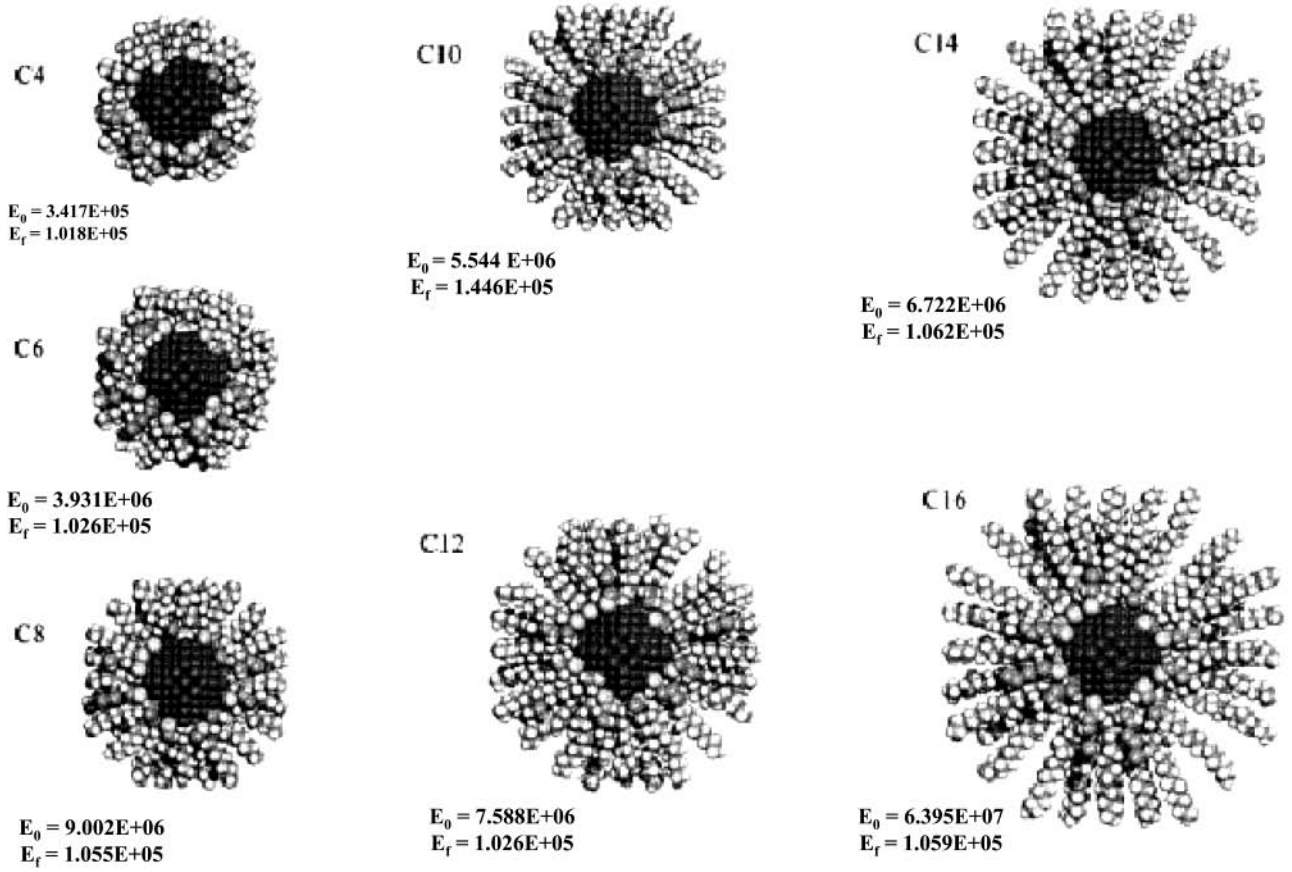

Figure 13. Stable configurations of AuNPs covered with *n*-alkanethiol molecules. The sequence shows $n = 4$ butanethiol, $n = 6$ hexanethiol, $n = 8$ octanethiol, $n = 10$ decanethiol, $n = 12$ dodecanethiol, $n = 14$ butanedecanethiol, and $n = 16$ hexanedecanethiol (n = number of C atoms). Reprinted with permission from ref 139 (José-Yacamán's group). Copyright 1998 Kluwer.

applied voltage and leads to the charging of a metal particle with at least one single electron.[148−150] Electrostatic trapping (ET) is a technique used to investigate isolated nanosize metal particles. It is based on moving a polarized particle in an electric field to the point of strongest field, which is the position between two electrodes (dipped in a solution of the particles) at a distance comparable to the particle diameter.[27,148,149]

The UV−vis and IR spectra provide an identification of the ligand that is also confirmed by NMR spectroscopy, except that the ligand atoms close to the core give broad signals. This latter phenomenon is due to (i) spin−spin relaxational (T_2) broadening (main factor), (ii) variations among the gold−sulfur bonding sites around the particle, and (iii) a gradient in the packing density of the thiolate ligands from the core region to the ligand terminus at the periphery.[151−153] The NMR spectra are very informative, as for all molecular compounds, for the part of the ligand remote from the core. The latter can also be more fully analyzed, if desired, after oxidative decomplexation using iodide.

IR spectroscopy shows that, as in SAMs,[154] the thiolate ligands of AuNPs are essentially in all-trans zigzag conformations, with 5−25% of gauche defects at both inner and terminal locations.[50,152] IR and NMR spectroscopies allow, together with differential scanning calorimetry (DSC),[152−155] the detection of order−disorder transitions in AuNPs in the solid state. The temperature of the transition increases with the chain length, and FTIR shows the increasing amount of gauche defects. Variable-temperature deuterium NMR in the solid state shows that the disorder, materialized by the increased proportion of gauche bonds, propagates from the chain terminus toward the middle of the chain, but not further to the ligand atom, and causes chain melting.[152] Calorimetric measurements led to the determination of the formation enthalpy of AuNPs in a water/sodium bis(2-ethylhexyl) sulfosuccinate/*n*-heptane microemulsion. The results indicated that the energetic states and the dimensions of the AuNPs were influenced by the radii and concentrations of the reversed micelles.[80]

Capillary zone electrophoresis in acetate buffer showed that the mobility of AuNPs with a given core diameter decreased with decreasing ionic strength. At the highest ionic strength investigated (6 mmol/L), a good linear dependence of the mobility on the reciprocal of the core radius allowed the characterization of the size of the AuNPs.[156]

The AFM images of AuNPs operating in the contact mode in air at room temperature showed an attractive interaction among the particles, leading to the formation of aggregates and a mean size that is a function of the size of the reverse micelle used for the synthesis. This was taken into account in terms of the formation of an adsorbed layer of surfactant molecules at the particle surface.[81]

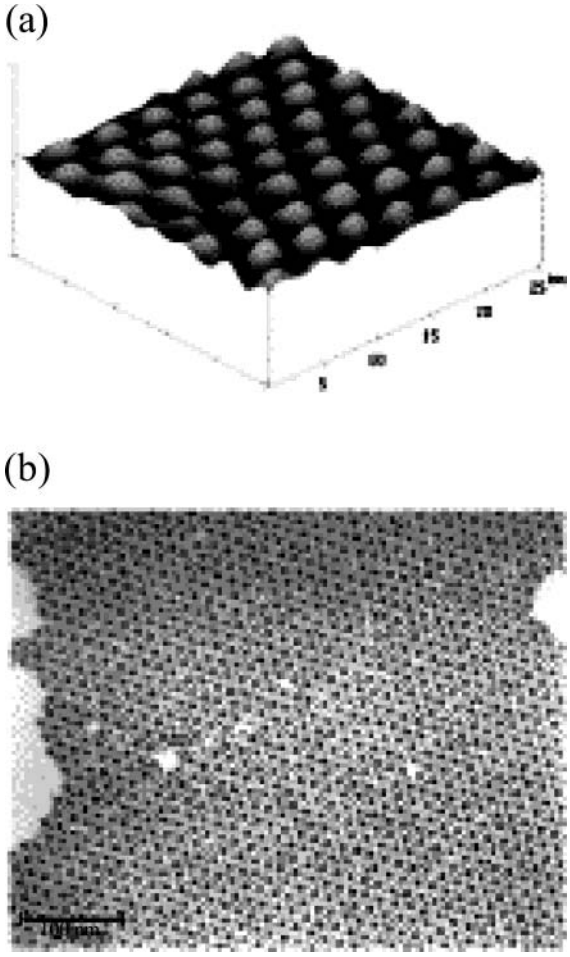

Figure 14. Nanostruture preparation from AuNPs: STM image of self-assembled superlattice of 3.5-nm gold particles on a HOPG substrate. The particles are stabilized by hexanethiol. TEM micrograph of an AB_2 superlattice of AuNPs having a bimodal size distribution (4.5 and 7.8 nm). The AuNPs are stabilized by decanethiol. Reprinted with permission from ref 27 (Brust's group). Copyright 2002 Elsevier.

The use of incoherent light experiments, performed in the vicinity of the surface plasmon resonance frequency, allowed measurement of the phase relaxation time and nonlinear susceptibility of AuNPs of 5−40 nm.[157]

Surface-enhanced Raman scattering (SERS)[70b] and XPS made it possible to analyze the chemisorptive properties of tetrathiol ligands and indicated that surface passivation was an important factor in the dispersibility of AuNPs in nonpolar solvents.[70c]

EXAFS allowed investigation of the size-dependent distance contraction in thiol-stabilized AuNPs, and the short metal−ligand bond found suggested a rather strong surface interaction.[158]

High-resolution time-of-flight mass spectroscopy analysis of alkanethiol-stabilized AuNPs allowed the assignment of the number of gold and sulfur atoms, although alkyl chains were not evident. Pure gold cluster ions of various sizes could be generated from the AuNPs in a two-laser experiment.[159]

Small-angle X-ray scattering, STM, and AFM were consistent with a small, monodisperse (2.4 nm diameter) gold core.[160a] The formation by physical vapor deposition and growth of AuNPs was studied by STM

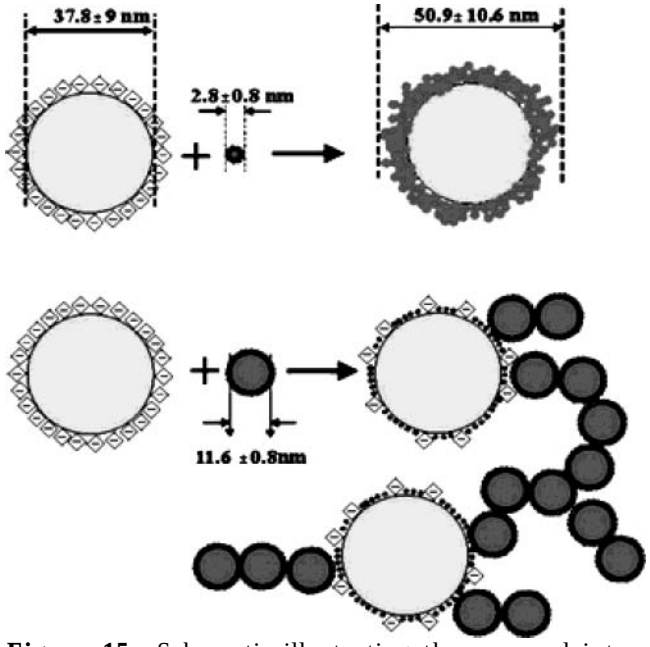

Figure 15. Schematic illustrating the proposed interactions of thiocyanate ion-coated 2.8 ± 0.8- and 11.6 ± 0.8-nm-diameter AuNPs with 37.8 ± 9-nm-diameter ethylenediaminetetraacetic acid (EDTA)-covered AgNPs. Reprinted with permission from ref 164 (Fendler's group). Copyright 2002 The Royal Society of Chemistry.

on TiO_2 (1,1,0) surfaces.[160b] The surface of AuNPs was analyzed using a phase reconstruction technique in TEM, extended to simultaneous correction of spherical aberration and two-fold astigmatism.[160c] The vacancy formation energy of AuNPs has been shown to decrease with decreasing particle size.[160d]

3.10. Bimetallic Nanoparticles

Bimetallic nanoparticles[20,37] containing gold as one of the elements have been synthesized in a variety of ways. Bimetallic AuNPs have been reported with Ag (Figure 15),[161−168] Pd (Figure 16),[97,161,166,167] Pt,[161,167] TiO_2,[99] Fe,[169−171] Zn,[168] Cu,[165,168] ZrO_2,[172] CdS,[173,174] Fe_2O_3,[175] and Eu.[176] Although bimetallic nanoparticles have been known for a long time, Schmid's group were the first to report the synthesis of core−shell bimetallic nanoparticles, the core−shell structure being demonstrated using HRTEM and energy-disperse X-ray (EDX) microanalysis. AuNPs of 18 nm diameter were covered with a Pd or Pt shell when an aqueous solution of these AuNPs was added to a solution of H_2PtCl_6 or H_2PdCl_4 and H_3NOHCl. The original color of the AuNPs then changed to brown-black. Addition of *p*-$H_2NC_6H_4SO_3Na$ stabilized the generated particles in the same manner as P(*m*-$C_6H_4SO_3Na)_3$ stabilized the AuNPs. The colloids showed a metallic luster and were of uniform 35 nm diameter. For instance, Au/Pt particles had an average gold content of 15% atom % located at the core surrounded by Pt crystals of about 5 nm that were pregrown before being added to the Au surface.[161] Stabilization of the bimetallic particles could be achieved using the Brust procedure in the presence of thiols. Such stable bimetallic particles were synthesized with group 10 (Pd, Pt) and group 11 (Cu, Ag, Au) metals, all containing Au as one of the two

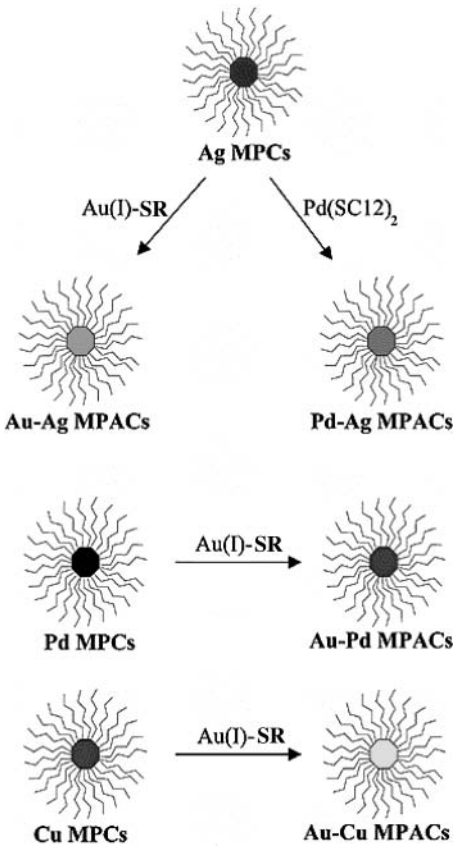

Figure 16. Cartoon diagram of core metal galvanic exchange reactions. MPC, monolayer-protected cluster; MPAC, monolayer-protected alloy cluster; SC12, $S(CH_2)_{11}CH_3$. Reprinted with permission from ref 166a (Murray's group). Copyright 2002 American Chemical Society.

metals, and were characterized using TEM, ^{1}H NMR line broadening, XPS, elemental analysis, and TGA. TEM showed that Pd/Au cores are small (1.7 nm) and relatively monodisperse (average 20% dispersity), while Ag/Au cores are larger (3.2 nm), and other bimetallic particles are of intermediate size. The mole ratios of metals both in and on the surface of the bimetallic cores differed significantly from the metal: salt ratio used in the bimetallic particle synthesis.[162] Partially segregated alloys indeed form easily, and more noble metals prefer the nonsurface (core) location.[20] Metal galvanic exchange reactions are yet another quite facile way to synthesize stable bimetallic particles. This procedure relies on reactions of alkanethiolate−metal particles or other metal particles (Ag, Pd, Cu) with the complexes $[Au^{I}SCH_2(C_6H_4)CMe_3]$ and $[Pd^{II}\{S(CH_2)_{11}Me\}_2]$.[163,166] Au core−Ag shell and Au core−Pt shell nanoparticles have been formed using photochemically reduced phosphotungstate Keggin ions.[168b] Specific properties and functions of bimetallic nanoparticles will be discussed in the appropriate sections devoted to catalytic, electronic, and optical properties.

3.11. Polymers

Since the report in Helcher's treatise in 1718,[3] indicating that starch stabilizes water-soluble gold particles, it has been known that such materials, recognized two centuries later as polymers, favor the isolation of AuNPs.[14,179] With the considerably improved recent understanding of the parameters leading to the stabilization of AuNPs and of their quantum-size-related interest, there has been a revival of activity in the field of polymer-stabilized AuNPs.[33,177,180−181] The most commonly used polymers for the stabilization of AuNPs are PVP and poly(ethylene glycol).[11b,14]

Although there are a variety of ways to achieve nanoparticle−polymer composites,[182,183] two different approaches dominate. The first one consists of the in situ synthesis of the nanoparticles in the polymer matrix either by reduction of the metal salts dissolved in that matrix[184] or by evaporation of the metals on the heated polymer surface.[185] The second one, less frequently used, involves polymerization of the matrix around the nanoparticles.[186] Recently, however, blending of *pre*made AuNPs into a *pre*synthesized polystyrene polymer (synthesized by anionic polymerization) bound to a thiol group was also reported.[187] Whereas the physical process involving mechanical crushing or pulverization of bulk metals and arc discharge yielded large nanoparticles with a wide size distribution, nanoparticles prepared by reduction of metal salts are small, with a narrow size distribution. This reduction processes most often use a reagent such as $NaBH_4$[188] which is added in situ, or the reductant can also be the solvent, such as an alcohol.[189,190] For instance, $HAuCl_4{\cdot}4H_2O$ gives stable AuNPs upon refluxing in methanol/water in the presence of PVP, even if NaOH is added subsequently to the preparation of the AuNPs.[191] In poly(acrylamide), $AuCl_4^-$ cannot be reduced by alcohol, but it can be reduced by $NaBH_4$.[192] Other reductants are generated involving radiolysis, photolysis,[193] or electrochemistry.[194] The polymer−nanoparticle composite can be generated from solution (the classic mode) or can involve the immobilization by a solid polymer such as poly(acrylic acid), poly(vinyl alcohol), or PVP frequently used. Reduction of metal ions in the presence of the polymer is most often chosen because the complexation of the metal cations by the ligand atoms of the polymer is crucial before reduction. In particular, it dramatically limits the particle size.[195]

The most important role of the stabilizing polymer is to protect the nanoparticles from coagulation. Toshima has expressed this function quantitatively by the "gold number", i.e. the number of milligrams of protective polymer that just prevents 10 mL of a red gold sol from changing color to violet upon addition of 1 mL of 10% aqueous NaCl. The "gold number" is smaller for protective polymers that are better stabilizers.[189] Core−shell PVP-stabilized Au/Pd[196] and Au/Pt[197,198] nanoparticles were prepared by Yonezawa and Toshima by simultaneous alcohol reduction of the two corresponding metal salts and characterized by EXAFS. The relative order of reduction in alcohol/water is seemingly controlled by the relative redox potentials, $HAuCl_4$ being reduced more rapidly than $Pd(OH)_2$ and $PtCl_6^{2-}$. The AuNPs form first, and then the Pd or Pt shell forms around the AuNPs to produce the core−shell bimetallic particles. In fact, the Pd^0 formed reduces $AuCl_4^-$ to Au^0 and thus acts as a mediator or redox catalyst for the reduction of $AuCl_4^-$, as long as any $AuCl_4^-$ is left in

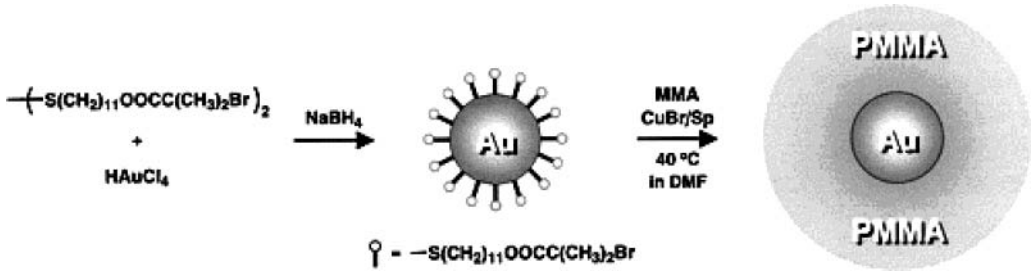

Figure 17. Schematic representation for the synthesis of polymer-coated AuNPs by surface-initiated living-radical polymerization (LRP). Reprinted with permission from ref 214 (Fukuda's group). Copyright 2002 American Chemical Society.

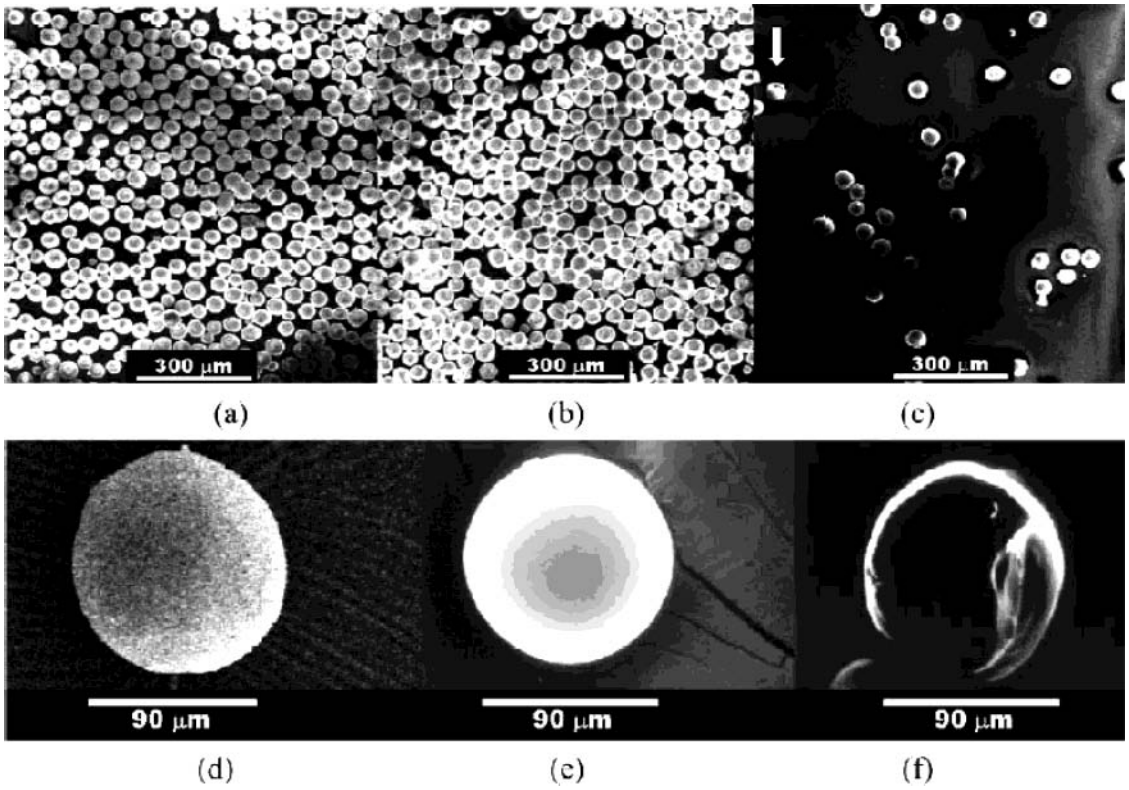

Figure 18. SEM image of (a) 50-μm ceramic hollow spheres (CHSs), (b)-50 μm gold-seeded CHSs, (c) 50-μm gold hollow spheres (GHSs) obtained by calcination and dissolution of gold-seeded CHSs, (d) a 100-μm CHS, (e) a 100-μm gold-seeded CHS, and (f) a 100-μm broken GHS. The arrow in (c) indicates a broken particle, which proves that it is hollow. From (f), it can be seen that the inside of GHS is empty. Reprinted with permission from ref 216b (Fendler's group). Copyright 2002 Elsevier.

the solution.[199,200] Attempts to synthesize Pd-core/Au-shell bimetallic particles led instead to a remarkable cluster-in-cluster structure because of this redox priority (Figure 16).[201]

Many ordered polymer−AuNPs are known. For instance, AuNPs in PVP were prepared by hydrazine reduction of incorporated $HAuCl_4$. The color of the solution of $HAuCl_4$-loaded block copolymer changed from yellow to purple, and then to bluish upon addition of a large excess of anhydrous hydrazine. The reduction can be stopped by addition of HCl, which protonates hydrazine in order to avoid coagulation of the AuNPs.[202,203] These phenomena were also obtained with (styrene-*block*-ethylene oxide).[204,205]

The use of a diaminotriazine-functionalized diblock copolymer led to size-controlled synthesis of AuNP aggregates in solution and in thin films with thymine functionality.[206] AuNPs were generated in polymeric micelles composed of amphiphilic block copolymers,[207,208] and amphilic star-block copolymers were an ideal choice to serve as a confined reaction vessel.[209] The formation of AuNPs was also controlled by using poly(methylphosphazene), whose lone pairs stabilized the AuNPs.[210] Functionalized polymers have also been used as stabilizers. Poly(ethylene glycol)-based polymer was used to fabricate an AuNP sensor that reversibly binds lectin for recognition and bioassay.[211] The so-called "grafting from" technique has been used to construct highly dense polymer brushes. For instance, several methods,[212−214] including the efficient living radical polymerization (LRP), have indeed been applied to the synthesis of AuNPs coated with such a high-density polymer brush. AuNP-based nanoscale architectures could be forecasted using this simple technique (Figure 17).[214]

Polymer hollow spheres have been synthesized with movable AuNPs at their interiors.[215] AuNPs can serve as templates for the synthesis of conductive capsules[216] (Figure 18) and for the oligomerization of L-cysteine in aqueous solution (Figure 19).[217]

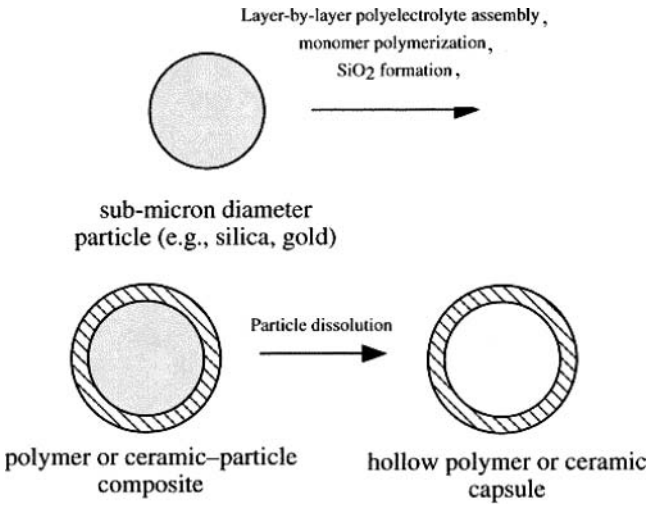

Figure 19. AuNPs as templates for the synthesis of hollow polymer capsules. Reprinted with permission from ref 216c (Feldheim's group). Copyright 1999 American Chemical Society.

Nanosized domains of block copolymers can be used as nanoreactors to synthesize AuNPs by expansion of the nanosized domains and period of block copolymers, such as polystyrene-*block*-poly(4-vinylpyridine) (PS−PVP) diblock copolymers.[218] Self-assemblies of AuNPs/polymer multilayer films have been formed using surface functionalization.[219,220] AuNPs of average size between 1 and 50 nm have also been stabilized by many water-soluble polymers, and some of then have been shown to be stable after 9 months in air. The most stable ones were obtained with polymers possessing hydrophobic backbones and side groups, allowing good interactions with the $AuCl_4^-$ ion. The preparations were carried out using either UV irradiation or KBH_4 to reduce $HAuCl_4$ in the presence of a mass ratio of polymer:gold 25:1.[221]

Linear polymers having cyano or mercapto groups stabilize AuNPs of 1.5−3 nm diameter and narrow size distributions.[222] AuNPs of Brust type with some thiol chain termini bearing *exo*-norbornene units were polymerized using ring-opening metathesis polymerization (ROMP) to produce a block copolymer shell.[223,224] Small AuNPs (5 nm diameter) stabilized with sodium citrate[225] were attached to the surface of silica nanoparticles protected by polymer layers to provide contrast in the final TEM image, a strategy also used to obtain TEM contrast for many types of molecular[97] and biological materials.[226] Solution behavior, i.e., transformation in the morphology from small spherical AuNPs to large anisotropic objects, was observed by decreasing the concentration of polystyrene-*block*-poly(2-vinylpyridine) micelles below the critical micelle concentration (Figure 20).[85]

Networks of AuNPs prepared in water were observed by TEM upon adding poly(acrylic acid) to AuNPs stabilized by thiolated poly(ethylene oxide) chains of high molecular weight (necessary to stabilize AuNPs in water). Moreover, thin and linear thermally robust arrangements were formed when chondroitin sulfate c sodium salt (a polysaccharide carrying sulfuric acid groups and carboxylic acid groups) was added (Figure 21).[227] AuNPs of about 20 nm size were formed upon reduction of $AuCl_3$ by polyaniline in *N*-methylpyrrolidinone.[228] An amine-functionalized polymer was used to simultaneously assemble carboxylic-acid-functionalized AuNPs and silica naoparticles into extended agregates.[229] Such a strategy also led to spherical silica templates (Figure 22).[226] Macroporous Au spheres with a diameter ~9 μm have been formed by employing porous organic bead templates and preformed AuNPs.[230] AuNPs were stabilized by the lone nitrogen pair on the backbone of polymethylphosphazene, $[Me(Ph)PN]_n$, and varying the ratio of $[Me(Ph)PN]_n$ to $HAuCl_4$

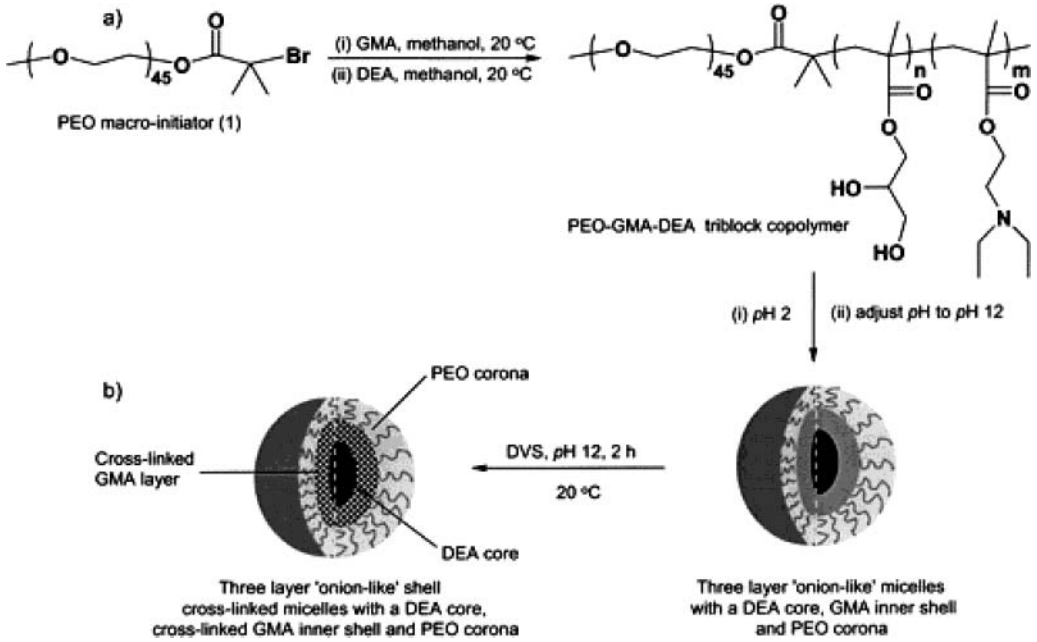

Figure 20. (a) Reaction scheme for the synthesis of the PEO-GMA-DEA$^{\alpha}$ triblock copolymers. (b) Schematic illustration of the formation of three-layer "onion-like" micelles and shell cross-linked micelles from PEO-GMA-DEA triblock copolymers. PEO-GMA-DEA, poly[(ethylene oxide)-*block*-glycerol monomethacrylate-*block*-2-(diethylamino)ethyl methacrylate]. Reprinted with permission from ref 85 (Armes's group). Copyright 2002 American Chemical Society.

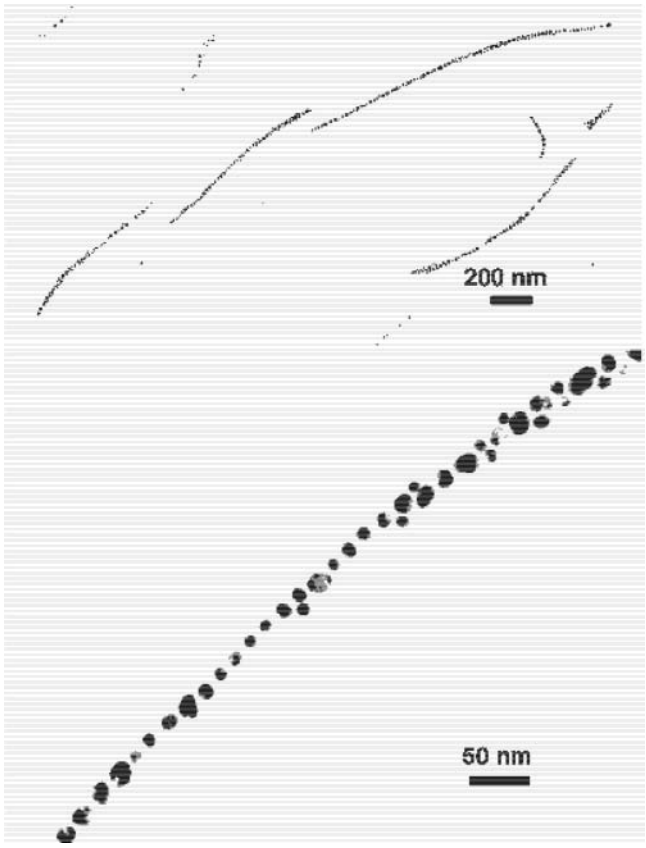

Figure 21. TEM images of AuNPs covered with PEGSH 2000, observed in the presence of chondroitin sulfate c sodium salt (polysaccharide carrying sulfuric acid groups and carboxylic acid groups, which are expected to interact with the PEG chain). Reprinted with permission from ref 228 (Ishiwatari's group). Copyright 2002 The Chemical Society of Japan.

prior to reduction allowed control of the AuNP size.[231] AuNPs (4−12 nm) were associated with thiol-functionalized polyoxometalates γ-$[SiW_{10}O_{36}(RSi)O]^{4-}$ (R = HSC_3H_6), where the R group played the role of both stabilizing the AuNPs via the thiolate ligand and forming a covalent link to the polyanion through the trimethoxysilane group.[232] The preparation of poly(*N*-isopropylacrylamide)-protected AuNPs has been carried out in a homogeneous phase using various methods, and this polymer was found to be a better passivant than alkanethiols.[233a]

AuNPs were prepared in both aqueous and organic systems by reducing $HAuCl_4$ with *o*-anisidine in the presence of 1:1 *N*-methyl-2-pyrrolidone/toluene.[233b] AuNPs of 6 nm diameter and narrow size distributions were stabilized by π-conjugated poly(dithiafulvene) polymers, and the oxidized form of this polymer induced a strong red shift of the absorption spectrum of the AuNPs to 550 nm (whereas the theory predicts 510−515 nm for the plasmon band in water).[234] AuNPs with improved stability against long-term aggregation up to one month were prepared using poly(styrene)-*block*-poly(2-vinylpyridine) star-block copolymer.[235]

Water-soluble polymer-stabilized AuNPs were prepared from citrate-capped AuNPs by simple contact with dilute aqueous solutions of hydrophilic nonionic polymers based on the monomers *N*-[tris(hydroxymethy)methyl]acrylamide and *N*-(isopropyl)acrylamide that were functionalized with disulfide anchoring groups. The resulting polymer-coated AuNPs could be stored in the dry state and redispersed in water to yield sterically stabilized AuNP suspensions. The disulfide-bearing polymers exhibited only a slightly larger affinity for the gold surface than those that do not have the disulfide groups. The polymer layers allowed the free diffusion of small solutes but efficiently minimized the nonspecific absorption of large molecules such as proteins, a promising property (Figure 23).[236a] AuNPs have been synthesized in graft copolymer micelles,[87] and the diffusion of AuNPs in a polymer matrix has been analyzed.[236b] Core−shell AuNPs have been prepared by the layer-by-layer technique, utilizing polyelectrolyte multilayers assembled onto polystyrene cores as thin films in which to infiltrate AuNPs, and hollow spheres were obtained by removal of the templated polystyrene cores.[236c]

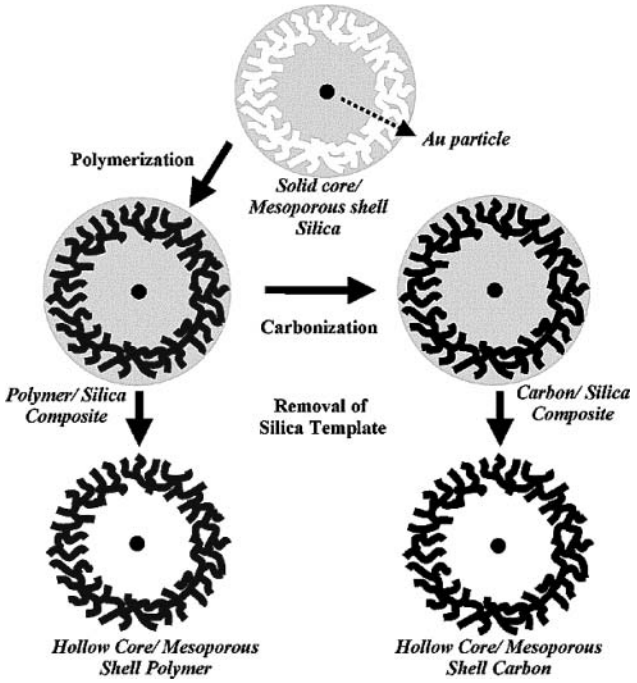

Figure 22. Schematic illustration for the synthesis of Au@HCMS (hollow core/mesoporous shell) polymer and carbon capsules. Reprinted with permission from ref 226 (Hyeon's group). Copyright 2002 American Chemical Society.

3.12. Dendrimers

A variety of assemblies between PAMAM dendrimers and AuNPs were reported in which the AuNPs were stabilized by the dendrimer that acted as both a polymer and a ligand. The AuNPs were stabilized only in the presence of excess PAMAM dendrimers and in solution, but PAMAM dendrimers functionalized with thiol termini could completely stabilize the AuNPs.[237] PAMAM dendrimers were also functionalized with hydrophobic groups for solubilization of the AuNPs in organic solvents.[238,368] Such dendrimer−AuNP assemblies were deposited as films on surfaces and used as sensors.[239−241] AuNPs were synthesized from $AuCl_3$ in DMF using PAMAM dendrimers that were modified with surface methyl ester groups.[242] The use of PAMAM dendrimers for the stabilization of AuNPs allowed control of the

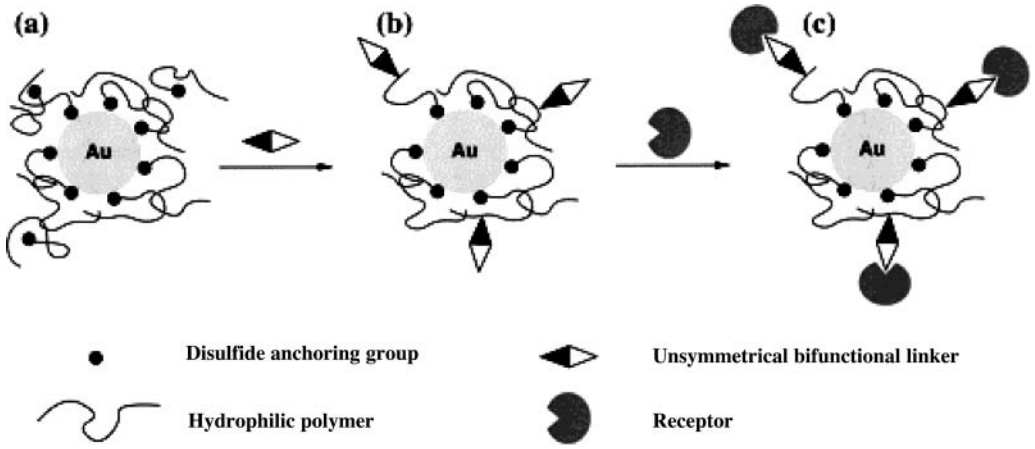

Figure 23. Stepwise "grafting-to" derivatization of AuNPs. (a) Fixation of the polymer with disulfide anchoring groups. (b) Activation of the polymer by unsymmetrical bifunctional linker groups. (c) Functionalization of the polymer by receptors. Step (b) is omitted when "activated" polymers are used. Reprinted with permission from ref 236a (Mangeney's group). Copyright 2002 American Chemical Society.

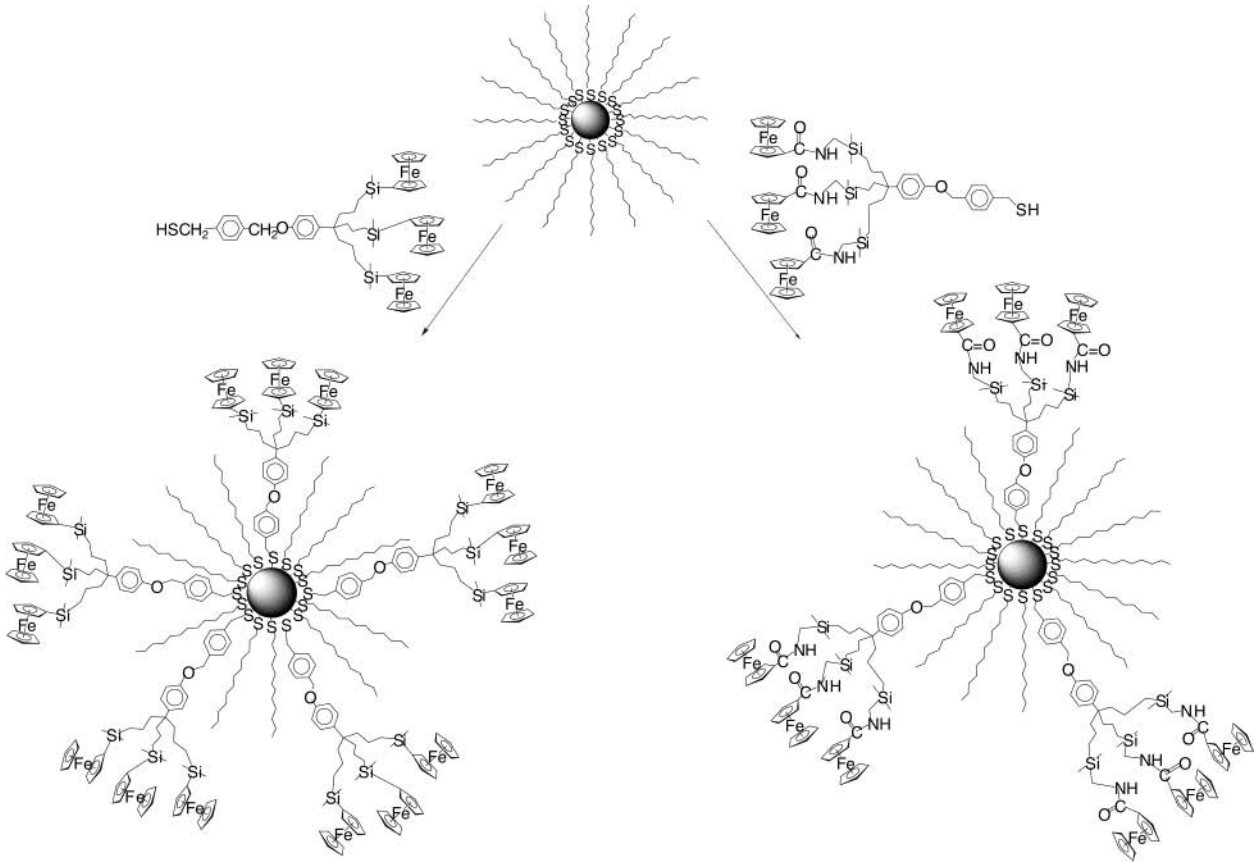

Figure 24. Syntheses of dendronized AuNPs using the thiol ligand substitution procedure. Reprinted with permission from ref 251 (Astruc's group). Copyright 2003 American Chemical Society.

interparticle distance.[243] PAMAM−dendrimer−AuNPs assemblies were incorporated into SiO_2 matrices.[244] The pH dependence of water-soluble PAMAM−dendrimer-stabilized AuNPs was examined,[245] and such assemblies were used for imaging in cells.[246] Bimetallic Au−Pd nanoparticles were synthesized by Crooks's group from PAMAM−dendrimer−Pd nanoparticles assemblies for a catalytic purpose.[247−249] Dendrimers containing a AuNP core were synthesized by using the Brust−Schiffrin technique with dendrons that were functionalized with thiols at the focal point (Figures 24 and 25).[250−254] PAMAM−dendrimer−AuNP composites were used as chemiresistor sensors for the detection of volatile organic compounds and studied by specular neutron reflectometry.[255a] AuNPs were formed in the presence of stiff polyphenylene dendrimer templates with 16 thiomethyl groups on the outside.[255b]

3.13. Surfaces, Films, Silica, and Other AuNP Materials

AuNPs were deposited on surfaces for a number of purposes, including physical studies[256−275] (Figures 26−28) and derivatization of self-assembled monolayers.[276−278] Privileged materials for deposition are

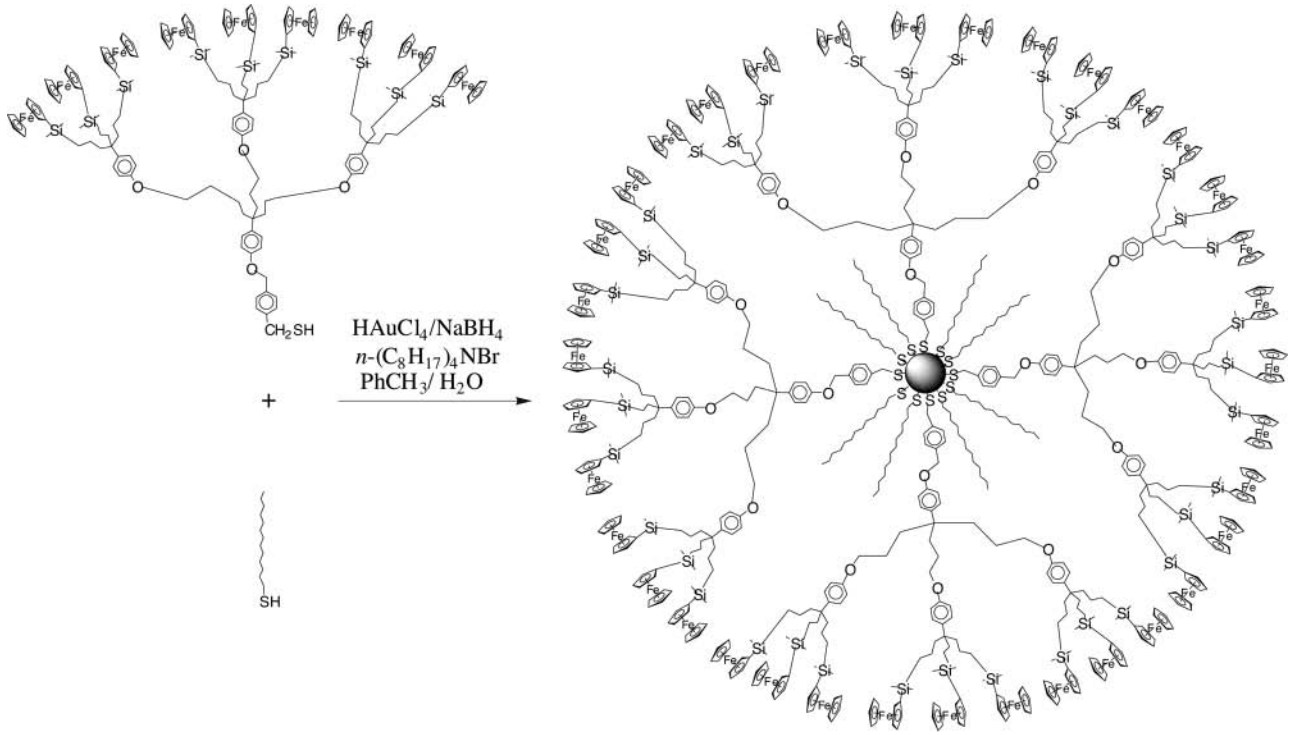

Figure 25. Direct syntheses of dendronized AuNPs containing a nonaferrocenyl thiol dendron (about 180 ferrocenyl groups). Reprinted with permission from ref 251 (Astruc's group). Copyright 2003 American Chemical Society.

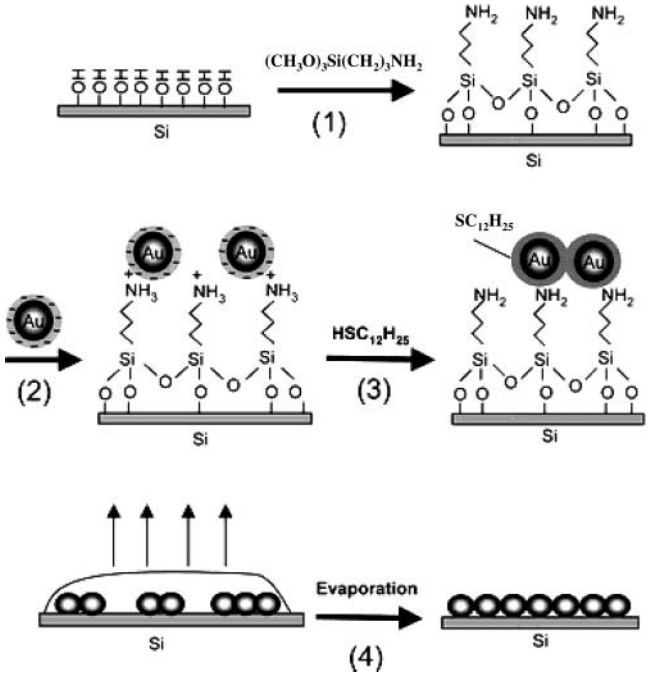

Figure 26. Schematic representation of the procedures developed for fabricating two-dimensional arrays of AuNPs on a silicon substrate in combination with self-assembly of an (aminopropyl)triethoxysilane monolayer, immobilization of nanoparticles, alkanethiol treatment, and solvent evaporation technique. Reprinted from ref 258 (Liu's group) by permission of the PCCP Owner Societies. Copyright 2002.

Si,[279] various molecular silicon substrates,[280] TiO_2 (Figure 29),[281−285a] $BaTiO_3$,[285b] $SrTiO_3$,[285c] Al_2O_3 (Figure 30),[286] ammonium salts,[287] and various forms of carbon[288−293] ([60] fullerene (Figure 31),[288,289] nanotubes,[290,291] and diamond[292]). AuNPs were also deposited together with [Ru^{II}tris(2,2′-bipyridine)] to

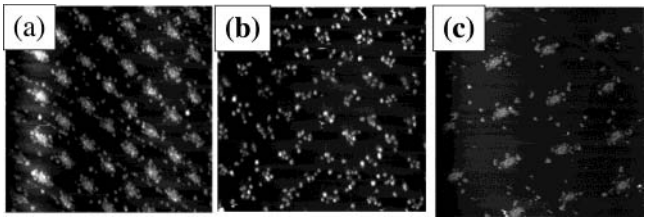

Figure 27. Tapping-mode AFM images (2 μm × 2 μm) of the morphologies of a 0.02-mL gold film deposited on focused ion beam patterned surfaces for different ion fluences I_f and periodicities l_{def}: (a) l_{def} = 300 nm, I_f = 37 500 ions per point; (b) l_{def} = 300 nm, I_f = 3750 ions per point; (c) l_{def} = 500 nm, I_f = 37 500 ions per point. Reprinted with permission from ref 262 (Bardotti's group). Copyright 2002 Elsevier.

form multistructures whose photocurrent responses were recorded.[294]

Thin films of AuNPs were prepared,[126,295−309] in particular LB films[310−319] (Figure 32) and monolayers[320] at the liquid interface[92,321] and from the gas phase.[322a] Typically, the Brust−Schiffrin method was used to synthesize alkanethiol-stabilized AuNPs that were subsequently spread on the water surface. These totally hydrophobic films could sustain reasonable pressures, and the compressibility was high. It appeared likely that multilayers were generated above 6−8 mN/m.[317] Films of several tens of cm^2 in width and several microns in thickness were formed by cross-linking AuNPs with alkanedithiols, followed by filtration onto nanoporous supports.[322b] A conducting AuNP film is simply produced by rinsing a polystyrene plate with ethanol and water, followed by stirring it at room temperature in an aqueous solution consisting of a thiol and a AuNP solution.[323] AuNPs were dispersed into Nylon-1,1 thin films, and the resulting materials were studied during heat treatment.[324−326] Phase transfer of AuNPs across a

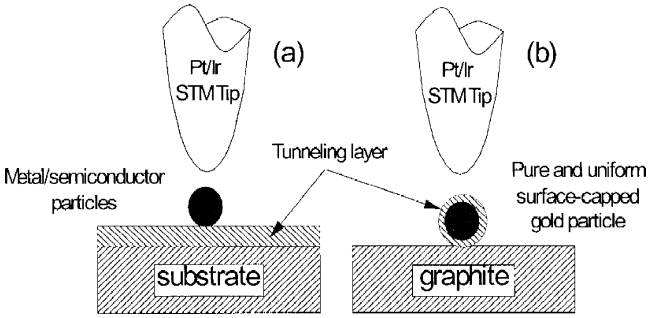

Figure 28. Schematic configuration of the experimental apparatus for measuring current−voltage characteristics by an STM tip. (a) Conventional structure of single-electron tunneling (SET) devices in which a small AuNP is separated from a substrate electrode by an ultrathin tunneling layer. (b) Current structure of the SET devices in which a small AuNP is separated from an HOPG ground plane by a surface-capped tunneling layer on the gold particle. Reprinted with permission from ref 272 (Huang's group). Copyright 1998 Elsevier.

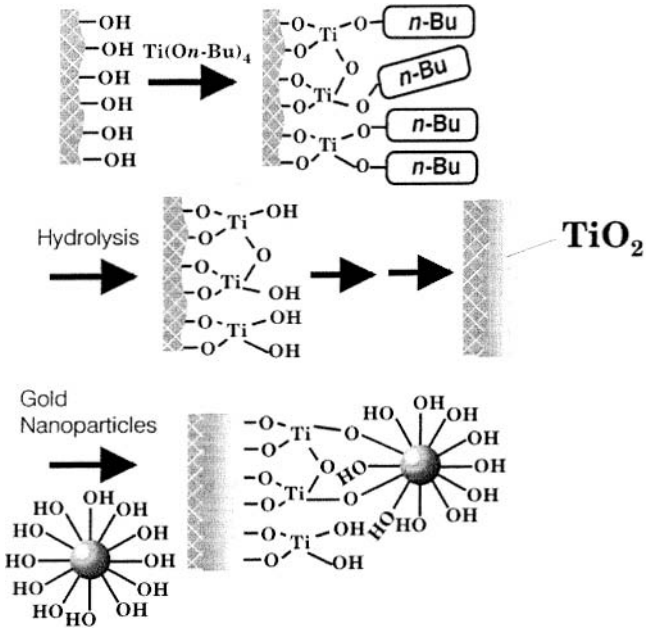

Figure 29. Schematic illustration of sequential surface sol−gel technique and alternate assembly. Reprinted with permission from ref 284a (Kunitake's group). Copyright 1999 American Chemical Society.

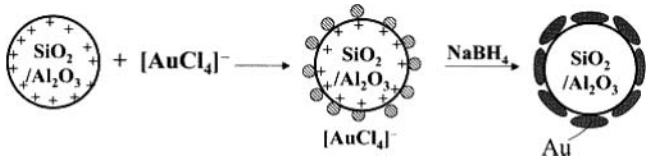

Figure 30. AuNP deposits on SiO_2/Al_2O_3 nanoparticles produced by reduction of $[AuCl_4]^-$ with freshly prepared sodium borohydride solution. Reprinted with permission from ref 115b (Kamat's group). Copyright 2000 American Chemical Society.

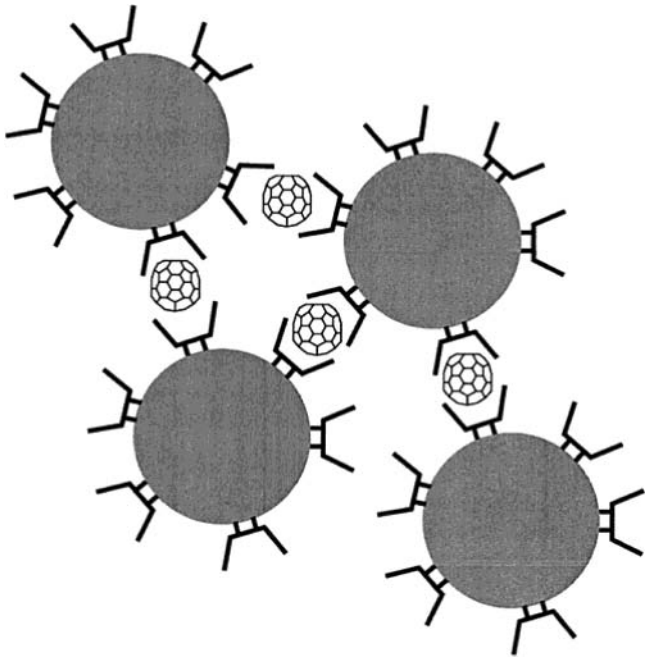

Figure 31. Fullerene-induced network of γ-cyclodextrin-capped AuNPs in aqueous solution. Reprinted with permission from ref 288a (Kaifer's group). Copyright 2001 American Chemical Society.

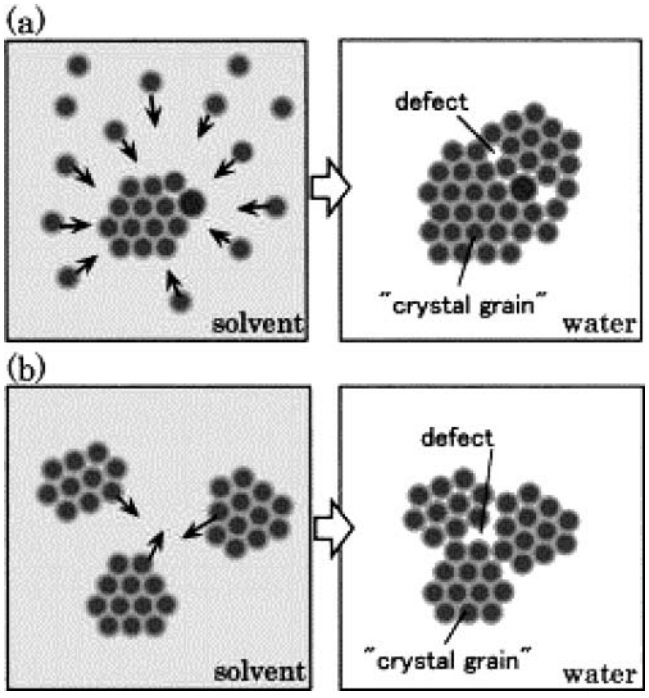

Figure 32. Schematics of the formation of the defects in LB monolayers prepared from (a) a low particle concentration and (b) a high AuNP concentration of LB spreading suspensions. Reprinted with permission from ref 312 (Huang's group). Copyright 2001 American Institute of Physics.

water/oil interface was achieved by stoichiometric ion-pair formation between carboxylate anions on particle surfaces and tetraoctylammonium cations and revealed by TEM, IR, UV−vis absorption, and EDX.[327a] Complete phase transfer of negatively charged ($-CO_2^-$ or $-SO_3^-$), surface-modified AuNPs from the aqueous phase to the organic phase was carried out by hydrophobization using primary amines.[327b] AuP nanowires that are between 100 and 200 nm wide could be formed by ultrashort laser pulses.[327c]

There are many reports of the preparation, characterization, and study of AuNPs dispersed within mesoporous silica, $Au@SiO_2$.[111−113,125,328−360] The influence of size, [328,329] the biofunctionalization,[331] the crystal growth,[332] the organization in high order

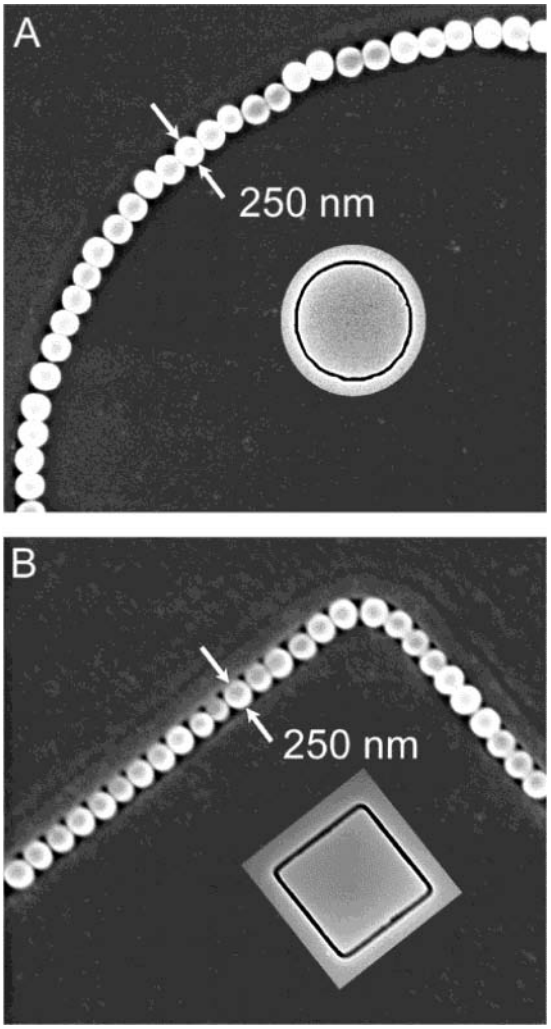

Figure 33. SEM images of plasmonic waveguide structures fabricated by assembling the Au@SiO_2 core−shell AuNP against templates (see insets) patterned in thin films of photoresist. These core−shell AuNPs had a core diameter of 50 nm and a shell thickness of ~100 nm. Reprinted with permission from ref 329a (Xia's group). Copyright 2002 American Chemical Society.

(Figure 33),[333] the influence of radiations on the nucleation,[342] and the sol−gel approach[354,359] have been examined in the preparations of Au@SiO_2. The two most common synthetic methods to form sol−gel matrices of AuNPs are the citrate route followed by stabilization by a (3-aminopropyl)trimethoxysilane (APTMS)-derived aminosilicate and the sol−gel processing in inverse micelles (Figure 34).[354] For instance, 2- and 5-nm AuNPs have been inserted in mesoporous silica materials MCM-41 and MCM-48 by the Somorjai group.[352] Another simple and successful method involves tetramethoxysilane, partially hydrolyzed tetrakis(hydroxymethyl)phosphonium chloride, and $HAuCl_4$ in aqueous solution to produce Au@SiO_2 containing up to 1% weight Au.[342] Reduction of $HAuCl_4$ using H_2 at 973 K for 1 h was also successfully used.[344] The sonochemical approach of $HAuCl_4$ reduction leads to the deposition of AuNPs on the surface of the silica spheres[113] or within the pores of mesoporous silica.[111,112] Some methods for the engineering of the AuNP surface have been described.[355] The homogeneous incorporation of silica-coated AuNPs into a transparent silica gel without

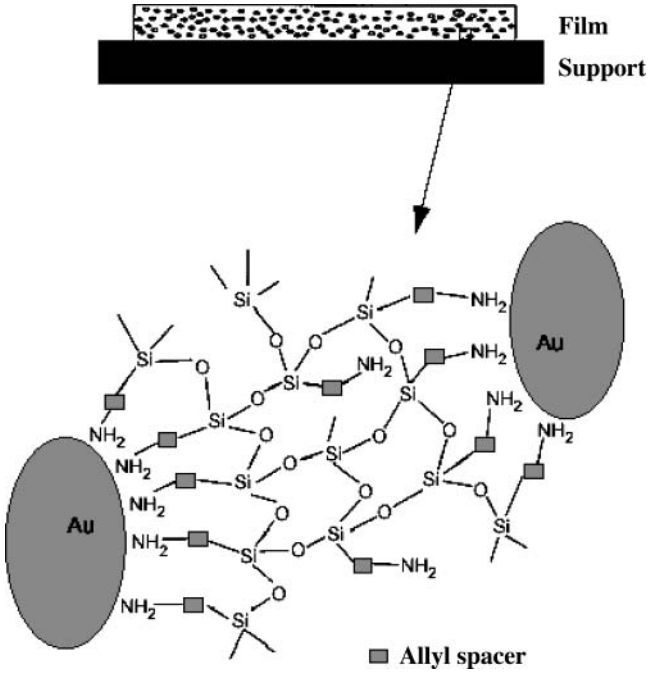

Figure 34. Schematic illustration of AuNPs in a silicate matrix. Reprinted with permission from ref 353 (Lev's group). Copyright 1997 The Royal Society of Chemistry.

any aggregation of particles has been reported.[335] There is growing interest for the assembly and study of AuNPs on silanized glass plates,[295,300,347,360,492,645−648]

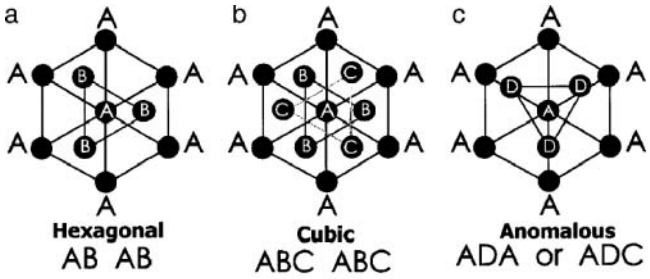

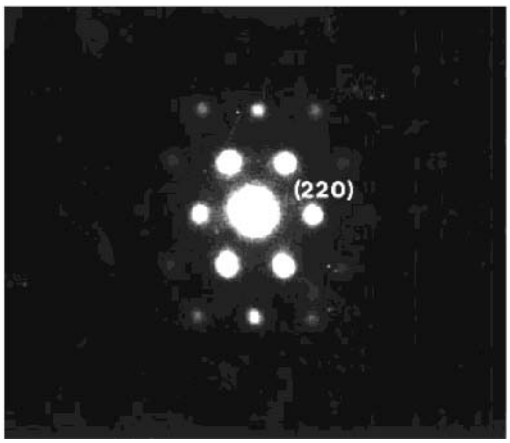

Figure 35. AuNP superlattices. (Top) Packing sequences observed in AuNP superlattices: (a) hexagonal close-packing ABAB, (b) cubic close-packing ABC ABC, and (c) anomalous packing in which AuNPs sit on two fold saddle positions D. The packing becomes ADA or ADC. (Bottom) High-dispersion diffraction patterns from an FCC AuNP superlattice on the [111] zone axis. The reflections (220), corresponding to the second row of reflections, correspond to the void superlattice. Reprinted with permission from ref 366 (José-Yacamán's group). Copyright 2000 Springer.

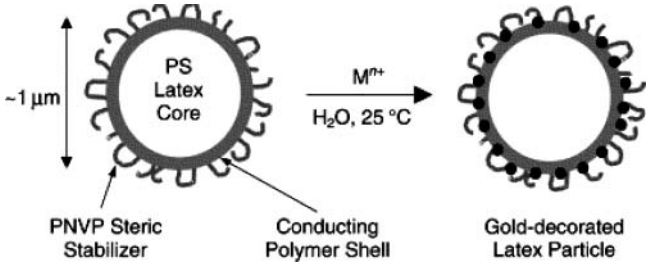

Figure 36. Synthesis of gold-decorated latexes via electroless deposition of gold from aqueous solution, using the conducting polymer overlayer as a redox template. PNVP, poly(*N*-vinylpyrrolidone). Reprinted with permission from ref 372a (Armes's group). Copyright 2001 The Royal Society of Chemistry.

and highly stable AuNPs have been prepared inside HY zeolite supercages.[361]

AuNPs have been manipulated to form highly ordered 1D,[65,362−364] 2D,[141,365] or 3D[59,366,367] (Figure 35) nanonetworks and superstructures.[60,368] Synthetic opals[369,370] were fabricated using a layer-by-layer process.[370] AuNPs have been formed in lipids following electrostatic entrapment of $AuCl_4^-$,[371] and biomolecular templating allowed site-specific organization of AuNPs.[372] AuNPs have been used to decorate latexes via conducting polymer templates (Figure 36).[373a] The spin-coating method was shown to be far superior to the traditional immersion method for the fast fabrication of AuNPs attached to APTMS-modified fused silica.[373b]

AuNP-containing materials, whose assembly is mentioned in this section, will be also discussed for their applications in the sensors and catalysis sections.

4. Physical Properties

4.1. The Surface Plasmon Band (SPB)

The deep-red color of AuNP sols in water and glasses reflects the surface plasmon band (SPB; see also section 2 for background), a broad absorption band in the visible region around 520 nm. The SPB is due to the collective oscillations of the electron gas at the surface of nanoparticles (6s electrons of the conduction band for AuNPs) that is correlated with the electromagnetic field of the incoming light, i.e., the excitation of the coherent oscillation of the conduction band. The study of the SPB has remained an area of very active research from both scientific and technological standpoints, especially when the particles are embedded in ionic matrices and glasses.[374,375] For instance, a driving force for this interest is the application to the photographic process.[376] Thus, the SPB provides a considerable body of information on the development of the band structure in metals and has been the subject of extensive study of optical spectroscopic properties of AuNPs.[375,377−379]

The nature of the SPB was rationalized in a master publication authored by Mie in 1908.[379] According to Mie theory, the total cross section composed of the SP absorption and scattering is given as a summation over all electric and magnetic oscillations. The resonances denoted as surface plasmons were described quantitatively by solving Maxwell's equations for spherical particles with the appropriate boundary conditions. Mie theory attributes the plasmon band of spherical particles to the dipole oscillations of the free electrons in the conduction band occupying the energy states immediately above the Fermi energy level.[380] All the numerous subsequent and recent reports correlate the spectroscopic behavior of AuNPs with the Mie theory.[24,375,380−383] The main characteristics of the SPB are (i) its position around 520 nm; (ii) its sharp decrease with decreasing core size for AuNPs with 1.4−3.2-nm core diameters due to the onset of quantum size effects that become important for particles with core sizes <3 nm in diameter and also cause a slight blue shift (the damping of the SP mode follows a 1/radius dependence due essentially to surface scattering of the conduction electrons;[381,384] this decrease of intensity of the SPB as particle size decreases is accompanied by broadening of the plasmon bandwidth); and (iii) steplike spectral structures indicating transitions to the discrete unoccupied levels of the conduction band with monodispersed AuNPs with core diameters between 1.1 and 1.9 nm.[382,383]

Thus, the SPB is absent for AuNPs with core diameter less than 2 nm, as well as for bulk gold. For AuNPs of mean diameter of 9, 15, 22, 48, and 99 nm, the SPB maximum λ_{max} was observed at 517, 520, 521, 533, and 575 nm, respectively, in aqueous media. The SPB maximum and bandwidth are also influenced by the particle shape, medium dielectric constant, and temperature. The refractive index of the solvent has been shown to induce a shift of the SPB, as predicted by Mie theory.[385,386] For instance, solutions of dodecanethiolate AuNPs of 5.2 nm average diameter reveal an 8-nm shift in SPB as the solvent refractive index is varied from $n_d^{20} = 1.33$ to 1.55. The ligand shell alters the refractive index and causes either a red or blue shift, so that the spectroscopic data obtained often deviate from the prediction of Mie theory that deals with naked nanoparticles. The agreement with Mie theory is obtained only when the shift induced by this ligand shell is taken into account. This shift is especially significant with thiolate ligands, which are responsible for a strong ligand field interacting with the surface electron cloud. In fact, since all AuNPs need some kind of stabilizing ligands or polymer, the band energy is rarely exactly as predicted by Mie theory if the shift of this stabilizer is not considered. With elliptical particles, the SPB is shifted to higher wavelength as the spacing between particles is reduced, and this shift is well described as an exponential function of the gap between the two particles. It becomes negligible when the gap is larger than about 2.5 times the short-axis length.[386c] A red shift for a polarization parallel to the long particle axis and a blue shift for the orthogonal polarization were reported and rationalized by a dipolar interaction mechanism.[386d] The optical thickness could be used as a measure of efficiency, this parameter being critically dependent on particle size and refractive index. Therefore, impurities can be easily detected since the refractive index of AuNPs greatly differs from that of gold oxide

or gold chloride.[386g]

Another influential parameter is the core charge. Excess electronic charge causes shifts to higher energy, whereas electron deficiency causes shifts to lower energy.[386,387] A convenient theoretical expression has been derived for the SPB position as a function of the changes in free electron concentration:

$$\lambda_{final}/\lambda_{initial} = (N_{initial}/N_{final})^{1/2}$$

For instance, in the AuNPs of 5.2 nm diameter containing 2951 Au atoms, the authors assume that there is one free electron per Au atom (e.g., $N_{initial}$ = 2951 free electrons per AuNP); AuNPs charged to +0.82 V vs Ag leads to the removal of 19 electrons per AuNP, and thus N_{final} is 19 electrons less (N_{final} = 2932). This corresponds to a predicted red shift of 1.7 nm, which is much smaller than that observed experimentally (9 nm from 516 to 525 nm, which would theoretically correspond to the removal of 100 electrons from the AuNP). The reason for this difference is not clear, and tentative explanations involve a much reduced number of free electrons and large shift amplification by the thiolate ligand shell.[386]

The SPB width was found to increase with decreasing size in the intrinsic size region (mean diameter smaller than 25 nm) and also to increase with increasing size in the extrinsic region (mean diameter larger than 25 nm). A small temperature effect was also found. It was proposed that the dominant electronic dephasing mechanism involves electron−electron interactions rather than electron−phonon coupling.[387a] Femtosecond light scattering of AuNPs of 80 nm diameter showed, on the other hand, that both electron−phonon and phonon−phonon coupling processes occur in the individual AuNPs.[387b] In Au−SiO_2 core−shell particles (Au@SiO_2), varying the SiO_2 shell thickness and the refractive index of the solvent allowed control over the optical properties of the dispersions, and the optical spectra were in good agreement with Mie theory.[356] The SPB position in Au@SiO_2 (including films) was accurately predicted by the Maxwell−Garnett model, and it was concluded that it is possible to synthesize composite materials with optical properties that lie anywhere between those of transparent glass and those of metallic gold.[388−390]

A near-field optical antenna effect was used to measure the line shape of the SPB in single AuNPs, and the results were found to be in agreement with Mie theory; double-peak shapes caused by electromagnetic coupling between close-lying particles were observed.[391]

From optical spectra of oriented AuNPs/polyethylene, the SPB extinction maxima of AuNPs for incident fields polarized parallel to the direction of nanoparticle orientation (λ_{max} − (0)) were found to be red-shifted relative to the extinction maxima for perpendicular polarization (λ_{max} − (90)).[392] For rodlike particles, the extinction maximum for incident electric fields polarized along the long axis occurs at a longer wavelength than the λ_{max} for polarization along the particle radius.[393] Selective suppression of

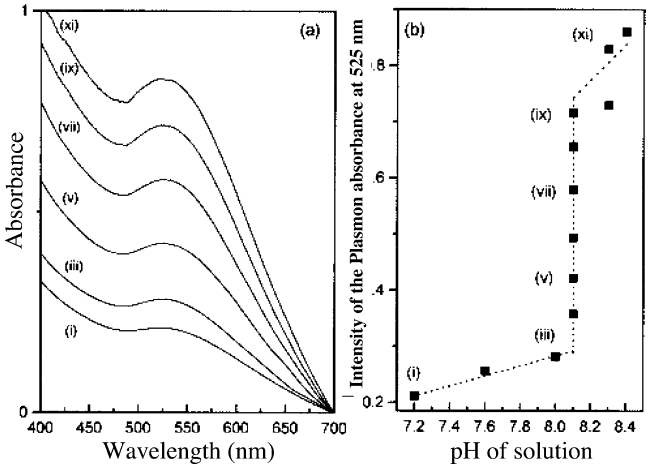

Figure 37. (a) UV/vis solution spectra of 4-mercaptobenzoic acid-capped AuNPs as a function of the addition of NaOH(aq) and (b) the variation of the intensity of the plasmon absorbance, at 525 nm, as a function of the pH of the solution. Points i, iii, v, vii, ix, and xi in (b) were obtained from curves i, iii, v, vii, ix, and xi in (a), respectively. Reprinted with permission from ref 93 (Evans's group). Copyright 1998 American Chemical Society.

extinction of the SPB was observed.[394,395] Picosecond dynamics of AuNPs was studied by laser excitation close to the SPB at 66 nm, leading to the formation of "hot" non-Fermi electronic distribution within the AuNPs.[396] Visible−laser-induced fusion and fragmentation could be induced by thionicotamide, and aggregation effects disappear following laser pulse excitation.[397a] Softening of the coherently excited breathing mode on AuNPs was observed by time-resolved spectroscopy, showing that the period of breathing mode increases with pump laser power.[397b] The coagulation (along with Oswald ripening) of AuNPs dispersed in organic liquids was dramatically accelerated by visible light, and the process was shown to be wavelength dependent; UV irradiation caused coalescence.[398] Laser irradiation at the SPB of suspended AuNPs in 2-propanol causes coagulation or dispersion, depending on concentration, the photochemical reaction being due to electron transfer from a solvent molecule to the AuNP.[399] AuNPs were pulverized into smaller AuNPs with a desired average diameter and a narrow distribution by a suitable selection of laser irradiation.[400] When a molecular linker, 4-aminobenzenethiol, attached several AuNPs together, the optical absorption differed, consistent with plasmon−plasmon interactions between the AuNPs of the assembly (Figure 37).[401]

Applications of the sensitivity of the position of the SPB are known, especially in the fields of sensors and biology. A shift of the SPB of AuNPs has been measured upon adsorption of gelatin, and quantitative yield measurements of the adsorbed amount were obtained.[402] Rhodamine 6G was shown to provoke morphological changes and particle growth upon laser irradiation of the SPB as a result of melting and fusion of AuNPs, and the multiphoton process leading to the fusion process has been elucidated using picosecond laser flash photolysis (Figure 38).[403] Increasing the solution temperature from 10 to 40 °C thermally triggered the reversible hydrophilic-to-hydrophobic phase transition of the adsorbed elastin-

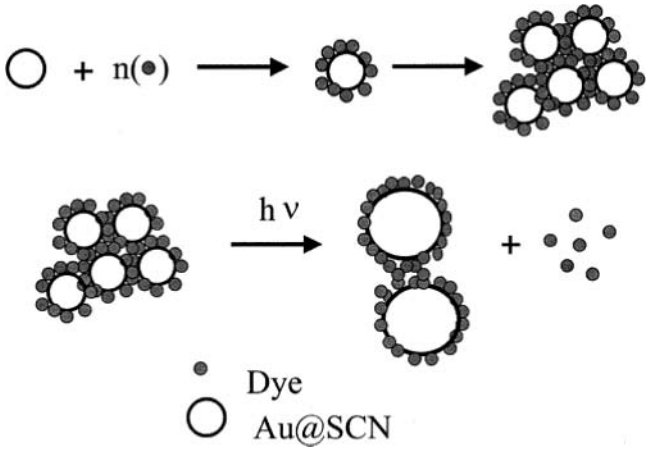

Figure 38. Schematic diagram illustrating the possible morphological changes associated with laser irradiation of the AuNP−dye assembly. Au@SCN, AuNPs obtained by reduction of $AuCl_4^-$ with SCN^-. Reprinted with permission from ref 402 (Kamat's group). Copyright 2000 American Chemical Society.

like polypeptide, a thermally responsive biopolymer.[404] Formation of large aggregates caused a reversible change in color of the AuNP suspension from red to violet due to coupling to surface plasmons in aggregated colloids. The SPB was used to study the dispersibility of AuNPs in a variety of solvents (Figure 39).[405] Phase transfer of dodecylamine-capped AuNPs dispersed in an organic solvent into water containing the surfactant cetyltrimethylammonium bromide (CTAB) was monitored by color changes initiated upon shaking.[406] Surface interaction of AuNPs with functional organic molecules was probed using the shifts of the SPB. For instance, a red shift was observed with an increase of the solvent dielectric constant with solvents that do not coordinate the gold core, but the SPB is unaffected in polar solvents that do not bind to the core.[407] AuNPs consisting of a mixture of triangular/hexagonal and smaller, close-to-spherical particles display two SPBs at 540 and 680 nm, respectively, as expected. UV−visible data indicate preferential adsorption of the flat AuNPs on polyelectrolyte films and the development of a new band at 650 nm as the number of bilayers increased.[408a] Compared to solid AuNPs of similar size, nanorings produced on soda−glass substrates using colloidal lithography exhibit a red-shifted localized SPB that could be tuned over an extended wavelength range by varying the ratio of the ring thickness to its radius.[408b]

The magnetic circular dichroism (MCD) spectra of AuNPs and $Au_9(PPh_3)_8^{3+}$ encapsulated in optically transparent xerogels have been shown to be temperature dependent between 5 and 295 K only for the former, and indicate that the MCD spectra of the latter reflect an excited-state phenomenon with a strong intermixing of the excited spin−orbit states.[382b] The hot electron dynamics of AuNPs was characterized using femtosecond two-color pump−probe spectroscopy in the SPB region.[382c]

4.2. Fluorescence

Fluorescence studies of AuNPs have been carried out under various conditions,[409−419] including femtosecond emission[410] and steady-state investigation of

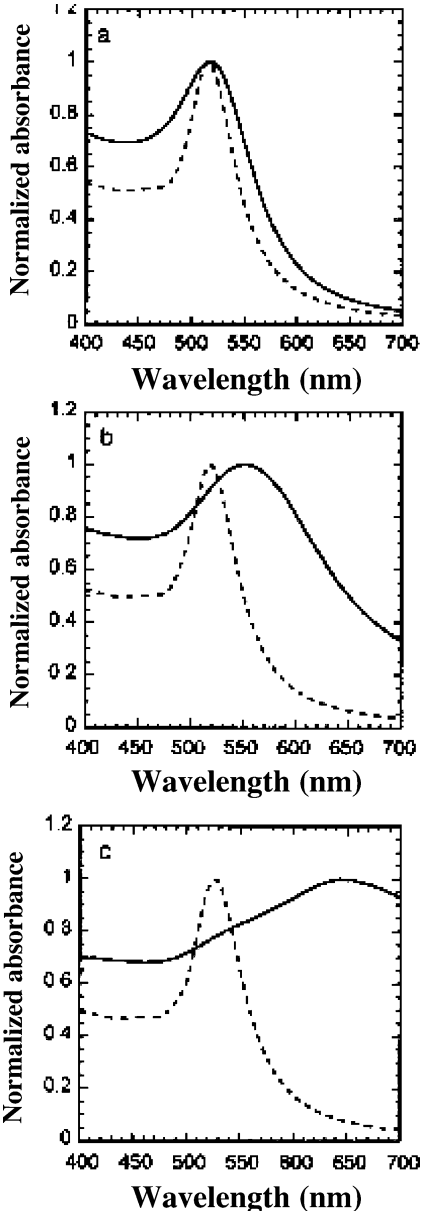

Figure 39. Optical absorption spectra of AuNPs 8.3 nm in diameter dispersed in (a) water, (b) ethanol, and (c) chloroform. The dashed lines represent the values calculated from the Mie equation. The solid lines represent the experimental data. Reprinted with permission from ref 404 (Huang's group). Copyright 2002 American Institute of Physics.

the interaction between thiolate ligands and the gold core.[411] Capping fluorescent groups are pyrenyl,[413] polyoctylthiophenyl,[415] fluorenyl,[419] and other probes.[414,416−418] Indeed, resonant energy transfer was observed in fluorescent ligand-capped AnNPs, this phenomenon being of great interest in biophotonics[420] and materials science.[421−423] Both radiative and nonradiative rates critically depend on the size and shape of the AuNPs, the distance between the dye molecules, the orientation of the dipole with respect to the dye−nanoparticle axis, and the overlap of the molecule's emission with the nanoparticle's absorption spectrum.[418] Orders-of-magnitude higher efficiencies were obtained with nanometer-dimension metal samples.[424−426] The observed increase in the fluorescence yield reflected the suppression of the

nonradiative decay upon binding to AuNPs.[414] Visible luminescence has been reported for water-soluble AuNPs, for which a hypothetical mechanism involving 5 $d^{10} \rightarrow 6\ (sp)^1$ interband transition has been suggested.[409] On the basis of the ability of discrete photoisomeric states of spiropyrans to exhibit distinct physical properties, photoswitchable AuNP assemblies of various amino acids were designed by anchoring spiropyrans to allow the release of the outer sphere of amino acids on irradiation.[427]

4.3. Electrochemistry

The electrochemistry of thiolate-stabilized AuNPs showing the formation of core charge has been indicated in section 2 (staircase blockade).[39,40] Moreover, the quantized capacitance charging of AuNPs self-assembled monolayers on electrode surfaces could be rectified by certain hydrophobic electrolyte ions, such as PF_6^-, in aqueous solution (Figure 40).[39c] In the presence of some *p*-nitrothiophenolate ligands, the peak spacings corresponding to the quantized capacitance charging were found to decrease slightly compared to those obtained in the absence of *p*-nitrothiophenolate ligands, corresponding to a small decrease of the particle capacitance due to the presence of more polar ligands.[428a] Magnetoelectrochemistry of AuNP quantized capacitance charging showed the influence of a magnetic field on the electrochemistry of AuNPs, and in particular the effect of electron parity upon their charging states.[428b] Double-layer capacitance was obtained in aqueous media by differential pulse voltammetry.[428c] The voltammetry of small AuNPs containing respectively 11[429a] and 38[429b] core Au atoms has been reported.

Viologen thiols and dithiols have been synthesized and connected to AuNPs.[430,431] In particular, viologen thiols have been used as redox-active linkers in order to study electron transfer between the linked AuNPs.[430a] AuNPs have been shown to tune the electrochemical properties of the electrode/solution interface using the $Fe(CN)_6^{3-/4-}$ redox system.[432]

The electrochemistry of functional AuNPs containing thiolate ligands bearing ferrocenyl[49b] or amido- or silylferrocenyl[140,250−252,433] and biferrocenyl groups has been reported, and these ferrocenyl- or biferrocenyl-derived AuNPs have been deposited on electrodes by scanning around the potential region around the Fe^{II}/Fe^{III} waves.[251,252] Nishihara's group has modified alkanethiol-stabilized AuNPs by thiol ligands bearing biferrocenyl[434−437] or anthraquinone[436,437] using the thiolate-exchange method. The second oxidation process of the biferrocenyl units of AuNPs−biferrocenylthiolate led to a uniform redox-active AuNP film on an electrode. AuNPs−anthraquinonethiolate was found to be aggregated by two-electron reduction of anthraquinone groups. These findings confirmed that AuNPs containing multiple redox molecules could assemble according to charge accumulation. The multielectron system seemed to be indispensable for these deposition phenomena, as they were not observed for AuNPs linked via thiolate ligands with a single redox species such as ferrocenyl.[49b] This property also allowed Yamada and Nishihara to construct alternating multilayed structures of palladium and gold nanoparticles connected with biferrocenyl groups (Figure 41).[440] Ferrocenyldendronized AuNPs also adsorb very well, a useful property for molecular recognition (vide infra).[251,252] C_{60}-functionalized AuNPs, synthesized using the ligand-exchange procedure, can form a derivatized electrode upon immersion of a gold electrode, and this modified electrode showed two peaks corresponding to the reduction of C_{60} that were stable upon scanning.[441a] The charge injection energetics between a solution redox couple and hexanethiol−AuNPs has been probed by scanning electrochemical microscopy.[441b] Altogether, electrochemistry has been used in several ways to fabricate and deposit AuNPs,[251,252,436−441] inter alia on porous silicon.[441c] A APTMS-supported AuNP electrode was constructed; therefore, the preparation procedure using 3-mercaptopropionic acid-bridged copper hexacyanoferrate multilayers on a planar macroelectrode was copied to the as-prepared AuNP electrode.[441d] AuNPs formed from ferrocenylthiophenol (2.5 nm) were studied inter alia by voltammetry, showing only 15% coverage with the composition $Au_{490}Fc_{80}$.[441e] AuNP microelectrodes have been prepared with uniform Pt group overlayers.[442a]

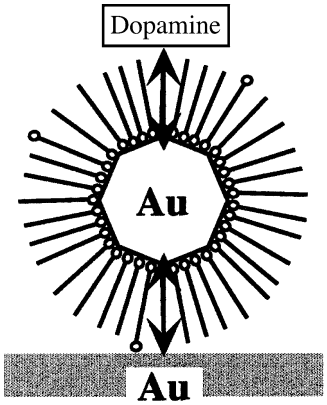

Figure 40. Schematic chart of electron tunneling through surface-confined AuNP layers. Reprinted with permission from ref 39c (Chen's group). Copyright 2001 American Chemical Society.

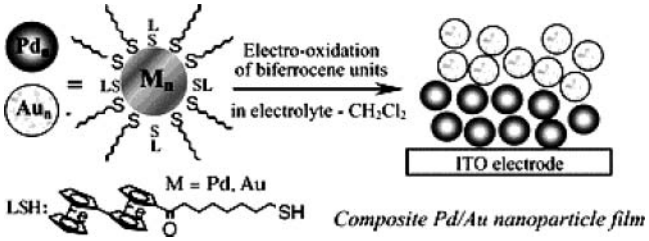

Figure 41. Combination of electro-oxidative deposition of PdNPs attached with biferrocene-terminated thiolates and that of AuNPs with the same thiolates, to form a thin redox-active film with a layered hybrid structure. Reprinted with permission from ref 440 (Nishihara's group). Copyright 2002 The Royal Society of Chemistry.

4.4. Electronic Properties Using Other Physical Methods

It was found that, for 2D superlattices consisting of large (5 nm) AuNPs, the electronic behavior was dominated by the Coulomb blockade effect at low temperature, while the $I-V$ response was ohmic at

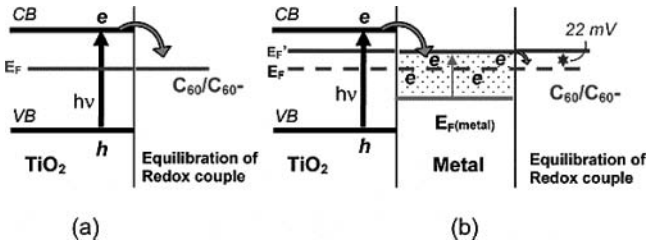

Figure 42. Charge distribution between TiO_2 and AuNPs, leading to equilibration with the C_{60}/C_{60}^- redox couple (a) in the absence and (b) in the presence of metal nanoparticles. E_F and E_F' refer to the Fermi levels of TiO_2 before and after attaining equilibrium, respectively. Reprinted with permission from ref 442b (Kamat's group). Copyright 2003 American Chemical Society.

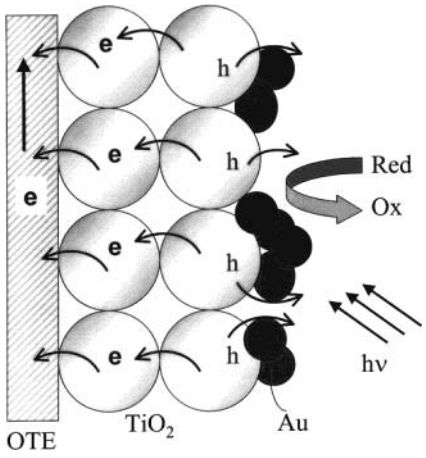

Figure 43. Charge separation in a AuNP-modified nanostructured TiO_2 electrode. OTE, optically transparent electrode. Reprinted with permission from ref 459 (Kamat's group). Copyright 2000 American Chemical Society.

room temperature.[61] TiO_2 nanoparticles exhibited a blue coloration due to stored electrons within the particles when subjected to UV. A partial disappearance of the blue color was seen upon contact with AuNPs as electrons were transferred from TiO_2 to AuNPs (Figure 42).[442b] TiO_2 films cast on conducting glass plates were modified by adsorbing AuNPs (5 nm diameter) from a toluene solution, and selective formation of Au islands and larger particles on the TiO_2 suface was observed by TEM and AFM (Figure 43).[459] A technique was described in which a AuNP was connected to two Cr electrodes, and electron transport in this sample could be fitted to orthodox theory of electron tunneling.[443a] Scanning electrochemical microscopy was used to investigate the kinetics of electron-transfer reactions between methyl viologen (MV^{2+}) and protons, giving H_2 and $MV^{+\bullet}$, catalyzed by AuNPs supported on an insulating substrate. This technique allows investigation of AuNP size effects on the kinetics and study of reactions at semiconductor nanoparticle surfaces in the absence of a metallic conductor.[443b] An electronic conductivity study of composites made from 1,10-decanethiol and AuNPs using pressed pellets between 1-μm electrode gaps showed that the $I-V$ curve was sigmoidal (Figure 44).[438] The rectifying effects of electrolyte ions on interfacial electron transfer were investigated with AuNP monolayers anchored by bifunctional chemical bridges containing viologen groups (Figure 45).[439] X-ray absorption near-edge structure (XANES) of 2-nm AuNPs capped with dendrimer and thiol revealed the gain of a 5d electron relative to the bulk when capped with weakly interacting dendrimers and the loss of a 5d electron when capped with strongly interacting thiol ligands.[444a] The chemical states of the self-assembled AuNPs absorbed onto the surface of a silane were studied by angle-resolved X-ray photoelectron spectroscopy, which made it possible to distinguish bound thiolate ligands and unbound thiols[444b] and to investigate the size-dependent systematics of lattice contraction and charge redistribution.[444c] Using a pump−probe technique, the dynamics of the hot carriers in nanodots induced by femtosecond laser pulses showed that

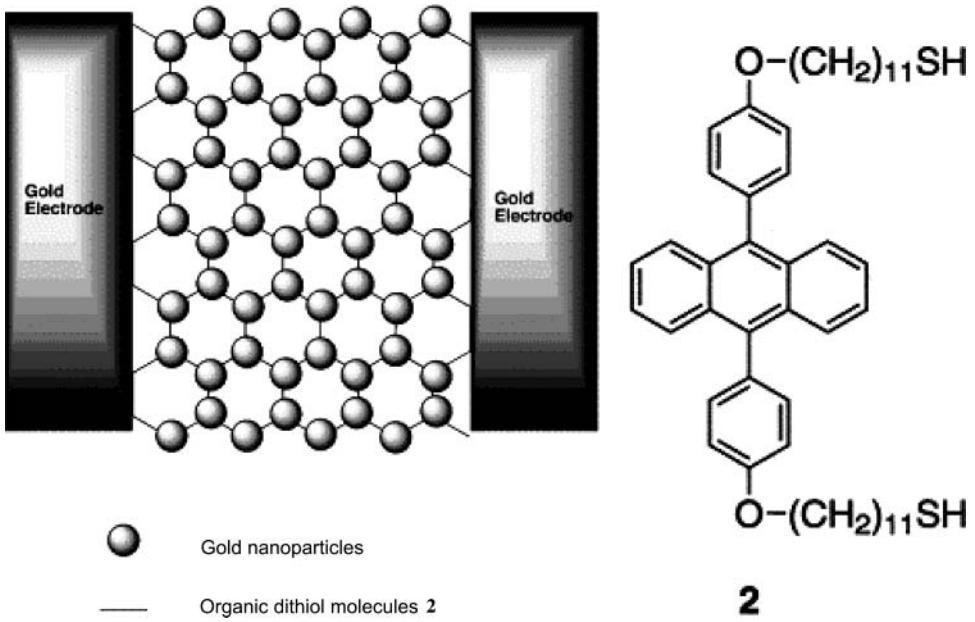

Figure 44. Schematic illustration of the micro-gap electrodes which are connected with the network of organic dithiols and AuNPs. Shaded circles indicate AuNPs, and lines indicate organic dithiol molecules. Reprinted with permission from ref 438 (Ogawa's group). Copyright 2001 Elsevier.

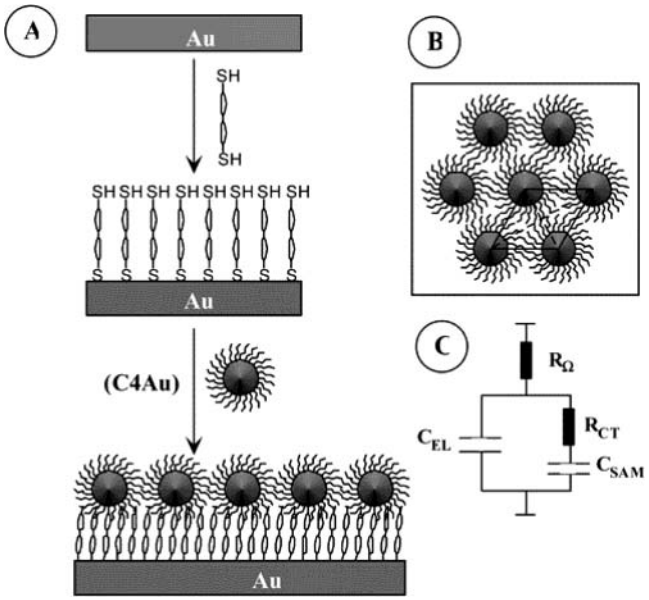

Figure 45. (A) Sequential anchoring of AuNPs to viologen dithiol self-assembled monolayers, (B) hypothetical hexagonal distribution of surface-immobilized AuNPs, and (C) Randle's equivalent circuit, where R_Ω is the solution (uncompensated) resistance, R_{CT} is the charge-transfer resistance, and C_{SAM} and C_{EL} are the interfacial capacitances from the collective contributions of all surface-anchored AuNPs and the interparticle void space, respectively. Reprinted with permission from ref 439 (Chen's group). Copyright 2002 American Chemical Society.

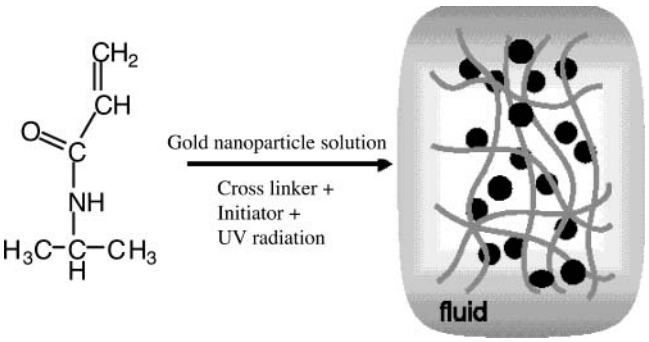

Figure 46. Scheme showing how the AuNPs are locked in the hydrogel network. Reprinted with permission from ref 445 (El-Sayed's group). Copyright 2001 Elsevier.

changing the surrounding matrix led to large variations in the relaxation times of both the electron−phonon and phonon−phonon coupling (Figure 46).[445] High-resolution electron energy loss spectroscopy (HREELS) was used to study low-energy electron impact on films of AuNPs passivated with dialkyl sulfide.[446a] Metal-containing molecular rods were self-assembled on a Au disk electrode, and AuNPs were deposited electrochemically; cyclic voltammetry indicated that the electron could transport rapidly through this structure between the Au electrode and $Fe(CN)_6^{3-/4-}$.[446b] The effect of spin−orbit scattering on discrete energy levels in AuNPs and other nanoparticles showed level-to-level fluctuations of the effective *g*-factor from Zeeman splitting, and the statistics were found to be well characterized by random matrix predictions.[447a] Energy transfer from a surface-bound arene to the gold core was observed upon photoirradiation.[419]

AuNPs have a remarkably low melting temperature (between 300 and 400 °C), due to the large ratio of surface atoms to inner atoms, compared to that of bulk gold (1064 °C). This property was used in the process of printing and laser-curing of AuNP solutions, a laser irradiation time of 1 ms being sufficient.[447b]

5. Chemical, Supramolecular, and Recognition Properties

5.1. Reactions of Thiolate-Stabilized AuNPs

Some of the thiolate ligands in alkanethiolate-stabilized AuNPs can be substituted by reaction with other thiols at rates depending on the chain length[50] and steric bulk[53] of the leaving thiolate and incoming thiols[448a] and on the charge of the AuNPs. For instance, oxidation of the AuNPs largely enhances the proportion of thiolate ligands that can be replaced.[448b] Various functional thiols could be partially incorporated into AuNPs using this efficient reaction. For instance, incorporation of 11-mercaptoundecanoic acid gave amphiphilic AuNPs that were soluble in basic aqueous media but aggregated in acidic media due to hydrogen-bonding. This property was controlled by adjusting the pH,[133] and in particular biomimetic ion-gating recognition has been reported.[449a] The chelating properties of the carboxylate group with metal have been used for metal detection[449b] and formation of AuNP films.[450,451] Complexation of pyridine-functionalized thiol AuNPs also led to solid substrate assembly,[452] and such bifunctional ligands were used to link AuNPs, which led to electron-hopping studies and applications as sensors.[453] Various other electroactive[45,455−460] and photoactive groups,[460−467] spin labels,[468] and catalysts,[469,470] as well as simple groups such as halides, nitriles, alkenes, and sulfonates,[48,471] were similarly introduced using this ligand-exchange reaction.[52c]

Nucleophilic substitution of bromide in *ω*-bromoalkanethiolate-functionalized AuNPs follows an S_N2 mechanism with alkylamines, the rate being largely dependent on the steric bulk (Figure 47). Similarly, nucleophilic substitution of the hydroxy group by alkyl halides could be carried out with *ω*-hydroxy-functionalized AuNPs.[52c] C_{60} was introduced into AuNPs by nucleophilic addition of 4-aminophenoxide ligands to C_{60} double bonds (Figure 48).[288] Nucleophilic addition of *ω*-maleimido thiol-AuNPs onto a sulfidryl group was used to attach AuNPs to proteins, peptides, and oligonucleotides.[472,473] The nucleophilic reaction of amino groups of SAMs on a gold surface with carbonyl groups of functional AuNPs was used to attach AuNPs onto the SAMs.[276] Nucleophilic reaction of the amino group of *ω*-aminothiol-AuNPs with the aldehyde group of glycoproteins, generated by oxidation of ribose cis-diols, could be used to label carbohydrates.[474] Carboxylic acid−alcohol coupling was used to link 2-naphthaleneethanol, ferrocenemethanol, phenothiazine, anthraquinone, α-D-glucose, and uridine to AuNPs.[475] Propionic anhydride reacted with *p*-mercatophenol−AuNPs, giving only partial esterification due to the steric constraint.[47]

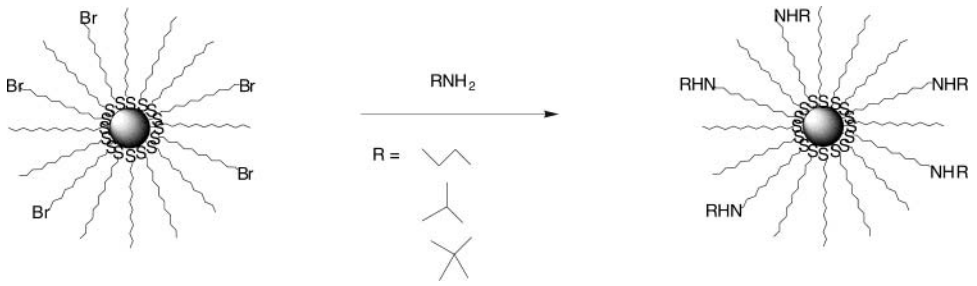

Figure 47. Nucleophilic substitution reaction between AuNPs containing alkanethiol bromide and alkylamines.

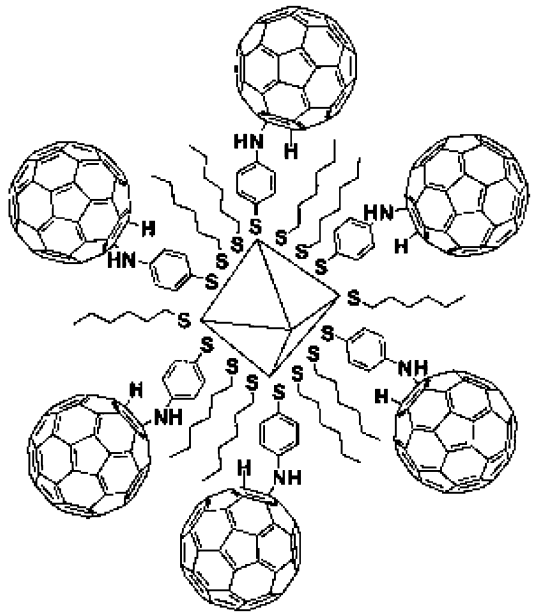

Figure 48. C_{60}-linked AuNPs. Reprinted with permission from ref 287 (Shon's group). Copyright 2002 The Royal Society of Chemistry.

The radical polymerization precursor 2-bromoisobutyronitrile bromide reacted with 11-mercaptoundecanol-AuNPs, providing the ester linkage.[476] Carboxylic acid−amine coupling was used to link TEMPO, pyridine, glutamic acid, pyrene, fluorescein,[50,475] carbon nanotubes,[477,478] ferrocenyl, and viologen to AuNPs (Figure 49).[479] AuNPs functionalized with sulfo-*N*-hydroxysuccinimide react with primary amines, which allows any protein bearing a primary amine to be linked to AuNPs. AuNPs could be polymerized when they bore a thiol functionalized with an atom-transfer-radical (ATR) polymerization initiator such as CuBr/tris(2-dimethylaminoethyl)amine[212] or CuBr/1,4,8,11-tetramehyl-1,4,8,11-tetraazacyclotetradecane.[476] AuNPs could be subjected to cationic polymerization, giving dense brushes if they were functionalized with ω-trifluoromethanesulfonate, using 2-phenyl-2-oxazoline or *N*,*N*-di-*n*-octadecylamine as a monomer and terminating agent, respectively. AuNPs functionalized with a thiolate ligand bearing a norbornyl group could be submitted to ROMP using Grubb's catalyst $[RuCl_2(PCy_3)_2(=CHPh)]$, and two kinds of electroactive ferrocenyl groups could be incorporated. Spherical hollow-sphere capsules were formed by ROMP of AuNPs functionalized with a tripodal ligand followed by etching.[480] Polymerization of ω-siloxane−AuNPs formed AuNPs that were surrounded by polysiloxane shells.[481]

The thiolate-stabilized AuNPs can be decomposed inter alia by reaction of cyanide to give mononuclear gold cyanide and the free thiols or by photoirradiation in the presence of bromine-containing trihalomethanes.[482]

5.2. Supramolecular Chemistry

Acid−base chemistry[483,484] has been involved in molecular recognition and has been studied using various techniques.[484,485] For instance, the structures formed by adsorption of carboxyalkylphosphonic acids on metal oxides were compared to those formed with ω-mercaptocarboxylic acids and AuNP cores using ^{1}H fast magic angle spinning (MAS), heteronuclear correlation (HETCOR), and ^{1}H double-quantum (DQ) MAS solid-state NMR.[486] Infrared reflection spectroscopic data were used to characterize the interfacial structures derived from the interfacial reactivity at the interconnecting linkages of core−shell nanoparticle networks and pH-tunable networks consisting of head-to-head hydrogen-bonded carboxylic acid terminals.[487,488] Nanoparticle arrays obtained by mixing anionic bilayer membranes and cationic, quaternary ammonium-stabilized AuNPs were immobilized densely into the hydrophilic interlayers of dispersed lamellar structures to form a quasi-1D structure.[489] A pseudorotaxane assembly was achieved at the surface of AuNPs, pointing to similarities with the binding of a drug molecule by the receptor sites on the surface of a cell (Figure 50).[490] Evidence for film formation was also found in the case of AuNPs terminated by carboxylic acid groups.[491−493]

For amide-functionalized AuNPs, IR and ^{1}H NMR studies revealed that intramolecular H-bonding was highly dependent on the distance of the amide from the core.[494] Polyhedral oligomeric silsesquioxanes functionalized by diaminopyridines self-assembled with complementary thymines into spherical aggregates.[495] IR spectroscopy and cyanide-mediated decomposition of the gold cores of amide-stabilized AuNPs showed a strong correlation between the strength of the intramolecular H-bonding and the rate of decomposition.[496] Interaction of nitroxyl radicals with AuNPs, monitored by paramagnetic probes, resulted in loss of the EPR signal, due to exchange interaction of the unpaired electron with conduction band electrons of the AuNPs. Catalytic oxidation of a probe was also found when dioxygen was present.[497]

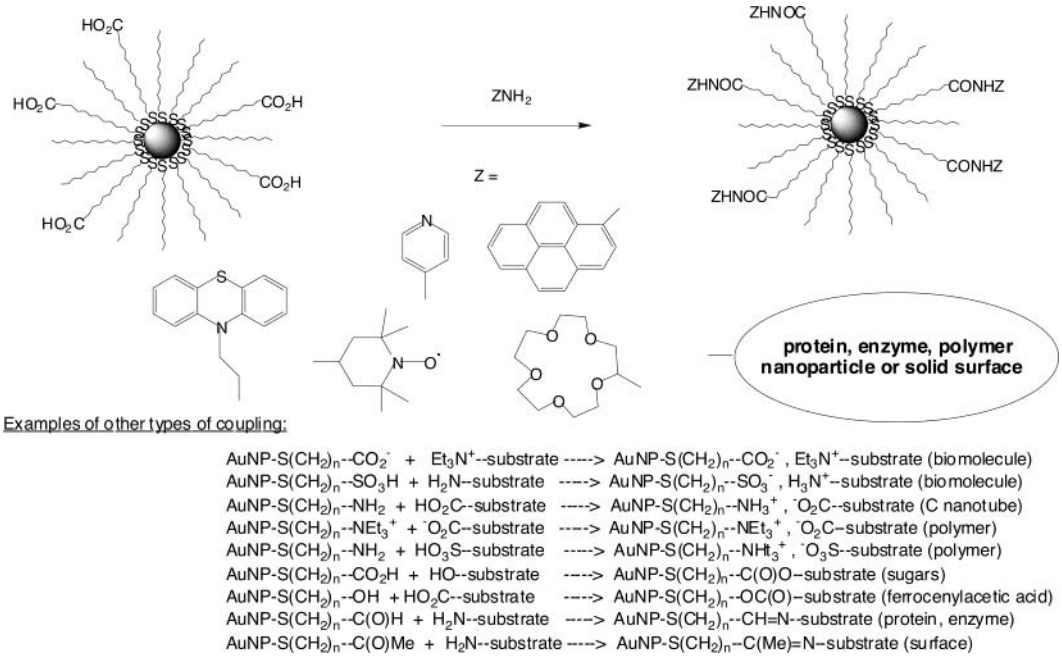

Figure 49. Examples of amide coupling reactions between AuNPs containing carboxylic acid termini and amine derivatives.

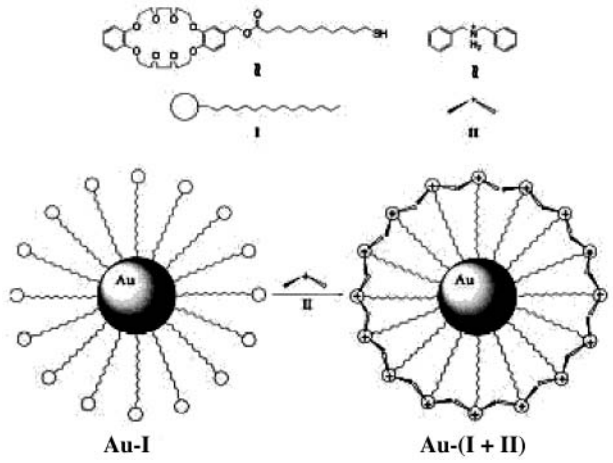

Figure 50. Programmed pseudorotaxane assembly at the surface of AuNPs by heterosupramolecular chemistry. Reprinted with permission from ref 490 (Fitzmaurice's group). Copyright 1999 Wiley-VCH.

5.3. Molecular Recognition

5.3.1. Redox Recognition Using Functionalized AuNPs as Exoreceptors

Alkanethiolate-stabilized AuNPs in which a proportion of the alkanethiolate ligands have been exchanged by amidoferrocenyl-alkanethiol recognize $H_2PO_4^-$ and HSO_4^- as their *n*-Bu_4N^+ salts using the variation of the ferrocenyl redox potential.[433] Thus, they are exo-receptors[501a] for these anions. These salts can be titrated by cyclic voltammetry using this variation of redox potential as a function of the addition of the salt, since a one-to-one interaction occurs between each amidoferrocenyl group and the anion. The case of $H_2PO_4^-$ corresponds to a square scheme with a strong interaction in the Echegoyen−Kaifer model, whereby a new ferrocenyl wave is obtained upon addition of the salt.[498] The difference of potential, $\Delta E° = E°_{free} - E°_{bound}$, between these two waves is 220 mV and provides access to the ratio of apparent association constants between the AuNPs and the salt in the ferrocenyl (K_0) and ferrocenium (K_+) forms:

$$\Delta E° = E°_{free} - E°_{bound} = 0.059 \log(K_+/K_0) = 6210 \pm 620 \quad \text{at 25 °C}$$

The hydrogen-bonding between the amido group and the $H_2PO_4^-$ anion and the electrostatic attraction between the anion and the cationic ferrocenium form upon anodic oxidation are two factors partly responsible for the variation of redox potential signifying recognition.[499] The addition of the salt [*n*-Bu_4N^+]-[$H_2PO_4^-$] to a monomeric amidoferrocenyl derivative that is not connected to the AuNP provokes only a weak shift of 45 mV. Thus, an additional key factor is the topological one created by the AuNP environment, i.e. the dense thiolate ligand shell that forces the anion to penetrate into a narrow channel between the thiolate ligands. This steric factor compares with that of a nonakis-amidoferrocenyl dendrimer, but is less marked than that in an 18-amidoferrocenyl dendrimer, because the recognition process follows a positive dendritic effect in dendrimers due to the increased steric bulk at the periphery.[500] AuNPs containing various proportions of amidoferrocenyl-alkanethiolates and similar ligands with various chain lengths were synthesized as well as analogues containing the pentamethylamidoferrocenyl-alkanethiolate ligand or the 1-acetyl-1′-amidoferrocenyl-alkanethiolate ligand in order to study the influence of the stereoelectronic factors on the recognition. The chain proportion and length did not show a significant influence, but the electron-withdrawing acetyl group of the amidoferrocenyl system favored the recognition, whereas the electron-releasing methyl

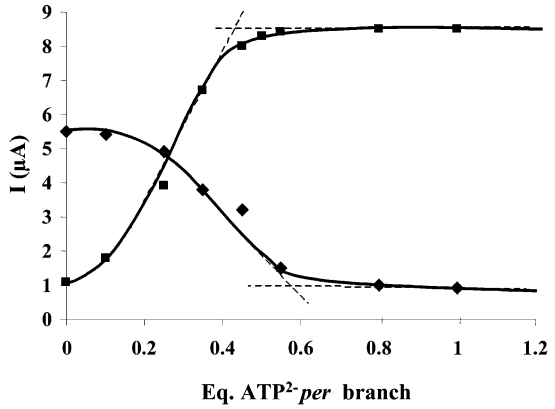

Figure 51. Titration of ATP^{2-} with ferrocenyl-dendronized AuNPs. Decrease of the intensity of the initial CV wave (◆) and increase of the intensity of the new CV wave (■) vs the number of equivalents of [*n*-Bu_4N]$_2$[ATP] added per ferrocenyl branch. Nanoparticles, 3.8×10^{-6} M in CH_2Cl_2. Conditions: supporting electrolyte, [*n*-Bu_4N][PF_6] 0.1 M; reference electrode, Ag; auxiliary and working electrodes, Pt; scan rate, 0.2 V/s; solution of [*n*-Bu_4N]$_2$[ATP], 5×10^{-3} M; internal reference, $FeCp_2$*. Reprinted with permission from ref 251 (Astruc's group). Copyright 2003 American Chemical Society.

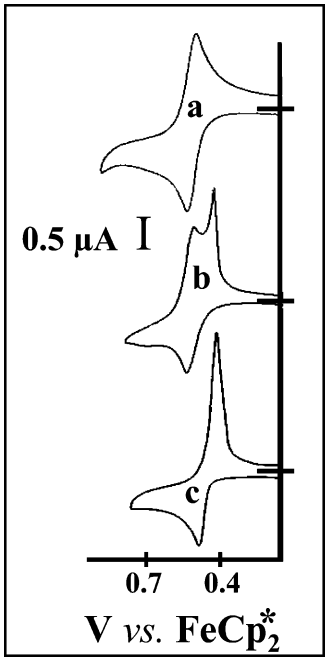

Figure 52. Titration of ATP^{2-} with dendronized AuNPs in the presence of [*n*-Bu_4N][Cl] and [*n*-Bu_4N][HSO_4] (both anions, 5×10^{-2} M, 0.5 equiv per ferrocenyl branch). Cyclic voltammograms of AuNPs (a) alone, (b) in the course of the titration, and (c) with an excess of [*n*-Bu_4N]$_2$[ATP]. Reprinted with permission from ref 251 (Astruc's group). Copyright 2003 American Chemical Society.

substituents provided a decrease of the $\Delta E°$ values. This latter finding indicated that the most important hydrogen-bonding interaction in the chelating group was that between the negatively charged oxygen atom of the anion and the positively charged NH group of the AuNP ligand.[140]

The case of HSO_4^- corresponds to the square scheme, with a weak interaction in the Echegoyen−Kaifer model ($K_0 \ll 1$), whereby there is no new ferrocenyl wave upon addition of the salt, but only a cathodic shift of the original wave. $\Delta E°$ is now the potential shift of this wave at the equivalence point, and its measure now gives access to the absolute value of K_+:[498]

$$\Delta E° = 0.059 \log [cK_+] \qquad \text{at } 25\ °C$$

This shift (30 mV) was smaller than that found in polyamidoferrocenyl dendrimers and only equal to that of a tripodal tris-amidoferrocenyl derivative, although it was larger than that in monoamidoferrocene (<10 mV). To combine the advantages of both AuNPs and dendrimers, dendronized AuNPs were synthesized with amidoferrocenyl groups or silylferrocenyl groups at the periphery. For this purpose, the direct synthetic method proved more useful than the place ligand substitution method, the latter being marred by the steric effect in this case. These ferrocenyl dendrimers with an AuNP core contained up to 360 ferrocenyl groups and were more efficient than the ferrocenyl-alkanethiolate-containing AuNPs. Positive dendritic effects were observed; i.e., AuNP-cored ferrocenyl dendrimers assembled with nonakis-silylferrocenyl dendrons showed larger values than those assembled with tris-silylferrocenyl dendrons (Figures 51 and 52). In addition, one of the most interesting properties of these AuNP-cored large ferrocenyl dendrimers was their great ability to adsorb on metal surfaces. For instance, very stable platinum electrodes modified with these AuNP-cored dendrimers were prepared upon cycling the potential region around the ferrocenyl redox potential. These platinum electrodes modified with the large AuNP-cored silyferrocenyl dendrimers easily and selectively recognize the anion in a mixture of several anions, such as HSO_4^- and halides. Gratifyingly, the recognized salt could be removed by washing with methylene chloride, but the attached AuNP-cored silylferrocenyl dendrimer remained attached, and the modified electrodes could be reused many times for the recognition procedure (Figure 53).[140]

5.3.2. Miscellaneous Recognition and Sensors

The controlled assembly of nanoparticles in solution based on supramolecular chemistry, i.e., noncovalent bonding,[501a] is a general strategy leading to well-organized AuNP materials. Thus, approaches have been reported using hydrogen-bonding,[501b] $\pi-\pi$,[501c] host−guest,[501d] van der Waals,[501e] electrostatic,[501f] charge-transfer,[501g] and antigen−antibody[501h] interactions.

Amide-functionalized AuNPs were also used as optical sensors for anions.[502] AuNPs functionalized with 15-crown-5 recognize K^+ in water,[503a] and Li^+ [503b] (Figure 54) and heavy metal ions[28,504] were recognized using AuNP-based sensors. The recognition properties based on H-bonding were used to assemble AuNPs into micelles using polymers (Figure 55).[505] AuNPs have also been used for vapor sensing.[507a,b] The sensitivity of the plasmon band with the core environment is obviously a source of sensing, and the optical response (SPB) has been modelized.[506] (See also the SPB section and that on biological applica-

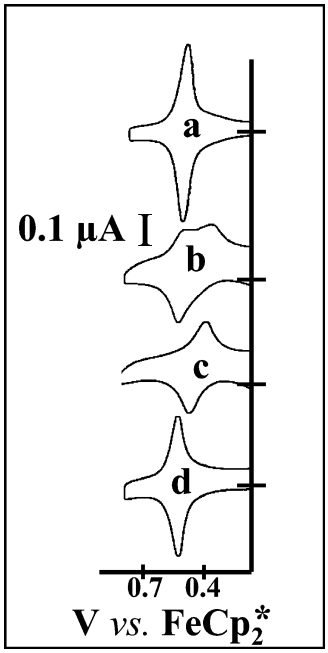

Figure 53. Recognition of ATP^{2-} with a Pt electrode modified with dendronized AuNPs. Cyclic voltammograms of dendronized AuNP-modified electrodes (a) alone, (b) in the course of the titration, (c) with an excess of $[n\text{-}Bu_4N]_2$-[ATP], and (d) after removal of ATP^{2-} by washing the modified electrode with CH_2Cl_2. Reprinted with permission from ref 251 (Astruc's group). Copyright 2003 American Chemical Society.

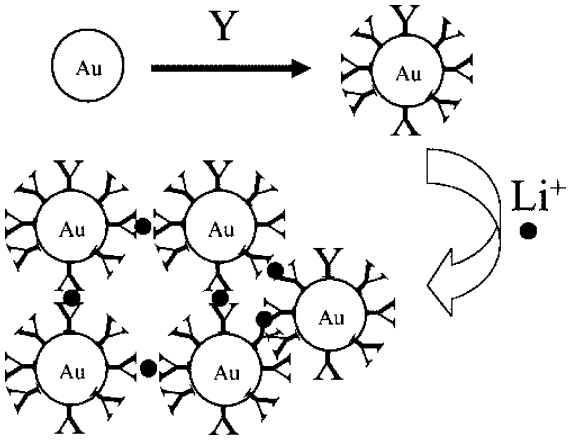

Figure 54. Detection scheme for Li^+ with functionalized AuNPs. AuNPs are surface-derivatized with a ligand Y that binds to lithium ions in a bidentate fashion. Upon introduction of lithium ion (small dark circles) into the solution, AuNP aggregation is induced, which is manifested as a visible color change in the solution. Reprinted with permission from ref 503b (Murphy's group). Copyright 2002 American Chemical Society.

tions, in particular the color sensitivity of the AuNP−DNA assemblies.) Electrochemical genosensors for the detection of the Factor V Leiden mutation from polymerase chain reaction amplicons using the oxidation signal of AuNPs at +1.20 V were described.[507c] DNA−AuNP assemblies, which are discussed in the next section, have also been used as colorimetric lead biosensors.[507d] *N*-Methylimidazole-functionalized AuNPs were reported to recognize bis- and tris-Zn-porphyrins.[507e]

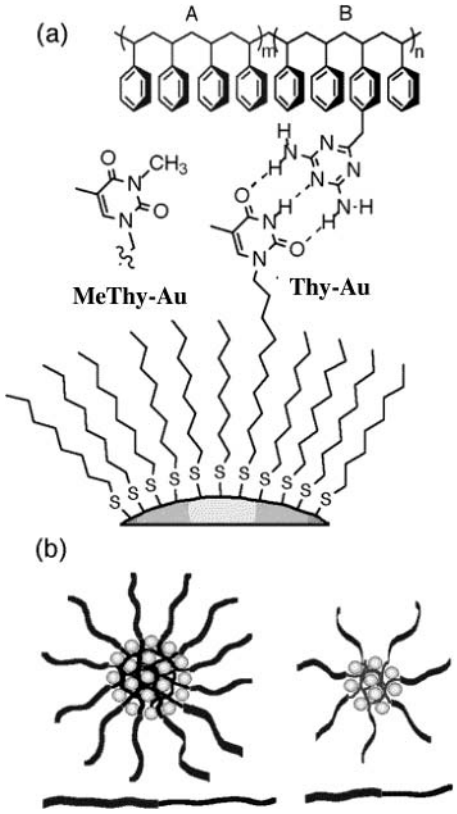

Figure 55. (a) Diblock copolymers 1−3, Thy-Au, and non-hydrogen-bonding control MeThy-Au. (b) Scheme demonstrating an increase in both core diameter and outer corona as the polymer size increases. Reprinted with permission from ref 505 (Rotello's group). Copyright 2002 American Chemical Society.

6. Biology

6.1. DNA−AuNPs Assemblies and Sensors

Conjugates of AuNPs−oligonucleotides are of great current interest because of the potential use of the programmability of DNA base-pairing to organize nanocrystals in space and the multiple ways of providing a signature for the detection of precise DNA sequences. Applications in the fields of biosensors, disease diagnosis, and gene expression are clearly called for. The two groups of Mirkin−Letsinger at Northwestern[508−516] and Alivisatos−Schultz at Berkeley[473] have pioneered strategies for the organization of functionalization of AuNPs with oligonucleotides. The former group used DNA as a linker to form macroscopic assemblies consisting in discrete 13-nm-diameter particles. The DNA attached to the nanoparticles retained its ability to hybridize with complementary DNA, and the annealing process was thermally reversible and nondestructive. The reaction was sequence-specific (Figure 56).[509] The latter group used DNA as a template to prepare nanocrystal molecules consisting of two or three 1.4-nm-diameter particles on a single oligonucleotide strand.[473] DNA-driven assemblies of AuNPs have indeed attracted considerable interest,[510−536] and a new colorimetric technique based on the sensitivity of the SPB to monitor DNA modification was designed by the Mirkin−Letsinger group.[508−517] In this strategy, AuNPs are used as building blocks, allowing the assembly of alkanethiol-capped oligonucleotides

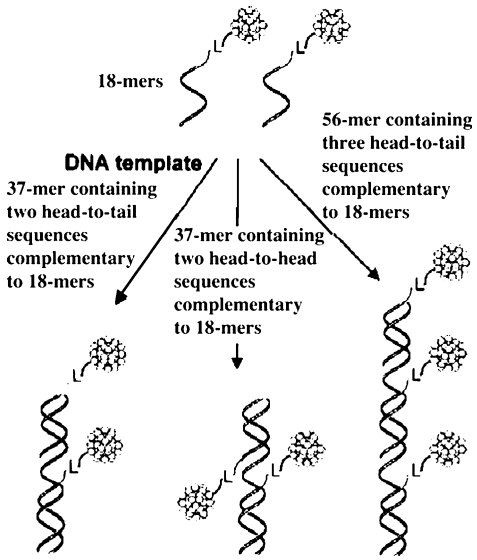

Figure 56. Preparation of "nanocrystal molecules" consisting of two or three DNA modified Au particles attached to a complementary DNA template, using phosphine-stabilized 1.40nm AuNPs modified with a single thiol-capped oligonucleotide and two different DNA template lengths and sequences. Reprinted with permission from ref 509 (Mirkin's group). Copyright 1997 Kluwer.

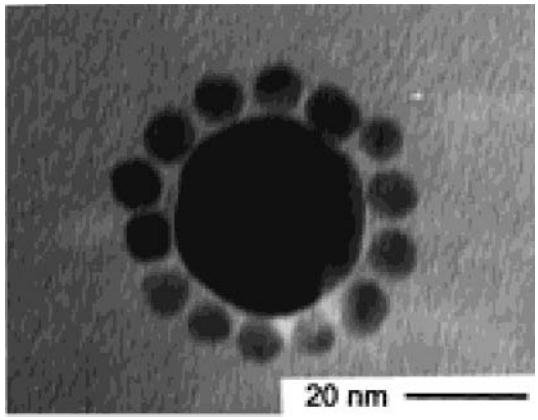

Figure 57. TEM images of the binary AuNPs network materials supported on holey carbon grids: a AuNP satellite structure obtained from the reaction involving 120/1 1-modified 8-nm particles/2-modified 31-nm AuNPs and linking oligonucleotide. Reprinted with permission from ref 511b (Mirkin's group). Copyright 1998 American Chemical Society.

such as single-stranded DNA and complementary linker oligonucleotide (DNA) strands (Figure 57).

Aggregation of AuNPs linked by the oligonucleotides provokes a red-to-blue color change (red shift from 520 to 600 nm of the SPB) that is most useful for this DNA-sensing method. The parameters that are controlled are the AuNP composition, the periodicity, and the aggregate thermal stability. These parameters are organized in order to influence the optical, mechanical, and electrical properties of the AuNPs. In particular, the optical properties due to the SPB of AuNPs from 13 to 17 nm diameter led to the development of a highly selective diagnostic method for DNA, based on the distance-related SPB of AuNPs (Figure 58). The effect of the length of the DNA strands that control the interparticle distance was studied, and it was found that the SPB frequency changes are inversely dependent on the oligonucleotide linker length (between 24 and 72 base pairs, i.e., from 80 to 24 Å). An interesting result was that the most important parameter that controls the SPB shift of these AuNPs−DNA materials is the aggregate size. This aggregate size is under kinetic control, and it is the growth rate that depends on the linker length. Annealing of the kinetic structures formed at temperatures just below their melting points lead to a SPB shift. This growth, leading to the red shift of the SPB, occurs through an Oswald ripening mechanism whereby larger aggregates grow at the expense of smaller ones.

Electrodynamics modeling contributes to show that these SPB shifts are much more consistent with changes in aggregate size than with interparticle distance. Thus, DNA linkers could be more useful as kinetic controllers of aggregate growth than as spacer units, a valuable indication for the development of quantitative assays for DNA.[515]

Another important characteristic of the AuNP-based pair detection is the "melting" transition of the complementary DNA strand. The AuNPs are linked in the presence of the complementary strand. These H-bonded connections of the links are broken at sufficiently high temperatures, which unzips the oligonucleotides, "melting" the DNA and releasing the particles.[513] Calculations using AuNP polarizabilities determined from Mie theory, an iterative conjugate-gradient solution algorithm, and fast Fourier transform methods for efficient solution of the electrodynamics of interacting AuNP equations show that the UV extinction lowering and the shift and broadening of the SPB of the DNA-linked AuNPs are explained as the collective electromagnetic response of thousands of AuNPs.[510]

Supramolecular aggregates were shown to form by self-assembly of DNA−streptavidin adducts.[519] Heterologous chemical systems including DNA have been scaffolded into precise 2D geometrical arrangements.[524] The conformation of oligonucleotides attached to AuNPs has been probed by the electrophoretic mobility determined on 2% agarose gels, and the effective diameter of the DNA−AuNP conjugates has been determined (Figure 59).[525]

Multiple thiolate and phosphine anchors improved the AuNP−nucleotide stability.[529,530] DNA was coated with cationic, metastable AuNPs.[537] Several reports indeed showed the efficacy of electrostatic AuNP−DNA assembly,[537−539] including for the fabrication of linear superstructures.[538] Interestingly, however, DNA also wraps around negatively charged AuNP cores.[530] Ring aggregation of AuNPs can be induced by DNA hybridization even without cross linking.[539c]

DNA−nucleotides and AuNP−DNA nanostructures were analyzed using electrochemical techniques,[540−546] including scanning electrochemical microscopy.[544a] Imaging of DNA−AuNPs assemblies by TEM, AFM, and near-field scanning optical microscopy was provided.[544b] Other techniques used were SPB (Figure 60),[510−514] luminescence,[420] Fourrier transform infrared and Raman spectroscopy,[533,540] surface-enhanced Raman spectroscopy,[547] labeling and scanning force microscopy,[533,548] differential light-

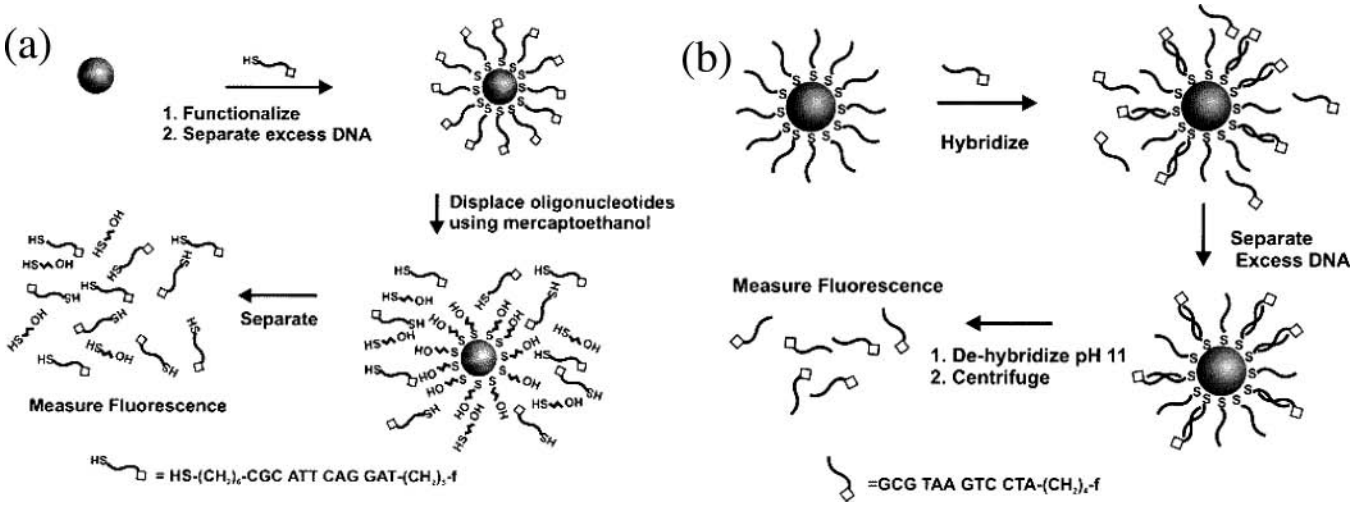

Figure 58. Fluorescence-based method for determining (a) the surface coverage and (b) the hybridization efficiency of thiol-capped oligonucleotides bound to gold thin films and AuNPs. Reprinted with permission from ref 516 (Mirkin's group). Copyright 2000 American Chemical Society.

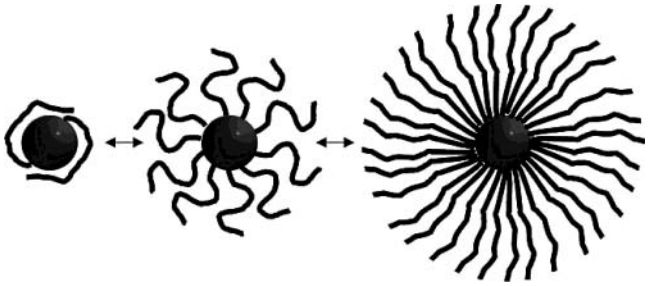

Figure 59. Different possible configurations of DNA molecules attached to the surface of AuNPs. Reprinted with permission from ref 525 (Alivisatos's group). Copyright 2003 American Chemical Society.

scattering spectroscopy,[549a] and quartz-crystal microbalance (QCM).[535,536,549] The latter technique was shown to be especially useful for the design of new DNA sensors[535,536] involving dendritic amplification of DNA analysis.[536] Using 50-nm-diameter AuNPs, with QCM it was also possible to reach a sensitivity of 10^{-14} M of DNA analyte, a fragment of P 53 gene near codon 248 which has significance in cancer diagnosis.[535] Microcantilevers were used to detect DNA strands with a specific sequence using AuNP-modified DNA. This method is analogous to QCM in the vibration−working mode, but it has various advantages over QCM.[549b] When the size of the AuNPs is 50 nm, a sensitivity of 10^{-15} M for single-base mutation detection has been achieved with this method.[549c] Dry-reagent strip-type biosensors based on AuNP−DNA interaction enabled visual detection within minutes, and quantitative data were obtained by densitometric analysis.[549d] AuNP−streptavidin conjugates covered with 6-ferrocenylhexanethiol were attached onto a biotinylated DNA detection probe of a sandwich DNA complex, and the amplified voltammetric signal was recorded. A detection level down to 2.0 pM for oligonucleotide was obtained.[549e] Single-stranded and double-stranded DNA were shown by electrophoresis and fluorescence to bind nonspecifically to the AuNP surface, despite their negative charge.[549f] Nonspecific binding of biological molecules can be eliminated, however, using ethylene glycol core protection.[549g]

6.2. AuNP-Enhanced Immuno-Sensing

Immunolabeling with AuNPs and imaging of cells, biomolecules, and other biological components have been extensively reviewed in the book edited by Hayat in 1989,[14] and this area continues to attract the attention of biochemists and biophysicists.[555] The recognition of proteins has been for some time the subject of research of biodevices for diagnostics based on the interaction between AuNP−antibody conjugates and their antigens.[14] Only recent progress is reviewed here. The great sensitivity of the SPB by AuNP adsorption led to their use in bioassay applications. The investigated AuNP−protein conjugate architectures involve either direct binding of antigen: AuNP−biocongugate to an antibody-modified surface or the exposure of an antibody-derived surface to free antigen and then to a secondary antibody−AuNP conjugate. This classic type of immunoassay allows the evaluation of AuNP tags in a standard mode of antigen detection.[550−552] Biosensors for immunoassays in human serum have been developed.[553,554]

6.3. AuNP Sugar Sensors

AuNPs coupled with biomolecules are attracting increasing attention because of the potential applications of these new materials in biology-related challenges.[555,556] Mannose-encapsulated AuNPs have been shown by TEM to specifically bind FimH adhesin of bacterial type 1 pili in *Escherichia coli*, and to do so more strongly than free mannose in the competition assay. This process represents a new method of labeling specific proteins on the cell surface using carbohydrate-conjugated AuNPs, whereby the visualization of the target receptor on the cell surface is relatively easy under an electron microscope.[55] AuNPs functionalized with a monolayer of 11-thioacetate-undecanol-derivatized neoglycoconjugates of lactose disaccharide and trisaccharide antigens can be used to mimic glycophosphinolipid clusters in plasma

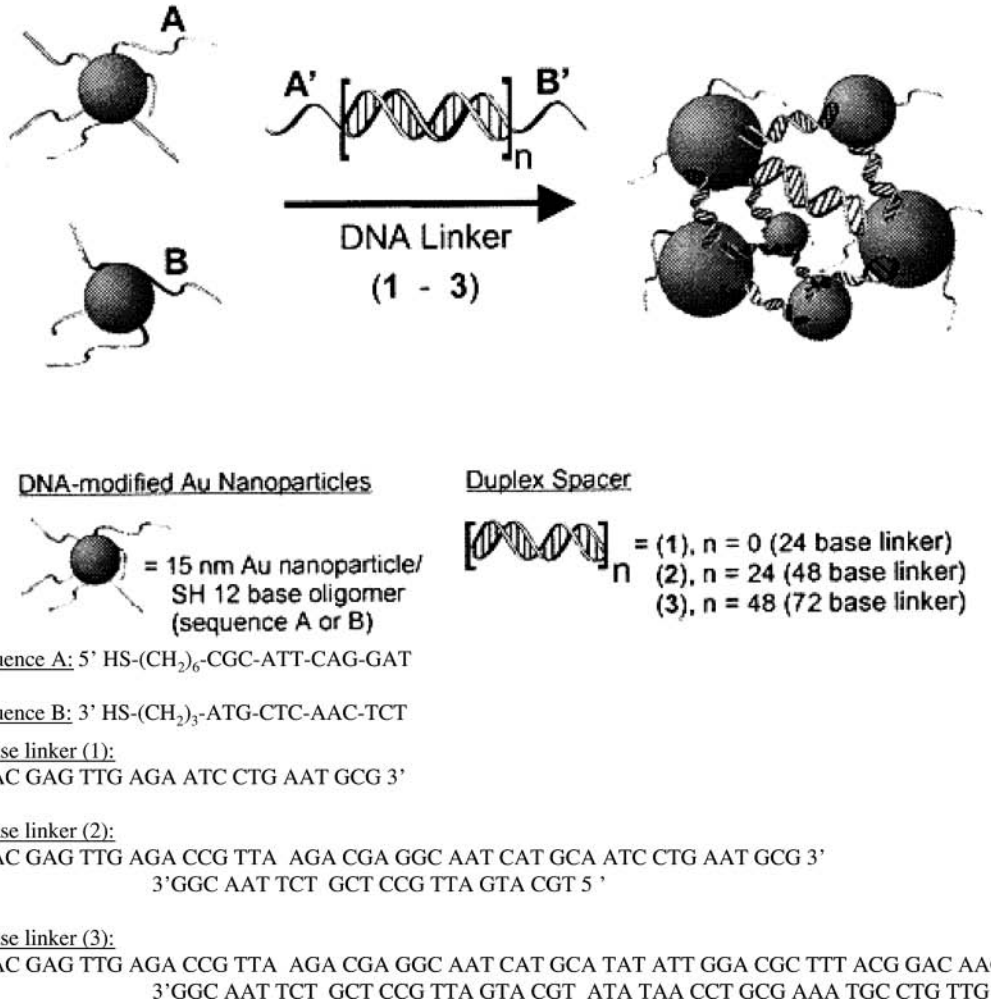

Figure 60. Control of the optical properties of DNA-linked AuNPs assemblies by modulating the length of the DNA linker molecule (1, 2, 3) and the thiol 12 base oligomer (A and B) one. Reprinted with permission from ref 514 (Mirkin's group). Copyright 2000 American Chemical Society.

membranes in order to investigate a new mechanism of cell adhesion through carbohydrate−carbohydrate interactions.[558,559] Spontaneous formation of AuNPs was observed in aqueous solutions of sugar-persubstituted PAMAM dendrimers without the addition of any additional reductant.[560] AuNPs coated with haptenated mercaptodextrans containing 15 mercapto groups bind specifically to paramagnetic beads coated with the corresponding antibody.[561a] A mannose derivative has been self-assembled onto preformed, citrate-capped water-soluble AuNPs, and, through the use of a C_2 tether, a rapid colorimetric detection test has been developed for the protein canavalinin A.[561b] Multivalent interactions of glycono-AuNPs containing galactosyl and glucosyl headgroups with the HIV-associated recombinant glycoprotein gp 120 have been studied.[561c]

6.4. Other AuNP Bioconjugates: Peptides, Lipids, Enzymes, Drugs, and Viruses

Phospholipids were used for the formation of AuNPs,[563−565] in particular as dispersants in the preparation of AuNPs.[562] Helically patterned arrays of AuNPs were formed using lipid tubules as templates.[563] The assembly of relatively short polypeptides on a template can provide protein-like complex structures and properties, especially in conjugates with AuNPs.[566,567] Water-soluble AuNPs based on thiopronin have been prepared.[568,569] Other Au−NP-based receptors providing H-bonds recognize flavin.[570,571] Ligand design optimizes bioconjugation in various AuNPs frameworks.[572−576] Enzymatic activity of fungal protease−AuNP bioconjugates was reported[577] as well as a method to construct a third-generation horseradish peroxidase biosensor by self-assembling AuNPs.[578] Phthalocyanine-stabilized AuNPs were shown to be a potential delivery vehicle for photodynamic therapy.[579] The biochemical preparation of AuNPs was reported whereby the biological organisms played the roles of reductant, protecting agent, and precipitating agent.[175b,580−582] AuNPs bound on APTMS-functionalized Na−Y zeolite could be used for the immobilization of pepsin, whose catalytic activity in the bioconjugate was comparable to that of the free enzyme.[583a] Assembly of AuNPs on polyurethane spheres could be used to immobilize enzymes such as pepsin; these bioconjugate catalysts can also be reused as free enzymes.[583b] Raleigh resonance spectroscopy was reported on single brome mosaic virus capsids (28 nm) with AuNPs (2.5−4.5 nm) inside.[583c]

Control over the morphology of ceramic crystals by biomimetic processes is of increasing interest. For instance, large changes in the morphology of barite crystals occur on templates of varying dimensionality.[584a] In a strategy aimed at nuclear targeting in biological systems mimicking viruses, the most capable peptides were combined on a 20-nm bovine serum albumin−AuNP platform, and the trajectories inside cells of these assemblies were monitored using a combination of video-enhanced color microscopy and differential interference contrast microscopy.[584b]

6.5. AuNP Biosynthesis

Macroscopic quantities of microorganisms such as fungi could be used as living templates with AuNPs to organize presynthesized nanoscale components into ordered structures.[584c] Reaction of $AuCl_4^-$ ions with the extract of geranium leaves and an endophytic fungus, *Colletotrichum* sp., present in the leaves, leads to the formation of AuNPs.[584d]

7. Catalysis

Gold is very popular for being chemically inert. It is indeed one of the most stable metals in the group 8 elements, and it is resistant to oxidation. In the 1970s, however, Parravano's group reported the investigation of the activity of gold in oxygen/hydrogen-transfer reactions[585,586] and the reduction of NO by dihydrogen,[587] but these studies remained isolated. Therefore, the discovery by Haruta et al., reported in 1989, that AuNPs supported on Co_3O_4, Fe_2O_3, or TiO_2 were highly active catalysts, under high dispersion, for CO and H_2 oxidation,[588,589] NO reduction,[590] water−gas shift reaction,[591] CO_2 hydrogenation,[592] and catalytic combustion of methanol[593] was a surprise, and was considered important by the chemical community. Catalysis with AuNPs, in particular the very active oxide-supported ones, is now an expanding area, and a large number of new catalytic systems for various reactions are now being explored.

7.1. Catalysis of CO Oxidation

Most of the recent research on the catalytic activity of oxide-supported AuNPs concerned CO oxidation.[588−621] In particular, the mechanism of the catalytic process was actively investigated, and particle size effects and metal/support interactions were examined. The gold cluster $[Au_9(PPh_3)_8(NO_3)_3]$ was highly dispersed by impregnating Mn, Fe, Co, Ni, Cu, or Cu hydroxide with a solution of this cluster, and activity in CO oxidation was found even at subambient temperatures (below 0 °C and even at −70 °C).[595] Further studies on the AuNP/$Fe(OH)_3$ system showed that the catalytic activity was extremely high after calcination, which was ascribed to the stabilization of $[Au(PPh_3)]^+$, leading to small particles.[596] Alternatively, it was suggested that the catalytic activity was due to the presence of ferrihydrate activating O_2,[597] and Au^+ species were found to be more active than Au^0 particles.[598] Small AuNPs were stabilized by insertion into zeolite supercages, and ^{129}Xe and DRIF studies showed the presence of $Au^{\delta+}$ species,[599] which were found to be highly active.[599,600] With AuNPs impregnated on $Mg(OH)_2$, it was indicated that, below 1 nm diameter, AuNPs have icosahedral symmetry, whereas above 1 nm, the AuNPs are in face-centered cubic cuboctahedral symmetry. This showed that the geometrical factor is also important in catalytic activity.[601] New methods for preparation of AuNPs for catalytic oxidation of CO include arc melting, chemical vapor deposition, cosputtering,[602] and pulsed laser deposition (PLD).[603] The exceptionally high catalytic activity of the AuNPs deposited onto Fe_2O_3, Co_2O_3, and TiO_2[604−607] supports was interpreted in terms of the formation of an active AuNP/support interface along the perimeter of AuNPs.[608,609] The morphology, electronic structure, and catalytic activity in CO oxidation over a Au/FeO_x/SiO_2/Si(100) model sample prepared by PLD have been investigated by X-ray photoelectron spectroscopy and TEM, which showed that activity in CO oxidation increased after oxidation, the higher activity being associated with amorphous iron oxide with Fe 2p binding energy = 711.3 eV.[610−613] The intrinsic catalytic activity of the AuNPs was shown to increase with decreasing particle size. When an Au/FeO_x interface was created by FeO_x deposition on large AuNPs, a significant increase in the rate of the CO oxidation was observed, and these data correlate the catalytic activity with the valence bond density of states of the AuNPs.[614] Spherical aberration-free phase image analysis showed that catalytically active AuNPs form single crystals having a cuboctahedral shape, and that the atomic structure on the surface and interface is largely deformed from the bulk structure by stress produced by the atom-missing structure, the reconstructed structure surface, and strong interaction with the substrate.[615] It has been suggested that a synergistic mechanism occurs at the AuNP−metal oxide interface, with the oxide support being part of the catalytic process. Adsorption of CO would proceed on the AuNP on a site adjacent to a metal oxide site occupied by an adsorbed O_2 molecule. The reaction would involve an intermediate carbonate-like species decomposing to CO_2 upon desorption from the surface.[593] AuNP−FeO_x catalysts, prepared by coprecipitation, containing ferrihydrite, a structurally disordered material with approximate composition $Fe_5HO_8{\cdot}4H_2O$, and a noncrystalline phase $AuOOH{\cdot}xH_2O$, showed 100% conversion after 20 min at room temperature.[616] AuNPs prepared by chemical vapor deposition (CVD) of dimethyl gold acetylacetonate are active catalysts for CO oxidation below 0 °C.[617] Extensively varying the conditions of preparation of AuNP−MO_x catalysts (M = Si, Ti, Zr, Al) of 1−6 nm size, followed by characterization using TEM, XPS, and EPR, made it possible to investigate the structure−reactivity of the catalysts.[618] AuNPs supported on a TiO_2 surface by calcination first at 500 °C under vacuum and then at 400 °C in air showed low-temperature activity on CO oxidation (Figure 61).[621] The size of the most active AuNPs was determined by low-frequency Raman modes, providing a signal at 11 ± 1 cm^{-1} that corresponded to a particle diameter of 8 ± 1 nm, and combination of this technique with microscopy techniques gave information on size distribution and structural 3D

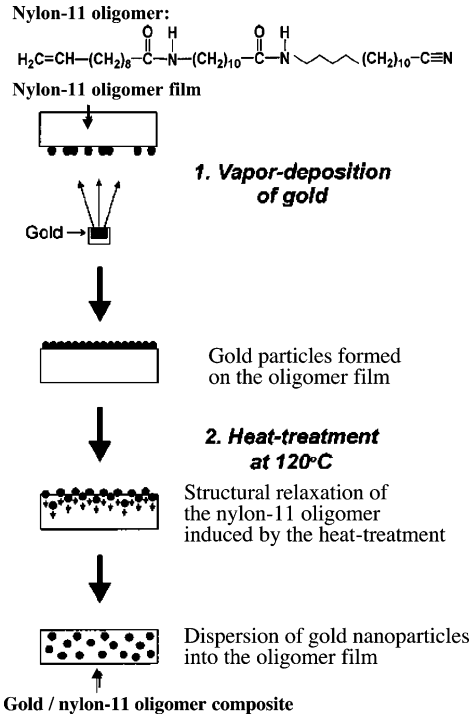

Figure 61. Novel method of preparation of a AuNP catalyst supported on TiO_2. Reprinted with permission from ref 621 (Sayo's group). Copyright 1999 Elsevier.

arrangement.[622] DFT calculation for O_2 chemisorption showed a typical binding energy of 0.5−1.5 eV, increasing for negatively charged clusters.[623]

7.2. Electrochemical Redox Catalysis of CO and CH_3OH Oxidation and O_2 Reduction

The electrooxidation of CO[624] and CH_3OH,[126,625,626] both leading to CO_2 (CO_3^{2-} in alkaline medium), i.e.,

$$CO + 2OH^- - 2e^- \rightarrow H_2O + CO_2 \qquad (CO_3^{2-} \text{ in alkaline})$$

$$CH_3OH + 6OH^- - 6e^- \rightarrow 5H_2O + CO_2 \qquad (CO_3^{2-} \text{ in alkaline})$$

has been reported using alkanethiolate−AuNPs that were precipitated onto a glassy carbon electrode by cross-linking the AuNPs with 9-nonanedithiol, leading to a 3D network thin film. The electrocatalytic processes were shown by cyclic voltammetry. A wave observed at +50 mV on the negative sweeping in the presence of CO was characteristic of CO oxidation, whereas a wave observed at +250 mV in the presence of MeOH was characteristic of MeOH oxidation. The oxidation current was found to increase with concentration of CO or MeOH, observed only after a potential polarization around +800 mV that provoked catalytic activation. This activation was confirmed by matching the oxidation potential with that of Au oxide formation, and by quartz-crystal microbalance, infrared reflection spectroscopy, and AFM experiments.[627a] This electrocatalytic CO oxidation was also demonstrated using AuNPs synthesized by block copolymer micelle encapsulation, whereby the dip-coating method of synthesis produced a highly dispense, quasi-regular array of AuNPs (diameter 4.8 ± 1.3 nm).[627b]

AuNPs electrodeposited on a gold electrode by applying a 5-s potential step from 1.1 to 0 V with a 0.5 M H_2SO_4 solution containing 0.11 mM $Na[AuCl_4]$ were shown to be very active catalysts for the reduction of O_2. Two electrocatalytic reduction waves recorded at +50 and −250 mV indicated a two-step, four-electron reduction path of O_2:[628a]

$$O_2 + 2H^+ + 2e^- \rightarrow H_2O_2$$

$$H_2O_2 + 2H^+ + 2e^- \rightarrow 2H_2O$$

AuNPs deposited on boron-doped diamond with an average diameter of 60 nm were shown to be 20 times more active than polycrystalline gold for the electrocatalytic O_2 reduction.[628a]

7.3. Catalysis of Hydrogenation of Unsaturated Substrates

More recent investigations have shown that AuNPs that were adsorbed and dispersed on oxide support by reduction of $AuCl_4^-$ or $AuCl_3$, and then calcinated, were also efficient catalysts for other reactions, including hydrogenation of unsaturated substrates. For instance, such AuNPs of 1−5 nm diameter, supported on titania or zirconia, were active in the regioselective hydrogenation of acrolein to allylic alcohol at 180−280 °C (total pressure, 2 MPa), a particularly difficult reaction. Following TEM and EPR studies, it was suggested that the origin of the selectivity of C=O vs C=C hydrogenation might be attributed to quantum size effects that alter the electronic properties of sufficiently small AuNPs.[629−631] Active sites were identified as edges.[631] AuNPs were prepared by dispersion on an amorphous silica support, wherein silanol groups of the surface of fumed silica spontaneously reduced $AuCl_4^-$ ions. These supported AuNPs were found to be catalytically active in the hydrogenation of cyclohexene at 80 °C and 200 psi H_2.[632] PVP-stabilized Au/Pd bimetallic nanoparticles[201] showed high activity for the hydrogenation of cycloocta-1,3-diene (COD), with 100% selectivity for cyclooctene formation. The high activity was ascribed to electronic deficiency of the active surface Pd atoms (required for π back-donation from the coordinated olefin) due to electron transfer to the gold atoms (Figure 62).[26,180] Reduction of eosin by $NaBH_4$ at 29 °C was catalyzed by AuNPs of 10−46 nm diameter, prepared by a seed-mediated growth method, and the reaction rates were shown to increase both above and below 15 nm diameter.[633]

7.4. Catalysis by Functional Thiolate-Stabilized AuNPs

Since imidazoles play a key role as catalysts in many hydrolytic systems, *N*-imidazole-functionalized thiolate−AuNPs were investigated as catalysts, in 6:4 methanol−water solution, for the cleavage of 2,4-dinitrophenyl acetate with more than an order-of-magnitude rate acceleration with respect to acetyl-*N*-methylhistamine.[470] A thiol terminated with a

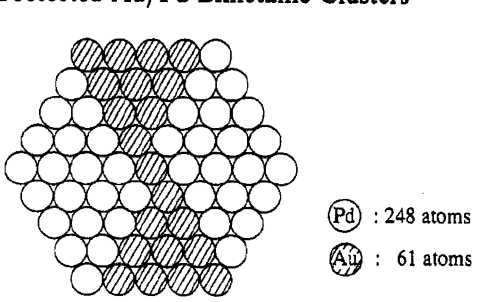

Figure 62. Cross section of a model for Au/Pt (1/4) AuNPs catalytically active for hydrogenation reaction, prepared by a successive (Pt then Au) reduction. Reprinted with permission from ref 196b (Toshima's group). Copyright 1993 American Chemical Society.

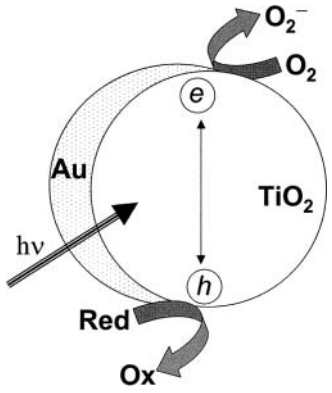

Figure 63. Interfacial charge-transfer processes in a metal−semiconductor nanoparticle. Reprinted with permission from ref 461b (Kamat's group). Copyright 2001 American Chemical Society.

hexadiene functionality was coordinated to alkanethiolate−AuNPs and to $RuCl_3$, and the functional AuNPs catalyzed the heterogeneous polymerization of norbornene. The FTIR spectra are consistent with the presence of Cl-bridged dimeric Ru catalytic species.[634]

7.5. Other Types of Catalysis

AuNPs supported on highly hydrophobic ethane-bridged Ti-incorporated mesoporous organosilica catalyzed vapor-phase epoxidation of propene using H_2 and O_2 at 90−120 °C.[635] Clear red-gold microemulsions of $Na[AuCl_4]$ and $NaBH_4$ supported on activated carbon were active catalysts for the oxidation of glycol to glycolate by O_2,[82] although Au/C catalysts of comparable medium-size particles show higher conversion.[636,637] Semiconductor/AuNP composites synthesized by reducing $HAuCl_4$ on the surface of preformed TiO_2 nanoparticles of 10−40 nm diameter were grown by laser-induced melting/fusion, and the particles modified by this treatment were shown to undergo photocatalytic charge transfer, probed using thiocyanate oxidation at the semiconductor interface (Figure 63).[461] Miscellaneous catalytic applications involve lithography,[638] synthesis of onions,[639a] combustion,[639b] and the reaction between CS_2 and $NaBH_4$.[69b] AuNPs−dendrimer composites prepared by laser irradiation were shown to catalyze the reduction of 4-nitrophenol by $NaBH_4$ at rates depending on the dendrimer structure (PPI more efficient than PAMAM).[640]

8. Nonlinear Optics (NLO)

Glasses, polymers, and other shell materials with NLO properties are becoming viable alternatives to the expensive inorganic crystals $LiNbO_3$, KH_2PO_4, and BaB_2O_4 to change the wavelength of laser light through parametric processes. Indeed, the latter crystals are also cumbersome to tailor into the waveguide configurations that are compatible with optical fiber systems. Besides organic chromophores, nanoparticles including AuNPs represent a very important category of NLO dopants.

The nonlinear response of glasses containing metal nanoparticles is dominated by two relaxation processes:[641] (i) a fast relaxation process due to electron−phonon coupling, leading to thermal equilibrium between the electron and lattice in a metal nanoparticle system after excitation of the hot electron by the incident pulse, and (ii) a slow relaxation process due to thermal diffusion of the excess heat from metal nanoparticles to the matrix.

AuNPs have a large third-order nonlinear susceptibility and a near-resonance nonlinear response[642] that is fast on the 50-ps time scale, and glass with dispersed AuNPs is therefore a candidate material for use in nonlinear optical devices.[643] Their production requires the dispersion of a large amount of AuNPs. Although the AuNP concentration is low in glasses prepared by conventional methods due to the vaporization and low solubility of raw materials, a large amount of AuNPs can be dispersed in matrices by ion implantation, because this technique is free of these restrictions.[644] Glass produced by ion implantation has a large third-order nonlinear optical susceptibility ($\chi^{(3)} = 1.2 \times 10^{-7}$ esu).[645] In glass with dispersed AuNPs, the growth of AuNPs leads to an increase in third-order optical susceptibility and concurrently an increase in absorption coefficient.[644] For practical applications, it is desirable to have a low absorption coefficient and a large third-order optical susceptibility. With silica glass in which AuNPs were synthesized by ion implantation, AuNPs were found to grow through an Ostwald ripening mechanism controlled by diffusion in the silica glass.[645,646] The third-order nonlinear optical susceptibility, $\chi^{(3)}$, of this glass was found to be proportional to the fourth power of the radius of the colloid particles or the fourth power of the absorption coefficient at the peak of the SPB when the total volume of the AuNPs was constant. $\chi^{(3)}$ was also inversely proportional to the third power of the total volume of AuNPs when the absorption coefficient of the SPB was constant.[646] Crystallization effects were found to influence the NLO response of transparent glass−ceramics with AuNP nuclei. The temporal absorption change at the SPB showed that the fast component of the relaxation process was hardly changed with crystallization, while the relaxation time of the tail component decreased with an increase in crystallite size.[647] The relaxation time was also found to increase with a decrease of the AuNP radius, and the tail of the decay curve due to the slow

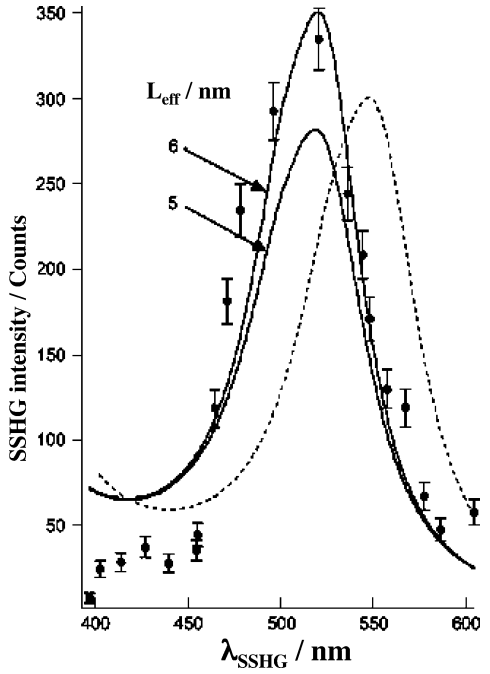

Figure 64. SSHG spectrum for the underivatived AuNPs at the air/toluene interface (circles). The adsorption band corresponds to surface plasmon excitations and has a maximum at 520 nm. The solid line represents the calculated SSHG spectrum for AuNPs in toluene, taking size effects into accounts (L_{eff} = 6 and 5 nm). The solid line is for λ_P = 138.5 nm, corresponding to bulk gold; the dotted line is for a material with a free electron concentration 10% lower than that of bulk gold, for $\lambda_P' = 146$ nm and $v_f' = 1.342 \times 10^6$ ms^{-1} (and L_{eff} = 6 nm). Reprinted with permission from ref 652 (Schiffrin's group). Copyright 1997 The Royal Society of Chemistry.

relaxation component increased with an increase of the AuNP size.[648] Dielectric periodic structures in which some frequencies of light cannot penetrate because photon modes at these frequencies do not exist in the structure were called photonic crystals. In such photonic crystals with AuNPs dispersed in layers as a defect structure, the defect mode shift could be attributed to the Kerr effect inside the defect structure. NLO effects were found in these photonic crystals.[649]

Although glass−AuNPs have attracted the most attention, other AuNP materials with interesting NLO properties are also known in which the AuNPs are in suspension[650] or embedded in other supports, such as pores of mesoporous silica,[112] polymer matrices,[651] and thiolate ligand shells.[652−656] Indeed, second-order NLO activity for liquid dispersion of AuNPs has been disclosed.[657,658] AuNPs in polydiacetylenes induce an enhancement of the third-order susceptibility, $\chi^{(3)}$, by 2 orders of magnitude in comparison with that of the polymer alone.[659] In addition, hyper-Raleigh scattering (HRS) has been used to study the NLO response of AuNP suspensions,[650] and molecularly bridged thiolate−AuNPs showed very large responses. Both symmetry and distance were found to be key factors in determining NLO behavior.[653] NLO-active chromophores have also been anchored onto AuNPs in order to combine the NLO properties of both the core and ligand components of thiolate-stabilized AuNPs.[651] Surface second harmonic generation (SSHG) was used as a new technique, sensitive to resonant plasmon excitation, to characterize AuNPs at the air/toluene interface. Wavelength analysis of these thiolate-stabilized AuNPs indicated the narrow frequency band of the AuNP surface plasmon (Figure 64).[652] NLO properties of C_{60}-containing nitrogen ligands bound to AuNPs were investigated, and optical limiting effects were measured for 8 ns at 532 nm. The NLO properties of these composites, investigated by the Z-scan technique, could be attributed to the strong excited-state absorption of the ligands and the SP resonance of the AuNPs. The main absorptive mechanisms are the nonlinear absorption and the absorption-induced nonlinear scattering. The stronger nonlinear refractions enhance further the refractive optical linear effects (Figure 65).[654−656]

9. Miscellaneous Applications

AuNPs have been used to manipulate the selectivity between solutes in capillary electrophoresis. Therefore, the AuNPs serve as large surface area platforms for organofunctional groups that interact with the capillary surface, the analytes, or both. The apparent mobilities of target analytes as well as the electro-

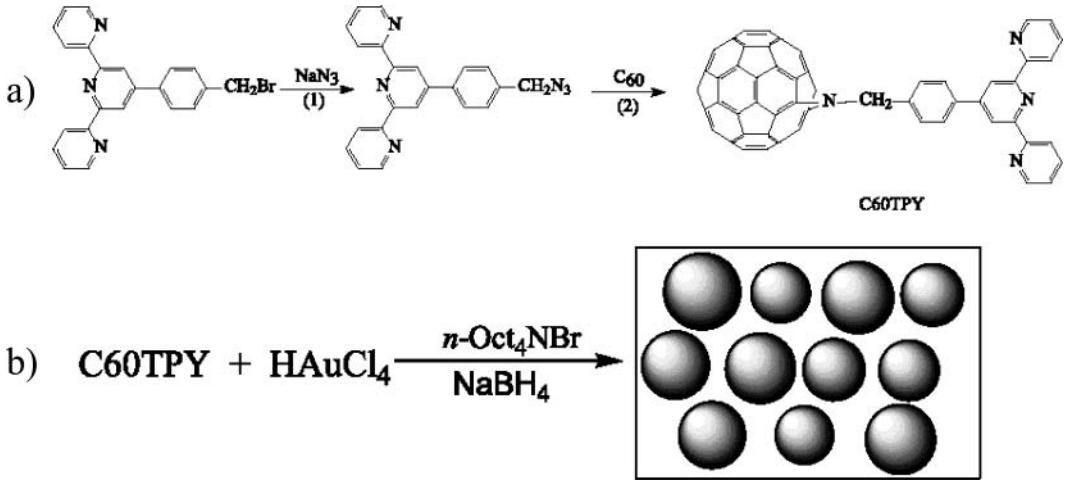

Figure 65. Synthetic routes leading to (a) a [60]fullerene-substituted oligopyridine and (b) the AuNPs stabilized by it. Reprinted with permission from ref 656 (Li's group). Copyright 2002 Elsevier.

osmotic flow could be altered, which led to enhanced selectivities.[660] The use of AuNPs has also been extended to chip-based capillary electrophoresis devices, the AuNPs in the microchannels acting as a rectifier.[661] Electromagnetic coupling effects with lithographically produced AuNPs were investigated by photon scanning tunneling microscopy. The surface plasmon propagation on microstructured metal thin films was examined in order to provide an interface between the nano-optical device and classical far-field optics.[662]

The optical manipulation of particles on waveguide surfaces offers a controllable tool for application to particle sorting, sensing, and atomic mirrors. In this context, potassium-ion-exchanged optical waveguides in glass for evanescent field propulsion of AuNPs were optimized.[663]

Encapsulation techniques are currently used to reduce photo-oxidation in commercial devices. In particular, utilization of AuNPs in optoelectronic devices often enhances the optical and electrical properties as well as the stability; this technique effectively inhibits photoluminescence decay.[664]

10. Conclusion and Perspectives

AuNPs, which have been known for 2500 years, are the subject of an exponentially increasing number of reports and are full of promises for optical, electronic, magnetic, catalytic, and biomedical applications in the 21st century, using the "bottom-up" approach with the hybrid organic−inorganic and biological−inorganic building blocks derived therefrom. From the fascination produced by the more or less virtual medical uses of soluble gold in the past millenaries, it remains at least that AuNPs are completely biocompatible. The reasons for the present excitement in AuNP research are also the stability of AuNPs, the extraordinary diversity of their modes of preparations (including biosynthetic modes and template synthesis) involving ceramics, glasses, polymers, ligands, surfaces, films, oxides, zeolithes, biomolecules, and bioorganisms, and their essential properties and role in nanoscience and future nanotechnology.

The classic Turkevitch−Frens synthesis with citrate stabilizer is practical and still very much used to prepare precursors. However, the stabilization of AuNPs by alkanethiolate and various functional thiolate ligands forming very stable, relatively monodisperse materials and the two-phase Schiffrin synthesis have been a breakthrough. These facile syntheses have been shown to be particularly favorable for easy manipulations, such as place-exchange reactions and extensive physical characterizations, formation of superlattices and crystals, and rich molecular chemistry. For instance, multiple redox states (up to 15!) of AuNP−alkanethiolate were beautifully characterized at room temperature as charge injection in the core is quantized, and 2D and 3D AuNP superlattices are now common, easily controlled assemblies that use supramolecular principles and are characterized by spectacular imaging and microscopy techniques.

Fascinating aspects are the optoelectronic properties of AuNPs related to the surface plasmon absorption, reflecting the collective oscillation of the conducting electrons of the gold core, a feature relevant to the quantum size effect. NLO applications of AuNPs are also rapidly growing. The combination of this photonics discipline with biology and medicine has already been demonstrated by the seminal work on AuNP−DNA assemblies and is very promising for future biomolecular manipulations and applications, such as labeling, detection, and transfer of drugs, including genetic materials.

Electronic conduction correlated with single-electron tunneling is a possible basis for future nanoelectronic digital circuits in connection with self-assembled monolayers, although the quantized capacitance involved will require ultrapure AuNP materials.

Excellent sensory and environmental devices are becoming available by tuning the spectroscopy, fluorescence, luminescence, and electrochemical characteristics of AuNPs with those of substrates including DNA, sugars, and other biological molecules or systems. Another promising electrochemical field that has just started to develop is that of AuNP ultramicroelectrodes. Thus, it is becoming possible to control molecules at a resolution well below that offered by photolithography. In particular, DNA is a candidate for this task because of its excellent specificity in base pairing, and it can be easily addressed at the nanoscale for applications in biosensing and bionanotechnology.

Finally, although bulk gold is well known for being inert, the reactivity of the gold cores in AuNPs has recently proven very useful in catalytic applications, even at subambient temperatures, and the field of AuNP-catalyzed CO and methanol oxidation and O_2 reduction is now also developing at a rapid rate. Here again, the variety of synthetic possibilities using AuNP components and the understanding of the AuNP nanostructures and their role on the catalytic events is a key toward future applications.

In conclusion, an extraordinary variety of structures, properties, and applications is available for AuNPs and will motivate fundamental studies and applications in connection with those of other molecular, inorganic, and biological nanomaterial components in interdisciplinary research involving chemistry, physics, biology, and medicine.[665]

11. Acknowledgment

The helpful assistance of Jocelyne Moncada for the preparation of this manuscript and financial support from the Institut Universitaire de France (IUF), the University Bordeaux I, and the Centre National de la Recherche Scientifique (CNRS) are gratefully acknowledged.

12. Abbreviations

2D	two-dimensional
3D	three-dimensional
AFM	atomic force microscopy
APTMS	(3-aminopropyl)trimethoxysilane

ATR	atom-transfer radical
Au@SiO2	Au−SiO_2 core−shell particles
AuNP	gold nanoparticle
BAM	Brewter angle microscopy
CVD	chemical vapor deposition
DFT	density functional theory
DNA	desoxyribonucleic acid
DPV	differential pulse voltammetry
DQ	double quantum
DSC	differential scanning calorimetry
EDX	energy-disperse X-ray
EPR	electronic paramagnetic resonance
ESCA	electron spectroscopy for chemical analysis
ET	electrostatic trapping
EXAFS	extended X-ray absorption fine structure
FTIR	Fourier transform infrared
HETCOR	heteronuclear correlation
HIV	human immunodeficiency virus
HOPG	highly ordered pyrolytic graphite
HREELS	high-resolution electron energy loss spectroscopy
HRS	hyper-Raleigh scattering
HRTEM	high-resolution transmission electron microscopy
LB	Langmuir−Blodgett
LDI-MS	laser desorption−ionization mass spectrometry
LRP	living radical polymerization
MAS	magic angle spinning
MCD	magnetic circular dichroism
MPC	monolayer-protected cluster
NLO	nonlinear optics
PAMAM	polyamidoamine
PLD	pulsed laser deposition
PRB	plasmon resonance band
PS−PVP	polystyrene-*block*-poly(4-vinylpyridine)
PVP	poly(*N*-vinyl-2-pyrrolidone)
QCM	quartz crystal microbalance
ROMP	ring-opening metathesis polymerization
SAM	self-assembled monolayer
SAXS	small-angle X-ray scattering
SEM	scanning electron microscopy
SERS	surface-enhanced Raman scattering
SFM	scanning force microscopy
SP	surface plasmon
SPB	surface plasmon band
SSHG	surface second harmonic generation
STM	scanning tunneling microscopy
STS	scanning tunneling spectroscopy
TEM	transmission electron microscopy
TEMPO	2,2,6,6-tetramethyl-1-piperidinyloxyl
TGA	thermogravimetric analysis
TOPO	tri-*n*-octylphosphine oxide
XANES	X-ray absorption near-edge structure
XPS	X-ray photoelectron spectroscopy

13. References

(1) Antonii, F. *Panacea Aurea-Auro Potabile*; Bibliopolio Frobeniano: Hamburg, 1618.

(2) (a) Kunckels, J. *Nuetliche Observationes oder Anmerkungen von Auro und Argento Potabili*; Schutzens: Hamburg, 1676. (b) Savage, G. *Glass and Glassware*; Octopus Book: London, 1975.

(3) Helcher, H. H. *Aurum Potabile oder Gold Tinstur*; J. Herbord Klossen: Breslau and Leipzig, 1718.

(4) *Dictionnaire de Chymie*; Lacombe: Paris, 1769.

(5) Fulhame, Mrs. *An Essay on Combustion with a View to a New Art of Dying and Painting*; J. Cooper: London, 1794.

(6) Ostwald, W. Zur Geschichte des Colloiden Goldes. *Kolloid Z.* **1909**, *4*, 5.

(7) Faraday, M. Experimental Relations of Gold (and other Metals) to Light. *Philos. Trans.* **1857**, *147*, 145−181.

(8) Graham, T. *Philos. Trans. R. Soc.* **1861**, *151*, 183−190.

(9) Kahn, R. L. Serum Diagnosis for Syphilis. In *Colloid Chemistry*; Alexander, J., Ed.; The Chemical Catalog Co.: New York, 1928; Vol. II, p 757.

(10) Hauser, E. A. Aurum Potabile. *J. Chem. Educ.* **1952**, 456−458.

(11) (a) Brown, D. H.; Smith, W. E. The Chemistry of the Gold Drugs Used in the Treatment of Rheumatoid Arthritis. *Chem. Soc. Rev.* **1980**, *9*, 217−240. (b) *Immuno-Gold Electron Microscopy in Virus Diagnosis and Research*; Hyatt, A. D., Eaton, B. T., Eds.; CRC Press: Boca Raton, FL, 1993.

(12) Turkevitch, J.; Stevenson, P. C.; Hillier, J. Nucleation and Growth Process in the Synthesis of Colloidal Gold. *Discuss. Faraday Soc.* **1951**, *11*, 55−75.

(13) Frens, G. Controlled Nucleation for the Regulation of the Particle Size in Monodisperse Gold Suspensions. *Nature: Phys. Sci.* **1973**, *241*, 20−22. For a more recent report on citrate-stabilized AuNPs, see ref 223.

(14) Hayat, M. A. *Colloidal Gold, Principles, Methods and Applications*; Academic Press: New York, 1989.

(15) *Clusters and Colloids*; Schmid, G., Ed.; VCH: Weinheim, 1994.

(16) Bradley, J. S. In *Clusters and Colloids*; Schmid, G., Ed.; VCH: Weinheim, 1994; Chapter 6, pp 459−544.

(17) Schmid, G. Large Clusters and Colloids. *Chem. Rev.* **1992**, *92*, 1709−1727.

(18) Fendler, J. H.; Meldrum, F. C. The Colloidal Chemical Approach to Nanostructured Materials. *Adv. Mater.* **1995**, *7*, 607−632.

(19) Schmid, G.; Chi, L. F. Metal Clusters and Colloids. *Adv. Mater.* **1998**, *10*, 515−527.

(20) Edelstein, A. S.; Cammarata, R. C. *Nanoparticle: Synthesis, Properties and Applications*; Institute of Physics Publishing: Bristol, 1996.

(21) Schmid, G. In *Nanoscale Materials in Chemistry*; Klabunde, K. J., Ed.; Wiley: New York, 2001.

(22) Bethell, D.; Brust, M.; Schiffrin, D. J.; Kiely, C. From Monolayers to Nanostructured Materials: An Organic Chemist's View of Self-Assembly. *J. Electroanal. Chem.* **1996**, *409*, 137−143.

(23) Matijevic, E. Controlled Colloid Formation. *Curr. Opin. Colloid Interface Sci.* **1996**, *1*, 176−183.

(24) *Optical Properties of Metal Clusters*; Freibig, U., Vollmer, M., Eds.; Springer-Verlag: New York, 1995.

(25) Ung, T.; Liz-Marzán, L. M.; Mulvaney, P. Gold Nanoparticle Thin Films. *Colloids Surf. A: Physicochem. Eng. Asp.* **2002**, *202*, 119−126.

(26) Yonezawa, T.; Toshima, N. Polymer-Stabilized Metal Nanoparticles: Preparation, Characterization and Applications. In *Advanced Functional Molecules and Polymers*; Nalwa, H. S., Ed.; Gordon & Breach: Reading, UK, 2001; Vol. 2, Chapter 3, pp 65−86.

(27) Brust, M.; Kiely, C. J. Some Recent Advances in Nanostructure Preparation from Gold and Silver: A Short Topical Review. *Colloids Surf. A: Physicochem. Eng. Asp.* **2002**, *202*, 175−186.

(28) *Metal Nanoparticles−Synthesis, Characterization and Applications*; Feldheim, D. L., Colby, A. F., Jr., Eds.; Marcel Dekker: New York, 2002.

(29) Alivisatos, A. P. Semiconductor Clusters, Nanocrystals, and Quantum Dots. *Science* **1996**, *271*, 933−937.

(30) (a) Schmid, G.; Bäumle, M.; Geerkens, M.; Heim, I.; Osemann, C.; Sawitowski, T. Current and Future Applications of Nanoclusters. *Chem. Soc. Rev.* **1999**, *28*, 179−185. (b) Schmid, G.; Corain, B. Nanoparticulated Gold: Syntheses, Structures, Electronics, and Reactivities. *Eur. J. Inorg. Chem.* **2003**, 3081−3098. (c) Zhang, H.; Schmid, G.; Hartmann, U. Reduced Metallic Properties of Ligand-Stabilized Small Metal Clusters. *Nano Lett.* **2003**, *3*, 305−307.

(31) Schmid, G.; Harms, M.; Malm, J. O.; Bovin, J. O.; Van Ruitenbeck, J.; Zandbergen, H. W.; Fu, W. T. Ligand-stabilized Giant Palladium Clusters: Promising Candidates in Heterogeneous Catalysis. *J. Am. Chem. Soc.* **1993**, *115*, 2046−2048.

(32) Andres, R. P.; Bein, T.; Dorogi, M.; Feng, S.; Jenderson, J. I.; Kubiak, C. P.; Mahoney, W.; Osifchin, R. G.; Reifenverger, R. "Coulomb Staircase" at Room Temperature in a Self-Assembled Molecular Nanostructure. *Science* **1996**, *272*, 1323−1325.

(33) (a) *Fine Particles Sciences and Technology−From Micro- to New Particles*; Pellizzetti, E., Ed.; Kluwer: Dordrecht, 1996. (b) Toshima, N. In *Fine Particles Sciences and Technology−From Micro- to New Particles*; Pellizzetti, E., Ed.; Kluwer: Dordrecht, 1996; pp 371−383.

(34) Beesley, J. E. *Colloidal Gold. A New Perpective for Cytochemical Marking*; Royal Microscopical Society Handbook 17; Oxford Science Publication, Oxford University Press: Oxford, 1989.

(35) Toshima, N.; Yonezawa, T. Bimetallic Nanoparticles-Novel Materials for Chemical and Physical Applications. *New J. Chem.* **1998**, 1179−1201.

(36) Fendler, J. H. Self-Assembled Nanostructured Materials. *Chem. Mater.* **1996**, *8*, 1616−1624.

(37) Henglein, A. Physicochemical Properties of Small Metal Particles and the Atom-to-Metal Transition. *J. Phys. Chem.* **1993**, *97*, 5457−5471.

(38) Belloni, J. Metal Nanocolloids. *Curr. Opin. Colloid Interface Sci.* **1996**, *1*, 184−196.

(39) (a) Chen, S.; Ingram, R. S.; Hostetler, M. J.; Pietron, J. J.; Murray, R. W.; Schaaff, T. G.; Khoury, J. T.; Alvarez, M. M.; Whetten, R. L. Gold Nanoelectrodes of Varied Size: Transition to Molecule-Like Charging. *Science* **1998**, *280*, 2098−2101. (b) Miles, D. T.; Murray, R. W. Temperature-Dependent Quantized Double Layer Charging of Monolayer-Protected Gold Clusters. *Anal. Chem.* **2003**, *75*, 1251−1257. (c) Chen, S.; Pei, R. Ion-Induced Rectification of Nanoparticle Quantized Capacitance Charging in Aqueous Solutions. *J. Am. Chem. Soc.* **2001**, *123*, 10607−10615.

(40) Quinn, B. M.; Liljeroth, P.; Ruiz, V.; Laaksonen, T.; Kontturi, K. Electrochemical Resolution of 15 Oxidation States for Monolayer Protected Gold Nanoparticles. *J. Am. Chem. Soc.* **2003**, *125*, 6644−6645.

(41) (a) Puddephat, R. J. *The Chemistry of Gold*; Elsevier: Amsterdam, 1978. (b) *Gold, Progress in Chemistry, Biochemistry and Technology*; Schmidbauer, H., Ed.; Wiley: Chichester, 1999.

(42) Laguna, A. In *Metal Clusters in Chemistry*; Braunstein, P., Oro, L., Raithby, P. R., Eds; Wiley-VCH: Weinheim, 1999.

(43) *Nanoparticles and Nanostructured Films*; Fendler, J. H., Ed.; Wiley-VCH: Weinheim, 1998.

(44) Yonezawa, T.; Kunitake, T. Practical Preparation of Anionic Mercapto Ligand-Stabilized Gold Nanoparticles and Their Immobilization. *Colloids Surf. A: Physicochem. Eng. Asp.* **1999**, *149*, 193−199.

(45) Schmid, G.; Pfeil, R.; Boese, R.; Bandermann, F.; Meyer, S.; Calis, G. H. M.; van der Velden, J. W. A. $[Au_{55}\{P(C_6H_5)_3\}_{12}Cl_6]$ − A Gold Cluster of Unusual Size. *Chem. Ber.* **1981**, *114*, 3634−3642.

(46) (a) Giersig, M.; Mulvaney, P. Preparation of ordered colloid monolayers by electrophoretic deposition. *Langmuir* **1993**, *9*, 3408−3413. (b) Hasan, M.; Bethell, D.; Brust, M. The Fate of Sulfur-Bound Hydrogen on Formation of Self-Assembled Thiol Monolayers on Gold: ^{1}H NMR Spectroscopic Evidence from Solutions of Gold Clusters. *J. Am. Chem. Soc.* **2003**, *125*, 1132−1133.

(47) (a) Brust, M.; Walker, M.; Bethell, D.; Schiffrin, D. J.; Whyman, R. J. Synthesis of Thiol-Derivatized Gold Nanoparticles in a Two-phase Liquid−Liquid System. *J. Chem. Soc., Chem. Commun.* **1994**, 801−802. (b) Brust, M.; Fink, J.; Bethell, D.; Schiffrin, D. J.; Kiely, C. J. Synthesis and Reactions of Functionalised Gold Nanoparticles. *J. Chem. Soc., Chem. Commun.* **1995**, 1655−1656.

(48) (a) Chen, S. 4-Hydroxythiophenol-Protected Gold Nanoclusters in Aqueous Media. *Langmuir* **1999**, *15*, 7551−7557. (b) Chen, S.; Murray, R. W. Arenethiolate Monolayer-Protected Gold Clusters. *Langmuir* **1999**, *15*, 682−689.

(49) (a) Hostetler, M. J.; Green, S. J.; Stokes, J. J.; Murray, R. W. Monolayers in Three Dimensions: Synthesis and Electrochemistry of ω-Functionalized Alkanethiolate-Stabilized Gold Cluster Compounds. *J. Am. Chem. Soc.* **1996**, *118*, 4212−4213. (b) Ingram, R. S.; Hostetler, M. J.; Murray, R. W. Poly-hetero-ω-functionalized Alkanethiolate-Stabilized Gold Cluster Compounds. *J. Am. Chem. Soc.* **1997**, *119*, 9175−9178.

(50) Templeton, A. C.; Wuelfing, W. P.; Murray, R. W. Monolayer-Protected Cluster Molecules. *Acc. Chem. Res.* **2000**, *33*, 27−36.

(51) Hostetler, M. J.; Wingate, J. E.; Zhong, C.-J.; Harris, J. E.; Vachet, R. W.; Clark, M. R.; Londono, J. D.; Green, S. J.; Stokes, J. J.; Wignall, G. D.; Glish, G. L.; Porter, M. D.; Evans, N. D.; Murray, R. W. Alkanethiolate Gold Cluster Molecules with Core Diameters from 1.5 to 5.2 nm: Core and Monolayer Properties as a Function of Core Size. *Langmuir* **1998**, *14*, 17−30.

(52) (a) Templeton, A. C.; Hostetler, M. J.; Kraft, C. T.; Murray, R. W. Reactivity of Monolayer-Protected Gold Cluster Molecules: Steric Effects. *J. Am. Chem. Soc.* **1998**, *120*, 1906−1911. (b) Hostetler, M. J.; Templeton, A. C.; Murray, R. W. Dynamics of Place-Exchange Reactions on Monolayer-Protected Gold Cluster Molecules. *Langmuir* **1999**, *15*, 3782−3789.

(53) Hostetler, M. J.; Templeton, A. C.; Murray, R. W. Dynamics of Place-Exchange Reactions on Monolayer-Protected Gold Cluster Molecules. *Langmuir* **1999**, *15*, 3782−3789.

(54) Waters, C. A.; Mills, A. J.; Johnson, K. A.; Schiffrin, D. J. Purification of Dodecanethiol Derivatized Gold Nanoparticles. *Chem. Commun.* **2003**, 540−541.

(55) Aslan, K.; Pérez-Luna, V. H. Surface Modification of Colloidal Gold by Chemisorption of Alkanethiols in the Presence of a Nonionic Surfactant. *Langmuir* **2002**, *18*, 6059−6065.

(56) Prasad, B. L. V.; Stoeva, S. I.; Sorensen, C. M.; Klabunde, K. J. Digestive Ripening of Thiolated Gold Nanoparticles: The Effect of Alkyl Chain Length. *Langmuir* **2002**, *18*, 7515−7520.

(57) Prasad, B. L. V.; Stoeva, S. I.; Sorensen, C. M.; Klabunde, K. J. Digestive-Ripening Agents for Gold Nanoparticles: Alternatives to Thiols. *Chem. Mater.* **2003**, *15*, 935−942.

(58) (a) Andres, R. P.; Bielefeld, J. D.; Henderson, J. I.; Janes, D. B.; Kolagunta, V. R.; Kubiak, C. P.; Mahoney, W. J.; O. R. G. Self-Assembly of a Two-Dimensional Superlattice of Molecularly Linked Metal Clusters. *Science* **1996**, *273*, 1690−1693. (b) Lin, X. M.; Sorensen, C. M. Ligand-Induced Gold Nanocrystal Superlattice Formation in Colloidal Solution. *Chem. Mater.* **1999**, *11*, 198−202.

(59) (a) Brown, L. O.; Hutchison, J. E. Formation and Electron Diffraction Studies of Ordered 2-D and 3-D Superlattices of Amine-Stabilized Gold Nanocrystals. *J. Phys. Chem. B* **2001**, *105*, 8911−8916. (b) Stoeva, S. I.; Prasad, B. L. V.; Uma, S.; Stoimenov, P. K.; Zaikovsky, V.; Sorensen, C. M.; Klabunde, K. J. Face-Centered Cubic and Hexagonal Closed-Packed Nanocrystal Superlattice of Gold Nanoparticles Prepared by Different Methods. *J. Phys. Chem. B* **2003**, *107*, 7441−7448.

(60) (a) Li, W.; Huo, L.; Wang, D.; Zeng, G.; Xi, S.; Zhao, B.; Zhu, J.; Wang, J.; Shen, Y.; Lu, Z. Self-Assembled Multilayers of Alternating Gold Nanoparticles and Dithiols: Approaching to Superlattice. *Colloids Surf.* **2000**, *175*, 217−223. (b) Wang, T.; Zhang, D.; Xu, W.; Zhu, D. Self-Organization of Gold Nanoparticles into 2D Superlattice through $\pi-\pi$ Interaction. *Synth. Met.* **2003**, *135−136*, 835−836.

(61) (a) Kanehara, M.; Oumi, Y.; Sano, T.; Teranishi, T. Formation of Low-Symmetric 2D Superlattices of Gold Nanoparticles through Surface Modification by Acid−Base Interaction. *J. Am. Chem. Soc.* **2003**, *125*, 8708. (b) Teranishi, T. Fabrication and Electronic Properties of Gold Nanoparticles. In *Dendrimers and Nanoscience*; Astruc, D., Ed.; Compte-Rendus Chimie, Elsevier: Paris, 2003 (in press).

(62) Dieluweit, S.; Pum, D.; Sleytr, U. B. Formation of a Gold Superlattice on an S−Layer with Square Lattice Symmetry. *Supramol. Sci.* **1998**, *5*, 15−19.

(63) (a) Sarathy, K. V.; Kulkarni, G. U.; Rao, C. N. R. A Novel Method of Preparing Thiol-Derivatised Nanoparticles of Gold, Platinum and Silver Forming Superstructures. *Chem. Commun.* **1997**, 537−538. (b) Ascencio, J. A.; Pérez, M.; José-Yacamán, M. A Truncated Icosahedral Structure Observed in Gold Nanoparticles. *Surf. Sci.* **2000**, *447*, 73−80. (c) Chushak, Y.; Bartell, L. S. Molecular Dynamics Simulations of the Freezing of Gold Nanoparticles. *Eur. Phys. J. D* **2001**, *16*, 43−46.

(64) (a) Yee, C. K.; Jordan, R.; Ulman, A.; White, H.; King, A.; Rafailovich, M.; Sokolov, J. Novel One-Phase Synthesis of Thiol-Functionalized Gold, Palladium, and Iridium Nanoparticles Using Superhydride. *Langmuir* **1999**, *15*, 3486−3491. (b) Selvakannan, P. R.; Mandal, S.; Pasricha, R.; Adyanthaya, S. D.; Sastry, M. One-Step Synthesis of Hydrophobized Gold Nanoparticles of Controllable Size by the Reduction of Aqueous Chloroaurate Ions by Hexedecylaniline at the Liquid−Liquid Interface. *Chem. Commun.* **2002**, 1334−1335.

(65) Wei, G.-T.; Liu, F.-K.; Wang, C. R. C. Shape Separation of Nanometer Gold Particles by Size-Exclusion Chromatography. *Anal. Chem.* **1999**, *71*, 2085−2091.

(66) Tzhayik, O.; Sawant, P.; Efrima, S.; Kovalev, E.; Klug, J. T. Xanthate Capping of Silver, Copper, and Gold Colloids. *Langmuir* **2002**, *18*, 3364−3369.

(67) Porter, L. A., Jr.; Ji, D.; Westcott, S. L.; Graupe, M.; Czernuszewicz, R. S.; Halas, N. J.; Lee, T. R. Gold and Silver Nanoparticles Functionalized by the Adsorption of Dialkyl Disulfides. *Langmuir* **1998**, *14*, 7378−7386.

(68) Yonezawa, T.; Yasui, K.; Kimizuka, N. Controlled Formation of Smaller Gold Nanoparticles by the Use of Four-Chained Disulfide Stabilizer. *Langmuir* **2001**, *17*, 271−273.

(69) (a) Manna, A.; Chen, P.-L.; Akiyama, H.; Wei, T.-X.; Tamada, K.; Knoll, W. Optimized Photoisomerization on Gold Nanoparticles Capped by Unsymmetrical Azobenzene Disulfides. *Chem. Mater.* **2003**, *15*, 20−28. (b) Torigoe, K.; Esumi, K. Preparation and Catalytic Effect of Gold Nanoparticles in Water Dissolving Carbon Disulfide. *J. Phys. Chem. B* **1999**, *103*, 2862−2866.

(70) (a) Resch, R.; Baur, C.; Bugacov, A.; Koel, B. E.; Echternach, P. M.; Madhukar, A.; Montoya, N.; Requicha, A. A. G.; Will, P. Linking and Manipulation of Gold Multinanoparticle Structures Using Dithiols and Scanning Force Mircroscopy. *J. Phys. Chem. B* **1999**, *103*, 3647−3650. (b) Félidj, N.; Aubard, J.; Lévi, G.; Krenn, J. R.; Hohenau, A.; Schider, G.; Leitner, A.; Aussenegg, F. R. Optimized Surface-Enhanced Raman Scattering on Gold Nanoparticle Arrays. *Appl. Phys. Lett.* **2003**, *82*, 3095−3097. (c) Tan, Y.; Li, Y.; Zhu, D. Fabrication of Gold Nanoparticles Using a Trithiol (Thiocyanuric Acid) as the Capping Agent. *Langmuir* **2002**, *18*, 3392−3395. (d) Balasubramanian, R.; Kim, B.; Tripp, S. L.; Wang, X.; Lieberman, M.; Wei, A. Dispersion and Stability Studies of Resorcinarene-Encapsulated Gold Nanoparticles. *Langmuir* **2002**, *18*, 3676−3681.

(71) Shelley, E. J.; Ryan, D.; Johnson, S. R.; Couillard, M.; Fitzmaurice, D.; Nellist, P. D.; Chen, Y.; Palmer, R. E.; Preece, J. A. Dialkyl Sulfides: Novel Passivating Agents for Gold Nanoparticles. *Langmuir* **2002**, *18*, 1791−1795.

(72) Li, X.-M.; de Jong, M. R.; Inoue, K.; Shinkai, S.; Huskens, J.; Reinhoudt, D. N. Formation of Gold Colloids Using Thioether Derivatives as Stabilizing Ligands. *J. Mater. Chem.* **2001**, *11*, 1919−1923. (b) Maye, M. M.; Chun, S. C.; Han, L.; Rabinovitch, D.; Zhong, C.-J. Novel Spherical Assembly of Gold Nanoparticles Mediated by a Tetradentate Thioether. *J. Am. Chem. Soc.* **2002**, *124*, 4958−4959.

(73) Sun, L.; Crooks, R. M.; Chechik, V. Preparation of Polycyclodextrin Hollow Spheres by Templating Gold Nanoparticles. *Chem. Commun.* **2001**, 359−360.

(74) (a) Weare, W. W.; Reed, S. M.; Warner, M. G.; Hutchison, J. E. Improved Synthesis of Small ($d_{CORE} \approx 1.5$ nm) Phosphine-Stabilized Gold Nanoparticles. *J. Am. Chem. Soc.* **2000**, *122*, 12890−12891. (b) Yamamoto, M.; Nakamoto, M. New Type of Monodispersed Gold Nanoparticles Capped by Myristate and PPh_3 Ligands Prepared by Controlled Thermolysis of [Au($C_{13}H_{27}$-COO)(PPh_3)]. *Chem. Lett.* **2003**, *32*, 452−453.

(75) (a) Heath, J. R.; Brandt, L.; Leff, D. V. Synthesis and Characterization of Hydrophobic, Organically-Soluble Gold Nanocrystals Functionalized with Primary Amines. *Langmuir* **1996**, *12*, 4723−4730. (b) Heath, J. R.; Knobler, C. M.; Leff, D. V. Pressure/Temperature Phase Diagrams and Superlattices of Organically Functionalized Metal Nanocrystal Monolayers: The Influence of Particle Size, Size Distribution, and Surface Passivant. *J. Phys. Chem. B* **1997**, *101*, 189−197.

(76) (a) Gomez, S.; Philippot, K.; Collière, V.; Chaudret, B.; Senocq, F.; Lecante, P. Gold Nanoparticles from Self-Assembled Gold (I) Amine Precursors. *Chem. Commun.* **2000**, 1945−1946. (b) Bardaji, M.; Uznanski, P.; Amiens, C.; Chaudret, B.; Laguna, A. Aurophilic Complexes as Gold Atom Sources in Organic Media. *Chem. Commun.* **2002**, 598−599. (c) Green, M.; O'Brien, P. A Simple One Phase Preparation of Organically Capped Gold Nanocrystals. *Chem. Commun.* **2000**, 183−184. (d) Selvakannan, P. R.; Mandal, S.; Phadtare, S.; Pasricha, R.; Sastry, M. Capping of Gold Nanoparticles by the Amino Acid Lysine Renders Them Water-Dispersible. *Langmuir* **2003**, *19*, 3545−3549. (e) Ahmad, A.; Senapati, S.; Khan, M. I.; Kumar, R.; Sastry, M. Extracellular Biosynthesis of Monodisperse Gold Nanoparticles by a Novel Extremophilic Actinomycete, *Thermomonospora* sp. *Langmuir* **2003**, *19*, 3550−3553. (f) Chen, J.; Calvet, L. C.; Reed, M. A.; Carr, D. W.; Grushiba, D. S.; Bennett, D. W. *Chem. Phys. Lett.* **1999**, *313*, 741. (g) Kim, H. S.; Lee, S. J.; Kim, N. H.; Yoon, J. K.; Park, H. K.; Kim, K. Adsorption Characteristics of 1,4-Phenylene Diisocyanide on Gold Nanoparticles: Infrared and Raman Spectroscopy Study. *Langmuir* **2003**, *19*, 6701−6710. (h) Joo, S.-W.; Kim, W.-J.; Yoon, W. S.; Choi, I. S. Adsorption of 4,4′-Biphenyl Diisocyanide on Gold Nanoparticle Surfaces Investigated by Surface-Enhanced Raman Scattering. *J. Raman Spectrosc.* **2003**, *34*, 271−275. (i) Li, G.; Lauer, M.; Schulz, A.; Boettcher, C.; Li, F.; Fuhrhop, J.-H. Spherical and Planar Gold (0) Nanoparticles with a Rigid Gold(I)-Anion or a Fluid Gold-(0)-Acetone Surface. *Langmuir* **2003**, *19*, 6483−6491. (j) Cheng, W.; Dong, S.; Wang, E. Iodine-Induced Gold Nanoparticle Fusion/Fragmentation/Aggregation and Iodine-Linked Nanostructured Assemblies on a Glass Substrate. *Angew. Chem., Int. Ed.* **2003**, *42*, 449−452.

(77) (a) Lattes, A.; Rico, I.; de Savignac, A.; Samii, A. Formamide, a Water Substitute in Micelles and Microemulsions: Structural Analysis Using a Diels−Alder Reaction as a Chemical Probe. *Tetrahedron* **1987**, *43*, 1725−1735. (b) Taleb, A.; Petit, C.; Pileni, M. P. J. Optical Properties of Self-Assembled 2D and 3D Superlattices of Silver Nanoparticles. *Phys. Chem. B* **1998**, *102*, 2214−2220. (c) Chen, F.; Xu, G.-Q.; Hor, T. S. A. Preparation and Assembly of Colloidal Gold Nanoparticles in CTAB−Stabilized Reverse Microemulsion. *Mater. Lett.* **2003**, *57*, 3282−3286.

(78) Sohn, B.-H.; Choi, J.-M.; Yoo, S., II; Yun, S.-H.; Zin, W.-C.; Jung, J. C.; Kanehara, M.; Hirata, T.; Teranishi, T. Directed Self-Assembly of Two Kinds of Nanoparticles Utilizing Monolayer Films of Diblock Copolymer Micelles. *J. Am. Chem. Soc.* **2003**, *125*, 6368−6369.

(79) Manna, A.; Imae, T.; Yogo, T.; Aoi, K.; Okazaki, M. Synthesis of Gold Nanoparticles in a Winsor II Type Microemulsion and Their Characterization. *J. Colloid Interface Sci.* **2002**, *256*, 297−303.

(80) Aliotta, F.; Arcoleo, V.; Buccoleri, S.; La Manna, G.; Liveri, V. T. Calorimetric Investigation on the Formation of Gold Nanoparticles in Water/AOT/*n*-heptane Microemulsions. *Thermochim. Acta* **1995**, *265*, 15−23.

(81) Arcoleo, V.; Liveri, V. T. AFM Investigation of Gold Nanoparticles Synthesized in Water/AOT/*n*-heptanes. *Chem. Phys. Lett.* **1996**, *258*, 223−227.

(82) Porta, F.; Prati, L.; Rossi, M.; Scarì, G. Synthesis of Au (0) Nanoparticles from W/O Microemulsions. *Colloids Surf.* **2002**, *211*, 43−48.

(83) Chiang, C.-L. Controlled Growth of Gold Nanoparticles in AOT/$C_{12}E_4$/Isooctane Mixed Reverse Micelles. *J. Colloid Surf. Sci.* **2001**, *239*, 334−341.

(84) Chiang, C.-L. Controlled Growth of Gold Nanoparticles in Aerosol-OT/Sorbitan Monooleate/Isooctane Mixed Reverse Micelles. *J. Colloid Interface Sci.* **2000**, *230*, 60−66.

(85) Liu, S.; Weaver, J. V. M.; Save, M.; Armes, S. P. Synthesis of p*H*-Responsive Shell Cross-Linked Micelles and Their Use as Nanoreactors for the Preparation of Gold Nanoparticles. *Langmuir* **2002**, *18*, 8350−8357.

(86) Mössmer, S.; Spatz, J. P.; Möller, M.; Aberle, T.; Schmidt, J.; Burchard, W. Solution Behavior of Poly(styrene)-*block*-poly(2-vinylpyridine) Micelles Containing Gold Nanoparticles. *Macromolecules* **2000**, *33*, 4791−4798.

(87) (a) Carrot, G.; Valmalette, J. C.; Plummer, C. J. G.; Scholz, S. M.; Dutta, J.; Hofmann, H.; Hilborn, J. G. Gold Nanoparticle Synthesis in Graft Copolymer Micelles. *Colloid Polym. Sci.* **1998**, *276*, 853−859. (b) Busbee, B. D.; Obare, S. O.; Murphy, C. J. An Improved Synthesis of High-Aspect-Ratio Gold Nanorods. *Adv. Mater.* **2003**, *15*, 414−416.

(88) Mandal, M.; Ghosh, S. K.; Kundu, S.; Esumi, K.; Pal, T. UV Photoactivation for Size and Shape Controlled Synthesis and Coalescence of Gold Nanoparticles in Micelles. *Langmuir* **2002**, *18*, 7792−7797.

(89) Jana, N. R.; Gearheart, L.; Murphy, C. J. Seeding Growth for Size Control of 5−40 nm Diameter Gold Nanoparticles. *Langmuir* **2001**, *17*, 6782−6786.

(90) Jana, N. R.; Gearheart, L.; Murphy, C. J. Seed-Mediated Growth Approach for Shape-Controlled Synthesis of Spheroidal and Rodlike Gold Nanoparticles Using a Surfactant Template. *Adv. Mater.* **2001**, *13*, 1389−1393.

(91) Markowitz, M. A.; Dunn, D. N.; Chow, G. M.; Zhang, J. The Effect of Membrane Charge on Gold Nanoparticle Synthesis via Surfactant Membranes. *J. Colloid Interface Sci.* **1999**, *210*, 73−85.

(92) Johnson, S. R.; Evans, S. D.; Mahon, S. W.; Ulman, A. Synthesis and Characterization of Surfactant-Stabilized Gold Nanoparticles. *Supramol. Sci.* **1997**, *4*, 329−333.

(93) Johnson, S. R.; Evans, S. D.; Brydson, R. Influence of a Terminal Functionality on the Physical Properties of Surfactant-Stabilized Gold Nanoparticles. *Langmuir* **1998**, *14*, 6639−6647.

(94) Hassenkam, T.; Nørgaard, K.; Iversen, L.; Kiely, C. J.; Bjørnholm, T. Fabrication of 2D Gold Nanowires by Self-Assembly of Gold Nanoparticles on Water Surfaces in the Presence of Surfactants. *Adv. Mater.* **2002**, *14*, 1126−1130.

(95) Kawai, T.; Neivandt, D. J.; Davies, P. B. Sum Frequency Generation on Surfactant-Coated Gold Nanoparticles. *J. Am. Chem. Soc.* **2000**, *122*, 12031−12032.

(96) Youk, J. H.; Locklin, J.; Xia, C.; Park, M.-K.; Advincula, R. Preparation of Gold Nanoparticles from a Polyelectrolyte Complex Solution of Terthiophene Amphiphiles. *Langmuir* **2001**, *17*, 4681−4683.

(97) Yonezawa, T.; Onoue, S.-Y.; Kunitake, T. Preparation of Cationic Gold Nanoparticles and Their Monolayer Formation on an Anionic Amphiphile Layer. *Chem. Lett.* **1999**, 1061−1062.

(98) Gittins, D. I.; Caruso, F. Tailoring the Polyelectrolyte Coating of Metal Nanoparticles. *J. Phys. Chem. B* **2001**, *105*, 6846−6852.

(99) Gohy, J.-F.; Varshney, S. K.; Jérôme, R. Morphology of Water-Soluble Interpolyelectrolyte Complexes Formed by Poly(2-vinylpyridinium)-*block*-poly(ethylene oxide) Diblocks and Poly(4-styrenesulfonate) Polyanions. *Macromolecules* **2001**, *34*, 2745−2747.

(100) Svergun, D. I.; Shtykova, E. V.; Dembo, A. T.; Bronstein, L. M.; Platonova, O. A.; Yakunin, A. N.; Valetsky, P. M.; Khokhlov, A. R. Size Distributions of Metal Nanoparticles in Polyelectrolyte Gels. *J. Chem. Phys.* **1998**, *109*, 111109−11116.

(101) Mayya, K. S.; Gittins, D. I.; Caruso, F. Gold-Titania Core−Shell Nanoparticles by Polyelectrolyte Complexation with a Titania Precursor. *Chem. Mater.* **2001**, *13*, 3833−3836.

(102) (a) Mayer, A. B. R.; Mark, J. E. Colloidal Gold Nanoparticles Protected by Cationic Polyelectrolytes. *Pure Appl. Chem.* **1997**, *11*, A34, 2151−2164. (b) Mayya, K. S.; Schoeler, B.; Caruso, F. Preparation and Organization of Nanoscale Polyelectrolyte-Coated Gold Nanoparticles. *Adv. Funct. Mater.* **2003**, *13*, 183−188.

(103) Jana, N. R.; Gearheart, L.; Murphy, C. J. Evidence for Seed-Mediated Nucleation in the Chemical Reduction of Gold Salts to Gold Nanoparticles. *Chem. Mater.* **2001**, *13*, 2313−2322.

(104) Sau, T. K.; Pal, A.; Jana, N. R.; Wang, Z. L.; Pal, T. Size Controlled Synthesis of Gold Nanoparticles Using Photochemically Prepared Seed Particles. *J. Nanopart. Res.* **2001**, *3*, 257−261.

(105) Meltzer, S.; Resch, R.; Koel, B. E.; Thompson, M. E.; Madhukar, A.; Requicha, A. A. G.; Will, P. Fabrication of Nanostructures by Hydroxylamine Seeding of Gold Nanoparticle Templates. *Langmuir* **2001**, *17*, 1713−1718.

(106) Mallick, K.; Wang, Z. L.; Pal, T. Seed-Mediated Successive Growth of Gold Particles Accomplished by UV Irradiation: a Photochemical Approach for Size-Controlled Synthesis. *J. Photochem. Photobiol.* **2001**, *140*, 75−80.

(107) Zhou, Y.; Wang, C. Y.; Zhu, Y. R.; Chen, Z. Y. A Novel Ultraviolet Irradiation Technique for Shape-Controlled Synthesis of Gold Nanoparticles at Room Temperature. *Chem. Mater.* **1999**, *11*, 2310−2312.

(108) (a) Niidome, Y.; Hori, A.; Sato, T.; Yamada, S. Enormous Size Growth of Thiol-passivated Gold Nanoparticles Induced by Near-IR Laser Light. *Chem. Lett.* **2000**, 310−311. (b) Reed, J. A.; Cook, A.; Halaas, D. J.; Parazolli, P.; Robinson, A.; Matula, T. J.; Griezer, F. The Effects of Microgravity on Nanoparticle Size Distributions Generated by the Ultrasonic Reduction of an Aqueous Gold-Chloride Solution. *Ultrason. Sonochem.* **2003**, *10*, 285−289.

(109) Okitsu, K.; Yue, A.; Tanabe, S.; Matsumoto, H.; Yobiko, Y. Formation of Colloidal Gold Nanoparticles in an Ultrasonic Field: Control of Rate of Gold (III) Reduction and Size of Formed Gold Particles. *Langmuir* **2001**, *17*, 7717−7720.

(110) Okitsu, K. Sonolytic Control of Rate of Gold (III) Reduction and Size of Formed Gold Nanoparticles: Relation between Reduction Rates and Sizes of Formed Nanoparticles. *Bull. Chem. Soc. Jpn.* **2002**, *75*, 2289−2296.

(111) Chen, W.; Cai, W. P.; Liang, C. H.; Zhang, L. D. Synthesis of Gold Nanoparticles Dispersed Within Pores of Mesoporous Silica Induced by Ultrasonic Irradiation and its Characterization. *Mater. Res. Bull.* **2001**, *36*, 335−342.

(112) Chen, W.; Cai, W.; Zhang, L.; Wang, G.; Zhang, L. Sonochemical Processes and Formation of Gold Nanoparticles within Pores of Mesoporous Silica. *J. Colloid Surf. Sci.* **2001**, *238*, 291−295.

(113) Pol, V. G.; Gedanken, A.; Calderro-Moreno, J. Deposition of Gold Nanoparticles on Silica Spheres: A Sonochemical Approach. *Chem. Mater.* **2003**, *15*, 1111−1118.

(114) Mizukoshi, Y.; Okitsu, K.; Maeda, Y.; Yamamoto, T. A.; Oshima, R.; Nagata, Y. Sonochemical Preparation of Bimetallic Nanoparticles of Gold/Palladium in Aqueous Solution. *J. Phys. Chem. B* **1997**, *101*, 7033−7037.

(115) (a) Henglein, A.; Meisel, D. Radiolytic Control of the Size of Colloidal Gold Nanoparticles. *Langmuir* **1998**, *14*, 7392−7396. (b) Dawson, A.; Kamat, P. V. Complexation of Gold Nanoparticles with Radiolytically Generated Thiocyanate Radicals $(SCN)_2^{\bullet-}$. *J. Phys. Chem. B* **2000**, *104*, 11842−11846.

(116) Gachard, E.; Remita, H.; Khatouri, J.; Keita, B.; Nadjo, L.; Belloni, J. Radiation-Induced and Chemical Formation of Gold Clusters. *New J. Chem.* **1998**, 1257−1265.

(117) Khomutov, G. B. Two-Dimensional Synthesis of Anisotropic Nanoparticles. *Colloids Surf.* **2002**, 243−267.

(118) (a) Nakamoto, M.; Yamamoto, M.; Fukusumi, M. Thermolysis of Gold (I) Thiolate Complexes Producing Novel Gold Nanoparticles Passivated by Alkyl Groups. *Chem. Commun.* **2002**, 1622−1623. (b) Shimizu, T.; Teranishi, T.; Hasegawa, S.; Miyake, M. Size Evolution of Alkanethiol-Protected Gold Nanoparticles by Heat Treatment in the Solid State. *J. Phys. Chem. B* **2003**, *107*, 2719−2724. (c) Teranishi, T.; Hasegawa, S.; Shimizu, T.; Miyake, M. Heat-Induced Size Evolution of Gold Nanoparticles in the Solid State. *Adv. Mater.* **2001**, *13*, 1699−1701.

(119) Bronstein, L.; Chernyshov, D.; Valetsky, P.; Tkachenko, N.; Lemmetyinen, H.; Hartmann, J.; Förster, S. Laser Photolysis Formation of Gold Colloids in Block Copolymer Micelles. *Langmuir* **1999**, *15*, 83−91.

(120) (a) Mafumé, F.; Kohno, J.-Y.; Takeda, Y.; Kondow, T. Full Physical Preparation of Size-Selected Gold Nanoparticles in Solution: Laser Ablation and Laser-Induced Size Control. *J. Phys. Chem. B* **2002**, *106*, 7575−7577. (b) Mafuné, F.; Kondow, T. Formation of Small Gold Clusters in Solution by Laser Excitation of Interband Transition. *Chem. Phys. Lett.* **2003**, *372*, 199−204.

(121) Mafumé, F.; Kohno, J.-Y.; Takeda, Y.; Kondow, T.; Sawabe, H. Formation of Gold Nanoparticles by Laser Ablation in Aqueous Solution of Surfactant. *J. Phys. Chem. B* **2001**, *105*, 5114−5120.

(122) Kawakami, Y.; Seto, T.; Yoshida, T.; Ozawa, E. Gold Nanoparticles and Films Produced by a Laser Ablation/Gas Deposition (LAGD) Methodology. *Appl. Surf. Sci.* **2002**, *197*−*198*, 587−593.

(123) Maye, M. M.; Zheng, W.; Leibowitz, F. L.; Ly, N. K.; Zhong, C.-J. Heating-Induced Evolution of Thiolate-Encapsulated Gold Nanoparticles: A strategy for Size and Shape Manipulations. *Langmuir* **2000**, *16*, 490−497.

(124) Magnusson, M. H. Gold Nanoparticles: Production, Reshaping, and Thermal Charging. *J. Nanopart. Res.* **1999**, *1*, 243−251.

(125) De Marchi, G.; Mattei, G.; Mazzoli, P.; Sada, C.; Miotello, A. Two Stages in the Kinetics of Gold Cluster Growth in Ion-Implanted Silica During Isothermal Annealing in Oxidizing Atmosphere. *J. Appl. Phys.* **2002**, *92*, 4249−4254.

(126) (a) Luo, J.; Jones, V. W.; Maye, M. M.; Han, L.; Kariuki, N. N.; Zhong, C.-J. Thermal Activation of Molecularly-Wired Gold Nanoparticles on a Substrate as Catalyst. *J. Am. Chem. Soc.* **2002**, *124*, 13988−13989. (b) Adachi, E. Coagulative Transition of Gold Nanoparticle Spheroids into Monolithic Colloids: Structure, Lifetime, and Transition Model. *Langmuir* **2001**, *17*, 3863−3870. (c) Nakaso, K.; Shimada, M.; Okuyama, K.; Deppert, K. Evaluation of the Change in the Morphology of Gold Nanoparticles During Sintering. *Aerosol Sci.* **2002**, *33*, 1061−1074.

(127) Yonezawa, T.; Onoue, S.-Y.; Kimizuka, N. Formation of Uniform Fluorinated Gold Nanoparticles and Their Highly Ordered Hexagonally Packed Monolayer. *Langmuir* **2001**, *17*, 2291−2293.

(128) Foos, E. E.; Snow, A. W.; Twigg, M. E.; Ancona, M. G. Thiol-Terminated Di-, Tri-, and Tetraethylene Oxide Functionalized Gold Nanoparticles: A Water-Soluble, Charge-Neutral Cluster. *Chem. Mater.* **2002**, *14*, 2401−2408.

(129) Kanaras, A. G.; Kamounah, F. S.; Schaumburg, K.; Kiely, C. J.; Brust, M. Thioalkylated Tetraethylene Glycol: a New Ligand for Water Soluble Monolayer Protected Gold Clusters. *Chem. Commun.* **2002**, 2294−2295.

(130) (a) Wuelfing, W. P.; Gross, S. M.; Miles, D. T.; Murray, R. W. Nanometer Gold Clusters Protected by Surface-Bound Monolayers of Thiolated Poly(ethylene glycol) Polymer Electrolyte. *J. Am. Chem. Soc.* **1998**, *120*, 12696−12697. (b) Chen, S.; Kimura, K. Synthesis and Characterization of Carboxylate-Modified Gold Nanoparticles Powders Dispersible in Water. *Langmuir* **1999**, *15*, 1075−1082. (c) Kimura, K.; Sato, S.; Yao, H. Particle Crystals of Surface Modified Gold Nanoparticles Grown From Water. *Chem. Lett.* **2001**, 372−373.

(131) Yonezawa, T.; Sutoh, M.; Kunitake, T. Practical Preparation of Size-Controlled Gold Nanoparticles in Water. *Chem. Lett.* **1997**, 619−620.

(132) Warner, M. G.; Reed, S. M.; Hutchison, J. E. Small, Water-Soluble, Ligand-Stabilized Gold Nanoparticles Synthesized by Interfacial Ligand Exchange Reactions. *Chem. Mater.* **2000**, *12*, 3316−3320.

(133) Simard, J.; Briggs, C.; Boal, A. K.; Rotello, V. M. Formation and p*H*-controlled Assembly of Amphiphilic Gold Nanoparticles. *Chem. Commun.* **2000**, 1943−1944.

(134) Yao, H.; Momozawa, O.; Hamatani, T.; Kimura, K. Stepwise Size-Selective Extraction of Carboxylate-Modified Gold Nanoparticles from an Aqueous Suspension into Toluene with Tetraoctylammonium Cations. *Chem. Mater.* **2001**, *13*, 4692−4697.

(135) Jana, N. R.; Peng, X. Single-Phase and Gram-Scale Routes toward Nearly Monodisperse Au and Other Noble Metal Nanocrystals. *J. Am. Chem. Soc.* **2003**, *125*, 14280−14281.

(136) Leff, D. V.; Ohara, P. C.; Heath, J. R.; Gelbart, W. M. Thermodynamic Control of Gold Nanocrystal Size: Experiment and Theory. *J. Phys. Chem.* **1995**, *99*, 7036−7041.

(137) (a) Nakamura, K.; Kawabata, T.; Mori, Y. Size Distribution Analysis of Colloidal Gold by Small-Angle X-ray Scattering and Light Absorbance. *Powder Technol.* **2003**, *131*, 120−128. (b) Cleveland, C. L.; Landman, U.; Shafigullin, M. N.; Stephens, P. M.; Whetten, R. L. Structural Evolution of Larger Gold Clusters. *Z. Phys. D* **1997**, *40*, 503−508. (c) Koga, K.; Sugawara, K. Population Statistics of Gold Nanoparticle Morphologies: Direct Determination by HRTEM Observations. *Surf. Sci.* **2003**, *529*, 23−35.

(138) Fenter, P.; Eberhardt, A.; Eisemberger, P. Self-Assembly of *n*-alkyl Thiols as Disulfides on Au(111). *Science* **1994**, *266*, 1216−1218.

(139) Gutiérrez-Wing, C.; Ascencio, J. A.; Pérez-Alvarez, M.; Marin-Almazo, M.; José-Yacamán, M. On the Structure and Formation of Self-Assembled Lattices of Gold Nanoparticles. *J. Cluster Sci.* **1998**, *9*, 529−545.

(140) Labande, A.; Ruiz, J.; Astruc, D. Supramolecular Gold Nanoparticles for the Redox Recognition of Oxoanions: Syntheses, Titrations, Stereoelectronic Effects, and Selectivity. *J. Am. Chem. Soc.* **2002**, *124*, 1782−1789.

(141) Whetten, R. L.; Khoury, J. T.; Alvarez, M.; Murthy, S.; Vezmar, I.; Wang, Z. L.; Stephens, P. W.; Cleveland, C. L.; Luetke, W. D.; Landman, U. Nanocrystal Gold Molecules. *Adv. Mater.* **1996**, *8*, 428−433.

(142) Whetten, R. L.; Shafigullin, M. N.; Khoury, J. T.; Schaaf, T. G.; Vezmar, I.; Alvarez, M. M.; Wilkinson, A. Crystal Structures of Molecular Gold Nanocrystal Arrays. *Acc. Chem. Res.* **1999**, *32*, 397−406.

(143) Kiely, C. J.; Fink, J.; Brust, M.; Bethell, D.; Schiffrin, D. J. Spontaneous Ordering of Bimodal Ensembles of Nanoscopic Gold Clusters. *Nature* **1998**, *396*, 444−446.

(144) (a) Schmid, G.; Meyer-Zaika, W.; Pugin, R.; Sawitowski, T.; Majoral, J. P.; Caminade, A. M.; Turrin, C. O. Naked Au_{55} Clusters: Dramatic Effect of a Thiol-Terminated Dendrimer. *Chem.*−*Eur. J.* **2000**, *6*, 1693−1697. (b) Wang, S.; Sato, S.; Kimura, K. Preparation of Hexagonal-Close-Packed Colloidal Crystals of Hydrophilic Monodisperse Gold Nanoparticles in Bulk Aqueous Solution. *Chem. Mater.* **2003**, *15*, 2445−2448.

(145) (a) Zanchet, D.; Hall, B. D.; Ugarte, D. Structure Population in Thiol-Passivated Gold Nanoparticles. *J. Phys. Chem. B* **2000**, *104*, 11013−11018. (b) Wang, S.; Sato, S.; Kimura, K. Influence of Organic Vapors on the Self-assembly of Gold Nanoparticles at Solution-gas Interfaces. *Chem. Lett.* **2003**, *32*, 520−521.

(146) Schön, G.; Simon, U. A Fascinating New Field in Colloid Science: Small Ligand-Stabilized Metal Clusters and Possible Application in Microelectronics. Part I. State of the Art. *Colloid Polym. Sci.* **1995**, *273*, 101−117.

(147) Schön, G.; Simon, U. A Fascinating New Field in Colloid Science: Small Lligand-Stabilized Metal Clusters and Their Possible Application in Microelectronics. Part II. Future Directions. *Colloid Polym. Sci.* **1995**, *273*, 202−218.

(148) Van Kempen, H.; Dubois, J. G. A.; Gerritsen, J. W.; Schmid, G. Small Metallic Particles Studied by Scanning Tunneling Microscopy. *Physica B* **1995**, *204*, 51−56.

(149) Dubois, J. G. A.; Gerritsen, J. W.; Shafranjuk, S. E.; Boon, E. F. G.; Schmid, G.; van Kempen. Coulomb Staircases and Quantum Size Effects in Tunneling Spectroscopy on Ligand-Stabilized Metal Clusters. *Europhys. Lett.* **1996**, *33*, 279−284.

(150) Bzryadin, A.; Dekker, C.; Schmid, G. Electrostatic Trapping of Single Conducting Nanoparticles Between Nanoelectrodes. *Appl. Phys. Lett.* **1997**, *71*, 1273−1275.
(151) Templeton, A. C.; Hostetler, M. J.; Kraft, C. T.; Murray, R. W. Reactivity of Monolayer-Protected Gold Cluster Molecules: Steric Effects. *J. Am. Chem. Soc.* **1998**, *120*, 1906−1911.
(152) Badia, A.; Cuccia, L.; Demers, L.; Morin, F.; Lennox, R. B. Structure and Dynamics in Alkanethiolate Monolayers Self-Assembled on Gold Nanoparticles: A DSC, FT-IR, and Deuterium NMR Study. *J. Am. Chem. Soc.* **1997**, *119*, 2682−2692.
(153) Badia, A.; Demers, L.; Dickinson, L.; Morin, F. G.; Lennox, R. B.; Reven, L. Gold−Sulfur Interactions in Alkylthiol Self-Assembled Monolayers Formed on Gold Nanoparticles Studied by Solid-State NMR. *J. Am. Chem. Soc.* **1997**, *119*, 11104−11105.
(154) Ulman, A. Formation and Structure of Self-Assembled Monolayers. *Chem. Rev.* **1996**, *96*, 1533−1554.
(155) de Dios, A. C.; Abraham, A. E. ^{13}C Chemical Shifts in Octanethiols Adsorbed on Gold: a Theoretical Study. *J. Mol. Struct.* **2002**, *602−603*, 209−214.
(156) Schnabel, U.; Fischer, C.-H.; Kenndler, E. Characterization of Colloidal Gold Nanoparticles According to Size by Capillary Zone Electrophoresis. *J. Microcolumn Sep.* **1997**, *9*, 529−534.
(157) Puech, K.; Henari, F. Z.; Blau, W. J.; Duff, D.; Schmid, G. Investigation of the Ultrafast Dephasing Time of Gold Nanoparticles Using Incoherent Light. *Chem. Phys. Lett.* **1995**, *247*, 13−17.
(158) Zanchet, D.; Tolentino, H.; Alves, M. C. M.; Alves, O. L.; Ugarte, D. Inter-Atomic Distance Contraction in Thiol-Passivated Gold Nanoparticles. *Chem. Phys. Lett.* **2000**, *323*, 167−172.
(159) Arnold, R. J.; Reilly, J. P. High-Resolution Time-of-Flight Mass Spectra of Alkanethiolate-Coated Gold Nanocrystals. *J. Am. Chem. Soc.* **1998**, *120*, 1528−1532.
(160) (a) Terrill, R. H.; Postlethwaite, T. A.; Chen, C.-H.; Poon, C.-D.; Terzis, A.; Chen, A.; Hutchison, J. E.; Clark, M. R.; Wignall, G.; Londono, J. D.; Superfine, R.; Falvo, M.; Johnson, C. S., Jr.; Samulski, E. T.; Murray, R. W. Monolayers in Three Dimensions: NMR, SAXS, Thermal, and Electron Hopping Studies of Alkanethiol Stabilized Gold Clusters. *J. Am. Chem. Soc.* **1995**, *117*, 12537−12548. (b) Kitchin, J. R.; Barteau, M. A.; Chen, J. G. A Comparison of Gold and Molybdenum Nanoparticles on TiO_2(110) 1 × 2 Reconstructed Single-Crystal Surfaces. *Surf. Sci.* **2003**, *526*, 323−331. (c) Kawasaki, T.; Takai, Y. Phase Reconstruction with Simultaneous Correction of Spherical and Astigmatic Aberrations by Three-Dimensional Fourier Filtering Methodology. *Surf. Interface Anal.* **2003**, *35*, 51−54. (d) Qi, W. H.; Wang, M. P. Size Dependence of Vacancy Formation Energy of Metallic Nanoparticles. *Physica B* **2003**, *334*, 432−435.
(161) Schmid, G.; Lehnert, A.; Malm, J.-O.; Bovin, J.-O. Ligand-Stabilized Bimetallic Colloids Identified by HRTEM and EDX. *Angew. Chem., Int. Ed. Engl.* **1991**, *30*, 874−876.
(162) Schierhorn, M.; Marzán-Liz, L. M. Synthesis of Bimetallic Colloids with Tailored Intermetallic Separation. *Nano Lett.* **2002**, *2*, 13−16.
(163) Cao, Y. W.; Jin, R.; Mirkin, C. A. DNA-Modified Core−Shell Ag/Au Nanoparticles. *J. Am. Chem. Soc.* **2001**, *123*, 7961−7962.
(164) Hutter, E.; Fendler, J. H. Size Quantized Formation and Self-Assembly of Gold Encased Silver Nanoparticles. *Chem. Commun.* **2002**, 378−379.
(165) Moskovits, M.; Srnová-Sloufová, I.; Vlcková, B. Bimetallic Ag−Au Nanoparticles: Extracting Meaningful Optical Constants from the Surface-Plasmon Extinction Spectrum. *J. Chem. Phys.* **2002**, *116*, 10435−10446.
(166) (a) Shon, Y.-S.; Dawson, G. B.; Porter, M.; Murray, R. W. Monolayer-Protected Bimetal Cluster Synthesis by Core Metal Galvanic Exchange Reaction. *Langmuir* **2002**, *18*, 3880−3885. (b) Huang, T.; Murray, R. W. Luminescence of Topronin Monolayer-Protected Silver Clusters Changes To That of Gold Clusters upon Galvanic Core Metal Exchange. *J. Phys. Chem. B* **2003**, *107*, 7434−7440.
(167) Hostetler, M. J.; Zhong, C.-J.; Yen, B. K. H.; Anderegg, J.; Gross, S. M.; Evans, N. D.; Porter, M.; Murray, R. W. Stable, Monolayer-Protected Metal Alloy Clusters. *J. Am. Chem. Soc.* **1998**, *120*, 9396−9697.
(168) (a) Shibata, T.; Bunker, B. A.; Zhang, Z.; Meisel, D.; Vardeman, C. F., II; Gezelter, J. D. Size-Dependent Spontaneous Alloying of Au−Ag Nanoparticles. *J. Am. Chem. Soc.* **2002**, *124*, 11989−11996. (b) Mandal, S.; Selvakannan, P. R.; Pasricha, R.; Sastry, M. Keggin Ions as UV−Switchable Reducing Agents in the Synthesis of Au Core-Ag Shell. Nanoparticles. *J. Am. Chem. Soc.* **2003**, *125*, 8440−8441.
(169) Norsten, T. B.; Frankamp, B. L.; Rotello, V. M. Metal Directed Assembly of Terpyridine-Functionalized Gold Nanoparticles. *Nano Lett.* **2002**, *2*, 1345−1348.
(170) Ravel, B.; Carpenter, E. E.; Harris, V. G. Oxidation of Iron in Iron/Gold Core/Shell Nanoparticles. *J. Appl. Phys.* **2002**, *91*, 8195−8197.
(171) Bian, B.; Hirotsu, Y. Preparation of Thin Films of Oriented Iron Nanocrystals. *Jpn. J. Appl. Phys.* **1997**, *36*, 1232−1235.
(172) Vacassy, R.; Lemaire, L.; Valmalette, J.-C.; Dutta, J.; Hofmann, H. Synthesis of Zirconia-Coated Gold Nanoparticles. *J. Mater. Sci. Lett.* **1998**, *17*, 1665−1667.
(173) Kolny, J.; Kornowski, A.; Weller, H. Self-Organization of Cadmium Sulfide and Gold Nanoparticles by Electrostatic Interaction. *Nano Lett.* **2002**, *2*, 361−364.
(174) Yang, Y.; Shi, J.; Chen, H.; Dai, S.; Liu, Y. Enhanced Off-Resonance Optical Nonlinearities of Au@CdS Core−Shell Nanoparticles Embedded in $BaTiO_3$ Thin Films. *Chem. Phys. Lett.* **2003**, *370*, 1−6.
(175) Horváth, D.; Toth, L.; Guczi, L. Gold Nanoparticles: Effect of Treatment on Structure and Catalytic Activity of Au/Fe_2O_3 Catalyst Prepared by Co−Precipitation. *Catal. Lett.* **2000**, *67*, 117−128.
(176) Ascencio, J. A.; Mejia, Y.; Liu, H. B.; Angeles, C.; Canizal, G. Bioreduction Synthesis of Eu−Au Nanoparticles. *Langmuir* **2003**, *19*, 5882−5886.
(177) Tuzar, Z.; Kratochvil, P. *Surface and Colloid Science*; Plenum Press: New York, 1993; Vol. 15.
(178) Birtcher, R. C.; McCormick, A. W.; Baldo, P. M.; Toyoda, N.; Yamada, I.; Matsuo, J. Gold Nanoparticles Sputtered by Single Ions and Clusters. *NIM Phys. Res. B* **2003**, *206*, 851−854.
(179) Napper, D. H. *Polymeric Stabilization of Colloidal Dispersions*; Academic Press: London, 1983.
(180) Mayer, A. B. R.; Mark, J. E. In *Nanotechnology, Molecularly Designed Materials*; Chow, G. M., Gonsalves, K. E., Eds.; ACS Symposium Series 622; American Chemical Society: Washington, DC, 1996.
(181) Roucoux, A.; Schulz, J.; Patin, H. Reduced Transition Metal Colloids: A Novel Family of Reusable Catalysts? *Chem. Rev.* **2002**, *102*, 3757−3778.
(182) Ziolo, R. F.; Giannelis, E. P.; Weinstein, B. A.; O'Horo, M. P.; Gamguly, B. N.; Mehrota, V.; Russel, M. W.; Huffman, D. R. Matrix-Mediated Synthesis of Nanocrystalline γ-Fe_2O_3: A New Optically Transparent Magnetic Material. *Science* **1992**, *257*, 219−223.
(183) Jordan, R.; West, N.; Chou, Y.-M.; Nuyken, O. Nanocomposites by Surface-Initiated Living Cationic Polymerization of 2-Oxazolines on Functionalized Gold Nanoparticles. *Macromolecules* **2001**, *34*, 1606−1611.
(184) Selvan, S. T.; Spatz, J. P.; Klock, H.-A.; Möller, M. Gold-Polypyrrole Core−Shell Particles in Diblock Copolymer Micelles. *Adv. Mater.* **1998**, *10*, 132−134.
(185) Sayo, K.; Deki, S.; Hayashi, S. A Novel Method of Preparing Nano-Sized Gold and Palladium Particles Dispersed in Composites That Uses the Thermal Relaxation Technique. *Eur. Phys. J. D* **1999**, *9*, 429−432.
(186) (a) Lee, J.; Sundar, V. C.; Heine, J. R.; Bawendi, M. G.; Jensen, K. F. Full Color Emission from II−VI Semiconductor Quantum Dot-Polymer Composites. *Adv. Mater.* **2000**, *12*, 1102−1105. (b) Teichroeb, J. H.; Forrest, J. A. Direct Imaging of Nanoparticle Embedding to Probe Viscoelasticity of Polymer Surfaces. *Phys. Rev. Lett.* **2003**, *91*, 016104-1−016104-4. (c) Raula, J.; Shan, J.; Nuopponen, M.; Niskanen, A.; Jiang, H.; Kauppinen, E. I.; Tenhu, H. Synthesis of Gold Nanoparticles Grafted with a Thermoresponsive Polymer by Surface-Induced Reversible-Addition-Fragmentation Chain-Transfer Polymerization. *Langmuir* **2003**, *19*, 3499−3504.
(187) Corbierre, M. K.; Cameron, N. S.; Sutton, M.; Mochrie, S. G. J.; Lurio, L. B.; Rühm, A.; Lennox, R. B. Polymer-Stabilized Gold Nanoparticles and Their Incorporation into Polymer Matrices. *J. Am. Chem. Soc.* **2001**, *123*, 10411−10412.
(188) Kolb, U.; Quaiser, S. A.; Winter, M.; Reetz, M. T. Investigation of Tetraalkylammonium Bromide Stabilized Palladium/Platinum Bimetallic Clusters Using Extended X-ray Absorption Fine Structure Spectroscopy. *Chem. Mater.* **1996**, *8*, 1889−1894.
(189) Hirai, H.; Toshima, N. In *Polymer-Attached Catalysts*; Iwasawa, Y., Ed.; Kluwer: Dordrecht, 1986.
(190) Toshima, N.; Yonezawa, T. Bimetallic Nanoparticles-Novel Materials for Chemical and Physical Applications. *New J. Chem.* **1998**, 1179−1201.
(191) Hirai, H.; Nakao, Y.; Toshima, N. Preparation of Colloidal Transition Metals in Polymers by Reduction with Alcohols or Ethers. *J. Macromol. Sci. Chem.* **1979**, *A13*, 727−750.
(192) Teranishi, T.; Miyake, M. Size Control of Metal Nanoparticles with Aid of Surface Protection by Polymer. *Hyomen* **1997**, *35*, 439−452.
(193) Esumi, K.; Susuki, A.; Aihara, N.; Usui, K.; Torigoe, K. Preparation of Gold Colloids with UV Irradiation Using Dendrimers as Stabilizer. *Langmuir* **1998**, *14*, 3157−3159.
(194) Reetz, M. T.; Helbig, W. Size-Selective Synthesis of Nanostructured Transition Metal Clusters. *J. Am. Chem. Soc.* **1994**, *116*, 7401−7402.
(195) Schaaf, T. G.; Whetten, R. L. Giant Gold-Glutathione Cluster Compounds: Intense Optical Activity in Metal-Based Transitions. *J. Phys. Chem. B* **2000**, *104*, 2630−2641.
(196) (a)Toshima, N.; Harada, M.; Yamazaki, Y.; Asakura, K. Catalytic Activity and Structural Analysis of Polymer-Protected Gold−Palladium Bimetallic Clusters Prepared by the Simultaneous

Reduction of Hydrogen Tetrachloroaurate and Palladium Dichloride. *J. Phys. Chem.* **1992**, *96*, 9927−9933. (b) Harada, M.; Asakura, K.; Toshima, N. Catalytic Activity and Structural Analysis of Polymer-Protected Au/Pd Bimetallic Clusters Prepared by the Successive Reduction of $HAuCl_4$ and $PdCl_2$. *J. Phys. Chem.* **1993**, *97*, 5103−5114.

(197) Toshima, N.; Yonezawa, T. Preparation of Polymer-Protected Gold/Platinum Bimetallic Clusters and Their Application to Visible Light-Induced Hydrogen Evolution. *Makromol. Chem., Macromol. Symp.* **1992**, *59*, 281−295.

(198) Yonezawa, T.; Toshima, N. Polymer- and Micelle-Protected Gold/Platinum Bimetallic Systems. Preparation, Application to Catalysis for Visible-Light-Induced Hydrogen Evolution, and Analysis of Formation Process with Optical Methods. *J. Mol. Catal.* **1993**, *83*, 167−181.

(199) Yoneazawa, T.; Toshima, N. Mechanistic Consideration of Formation of Polymer-Protected Nanoscopic Bimetallic Clusters. *J. Chem. Soc., Faraday Trans.* **1995**, *91*, 4111−4119.

(200) Astruc, D. Redox Catalysis. *Electron Transfer and Radical Processes in Transition Metal Chemistry*; VCH: New York, 1995; Chapter 7.

(201) Harada, M.; Asakura, K.; Toshima, N. J. Catalytic Activity and Structural Analysis of Polymer-Protected Gold/Palladium Bimetallic Clusters Prepared by the Successive Reduction of Hydrogen Tetrachloroaurate(III) and Palladium Dichloride. *J. Phys. Chem.* **1993**, *97*, 5103.

(202) Spatz, J. P.; Mössmer, S.; Möller, M. Mineralization of Gold Nanoparticles in a Block Copolymer Microemulsion. *Chem.−Eur. J.* **1996**, *12*, 1552−1555.

(203) Spatz, J. P.; Mössmer, S.; Möller, M. Metastable Reverse Globular Micelles and Giant Micellar Wires from Block Copolymers. *Angew. Chem., Int. Ed. Engl.* **1996**, *35*, 1510−1512.

(204) Spatz, J. P.; Roescher, A.; Möller, M. Gold Nanoparticles in Micellar Poly(Styrene)-*b*-Poly(-Ethyleneoxide) Films. *Adv. Mater.* **1996**, *8*, 337−340.

(205) Bronstein, L. M.; Chernyshov, D. M.; Timofeeva, G. I.; Dubrovina, L. V.; Valetsky, P. M.; Obolonkova, E. S.; Khokhlov, A. R. Interaction of Polystyrene-Block-Poly(Ethylene Oxide) Micelles with Cationic Surfactant in Aqueous Solutions. Metal Colloid Formation in Hybrid Systems. *Langmuir* **2000**, *16*, 3626−3632.

(206) Frankamp, B. L.; Uzun, O.; Ilhan, F.; Boal, A. K.; Rotello, V. M. Recognition-Mediated Assembly of Nanoparticles into Micellar Structures with Diblock Copolymers. *J. Am. Chem. Soc.* **2002**, *124*, 892−893.

(207) Spatz, J. P.; Mössmer, S.; Harmann, C.; Möller, M.; Herzog, T.; Krieger, M.; Boyen, H.-G.; Ziemann, P.; Kabius, B. Ordered Deposition of Inorganic Clusters from Micellar Block Copolymer Films. *Langmuir* **2000**, *16*, 407−415.

(208) Gohy, J. F.; Willet, N.; Varshney, S.; Zhang, J.-X.; Jérôme, R. Core−Shell-Corona Micelles with a Responsive Shell. *Angew. Chem., Int. Ed.* **2001**, *40*, 3214−3216.

(209) Youk, J. H.; Park, M. K.; Locklin, J.; Advincula, R.; Yang, J.; Mays, J. Preparation of Aggregation Stable Gold Nanoparticles Using Star-Block Copolymers. *Langmuir* **2002**, *18*, 2455−2458.

(210) Walker, C. H.; St John, J. V.; Wisian-Neilson, P. Synthesis and Size Control of Gold Nanoparticles Stabilized by Poly(Methylphenylphosphazene). *J. Am. Chem. Soc.* **2001**, *123*, 3846−3847.

(211) Otsuka, H.; Akiyama, Y.; Nagasaki, Y.; Kataoka, K. Quantitative and Reversible Lectin-Induced Association of Gold Nanoparticles Modified with −Lactosyl-Mercapto-Poly(Ethylene Glycol). *J. Am. Chem. Soc.* **2001**, *123*, 8226−8230.

(212) Nuss, S.; Böttcher, H.; Wurm, H.; Hallensleben, M. L. Gold Nanoparticles with Covalently Attached Polymer Chains. *Angew. Chem., Int. Ed.* **2001**, *40*, 4016−4018.

(213) Mandal, T. K.; Fleming, M. S.; Walt, D. R. Preparation of Polymer Coated Gold Nanoparticles by Surface-Confined Living Radical Polymerization at Ambient Temperature. *Nano Lett.* **2002**, *2*, 3−7.

(214) Ohno, K.; Hoh, K.-m.; Tsuji, Y.; Fukuda, T. Synthesis of Gold Nanoparticles Coated with Well-Defined, High-Density Polymer Brushes by Surface-Initiated Living Radical Polymerization. *Macromolecules* **2002**, *35*, 8989−8993.

(215) Kamata, K.; Lu, Y.; Xia, Y. Synthesis and Characterization of Monodispersed Core−Shell Spherical Colloids with Movable Cores. *J. Am. Chem. Soc.* **2003**, *125*, 2384−2385.

(216) (a) Marinakos, S. M.; Shultz, D. A.; Feldheim, D. L. Gold Nanoparticles as Templates for the Synthesis of Hollow Nanometer-Sized Conductive Polymer Capsules. *Adv. Mater.* **1999**, *11*, 34−37. (b) Chah, S.; Fendler, J. H.; Yi, J. Nanostructured Gold Hollow Microspheres Prepared on Dissolvable Ceramic Hollow Sphere Templates. *J. Colloid Interface Sci.* **2002**, *250*, 142−148. (c) Marinakos, S. M.; Novak, J. P.; Brousseau, L. C., III; House, A. B.; Edeki, E. M.; Feldhaus, J. C.; Feldheim, D. L. Gold Particles as Templates for the Synthesis of Hollow Polymer Capsules. Control of Capsule Dimensions and Guest Encapsulation. *J. Am. Chem. Soc.* **1999**, *121*, 8518−8522.

(217) Naka, K.; Itoh, H.; Chujo, Y. Effect of Gold Nanoparticles as a Support for the Oligomerization of L-Cysteine in an Aqueous Solution. *Langmuir* **2003**, *19*, 5546−5549.

(218) Sohn, B.-H.; Seo, B.-W.; Yoo, S.-I. Changes of the Lamellar Period by Nanoparticles in the Nanoreactor Scheme of Thin Films of Symmetric Diblock Copolymers. *J. Mater. Chem.* **2002**, *12*, 1730−1734.

(219) Cant, N. E.; Critchley, K.; Zhang, H.-L.; Evans, S. D. Surface Functionalization for the Self-Assembly of Nanoparticle/Polymer Multilayer Films. *Thin Solid Films* **2003**, *426*, 31−39.

(220) Gonsalves, K. E.; Carlson, G.; Chen, X.; Kumar, J.; Aranda, F.; Perez, R.; Jose-Yacaman, M. Surface-Functionalized Nanostructured Gold/Polymer Composite Films. *J. Mater. Sci. Lett.* **1996**, *15*, 948−951.

(221) Mayer, A. B. R.; Mark, J. E. Colloidal Gold Nanoparticles Protected by Water-Soluble Homopolymers and Random Copolymers. *Eur. Polym. J.* **1998**, *34*, 103−108.

(222) Teranishi, T.; Kiyokawa, I.; Miyake, M. Synthesis of Monodisperse Gold Nanoparticles Using Linear Polymers as Protective Agents. *Adv. Mater.* **1998**, *10*, 596−599.

(223) Watson, K. J.; Zhu, J.; Nguyen, S. B. T.; Mirkin, C. A. Hybrid Nanoparticles with Block Copolymer Shell Structures. *J. Am. Chem. Soc.* **1999**, *121*, 462−463.

(224) Watson, K. J.; Zhu, J.; Nguyen, S. B. T.; Mirkin, C. A. Redox-Active Polymer-Nanoparticle Hybrid Materials. *Pure Appl. Chem.* **2000**, *72*, 67−72.

(225) Grabar, K. C.; Allison, K. J.; Baker, B. E.; Bright, R. M.; Brown, K. R.; Freeman, R. G.; Fox, A. P.; Keating, C. D.; Musick, M. D.; Natan, M. J. Two-Dimensional Arrays of Colloidal Gold Particles: A Flexible Approach to Macroscopic Metal Surfaces. *Langmuir* **1996**, *12*, 2353−2361.

(226) Kim, M.; Sohn, K.; Na, H. B.; Hyeon, T. Synthesis of Nanorattles Composed of Gold Nanoparticles Encapsulated in Mesoporous Carbon and Polymer Shells. *Nano Lett.* **2002**, *2*, 1383−1387.

(227) Wolfe, D. B.; Oldenburg, S. J.; Westcott, S. L.; Jackson, J. B.; Paley, M. S.; Halas, N. J. Photodeposition of Molecular Layers on Nanoparticle Substrates. *Langmuir* **1999**, *15*, 2745−2748.

(228) Takagi, K.; Ishiwatari, T. Polymer Chain-Guided Arrangement of Gold Nanoparticles. *Chem. Lett.* **2002**, 990−991.

(229) Wang, J.; Neoh, K. G.; Kang, E. T. Preparation of Nanosized Metallic Particles in Polyaniline. *J. Colloid Surf. Sci.* **2001**, *239*, 78−86.

(230) Shchukin, D. G.; Caruso, R. A. Template Synthesis of Porous Gold Microspheres. *Chem. Commun.* **2003**, 1478−1479.

(231) Walker, C. H.; St. John, J. V.; Wisian-Neilson, P. Synthesis and Size Control of Gold Nanoparticles Stabilized by Poly(methylphenylphosphazene). *J. Am. Chem. Soc.* **2001**, *123*, 3846−3847.

(232) (a) Mayer, C. R.; Neveu, S.; Cabuil, V. A Nanoscale Hybrid System Based on Gold Nanoparticles and Heteropolyanions. *Angew. Chem., Int. Ed.* **2002**, *41*, 501−503. (b) Mayer, C. R.; Neveu, S.; Simonnet-Jégat, C.; Debiemme-Chouvry, C.; Cabuil, V.; Secheresse, F. Nanocomposite Systems Based on Gold Nanoparticles and Thiometalates. From Colloids to Networks. *J. Mater. Chem.* **2003**, *13*, 338−341.

(233) (a) Shan, J.; Nuopponen, M.; Jiang, H.; Kauppinen, E.; Tenhu, H. Preparation of Poly(*N*-isopropylacrylamide)-Monolayer-Protected Gold Clusters: Synthesis Methods, Core Size, and Thickness of Monolayer. *Macromolecules* **2003**, *36*, 4526−4533. (b) Dai, X.; Tan, Y.; Xu, J. Formation of Gold Nanoparticles in the Presence of *o*-Anisidine and the Dependence of the Structure of Poly(*o*-anisidine) on Synthetic Conditions. *Langmuir* **2002**, *18*, 9010−9016.

(234) Zhou, Y.; Itoh, H.; Uemura, T.; Naka, K.; Chujo, Y. Preparation of π-Conjugated Polymer-Protected Gold Nanoparticles in Stable Colloidal Form. *Chem. Commun.* **2001**, 613−614.

(235) Youk, J. H.; Park, M.-K.; Locklin, J.; Advincula, R.; Yang, J.; Mays, J. Preparation of Aggregation Stable Gold Nanoparticles Using Star-Block Copolymers. *Langmuir* **2002**, *18*, 2455−2458.

(236) (a) Mangeney, C.; Ferrage, F.; Aujard, I.; Marchi-Artzner, V.; Jullien, L.; Ouari, O.; El Rekai, D.; Laschewsky, A.; Vikholm, I.; Sadowski, J. W. Synthesis and Properties of Water-Soluble Gold Colloids Covalently Derivatized with Neutral Polymer Monolayers. *J. Am. Chem. Soc.* **2002**, *124*, 5811−5821. (b) Cole, D. H.; Shull, K. R.; Rehn, L. E.; Baldo, P. M. RBS Analysis of the Diffusion of Nano-Size Spheres in a Polymer Matrix. *Nucl. Instrum. Methods Phys. Res. B* **1998**, *136−138*, 283−289. (c) Liang, Z.; Susha, A.; Caruso, F. Gold Nanoparticle-Based Core−Shell and Hollow Spheres and Ordered Assemblies Thereof. *Chem. Mater.* **2003**, *15*, 3176−3183.

(237) Chechik, V.; Crooks, R. M. Monolayers of Thiol-Terminated Dendrimers on the Surface of Planar and Colloidal Gold. *Langmuir* **1999**, *15*, 6364−6369.

(238) Esumi, K.; Hosoya, T.; Suzuki, A.; Torigoe, K. Preparation of Hydrophobically Modified Poly(amidoamine) Dendrimer-Encapsulated Gold Nanoparticles in Organic Solvents. *J. Colloid Interface Sci.* **2000**, *229*, 303−306.

(239) Krasteva, N.; Besnard, I.; Guse, B.; Bauer, R. E.; Müllen, K.; Yasuda, A.; Vossmeyer, T. Self-Assembled Gold Nanoparticle/

Dendrimer Composite Films for Vapor Sensing Applications. *Nano Lett.* **2002**, *2*, 551−555.
(240) He, J.-A.; Valluzzi, R.; Yang, K.; Dolukhanyan, T.; Sung, C.; Kumar, J.; Tripathy, S. K. Electrostatic Multilayer Deposition of a Gold-Dendrimer Nanocomposite. *Chem. Mater.* **1999**, *11*, 3268−3274.
(241) Won, J.; Ihn, K. J.; Kang, Y. S. Gold Nanoparticle Patterns of Polymer Films in the Presence of Poly(amidoamine) Dendrimers. *Langmuir* **2002**, *18*, 8246−8249.
(242) Esumi, K.; Kameo, A.; Suzuki, A.; Torigoe, K. Preparation of Gold Nanoparticles in Formamide and *N*,*N*-dimethylformamide in the Presence of Poly(amidoamine) Dendrimers with Surface Methyl Ester Groups. *Colloids Surf.* **2001**, *189*, 155−161.
(243) Frankamp, B. L.; Boal, A. K.; Rotello, V. M. Controlled Interparticle Spacing through Self-Assembly of Au Nanoparticles and Poly(amidoamine) Dendrimers. *J. Am. Chem. Soc.* **2002**, *124*, 15146−15147.
(244) Zhou, Y.; Ma, C.; Itoh, H.; Naka, K.; Chujo, Y. A Simple In Situ Hydrogen Interaction to Homogeneous Dispersion of Gold Nanoparticles in SiO_2 Matrix Using Dendrimer as Template. *Chem. Lett.* **2002**, 1170−1171.
(245) Zheng, J.; Stevenson, M. S.; Hikida, R. S.; Van Patten, G. P. Influence of pH on Dendrimer-Protected Nanoparticles. *J. Phys. Chem. B* **2002**, *106*, 1252−1255.
(246) Bielinska, A.; Eichman, J. D.; Lee, I.; Baker, J. R., Jr.; Balogh, L. Imaging {Au^0-PANAM} Gold-Dendrimer Nanocomposites in Cells. *J. Nanopart. Res.* **2002**, *4*, 395−403.
(247) (a) Zhao, M.; Crooks, R. M. Intradendrimer Exchange of Metal Nanoparticles. *Chem. Mater.* **1999**, *11*, 3379−3385. (b) Gröhn, F.; Bauer, B. J.; Akpalu, Y. A.; Jackson, C. L.; Amis, E. J. Dendrimer Templates for the Formation of Gold Nanoclusters. *Macromolecules* **2000**, *33*, 6042−6050.
(248) Crooks, R. M.; Zhao, M.; Sun, L.; Chechik, V.; Yeung, L. K. Dendrimers-Encapsulated Metal Nanoparticles: Synthesis, Characterization, and Applications to Catalysis. *Acc. Chem. Res.* **2001**, *34*, 181−190.
(249) Niu, Y.; Crooks, R. M. Dendrimer-Encapsulated Metal Nanoparticles and Their Applications to Catalysis. In *Dendrimers and Nanoscience*; Astruc, D., Ed.; Compte-Rendus Chimie, Elsevier: Paris, 2003; in press.
(250) Daniel, M.-C.; Ruiz, J.; Nlate, J.; Palumbo, J.; Blais, J.-C.; Astruc, D. Gold Nanoparticles Containg Redox-Active Supramolecular Dendrons that Recognize $H_2PO_4^-$. *Chem. Commun.* **2001**, 2000−2001.
(251) Daniel, M.-C.; Ruiz, J.; Nlate, S.; Blais, J.-C.; Astruc, D. Nanoscopic Assemblies Between Supramolecular Redox Active Metallodendrons and Gold Nanoparticles: Synthesis, Characterisation and Selective Recognition of $H_2PO_4^-$, HSO_4^- and Adenosine-5′-Triphosphate (ATP^{2-}) Anions. *J. Am. Chem. Soc.* **2003**, *125*, 2617−2628.
(252) Astruc, D.; Blais, J.-C.; Daniel, M.-C.; Nlate, S.; Ruiz, J. Metallodendrimers and Dendronized Gold Colloids as Nanocatalysts, Nanosensors and Nanomaterials for Moleculars Electronics. In *Dendrimers and Nanosciences, Comptes Rendus Chimie*; Astruc, D., Ed.; Elsevier: Paris, 2003; in press.
(253) Wang, R.; Yang, J.; Zheng, Z.; Carducci, M. D.; Jiao, J.; Seraphin, S. Dendron-Controlled Nucleation and Growth of Gold Nanoparticles. *Angew. Chem., Int. Ed.* **2001**, *40*, 549−552.
(254) Kim, M.-K.; Jeon, Y.-M.; Jeon, W. S.; Kim, H.-J.; Hong, S. G.; Park, C. G.; Kim, K. Novel Dendron-Stabilized Gold Nanoparticles with High Stability and Narrow Size Distribution. *Chem. Commun.* **2001**, 667−668. (b) Gopidas, K. R.; Whitesell, J. K.; Fox, M.-A. Nanoparticle-Cored Dendrimers: Synthesis and Characterization. *J. Am. Chem. Soc.* **2003**, *125*, 6491−6502.
(255) (a) Krastena, N.; Krustev, R.; Yasuda, A.; Vossmeyer, T. Vapor Sorption in Self-Assembled Gold Nanoparticle/Dendrimer Films Studied by Specular Neutron Reflectometry. *Langmuir* **2003**, *19*, 7754−7760. (b) Kimura, K.; Takashima, S.; Ohshima, H. Molecular Approach to the Surface Potential Estimate of Thiolate-Modified Gold Nanoparticles. *J. Phys. Chem. B* **2002**, *106*, 7260−7266. (c) Taubert, A.; Wiesler, U.-M.; Müllen, K. Dendrimer-Controlled One-Pot Synthesis of Gold Nanoparticles with a Bimodal Size Distribution and their Self-Assembly in the Solid State. *J. Mater. Chem.* **2003**, *13*, 1090−1093.
(256) Bhat, R. R.; Fischer, D. A.; Genzer, J. Fabricating Planar Nanoparticle Assemblies with Number Density Gradients. *Langmuir* **2002**, *18*, 5640−5643.
(257) Nagle, L.; Ryan, D.; Cobbe, S.; Fitzmaurice, D. Templated Nanoparticle Assembly on the Surface of a Patterned Nanosphere. *Nano Lett.* **2003**, *3*, 51−53.
(258) Liu, S.; Zhu, T.; Hu, R.; Liu, Z. Evaporation-Induced Self-Assembly of Gold Nanoparticles Into a Highly Organized Two-Dimensional Array. *Phys. Chem. Chem. Phys.* **2002**, *4*, 6059−6062.
(259) Radnik, J.; Mohr, C.; Claus, P. On the Origin of Binding Energy Shifts of Core Levels of Supported Gold Nanoparticles and Dependence of Pretreatment and Material Synthesis. *Phys. Chem. Chem. Phys.* **2003**, *5*, 172−177.
(260) Paraschiv, V.; Zapotoczny, S.; de Jong, M. R.; Vancso, G. J.; Huskens, J.; Reinhoudt, D. N. Functional Group Transfer from Gold Nanoparticles to Flat Gold Surfaces for the Creation of Molecular Anchoring Points on Surfaces. *Adv. Mater.* **2002**, *14*, 722−726.
(261) Geng, J.; Johnson, B. F. G.; Thomas, M. D. R.; Shephard, D. S.; Jiang, L. Behaviour of Two-Dimensional Arrays of Gold Nanoparticles Under H_2S: Agglomeration and Regeneration. *Inorg. Chim. Acta* **2002**, *330*, 33−37.
(262) Bardotti, L.; Prével, B.; Jensen, P.; Treilleux, M.; Mélinon, P.; Perez, A.; Gierak, J.; Faini, G.; Mailly, D. Organizing Nanoclusters on Functionalized Surfaces. *Appl. Surf. Sci.* **2002**, *191*, 205−210.
(263) Haidara, H.; Mougin, K.; Schultz, J. Spontaneous Growth of Two-Dimensional Complex Patterns of Nanoparticles at Model Molecular Surfaces. *Langmuir* **2001**, *17*, 659−663.
(264) Mougin, K.; Haidara, H.; Castelein, G. Controlling the Two-dimensional Adhesion and Organization of Colloidal Gold Nanoparticles. *Colloids Surf.* **2001**, *193*, 231−237.
(265) Ito, S.; Yoshikawa, H.; Masuhara, H. Laser Manipulation and Fixation of Single Gold Nanoparticles in Solution at Room Temperature. *J. Appl. Phys.* **2002**, *80*, 482−484.
(266) Murakoshi, K.; Nakato, Y. Formation of Linearly Arrayed Gold Nanoparticles on Gold Single-Crystal Surfaces. *Adv. Mater.* **2000**, *12*, 791−795.
(267) Resch, R.; Lewis, D.; Meltzer, S.; Montoya, N.; Koel, B. E.; Madhukar, A.; Requicha, A. A. G.; Will, P. Manipulation of Gold Nanoparticles in Liquid Environments Using Scanning Force Microscopy. *Ultramicroscopy* **2000**, *82*, 135−139.
(268) Lei, S.; Zhao, S.; Chen, S.; Ai, Z.; Wang, S. Effect of Square Wave Pulse on the Deposition Structure of Gold Nanoparticles. *J. Serb. Chem. Soc.* **1999**, *64*, 259−263.
(269) Rudoy, V. M.; Dement'eva, O. V.; Yaminskii, I. V.; Sukhov, V. M.; Kartseva, M. E.; Ogarev, V. A. Metal Nanoparticles on Polymer Surfaces: 1. A New Method of Determining Glass Transition Temperature of the Surface Layer. *Colloid J.* **2002**, *64*, 746−754.
(270) Schulz, F.; Franzka, S.; Schmid, G. Nanostructured Surfaces by Deposition of Metal Nanoparticles by Means of Spray Techniques. *Adv. Funct. Mater.* **2002**, *12*, 532−536.
(271) Baur, C.; Gazen, B. C.; Koel, B.; Ramachandran, T. R.; Requicha, A. A. G.; Zini, L. Robotic Nanomanipulation with a Scanning Probe Microscope in a Networked Computing Environment. *J. Vac. Sci. Technol. B* **1997**, *15*, 1577−1580.
(272) Han, M. Y.; Zhou, L.; Quek, C. H.; Li, S. F. Y.; Huang, W. Room-Temperature Coulomb Staircase on Pure and Uniform Surface-Capped Gold Nanoparticles. *Chem. Phys. Lett.* **1998**, *287*, 47−52.
(273) Garno, J. C.; Yang, Y.; Amro, N. A.; Cruchon-Dupeyrat, S.; Chen, S.; Liu, G.-Y. Precise Positioning of Nanoparticles on Surfaces Using Scanning Probe Lithography. *Nano Lett.* **2003**, *3*, 389−395.
(274) Zhu, T.; Fu, X.; Mu, T.; Wang, J.; Liu, Z. p*H*-Dependent Adorption of Gold Nanoparticles on *p*-Aminothiophenol-Modified Gold Substrates. *Langmuir* **1999**, *15*, 5197−5199.
(275) Chan, E. W. L.; Yu, L. Chemoselective Immobilization of Gold Nanoparticles onto Self-Assembled Monolayers. *Langmuir* **2002**, *18*, 311−313.
(276) Menzel, H.; Mowery, M. D.; Cai, M.; Evans, C. E. Surface-Confined Nanoparticles as Substrates for Photopolymerizable Self-Assembled Monolayers. *Adv. Mater.* **1999**, *11*, 131−134.
(277) Zhu, T.; Zhang, X.; Wang, J.; Fu, X.; Liu, Z. Assembling Colloidal Au Nanoparticles with Functionalized Self-Assembled Monolayers. *Thin Solid Films* **1998**, *327−329*, 595−598.
(278) (a) Li, Q.; Zheng, J.; Liu, Z. Site-Selective Assemblies of Gold Nanoparticles on an AFM Tip-Defined Silicon Template. *Langmuir* **2003**, *19*, 166−171. (b) Zheng, J.; Chen, Z.; Liu, Z. Atomic Force Microscopy-Based Nanolithography on Silicon Using Colloidal Au Nanoparticles As a Nanooxidation Mask. *Langmuir* **2000**, *16*, 9673−9676. (c) Lee, K.-B.; Lim, J.-H.; Mirkin, C. A. Protein Nanostructures Formed via Direct-Write Dip-Pen Nanolithography. *J. Am. Chem. Soc.* **2003**, *125*, 5588−5589.
(279) Tilley, R. D.; Saito, S. Preparation of Large Scale Monolayers of Gold Nanoparticles on Modified Silicon Substrates Using a Controlled Pulling Methodology. *Langmuir* **2003**, *19*, 5115−5120.
(280) Zanella, R.; Giorgio, S.; Henry, C. R.; Louis, C. Alternative Methods for the Preparation of Gold Nanoparticles Supported on TiO_2. *J. Phys. Chem. B* **2002**, *106*, 7634−7642.
(281) Schaaff, T. G.; Blom, D. A. Deposition of Au−Nanocrystals on TiO_2 Crystallites. *Nano Lett.* **2002**, *2*, 507−511.
(282) Boccuzzi, F.; Chiorino, A.; Manzoli, M. FTIR Study of the Cationic Effects of CO adsorbed on Gold Nanoparticles Supported on Titania. *Surf. Sci.* **2000**, *454−456*, 942−946.
(283) Qian, W.; Lin, L.; Deng, Y. J.; Xia, Z. J.; Zou, Y. H.; Wong, G. K. L. Femtosecond Studies of Coherent Acoustic Phonons in Gold Nanoparticles Embedded in TiO_2 Thin Films. *J. Appl. Phys.* **2000**, *87*, 612−614.

(284) (a) Yonezawa, T.; Matsune, H.; Kunitake, T. Layered Nanocomposite of Close-Packed Gold Nanoparticles and TiO_2 Gel Layers. *Chem. Mater.* **1999**, *11*, 33−35. (b) Yang, Y.; Shi, J.; Huang, W.; Dai, S.; Wang, L. Preparation and Optical Properties of Gold Nanoparticles Embedded in Barium Titanate Thin Films. *J. Mater. Sci.* **2003**, *38*, 1243−1248. (c) Lengl, G.; Ziemann, P.; Banhart, F.; Walther, P. Anomalous Behavior of Gold Nanoislands on Top of $SrTiO_3$(001) During their Overgrowth by Thin YBaCuO Films. *Physica C* **2003**, *390*, 175−184.

(285) (a) Winkler, C.; Carew, A. J.; Haq, S.; Raval, R. Carbon Monoxide on γ-Alumina Single-Crystal Surfaces with Gold Nanoparticles. *Langmuir* **2003**, *19*, 717−721. (b) Hulteen, J. C.; Patrissi, C. J.; Miner, D. L.; Crosthwait, E. R.; Oberhauser, E. B.; Martin, C. R. Changes in the Shape and Optical Properties of Gold Nanoparticles Contained Within Alumina Membranes Due to Low-Temperature Annealing. *J. Phys. Chem. B* **1997**, *101*, 7727−7731. (c) García-Serrano, J.; Pal, U. Synthesis and Characterization of Au Nanoparticles in Al_2O_3 Matrix. *Hydrogen Energy* **2003**, *28*, 637−640.

(286) Yonezawa, T.; Onoue, S-y.; Kunitake, T. Growth of Closely Packed Layers of Gold Nanoparticles on an Aligned Ammonium Surface. *Adv. Mater.* **1998**, *10*, 414−416.

(287) Shon, Y.-S.; Choo, H. [60]Fullerene-Linked Gold Nanoparticles: Synthesis and Layer-by-Layer Growth on a Solid Surface. *Chem. Commun.* **2002**, 2560−2561.

(288) (a) Liu, J.; Alvarez, J.; Ong, W.; Kaifer, A. E. Network Aggregates Formed by C_{60} and Gold Nanoparticles Capped with γ-Cyclodextrin Hosts. *Nano Lett.* **2001**, *1*, 57−60. (b) Zhu, D.; Li, Y.; Wang, S.; Shi, Z.; Du, C.; Xiao, S.; Fang, H.; Zhou, Y. Design, Synthesis and Properties of Functional Materials Based on Fullerene. *Synth. Met.* **2003**, *133−134*, 679−683.

(289) Liu, L.; Wang, T.; Li, J.; Guo, Z.-X.; Dai, L.; Zhang, D.; Zhu, D. Self-Assembly of Gold Nanoparticles to Carbon Nanotubes Using a Thiol-Terminated Pyrene as Interlinker. *Chem. Phys. Lett.* **2003**, *367*, 747−752.

(290) Jiang, K.; Eitan, A.; Schadler, L. S.; Ajayan, P. M.; Siegel, R. W.; Grobert, N.; Mayne, M.; Reyes-Reyes, M.; Terrones, H.; Terrones, M. Selective Attachment of Gold Nanoparticles to Nitrogen-Doped Carbon Nanotubes. *Nano Lett.* **2003**, *3*, 275−277.

(291) Boyen, H.-G.; Herzog, Th.; Käqrle, G.; Weigl, F.; Ziemann, P. X-Ray Photoelectron Spectroscopy Study on Gold Nanoparticles Supported on Diamond. *Phys. Rev. B* **2002**, *65*, 0754121−0754125.

(292) Teranishi, T.; Sugawara, A.; Shimizu, T.; Miyake, M. Planar Array of 1D Gold Nanoparticles on Ridge-and-Valley Structured Carbon. *J. Am. Chem. Soc.* **2002**, *124*, 4210−4211.

(293) (a) Kuwahara, Y.; Akiyama, T.; Yamada, S. Construction of Gold Nanoparticle-Ruthenium (II) Tris(2,2′-bipyridine) Self-Assembled Multistructures and Their Photocurrent Responses. *Thin Solid Films* **2001**, *393*, 273−277. (b) Gittins, D. I.; Susha, A. S.; Schoeler, B.; Caruso, F. Dense Nanoparticulate Thin Films via Gold Nanoparticle Self-Assembly. *Adv. Mater.* **2002**, *14*, 508−512.

(294) (a) Seitz, O.; Chehimi, M. M.; Cabet-Deliry, E.; Truong, S.; Felidj, N.; Perruchot, C.; Greaves, S. J.; Watts, J. F. Preparation and Characterization of Gold Nanoparticles Assemblies on Silanised Glass Plates. *Colloids Surf.* **2003**, *218*, 225−239. (b) Hrapovic, S.; Liu, Y.; Enright, G.; Bensebaa, F.; Luong, J. H. T. New Strategy for Preparing Thin Gold Films on Modified Glass Surfaces by Electroless Deposition. *Langmuir* **2003**, *19*, 3958−3965.

(295) Gu, Z.-Z.; Horie, R.; Kubo, S.; Yamada, Y.; Fujishima, A.; Sato, O. Fabrication of a Metal-Coated Three-Dimensionally Ordered Macroporous Film and its Application as a Refractive Index Sensor. *Angew. Chem., Int. Ed.* **2002**, *41*, 1153−1156.

(296) He, T.; Ma, Y.; Cao, Y.-A. C.; Yang, W.-S.; Yao, J.-N. Improved Photochromism of WO_3 Thin Films by Addition of Au Nanoparticles. *Phys. Chem. Chem. Phys.* **2002**, *4*, 1637−1639.

(297) (a) Deki, S.; Ko, H. Y. Y.; Fujita, T.; Akamatsu, K.; Mizuhata, M.; Kajinami, A. Synthesis and Microstructure of Metal Oxide Thin Films Containing Metal Nanoparticles by Liquid-Phase Deposition (LPD) Methodology. *Eur. Phys. J. D* **2001**, *16*, 325−328. (b) Deki, S.; Nabika, H.; Akamatsu, K.; Mizuhata, M.; Kajinami, A.; Tomita, S.; Fujii, M.; Hayashi, S. Fabrication and Characterization of PAN-Derived Carbon Thin Films Containing Au Nanoparticles. *Thin Solid Films* **2002**, *408*, 59−63.

(298) (a) Raguse, B.; Müller, K.-H.; Wieczorek, L. Nanoparticle Actuators. *Adv. Mater.* **2003**, *15*, 922−926. (b) Zhang, H.-L.; Evans, S. D.; Henderson, J. R. Spectroscopic Ellipsometric Evaluation of Gold Nanoparticle Thin Films Fabricated Using Layer-by-Layer Self-Assembly. *Adv. Mater.* **2003**, *15*, 531−534.

(299) Yanagi, H.; Ohno, T. Nanofabrication of Gold Particles in Glass Films by AFM-Assisted Local Reduction. *Langmuir* **1999**, *15*, 4773−4776.

(300) Huang, W.; Shi, J. Synthesis and Properties of ZrO_2 Films Dispersed with Au Nanoparticles. *J. Sol-Gel Sci. Technol.* **2001**, *20*, 145−151.

(301) Diao, J. J.; Qiu, F. S.; Chen, G. D.; Reeves, M. E. Surface Vertical Deposition of Gold Nanoparticle Film. *J. Phys. D: Appl. Phys.* **2003**, *36*, L25−L27.

(302) Ko, H. Y. Y.; Mizuhata, M.; Kajinami, A.; Deki, S. Fabrication of High Performance Thin Films from Metal Fluorocomplex Aqueous Solution by the Liquid-Phase Deposition. *J. Fluorine Chem.* **2003**, *120*, 157−163.

(303) Lu, A. H.; Lu, G. H.; Kessinger, A. M.; Foss, C. A., Jr. Dichroic Thin Layer Films Prepared from Alkanethiol-Coated Gold Nanoparticles. *J. Phys. Chem. B* **1997**, *101*, 9140−9142.

(304) Yang, W.; Inoue, H.; Chow, T. Y.; Samura, H.; Saegusa, T. Metal Oxide Thin Films Containing Au Nano-Particles Prepared with Gas Diffusion Methodology. *J. Sol-Gel Sci. Technol.* **1998**, *11*, 117−124.

(305) Compagnini, G.; Scalisi, A. A.; Puglisi, O. Ablation of Noble Metals in Liquids: a Method to Obtain Nanoparticles in a Thin Polymeric Film. *Phys. Chem. Chem. Phys.* **2002**, *4*, 2787−2791.

(306) Kariuki, N. N.; Han, L.; Ly, N. K.; Patterson, M. J.; Maye, M. M.; Liu, G.; Zhong, C.-J. Preparation and Characterization of Gold Nanoparticles Dispersed in Poly(2-hydroxyethyl methacrylate). *Langmuir* **2002**, *18*, 8255−5259.

(307) (a) He, T.; Ma, Y.; Cao, Y.; Jiang, P.; Zhang, X.; Yang, W.; Yao, J. Enhancement Effect of Gold Nanoparticles on the UV−Light Photochromism of Molybdenum Trioxide Thin Films. *Langmuir* **2001**, *17*, 8024−8027. (b) Hussain, I.; Brust, M.; Papworth, A. J.; Cooper, A. I. Preparation of Acrylate-Stabilized Gold and Silver Hydrosols and Gold-Polymer Composite Films. *Langmuir* **2003**, *19*, 4831−4835.

(308) (a) Gittins, D. I.; Susha, A. S.; Schoeler, B.; Caruso, F. Dense Nanoparticulate Thin Films via Gold Nanoparticle Self-Assembly. *Adv. Mater.* **2002**, *14*, 508−512. (b) Joseph, Y.; Besnard, I.; Rosenberger, M.; Guse, B.; Nothofer, H.-G.; Wessels, J.-M.; Ute, W.; Knop-Gericke, A.; Su, D.; Schlögl, R.; Yasuda, A.; Vossmeyer, T. Self-assembled Gold Nanoparticles/Alkanedithiol Films: Preparation, Electron Microscopy, XPS-Analysis, Charge Transport, and Vapor-Sensing Properties. *J. Phys. Chem. B* **2003**, *107*, 7406−7413.

(309) (a) Werts, M. H.; Lambert, M.; Bourgoin, J.-P.; Brust, M. Nanometer Scale Patterning of Langmuir-Blogett Films of Gold Nanoparticles by Electron Beam Lithography. *Nano Lett.* **2002**, *2*, 43−47. (b) Paul, S.; Pearson, C.; Molloy, A.; Cousins, M. A.; Green, M.; Kolliopoulou, S.; Dimitrakis, P.; Normand, P.; Tsoukalas, D.; Petty, M. C. Langmuir−Blodgett Film Deposition of Metallic Nanoparticles and Their Application to Electronic Memory Structures. *Nano Lett.* **2003**, *3*, 533−536.

(310) Brust, M.; Stuhr-Hansen, N.; Nørgaard, K.; Christensen, J. B.; Nielsen, L. K.; Bjørnholm, T. Langmuir−Blodgett Films of Alkane Chalcogenide (S, Se, Te) Stabilized Gold Nanoparticles. *Nano Lett.* **2001**, *1*, 189−191.

(311) Sastry, M.; Gole, A.; Patil, V. Lamellar Langmuir-Blogett Films of Hydrophobized Colloidal Gold Nanoparticles by Organization at the Air−Water Interface. *Thin Solid Films* **2001**, *384*, 125−131.

(312) Huang, S.; Tsutsui, G.; Sakaue, H.; Shingubara, S.; Takahagi, T. Experimental Conditions for a Highly Ordered Monolayer of Gold Nanoparticles Fabricated by the Langmuir-Blogett Methodology. *J. Vac. Sci. Technol. B* **2001**, *19*, 2045−2049.

(313) Kalinina, M. A.; Arslanov, V. V.; Tsar'kova, L. A.; Dolzhikova, V. D.; Rakhnyanskaya, A. A. Langmuir-Blogett Monolayers and Films of Alkylated Tetraazacrowns Containing Metal Ions and Nanoparticles. *Colloid J.* **2001**, *63*, 312−317.

(314) Sbrana, F.; Parodi, M. T.; Ricci, D.; Di Zitti, E. Langmuir Films of Thiolated Gold Nanoparticles Transferred onto Functionalized Substrate: 2-D Local Organization. *Mater. Sci. Eng. C* **2002**, *22*, 187−191.

(315) Ravaine, S.; Fanucci, G. E.; Seip, C. T.; Adair, J. H.; Talham, D. R. Photochemical Generation of Gold Nanoparticles in Langmuir−Blodgett Films. *Langmuir* **1998**, *14*, 708−713.

(316) (a) Bourgoin, J.-P.; Kergueris, C.; Lefèvre, E.; Palacin, S. Langmuir−Blodgett Films of Thiol-Capped Gold Nanoclusters: Fabrication and Electrical Properties. *Thin Solid Films* **1998**, *327−329*, 515−519. (b) Swami, A.; Kumar, A.; Selvakannan, P. R.; Mandal, S.; Sastry, M. Langmuir−Blodgett Films of Laurylamine-Modified Hydrophobic Gold Nanoparticles Organized at the Air−Water Interface. *J. Colloid Interface Sci.* **2003**, *260*, 367−373.

(317) (a) Brown, J. J.; Porter, J. A.; Daghlian, C. P.; Gibson, U. J. Ordered Arrays of Amphiphilic Gold Nanoparticles in Langmuir Monolayers. *Langmuir* **2001**, *17*, 7966−7969. (b) Sbrana, F.; Parodi, M. T.; Ricci, D.; Di Zitti, E.; Natale, C.; Thea, S. Assembling Thiolated Gold Nanoparticles in Compact Patterns: a Transmission Electron Microscopy and Scanning Probe Microscopy Investigation. *Mater. Sci. Eng. B* **2002**, *96*, 193−198.

(318) Khomutov, G. B.; Kislov, V. V.; Gainutdinov, R. V.; Gubin, S. P.; Obydenov, A. Y.; Pavlov, S. A.; Sergeev-Cherenkov, A. N.; Soldatov, E. S.; Tolstikhina, A. L.; Trifonov, A. S. The Design, Fabrication and Characterization of Controlled-Morphology Nanomaterials and Functional Planar Molecular Nanocluster-Based Nanostructures. *Surf. Sci.* **2003**, *532−535*, 287−293.

(319) (a) Zhao, S.-Y.; Lei, S.-B.; Chen, S.-H.; Ma, H.-Y.; Wang, S.-Y. Assembly of Two-Dimensional Ordered Monolayers of Nanoparticles by Electrophoretic Deposition. *Colloid Polym. Sci.* **2002**, *278*, 682−686. (b) Tanaka, H.; Mitsuishi, M.; Miyashita, T. Tailored-Control of Gold Nanoparticle Adsorption onto Polymer Nanosheets. *Langmuir* **2003**, *19*, 3103−3105.

(320) Kumar, A.; Mandal, S.; Mathew, S. P.; Selvakannan, P. R.; Mandale, A. B.; Chaudhari, R. V.; Sastry, M. Benzene- and Anthracene-Mediated Assembly of Gold Nanoparticles at the Liquid Interface. *Langmuir* **2002**, *18*, 6478−6483.

(321) (a) Krinke, T. J.; Deppert, K.; Magnusson, M. H.; Schmidt, F.; Fissan, H. Microscopic Aspects of the Deposition of Nanoparticles From the Gas Phase. *Aerosol Sci.* **2002**, *33*, 1341−1359. (b) Raguse, B.; Herrmann, J.; Stevens, G.; Myers, J.; Baxter, G.; Müller, K.-H.; Reda, T.; Molodyk, A.; Braach-Maksvytis, V. Hybrid Nanoparticle Film Material. *J. Nanopart. Res.* **2002**, *4*, 137−143.

(322) Shiigi, H.; Yamamoto, Y.; Yakabe, H.; Tokonami, S.; Nagaoka, T. Electrical Property and Water Repellency of a Networked Monolayer Film Prepared from Au Nanoparticles. *Chem. Commun.* **2003**, 1038−1039.

(323) Akamatsu, K.; Deki, S. Characterization and Optical Properties of Gold Nanoparticles Dispersed in Nylon 11 Thin Films. *J. Mater. Chem.* **1997**, *7*, 1773−1777.

(324) Akamatsu, K.; Deki, S. Dispersion of Gold Nanoparticles Into a Nylon 11 Thin Film During Heat Treatment: in situ Optical Transmission Study. *J. Mater. Chem.* **1998**, *8*, 637−640.

(325) (a) Akamatsu, K.; Deki, S. TEM Investigation and Electron Diffraction Study on Dispersion of Gold Nanoparticles into a Nylon 11 Thin Film During Heat Treatment. *J. Colloid Interface Sci.* **1999**, *214*, 353−361. (b) Inoue, Y.; Fujii, M.; Inata, M.; Hayashi, S.; Yamamoto, K.; Akamatsu, K.; Deki, S. Single-Electron Tunneling Effects in Thin Nylon 11 Films Containing Gold Nanoparticles. *Thin Solid Films* **2000**, *372*, 169−172.

(326) (a) Yao, H.; Momozawa, O.; Hamatani, T.; Kimura, K. Phase Transfer of Gold Nanoparticles Across a Water/Oil Interface by Stoichiometric Ion-Pair Formation on Particle Surfaces. *Bull. Chem. Soc. Jpn.* **2000**, *73*, 2675−2678. (b) Mayya, K. S.; Caruso, F. Phase Transfer of Surface-Modified Gold Nanoparticles by Hydrophobization with Alkylamines. *Langmuir* **2003**, *19*, 6987−6993. (c) Kaempfe, M.; Graener, H.; Kiesow, A.; Heilmann, A. Formation of Metal Particle Nanowires Induced by Ultrashort Laser Pulses. *Appl. Phys. Lett.* **2001**, *79*, 1876−1879.

(327) (a) Dick, K.; Dhanasekaran, T.; Zhang, Z.; Meisel, D. Size-Dependent Melting of Silica-Encapsulated Gold Nanoparticles. *J. Am. Chem. Soc.* **2002**, *124*, 2312−2317. (b) Fu, G.; Cai, W.; Kann, C.; Li, C.; Fang, Q. Optical Study of the Ultrasonic Formation Process of Noble Metal Nanoparticles Dispersed Inside the Pores of Monolithic Mesoporous Silica. *J. Phys. D: Appl. Phys.* **2003**, *36*, 1382−1387.

(328) (a) Sadtler, B.; Wei, A. Spherical Ensembles of Gold Nanoparticles on Silica: Electrostatic and Size Effects. *Chem. Commun.* **2002**, 1604−1605. (b) Zhu, H.; Lee, B.; Dai, S.; Oberbury, S. H. Co−Assembly Synthesis of Ordered Mesoporous Silica Materials Containing Au Nanoparticles. *Langmuir* **2003**, *19*, 3974−3980.

(329) (a) Lu, Y.; Yin, Y.; Li, Z.-Y.; Xia, Y. Synthesis and Self-Assembly of Au@SiO_2 Core−Shell Colloids. *Nano Lett.* **2002**, *2*, 785−788. (b) Lu, X.; Hanrath, T.; Johnston, K. P.; Korgel, B. A. Growth of Single-Crystal Silicon Nanowires in Supercritical Solution from Tethered Gold Particles on a Silicon Substrate. *Nano Lett.* **2003**, *3*, 93−99.

(330) (a) Schroedter, A.; Weller, H. Biofunctionalization of Silica-Coated CdTe and Gold Nanocrystals. *Nano Lett.* **2002**, *2*, 1363−1367. (b) Hu, M.; Wang, X.; Hartland, G. V.; Salgueiriño-Maceira, V.; Liz-Marzán, L. M. Heat Dissipation in Gold-Silica Core−Shell Nanoparticles. *Chem. Phys. Lett.* **2003**, *372*, 767−772.

(331) Guari, Y.; Thieuleux, C.; Mehdi, A.; Reyé, C.; Corriu, R. J. P.; Gomez-Gallardo, S.; Philippot, K.; Chaudret, B. In Situ Formation of Gold Nanoparticles within Thiol Functionalized HMS−C_{16} and SBA-15 Type Materials via an Organometallic Two-Step Approach. *Chem. Mater.* **2003**, *15*, 2017−2024.

(332) (a) Nooney, R. I.; Dhanasekaran, T.; Chen, Y.; Josephs, R.; Ostafin, A. E. Self-Assembled Highly-Ordered Spherical Mesoporous Silica/Gold Nanocomposites. *Adv. Mater.* **2002**, *14*, 529−532. (b) Chen, W.; Zhang, J.-Y.; Di, Y.; Boyd, I. W. Photochemical Production of Gold Nanoparticles in Monolithic Porous Silica by Using a Novel Excimer Ultraviolet Source. *Inorg. Chem. Commun.* **2003**, *6*, 950−952.

(333) (a) Fleming, M. S.; Walt, D. R. Stability and Exchange Studies of Alkanethiol Monolayers on Gold-Nanoparticle-Coated Silica Microspheres. *Langmuir* **2001**, *17*, 4836−4843. (b) Cheng, S.; Wei, Y.; Feng, Q.; Qiu, K.-Y.; Pang, J.-B.; Jansen, S. A.; Yin, R.; Ong, K. Facile Synthesis of Mesoporous Gold-Silica Nanocomposite Materials via Gold-Gel Process with Nonsurfactant Templates. *Chem. Mater.* **2003**, *15*, 1560−1566.

(334) (a) Kobayashi, Y.; Correra-Durante, M. A.; Liz-Marzán, L. M. Sol−Gel Processing of Silica-Coated Gold Nanoparticles. *Langmuir* **2001**, *17*, 6375−6379. (b) Lim, Y. T.; Park, O O.; Jung, H.-T. Gold Nanolayer-Encapsulated Silica Particles Synthesized by Surface Seeding and Shell Growing Method: Near Infrared Responsive Materials. *J. Colloid Interface Sci.* **2003**, *263*, 449−453.

(335) Pető, G.; Molnár, G. L.; Pászti, Z.; Geszti, O.; Beck, A.; Guczi, L. Electronic Structure of Gold Nanoparticles Deposited on SiO/Si(100). *Mater. Sci. Eng. C* **2002**, *19*, 95−99.

(336) Caruso, F.; Spasova, M.; Salgueiri-o-Maceira, V.; Liz-Marzán, L. M. Multilayer Assemblies of Silica-Encapsulated Gold Nanoparticles on Decomposable Colloid Templates. *Adv. Mater.* **2001**, *13*, 1090−1094.

(337) García-Santamaría, F.; Salgueiriño-Maceira, V.; López, C.; Liz-Marzán, L. M. Synthetic Opals Based on Silica-Coated Gold Nanoparticles. *Langmuir* **2002**, *18*, 4519−4522.

(338) Chen, W.; Cai, W.; Wang, G.; Zhang, L. Effects of Interface Interaction on the Mie Resonance Absorption of Gold Nanoparticles Dispersed within Pores of Mesoporous Silica. *Appl. Surf. Sci.* **2001**, *174*, 51−54.

(339) Papernov, S.; Schmid, A. W. Correlations between Embedded Single Gold Nanoparticles in SiO_2 Thin Film and Nanoscale Crater Formation Induced by Pulsed-Laser Radiation. *J. Appl. Phys.* **2002**, *92*, 5720−5728.

(340) Chen, W.; Cai, W.; Zhang, Z.; Zhang, L. A Convenient Synthetic Route to Gold Nanoparticles Dispersed within Mesoporous Silica. *Chem. Lett.* **2001**, 152−153.

(341) Ila, D.; Williams, E. K.; Zimmerman, R. L.; Poker, D. B.; Hensley, D. K. Radiation Induced Nucleation of Nanoparticles in Silica. *Nucl. Instrum. Methods Phys. Res. B* **2002**, *166−167*, 845−850.

(342) Abis, L.; Armelao, L.; Dell'Amico, D. B.; Calderazzo, F.; Garbassi, F.; Merigo, A.; Quadrelli, E. A. Gold Molecular Precursors and Gold-Silica Interactions. *J. Chem. Soc., Dalton Trans.* **2001**, 2704−2709.

(343) Shi, H.; Zhang, L.; Cai, W. Preparation and Optical Absorption of Gold Nanoparticles within Pores of Mesoporous Silica. *Mater. Res. Bull.* **2000**, *35*, 1689−1695.

(344) Selvan, S. T.; Nogami, M.; Nakamura, A.; Hamanaka, Y. A Facile Sol−Gel Method for the Encapsulation of Gold Nanoparticles in Silica Gels and their Optical Properties. *J. Non-Cryst. Solids* **1999**, *255*, 254−258.

(345) Ghosh, A.; Patra, C. R.; Mukherjee, P.; Sastry, M.; Kumar, R. Preparation and Stabilization of Gold Nanoparticles Formed by in situ Reduction of Aqueous Chloroaurate Ions within Surface-Modified Mesoporous Silica. *Microporous Mesoporous Mater.* **2003**, *58*, 201−211.

(346) Battaglin, G.; Boscolo-Boscoletto, A.; Mazzoldi, P.; Meneghini, C.; Arnold, G. W. Gold Nanocluster Formation in Silicate Glasses by Low Fluence Ion Implantation and Annealing. *Nucl. Instrum. Methods Phys. Res. B* **1996**, *116*, 527−530.

(347) Innocenti, P.; Brusatin, G.; Martucci, A.; Urabe, K. Microstructural Characterization of Gold-Doped Silica−Titania Sol−Gel Films. *Thin Solid Films* **1996**, *279*, 23−28.

(348) Coultard, I.; Degen, S.; Zhu, Y.-J.; Sham, T. K. Gold Nanoclusters Reductively Deposited on Porous Silicon: Morphology and Electronic Structures. *Can. J. Chem.* **1998**, *76*, 1707−1716.

(349) Aihara, N.; Torigoe, K.; Esumi, K. Preparation and Characterization of Gold and Silver Nanoparticles in Layered Laponite Suspensions. *Langmuir* **1998**, *14*, 4945−4949.

(350) Wescott, S. L.; Oldenburg, S. J.; Lee, T. R.; Halas, N. J. Formation and Adsorption of Clusters of Gold Nanoparticles onto Functionalized Silica Nanoparticle Surfaces. *Langmuir* **1998**, *14*, 5396−5401.

(351) Kónya, Z.; Puntes, V. F.; Kiricsi, I.; Zhu, J.; Ager, J. W., III; Ko, M. K.; Frei, H.; Alivisatos, P.; Somorjai, G. A. Synthetic Insertion of Gold Nanoparticles into Mesoporous Silica. *Chem. Mater.* **2003**, *15*, 1242−1248.

(352) Wang, J.; Zhu, T.; Song, J.; Liu, Z. Gold Nanoparticulate Films Bound to Silicon Surface with Self-Assembled Monolayers. *Thin Solid Films* **1998**, *327−329*, 591−594.

(353) Bharathi, S.; Lev, O. Direct Synthesis of Gold Nanodispersions in Sol−Gel Derived Silicate Sols, Gels and Films. *Chem. Commun.* **1997**, 2303−2304.

(354) Caruso, F. Nanoengineering of Particle Surfaces. *Adv. Mater.* **2001**, *13*, 11−22.

(355) Liz-Marsan, L. M.; Griersig, M.; Mulvaney, P. Synthesis of Nanosized Gold-Silica Core−Shell Particles. *Langmuir* **1996**, *12*, 4329−4335.

(356) Hall, S. R.; Davis, S. A.; Mann, S. Co−Condensation of Organosilica Hybrid Shells on Nanoparticle Templates: A Direct Synthetic Route to Functionalized Core−Shell Colloids. *Langmuir* **2000**, *16*, 1454−1456.

(357) González-Rodríguez, B.; Salgueiri-o-Maceira, V.; García-Santamaría, F.; Liz-Marzán, L. M. Fully Accessible Gold Nanoparticles within Ordered Macroporous Solids. *Nano Lett.* **2002**, *2*, 471−473.

(358) Guari, Y.; Thieuleux, C.; Mehdi, A.; Reyé, C.; Corriu, R. J. P.; Gomez-Gallardo, S.; Philippot, K.; Chaudret, B.; Dutartre, R. In situ Formation of Gold Nanoparticles within Functionalized Ordered Mesoporous Silica via an Organometallic 'Chimie Douce' Approach. *Chem. Commun.* **2001**, 1374−1375.

(359) Epifani, M.; Carlino, E.; Blasi, C.; Giannini, C.; Tapfer, L.; Vasanelli, L. Sol−Gel Processing of Au Nanoparticles in Bulk 10% B_2O_3-90% SiO_2 Glass. *Chem. Mater.* **2001**, *13*, 1533−1539.

(360) Horváth, D.; Thfoin-Polisset, M.; Fraissard, J.; Guczi, L. Novel Preparation Method and Characterization of Au−Fe/HY Zeolite Containing Highly Stable Gold Nanoparticles Inside Zeolite Supercages. *Solid State Ionics* **2001**, *141*−*142*, 153−156.

(361) Ng, L. N.; Zervas, M. N.; Wilkinson, J. S.; Luff, B. J. Manipulation of Colloidal Gold Nanoparticles in the Evanescent Field of a Channel Waveguide. *Appl. Phys. Lett.* **2000**, *76*, 1993−1995.

(362) Oku, T.; Suganuma, K. Carbon Nanocage Structures Formed by One-Dimensional Self-Organization of Gold Nanoparticles. *Chem. Commun.* **1999**, 2355−2356.

(363) Sawitowski, T.; Miquel, Y.; Heilmann, A.; Schmid, G. Optical Properties of Quasi One-Dimensional Chains of Gold Nanoparticles. *Adv. Funct. Mater.* **2001**, *11*, 435−440.

(364) Reuter, T.; Vidoni, O.; Torma, V.; Schmid, G. Two-Dimensional Networks via Quasi One-Dimensional Arrangements of Gold Clusters. *Nano Lett.* **2002**, *2*, 709−711.

(365) Blonder, R.; Sheeney, L.; Willner, I. Three-Dimensional Redox-Active Layered Composites of Au−Au, Ag−Ag and Au−Ag Colloids. *Chem. Commun.* **1998**, 1393−1394.

(366) Gutiérrez-Wing, C.; Santiago, P.; Ascencio, J. A.; Camacho, A.; José-Yacamán, M. Self-Assembling of Gold Nanoparticles in One, Two, and Three Dimensions. *Appl. Phys. A* **2000**, *71*, 237−243.

(367) Mafuné, F.; Kohno, J-y.; Takeda, Y.; Kondow, T. Nanoscale Soldering of Metal Nanoparticles for Construction of Higher-Order Structures. *J. Am. Chem. Soc.* **2003**, *125*, 1686−1687.

(368) Oh, S.-K.; Kim, Y.-G.; Ye, H.; Crooks, R. M. Synthesis, Characterization, and Surface Immobilization of Metal Nanoparticles Encapsulated within Bifunctionalized Dendrimers. *Langmuir* **2003**, *19*, 10420−10425.

(369) Liang, Z.; Susha, A. S.; Caruso, F. Metallodielectric Opals of Layer-by-Layer Processed Coated Colloids. *Adv. Mater.* **2002**, *14*, 1160−1164.

(370) Powell, C.; Fenwick, N.; Bresme, F.; Quirke, N. Wetting of Nanoparticles and Nanoparticle Arrays. *Physicochem. Eng. Asp.* **2002**, *206*, 241−251.

(371) Hall, S. R.; Shenton, W.; Engelhardt, H.; Mann, S. Site-Specific Organization of Gold Nanoparticles by Biomolecular Templating. *ChemPhysChem* **2001**, n° 3, 184−186.

(372) (a) Khan, M. A.; Perruchot, C.; Armes, S. P.; Randall, D. P. Synthesis of Gold-Decorated Latexes via Conducting Polymer Redox Templates. *J. Mater. Chem.* **2001**, *11*, 2363−2372. (b) Liu, F.-K.; Chang, Y.-C.; Ko, F.-H.; Chu, T.-C.; Dai, B.-T. Rapid Fabrication of High Quality Self-Assembled Nanometer Gold Particles by Spin Coating Methodology. *Microelectron. Eng.* **2003**, *67*−*68*, 702−709.

(373) Mott, N. F.; Gurney, N. W. *Electronic Processes in Ionic Crystals*; Oxford University Press: Oxford, 1948.

(374) (a) Mulvaney, P. Surface Plasmon Spectroscopy of Nanosized Metal Particles. *Langmuir* **1996**, *12*, 788−800. (b) Mulvaney, P. In *Semiconductor Nanoclusters*−*Physical, Chemical and Catalytic Aspects*; Kamat, P. V., Meisel, D., Eds.; Elsevier: Amsterdam, 1997; pp 99−123.

(375) *The Theory of the Photographic Process*, 4th ed; James, T. H., Ed.; MacMillan Press: New York, 1977.

(376) Van der Hulst, H. C. *Light Scattering by Small Metal Particles*; Wiley: New York, 1957.

(377) Kerker, M. *The Scattering of Light and Other Electromagnetic Radiation*; Academic Press: New York, 1969.

(378) Bohren, C. F.; Huffman, D. R. *Absorption of Light by Small Particles*; Wiley: New York, 1983.

(379) Mie, G. Beiträge zur Optik Trüber Medien, Speziell Kolloidaler Metallösungen. *Ann. Phys.* **1908**, *25*, 377−445.

(380) Alvarez, M. M.; Khoury, J. T.; Schaaff, T. G.; Shafigullin, M. N.; Vezmar, I.; Whetten, R. L. Optical Absorption Spectra of Nanocrystal Gold Molecules. *J. Phys. Chem. B* **1997**, *101*, 3706−3712.

(381) Logunov, S. L.; Ahmadi, T. S.; El-Sayed, M. A.; Khoury, J. T.; Whetten, R. L. Electron Dynamics of Passivated Gold Nanocrystals Probed by Subpicosecond Transient Absorption Spectroscopy. *J. Phys. Chem. B* **1997**, *101*, 3713−3719.

(382) (a) Schaaf, T. G.; Shafigullen, M. N.; Khoury, J. T.; Vezmar, I.; Whetten, R. L.; Cullen, W. G.; First, P. N.; Guttierrez-Wing, C.; Ascencio, J.; Jose-Yacamun, M. J. Isolation of Smaller Nanocrystal Au Molecules: Robust Quantum Effects in Optical Spectra. *J. Phys. Chem. B* **1997**, *101*, 7885−7891. (b) Zaitoun, M. A.; Mason, W. R.; Lin, C. T. Magnetic Circular Dichroism Spectra for Colloidal Gold Nanoparticles in Xerogels at 5.5 K. *J. Phys. Chem. B* **2001**, *105*, 6780−6784.

(383) Melinger, J. S.; Kleiman, V. D.; McMorrow, D.; Gröhn, F.; Bauer, B. J.; Amis, E. Ultrafast Dynamics of Gold-Based Nanocomposite Materials. *J. Phys. Chem. A* **2003**, *107*, 3424−3431.

(384) Papavassiliou, G. C. Optical Properties of Small Inorganic and Organic Metal Particles. *Prog. Solid State Chem.* **1979**, *12*, 185−271.

(385) Templeton, A. C.; Pietron, J. J.; Murray, R. W.; Mulvaney, P. Solvent Refractive Index and Core Charge Influences on the Surface Plasmon Adsorbance of Alkanethiolate Monolayer-Protected Gold Clusters. *J. Phys. Chem. B* **2000**, *104*, 564−570.

(386) (a) Link, S.; El-Sayed, M. A. Size and Temperature Dependence of the Plasmon Absorption of Colloidal Gold Nanoparticles. *J. Phys. Chem. B* **1999**, *103*, 4212−4217. (b) Itoh, T.; Asahi, T.; Masuhara, H. Femtosecond Light Scattering Spectroscopy of Single Gold Nanoparticles. *Appl. Phys. Lett.* **2001**, *79*, 1667−1669. (c) Su, K.-H.; Wei, Q.-H.; Zhang, X.; Mock, J. J.; Smith, D. R.; Schulz, S. Interparticle Coupling Effects on Plasmon Resonance of Nanogold Particles. *Nano Lett.* **2003**, *3*, 1087−1090. (d) Rechberger, W.; Hohenau, A.; Leitner, A.; Krenn, J. R.; Lamprecht, B.; Aussenegg, F. R. Optical Properties of Two Interacting Gold Nanoparticles. *Opt. Commun.* **2003**, *220*, 137−141. (e) Link, S.; Mohamed, M. B.; El-Sayed, M. A. Simulation of the Optical Absorption Spectra of a Gold Nanorods as a Function of their Aspect Ratio and the Effect of the Medium Dielectric Constant *J. Phys. Chem. B* **1999**, *103*, 3073. (f) Yan, B.; Yang, Y.; Wang, Y. Comment on "Simulation of the Optical Absorption Spectra of a Gold Nanorods as a Function of their Aspect Ratio and the Effect of the Medium Dielectric Constant" *J. Phys. Chem. B* **2003**, *107*, 9159. (g) Swanson, N. L.; Billard, B. D. Optimization of Extinction from Surface Plasmon Resonances of Gold Nanoparticles. *Nanotechnology* **2003**, *14*, 353−357.

(387) Ung, T.; Liz-Marzán, L. M.; Mulvaney, P. Gold Particles Thin Films. *Colloids Surf. A: Physicochem. Eng. Asp.* **2002**, *202*, 119−126.

(388) Ung, T.; Giersig, M.; Dunstan, D.; Mulvaney, P. Spectroelectrochemistry of Colloidal Silver. *Langmuir* **1997**, *13*, 1773−1782.

(389) Ung, T.; Liz-Marzán, L. M.; Mulvaney, P. Optical Properties of Thin Films of Au@SiO_2 Particles. *J. Phys. Chem. B* **2001**, *105*, 3441−3452.

(390) Klar, T.; Perner, M.; Grosse, S.; von Plessen, G.; Spirkl, W.; Feldmann, J. Surface-Plasmon Resonances in Single Metallic Nanoparticles. *Phys. Rev. Lett.* **1998**, *80*, 4249−4252.

(391) Al-Rawashdeh, N.; Foss, C. A., Jr. UV/Visible and Infrared Spectra of Polyethylene/Nanoscopic Gold Rod Composite Films: Effects of Gold Particle Size, Shape and Orientation. *Nanostruct. Mater.* **1997**, *9*, 383−386.

(392) Al-Rawashdeh, N. A. F.; Sandrock, M. L.; Seugling, C. J.; Foss, C. A., Jr. Visible Region Polarization Spectroscopic Studies of Template-Synthesized Gold Nanoparticles Oriented in Polyethylene. *J. Phys. Chem. B* **1998**, *102*, 361−371.

(393) Linden, S.; Christ, A.; Kuhl, J.; Giessen, H. Selective Suppression of Extinction within the Plasmon Resonance of Gold Nanoparticles. *Appl. Phys. B* **2001**, *73*, 311−316.

(394) Linden, S.; Kuhl, J.; Giessen, H. Controlling the Interaction between Light and Gold Nanoparticles: Selective Suppression of Extinction. *Phys. Rev. Lett.* **2001**, *86*, 4688−4691.

(395) (a) Ahmadi, T. S.; Logunov, S. L.; El-Sayed, M. A. Picosecond Dynamics of Colloidal Gold Nanoparticles. *J. Phys. Chem. B* **1999**, *100*, 8059−8056. (b) Logunov, S. L.; Ahmadi, T. S.; El-Sayed, M. A. Electron Dynamics of Passivated Gold Nanocrystals Probed by Subpicosecond Transient Absorption Spectroscopy. *J. Phys. Chem. B* **1997**, *101*, 3713−3719. (c) Hartland, G. V.; Hu, M.; Sader, J. E. Softening of the Symmetric Breathing Mode in Gold Particles by Laser-Induced Heating. *J. Phys. Chem. B* **2003**, *107*, 7472−7478.

(396) (a) Fujiwara, H.; Yanagida, S.; Kamat, P. V. Visible Laser Induced Fusion and Fragmentation of Thionicotinamide-Capped Gold Nanoparticles. *J. Phys. Chem. B* **1999**, *103*, 2589−2591.

(397) Takeuchi, Y.; Ida, T.; Kimura, K. Colloidal Stability of Gold Nanoparticles in 2-Propanol Under Laser Irradiation. *J. Phys. Chem. B* **1997**, *101*, 1322−1327.

(398) Satoh, N.; Hasegawa, H.; Tsujii, K.; Kimura, K. Photoinduced Coagulation of Au Nanocolloids. *J. Phys. Chem.* **1994**, *98*, 2143−2147.

(399) Mafuné, F.; Kohno, J.-Y.; Takeda, Y.; Kondow, T. Dissociation and Aggregation of Gold Nanoparticles under Laser Irradiation. *J. Phys. Chem. B* **2001**, *105*, 9050−9056.

(400) Westcott, S. L.; Oldenburg, S. J.; Lee, T. R.; Halas, N. J. Construction of Simple Gold Nanoparticle Aggregates with Controlled Plasmon-Plasmon Interactions. *Chem. Phys. Lett.* **1999**, *300*, 651−655.

(401) Eck, D.; Helm, C. A.; Wagner, N. J.; Vaynberg, K. A. Plasmon Resonance Measurements of the Adsorption and Adsorption Kinetics of a Biopolymer onto Gold Nanocolloids. *Langmuir* **2001**, *17*, 957−960.

(402) Chandrasekharan, N.; Kamat, P. V.; Hu, J.; Jones, G., II. Dye-Capped Gold Nanoclusters: Photoinduced Morphological Changes in Gold/Rhodamine 6G Nanoassemblies. *J. Phys. Chem. B* **2000**, *104*, 11103−11109.

(403) Nath, N.; Chilkoti, A. Interfacial Phase Transition of an Environmentally Responsive Elastin Biopolymer Adsorbed on Functionalized Gold Nanoparticles Studied by Colloidal Surface Plasmon Resonance. *J. Am. Chem. Soc.* **2001**, *123*, 8197−8202.

(404) Huang, S.; Minami, K.; Sakaue, H.; Shingubara, S.; Takahagi, T. Optical Spectroscopic Studies of the Dispersibility of Gold Nanoparticle solutions. *J. Appl. Phys.* **2002**, *92*, 7486−7490.

(405) Swami, A.; Kumar, A.; Sastry, M. Formation of Water-Dispersible Gold Nanoparticles Using a Technique Based on Surface-Bound Interdigitated Bilayers. *Langmuir* **2003**, *19*, 1168−1172.
(406) Thomas, K. G.; Zajicek, J.; Kamat, P. V. Surface Binding Properties of Tetraoctylammonium Bromide-Capped Gold Nanoparticles. *Langmuir* **2002**, *18*, 3722−3727.
(407) (a) Malikova, N.; Pastoriza-Santos, I.; Schierhorn, M.; Kotov, N. A.; Liz-Marzán, L. M. Layer-by-Layer Assembled Mixed Spherical and Planar Gold Nanoparticles: Control of Interparticle Interactions. *Langmuir* **2002**, *18*, 3694−3697. (b) Aizpurua, J.; Hanarp, P.; Sutherland, D. S.; Käll, M.; Bruant, G. W.; Garcia de Abajo, F. J. Optical Properties of Gold Nanorings. *Phys. Rev. Lett.* **2003**, *90*, 057401-1−057401-4.
(408) Huang, T.; Murray, R. W. Visible Luminescence of Water-Soluble Monolayer-Protected Gold Clusters. *J. Phys. Chem. B* **2001**, *105*, 12498−12502.
(409) Hwang, Y.-N.; Jeong, D. H.; Shin, H. J.; Kim, D.; Jeoung, S. C.; Han, S. H.; Lee, J.-S.; Cho, G. Femtosecond Emission Studies of Gold Nanoparticles. *J. Phys. Chem. B* **2002**, *106*, 7581−7584.
(410) Chen, M. M. Y.; Katz, A. Steady-State Fluorescence-Based Investigation of the Interaction between Protected Thiols and Gold Nanoparticles. *Langmuir* **2002**, *18*, 2413−2420.
(411) Hu, J.; Zhang, J.; Liu, F.; Kittredge, K.; Whitesell, J. K.; Fox, M. A. Competitive Photochemical Reactivity in a Self-Assembled Monolayer on a Colloidal Gold Cluster. *J. Am. Chem. Soc.* **2001**, *123*, 1464−1470.
(412) Wang, T.; Zhang, D.; Xu, W.; Yang, J.; Han, R.; Zhu, D. Preparation, Characterization, and Photophysical Properties of Alkanethiols with Pyrene Units-Capped Gold Nanoparticles: Unusual Fluorescence Enhancement for the Aged Solutions of These Gold Nanoparticles. *Langmuir* **2002**, *18*, 1840−1848.
(413) Thomas, K. G.; Kamat, P. V. Making Gold Nanoparticles Glow: Enhanced Emission from a Surface-Bound Fluoroprobe. *J. Am. Chem. Soc.* **2000**, *122*, 2655−2656.
(414) Sarathy, V. K.; Narayan, K. S.; Kim, J.; White, J. O. Novel Fluorescence and Morphological Structures in Gold Nanoparticles-Polyoctylthiophene Based Thin Films. *Chem. Phys. Lett.* **2000**, *318*, 543−548.
(415) Xu, P.; Yanagi, H. Fluorescence Patterning in Dye-Doped Sol−Gel Films by Generation of Gold Nanoparticles. *Chem. Mater.* **1999**, *11*, 2626−2628.
(416) Makarova, O. V.; Ostafin, A. E.; Miyoshi, H.; Norris, J. R., Jr.; Meisel, D. Adsorption and Encapsulation of Fluorescent Probes in Nanoparticles. *J. Phys. Chem. B* **1999**, *103*, 9080−9084.
(417) Dulkeith, E.; Morteani, A. C.; Niedereichholz, T.; Klar, T. A.; Feldmann, J. Fluorescence Quenching of Dye Molecules near Gold Nanoparticles: Radiative and Nonradiative Effects. *Phys. Rev. Lett.* **2002**, *89*, 203002-1−203002-4.
(418) Gu, T.; Whitesell, J. K.; Fox, M. A. Energy Transfer from a Surface-Bound Arene to the Gold Core in ω-Fluorenyl-Alkane-1-Thiolate Monolayer-Protected Gold Clusters. *Chem. Mater.* **2003**, *15*, 1358−1366.
(419) Dubertret, B.; Calame, M.; Libchaber, A. J. Single-Mismatch Detection Using Gold-Quenched Fluorescent Oligonucleotides. *Nat. Biotechnol.* **2001**, *19*, 365−370.
(420) Imahori, H.; Fukuzumi, S. Porphyrin Monolayer-Modified Gold Clusters as Photoactive Materials. *Adv. Mater.* **2001**, *13*, 1197−1199.
(421) Imahori, H.; Arimura, M.; Hanada, T.; Nishimura, Y.; Yamazaki, I.; Sakata, Y.; Fukuzumi, S. Photoactive Three-Dimensional Monolayers: Porphyrin-Alkanethiolate-Stabilized Gold Clusters. *J. Am. Chem. Soc.* **2001**, *123*, 335−336.
(422) Lakowitcz, J. R. *Principles of Fluorescence Spectroscopy*; Kluwer: New York, 1999.
(423) Wilcoxon, J. P.; Martin, J. E.; Parsapour, F.; Wiedenman, B.; Kelley, D. F. Photoluminescence From Nanosize Gold Clusters. *J. Chem. Phys.* **1998**, *108*, 9137−9143.
(424) Mohamed, M. B.; Volkov, V.; Link, S.; El-Sayed, M. A. The 'lightning' Gold Nanorods: Fluorescence Enhancement of Over a Million Compared to the Gold Metal. *Chem. Phys. Lett.* **2000**, *317*, 517−523.
(425) Bigioni, T. P.; Whetten, T. P.; Dag, O. Near-Infrared Luminescence from Small Gold Nanocrystals. *J. Phys. Chem. B* **2000**, *104*, 6983−6986.
(426) Link, S.; El-Sayed, M. A. Shape and Size Dependence of Radiative, Non-Radiative and Photothermal Properties of Gold Nanocrystals. *Int. Rev. Phys. Chem.* **2000**, *19*, 3, 409−453.
(427) Ipe, B. I.; Mahima, S.; Thomas, K. G. Light-Induced Modulation of Self-Assembly on Spiropyran-Capped Gold Nanoparticles: A Potential System for the Controlled Release of Amino Acid Derivatives. *J. Am. Chem. Soc.* **2003**, *125*, 7174−7175.
(428) (a) Chen, S.; Huang, K. Electrochemical and Spectroscopic Studies of Nitrophenyl Moieties Immobilized on Gold Nanoparticles. *Langmuir* **2000**, *16*, 2014−2018. (b) Chen, S.; Yang, Y. Magnetoelectrochemistry of Gold Nanoparticle Quantized Capacitance Charging. *J. Am. Chem. Soc.* **2002**, *124*, 5280−5281. (c) Li, D.; Li, J. Preparation, Characterization and Quantized Capacitance of 3-Mercapto-1,2-Propanediol Monolayer Protected Gold Nanoparticles. *Chem. Phys. Lett.* **2003**, *372*, 668−673.
(429) (a) Yang, Y.; Chen, S. Surface Manipulation of the Electronic Energy of Subnanometer-Sized Gold Clusters: An Electrochemical and Spectroscopic Investigation. *Nano Lett.* **2003**, *3*, 75−79. (b) Lee, D.; Donkers, R. L.; DeSimone, J. M.; Murray, R. W. Voltammetry and Electron-Transfer Dynamics in a Molecular Melt of a 1.2 nm Metal Quantum Dot. *J. Am. Chem. Soc.* **2003**, *125*, 1182−1183.
(430) (a) Gittins, D. I.; Bethell, D.; Nichols, R. J.; Schiffrin, D. J. Redox-Connected Multilayers of Discrete Gold Particles: A Novel Electroactive Nanomaterial. *Adv. Mater.* **1999**, *11*, 737−740. (b) Sagara, T.; Kato, N.; Toyota, A.; Nakashima, N. Anomalous Electroreflectance and Absorption Spectra of Viologen Radical Cation in Close Proximity of Gold Nanoparticles at Electrified Interfaces. *Langmuir* **2002**, *18*, 6995−7001.
(431) Kuwahara, Y.; Akiyama, T.; Yamada, S. Facile Fabrication of Photoelectrochemical Assemblies Consisting of Gold Nanoparticles and a Tris(2,2′-bipyridine)ruthenium(II)-Viologen Linked Thiol. *Langmuir* **2001**, *17*, 5714−5716.
(432) Cheng, W.; Dong, S.; Wang, E. Gold Nanoparticles as Fine Tuners of Electrochemical Properties of the Electrode/Solution Interface. *Langmuir* **2002**, *18*, 9947−9952.
(433) Labande, A.; Astruc, D. Colloids as Redox Sensors: Recognition of $H_2PO_4^-$ and HSO_4^- by Amidoferrocenylalkylthiol-Gold-Nanoparticles. *Chem. Commun.* **2000**, 1007−1008.
(434) Horikoshi, T.; Itoh, M.; Kurihara, M.; Kubo, K.; Nishihara, H. Synthesis, Redox Behavior and Electrodeposition of Biferrocene-modified Gold Clusters. *J. Electroanal. Chem.* **1999**, *473*, 113−116.
(435) Yamada, M.; Tadera, T.; Kubo, K.; Nishihara, H. *J. Phys. Chem. B* **2003**, *107*, 3703−3711.
(436) Yamada, M.; Kubo, K.; Nishihara, H. Electroreductive Deposition of An Clusters Modified with an Anthraquinone Derivative. *Chem. Lett.* **1999**, 1335−1336.
(437) Yamada, M.; Nishihara, H. Electrochemical Deposition of Metal Nanoparticles Functionalized with Multiple Redox Molecules. In *Dendrimers and Nanoscience*; Astruc, D., Ed.; Compte-Rendus Chimie, Elsevier: Paris, 2003.
(438) Ogawa, T.; Kobayashi, K.; Masuda, G.; Takase, T.; Maeda, S. Electronic Conductive Characteristics of Devices Fabricated with 1,10-Decanedithiol and Gold Nanoparticles Between 1-μm Electrode Gaps. *Thin Solid Films* **2001**, *393*, 374−378.
(439) Chen, S.; Deng, F. Rectifying Nanoscale Electron Transfer by Viologen Moieties and Hydrophobic Electrolyte Ions. *Langmuir* **2002**, *18*, 8942−8948.
(440) Yamada, M.; Nishihara, H. Electrochemical Construction of an Alternating Multi-Layered Structure of Palladium and Gold Nanoparticles Attached with Biferrocene Moieties. *Chem. Commun.* **2002**, 2578−2579.
(441) (a) Fujihara, H.; Nakai, H. Fullerenethiolate-Functionalized Gold Nanoparticles: A New Class of Surface-Confined Metal-C_{60} Nanocomposites. *Langmuir* **2001**, *17*, 6393−6395. (b) Liljeroth, P.; Quinn, B. M.; Ruiz, V.; Kontturi, K. Charge Injection and Lateral Conductivity in Monolayers of Metallic Nanoparticles. *Chem. Commun.* **2003**, 1570−1571. (c) Zhang, P.; Kim, P. S.; Sham, T. K. Electrochemical Route for the Fabrication of Alkanethiolate-Capped Gold Nanoparticles. *Appl. Phys. Lett.* **2003**, *82*, 1470−1472. (d) Cheng, W.; Dong, S.; Wang, E. Site-Selective Self-Assembly of MPA-Bridged CuHCF Multilayers on APTMS−Supported Gold Colloid Electrodes. *Chem. Mater.* **2003**, *15*, 2495−2501. (e) Li, D.; Zhang, Y.; Li, J. Electrochemical Study of 4-Ferrocene Thiophenol Monolayers Assembled on Gold Nanoparticles. *Microelectron. Eng.* **2003**, *66*, 91−94.
(442) (a) Park, S.; Yang, P.; Coordor, P.; Weaver, M. J. Transition Metal-Coated Nanoparticle Films: Vibrational Characterization with Surface-Enhanced Raman Scattering. *J. Am. Chem. Soc.* **2002**, *124*, 2428−2429. (b) Jakob, M.; Levanon, H.; Kamat, P. V. Charge Distribution between UV−Irradiated TiO_2 and Gold Nanoparticles: Determination of Shift in the Fermi Level. *Nano Lett.* **2003**, *3*, 353−358.
(443) (a) Davidovic, D.; Tinkham, M. Coulomb Blockade and Discrete Energy Levels in Au Nanoparticles. *Appl. Phys. Lett.* **1998**, *73*, 3959−3961. Davidovic, D.; Tinkham, M. Spectroscopy, Interactions, and Level Splittings in Au Nanoparticles. *Phys. Rev. Lett.* **1999**, *83*, 1644−1647. (b) Zhang, J.; Lahtinen, R. M.; Kontturi, K.; Unwin, P. R.; Schriffin, D. J. Electron-Transfer Reactions at Gold Nanoparticles. *Chem. Commun.* **2001**, 1818−1819.
(444) (a) Zhang, P.; Sham, T. K. Tuning the Electronic Behavior of Au Nanoparticles with Capping Molecules. *Appl. Phys. Lett.* **2002**, *81*, 736−738. (b) Zhang, P.; Sham, T. K. X-Ray Studies of the Structure and Electronic Behavior of Alkanethiolate-Capped Gold Nanoparticles: The Interplay of Size and Surface Effects. *Phys. Rev. Lett.* **2003**, *90*, 245502-1−245502-4. (c) Huang, X.; Huang, H.; Wu, N.; Hu, R.; Zhu, T.; Liu, Z. Investigation of Structure and Chemical States of Self-Assembled Au Nanoscale Particles by Angle-Resolved X-Ray Photoelectron Spectroscopy. *Surf. Sci.* **2000**, *459*, 183−190.

(445) Mohamed, M. B.; Ahmadi, T. S.; Link, S.; Braun, M.; El-Sayed, M. A. Hot Electron and Phonon Dynamics of Gold Nanoparticles Embedded in a Gel Matrix. *Chem. Phys. Lett.* **2001**, *343*, 55−63.
(446) (a) Chen, Y.; Palmer, R. E.; Shelley, E. J.; Preece, J. A. HREELS Studies of Gold Nanoparticles with Dialkyl Sulphide Ligands. *Surf. Sci.* **2002**, *502*−*503*, 208−213. (b) Lin, H.-W.; Wang, X.-H.; Zhao, X.-J.; Li, J.; Wang, F.-S. Metal-Containing Molecular Wires and Their Electron Transportation Properties. *Synth. Met.* **2003**, *135*−*136*, 239−240.
(447) (a) Petta, J. R.; Ralph, D. C. Studies of Spin−Orbit Scattering in Noble-Metal Nanoparticles Using Energy-Level Tunneling Spectroscopy. *Phys. Rev. Lett.* **2001**, *87*, 266801-1−266801-4. (b) Bieri, N. R.; Chung, J.; Haferl, S. E.; Poulikakos, D.; Grigoropoulos, C. P. Microstructuring by Printing and Laser Curing of Nanoparticle Solutions. *Appl. Phys. Lett.* **2003**, *82*, 3529−3531.
(448) (a) Montalti, M.; Prodi, L.; Zaccheroni, N.; Baxter, R.; Teobaldi, G.; Zerbetto, F. Kinetics of Place-Exchange Reactions of Thiols on Gold Nanoparticles. *Langmuir* **2003**, *19*, 5172−5174. (b) Song, Y.; Murray, R. W. Dynamics and Extent of Ligand Exchange Depend on Electronic Charge of Metal Nanoparticles. *J. Am. Chem. Soc.* **2002**, *124*, 7096−7102.
(449) Zheng, W.; Maye, M. M.; Leibowitz, F. L.; Zhong, C.-J. Imparting Biomimetic Ion-Gating Recognition Properties to Electrodes with a Hydrogen-Bonding Structured Core−Shell Nanoparticle Network. *Anal. Chem.* **2000**, *72*, 2190−2199.
(450) Zamborini, F. P.; Hicks, J. F.; Murray, R. W. Quantized Double Layer Charging of Nanoparticle Films Assembled Using Carboxylate/(Cu^{2+} or Zn^{2+})/Carboxylate Bridges. *J. Am. Chem. Soc.* **2000**, *122*, 4514−4515.
(451) Wuelfing, W. P.; Zamborini, F. P.; Templeton, A. C.; Wen, X.; Yoon, H.; Murray, R. W. Monolayer-Protected Clusters: Molecular Precursors to Metal Films. *Chem. Mater.* **200**1, *13*, 87−95.
(452) Chen, S.; Pei, R.; Dyer, D. J. Gold Nanoparticle Assemblies by Metal Ion-Pyridine Complexation and Their Rectified Quantized Charging in Aqueous Solutions. *J. Phys. Chem. B* **2002**, *106*, 1903−1908.
(453) McIntosh, C. M.; Esposito, E. A.; Boal, A. K.; Simard, J. M.; Martin, C. T.; Rotello, V. M. Inhibition of DNA Transcription Using Cationic Mixed Monolayer Protected Gold Clusters. *J. Am. Chem. Soc.* **2001**, *123*, 7626−7629.
(454) Pietron, J. J.; Murray, R. W. Mediated Electrocatalysis with Polyanthraquinone-Functionalized Monolayer-Protected Clusters. *J. Phys. Chem. B* **1999**, *103*, 4440−4446.
(455) Miles, D. T.; Murray, R. W. Redox and Double-Layer Charging of Phenothiazine Functionalized Monolayer-Protected Clusters. *Anal. Chem.* **200**1, *73*, 921−929.
(456) Brousseau, L. C., III; Zhao, D. A.; Shulz, D. A.; Felheim, D. L. p*H*-Gated Single-Electron Tunneling in Chemically Modified Gold Nanoclusters. *J. Am. Chem. Soc.* **1998**, *120*, 7645−7646.
(457) Nakai, H.; Yoshihara, M.; Fujihara, H. New Electroactive Tetrathiafulvalene-Derivatized Gold Nanoparticles and Their Remarkably Stable Nanoparticle Films on Electrodes. *Langmuir* **1999**, *15*, 8574−8576.
(458) Chen, S.; Huang, K. Electrochemical and Spectroscopic Studies of Nitrophenyl Moieties Immobilized on Gold Nanoparticles. *Langmuir* **2000**, *16*, 2014−2018.
(459) Chandrasekharan, N.; Kamat, P. V. Improving the Photoelectrochemical Performance of Nanostructured TiO_2 Films by Adsorption of Gold Nanoparticles. *J. Phys. Chem. B* **2000**, *104*, 10851−10857.
(460) (a) Sudeep, P. K.; Ipe, B. I.; Thomas, K. G.; George, M. V.; Barazzouk, S.; Hotchandani, S.; Kamat, P. V. Fullerene-Functionalized Gold Nanoparticles. A Self-Assembled Photoactive Antenna-Metal Nanocore Assembly. *Nano Lett.* **2002**, *2*, 29−35. (b) Thomas, K. G.; Ipe, B. I.; Sudeep, P. K. Photochemistry of Chromophore-Functionalized Gold Nanoparticles. *Pure Appl. Chem.* **2002**, *74*, 1731−1738.
(461) (a) Kamat, P. V. Photophysical, Photochemical and Photocatalytic Aspects of Metal Nanoparticles. *J. Phys. Chem. B* **2002**, *2*, 7729−7744. (b) Dawson, A.; Kamat, P. V. Semiconductor-Metal Nanocomposites. Photoinduced Fusion and Photocatalysis of Gold-Capped TiO_2 (TiO_2/Gold) Nanoparticles. *J. Phys. Chem. B* **2001**, *105*, 960−966.
(462) Hu, J.; Zhang, J.; Liu, F.; Kittredge, K.; Whitesell, J. K.; Fox, M. A. Competitive Photochemical Reactivity in a Self-Assembled Monolayer on a Colloidal Gold Cluster. *J. Am. Chem. Soc.* **2001**, *123*, 1464−1470.
(463) Wang, G.; Zhang, J.; Murray, R. W. DNA Binding of an Ethidium Intercalator Attached to a Monolayer-Protected Gold Cluster. *Anal. Chem.* **2002**, *74*, 4320−4327.
(464) Aguila, A.; Murray, R. W. Monolayer-Protected Clusters with Fluorescent Dansyl Ligands. *Langmuir* **2000**, *16*, 5949−5964.
(465) Ipe, B. I.; Thomas, K. G.; Barazzouk, S.; Hotchandani, S.; Kamat, P. V. Photoinduced Charge Separation in a Fluorophore-Gold Nanoassembly. *J. Phys. Chem. B* **2002**, *106*, 18−21.
(466) Evans, S. D.; Johnson, S. R.; Ringsdorf, R.; Williams, L. M.; Wolf, H. Photoswitching of Azobenzene Derivatives Formed on Planar and Colloidal Gold Surfaces. *Langmuir* **1998**, *14*, 6436−6440.
(467) Imahori, H.; Arimura, M.; Hanada, T.; Nishimura, Y.; Yamazaki, I.; Sakata, Y.; Fukuzumi, S. Photoactive Three-Dimensional Monolayers: Porphyrin-Alkanethiolate-Stabilized Gold Clusters. *J. Am. Chem. Soc.* **2001**, *123*, 335−336.
(468) Ionita, P.; Carageorgheopol, A.; Gilbert, B. C.; Chechik, V. EPR Study of a Place-Exchange Reaction on Au Nanoparticles: Two Branches of a Disulfide Molecule Do Not Adsorb Adjacent to Each Other. *J. Am. Chem. Soc.* **2002**, *124*, 9048−9049.
(469) Li, H.; Luk, Y.-Y.; Mrksich, M. Catalytic Asymmetric Dihydroxylation by Gold Colloids Functionalized with Self-Assembled Monolayers. *Langmuir* **1999**, *15*, 4957−4959.
(470) Pasquato, L.; Rancan, F.; Scrimin, P.; Mancin, F.; Frigeri, C. *N*-Methylimidazole-Functionalized Gold Nanoparticles as Catalysts for Cleavage of a Carboxylic Acid Ester. *Chem. Commun.* **2000**, 2253−2254.
(471) Warner, M. G.; Reed, S. M.; Hutchison, J. E. Small, Water-Soluble, Ligand-Stabilized Gold Nanoparticles Synthesized by Interfacial Ligand Exchange Reactions. *Chem. Mater.* **2000**, *12*, 3316−3320.
(472) Gregori, L.; Hainfeld, J. F.; Simon, M. N.; Golbager, D. Binding of Amyloid β Protein to the 20 S Proteasome. *J. Biol. Chem.* **1997**, *272*, 58−62.
(473) Alivisatos, A. P.; Johnsson, K. P.; Peng, X.; Wilson, T. E.; Loweth, C. J.; Bruchez, M. P., Jr.; Schultz, P. G. Organization of Nanocrystal Molecules Using DNA. *Nature* **1996**, *382*, 609−611.
(474) Lipka, J. J.; Hainfeld, J. F.; Wall, J. S. Undecagold Labeling of a Glycoprotein: STEM Visualization of an Undecagoldphosphine Cluster Labeling the Carbohydrate Sites of Human Haptoglobin-Hemoglobin Complex. *J. Ultrastruct. Res.* **1983**, *84*, 120−129.
(475) Templeton, A. C.; Hostetler, M. J.; Warmoth, E. K.; Chen, S.; Hartshorn, C. M.; Krishnamurthy, V. M.; Forbes, M. D. E.; Murray, R. W. Gateway Reactions to Diverse, Polyfunctional Monolayer-Protected Gold Clusters. *J. Am. Chem. Soc.* **1998**, *120*, 4845−4849.
(476) Mandal, T. K.; Fleming, M. S.; Walt, D. R. Preparation of Polymer Coated Gold Nanoparticles by Surface-Confined Living Radical Polymerization at Ambient Temperature. *Nano Lett.* **2002**, *2*, 3−7.
(477) Banerjee, S.; Wong, S. S. Synthesis and Characterization of Carbon Nanotube-Nanocrystal Heterostructures. *Nano Lett.* **2002**, *2*, 195−200.
(478) Liu, J.; Rinzler, A. G.; Dai, H.; Hafner, J. H.; Bradley, R. K.; Boul, P. J.; Lu, A.; Iverson, T.; Shelimov, K.; Huffmann, C. B.; Rodriguez-Macias, F.; Shon, Y.-S.; Lee, T. R.; Colbert, R. E.; Smalley, R. E. Fullerene Pipes. *Science* **1998**, *280*, 1253−1256.
(479) Ronit, H.; Katz, E.; Willner, I. Magneto-Switchable Bioelectrocatalysis. *J. Am. Chem. Soc.* **2000**, *122*, 12053−12054.
(480) Wu, M.; O'Neill, S. A.; Brousseu, L. C.; McConnell, W. P.; Schulz, D. A.; Linderman, R. J.; Feldheim, D. L. Synthesis of Nanometer-Sized Hollow Polymer Capsules from Alkanethiol-Coated Gold Particles. *Chem. Commun.* **2000**, 775−776.
(481) Buining, P. A.; Humbel, B. M.; Philipse, A. P.; Verkleij, A. J. Preparation of Functional Silane-Stabilized Gold Colloids in the (Sub)nanometer Size Range. *Langmuir* **1997**, *13*, 3921−3926.
(482) Pal, A. Photochemical Dissolution of Gold Nanoparticles by Bromine Containing Trihalomethanes (THMs) in an Aqueous Triton X-100 Medium and its Analytical Application. *J. Photochem. Photobiol.* **2001**, *142*, 59−65.
(483) Sastry, M.; Rao, M.; Ganesh, K. N. Electrostatic Assembly of Nanoparticles and Biomacromolecules. *Acc. Chem. Res.* **2002**, *35*, 847−855.
(484) Boal, A. K.; Rotello, V. M. Radial Control of Recognition and Redox Processes with Multivalent Nanoparticle Hosts. *J. Am. Chem. Soc.* **2002**, *124*, 5019−5024.
(485) Fullam, S.; Rao, S. N.; Fitzmaurice, D. Noncovalent Self-Assembly of Silver Nanocrystal Aggregates in Solution. *J. Phys. Chem. B* **2000**, *104*, 6164−6173.
(486) Pawsey, S.; McCormick, M.; De Paul, S.; Graf, R.; Lee, Y. S.; Reven, L.; Spiess, H. W. ^{1}H Fast MAS NMR Studies of Hydrogen-Bonding Interactions in Self-Assembled Monolayers. *J. Am. Chem. Soc.* **2003**, *125*, 4174−4184.
(487) Zheng, W.; Maye, M. M.; Leibowitz, F. L.; Zhong, C.-J. An Infrared Reflectance Spectroscopic Study of a p*H*-tunable Network of Nanoparticles Linked by Hydrogen Bonding. *Analyst* **2000**, *125*, 17−20.
(488) Zhang, F. X.; Zheng, W.; Maye, M. M.; Lou, Y.; Li, H.; Zhong, C.-J. An Infrared Reflection Spectroscopic Assessment of Interfacial Derivatization and Reactivity at Inter-Shell Linked Nanoparticle Films. *Langmuir* **2000**, *16*, 9639−9644.
(489) Yonezawa, T.; Onoue, S.-Y.; Kimizuka, N. Formation of Nanoparticle Arrays at the Interlayer of Aqueous Phosphate Bilayers. *Chem. Lett.* **2002**, 528−529.
(490) Fitzmaurice, D.; Rao, S. N.; Preece, J. A.; Stoddart, J. F.; Wenger, S.; Zaccheroni, N. Heterosupramolecular Chemistry: Programmed Pseudorotaxane Assembly at the Surface of a Nanocrystal. *Angew. Chem., Int. Ed.*. **1999**, *38*, 1147−1150.
(491) Hicks, J. F.; Shon, Y. S.; Murray, R. W. Layer-by-Layer Growth of Polymer/Nanoparticle Films Containing Monolayer-Protected Gold Clusters. *Langmuir* **2002**, *18*, 2288−2294.

(492) Kumar, A.; Mandale, A. B.; Sastry, M. Sequential Electrostatic Assembly of Amine-Derivatized Gold and Carboxylic Acid-Derivatized Silver Colloidal Particles on Glass Substrates. *Langmuir* **2000**, *16*, 6921−6926.
(493) Schmid, G.; Bäumle, M.; Beyer, N. Ordered Two-Dimensional Monolayers of Au_{55} Clusters. *Angew. Chem., Int. Ed.* **2000**, *39*, 181−183.
(494) Boal, A. K.; Rotello, V. M. *Intra*- and *Inter*monolayer Hydrogen Bonding in Amide-Functionalized Alkanethiol Self-Assembled Monolayers on Gold Nanoparticles. *Langmuir* **2000**, *16*, 9527−9532.
(495) Carroll, J. B.; Frankamp, B. L.; Rotello, V. M. Self-Assembly of Gold Nanoparticles Through Tandem Hydrogen Bonding and Polyoligosilsequioxane (POSS)-POSS Recognition Processes. *Chem. Commun.* **2002**, 1892−1893.
(496) Paulini, R.; Frankamp, B. L.; Rotello, V. M. Effects of Branched Ligands on the Structure and Stability of Monolayers on Gold Nanoparticles. *Langmuir* **2002**, *18*, 2368−2373.
(497) Zhang, Z.; Berg, A.; Levanon, H.; Fessenden, R. W.; Meisel, D. On the Interactions of Free Radicals with Gold Nanoparticles. *J. Am. Chem. Soc.* **2003**, *125*, 7959−7963.
(498) Miller, S. R.; Gustowski, D. A.; Chen, Z.-H.; Gokel, G. W.; Echegoyen, L.; Kaifer, A. E. Rationalization of the Unusual Electrochemical Behavior Observed in Lariat Ethers and Other Reducible Macrocyclic Systems. *Anal. Chem.* **1988**, *60*, 2021−2024.
(499) Beer, P. D.; Gale, P. A. Anion Recognition and Sensing: The State of the Art and Future Perspectives. *Angew. Chem., Int. Ed.* **2001**, *40*, 486−516.
(500) Valério, C.; Fillaut, J.-L.; Ruiz, J.; Guitard, J.; Blais, J.-C.; Astruc, D. The Dendritic Effect in Molecular Recognition: Ferrocene Dendrimers and their Use as Supramolecular Redox Sensors for the Recognition of Small Inorganic Anions. *J. Am. Chem. Soc.* **1997**, *119*, 2588−2589.
(501) (a) Lehn, J.-M. *Supramolecular Chemistry: Concepts and Perspectives*; VCH: Weinheim, 1995. (b) Boal, A.; Ilhan, F.; Derouchey, J. E.; Thurn-Albrecht, T.; Russell, T. P.; Rotello, V. Self-assembly of nanoparticles into structured spherical and network aggregates. *Nature* **2000**, *404*, 746−748. (c) Jin, J.; Iyoda, T.; Cao, C.; Song, Y.; Jiang, L.; Li, T. J.; Zhu, D. B. Self-Assembly of Uniform Spherical Aggregates of Magnetic Nanoparticles through π-π Interactions. *Angew. Chem., Int. Ed.* **2001**, *40*, 2135−2138. (d) Liu, J.; Mendoza, S.; Roman, E.; Lynn, M. J.; Xu, R.; Kaifer, A. E. Cyclodextrin-Modified Gold Nanospheres. Host−Guest Interactions at Work to Control Colloidal Properties. *J. Am. Chem. Soc.* **1999**, *121*, 4304−4305. (e) Patil, V.; Mayya, K. S.; Pradhan, S. D.; Satry, M. Evidence for Novel Interdigitated Bilayer Formation of Fatty Acids during Three-Dimensional Self-Assembly on Silver Colloidal Particles. *J. Am. Chem. Soc.* **1997**, *119*, 9281−9282. (f) Caruso, F.; Caruso, R. A.; Mohwald, H. Nanoengineering of Inorganic and Hybrid Hollow Spheres by Colloidal Templating. *Science* **1998**, *282*, 1111−1114. (g) Naka, K.; Itoh, H.; Chujo, Y. Temperature-Dependent Reversible Self-Assembly of Gold Nanoparticles into Spherical Aggregates by Molecular Recognition between Pyrenyl and Dinitrophenyl Units. *Langmuir* **2003**, *19*, 5496−5501. (h) Shenton, W.; Davies, S. A.; Mann, S. Directed Self-Assembly of Nanoparticles into Macroscopic Materials Using Antibody−Antigen Recognition. *Adv. Mater.* **1999**, *11*, 449−452.
(502) Watanabe, S.; Sonobe, M.; Arai, M.; Tazume, Y.; Matsuo, T.; Nakamura, T.; Yoshida, K. Enhanced Optical Sensing of Anions with Amide-Functionalized Gold Nanoparticles. *Chem. Commun.* **2002**, 2866−2867.
(503) (a) Lin, S.-Y.; Liu, S.-W.; Lin, C.-M.; Chen, C.-H. Recognition of Potassium Ion in Water by 15-Crown-5 Functionalized Gold Nanoparticles. *Anal. Chem.* **2002**, *74*, 330−335. (b) Obare, S. O.; Hollowell, R. E.; Murphy, C. J. Sensing Strategy for Lithium Ion Based on Gold Nanoparticles. *Langmuir* **2002**, *18*, 10407−10410.
(504) Kim, Y.; Johnson, R. C.; Hupp, J. T. Gold Nanoparticle-Based Sensing of "Spectroscopically Silent" Heavy Metal Ions. *Nano Lett.* **2001**, *1*, 165−167.
(505) Frankamp, B. L.; Uzun, O.; Ilhan, F.; Boal, A. K.; Rotello, V. M. Recognition-Mediated Assembly of Nanoparticles into Micellar Structures with Diblock Copolylmers. *J. Am. Chem. Soc.* **2002**, *124*, 892−893.
(506) Xu, H.; Käll, M. Modeling the Optical Response of Nanoparticle-Based Surface Plasmon Resonance Sensors. *Sens. Actuators B* **2002**, *87*, 244−249.
(507) (a) Zhang, H.-L.; Evans, S. D.; Henderson, J. R.; Miles, R. E.; Shen, T.-H. Vapour Sensing Using Surface Functionalized Gold Nanoparticles. *Nanotechnology* **2002**, *13*, 439−444. (b) Evans, S. D.; Johnson, S. R.; Cheng, Y. L.; Shen, T. Vapour Sensing Using Hybrid Organic−Inorganic Nanostructured Materials. *J. Mater. Chem.* **2000**, *10*, 183−188. (c) Ozsoz, M.; Erdem, A.; Kerman, K.; Ozkan, D.; Tugrul, B.; Topcuoglu, N.; Ekren, H.; Taylan, M. Electrochemical Genosensor Based on Colloidal Gold Nanoparticles for the Detection of Factor V Leiden Mutation Using Disposable Pencil Graphite Electrodes. *Anal. Chem.* **2003**, *75*, 2181−2187. (d) Liu, J.; Lu, Y. A Colorimetric Lead Biosensor Using DNAzyme-Directed Assembly of Gold Nanoparticles. *J. Am. Chem. Soc.* **2003**, *125*, 6642−6643. (e) Fantuzzi, G.; Pengo, P.; Gomila, R.; Ballester, P.; Hunter, C. A.; Pasquato, L.; Scrimin, P. Multivalent Recognition of bis- and tris-Zn−Porphyrins by *N*-Methylimidazole Functionalized Gold Nanoparticles. *Chem. Commun.* **2003**, 1004−1005.
(508) Mirkin, C. A.; Letsinger, R. L.; Mucic, R. C.; Storhoff, J. J. DNA-Based Method for Rationally Assembling Nanoparticles into Macroscopic Materials. *Nature* **1996**, *382*, 607−609.
(509) Storhoff, J. J.; Mucic, R. C.; Mirkin, C. A. Strategies for Organizing Nanoparticles into Aggregate Structures and Functional Materials. *J. Clust. Sci.* **1997**, *8*, 179−216.
(510) Elghanian, R.; Storhoff, J. J.; Mucic, R. C.; Letsinger, R. L.; Mirkin, C. A. Selective Colorimetric Detection of Polynucleotides Based on the Distance-Dependent Optical Properties of Gold Nanoparticles. *Science* **1997**, *277*, 1078−1081.
(511) (a) Storhoff, J. J.; Elghanian, R.; Mucic, R. C.; Mirkin, C. A.; Letsinger, R. L. One-Pot Colorimetric Differentiation of Polynucleotides with Single Base Imperfections Using Gold Nanoparticle Probes. *J. Am. Chem. Soc.* **1998**, *120*, 1959−1964. (b) Mucic, R. C.; Storhoff, J. J.; Mirkin, C. A.; Letsinger, R. L. DNA-Directed Synthesis of Binary Nanoparticles Network Materials. *J. Am. Chem. Soc.* **1998**, *120*, 12674−12675.
(512) Mitchell, G. P.; Mirkin, C. A.; Letsinger, R. L. Programmed Assembly of DNA Functionalized Quantum Dots. *J. Am. Chem. Soc.* **1999**, *121*, 8122−8123.
(513) Reynolds, R. A.; Mirkin, C. A.; Letsinger, R. L. Homogeneous, Nanoparticle-Based Quantitative Colorimetric Detection of Oligonucleotides. *J. Am. Chem. Soc.* **2000**, *122*, 3795−3796.
(514) Storhoff, J. J.; Lazarides, A. A.; Music, R. C.; Mirkin, C. A.; Letsinger, R. L.; Schatz, G. C. What Controls the Optical Properties of DNA-Linked Gold Nanoparticle Assemblies. *J. Am. Chem. Soc.* **2000**, *122*, 4640−4650.
(515) Taton, T. A.; Mucic, R. C.; Mirkin, C. A.; Letsinger, R. L. The DNA-Mediated Formation of Supramolecular Mono- and Multilayered Nanoparticle Structures. *J. Am. Chem. Soc.* **2000**, *122*, 6305−6306.
(516) Demers, L. M.; Mirkin, C. A.; Mucic, R. C.; Reynolds, R. A., III; Letsinger, R. L.; Elghanian, R.; Viswanadham, G. A Fluorescence-Based Method for Determining the Surface Coverage and Hybridization Efficiency of Thiol-Capped Oligonucleotides Bound to Gold Thin Films and Nanoparticles. *Anal. Chem.* **2000**, *72*, 5535−5541.
(517) Storhoff, J. J.; Mirkin, C. A. Programmed Materials Synthesis with DNA. *Chem. Rev.* **1999**, *99*, 1849−1862.
(518) (a) Lazarides, A. A.; Schatz, G. C. DNA-Linked Metal Nanosphere Materials: Structural Basis for the Optical Properties. *J. Phys. Chem. B* **2000**, *104*, 460−467. (b) Lazarides, A. A.; Schatz, G. C. DNA-Linked Metal Nanosphere Materials: Fourier Transform Solutions for the Optical Response. *J. Chem. Phys.* **2000**, *112*, 2987−2993.
(519) Niemeyer, C. M.; Burger, W.; Peplies, J. Covalent DNA-Streptavidin Conjugates as Building Blocks for Novel Biometallic Nanostructures. *Angew. Chem., Int. Ed.* **199**8, *37*, 2265−2268.
(520) (a) Niemeyer, C. M.; Ceyhan, B.; Gao, S.; Chi, L.; Peschel, S.; Simon, U. Site-Selective Immobilization of Gold Nanoparticles Functionalized with DNA Oligomers. *Colloid Polym. Sci.* **2001**, *279*, 68−72. (b) Peschel, S.; Ceyhan, B.; Niemeyer, C. M.; Gao, S.; Chi, L.; Simon, U. Immobilization of Gold Nanoparticles on Solid Supports Utilizing DNA Hybridization. *Mater. Sci. Eng. C* **2002**, *19*, 47−50.
(521) Hölzel, R.; Gajovic-Eichelmann, N.; Bier, F. F. Oriented and Vectorial Immobilization of Linear M13 dsDNA between Interdigitated Electrodes Towards Single Molecule DNA Nanostructures. *Biosens. Bioelectron.* **2003**, *1*8, 555−564.
(522) Simon, U. In *Metal Clusters in Chemistry*; Braunstein, P., Oro, L., Raithby, P. R., Eds.; Wiley-VCH: Weinheim, 1999; p 1342.
(523) Simon, U.; Schön, G. In *Handbook of Nanostructured Materials and Nanotechnology*; Nalwa, H. S., Ed.; Academic Press: San Diego, 1999; p 131.
(524) Xiao, S.; Liu, F.; Rosen, A. E.; Hainfeld, J. F.; Seeman, N. C.; Musier-Forsyth, K.; Kiehl, R. A. Self-Assembly of Metallic Nanoparticle Arrays by DNA Scaffolding. *J. Nanopart. Res.* **2002**, *4*, 313−317.
(525) Parak, W. J.; Pellegrino, T.; Micheel, C. M.; Gerion, D.; Williams, S. C.; Alivisatos, A. P. Conformation of Oligonucleotides Attached to Gold Nanocrystals Probed by Gel Electrophoresis. *Nano Lett.* **2003**, *3*, 33−36.
(526) Storhoff, J. J.; Elghanian, R.; Mirkin, C. A.; Letsinger, R. L. Sequence-Dependent Stability of DNA-Modified Gold Nanoparticles. *Langmuir* **2002**, *18*, 6666−6670.
(527) Park, S.-J.; Lazarides, A. A.; Mirkin, C. A.; Letsinger, R. L. Directed Assembly of Periodic Materials from Protein and Oligonucleotide-Modified Nanoparticle Building Blocks. *Angew. Chem., Int. Ed.* **2001**, *40*, 2909−2912.

(528) Reynolds, R. A., III; Mirkin, C. A.; Letsinger, R. L. A Gold Nanoparticle/Latex Microsphere-Based Colorimetric Oligonucleotide Detection Methodology. *Pure Appl. Chem.* **2000**, *72*, 229−235.
(529) Li, Z.; Jin, R.; Mirkin, C. A.; Letsinger, R. L. Multiple Thiol-Anchor Capped DNA-Gold Nanoparticle Conjugates. *Nucleic Acids Res.* **2002**, *30*, 1558−1562.
(530) Harnack, O.; Ford, W. E.; Yasuda, A.; Wessels, J. M. Tris(hydroxymethyl)phosphine-Capped Gold Particles Templated by DNA as Nanowire Presursors. *Nano Lett.* **2002**, *2*, 919−923.
(531) Maeda, Y.; Tabata, H.; Kawai, T. Two-Dimensional Assembly of Gold Nanoparticles with a DNA Network Template. *Appl. Phys. Lett.* **2001**, *79*, 1181−1183.
(532) Liu, T.; Tang, J.; Zhao, H.; Deng, Y.; Jiang, L. Particle Size Effect of the DNA Sensor Amplified with Gold Nanoparticles. *Langmuir* **2002**, *18*, 5624−5626.
(533) Sauthier, M. L.; Carroll, R. L.; Gorman, C. B.; Franzen, S. Nanoparticle Layers Assembled through DNA Hybridization: Characterization and Optimization. *Langmuir* **2002**, *18*, 1825−1830.
(534) Han, S.; Lin, J.; Satjapipat, M.; Baca, A. J.; Zhou, F. A Three-Dimensional Heterogeneous DNA Sensing Surface Formed by Attaching Oligodeoxynucleotide-Capped Gold Nanoparticles Onto a Gold-Coated Quartz Crystal. *Chem. Commun.* **2001**, 609−610.
(535) Zhao, H. Q.; Lin, L.; Li, J. R.; Tang, J. A.; Duan, M. X.; Jiang, L. DNA Biosensor with High Sensitivity Amplified by Gold Nanoparticles. *J. Nanopart. Res.* **2001**, *3*, 321−323.
(536) Patolsky, F.; Ranjit, K. T.; Lichtenstein, A.; Willner, I. Dendritic of DNA Analysis by Oligonucleotide-Functionalized Au−Nanoparticles. *Chem. Commun.* **2000**, 1025−1026.
(537) Yonezawa, T.; Onoue, S.-Y.; Kimizuka, N. Metal Coating of DNA Molecules by Cationic, Metastable Gold Nanoparticles. *Chem. Lett.* **2002**, 1172−1173.
(538) Kumar, A.; Pattarkine, M.; Bhadbhade, M.; Mandale, A. B.; Ganesh, K. N.; Datar, S. S.; Dharmadhikari, C. V.; Sastry, M. Linear Superclusters of Colloidal Gold Particles by Electrostatic Assembly on DNA Templates. *Adv. Mater.* **2001**, *13*, 341−344.
(539) (a) Sastry, M.; Kumar, A.; Datar, S.; Dharmadhikari, C. V.; Ganesh, K. DNA-Mediated Electrostatic Assembly of Gold Nanoparticles Into Linear Arrays by a Simple Drop-Coating Procedure. *Appl. Phys. Lett.* **2001**, *78*, 2943−2945. (b) Hussain, N.; Singh, B.; Sakthivel, T.; Florence, A. T. Formulation and Stability of Surface-Tethered DNA-Gold-Dendron Nanoparticles. *Int. J. Pharm.* **2003**, *254*, 27−31. (c) Sato, K.; Hosokawa, K.; Maeda, M. Rapid Aggregation of Gold Nanoparticles Induced by Non-Cross-Linking DNA Hybridization. *J. Am. Chem. Soc.* **2003**, *125*, 8102−8103.
(540) (a) Cao, Y. W. C.; Jin, R.; Mirkin, C. A. Nanoparticles with Raman Spectroscopic Fingerprints for DNA and RNA Detection. *Science* **2002**, *297*, 1536−1540.
(541) (a) Park, S.-J.; Taton, T. A.; Mirkin, C. A. Array-Based Electrical Detection of DNA with Nanoparticle Probes. *Science* **2002**, *295*, 1503−1506. (b) Dong, W.-F.; Sukhorukov, G. B.; Möhwald, H. Enhanced Raman Imaging and Optical Spectra of Gold Nanoparticle Doped Microcapsules. *Phys. Chem. Chem. Phys.* **2003**, *5*, 3003−3012.
(542) Hashimoto, K.; Ito, K.; Ishimori, Y. Sequence-Specific Gene Detection with a Gold Electrode Modified with DNA Probes and an Electrochemically Active Dye. *Anal. Chem.* **1994**, *66*, 3830−3833.
(543) Millan, K. M.; Saraullo, A.; Mikkelsen, S. R. Voltammetric DNA Biosensor for Cystic Fibrosis Based on a Modified Carbon Paste Electrode. *Anal. Chem.* **1994**, *66*, 2943−2948.
(544) (a) Wang, J.; Song, F.; Zhou, F. Silver-Enhanced Imaging of DNA Hybridization at DNA Microarrays with Scanning Electrochemical Microscopy. *Langmuir* **2002**, *18*, 6653−6658. (b) Iacopino, D.; Ongaro, A.; Nagle, L.; Eritja, R.; Fitzmaurice, D. Imaging the DNA and Nanoparticle Components of a Self-Assembled Nanoscale Architecture. *Nanotechnology* **2003**, *14*, 447−452.
(545) Cai, H.; Wang, Y.; He, P.; Fang, Y. Electrochemical Detection of DNA Hybridisation Based on Silver-Enhanced Gold Nanoparticle Label. *Anal. Chim. Acta* **2002**, *469*, 165−172.
(546) Wang, J.; Xu, D.; Kawde, A.-N.; Polsky, R. Metal Nanoparticle-Based Electrochemical Stripping Potentiometric Detection of DNA Hybridization. *Anal. Chem.* **2001**, *73*, 5576−5581.
(547) Gearheart, L. A.; Ploehn, H. J.; Murphy, C. J. Oligonucleotide Adsorption to Gold Nanoparticles: A Surface-Enhanced Raman Spectroscopy Study of Intrinsically Bent DNA. *J. Phys. Chem. B* **2001**, *105*, 12609−12615.
(548) Csáki, A.; Möller, R.; Straube, W.; Köhler, J. M.; Fritzsche, W. DNA Monolayer on Gold Substrates Characterized by Nanoparticle Labeling and Scanning Force Microscopy. *Nucleic Acids Res.* **2001**, *29*, 1−5.
(549) (a) Bogatyrev, V. A.; Dykman, L. A.; Krasnov, Ya. M.; Plotnikov, V. K.; Khlebtsov, N. G. Differential Light Scattering Spectroscopy for Studying Biospecific Assembling of Gold Nanoparticles with Protein or Oligonucleotide Probes. *Colloid J.* **2002**, *64*, 671−680. (b) Su, M.; Li, S.; Dravid, V. P. Microcantilever Resonance-Based DNA Detection with Nanoparticle Probes. *Appl. Phys. Lett.* **2003**, *82*, 3562−3564. (c) Liu, T.; Tang, J.; Han, M.; Jiang, L. A Novel Microgravimetric DNA Sensor with High Sensivity. *Biochem. Biophys. Res. Commun.* **2003**, *304*, 98−100. (d) Glynou, K.; Ioannou, P. C.; Christopoulos, T. K.; Syriopoulou, V. Oligonucleotide-Functionalized Gold Nanoparticles as Probes in a Dry-Reagent Strip Biosensor for DNA Analysis by Hybridization. *Anal. Chem.* **2003**, *75*, 4155−4160. (e) Wang, J.; Li, J.; Baca, A.; Hu, J.; Zhou, F.; Yan, W.; Pang, D.-W. Amplified Voltammetric Detection of DNA Hybridization via Oxidation of Ferrocene Caps on Gold Nanoparticles/Streptavidin Conjugates. *Anal. Chem.* **2003**, *75*, 3941−3945. (f) Sandström, P.; Boncheva, M.; Åkerman, B. *Langmuir* **2003**, *19*, 6066−6071. (g) Zheng, M.; Davidson, F.; Huang, X. Ethylene Glycol Monolayer Protected Nanoparticles for Eliminating Nonspecific Binding with Biological Molecules. *J. Am. Chem. Soc.* **2003**, *125*, 7790−7791.
(550) Natan, M. J.; Lyon, L. A. Surface Plasmon Resonnance Biosensing with Colloidal Au Amplification. In *Metal Nanoparticles—Synthesis, Characterization and Applications*; Feldheim, D. L., Colby, A. F., Jr., Eds.; Marcel Dekker: New York, 2002; pp 183−205.
(551) Thanh, N. T. K.; Rosenzweig, Z. Development of an Aggregation-Based Immunoassay for Anti-Protein A Using Gold Nanoparticles. *Anal. Chem.* **2002**, *74*, 1624−1628.
(552) Zhang, C.; Zhang, Z.; Yu, B.; Shi, J.; Zhang, X. Application of the Biological Conjugate between Antibody and Colloid Au Nanoparticles as Analyte to Inductively Coupled Plasma Mass Spectrometry. *Anal. Chem.* **2002**, *74*, 96−99.
(553) Schneider, B. H.; Dickinson, E. L.; Vach, M. D.; Hoijer, J. V.; Howard, L. V. Highly Sensitive Optical Chip Immunoassays in Human Serum. *Biosens. Bioelectron.* **2000**, *15*, 13−22.
(554) Schneider, B. H.; Dickinson, E. L.; Vach, M. D.; Hoijer, J. V.; Howard, L. V. Optical Chip Immunoassay for hCG in Human Whole Blood. *Biosens. Bioelectron.* **2000**, *15*, 497−604.
(555) Niemeyer, C. M. Nanoparticles, Proteins, and Nucleic Acids: Biotechnology Meets Materials Science. *Angew. Chem., Int. Ed.* **2001**, *40*, 4128−4158.
(556) Taton, T. A. Nanostructures as Tailored Biological Probes. *Trends Biotechnol.* **2002**, *20*, 277−279.
(557) Lin, C.-C.; Yeh, Y.-C.; Yang, C.-Y.; Chen, C.-L.; Chen, G.-F.; Chen, C.-C.; Wu, Y.-C. Selective Binding of Mannose-Encapsulated Gold Nanoparticles to Type 1 Pili in *Escherichia coli*. *J. Am. Chem. Soc.* **2002**, *124*, 3508−3509.
(558) De la Fuente, J. M.; Barrientos, A. G.; Rojas, T. C.; Rojo, J.; Cañada, A.; Fernandez, A.; Penadés, S. Gold Glyconanoparticles as Water-Soluble Polyvalent Models To Study Carbohydrate Interactions. *Angew. Chem., Int. Ed. Engl.* **2001**, *40*, 2257−2261.
(559) Rojas, T. C.; de la Fuente, J. M.; Barrientos, A. G.; Penadés, S.; Ponsonnet, L.; Fernández, A. Gold Glyconanoparticles as Building Blocks for Nanomaterials Design. *Adv. Mater.* **2002**, *14*, , 585−588.
(560) Esumi, K.; Hosoya, T.; Suzuki, A.; Torigoe, K. Spontaneous Formation of Gold Nanoparticles in Aqueous Solution of Sugar-Persubstituted Poly(amidoamine)dendrimers. *Langmuir* **2000**, *16*, 2978−2980.
(561) (a) Wilson, R. Haptenylated Mercaptodextran-Coated Gold Nanoparticles for Biomolecular Assays. *Chem. Commun.* **2003**, 108−109. (b) Hone, D. C.; Haines, A. H.; Russell, D. A. Rapid, Quantitative Colorimetric Detection of a Lectin Using Mannose-Stabilized Gold Nanoparticles. *Langmuir* **2003**, *19*, 7141−7144. (c) Nolting, B.; Yu, J.-J.; Liu, G-y.; Cho, S.-J.; Kauzlarich, S.; Gervay-Hague, J. Synthesis of Gold Glyconanoparticles and Biological Evaluation of Recombinant Gp 120 Interactions. *Langmuir* **2003**, *19*, 6465−6473.
(562) Chow, G. M.; Markowitz, M. A.; Rayne, R.; Dunn, D. N.; Singh, A. Phospholipid Mediated Synthesis and Characterization of Gold Nanoparticles. *J. Colloid Interface Sci.* **1996**, *183*, 135−142.
(563) Burkett, S. L.; Mann, S. Spatial Organization and Patterning of Gold Nanoparticles on Self-Assembled Biolipid Tubular Templates. *Chem. Commun.* **1996**, 321−322.
(564) Forstner, M. B.; Käs, J.; Martin, D. Single Lipid Diffusion in Langmuir Monolayers. *Langmuir* **2001**, *17*, 567−570.
(565) (a) Rautaray, D.; Kumar, A.; Reddy, S.; Sainkar, S. R.; Sastry, M. Morphology of $BaSO_4$ Crystals Grown on Templates of Varying Dimensionality: The Case of Cysteine-Capped Gold Nanoparticles (0-D), DNA (1-D), and Lipid Bilayer Stacks (2-D). *Cryst. Growth Des.* **2002**, *2*, 197−203. (b) Bhattacharya, S.; Srivastava, A. Synthesis and Characterization of Novel Cationic Lipid and Cholesterol-Coated Gold Nanoparticles and Their Interactions with Dipalmitoylphosphatidylcholine Membranes. *Langmuir* **2003**, *19*, 4439−4447.
(566) Wong, M. S.; Cha, J. N.; Choi, K.-S.; Deming, T. J.; Stucky, G. D. Assembly of Nanoparticles into Hollow Spheres Using Block Copolypeptides. *Nano Lett.* **2002**, *2*, 583−587.
(567) (a) Pengo, P.; Broxterman, Q. B.; Kaptein, B.; Pasquato, L.; Scrimin, P. Synthesis of a Stable Helical Peptide and Grafting on Gold Nanoparticles. *Langmuir* **2003**, *19*, 2521−2524. (b) Fan, J.; Chen, S.; Gao, Y. Coating Gold Nanoparticles with Peptide

Molecules via a Peptide Elongation Approach. *Colloids Surf.* **2003**, *28*, 199−207.
(568) Templeton, A. C.; Chen, S.; Gross, S. M.; Murray, R. W. Water-Soluble, Isolable Gold Clusters Protected by Tiopronin and Coenzyme A Monolayers. *Langmuir* **1999**, *15*, 66−76.
(569) Templeton, A. C.; Cliffel, D. E.; Murray, R. W. Redox and Fluorophore Functionalization of Water-Soluble, Tiopronin-Protected Gold Clusters. *J. Am. Chem. Soc.* **1999**, *121*, 7081−7089.
(570) Boal, A. K.; Rotello, V. M. Fabrication and Self-Optimization of Multivalent Receptors on Nanoparticle Scaffolds. *J. Am. Chem. Soc.* **2000**, *122*, 734−735.
(571) Boal, A. K.; Rotello, V. M. Redox-Modulated Recognition of Flavin by Functionalized Gold Nanoparticles. *J. Am. Chem. Soc.* **1999**, *121*, 4914−4915.
(572) Schroedter, A.; Weller, H. Ligand Design and Bioconjugation of Colloidal Gold Nanoparticles. *Angew. Chem., Int. Ed.* **2002**, *41*, 3218−3221.
(573) Grabar, C. C.; Freeman, R. G.; Hommer, M. B.; Natan, M. J. Preparation and Characterization of Au Colloid Monolayers. *Anal. Chem.* **1995**, *67*, 735−743.
(574) Su, X.; Yau Li, S. F.; O'Shea, S. J. Au Nanoparticle- and Silver-Enhancement Reaction-Amplified Microgravimetric Biosensor. *Chem. Commun.* **2001**, 755−756.
(575) Himmelhaus, M.; Takei, H. Cap-Shaped Gold Nanoparticles for an Optical Biosensor. *Sens. Actuators B* **2000**, *63*, 24−30.
(576) Bharathi, S.; Lev, O. Sol−Gel-Derived Nanocrystalline Gold-Silicate Composite Biosensor. *Anal. Commun.* **1998**, *35*, 29−31.
(577) Gole, A.; Dash, C.; Soman, C.; Sainkar, S. R.; Rao, M.; Sastry, M. On the Preparation, Characterization, and Enzymatic Activity of Fungal Protease-Gold Colloid Bioconjugates. *Bioconjugate Chem.* **2001**, *12*, 684−690.
(578) Jia, J.; Wang, B.; Wu, A.; Cheng, G.; Li, Z.; Dong, S. A Method to Construct a Third-Generation Horseradish Peroxidase Biosensor: Self-Assembling Gold Nanoparticles to Three-Dimensional Sol−Gel Network. *Anal. Chem.* **2002**, *74*, 2217−2223.
(579) Hone, D. C.; Walker, P. I.; Evans-Gowing, R.; FitzGerald, S.; Beeby, A.; Chambrier, I.; Cook, M. J.; Russell, D. A. Generation of Cytotoxic Singlet Oxygen via Phthalocyanine-Stabilized Gold Nanoparticles; A Potential Delivery Vehicle for Photodynamic Therapy. *Langmuir* **2002**, *18*, 2985−2987.
(580) Gardea-Torresdey, J. L.; Parsons, J. G.; Gomez, E.; Peralta-Videa, J.; Troiani, H. E.; Santiago, P.; Yacaman, M. J. Formation and Growth of Au Nanoparticles inside Live Alfalfa Plants. *Nano Lett.* **2002**, *2*, 397−401.
(581) Mukherjee, P.; Ahmad, A.; Mandal, D.; Senapati, S.; Sainkar, S. R.; Khan, M. I.; Ramani, R.; Parischa, R.; Ajayakumar, P. V.; Alam, M.; Sastry, M.; Kumar, R. Bioreduction of $AuCl_4^-$ Ions by the Fungus, *Verticillium sp.* and Surface Trapping of the Gold Nanoparticles Formed. *Angew. Chem., Int. Ed.* **2001**, *40*, 3585−3588.
(582) (a) Hillyer, J. F.; Albrecht, R. M. Gastrointestinal Persorption and Tissue Distribution of Differently Sized Colloidal Gold Nanoparticles. *J. Pharm. Sci.* **2001**, *90*, 1927−1936. (b) Gardea-Torresdey, J. L.; Tiemann, K. J.; Dokken, K.; Tehuacanero, S.; José-Yacamán, M. Gold Nanoparticles Obtained by Bio-Precipitation from Gold (III) Solutions. *J. Nanopart. Res.* **1999**, *1*, 397−404. (c) Mukherjee, P.; Senapati, S.; Mandal, D.; Ahmad, A.; Khan, M. I.; Kumar, R.; Sastry, M. Extracellular Synthesis of Gold Nanoparticles by the Fungus *Fusarium oxysporum*. *ChemBioChem* **2002**, 461−463.
(583) (a) Mukhopadhyay, K.; Phadtare, S.; Vinod, V. P.; Kumar, A.; Rao, M.; Chaudhari, R. V.; Sastry, M. Gold Nanoparticles Assembled on Amine-Functionalized Na−Y Zeolite: A Biocompatible Surface for Enzyme Immobilization. *Langmuir* **2003**, *19*, 3858−3863. (b) Phadtare, S.; Kumar, A.; Vinod, V. P.; Dash, C.; Palaskar, D. V.; Rao, M.; Shukla, P. G.; Sivaram, S.; Sastry, M. Direct Assembly of Gold Nanoparticle "Shells" on Polyurethane Microsphere "Cores" and Their Application as Enzyme Immobilization Templates. *Chem. Mater.* **2003**, *15*, 1944−1949. (c) Dragnea, B.; Chen, C.; Kwak, E.-S.; Stein, B.; Kao, C. C. Gold Nanoparticles as Spectroscopic Enhancers for in Vitro Studies on Single Viruses. *J. Am. Chem. Soc.* **2003**, *125*, 6374−6375.
(584) (a) Rautaray, D.; Kumar, A.; Reddy, S.; Sainkar, S. R.; Sastry, M. Morphology of $BaSO_4$ Crystals Grown on Templates of Varying Dimensionality: The Case of Cysteine-Capped Gold Nanoparticles (0-D), DNA (1-D), and Lipid Bilayer Stacks (2-D). *Cryst. Growth Des.* **2002**, *2*, 197−203. (b) Tchachenko, A. G.; Xie, H.; Coleman, D.; Glomm, W.; Ryan, J.; Anderson, M. F.; Franzen, S.; Feldheim, D. L. Multifunctional Gold Nanoparticle-Peptide Complexes for Nuclear Targeting. *J. Am. Chem. Soc.* **2003**, *125*, 4700−4701. (c) Li, Z.; Chung, S.-W.; Nam, J.-M.; Ginger, D. S.; Mirkin, C. A. Living Templates for the Hierarchical Assembly of Gold Nanoparticles. *Angew. Chem., Int. Ed.* **2003**, *42*, 2306−2309. (d) Shankar, S. S.; Ahmad, A.; Pasricha, R.; Sastry, M. Bioreduction of Chloroautate ions by Geranium Leaves and its Endophytic Fungus Yields Gold Nanoparticles of Different Shapes. *J. Mater. Chem.* **2003**, *13*, 1822−1826.
(585) Cha, D. Y.; Parravano, G. Surface Reactivity of Supported Gold. I. Oxygen Transfer Between Carbon Monoxide and Carbon Dioxide. *J. Catal.* **1970**, *18*, 200−211.
(586) Parravano, G. Surface Reactivity of Supported Gold. II. Hydrogen Transfer Between Benzene and Cyclohexane. *J. Catal.* **1970**, *18*, 320−328.
(587) Schwank, J.; Galvano, S.; Parravano, G. Isotopic Oxygen Exchange on Supported Ruthenium and Gold Catalysts. *J. Catal.* **1980**, *63*, 415−424.
(588) Galvagno, S.; Parravano, G. Chemical Reactivity of Supported Gold. IV. Reduction of Nitric Oxide by Hydrogen. *J. Catal.* **1978**, *55*, 178−190.
(589) (a) Haruta, M.; Kobayashi, T.; Sano, H.; Yamada, N. Novel Gold Catalysts for the Oxidation of Carbon Monoxide at a Temperature far below 0 °C. *Chem. Lett.* **1987**, 405−406. (b) Haruta, M.; Yamada, N.; Kobayashi, T.; Ijima, S. Gold Catalysts Prepared by Coprecipitation for Low-Temperature Oxidation of Hydrogen and of Carbon Monoxide. *J. Catal.* **1989**, *115*, 301−309.
(590) Haruta, M. Size- and Support-Dependency in the Catalysis of Gold. *Catal. Today* **1997**, *36*, 153−166.
(591) Ueda, A.; Oshima, T.; Haruta, M. Reduction of Nitrogen Monoxide with Propene in the Presence of Oxygen and Moisture Over Gold Supported on Metal Oxides. *Appl. Catal. B* **1997**, *12*, 81−93.
(592) Andreeva, D.; Tabakova, T.; Idakiev, V.; Chistov, P.; Giovanoli, R. $Au-Fe_2O_3$ Catalyst for Water-Gas Shift Reaction Prepared by Deposition-Precipitation. *Appl. Catal. A* **1998**, *169*, 9−14.
(593) Sakurai, H.; Haruta, M. Synergism in Methanol Synthesis from Carbon Dioxide Over Gold Catalysts Supported on Metal Oxides. *Catal. Today* **1996**, *29*, 361−365.
(594) Valden, M.; Lai, X.; Goodman, D. W. Onset of Catalytic Activity of Gold Clusters on Titania with the Appearance of Nonmetallic Properties. *Science* **1998**, *281*, 1647−1650.
(595) Haruta, M.; Ueda, A.; Tsubota, S.; Torres Sanchez, R. M. Low-Temperature Catalytic Combustion of Methanol and its Decomposed Derivatives Over Supported Gold Catalysts. *Catal. Today* **1996**, *29*, 443−447.
(596) Yuan, Y.; Asakura, K.; Wan, H.; Tsai, K.; Iwasawa, Y. Supported Gold Catalysts Derived from Gold Complexes and As−Precipitated Metal Hydroxides, Highly Active for Low-Temperature CO Oxidation. *Chem. Lett.* **1996**, *9*, 755−756.
(597) Kozlova, P.; Kozlov, I.; Sugiyama, S.; Matsui, Y.; Asakura, K.; Iwasawa, Y. Study of Gold Species in Iron-Oxide-Supported Gold Catalysts Derived from Gold-Phosphine Complex $Au(PPh_3)(NO_3)$ and As−Precipitated Wet $Fe(OH)_3$. *J. Catal.* **1999**, *181*, 37−48.
(598) Wagner, F. E.; Galvano, S.; Milone, C.; Visco, A. M. Mössbauer Characterization of Gold/Iron Oxide Catalysts. *J. Chem. Soc., Faraday Trans.* **1997**, *93*, 3403−3409.
(599) Minico, S.; Sciere, S.; Crisafulli, C.; Visco, A. M.; Galvano, S. FT-IR Study of Au/Fe_2O_3 Catalysts for CO Oxidation at Low Temperature. *Catal. Lett.* **1997**, *47*, 273−276.
(600) Guillemot, D.; Borovkov, V. B.; Polisset-Thofin, M.; Fraissard, J. Surface Characterization of Au/HY by ^{129}Xe NMR and Diffuse Reflectance IR Spectroscopy of Adsorbed CO. Formation of Electron-Deficient Gold Particles Inside HY Cavities. *J. Chem. Soc., Faraday Trans.* **1997**, *93*, 3587−3591.
(601) Salmama, T. M.; Ohnishi, R.; Shido, T.; Ichikawa, M. Highly Selective Catalytic Reduction of NO by H_2 over Au(0) and Au(I) Impregnated in NaY Zeolite Catalysts. *J. Catal.* **1996**, *162*, 169−178.
(602) Cunningham, D. A.; Vogel, W.; Kageyama, H.; Tsubota, S.; Haruta, M. The Relationship Between the Structure and Activity of Nanometer Size Gold When Supported on $Mg(OH)_2$. *J. Catal.* **1998**, *177*, 1−10.
(603) Haruta, M. Novel Catalysis of Gold Deposited on Metal Oxides. *Catal. Surveys Jpn.* **1997**, *1*, 61−73.
(604) Schubert, M. M.; Hacjenberg, S.; van Vee, A. C.; Muhler, M.; Plzak, V.; Behm, R. CO Oxidation over Supported Gold Catalysts-"Inert" and "Active" Support Materials and Their Role for the Oxygen Supply during Reaction. *J. Catal.* **2001**, *197*, 113−122.
(605) Haruta, M.; Daté, M. Advances in the Catalysis of Au Nanoparticles. *Appl. Catal. A* **2001**, *222*, 427−437.
(606) Bera, P.; Hedge, M. S. Characterization and Catalytic Properties of Combustion Synthesized Au/CeO_2 Catalyst. *Catal. Lett.* **2002**, *79*, 75−81.
(607) (a) Bond, G. C.; Thompson, D. T. Catalysis by Gold. *Catal. Rev.-Sci. Eng.* **1999**, *41*, 319−388. (b) Bond, G. C.; Thompson, D. T. Gold-Catalyzed Oxidation of Carbon Monoxide. *Gold Bull.* **2000**, *33*, 41−51. (c) Fan, L.; Ichikuni, N.; Shimazu, S.; Uematsu, T. Preparation of Au/TiO_2 Catalysts by Suspension Spray Reaction Method and Their Catalytic Property for CO Oxidation. *Appl. Catal.* **2003**, *246*, 87−95.
(608) Kozlov, A. I.; Kozlova, A. P.; Liu, H.; Iwasawa, Y. A New Approach to Active Supported Au Catalysts. *Appl. Catal. A* **1999**, *182*, 9−28.
(609) Serna, R.; Missana, T.; Afonso, C. N.; Ballesteros, J. M.; Petford-Long, A. K.; Doole, R. C. Bi Nanocrystals Embedded in an

Amorphous Ge Matrix Grown by Pulsed Laser Deposition. *Appl. Phys. A* **1998**, *66*, 43−47.
(610) Horváth, D.; Tóth, L.; Guczi, L. Gold Nanoparticles: Effect of Treatment on Structure and Catalytic Activity of Au/Fe_2O_3 Catalyst Prepared by Co−Precipitation. *Catal. Lett.* **2000**, *67*, 117−128.
(611) Guczi, L.; Horváth, D.; Pászti, Z.; Tóth, L.; Horváth, Z. E.; Karacs, A.; Petõ, G. Modeling Gold Nanoparticles: Morphology, Electron Structure, and Catalytic Activity in CO Oxidation. *J. Phys. Chem. B* **2000**, *104*, 3183−3193.
(612) Guczi, L.; Horváth, D.; Pászti, Z.; Petõ, G. Effect of Treatments on Gold Nanoparticles Relation Between Morphology, Electron Structure and Catalytic Activity in CO Oxidation. *Catal. Today* **2002**, *72*, 101−105.
(613) Petó, G.; Molnár, G. L.; Pászti, Z.; Geszti, O.; Beck, A.; Guczi, L. Electronic Structure of Gold Nanoparticles Deposited on SiO/Si(100). *Mater. Sci. Eng. C* **2002**, *19*, 95−99.
(614) Guczi, L.; Petö, G.; Beck, A.; Frey, K.; Geszti, O.; Molnár, G.; Daróczi, C. Gold Nanoparticles Deposited on SiO_2/Si(100): Correlation Between Size, Electron Structure, and Activity in CO Oxidation. *J. Am. Chem. Soc.* **2003**, *125*, 4332−4337.
(615) Kawasaki, T.; Takai, Y.; Shimizu, R. Distorted Surface and Interface Structures of Catalytic Gold Nanoparticles Observed by Spherical Aberration-Free Phase Electron Microscopy. *Appl. Phys. Lett.* **2001**, *79*, 3509−3511.
(616) Finch, R. M.; Hodge, N. A.; Hutchings, G. J.; Meagher, A.; Pankhurst, Q. A.; Siddiqui, M. R. H.; Wagner, F. E.; Whyman, R. Identification of Active Phases in Au−Fe Catalysts for Low-Temperature CO Oxidation. *Phys. Chem. Chem. Phys.* **1999**, *1*, 485−489.
(617) Okumura, M.; Tsubota, S.; Iwamoto, M.; Haruta, M. Chemical Vapor Deposition of Gold Nanoparticles on MCM-41 and Their Catalytic Activities for the Low-Temperature Oxidation of CO and of H_2. *Chem. Lett.* **1998**, 315−316.
(618) Schimpf, S.; Lucas, M.; Mohr, C.; Rodemerck, U.; Brückner, A.; Radnik, J.; Hofmeister, H.; Claus, P. Supported Gold Nanoparticles: in Depth Catalyst Characterization and Application in Hydrogenation and Oxidation Reactions. *Catal. Today* **2002**, *72*, 63−78.
(619) Grunwaldt, J.-D.; Kiener, C.; Wogerbauer, C.; Baiker, A. Preparation of Supported Gold Catalysts for Low-Temperature CO Oxidation via "Size-Controlled" Gold Colloids. *J. Catal.* **1999**, *181*, 223−232.
(620) Boccuzzi, C. A.; Manzola, M. Au/TiO_2 Nanostructured Catalyst: Effects of Gold Particle Sizes on CO Oxidation at 90 K. *Mater. Sci. Eng. C* **2001**, *15*, 215−217.
(621) Sayo, K.; Deki, S.; Hayashi, S. Novel Method for Preparation of a Nanosized Gold Catalyst Supported on TiO_2. *J. Colloid Interface Sci.* **1999**, *212*, 597−599.
(622) Cataliotti, R. S.; Compagnini, G.; Crisafulli, C.; Minicò, S.; Pignataro, B.; Sassi, P.; Scirè, S. Low-Frequency Raman Modes and Atomic Force Microscopy for the Size Determination of Catalytic Gold Clusters Supported on Iron Oxide. *Surf. Sci.* **2001**, *494*, 75−82.
(623) Franceschetti, A.; Pennycook, S. J.; Pantelides, S. T. Oxygen Chemisorption on Au Nanoparticles. *Chem. Phys. Lett.* **2003**, *374*, 471−475.
(624) Maye, M. M.; Lou, Y.; Zhong, C.-J. Core−Shell Gold Nanoparticle Assembly as Novel Electrocatalyst of CO Oxidation. *Langmuir* **2000**, *16*, 7520−7523.
(625) Lou, Y.; Maye, M. M.; Han, L.; Luo, J.; Zhong, C. J. Gold−Platinum Alloy Nanoparticle Assembly as Catalyst for Methanol Electrooxidation. *Chem. Commun.* **2001**, 473−474.
(626) Luo, J.; Maye, M. M.; Lou, Y.; Han, L.; Hepel, M.; Zhong, C. J. Catalytic Activation of Core−Shell Assembled Gold Nanoparticles as Catalyst for Methanol Electrooxidation. *Catal. Today* **2002**, *77*, 127−138.
(627) (a) Luo, J.; Lou, Y.; Maye, M. M.; Zhong, C. J.; Hepel, M. An EQCN Assessment of Electrocatalytic Oxidation of Methanol at Nanostructured Au−Pt Alloy Nanoparticles. *Electrochem. Commun.* **2001**, *3*, 172−176. (b) Jaramillo, T. F.; Baeck, S.-H.; Cuenya, B. R.; McFarland, E. W. Catalytic Activity of Supported Au Nanoparticles Deposited from Block Copolymer Micelles. *J. Am. Chem. Soc.* **2003**, *125*, 7148−7149.
(628) (a) Zhong, C.-J.; Maye, M. M. Core−Shell Assembled Nanoparticles as Catalysts. *Adv. Mater.* **2001**, *13*, n° 19, 1507−1511. (b) Zhang, Y.; Asahina, S.; Yoshihara, S.; Shirakashi, T. Oxygen Reduction on Au Nanoparticle Deposited Boron-Doped Diamond Films. *Electrochim. Acta* **2003**, *48*, 741−747.
(629) El-Deab, M. S.; Ohsaka, T. An Extraordinary Electrocatalytic Reduction of Oxygen on Gold Nanoparticles-Electrodeposited Gold Electrodes. *Electrochem. Commun.* **2002**, *4*, 288−292.
(630) Claus, P.; Brückner, A.; Mohr, C.; Hofmeister, H. Supported Gold Nanoparticles from Quantum Dot to Mesoscopic Size Scale: Effect of Electronic and Structural Properties on Catalytic Hydrogenation of Conjugated Functional Groups. *J. Am. Chem. Soc.* **2000**, *122*, 11430−11439.
(631) Mohr, C.; Hofmeister, H.; Claus, P. The Influence of Real Structure of Gold Catalysts in the Partial Hydrogenation of Acrolein. *J. Catal.* **2002**, *213*, 86−94.
(632) Mohr, C.; Hofmeister, H.; Radnik, J.; Claus, P. Identification of Active Sites in Gold-Catalyzed Hydrogenation of Acrolein. *J. Am. Chem. Soc.* **2003**, *125*, 1905−1911.
(633) Mukherjee, P.; Patra, C. R.; Ghosh, A.; Kumar, R.; Sastry, M. Characterization and Catalytic Activity of Gold Nanoparticles Synthesized by Autoreduction of Aqueous Chloroaurate Ions with Fumed Silica. *Chem. Mater.* **2002**, *14*, 1678−1684.
(634) Bartz, M.; Küther, J.; Seshadri, R.; Tremel, W. Colloid-Bound Catalysts for Ring-Opening Metathesis Polymerization: A Combination of Homogeneous and Heterogeneous Properties. *Angew. Chem., Int. Ed.* **1998**, *37*, 2466−2468.
(635) Kapoor, M. P.; Sinha, A. K.; Seelan, S.; Inagaki, S.; Tsubota, S.; Hoshida, H.; Haruta, M. Hydrophobicity Induced Vapor-Phase Oxidation of Propene Over Gold Supported on Titanium Incorporated Hybrid Mesoporous Silsesquioxane. *Chem. Commun.* **2002**, 2902−2903.
(636) Bianchi, C. L.; Porta, F.; Prati, L.; Rossi, M. Selective Liquid-Phase Oxidation Using Gold Catalysts. *Topics Catal.* **2000**, *13*, 231−236.
(637) Porta, F.; Prati, L.; Rossi, M. Metal Sols as a Useful Tool for Heterogeneous Gold Catalyst Preparation: Reinvestigation of a Liquid-Phase Oxidation. *Catal. Today* **2000**, *61*, 165−172.
(638) Li, X.-M.; Paraschiv, V.; Huskens, J.; Reinhoudt, D. N. Sulfonic Acid-Functionalized Gold Nanoparticles: A Colloid-Bound Catalyst for Soft Lithographic Application on Self-Assembled Monolayers. *J. Am. Chem. Soc.* **2003**, *125*, 4279−4284.
(639) (a) Troiani, H. E.; Camacho-Bragado, A.; Armendariz, V.; Torresday, J. L. G.; Yacaman, M. J. Synthesis of Carbon Anions by Gold Nanoparticles and Electron Irradiation. *Chem. Mater.* **2003**, *15*, 1029−1031. (b) Scirè, S.; Minicò, S.; Crisafulli, C.; Satriano, C.; Pistone, A. Catalytic Combustion of Volatile Organic Compounds on Gold/Cerium Oxide Catalysts. *Appl. Catal. B: Environmental* **2003**, *40*, 43−49.
(640) Hayakawa, K.; Yoshimura, T.; Esumi, K. Preparation of Gold Dendrimer Nanocomposites by Laser Irradiation and Their Catalytic Reduction of 4-Nitrophenol. *Langmuir* **2003**, *19*, 5517−5521.
(641) Inouye, H.; Tanaka, K.; Tanahashi, I.; Hirao, K. Ultrafast Dynamics of Nonequilibrium Electrons in a Gold Nanoparticle System. *Phys. Rev. B* **1998**, *57*, 11334−11340.
(642) Shen, Y. R. *The Principles of Nonlinear Optics*; Wiley: New York, 1984.
(643) Ricard, D.; Roussignol, Ph.; Flytzanis, C. Surface-Mediated Enhancement of Optical Phase Conjugation in Metal Colloids. *Opt. Lett.* **1985**, *10*, 511−513.
(644) Hache, F.; Ricard, D.; Flytzanis, C.; Kreibig, U. The Optical Kerr Effect in Small Metal Particles and Metal Colloids: The Case of Gold. *Appl. Phys. A* **1988**, *47*, 347−357.
(645) Fukumi, K.; Chayahara, A.; Kadono, K.; Sakagushi, T.; Horino, Y.; Miya, M.; Hahakawa, J.; Satou, M. Au^+−Ion-Implanted Silica Glass with Non-Linear Optical Property. *Jpn. J. Appl. Phys.* **1991**, *30*, L742−L744.
(646) Fukumi, K.; Chayahara, A.; Kadono, K.; Sakaguchi, T.; Horino, Y.; Miya, M.; Fujii, K.; Hayakawa, J.; Satou, M. Gold Nanoparticles Ion Implanted in Glass with Enhanced Nonlinear Optical Properties. *J. Appl. Phys.* **1994**, *75*, 3075−3080.
(647) Sasai, J.; Hirao, K. Crystallization Effect on Non-Linear Optical Response of Silicate Glass and Glass-Ceramics Containing Gold Nanoparticles. *J. Non-Cryst. Solids* **2001**, *290*, 49−56.
(648) Sasai, J.; Hirao, K. Relaxation Behavior of Nonlinear Optical Response in Borate Glasses Containing Gold Nanoparticles. *J. Appl. Phys.* **2001**, *89*, 4548−4553.
(649) Inouye, H.; Kanemitsu, Y. Direct Observation of Nonlinear Effects in a One-Dimensional Photonic Crystal. *Appl. Phys. Lett.* **2003**, *82*, 1155−1157.
(650) Shen, Y.-C.; Tang, Z.; Gui, M.; Cheng, J.; Wang, X.; Lu, Z. Nonlinear Optical Response of Colloidal Gold Nanoparticles Studied by Hyper-Rayleigh Scattering Technique. *Chem. Lett.* **2000**, 1140−1141.
(651) Vargas-Baca, I.; Brown, A. P.; Andrews, M. P.; Galstian, T.; Li, Y.; Vali, H.; Kuzyk, M. G. Linear and Nonlinear Optical Responses of a Dye Anchored to Gold Nanoparticles Dispersed in Liquid and Polymeric Matrixes. *Can. J. Chem.* **2002**, *80*, 1625−1633.
(652) Antoine, R.; Brevet, P. F.; Girault, H. H.; Bethell, D.; Schiffrin, D. J. Surface Plasmon Enhanced Non-Linear Optical Response of Gold Nanoparticles at the Air/Toluene Interface. *Chem. Commun.* **1997**, 1901−1902.
(653) Novak, J. P.; Brousseau, L. C., III; Vance, F. W.; Johnson, R. C.; Lemon, B. I.; Hupp, J. T.; Feldheim, D. L. Nonlinear Optical Properties of Molecularly Bridged Gold Nanoparticle Arrays. *J. Am. Chem. Soc.* **2000**, *122*, 12029−12030.
(654) Qu, S.; Song, Y.; Du, C.; Wang, Y.; Gao, Y.; Liu, S.; Li, Y.; Zhu, D. Nonlinear Optical Properties in Three Novel Nanocomposites with Gold Nanoparticles. *Opt. Commun.* **2001**, *196*, 317−323.

(655) Qu, S.; Du, C.; Song, Y.; Wang, Y.; Gao, Y.; Liu, S.; Li, Y.; Zhu, D. Optical Nonlinearities and Optical Limiting Properties in Gold Nanoparticles Protected by Ligands. *Chem. Phys. Lett.* **2002**, *356*, 403−408.
(656) Fang, H.; Du, C.; Qu, S.; Li, Y.; Song, Y.; Li, H.; Liu, H.; Zhu, D. Self-Assembly of the [60] Fullerene-Substituted Oligopyridines on Au Nanoparticles and the Optical Nonlinearities of the Nanoparticles. *Chem. Phys. Lett.* **2002**, *364*, 290−296.
(657) Vance, F. W.; Lemon, B. I.; Hupp, J. T. Enormous Hyper-Rayleigh Scattering from Nanocrystalline Gold Particle Suspensions. *J. Phys. Chem. B* **1998**, *102*, 10091−10093.
(658) Galletto, P.; Brevet, P. F.; Girault, H. H.; Antoine, R.; Broyer, M. Size Dependence of the Surface Plasmon Enhanced Second Harmonic Response of Gold Colloids: Towards a New Calibration Methodology. *Chem. Commun.* **1999**, 581−582.
(659) Olsen, A. W.; Kafafi, Z. H. Gold Cluster-Laden Polydiacetylenes: Novel Materials for Nonlinear Optics. *J. Am. Chem. Soc.* **1991**, *113*, 7758−7760.
(660) Neiman, B.; Grushka, E.; Lev, O. Use of Gold Nanoparticles to Enhance Capillary Electrophoresis. *Anal. Chem.* **2001**, *73*, 5220−5227.
(661) Pumera, M.; Wang, J.; Grushka, E.; Polsky, R. Gold Nanoparticle-Enhanced Microchip Capillary Electrophoresis. *Anal. Chem.* **2001**, *73*, 5625−5628.
(662) Krenn, J. R.; Salerno, M.; Felidj, N.; Lamprecht, B.; Schider, G.; Leitner, A.; Aussenegg, F. R.; Weeber, J. C.; Dereux, A.; Goudonnet, J. P. Light Field Propagation by Metal Micro- and Nanostructures. *J. Microsc.* **2001**, *202*, 122−128.
(663) Ng, L. N.; Luff, B. J.; Zervas, M. N.; Wilkinson, J. S. Propulsion of Gold Nanoparticles on Optical Waveguides. *Opt. Commun.* **2002**, *208*, 117−124.
(664) Park, J. H.; Lim, Y. T.; Park, O. O.; Kim, Y. C. Enhancement of Photostability in Blue-Light-Emitting Polymers Doped with Gold Nanoparticles. *Macromol. Rapid Commun.* **2003**, *24*, 331−334.
(665) Recent miscellaneous references added in proof: (a) Lowe, L. B.; Brewer, S. H.; Krämer, S.; Fuierer, R. R.; Qian, G.; Agbasi-Porter, O.; Moses, C.; Franzen, S.; Feldheim, D. L. Laser-Induced Temperature Jump Electrochemistry on Gold Nanoparticles-Coated Electrodes. *J. Am. Chem. Soc.* **2003**, *125*, 14258−14259. (b) Olofsson, L.; Rindzevicius, T.; Pfeiffer, I.; Käll, M.; Höök, F. Surface-Based Gold Nanoparticle Sensors for Specific and Quantitative DNA Hybridization Detection. *Langmuir* **2003**, *19*, 10414−10419. (c) Wurz, G. A.; Hranisavljevic, J.; Wiederrecht, G. P. Electromagnetic Scattering Pathways for Metallic Nanoparticles: A Near-Field Optical Study. *Nano Lett.* **2003**, *3*, 1511−1516. (d) Addition, Suppression, and Inhibition in the Electrophoretic Deposition of Nanocrystal Mixture Films for CdSe Nanocrystals with gamma-Fe_2O_3 and Au Nanocrystals. Islam, M. A.; Xia, Y.; Steigerwald, M. L.; Yin, M.; Liu, Z.; O'Brien, S.; Levicky, R.; Herman, I. P. *Nano Lett.* **2003**, *3*, 1603−1606.

CR030698+